

# Application of Visible Light Mediated Photocatalysis in the Synthesis of Biologically Active Molecules



Dissertation zur Erlangung des Doktorgrades der Naturwissenschaften

Dr. rer. nat.

der Fakultät für Chemie und Pharmazie

der Universität Regensburg

vorgelegt von

Simon Budde

aus Kienlohe

im Jahr 2020

Diese Arbeit wurde angeleitet von:

Prof. Dr. Oliver Reiser

Promotionsgesuch eingereicht am:

01.12.2020

Promotionskolloquium am:

28.01.2021

Prüfungsausschuss:

Vorsitz: Prof. Dr. Rainer Müller

1.Gutachter: Prof. Dr. Oliver Reiser

2.Gutachter: Prof. Dr. Julia Rehbein

3.Prüfer: Prof. Dr. Arno Pfitzner

Der experimentelle Teil der vorliegenden Arbeit wurde in der Zeit von November 2015 bis Oktober 2019 unter der Leitung von Prof. Dr. Oliver Reiser am Institut für Chemie und Pharmazie der Universität Regensburg angefertigt.

Herrn Prof. Dr. Oliver Reiser danke ich herzlich für die interessante Themenstellung und seine stete Unterstützung während der Durchführung der vorliegenden Arbeit.





Meiner Familie

*„Die Hoffnung ist der Regenbogen über dem  
herabstürzenden Bach des Lebens.“*

Friedrich Wilhelm Nietzsche

## Contents

1.	Overview.....	1
1.1	Summary.....	1
1.2	Zusammenfassung.....	3
2.	General Introduction .....	5
2.1	Basics of Visible Light Mediated Photochemistry .....	5
2.2	Photochemical Decarboxylations.....	11
3.	Smiles Rearrangement .....	14
3.1	Introduction.....	14
3.2	Studies on Visible Light Mediated Smiles Rearrangement <sup>x</sup> .....	16
3.2.1	Initial Studies: Phenylethylamines, Tetrahydroisoquinolines and Benzoazepinones <sup>y</sup> .....	16
3.2.2	Broadening the Substrate Scope: Amphetamines and More <sup>z</sup> .....	23
3.2.3	Consecutive Studies: Incorporating Aspartic and Glutamic acid.....	29
3.3	Decarboxylative Transformations of Oxazolidinone Protected Natural Amino Acids .....	31
3.4	The Hydantoin Group as Alternative to Oxazolidinone Protecting Group.....	34
3.5	Conclusion .....	39
3.6	Experimental Section.....	40
3.6.1	General Information .....	40
3.6.2	Fluorescence Quenching .....	42
3.6.3	Synthesis of Starting Materials for the Amphetamine Synthesis.....	44
3.6.4	Synthesis of Boc-amphetamines .....	52
3.6.5	Synthesis of Hydantoins .....	54
3.6.6	Spectra.....	63
3.7	Literature .....	81
4.	Visible Light Mediated Oxidative Ring Expansion of Cyclopropanes <sup>†</sup> .....	86
4.1	The Endoperoxide Moiety .....	86
4.2	Preliminary Studies.....	93
4.3	Optimization.....	94
4.4	Substrate Scope.....	97
4.5	Stability of the Endoperoxides .....	106
4.6	Transformations of the Endoperoxides.....	107
4.7	Mechanistic Studies.....	108
4.8	Biological Tests.....	119
4.9	Conclusions.....	121
4.10	Experimental Section Endoperoxides.....	122

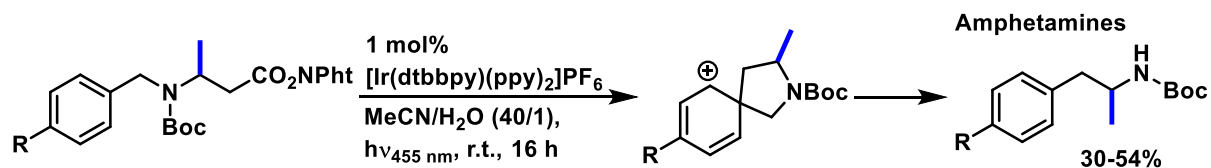
4.10.1	General Information .....	122
4.10.2	Biological Testing .....	125
4.10.3.	Thermogravimetric Analysis .....	128
4.10.4.	Cyclovoltammetry .....	131
4.10.5.	Fluorescence Quenching .....	135
4.10.6.	MM2 Minimization: Structure Analysis .....	137
4.10.7.	Games Optimization and Orbital Simulation .....	141
4.10.8.	Synthesis of Starting Materials .....	143
4.10.9.	Synthesis of Hydroperoxides .....	184
4.10.10.	Synthesis of Butyrolactones from Endoperoxides .....	186
4.10.11.	Crystal Structures .....	188
4.10.12.	Chiral HPLC .....	205
4.10.13.	NMR Spectra .....	207
4.11	Literature .....	264
5.	List of Abbreviations .....	268
6.	Curriculum Vitae .....	270
7.	Acknowledgements .....	272
8.	Declaration .....	275

# 1. Overview

## 1.1 Summary

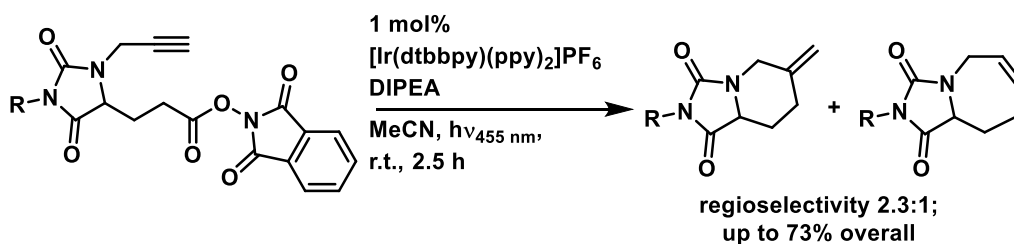
The work presented herein achieved the application of different facets of visible light mediated photocatalysis towards the synthesis of biologically active and hence pharmaceutically relevant molecules. It is divided in two parts.

The first part deals with harvesting the powers of the long known photochemical decarboxylation. By means of *N-O* esters, *i.e.* *N*-hydroxyphthalimide esters, primary carboxylic acids can be sufficiently activated to be decarboxylated by photochemical means. Using this technique, the scope of a Smiles rearrangement initiated by visible light mediated decarboxylation previously discovered in this workgroup was expanded. Additionally to the compound range shown by Christian Faderl, a scope of various amphetamines was synthesized (Scheme 1). In the course of this the possibility for incorporation and conservation of enantiomeric information was investigated and successfully demonstrated with the synthesis of enantiomerically pure (*S*)-amphetamine, a widely administered ADHD therapeutic.



Scheme 1: Synthesis of amphetamines *via* visible light initiated decarboxylation/Smiles rearrangement cascade.

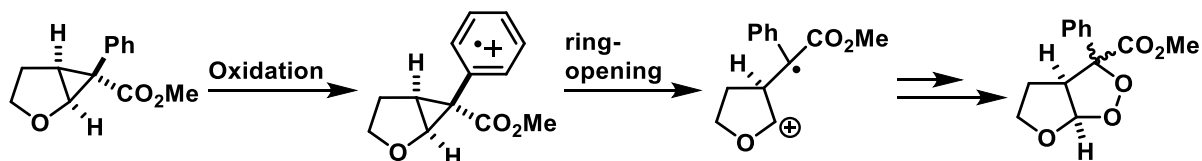
As the general build of the starting material required for such transformation implicated that natural aspartic acid could be a viable building block, this possibility was examined. Initial results were negative, but sparked the idea of using aspartic acid and its homologue, glutamic acid, in decarboxylations. While in literature the latter was target for the decarboxylation of its  $\alpha$ -carboxy group, its  $\gamma$ -carboxy group, representing a primary acid, was the focus of this work. Adequate starting materials based on glutamic acid were synthesized, using different protection strategies for  $\alpha$ -carboxylic acid and amine. The formation of an oxazolidinone or a hydantoin heterocycle was key to a successful protection of the two functionalities and conservation of the stereoinformation brought in by the naturally enantiopure glutamic acid.



Scheme 2: Substituted hydantoin derived from glutamic acid used for photochemical decarboxylation.

While the oxazolidinone protection strategy was used in decarboxylative *intermolecular* reactions and further explored by Christian Eichinger, the hydantoin protection strategy was successfully applied for an *intramolecular* cyclization, giving rise to six-membered ring systems (Scheme 2).

The second part deals with a photochemical oxygenation of cyclopropanated (hetero-) cycles giving rise to annelated peroxides. Suitable starting materials require an aromatic system adjacent to the tricycle, which can be oxidized in presence of air and Fukuzumi's catalyst. This generates a radical next to the cyclopropyl group, triggering its opening and subsequently leading to the incorporation of oxygen, therefore expanding the cyclopropane to a five-membered endoperoxide (Scheme 3).



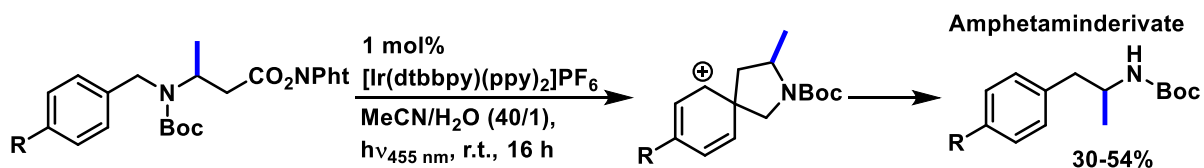
Scheme 3: Synthesis of endoperoxides from cyclopropanated furan.

Following the exploration of a broad range of substrates, including differently substituted cyclopropanated *O*- and *N*-heterocycles as well as carbocycles, an array of endoperoxides was tested for activity against the malaria pathogen *plasmodium falciparum* at the Max Planck Institute of colloids and interfaces by Felix Goerdeler of the research group of Prof. P. H. Seeberger. The results showed a positive correlation between activity and lipophilicity of the tested endoperoxides, revealing the carbocyclic derivatives to be most active. While the best IC<sub>50</sub> values were found to be in the low micromolar range and thus a factor 1000 higher than the current state-of-the-art malaria therapeutic artesunate, these initial results demonstrate the biological activity of the generated endoperoxides and point the way to possible further research.

## 1.2 Zusammenfassung

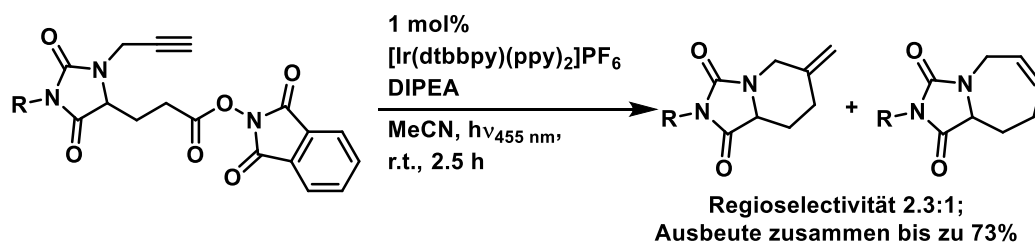
Im Rahmen der nachfolgend vorgestellten Arbeit wurde die Anwendung unterschiedlicher Facetten der Photokatalyse mit sichtbarem Licht in der Synthese biologisch aktiver Moleküle von pharmazeutischer Relevanz erreicht. Die Arbeit teilt sich in zwei Teile.

Der erste Teil beschreibt die Verwendung der lange bekannten photochemischen Decarboxylierung. Mittels der Aktivierung der Carboxylgruppe als *N*-*O*-ester, hier: als *N*-Acyloxyphthalimid, können primäre Carboxylgruppen mittels sichtbaren Lichts decarboxyliert werden. Durch die Anwendung dieser Strategie konnte die Substratbreite einer durch Decarboxylierung eingeleiteten Smiles-Umlagerung, welche schon zuvor im Arbeitskreis Reiser untersucht wurde, erweitert werden. Zusätzlich zu den Substraten, an denen durch Christian Faderl die Umlagerung erfolgreich durchgeführt wurde, konnte diese auch erfolgreich zur Synthese einiger Amphetamin-Derivate eingesetzt werden (Schema 1). Im Zuge dessen konnte anhand der erfolgreichen Synthese von enantiomerenreinen (*S*)-Amphetamin, welches zur Therapie von ADHS eingesetzt wird, gezeigt werden, dass in diesem Falle die Stereoinformation des Startmaterials erhalten bleibt.



Schema 1: Synthese von Amphetaminderivaten mittels einer Kaskade von Decarboxylierung und Smiles-Umlagerung.

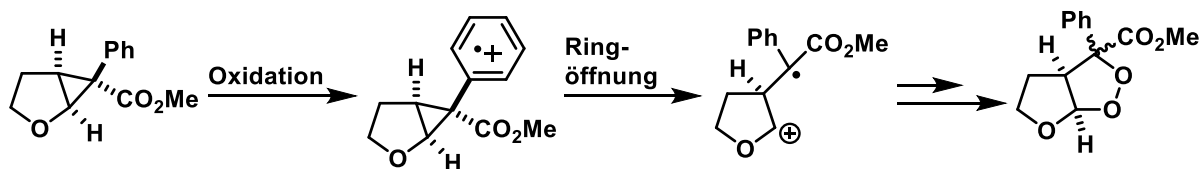
Da die natürliche Aminosäuren Asparaginsäure und Glutaminsäure die grundsätzlichen Voraussetzungen für eine Verwendung als Teil eines geeigneten Startmaterials erfüllen, und erhebliche Vorteile wie geringe Kosten und inhärente optische Reinheit mit sich bringen, wurden sie als Ziel weiterer Untersuchungen ausgewählt. Während einige Literatur zur Decarboxylierung der  $\alpha$ -Carboxylgruppe von Asparaginsäure und Glutaminsäure, dem um eine CH<sub>2</sub>-Gruppe verlängerten Homolog, verfügbar ist, wurde im Folgenden auf die Decarboxylierung der primären Säuregruppe der beiden Di-Säuren mittels Aktivierung als *N*-Acyloxyphthalimid abgezielt. Für Amin und  $\alpha$ -Säuregruppe wurden verschiedene Schutzgruppen getestet. Hierzu wurden Oxazolidinon- und Hydantoinheterocyclen gebildet, welche erfolgreich die beiden unbeteiligten funktionellen Gruppen und die Stereoinformation der natürlichen Aminosäuren bewahren.



Schema 2: Glutaminsäurebasiertes Hydantoinderivat als Startmaterial einer photochemischen Decarboxylierung.

Während die Oxazolidinon-Schutzgruppe in decarboxylativen *intermolekularen* Reaktionen verwendet wurde, welche von Christian Eichinger näher untersucht wurden, wurde ein geeignetes glutaminsäurebasiertes Hydantoin-Derivat erfolgreich bei einer *intramolekularen* Cyclisierung zu einem sechsgliedrigen Heterozyklus eingesetzt (Schema 2).

Im zweiten Teil dieser Dissertation wird die photochemische Oxygenierung von cyclopropanierten (Hetero-)zyklen zu annelierten Endoperoxiden beschrieben. Geeignete Startmaterialien für eine derartige Reaktion benötigen ein aromatisches System neben dem dreigliedrigen Ring, welcher in Gegenwart sichtbaren Lichtes, (Luft)sauerstoff und Fukuzumi-Katalysator oxidiert werden kann. Dabei wird ein Radikalzentrum neben dem Cyclopropanring gebildet, welcher dessen Öffnung auslöst. Diese Öffnung wird schließlich von Disauerstoff überbrückt, was zur Bildung eines fünfgliedrigen Endoperoxids führt (Schema 3).



Schema 3: Synthese von Endoperoxiden aus cyclopropaniertem Furan.

Aus der Reihe verschiedenster auf diesem Wege synthetisierter Endoperoxide wurde eine Auswahl am Max Planck Institut für Kolloid- und Grenzflächenforschung von Felix Gördeler aus der Arbeitsgruppe von Prof. P. H. Seeberger auf Aktivität gegen den Malaria-Erreger *plasmodium falciparum* untersucht. Die Ergebnisse zeigen eine positive Korrelation zwischen Aktivität und Lipophilie der untersuchten Endoperoxide, mit einem annelierten Carbocyclus als bestem Derivat. Während die gefundenen IC50-Werte im mikromolaren Bereich liegen, belegen sie doch die Wirksamkeit der synthetisierten Endoperoxide und zeigen den Weg zu möglichen weiteren Untersuchungen.



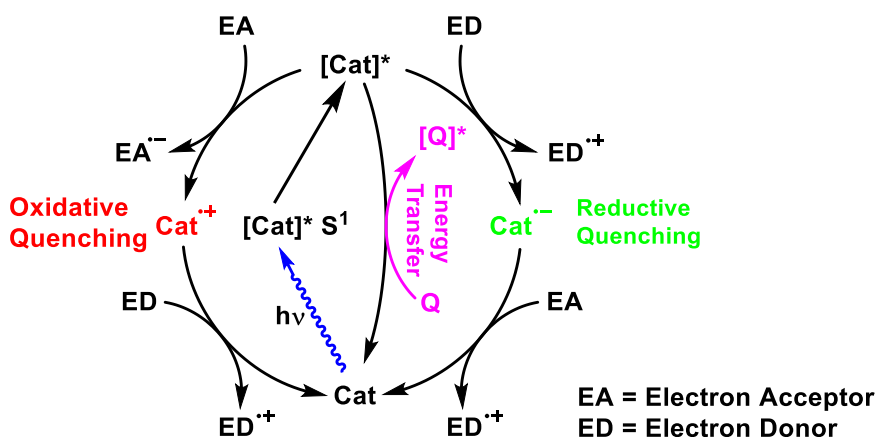
## 2. General Introduction

### 2.1 Basics of Visible Light Mediated Photochemistry

In the last two decades, visible light mediated photochemistry saw a rapid ascent in popularity<sup>1</sup>, as indicated by the number of publications in this field. It has become a widely established activation method, which provides selectivity and versatility and yet is operationally simple. Supported by the development of efficient light sources with narrow emission bands in the visible region, namely LED-lamps, in the 1990s, photochemistry is now commonly found even in industrial-scale processes. Controlled irradiation at a certain wavelength with a defined power allows for reproducibility and combined with flow-chemistry, visible light photochemistry is a valuable tool for greener processes in industrial syntheses, as covered in various reviews.<sup>2-7</sup>

For a long time, with some notable exceptions<sup>8</sup>, photochemistry relied on the use of UV-light, generated by high-pressure mercury lamps, posing a costly safety hazard. Some intriguing transformations were achieved<sup>8-10</sup>, but the applicability was low due to the incompatibility of many functional groups with high-energy UV-light and the inconvenient reaction setup.

However, the use of visible light generated by efficient light sources was not only an operational improvement, but also paved the path to completely new mechanisms and therefore transformations. While UV-light can directly excite organic molecules, these usually do not absorb in the visible region, making the use of catalysts mandatory. These colored organic dyes<sup>11</sup> and transition metal complexes<sup>12</sup> can harvest photons from the visible spectrum with a wavelength between 400 and 800 nm and then catalyze reactions in colorless substrates *via* different pathways. Combinations with other catalyst systems are possible, giving way to an entirely new playground for organic chemists.<sup>13-17</sup>



Scheme 4: Generic mechanism for photocatalytic reactions.

Said pathways are categorized either as single electron transfer (SET)<sup>6</sup> or energy transfer (ET) mechanisms (Scheme 4).<sup>18</sup> The single electron transfer mechanisms are usually called photoredox catalysis, which utilizes the ability of the excited catalyst  $[\text{Cat}]^*$  to either take up an electron from a given substrate and therefore act as oxidant (Oxidative Quenching), or donate an electron to function as one-electron reductant (Reductive Quenching). To close the catalytic cycle, the catalyst then has to take or respectively give an electron to return in its ground state, as shown in Scheme 4.

The energy transfer pathway in contrary does not necessarily produce a charged species, but brings the substrate molecule (Q) in an excited state  $[\text{Q}]^*$ , which can trigger *e.g.* intramolecular electron transfer between two functional groups within the substrate molecule, generating (di-)radicals.<sup>18-19</sup>

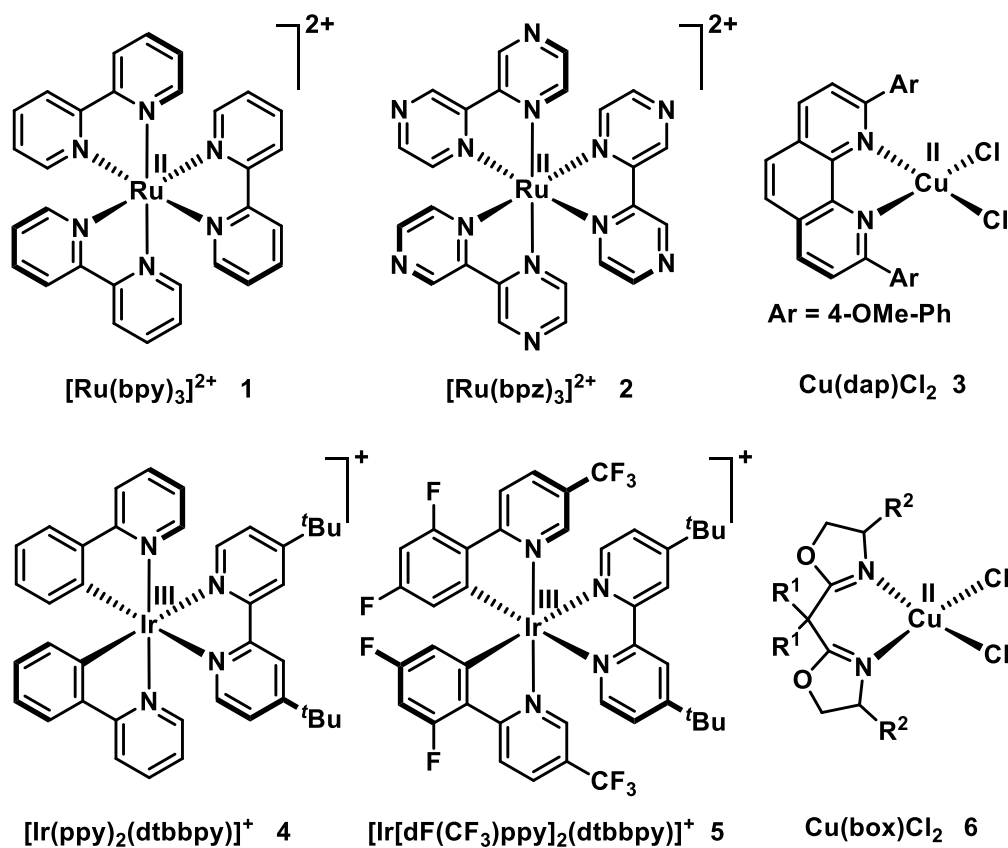
For the single electron pathway, the above described routes are differentiated by choosing the reaction conditions accordingly. To determine these conditions, knowledge about the reduction and oxidation potentials<sup>20</sup> of all the components in the reaction is required, including the catalyst in its ground- and excited state. Only then, the following questions can be answered:

- Does the potential of the catalyst match the potential of the substrate, *i.e.* can a SET between them take place?
- Does the reaction require a sacrificial electron donor, and if so, which one?
- Is the desired product stable under the conditions, or will it react further because it can also undergo a SET?

Analytical methods originally established in the field of electrochemistry and physical chemistry give access to the required numbers<sup>21</sup>, *e.g.* cyclic voltammetry for the elucidation of redox potentials.

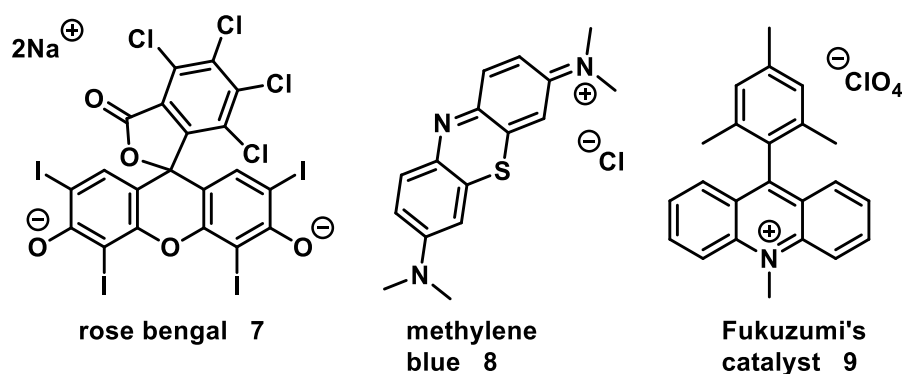
The toolbox available for adjusting the reaction conditions holds a variety of catalysts, covering a broad range of potentials. Several characteristics determine if a colored molecule can become an effective photocatalyst: The molecule needs a high absorption coefficient, which shows that of all the incoming photons, a large part is absorbed and can power the catalytic cycle. Upon absorption, a potential catalyst is transferred to its excited state, with the mechanism differing greatly between heterogeneous<sup>22</sup> and homogeneous catalysts, and in the latter group again between transition metal based and solely organic catalysts<sup>23</sup>. It needs to remain in the excited state for a sufficiently long time (so-called lifetime) without unproductive relaxation to enable interaction with the substrate, as this requires a close encounter of the two (distance under 10 Å). All of these properties can be tuned, by so-called “doping” in heterogeneous inorganic catalysts, changing ligands in transition metal complexes or substituents in organic dyes.

Most commonly employed are transition metal catalysts, which are known for their superior stability (Scheme 5). Their properties are determined by the ligands attached. The costly ruthenium<sup>24-25</sup> (*e.g.* **1**, **2**) and iridium<sup>26</sup> (*e.g.* **4**, **5**) based catalysts operate with an outer sphere mechanism, where the radicals generated do not interact with the metal centre. Copper-based catalysts (*e.g.* **3**, **6**) have shown extraordinary versatility, allowing for additional interaction: Substrates can coordinate to the copper and undergo visible light induced homolysis, or the radical formed during the reaction can coordinate to the copper, and therefore give rise to an inner sphere mechanism. The details of copper photocatalysis are discussed in detail in a recent review by Reiser *et al.*<sup>27</sup>



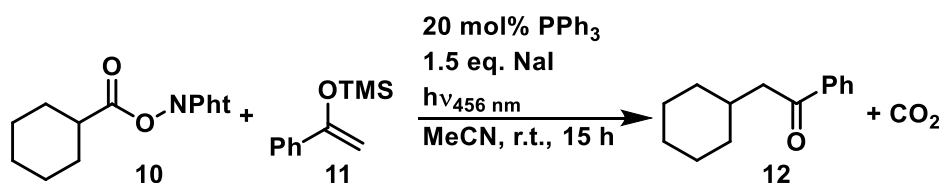
Scheme 5: Transition metal photocatalysts.

Next to transition metal catalysts, organic dyes stand as viable alternative (Scheme 6). Despite being less stable, they can be used in larger quantities than *e.g.* Ir-based catalysts, as they are more often than not inexpensive and produced in large scale by industry.



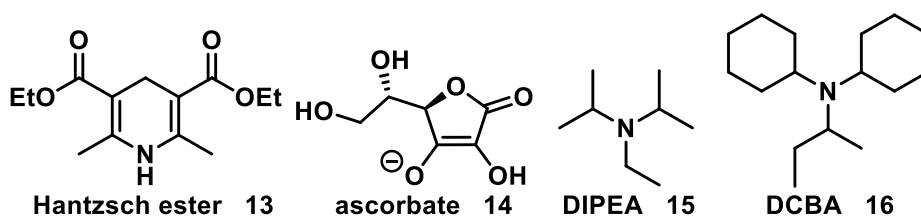
Scheme 6: Organic dyes used as photocatalysts.

The broad range is further enhanced by compounds that cannot be summarized under the two groups of catalysts discussed above, such as the heterogeneous anatase modification of titanium dioxide<sup>28-29</sup> or rather exotic cases, *e.g.* sodium iodide in combination with triphenylphosphine, which has been used as a photocatalyst by Fu *et al.* (Scheme 7).<sup>30</sup>



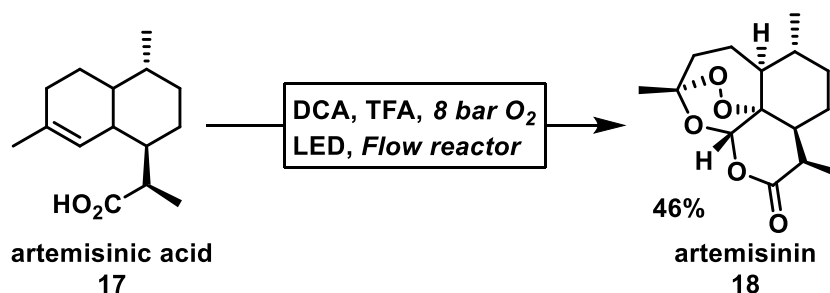
Scheme 7: Visible light mediated decarboxylative alkylation with iodide as catalyst.

Not only tailored catalysts, but also sacrificial electron donors tuned to specific demands – *i.e.* less prone to side reactions, good solubility or with a special redox potential – are available (Scheme 8). In terms of green chemistry, atom efficiency needs to be improved: The sacrificial electron donor should be of low molecular weight, recoverable and recyclable, easily accessible or ideally not “sacrificial” at all, but also transformed into a useful chemical.



Scheme 8: Assorted sacrificial electron donors used in photocatalysis.<sup>31</sup>

While a wide range of transformations can be performed using photocatalysis, its utilization in industry was hindered due to issues when upscaling lab-scale reactions. Traditional activation methods such as heating have been used for a long period of time; hence the knowledge on key points to solve in upscaling is there. Photochemistry however requires additional thought given to issues such as light penetration into vessels, which is dependent on the concentration and on the amount of volume, and cooling when strong lights are used. Several methods exist to improve lighting – *e.g.* lighting from the inside, or the use of flow techniques<sup>32-35</sup>, which in fact combine well with photocatalytic reactions.



Scheme 9: Synthesis of artemisinin by Seeberger *et al.*<sup>36</sup>

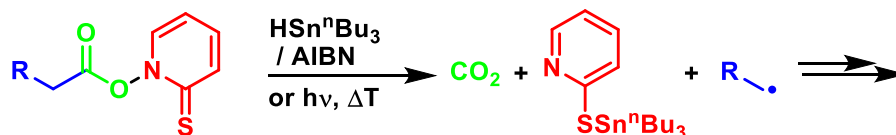
Even two-phase (liquid/liquid *and* liquid/gas) reactions can be performed in flow<sup>37</sup>, as shown by the continuous flow synthesis of the antimalarial pharmaceutical artemisinin **18** from its precursor artemisinic acid **17** by photochemical oxidation in presence of oxygen (Scheme

9).<sup>36</sup> This process allows for large scale synthesis of the drug, and as the precursor is extracted from a plant, the chlorophyll contained in the extraction mixture can be used as photocatalyst, making this a prime example of green chemistry. Hence, this much desired treatment for the malaria-disease becomes available at a reasonable price to the people even in third-world countries.

## 2.2 Photochemical Decarboxylations

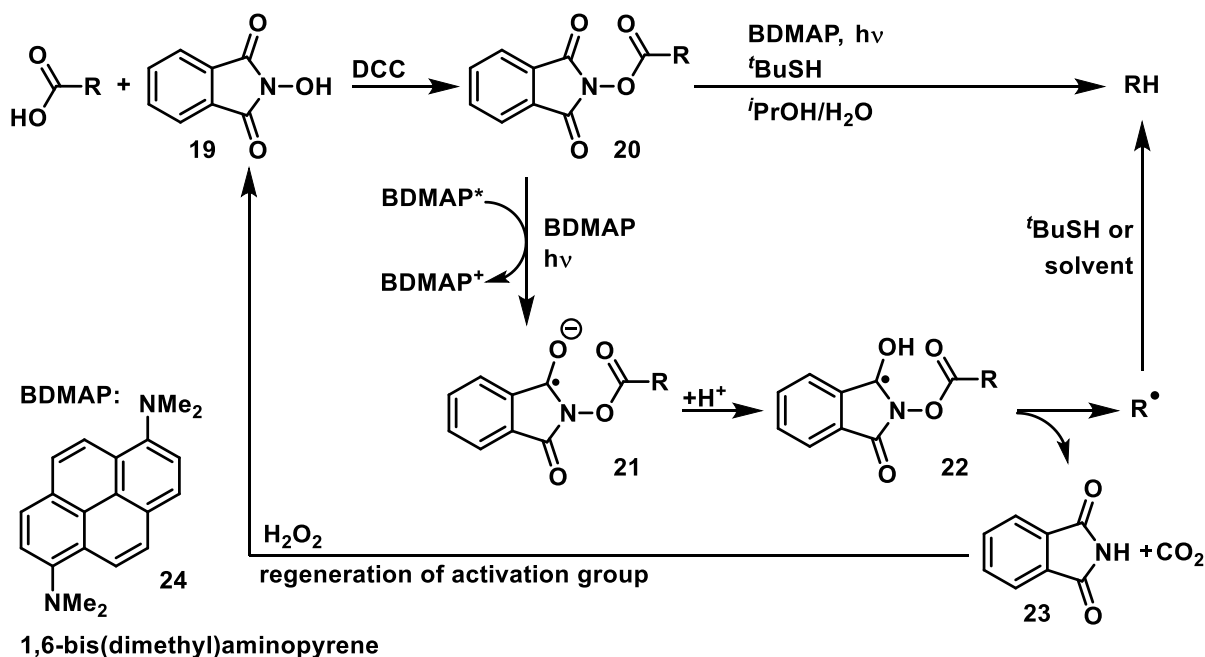
Decarboxylations are important reactions in nature and in synthetic chemistry. In nature, catalytic decarboxylation is a key reaction in most lifeforms, supplying energy *via* the Krebs cycle.<sup>38</sup> In chemistry, decarboxylations are useful reactions due to various carboxylic acids being available in large scale but at low cost (amino acids, fatty acids), and therefore a variety of starting materials are commercially available. In the laboratory, the extrusion of CO<sub>2</sub> from carboxylic acids can be achieved by a number of ways, including heating<sup>39</sup>, electrochemical methods<sup>40-41</sup>, use of various catalysts<sup>42</sup>, UV-irradiation<sup>43</sup> and photoredox catalysis<sup>44</sup>, the latter being the focus of this thesis and therefore discussed in more detail in the following.

Barton *et al.* first described decarboxylations of active esters by thermal means and upon addition of tributylstannane/AIBN as radical source (Scheme 10).<sup>45-46</sup> The radicals could be added either to *e.g.* double bonds, selenides<sup>46</sup>, or simply abstract hydrogen atoms. With further development by Bartons successors, among them Samir Z. Zard, this style of decarboxylation became widely used, even more so as the use of toxic tin-based radical-sources could be avoided by using an alternative “radical source” capable of inducing homolytic cleavage of the active ester.<sup>47</sup> This “radical source” is of course light, which makes the use of the *N-O*-esters developed by Barton viable even today.<sup>48</sup>



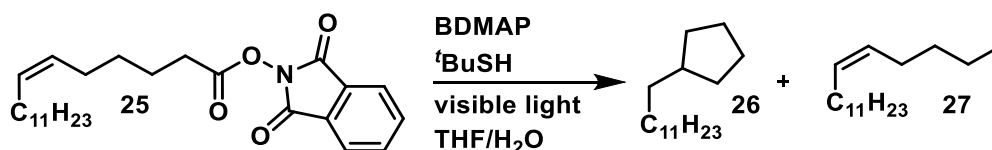
Scheme 10: Decarboxylation of active esters as described by Barton *et al.*<sup>45</sup>

An important contribution in the area of photochemical decarboxylations was made by the group of Okada *et al.*, who used a different activation group constructed from *N*-hydroxyphthalimide **19**, which is more easily introduced and can be regenerated after completion of the reaction (Scheme 11).<sup>49</sup>



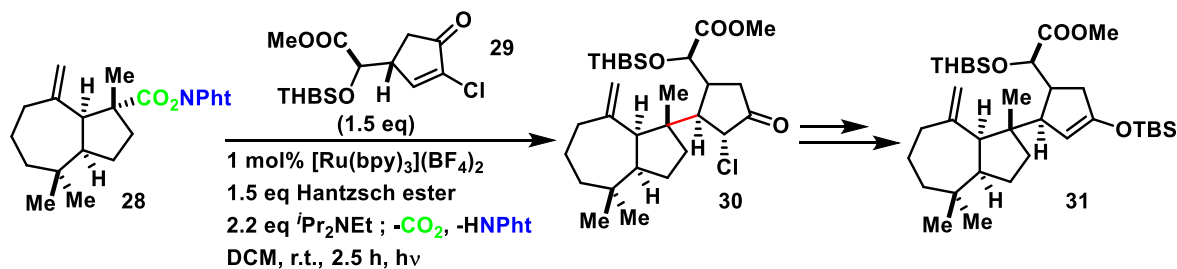
Scheme 11: Decarboxylation of *N*-acyloxyphthalimides as described by Okada *et al.*<sup>49</sup>

This decarboxylation generates free radicals, which can undergo various transformations, *intramolecular* and *intermolecular* (Scheme 12).



Scheme 12: Application of Okada's decarboxylation.<sup>49</sup>

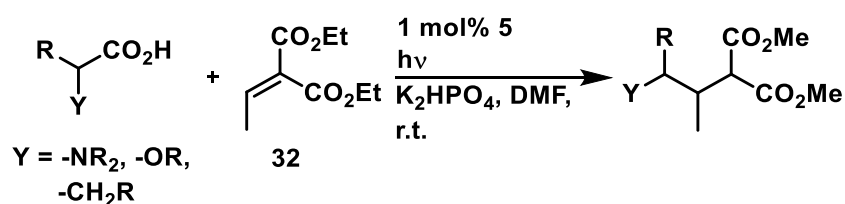
Even though new techniques were developed which avoid the use of active-esters altogether, the decarboxylation of *N*-acyloxyphthalimides remains viable due to the ease of preparation of the required *N*-*O*-esters and the compatibility with modern photoredox chemistry. In the example shown below (Scheme 13), Overman *et al.* use  $[\text{Ru}(\text{bpy})_3]^{2+}$  as photocatalyst instead of BDMAP, and use a combination of Hantzsch ester **13** and DIPEA **15** as sacrificial electron donors to facilitate the key step in their synthesis of (-)-aplyviolene **31**.<sup>50</sup>



Scheme 13: Synthesis of aplyviolene **31** by Overman *et al.*<sup>50</sup>



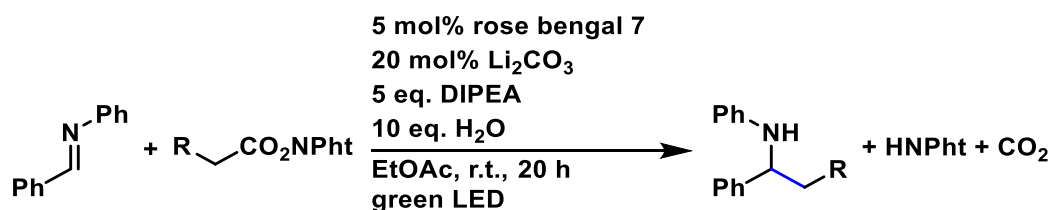
For a long time, the use of activation groups was mandatory to achieve successful decarboxylation under photoredox conditions, until in 2014 the group of MacMillan *et al.* demonstrated the visible light mediated photocatalytic decarboxylation of plain carboxylic acids without the work-around of active esters.<sup>51</sup> Employing highly oxidizing fluorinated [Ir(dF(CF<sub>3</sub>)ppy)<sub>2</sub>(dtbbpy)]PF<sub>6</sub> catalyst, salts of carboxylic acids in activated positions (*e.g.* α to a heteroatom group, secondary or tertiary acids) were decarboxylated upon irradiation. Among the tested bases, which were used to deprotonate the acids, forming their respective carboxylates, K<sub>2</sub>HPO<sub>4</sub> gave the best results (Scheme 14).



Scheme 14: Decarboxylation as described by MacMillan *et al.*<sup>51</sup>

Since its first description in literature, this technique has been applied as the key step in a number of syntheses.<sup>52-53</sup>

However, this active-ester free approach fails for unactivated primary carboxylic acids, *e.g.* most fatty acids from natural sources. In contrast, the decarboxylation of *N*-hydroxyphthalimide esters is possible also with such substrates and in general requires less oxidizing conditions and hence may be more suitable to sensitive substrates. A relevant up-to-date example is depicted in Scheme 15: Rüping *et al.* employed radicals generated *via* visible light photoredox decarboxylation from various acyloxyphthalimides for an addition to imines<sup>54</sup>, a transformation for which traditionally organometallic reagents would be employed.



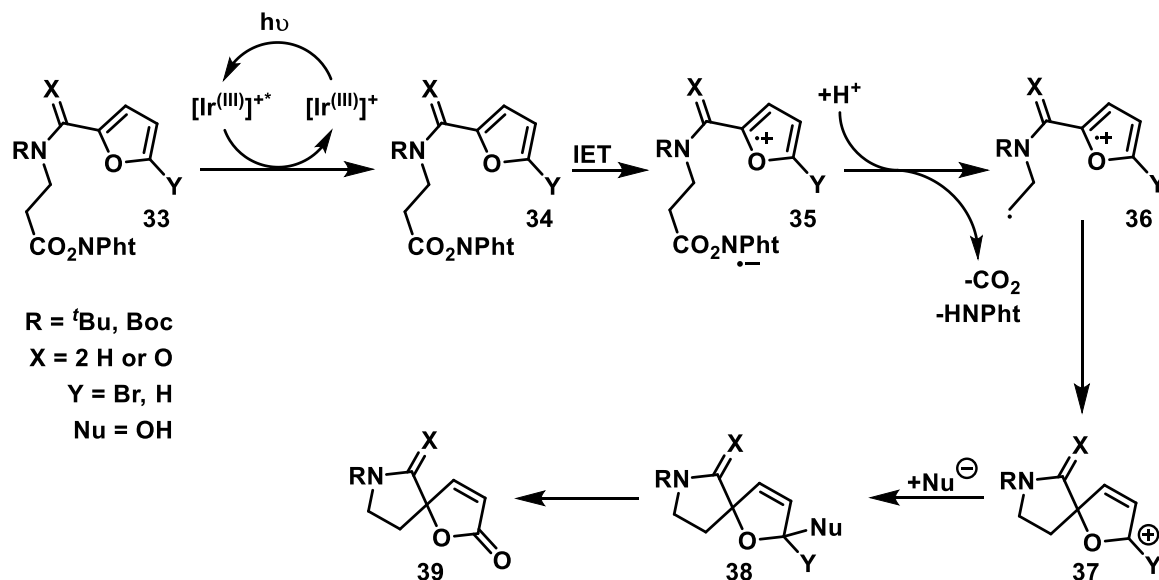
Scheme 15: Decarboxylation of *N*-acyloxyphthalimides for the construction of amines by Rüping *et al.*<sup>54</sup>

In conclusion, visible light mediated decarboxylation represents an important technique in the synthesis of complex molecules and an alternative to other activation methods, filling with life the term “traceless activation group” coined by D. W. C. MacMillan.<sup>51</sup>

### 3. Smiles Rearrangement

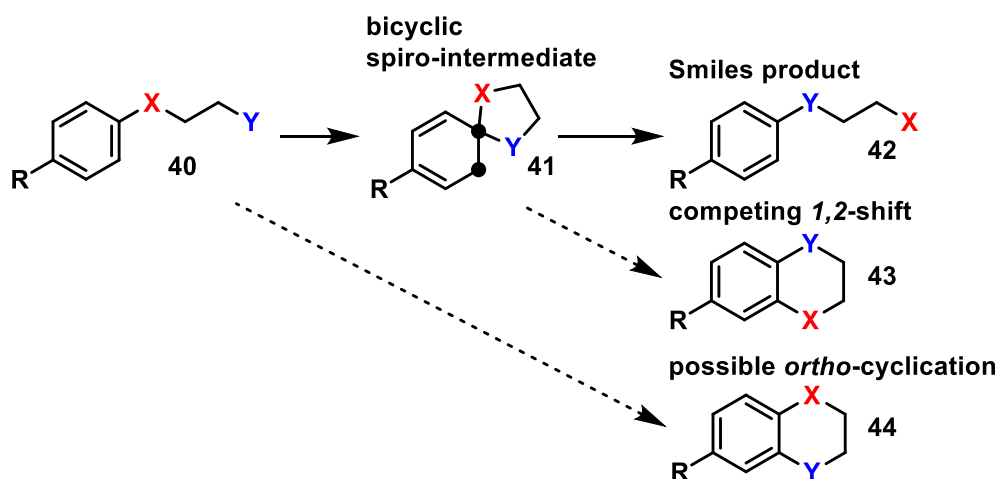
#### 3.1 Introduction

The visible light mediated decarboxylation elaborated on in the previous chapter was applied by Reiser *et al.* for a so-called Smiles rearrangement (Scheme 16).<sup>55</sup>



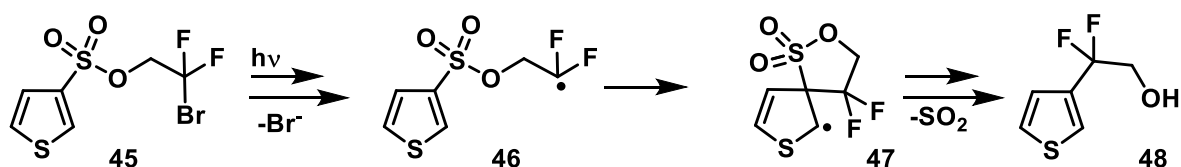
Scheme 16: Visible light mediated decarboxylation and consecutive rearrangement published by Reiser *et al.*<sup>55</sup>

The term is named after a rearrangement described by Samuel Smiles in 1931<sup>56</sup> and used to describe reactions where a chain on an aromatic system switches its start and end point, most commonly *via* a bicyclic intermediate (**41**, Scheme 17). As the reaction pathway involves an *ipso*-cyclization, the reaction is only feasible for certain chain lengths. Typically five or six-membered intermediates give the best results, with longer chains being disfavored and shorter chains nearly impossible as *per* the Baldwin rules.<sup>57</sup> Driving force is the higher stability of the newly formed bond, and the rearrangement is often triggered by reactions releasing volatile groups such as CO<sub>2</sub> (compare Scheme 16) or SO<sub>2</sub>.<sup>58</sup> From the spiro-intermediate an *1,2* shift (**43**) is competing with the ring opening, which can be differentiated from a possible *ortho*-cyclization (**44**) only in presence of other substituents.



Scheme 17: Basic representation of a Smiles rearrangement.

The Smiles rearrangement has been<sup>59</sup> and still is<sup>60</sup> an interesting option for the construction of side-chains of aromatic systems, even more so as visible light mediated photocatalysis presents a powerful and selective method to facilitate these reactions in highly functionalized molecules.<sup>61</sup> Among a number of contemporary examples<sup>e.g.62-63</sup>, one reported by Stephenson *et al.*<sup>64</sup> is shown in Scheme 18, where the reaction is initiated by radical formation *via* visible light mediated photoredox catalysis.



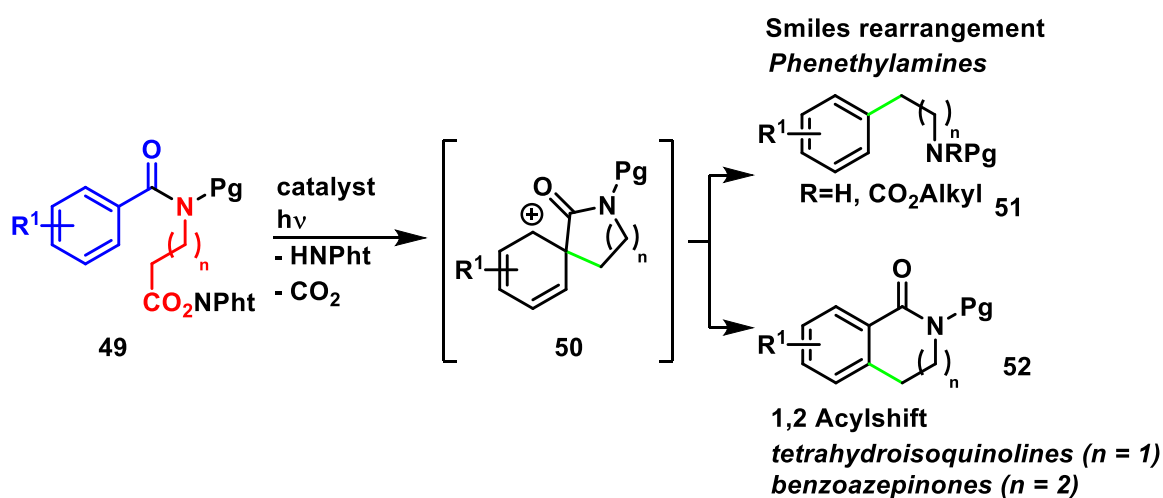
Scheme 18: Smiles rearrangement as key step in the synthesis of an ORL-1 antagonist.<sup>64</sup>

Following the previous work of the Reiser group on this topic (Scheme 16) and drawing inspiration from the literature, visible light mediated decarboxylation was applied as key step, initiating a Smiles-rearrangement, in the synthesis of bioactive compounds and some derivatives.

## 3.2 Studies on Visible Light Mediated Smiles Rearrangement <sup>‡</sup>

### 3.2.1 Initial Studies: Phenylethylamines, Tetrahydroisoquinolines and Benzoazepinones <sup>‡</sup>

The results described in this first sub-chapter are results of C. Faderls work, which have been published as his Ph.D thesis<sup>65</sup>, and which are the foundation for the following work of the author of this thesis. They are given within this thesis to present a reasonably complete view and proper introduction on the subject of the Smiles rearrangement triggered by photocatalytic decarboxylation.



Scheme 19: Visible light mediated photocatalysis initiating a Smiles rearrangement.

It was envisioned that the classes of biologically important phenylethylamines<sup>66</sup> (**51**), tetrahydroisoquinolines<sup>67</sup> (**52**, n = 1), or benzoazepinones (**52**, n = 2) could be accessed *via* a Smiles rearrangement from readily available starting materials **49** making use of renewable resources, *i.e.* benzoic and amino acids (Scheme 19).<sup>58, 63, 68-70</sup> A photochemical decarboxylation of a primary carboxylic acid should trigger the rearrangement, therefore an active ester, *i.e.* an *N*-acyloxyphthalimide, was used as starting material (**49**). Furthermore, the starting material was comprised from 4-methoxy benzoate, which was linked to  $\beta$ -alanin *via* an amide bond. On the amide-nitrogen, a <sup>t</sup>butyl group was attached to ensure a correct conformation, as this bulky group forces the starting material into a desirable conformation, bringing in close proximity the aromatic systems of the phthalimide and the benzoate (Figure 1).

<sup>‡</sup> Parts of this chapter are reproduced from C. Faderl, S. Budde, G. Kachkovskiy, D. Rackl and O. Reiser, *J. Org. Chem.*, **2018**, *19*, 12192-12206; Copyright 2018 American Chemical Society.

<sup>‡</sup> The work presented in this subchapter is work performed by Christian Faderl and was published in his Ph.D thesis.

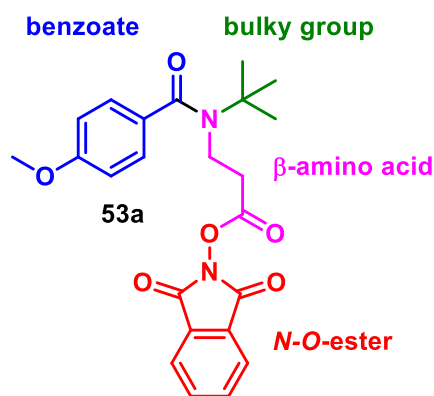
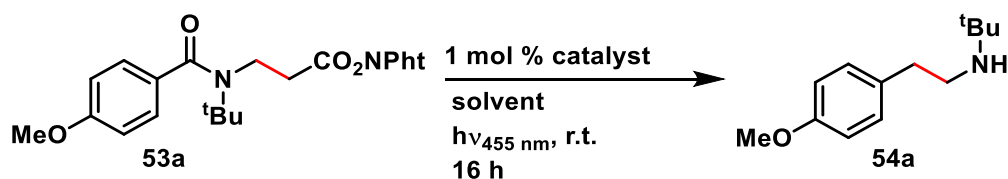


Figure 1: Model substrate for photochemical Smiles-rearrangement.

Under irradiation with a blue LED ( $\lambda_{\text{max}} = 455 \text{ nm}$ ) an iridium based photocatalyst  $[\text{Ir}(\text{dtbbpy})(\text{ppy})_2]\text{PF}_6$  was able to transform the model substrate **53a**, yielding the desired rearrangement product **54a** in 41% yield (Table 1 *vide infra*). As a competing process, a considerable amount of ester hydrolysis was observed, accounting for the complete conversion of **53a**. A screening of reaction conditions revealed that some amount of water in a polar organic solvent is beneficial for the reaction, as the water is coordinating to the phthalimide-portion of the molecule, reducing its oxidation potential.<sup>71</sup>

Common photocatalysts such as  $[\text{Ru}(\text{bpy})_3]\text{Cl}_2 \cdot 6 \text{ H}_2\text{O}$  or the dye perylene did not facilitate the desired rearrangement, while further control experiments suggested that the decarboxylation reaction is indeed a photochemically mediated process: In absence of the photocatalyst or light or in presence of air, no product formation was observed (entries 9-11). Under UV irradiation in absence of a catalyst the reaction proceeded to give the desired product in a comparable yield (entry 12) to the visible light / Ir-photocatalyst conditions (entry 3). It can therefore be concluded that neither an oxidative nor a reductive quenching cycle, but rather energy transfer is operative in this transformation. Either the catalyst can trigger the energy transfer, or it takes place intramolecularly under UV-conditions.

Table 1: Screening of reaction conditions.<sup>a</sup>

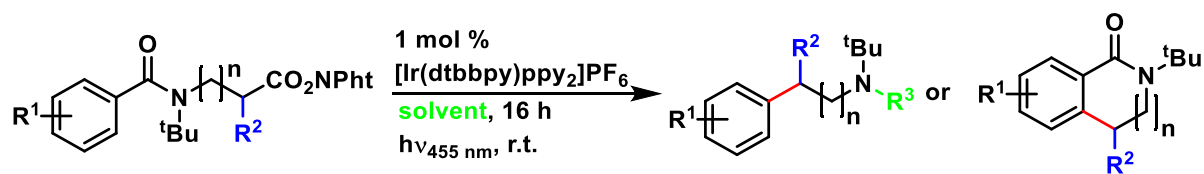


entry	catalyst	conditions	yield (%) <sup>b</sup>
1	[Ir(dtbbpy)(ppy) <sub>2</sub> PF <sub>6</sub>	MeCN	traces
2	[Ir(dtbbpy)(ppy) <sub>2</sub> PF <sub>6</sub>	MeCN/H <sub>2</sub> O (10/1)	41
3	[Ir(dtbbpy)(ppy) <sub>2</sub> PF <sub>6</sub>	MeCN/H <sub>2</sub> O (40/1)	61
4	[Ir(dtbbpy)(ppy) <sub>2</sub> PF <sub>6</sub>	MeCN/H <sub>2</sub> O (50/1)	48
5	[Ru(bpy) <sub>3</sub> ]Cl <sub>2</sub>	MeCN/H <sub>2</sub> O (40/1)	0
6	Perylene	MeCN/H <sub>2</sub> O (40/1)	0
7 <sup>c</sup>	[Ir(dtbbpy)(ppy) <sub>2</sub> PF <sub>6</sub>	40 °C	40
8 <sup>c</sup>	[Ir(dtbbpy)(ppy) <sub>2</sub> PF <sub>6</sub>	80 °C	17
9 <sup>c</sup>	[Ir(dtbbpy)(ppy) <sub>2</sub> PF <sub>6</sub>	no degassing	0
10 <sup>c</sup>	[Ir(dtbbpy)(ppy) <sub>2</sub> PF <sub>6</sub>	no light	0
11 <sup>c</sup>	-	no catalyst	0
12 <sup>d</sup>	-	UV /λ ≥ 250 nm	58

<sup>a</sup>Unless otherwise specified: **53a** (0.1 mmol), photocatalyst (1 mol %), degassed solvent (2 ml), ratio of mixed solvent in v/v, room temp., 16 h. <sup>b</sup>Yields were determined by <sup>1</sup>H NMR spectroscopy of the crude products with 4-nitrobenzaldehyde as internal standard. <sup>c</sup>Solvent: MeCN/H<sub>2</sub>O (40/1). <sup>d</sup>Acetone/H<sub>2</sub>O (20:1), room temp., 6 h.

With optimized conditions in hands, the reaction scope was evaluated (Table 2). An array of different β-phenylethylamines **54a-k** was synthesized by introduction of substituents on the phenyl ring. These substituents were tolerated well, regardless of the position (*para*-, *meta*-, *ortho*-), but electron donating substituents gave higher yields (**54a**). With respect to variations on the alkyl chain, β-substitution was feasible as demonstrated with the synthesis of **54j**. Changing water to alcohols (primary, secondary or tertiary) in the solvent mixture allowed the isolation of the corresponding carbamates **54a-R<sup>3</sup>**, **54b-R<sup>3</sup>** and **54f-Me**.

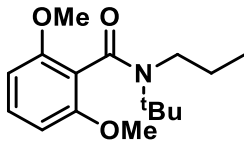
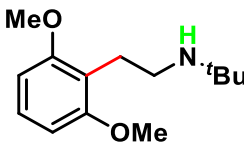
Table 2: Substrate scope of the Smiles rearrangement initiated by decarboxylation.



#	n	SM	R <sup>1</sup>	R <sup>2</sup>	R <sup>3</sup>	product	outcome
1	1	<b>53a</b>	4-OMe	H	H		<b>54a</b> , 61%
		<b>53b</b>	4-Cl				<b>54b</b> , 45%
		<b>53c</b>	4-Br				<b>54c</b> , 49%
		<b>53d</b>	4-Me				<b>54d</b> , 45%
		<b>53e</b>	4-H				<b>54e</b> , 29%
2	1	<b>53f</b>	2-OMe	H	H		<b>54f</b> , 43%
		<b>53g</b>	3-OMe				<b>54g</b> , 33%
		<b>53h</b>	3-Cl				<b>54h</b> , 21%
3	1	<b>53i</b>	3-Cl, 4-OMe	H	H		<b>54i</b> , 53%
4	1	<b>53j</b>	4-OMe	Me	H		<b>54j</b> , 53%
5	1	<b>53a</b>	4-OMe	H	CO <sub>2</sub> Me CO <sub>2</sub> <sup>i</sup> Pr CO <sub>2</sub> <sup>t</sup> Bu		<b>54a-Me</b> , 64%
6	1	<b>53b</b>	4-Cl	H	CO <sub>2</sub> Et CO <sub>2</sub> <sup>i</sup> Pr CO <sub>2</sub> <sup>t</sup> Bu CO <sub>2</sub> <sup>t</sup> Bn		<b>54a-<sup>i</sup>Pr</b> , 35%
							<b>54a-<sup>t</sup>Bu</b> , 37%
						<b>54b-Et</b> , 70%	
						<b>54b-<sup>i</sup>Pr</b> , 56%	
<b>54b-<sup>t</sup>Bu</b> , 35%							
<b>54b-Bn</b> , 60%							
7	1	<b>53f</b>	2-OMe	H	CO <sub>2</sub> Me		<b>54f-Me</b> , 38%
8	1	<b>53k</b>	3, 4-OMe	H	-		<b>55a</b> , 82%
9	1	<b>53l</b>	3, 4, 5-OMe	H	-		<b>55b</b> , 75%
10	2	<b>56a</b>	4-H	H	-		<b>57a</b> , 43%
		<b>56b</b>	4-OMe				<b>57b</b> , 60%
		<b>56c</b>	3, 4-OMe				<b>57c</b> , 58%
		<b>56d</b>	3,4,5-OMe				<b>57d</b> , 43%
		<b>56e</b>	4-OMe, 3-Cl				<b>57e</b> , 62%
		<b>56f</b>	Pyridine				<b>57f</b> , 35%

continue next page

notable results:

11 <sup>a</sup>	2	<b>56g</b>	2, 5-OMe	H	-		<b>58</b> , 45%; No rearrangement
12	1	<b>53m</b>	2, 5-OMe	H	H		<b>54l</b> , 38%; rearrangement

Reaction scale: **SM** (1 mmol), [Ir(dtbbpy)(ppy)<sub>2</sub>]PF<sub>6</sub> (1 mol %), 10 ml MeCN (degassed), with up to 13.5 equiv. AlkylOH or a mixture of MeCN/H<sub>2</sub>O ratio 40/1, room temp., hv (455 nm), 16 h. Isolated yields are given.

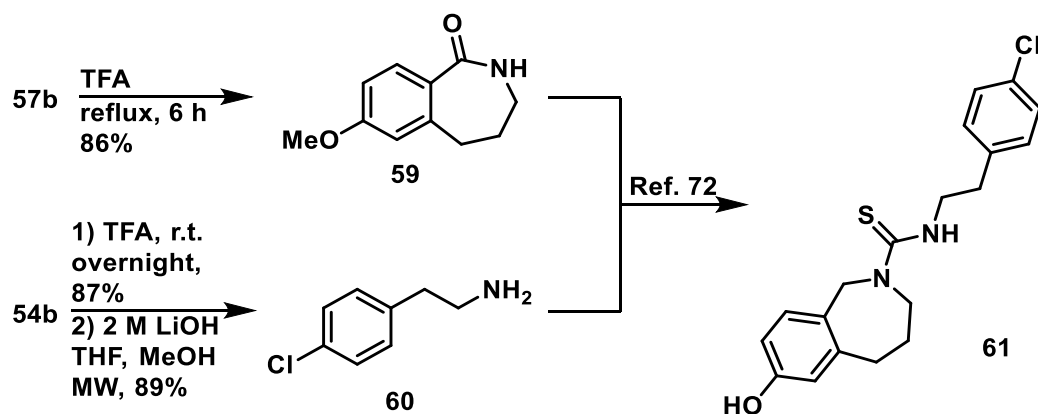
<sup>a</sup>Incomplete conversion after 24 h.

A further increase of the electron density in the arene ring by introduction of two (**53k**), or even three (**53l**) methoxy groups led to the exclusive formation of dihydroisoquinolinones **55a** and **55b**, the latter being established by X-ray structure analysis. This supports the proposed mechanism, as these products arise from the *1,2*-acyl shift in the spiro radical intermediate (compare Scheme 17, compd. **41**) rather than an *ortho*-cyclization which occurs regioselectively towards the sterically less hindered site if an unsymmetrical starting material such as **53k** is employed. Such a pathway is not feasible when both *ortho*-positions are blocked (**53l**); in this case, the Smiles rearrangement is observed (**54m**), albeit in low yield.

Substrates **56a-f**, comprising an alkyl chain in the amine elongated by one methylene unit compared to **53**, formed tetrahydrobenzazepinones **57**. No products arising from rearrangement or *1,2*-acyl shift were detected, indicating that these substrates followed a different mechanistic pathway, which is likely a direct *7-exo/endo*-trig ring closure. This change in mechanism is supported by the formation of **58** from a substrate where both *ortho*-positions are blocked: No rearrangement, but only formal reduction is observed, while the analogous reaction towards  $\beta$ -phenylethylamine **54l** follows the spirocyclization route. Notably, also electron deficient pyridine derivative **56f** was successfully transformed to **57f**, while no such reaction was observed for the analogous derivative with a shorter chain.

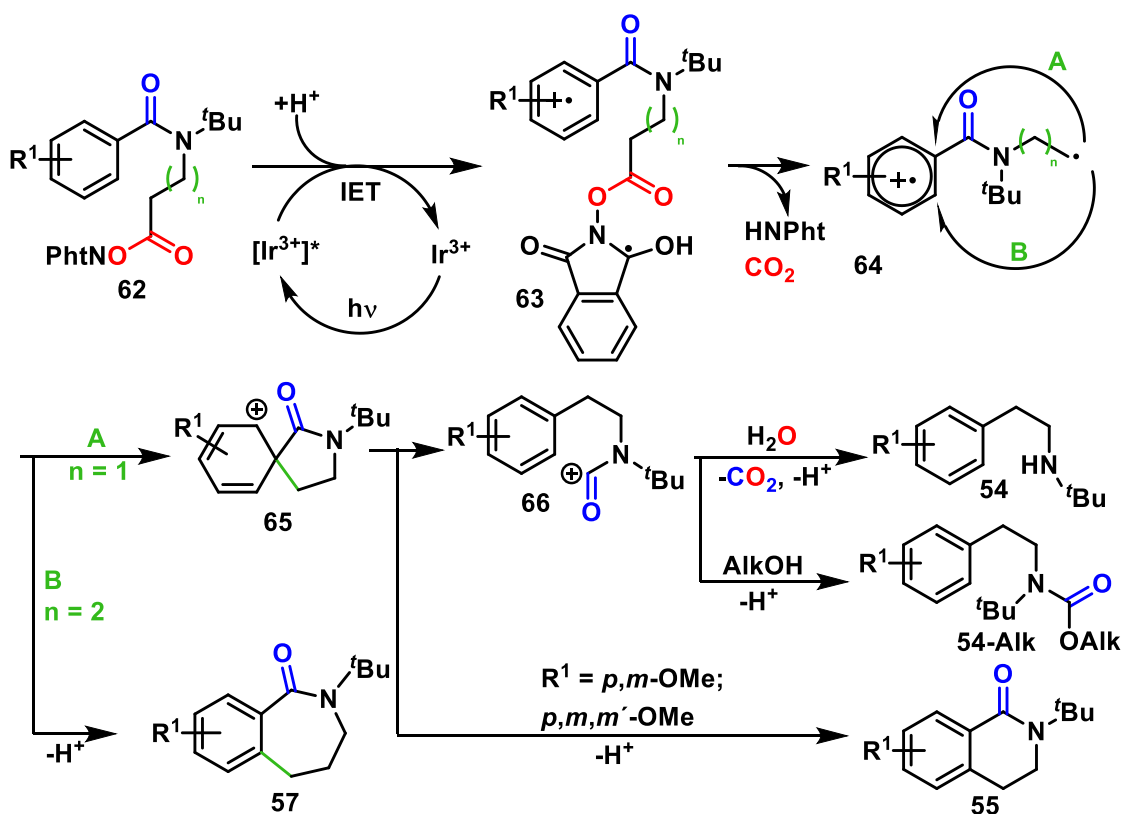
Both major product groups formed by the discussed decarboxylation, *i.e.* phenylethylamines and benzoazepinones, are core parts of a class of natural compounds called capsazepines<sup>72</sup> with anti-inflammatory and anti-nociceptive effects.<sup>73</sup> Therefore, a formal synthesis of capsazepinoid **61** was developed (Scheme 20, *vide infra*). Compounds **57b** and **54b**, being obtained from the photorearrangement of **56b** and **53b** (Table 2) could be readily converted to the key intermediates **59** and **60**, which can be transformed into the desired capsazepinoid.





Scheme 20: Formal synthesis of capsazepinoid **61** according to Sterner *et al.*<sup>72</sup>

The reduction potential of  $[\text{Ir}(\text{dtbbpy})(\text{ppy})_2]\text{PF}_6$  photocatalyst ( $E_{1/2}(\text{Ir}^{\text{IV}/\text{III}}) = -0.96 \text{ V vs. SCE}$ ) on its own is insufficient to enable an electron transfer to the *N*-acyloxyphthalimides (e.g.  $E_{1/2} = -1.32 \text{ V vs. SCE}$  for **53a**). Albeit the water required for successful transformation has been demonstrated to lower the reduction potential of the phthalimides, a photoredox mechanism remains unlikely in this case. Instead, an energy transfer mechanism seems more plausible. This proposal is supported by the fact that the reaction proceeds under UV-irradiation in absence of the catalyst (Table 1, entry 12). Furthermore, Schütz *et al.* calculated the analytic energy gradients for the ground and excited states in **53**, which showed that the  $S_1$  and  $T_1$  state of the excited molecule **62** can undergo such a charge transfer.<sup>74</sup> Upon energy transfer, *N-O* bond cleavage triggers the decarboxylation, forming radical **63** and releasing a neutral phthalimide molecule (Scheme 21, *vide infra*). Depending on the length of the alkyl chain, a *7-endo/exo*-trig cyclization leads to products **57**, or the key intermediate **65** is formed *via* spirocyclization. Following the analysis put forward by Chuang<sup>75</sup> and Tchabanenko<sup>70</sup> for spiroradical intermediates, rearomatization of **65** could be accompanied either by a direct *1,2*-acyl shift to the *ortho*-position of the phenyl ring (observed for electron rich substrates **53k**, **1**), or more likely, by ring cleavage. The latter gives rise to carbamoyl cation **66**, which then transforms to the different types of products depending on the electronic nature of the aryl ring (**54**, **54-alk**, **55**) and the solvent. In case of water trapping the carbamoyl cation, another decarboxylation occurs spontaneously under the reaction conditions, leading to products **54**. When instead of water an alcohol reacts with the carbamoyl cation, a stable urethane is formed (products **54-Alk**).

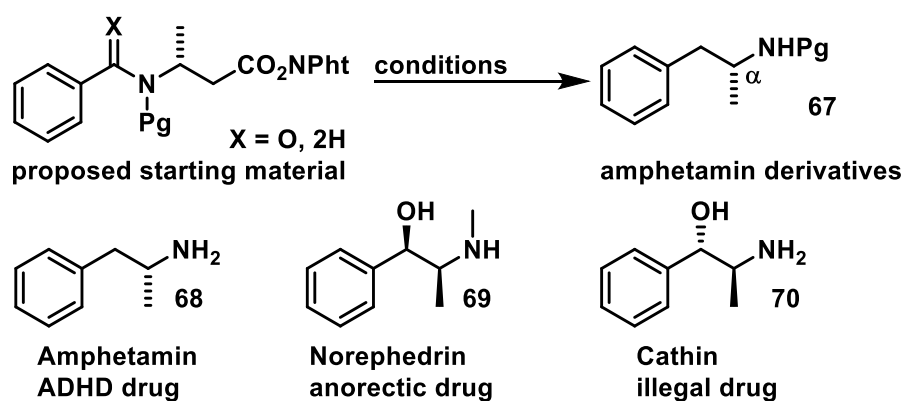


Scheme 21: Mechanistic proposal for Smiles rearrangement triggered by decarboxylation.

In summary, the photocatalyzed transformation of  $\omega$ -aryl-*N*-acyloxyphthalimides in presence of [Ir(dtbbpy)(ppy)<sub>2</sub>]<sup>+</sup>PF<sub>6</sub><sup>-</sup> may lead to three different types of products, depending on several key structural elements of the starting material:  $\beta$ -phenylethylamines **54**, dihydroisoquinolinones **55** and tetrahydrobenzoazepinones **57**. The preparation of two key intermediates for the convergent synthesis of the bronchodilator capsazepinoid **61**, distinguishing the reactivity of two  $\omega$ -aryl-*N*-acyloxyphthalimides with different chain lengths, shows the power of this synthetic strategy.

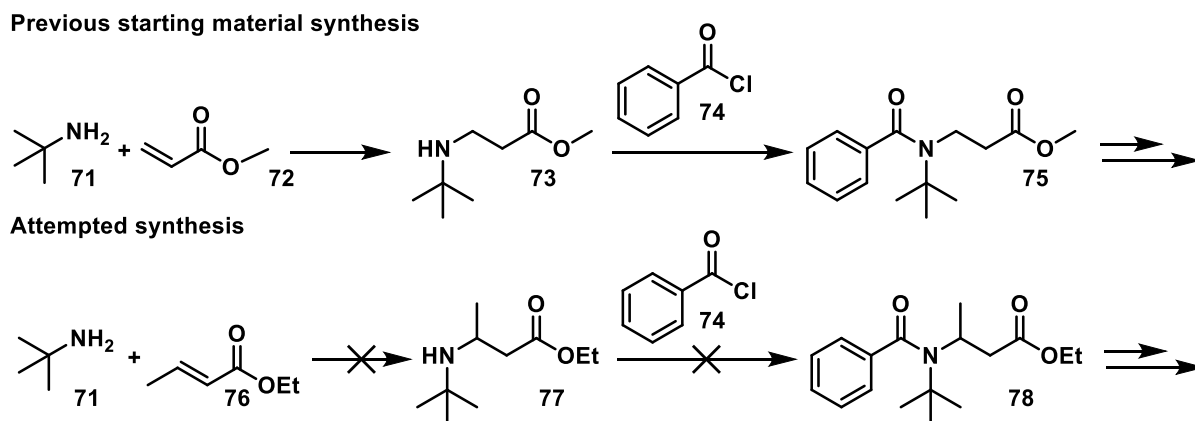
### 3.2.2 Broadening the Substrate Scope: Amphetamines and More <sup>§</sup>

Members of the phenylethylamin substance class, accessible by the Smiles rearrangement presented above (Table 2), exhibit remarkable biological activity. Among these substances, a subset of molecules with a special substitution pattern stands out: Amphetamines, which have gained widespread attention both as useful pharmaceuticals for the treatment of various diseases (ADHD, morbid obesity, *etc.*) as well as illegal stimulating drugs.<sup>66, 76</sup> Members of this substance class have in common a methyl substituent in  $\alpha$ -position to the amino group. In principal, they should be accessible by the Smiles rearrangement discussed herein (Scheme 22).



Scheme 22: Amphetamines possibly accessible *via* Smiles rearrangement.

However, the preparation of the required starting material *via* the previous route was unsuccessful (Scheme 23). Neither does the addition of *tert*-butylamine **71** to crotonate **76** take place as readily as to acrylate **72**, nor is the coupling of the benzoyl chloride **74** to the respective starting material sterically feasible.

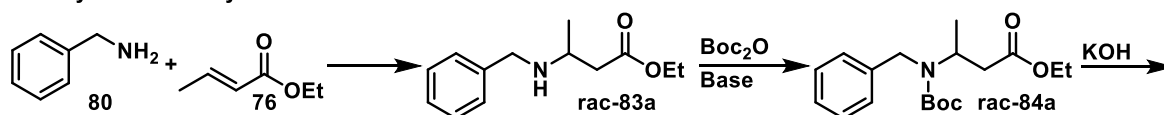


Scheme 23: Attempted starting material synthesis.

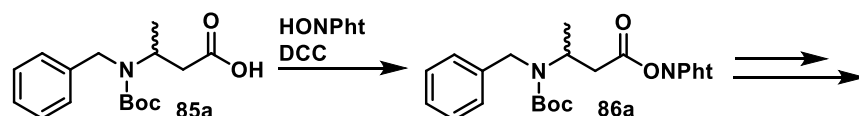
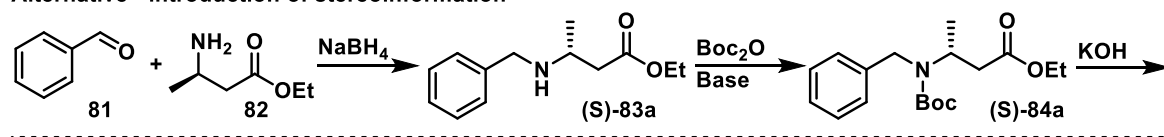
<sup>§</sup>The following work was performed by S. Budde as continuation of the work of C. Faderl presented in the previous sub-chapter.

An analysis of the key requirements of the starting material determined so far showed the necessity of an aromatic group, a sterically demanding substituent on the amine, and a suitable chain length for the carboxylic acid (compare Figure 1). Furthermore at least one of the substituents on the amine should be electron withdrawing (*e.g.* Boc, Ts), so to prevent the nitrogen from being oxidized under the photochemical conditions (*i.e.* act as electron donor, comparable to the often used DIPEA). Switching the benzoyl part for a benzyl group and exchanging the *tert*-butyl group for a Boc-protection group seemed a reasonable start for the investigation. This change would also open up the reaction for introducing chirality in the key substituent in  $\alpha$ -position to the amine, significantly improving the previous approach (Scheme 24).

**New synthesis - easy and cost effective**

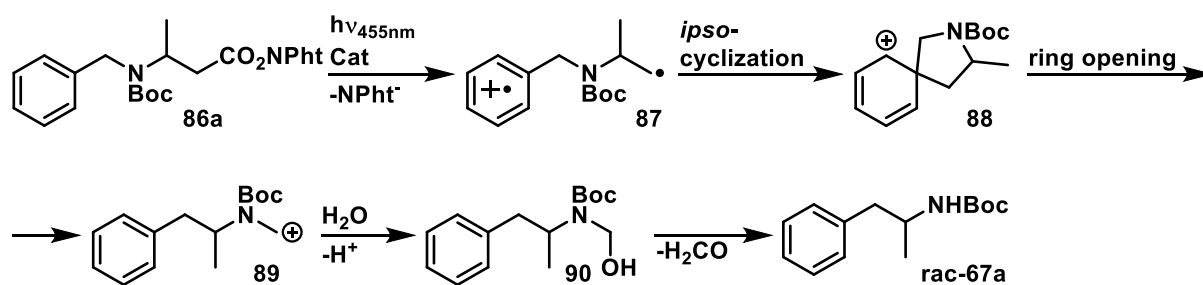


**Alternative - introduction of stereoinformation**



Scheme 24: New starting material synthesis for accessing phenethylamines.

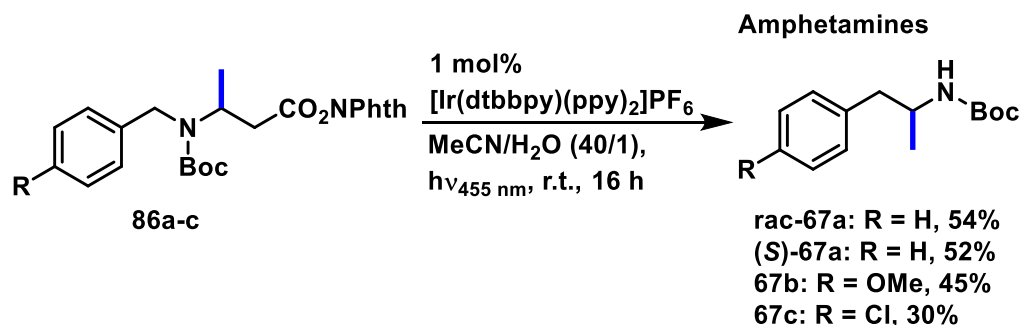
Transferring the key components of the mechanism suggested for the Smiles photoreaction (Scheme 21) on this new substrate (Scheme 25) showed one possible hindrance for the Smiles rearrangement. Upon decarboxylation, an *ipso* cyclization (**87**) would lead to a product (**88**), where both bonds of the spirocycle that do not derive from the aromatic system are alkyl bonds, connecting to a  $\text{CH}_2\text{-R}$  group, whereas with the previous substrate, one of the bonds would connect to a carbonyl (Scheme 21). For the rearrangement to proceed, an opening of the spirocycle **88** is required, and the differentiation between the two bonds would be less distinct with the starting material being derived from a benzyl- rather than a benzoyl group.



Scheme 25: Proposed mechanism for the Smiles rearrangement leading to amphetamines.

Also in this reaction water plays a critical role, as it traps the carbocation **88**, releasing formaldehyde instead of another molecule of carbon dioxide as in the mechanism for the other substrate classes (Scheme 21).

Both possible routes (Scheme 24) for the synthesis of suitable starting materials were completed successfully (**86a**), and to our delight, the Smiles rearrangement took place under irradiation in presence of a [Ir] catalyst, so to synthesize Boc-protected racemic (**rac-67a**) and (*S*)-amphetamine ((*S*)-**67a**) in mediocre to good yields (Scheme 26). Consecutively two different substituents on the aromatic system were introduced (**67b**, **c**), where the electron deficient (**67c**) substrate gave significantly lower yield.



Scheme 26: Synthesis of amphetamines *via* Smiles rearrangement.

In order to prove that the stereoinformation introduced by using chiral starting materials is conserved, both Boc-amphetamines were subjected to chiral HPLC analysis (Figure 2).

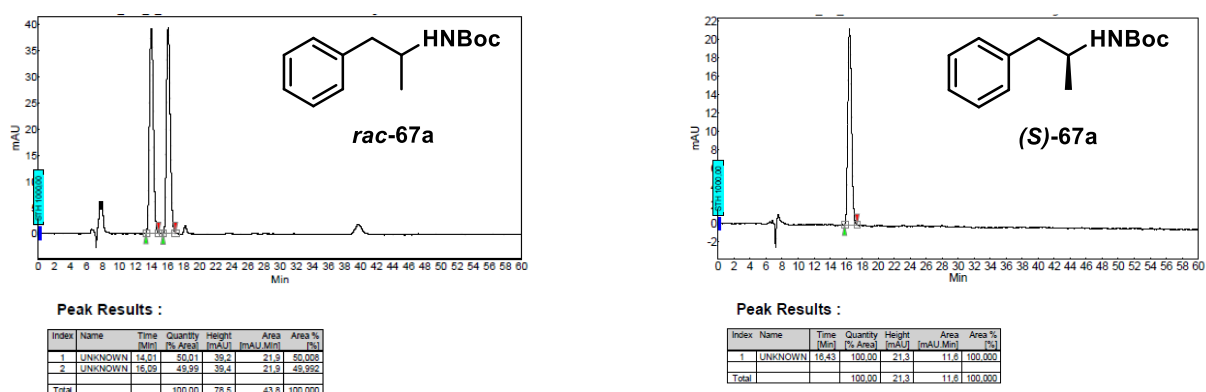


Figure 2: HPLC analysis of Boc-amphetamines.

In addition, more research towards the mechanism was performed by analyzing intensity- and lifetime-quenching of mixtures of the catalyst and the substrate. By comparison with a *N*-acyloxyphthalimide exhibiting similar core structure, but lacking the bulky substituent on the amine, this was thought to give better insight into why the Smiles rearrangement demonstrated above is feasible for these starting materials.<sup>77-78</sup> For this comparison, *N*-hydroxyphthalimide ester of hippuric acid (**91**) was chosen.

For the graphs below, the intensity at 560 nm ( $F$ ) was divided by the intensity of the pure catalyst solution ( $F_0$ ) and plotted against  $n_{\text{quencher}}/n_{\text{cat}}$ , which corresponds to the equivalents of substrate respective to the catalyst. Similarly, the lifetime of each sample ( $\tau$ ) was divided by the lifetime of the pure catalyst ( $t_0$ ) and plotted against the equivalents of substrate respective to the catalyst.

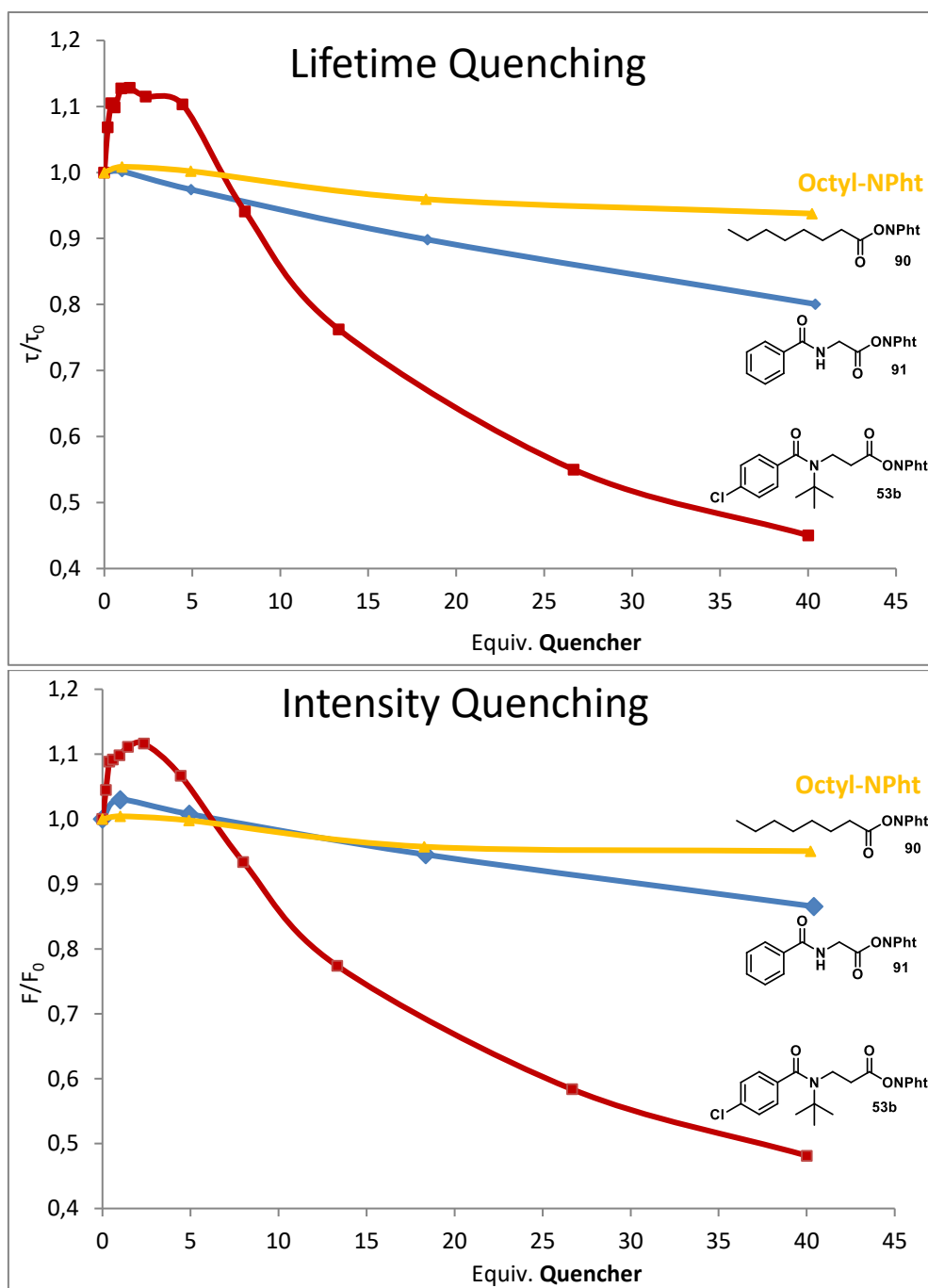


Figure 3: Fluorescence lifetime and intensity-quenching of selected substrates.

As seen from the graphs above, until addition of about 1 equiv. **53b**, the fluorescence intensity and lifetime of the [Ir] catalyst increase slightly, indicating the formation of a catalyst-substrate complex, but then drop drastically upon addition of more quencher. For **91**, a very small increase at the beginning is observed, but only poor quenching upon addition of more **91**. We conclude that a successful interaction between the catalyst and the substrate is only possible when the *N*-acyloxypthalimide is in a favorable conformation due to the presence of the bulky <sup>t</sup>Butyl group, or the Boc-group, respectively. However, the quenching of **53b** did

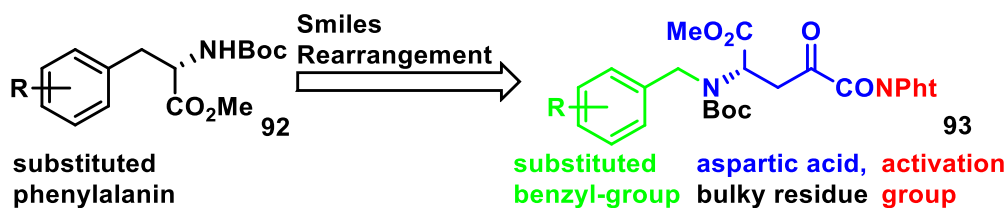
not follow a Stern-Volmer type quenching, indicating that more than just one pathway might be operative.

Octyl-NPht **90** ( $E_{1/2}^{\text{red}} = -1.25 \text{ V vs. SCE}$ , irreversible peak) was also investigated as completely neutral reference compound. If photoelectron transfer from the photocatalyst would occur, it would be expected that fluorescence quenching would be observable for Octyl-NPht, which was not the case, supporting our hypothesis of an electron transfer mechanism.



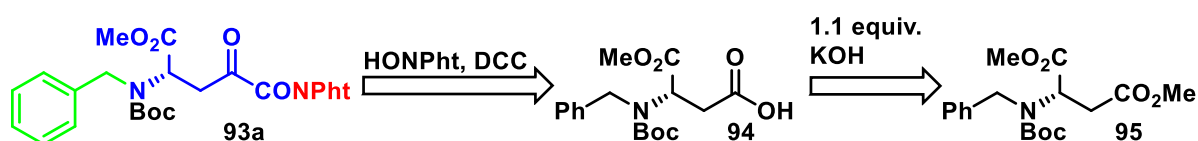
### 3.2.3 Consecutive Studies: Incorporating Aspartic and Glutamic acid

In an attempt to further broaden the substrate scope and to employ easily available starting materials, optically pure aspartic acid was envisaged as an ideal starting material for the Smiles rearrangement. This amino acid would be an affordable source with chiral information, leading to phenyl alanin **92** and derivatives, depending on the substituents on the aromatic ring (Scheme 27).



Scheme 27: Smiles rearrangement leading to substituted phenylalanines.

A possible synthesis for the suitable starting material **93a** called for the selective hydrolysis of the  $\gamma$ -ester of aspartic acid dimethyl ester **95** to the free acid **94** (Scheme 28). While a first guess would be, that this ester group is less activated than the  $\alpha$ -ester, the experiment showed that the desired ester is indeed preferentially hydrolyzed in reasonable selectivity.



Scheme 28: Envisioned starting material synthesis.

Di-ester **95** is synthesized from aspartic acid by benzylation and consecutive protection of the amine with a sterically demanding Boc-group. These two steps were attempted consecutively and also in one pot, as they both require similar basic conditions. However, while the benzylation was successful, a further substitution with a Boc-protection group on this amine could not be achieved. Several different bases were tested, and even the reverse order, first Boc-protection with consecutive benzylation, was attempted, all unsuccessful. Presumably high steric crowding prevented the double substitution at the amine, where in comparison with the singular methyl substituent (**84**, Scheme 23), the methyl carboxylate requires significantly more space.

Hence, the unprotected substrate was tested for possible photoreaction under the standard conditions established in the previous chapter, but no desired rearrangement product, but only a complex mixture was observed, from which mainly the free acid, stemming from ester hydrolysis, was identified.

After the miscarriage of this endeavor to incorporate a natural amino acid into the previously developed Smiles rearrangement, it was obvious that more drastic changes to the possible starting material synthesis were required.

Summarizing the results so far, a bulky substituent is required to force the starting material into the right conformation. Only when the phthalimide and the aromatic residue where the rearrangement is to occur are in close proximity, a reaction can take place. High steric crowding at the amine may prevent a successful starting material synthesis from natural amino acids, calling for different protection strategies.

Consecutively, other methods were envisioned to incorporate aspartic or glutamic acid into a rigid skeleton, borrowing from the Schöllkopf synthesis and others.<sup>79-80</sup> These investigations are described in the next chapter.

### 3.3 Decarboxylative Transformations of Oxazolidinone Protected Natural Amino Acids

Oxazolidinones, which are comparably easy to construct from aspartic and glutamic acid<sup>81</sup>, provide a rigid structure, protect the amine from oxidation, protect the  $\alpha$ -carboxylic group of the two di-acids, and offer the possibility for introduction of an aromatic residue on the amine.

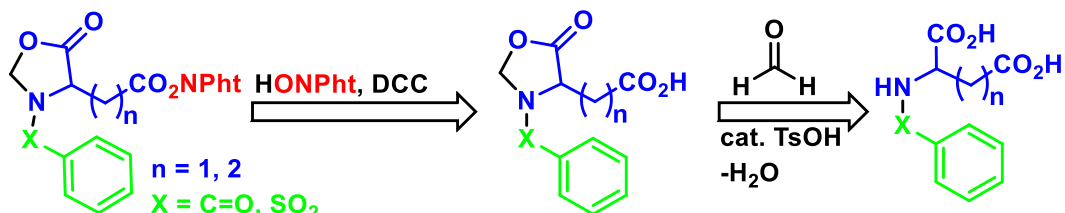
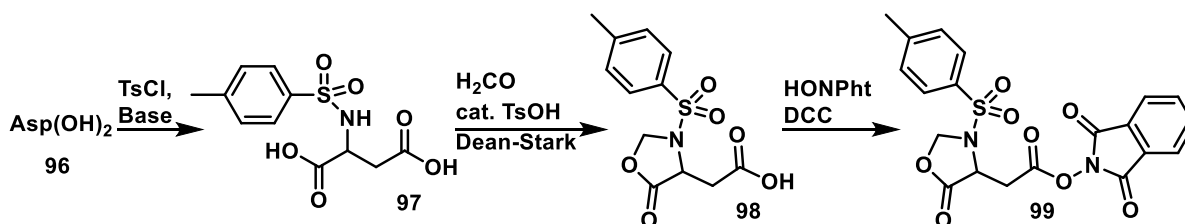


Figure 4: Envisioned synthesis of suitable precursors incorporating aspartic or glutamic acid within an oxazolidinone.

A possible synthetic route (Figure 4) calls for a condensation reaction of (natural)  $\alpha$ -amino acids with formaldehyde in presence of an acid catalyst such as toluenesulfonic acid. Employing a Dean-Stark apparatus under reflux conditions removes the water and in general results in good yields. In case of sensitive starting materials, an inverse Dean-Stark apparatus, allowing the use of Chloroform or DCM as refluxing solvent may be used. However, oxazolidinones only become stable when the amine is substituted with another electron withdrawing group, such as a toluenesulfonate, which need to be introduced beforehand.<sup>82</sup>

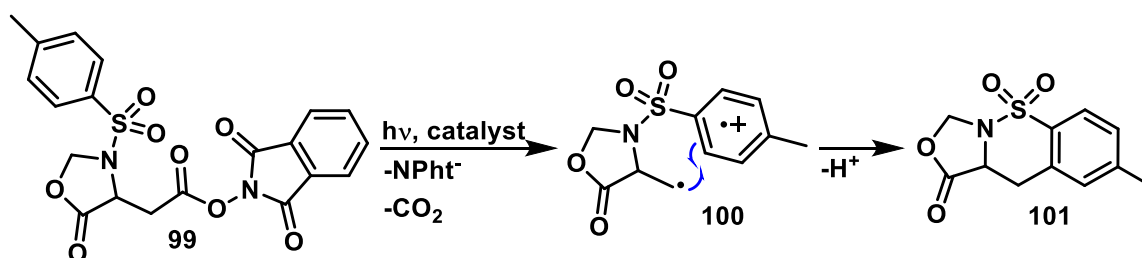
Based on the oxazolidinones formed from aspartic and glutamic acid, a photochemically initiated decarboxylation may give rise to inter- and intramolecular radical additions or rearrangements.<sup>83</sup>

First, starting from aspartic acid **96**, a derivative suitable for decarboxylation and possible subsequent intramolecular cyclization (**99**) was synthesized (Scheme 29). Compound **99** proved to be very polar and hardly dissolving in the solvent mixture acetonitrile: water 40:1 determined to be the best conditions for such decarboxylations.



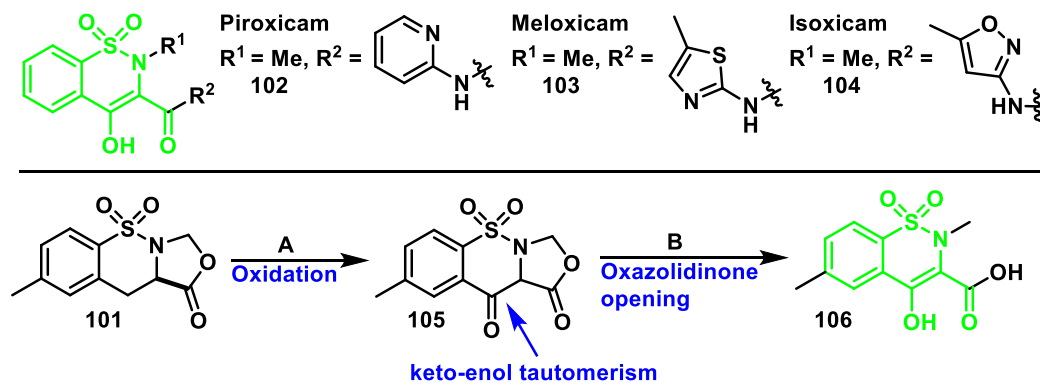
Scheme 29: Synthesis of a tosyl protected oxazolidinone **99** based on aspartic acid **96** as precursor for photochemical decarboxylation.

However, adding DMSO increased the solubility, and allowed for some test reactions. A new compound was isolable, which could not entirely be purified from residues of the phthalimide byproduct. However, mass spectroscopy and 2D-NMR allowed for the identification of product **101**, which is a cyclic sulfonamide (Scheme 30). This product derives from the starting material by *ortho*-cyclization initiated by decarboxylation (**100**), which had been observed for a different class of substrates in the previously discussed Smiles rearrangement (Table 2). It can be hypothesized, that due to the rigidity of the oxazolidinone, an *ipso*-cyclization is prevented, and therefore no rearrangement can take place. While the yield was rather low, and the final product could not be completely purified, the observed product skeleton sparked interest as it is found as part of widely used non-steroidal anti-inflammatory drugs (NSAIDs).<sup>84-85</sup> Apart from being NSAIDs, these compounds were also shown to inhibit the growth of certain cancer types.<sup>86</sup>



Scheme 30: Synthesis of cyclic sulfonamide *via* visible light mediated decarboxylation.

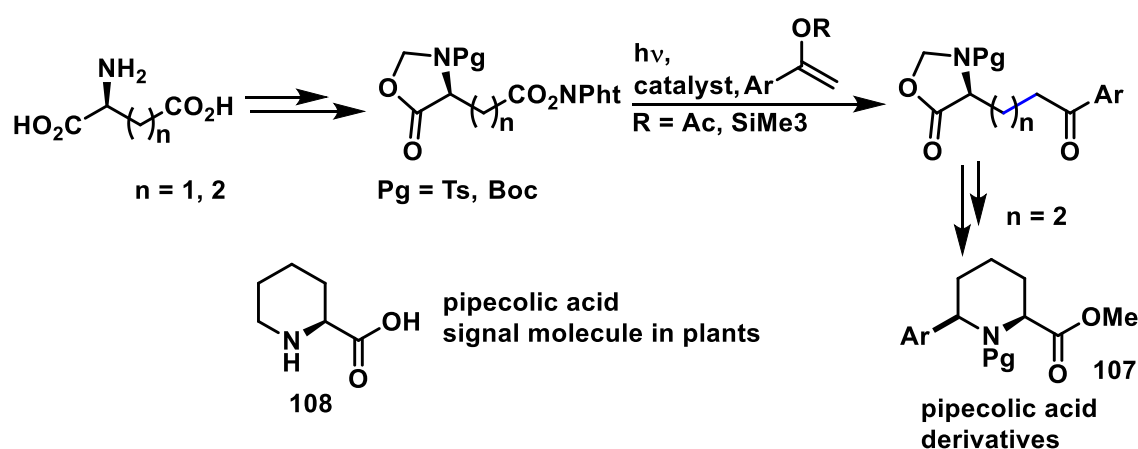
Starting from this compound, the core structure of several pharmaceutically used cyclic sulfonamides is accessible (**102-104**, Scheme 31). A possible synthetic route includes an oxidation in the first step (A), *e.g.* *via* photochemical oxygenation<sup>87</sup>, followed by opening of the oxazolidinone (B), *e.g.* using zinc bromide in combination with triethylsilane<sup>88</sup>, which directly leads to the methyl substituent on the amine found in many biologically active cyclic sulfonamides.



Scheme 31: Some pharmaceutically relevant cyclic sulfonamides and a possible synthesis of their core structure from compound **101**.

The oxidation is essential, as the carbonyl involved in the keto-enol tautomerism is key to biological activity of this substance class, but also it nullifies the stereochemical information introduced by using chiral starting materials. After all, this substance class is much easier accessible *via* traditional chemistry, involving a Friedel-Crafts acylation, avoiding laborious starting material synthesis. Therefore, no further research on the intramolecular cyclization found for the oxazolidinone derived from aspartic acid was carried out.

In contrast, possible *intermolecular* reactions of oxazolidinones derived from aspartic and glutamic acids were investigated, in part as collaboration of Simon Budde with Christian Eichinger (Scheme 32). This research is part of the thesis of Christian Eichinger and discussed in depth *ibidem*.<sup>89</sup>



Scheme 32: Intermolecular reactions induced by photochemical decarboxylation of suitably protected natural amino acids developed by C. Eichinger.

The synthesis developed gave access to pipercolic acid derivatives **107**. Pipercolic acid **108** is a signal molecule in plants, which plays an important role in defensive activity of plants *e.g.* when being attacked by pests.<sup>90-91</sup> Its synthesis has sparked interest, as it might find some application in agriculture or as structurally rigid part of peptides.<sup>92-93</sup>

### 3.4 The Hydantoin Group as Alternative to Oxazolidinone Protecting Group

Focus of this work remained on the *intramolecular* reactions of natural amino acid derivatives; in particular, an alternative to Smiles-type reactions and to aromatic residues as part of the core skeleton in general was researched. An intramolecular cyclization to a suitable residue of a substituent on the nitrogen was desirable, and this substituent should not be an amide, *i.e.* electron withdrawing, so that in the final product, a basic nitrogen-containing heterocycle would be formed. As oxazolidinones proved to be adequate protection groups, able to conserve the stereochemical information from the starting material, a similar cyclic protection group for  $\alpha$ -amino acids should be used. Depending on the ring size, either piperidine or azepane rings would be accessible, which represent core structures of many biologically active compounds (Figure 5).<sup>94-95</sup>

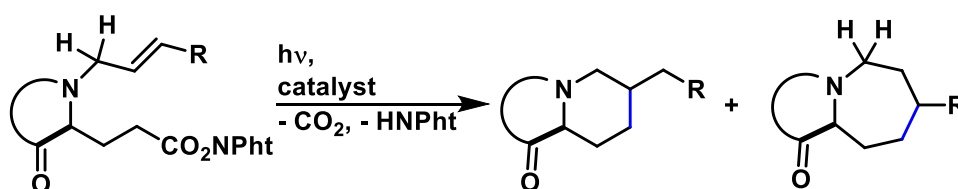


Figure 5: Envisioned intramolecular cyclization of glutamic acid derivatives.

Three cyclic protection groups for  $\alpha$ -amino acids were compared in respect of ease of synthesis, stability and possible functionalization (Figure 6). While 1,3-oxazolidin-4-one derivatives are generally regarded as less stable when the nitrogen is substituted with an alkyl group (in contrast to an electron withdrawing group such as Boc or Ts), the closely related *N*-carboxy anhydrides have found use in transformations of  $\alpha$ -amino acids.

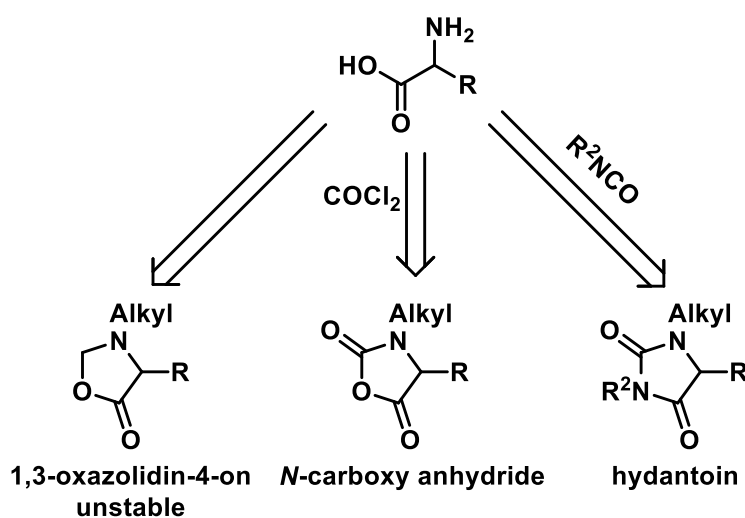


Figure 6: Possible cyclic protection groups for  $\alpha$ -amino acids.

Alternatively, hydantoin, which represent an urea derived structure, can be formed from  $\alpha$ -amino acids by the use of potassium cyanate (route **A**, Figure 7).<sup>96</sup> The two nitrogens vary in basicity and can be functionalized separately, or the diacylamine is already introduced with a substituent by using organo-cyanates<sup>94</sup> instead of cyanate salt.

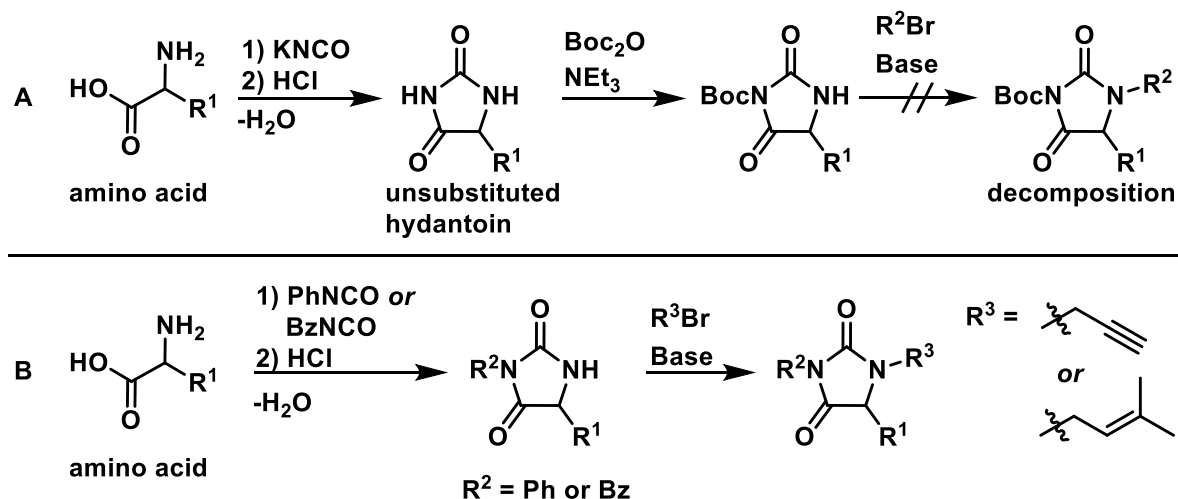


Figure 7 Synthesis of substituted hydantoin.

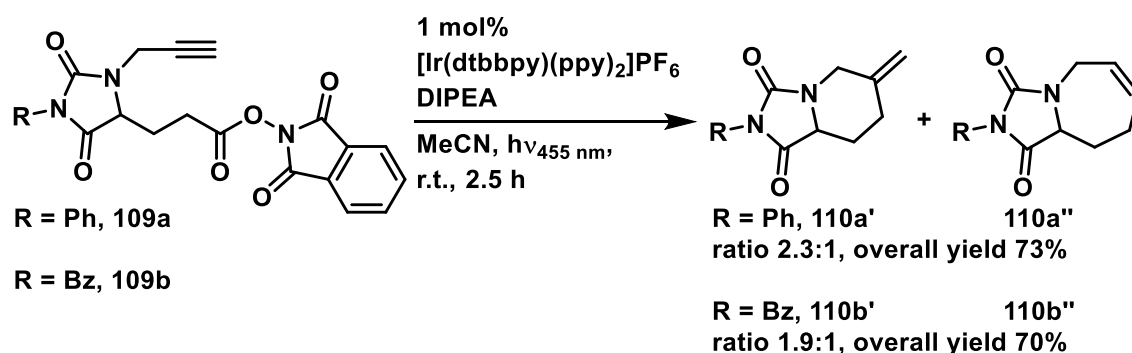
While the hydantoin-formation proceeds well in both routes, the third substituent of the diacylated nitrogen is key to the stability of the protection group.<sup>97-98</sup> Introducing a Boc group is achieved under relatively mild conditions. However, under the strongly basic conditions required for the introduction of an alkyl group on the other nitrogen, the hydantoin group decomposes and is cleaved.

Therefore, route **B**, introducing an aryl or benzyl group, was chosen. The first of which leads to the most stable hydantoin, but in consequence is most difficult to remove in the end, while the benzyl group is stable in the following steps but requires different and less harsh conditions to remove.

For this thesis, two different alkyl substituents as targets for the envisioned synthesis were chosen: a propargyl and a dimethylallyl group, the first of which would avoid the formation of a new stereocenter altogether, the latter only creates one new stereocenter. This would be the probe for possible stereinduction by the chiral information brought into the synthesis by employing optically pure glutamic acid. As it is suspected that a bulkier substituent such as the dimethylallyl group would be more susceptible to chiral induction, it was chosen over a simple allyl group.

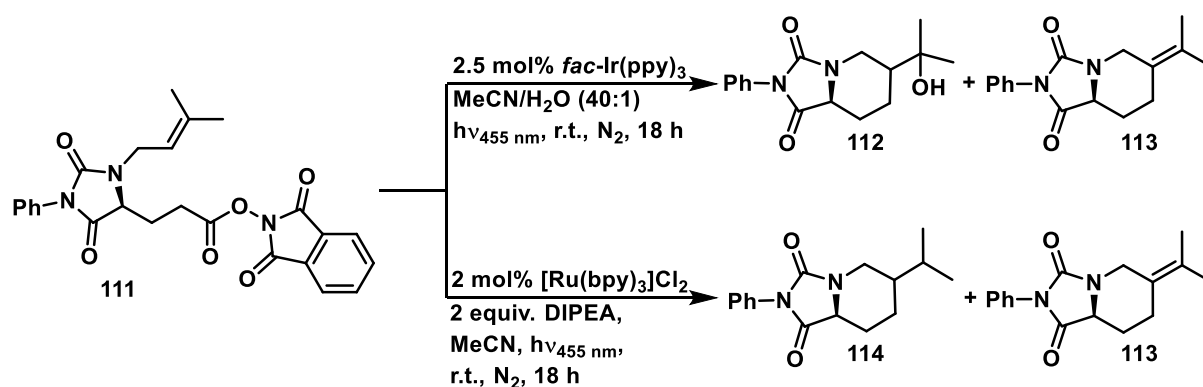
Also, the influence of the phenyl or benzyl group were considered: The phenyl substituent forces the hydantoin to take a very flat configuration due to conjugation of  $sp^2$ -centers (both nitrogens exhibit high  $sp^2$ -character), while the benzyl group allows for more flexibility,

which might have an impact on stereoinduction. As an energy transfer mechanism was not feasible in this case, and the oxidative route described by Glorius *et al.*<sup>71</sup> did not result in any conversion, the well-known reductive quenching cycle of [Ru(bpy)<sub>3</sub>]Cl<sub>2</sub> was employed with DIPEA **15** as sacrificial electron donor (Scheme 33). Commonly employed conditions analogous to reports from Overman *et al.*<sup>50</sup> were adapted, and gave a mixture of two compounds in excellent yields (Scheme 33). While the two compounds were inseparable by column chromatography, they were successfully identified by 2D-NMR techniques. The regioisomer which was formed in higher yields was found to be the product of a 6-exo-dig cyclization (**110a'**, **110b'**), while the minor regioisomer was derived from a 7-endo-dig cyclization (**110a''**, **110b''**). Both cyclizations are feasible in accordance to the Baldwin-rules<sup>57</sup>, yet the formation of the seven-membered compound was not expected to occur in the observed amount. The difference between phenyl and benzyl substituted hydantoin was found to be rather small, as the overall yield was in the same range, and the ratio of regioisomers was comparable.



Scheme 33: Intramolecular cyclization of glutamic acid derived hydantoin involving a propargyl residue.

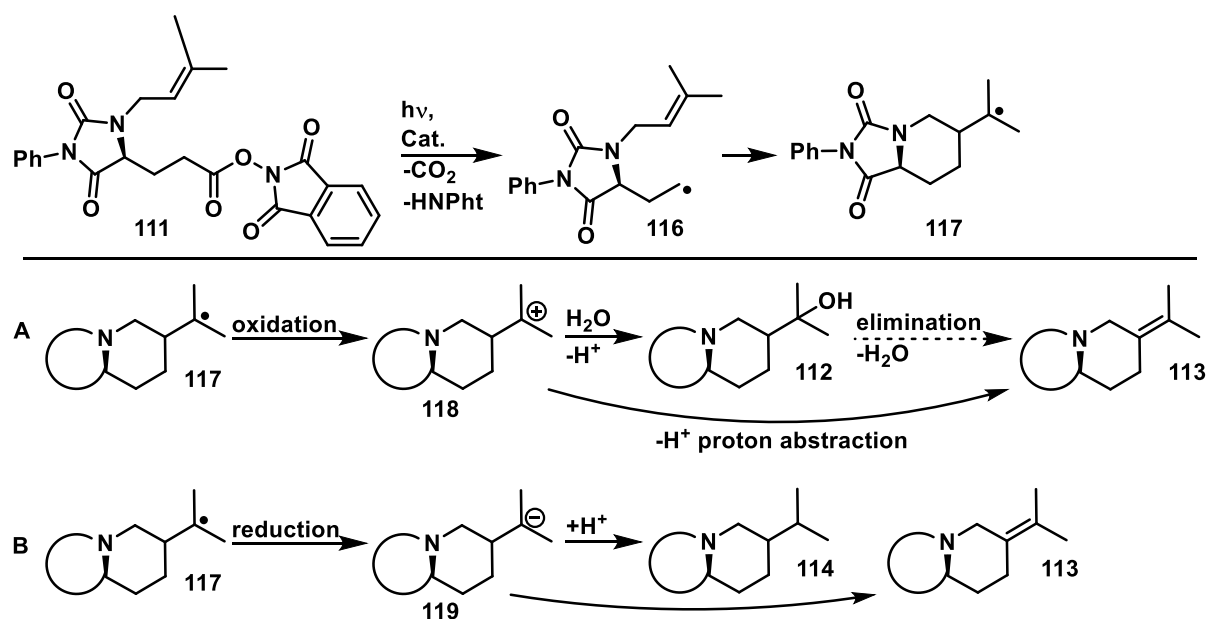
The starting material containing a dimethylallyl-residue **111** as target of the cyclization was also subjected to both oxidative and reductive conditions, but in contrast to the propargyl-substituted compound, conversion was observed under both conditions (Scheme 34).



Scheme 34: Intramolecular cyclization of glutamic acid derived hydantoin involving a dimethylallyl residue.



In this case, no 7-membered product was observed, but still a mixture of two compounds was isolated. For the oxidative reaction, compound **112** incorporating a hydroxyl group was formed as expected, but apparently this hydroxyl group is eliminated comparably easily, so that unsaturated product **113** derived from such reaction is also observed in considerable amounts. Elimination may proceed during column chromatography, as the product ratio was observed to change. Also, in case of the reductive pathway two cyclization products are formed, one being identified as the same unsaturated compound **113** as in the oxidative pathway, and one being the expected saturated compound **114**. A possible mechanism, explaining the formation of each compound, is shown below (Scheme 35).



Scheme 35: Depiction of possible pathways for oxidative (A) and reductive (B) conditions.

The initial generation of the radical and subsequent decarboxylation is different for oxidative and reductive pathway (compare Scheme 4), but both lead to the same intermediate **117** upon initial cyclization. From there, pathway **A** depicts the regeneration of the catalyst by oxidation of the cyclized radical (oxidative pathway), whereupon the resulting carbocation **118** may be trapped by water (**112**), which can be eliminated in the following, or the carbocation loses a proton directly, both of which leading to the unsaturated product **113**.

In contrast, pathway **B** calls for the regeneration of the catalyst by reduction of the cyclized radical (reductive pathway). The resulting anion **119** may be trapped by a proton, giving the saturated product **114**. Alternatively, the unsaturated product **113** may be formed by a different pathway from the carbanion or even the radical intermediate by abstraction of a hydrogen radical or cation, respectively. This involves complementary charged species formed from DIPEA (**15**) under the reaction conditions.

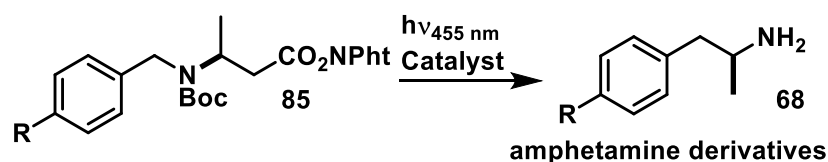
In either case, the compound mixture may be homogenized by transforming one of the compounds in each mixture to the other. For the oxidative pathway, the unsaturated product is accessible from the hydroxyl-compound by acid catalyzed elimination, while for the reductive reaction a hydrogenation may lead to solely the saturated compound.

### 3.5 Conclusion

The decarboxylation of carboxylic acids, one of the oldest and arguably most useful reactions in the toolbox of photochemistry has been brought to a renaissance by the application of new techniques focused on the combination of visible light and organic or transition metal catalysts. This allows for a simple reaction setup and smoothes the way to three different mechanisms, which depend on the conditions the reaction is performed under: Energy transfer, oxidative or reductive pathway (Scheme 4).

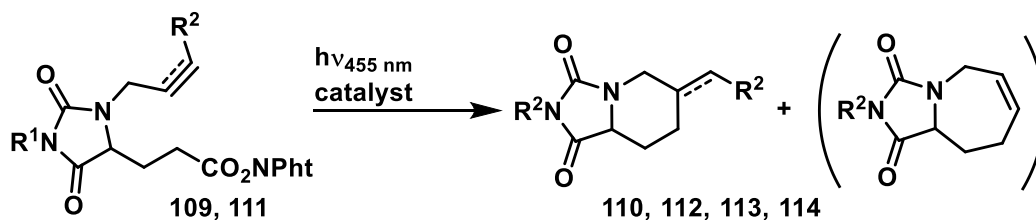
All three pathways were employed as key step in the synthesis of potentially biologically active substances or their key skeleton, initiating a decarboxylation of primary *N*-acyloxyphthalimides.

Suitably substituted  $\beta$ -amino acids were decarboxylated, resulting in a Smiles rearrangement leading to amphetamine derivatives (Scheme 36).



Scheme 36: Synthesis of amphetamine derivatives *via* Smiles rearrangement induced by visible light mediated decarboxylation.

Consecutively, the natural  $\beta$ - and  $\gamma$ -amino acids aspartic and glutamic acid were investigated as possible starting material for intramolecular cyclizations. Working with these di-acids required suitable protection strategies for the  $\alpha$ -amino acid part of the starting material. This resulted in the synthesis of oxazolidinones and hydantoin as protection group. The first of which was explored in cooperation with C. Eichinger and is described at length in his thesis, the latter was used for the construction of piperidines and also azepanes from glutamic acid derivatives (Scheme 37).



Scheme 37: Synthesis of piperidines and azepanes from hydantoin protected glutamic acid.

Thereby it was shown that visible light mediated decarboxylation of *N*-acyloxyphthalimides today is a viable method applicable in the synthesis of pharmacophores.

## 3.6 Experimental Section

### 3.6.1 General Information

#### Solvents and chemicals

All commercially available compounds were used as received. Anhydrous solvents were prepared by established laboratory procedures. Ethyl acetate, hexanes (40/60) and DCM were distilled prior to use in chromatography.  $[\text{Ir}(\text{dtbbpy})(\text{ppy})_2]\text{PF}_6$  was prepared as described in the literature.<sup>99</sup>

#### Light source in photoreactions

As light source in batch process CREE XLamp XP-E D5-15 LED ( $\lambda = 450 - 465 \text{ nm}$ ) were used.

#### NMR-spectroscopy

$^1\text{H}$ -NMR spectra were recorded on BRUKER Avance 300 (300 MHz), BRUKER Avance III 400 “Nanobay” (400 MHz) spectrometers.  $^{13}\text{C}$ -NMR spectra were recorded on BRUKER Avance 300 (75 MHz) and BRUKER Avance III 400 “Nanobay” (100 MHz) spectrometers. The spectra were recorded in  $\text{CDCl}_3$  unless otherwise noted. The Chemical shifts for  $^1\text{H}$  NMR were reported as  $\delta$ , parts per million, relative to the signal of  $\text{CHCl}_3$  at 7.26 ppm. The Chemical shifts for  $^{13}\text{C}$  NMR were reported as  $\delta$ , parts per million, relative to the center line signal of the  $\text{CDCl}_3$  triplet at 77.0 ppm.

#### Mass spectroscopy

Mass spectra were recorded at Central Analytical Laboratory of the University of Regensburg on a Varian MAT 311A, Finnigan MAT 95, Thermoquest Finnigan TSQ 7000 or Agilent Technologies 6540 UHD Accurate-Mass Q-TOF LC/MS.

#### Chromatography

For the column purification silica gel (Merck, Geduran 60, 0.063-0.200 mm particle size) and flash silica gel 60 (Merck, 0.040-0.063 mm particle size) was used. The TLC analysis was performed on silica gel 60 F254 (Merck) coated on aluminum sheets and visualized with UV, ninhydrin or  $\text{KMnO}_4$ .

#### FT-IR spectroscopy

ATR-IR spectroscopy was carried out on a Biorad Excalibur FTS 3000 spectrometer, equipped with a Specac Golden Gate Diamond Single Reflection ATR-System.

**Melting points** were measured with a Büchi SMP-20 apparatus in silicon oil bath.

**Cyclic voltammetry** was measured on an Autolab PGSTAT 302N setup at 20°C in MeCN containing  $n\text{Bu}_4\text{NBF}_4$  as supporting electrolyte. The electrochemical cell consisted of a glassy carbon working electrode, a platinum wire as counterelectrode and a silver wire as reference electrode. The solvent was degassed by  $\text{N}_2$  sparging prior to the measurements, and the redox potentials were referenced against ferrocene as internal standard. The values were then calculated and reported in reference to SCE electrode.

**Optical Rotation** was measured using an Anton Paar MCP500 Polarimeter at 589 nm in the specified solvent.

**Chiral HPLC** was carried out on a Varian 920-LC with Chiralpak AS-H, Phenomenex Lux Cellulose-1 or 2 as chiral stationary phase (as specified), using mixtures of  $n$ -heptane and  $i$ -PrOH as eluent.

**Fluorescence intensity** was measured with a Horiba Scientific FluoroMax4 Spectrofluorometer.

**Fluorescence lifetime** was measured with a Horiba DeltaPro Fluorescence Lifetime System equipped with a 370 nm Deltadiode DD-370.

### 3.6.2 Fluorescence Quenching

For the graphs below, the intensity at 560 nm (F) was divided by the intensity of the pure catalyst solution ( $F_0$ ) and plotted against  $n_{\text{quencher}}/n_{\text{cat}}$ , which corresponds to the equivalents of **53b** respective to the catalyst. Similarly, the lifetime of each sample ( $\tau$ ) was divided by the lifetime of the pure catalyst ( $t_0$ ) and plotted against the equivalents of **53b** respective to the catalyst. As seen from the graphs (Figure 3), until addition of about 1 equiv. **53b**, the fluorescence intensity and lifetime of the [Ir] catalyst increase slightly, indicating the formation of a catalyst-substrate complex, but then drop upon addition of more quencher. For **53b**, a very small increase at the beginning is observed, but only poor quenching upon addition of more **91**. It can be concluded, that a successful interaction between the catalyst and the substrate is only possible when the *N*-acyloxypthalimide is in a favorable conformation due to the presence of the bulky 'Butyl group. Furthermore, the quenching of **53b** did not follow a Stern-Volmer type quenching, indicating that more than just one pathway might be operative.

Table 3: Data for substrate **53b**.

Intensity F	1705770,0	1782416,7	1856883,3	1862493,3	1873110,0	1895170,0
lifetime $\tau$ [ $\mu$ s]	4,5846	4,8976	5,0649	5,0366	5,1683	5,1712
chi <sup>2</sup>	0,849	0,958	0,999	1,025	1,202	0,999
V total [L]	0,002000	0,002010	0,002020	0,002030	0,002050	0,002075
V add [L]	-	0,000010	0,000020	0,000030	0,000050	0,000075
$n_{\text{cat}}$ [mmol]	0,0001200	0,0001206	0,0001212	0,0001218	0,0001230	0,0001245
$n_{\text{1b}}$ [mmol]	0,0000000	0,0000240	0,0000480	0,0000720	0,0001200	0,0001801
$n_{\text{1b}}/n_{\text{cat}}$	0,00	0,20	0,40	0,59	0,98	1,45
F/ $F_0$	1,0000	1,0449	1,0886	1,0919	1,0981	1,1110
$\tau/\tau_0$	1,0000	1,0683	1,1048	1,0986	1,1273	1,1279

Intensity F	1904283,3	1819480,0	1592940,0	1320006,7	995600,0	820910,0
lifetime $\tau$ [ $\mu$ s]	5,1123	5,0565	4,3125	3,4935	2,5213	2,0638
chi <sup>2</sup>	1,003	1,016	0,856	0,840	0,918	0,936
V total [L]	0,00213	0,00225	0,00250	0,00300	0,00300	0,00300
V add [L]	0,00013	0,00025	0,00050	0,00100	0,00200	0,00300
$n_{\text{cat}}$ [mmol]	0,0001275	0,0001350	0,0001501	0,0001801	0,0001801	0,0001801
$n_{\text{1b}}$ [mmol]	0,0003001	0,0006002	0,0012005	0,0024009	0,0048037	0,0072056
$n_{\text{1b}}/n_{\text{cat}}$	2,35	4,44	8,00	13,33	26,68	40,02
F/ $F_0$	1,1164	1,0667	0,9339	0,7738	0,5837	0,4813
$\tau/\tau_0$	1,1151	1,1029	0,9406	0,7620	0,5500	0,4502

Table 4: Data for *N*-(Octanoyloxy)phthalimide **90**.

Intensity F	1966603,3	1975056,7	1962646,7	1882810,0	1869390,0
Lifetime $\tau$ [ $\mu$ s]	5,0820	5,1253	5,0915	4,8762	4,7654
$\chi^2$	0,975	0,996	0,9975405	0,967	0,975
V total [L]	0,00200	0,00201	0,00205	0,00220	0,00250
V add [L]	0,00000	0,00001	0,00005	0,00020	0,00050
n cat [mmol]	0,0001200	0,0001206	0,0001230	0,0001320	0,0001501
n <sub>1q</sub> [mmol]	0,0000000	0,0001207	0,0006035	0,0024141	0,0060353
n <sub>1q</sub> /n <sub>cat</sub>	0,00	1,00	4,90	18,28	40,22
F/F <sub>0</sub>	1,0000	1,0043	0,9980	0,9574	0,9506
$\tau/\tau_0$	1,0000	1,0085	1,0019	0,9595	0,9377

Octyl-NPht (**90**, -1.25 V vs. SCE, irreversible peak) was chosen as a reference compound. If photoelectron transfer from the photocatalyst would occur, it would be expected that fluorescence quenching would be observable for Octyl-NPht, which was not the case.

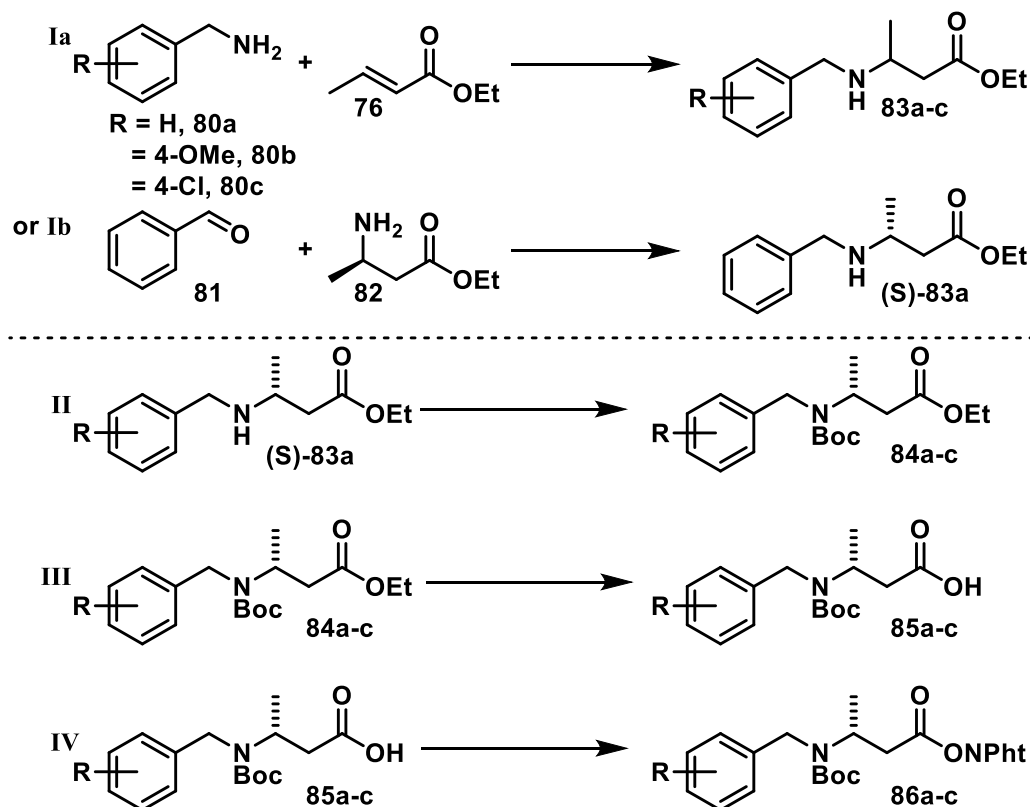
Table 5: Data for hippuric acid derivative **91**.

Intensity F	1903946,7	1961056,7	1918750,0	1799730,0	1647613,3
Lifetime $\tau$ [ $\mu$ s]	5,1625	5,1709	5,0286	4,6374	4,1329
$\chi^2$	0,968	1,048	1,058	0,905	0,888
V total [L]	0,00200	0,00201	0,00205	0,00220	0,00250
V add [L]	0,00000	0,00001	0,00005	0,00020	0,00050
n <sub>cat</sub> [mmol]	0,0001200	0,0001206	0,0001230	0,0001320	0,0001501
n <sub>1q</sub> [mmol]	0,0000000	0,0001213	0,0006064	0,0024254	0,0060635
n <sub>1q</sub> /n <sub>cat</sub>	0,00	1,01	4,93	18,37	40,41
F/F <sub>0</sub>	1,0000	1,0300	1,0078	0,9453	0,8654
$\tau/\tau_0$	1,0000	1,0016	0,9741	0,8983	0,8006

The *N*-hydroxyphthalimide ester of hippuric acid (**91**) tested, because it closely resembles the successful starting material **53b**, except that its amine is not functionalized with a bulky group. Therefore its two aromatic systems, phenyl ring and phthalimide moiety, are not in close proximity, preventing an IET. Thus, no transformation according to the suggested mechanism is possible, which is in line with the observed experimental results.

### 3.6.3 Synthesis of Starting Materials for the Amphetamine Synthesis

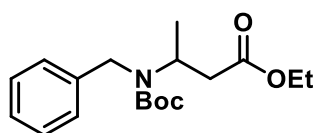
Substrates **83a-c** were synthesized by one-pot addition of benzyl amines to ethyl crotonate (Scheme 38, step **Ia**) or reductive amination of benzaldehyde with ethyl (*S*)-3-aminobutanoate (step **Ib**) and successive Boc-protection (step **II**) in a one-pot procedure, giving **84a-c**.



Scheme 38: Synthesis procedure for the synthesis of amphetamine precursors.

Following the saponification of **84a-c** to the corresponding acids **85a-c** (step **III**), the desired *N*-acyloxyphthalimides **86a-c** were obtained by esterification with *N*-hydroxyphthalimide (step **IV**).

#### Ethyl 3-(benzyl(*tert*-butoxycarbonyl)amino)butanoate ( $\pm$ )-**84a**

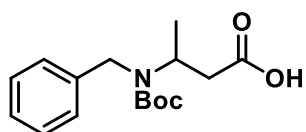


Compound ( $\pm$ )-**84a** was prepared by stirring benzyl amine **80a** (2 mL, 18 mmol, 1 equiv.) with ethyl crotonate **76**, (2.3 mL, 18 mmol, 1 equiv.) for 3 days without additional solvent at ambient temperature. Afterwards, the reaction mixture was diluted with 100 mL THF/H<sub>2</sub>O (1/1) and NaHCO<sub>3</sub> was added (7.56 g, 90 mmol, 5 equiv.). Upon cooling to 0 °C, Boc<sub>2</sub>O



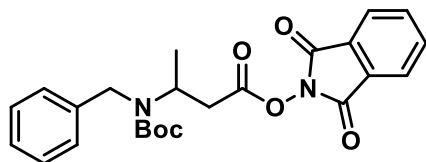
(4.53 g, 22 mmol, 1.2 equiv.) was added as solution in 20 mL THF. The reaction mixture was stirred for 24 h at ambient temperature, then THF was evaporated under reduced pressure and the remaining aqueous phase extracted with EtOAc (3x25 mL). The organic phase was washed with 1M HCl and brine, dried over Na<sub>2</sub>SO<sub>4</sub>, filtered and the solvent was removed under reduced pressure, yielding 5.07 g clear viscous oil, which was used in the next step without further purification.

### 3-(benzyl(*tert*-butoxycarbonyl)amino)butanoic acid (±)-85a



Compound (±)-85a was prepared from ester (±)-84a (5.00 g, 15.6 mmol, 1 equiv.) and potassium hydroxide (1.1 g, 20 mmol, 1.26 equiv.), which was dissolved in 10 mL H<sub>2</sub>O and slowly added to a solution of the ester in 100 mL EtOH. After 3 h vigorous stirring the mixture was acidified and extracted with 3x25 mL EtOAc. The organic phases were dried with MgSO<sub>4</sub> and the solvent evaporated under reduced pressure, yielding 3.8 g of viscous oil, which was used in the next step without further purification.

### 1,3-dioxoisindolin-2-yl 3-(benzyl(*tert*-butoxycarbonyl)amino)butanoate (±)-86a



Compound (±)-86a was prepared from acid (±)-85a (7.8 g, 26.5 mmol, 1 equiv.), *N*-hydroxyphthalimide (5.7 g, 27.8 mmol, 1.05 equiv.), and DCC (4.5 g, 27.8 mmol, 1.05 equiv.) by stirring in 100 mL dry DCM over night. After reaction completion, the mixture was cooled to 0 °C and precipitated DCU was filtered off. Column chromatography (hexanes:EtOAc = 4:1 to 1:1) and recrystallization from EtOH gave 6.15 g (14 mmol, 31% over three steps) offwhite solid.

**R<sub>f</sub>** (hexanes:EtOAc = 2:1) = 0.23.

**m.p.** = 107-108 °C.

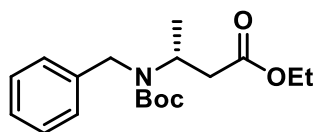
**IR** (neat): 2978, 1825, 1785, 1736, 1684, 1464, 1435, 1341, 1252 1222, 1162, 1133, 1114, 693 cm<sup>-1</sup>.

**<sup>1</sup>H NMR** (400 MHz, CDCl<sub>3</sub>): δ 7.82 (dd, J = 5.5, 3.1 Hz, 2H), 7.73 (dd, J = 5.5, 3.1 Hz, 2H), 7.31 – 7.18 (m, 5H), 4.64 (broad d, 1H), 4.21 (broad m, 2H), 3.05 (broad d, 1H), 2.75 (s, 1H), 1.42 (s, 9H), 1.25 (s, 3H).

**<sup>13</sup>C NMR** (101 MHz, CDCl<sub>3</sub>): δ 167.7, 161.9 (2 C), 154.9 (2 C), 139.2 (2 C), 134.9 (2 C), 128.9 (2 C), 128.6, 127.8, 127.5, 124.0 (2 C), 80.4, 76.8, 50.3, 49.7, 37.3, 28.5 (3 C), 18.5.

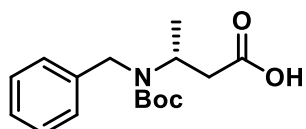
**HR-MS** (ESI-EIC) m/z calculated for C<sub>24</sub>H<sub>27</sub>N<sub>2</sub>O<sub>6</sub> [M+Na<sup>+</sup>]: 461.1683, found 461.1685.

**Ethyl (S)-3-(benzyl(*tert*-butoxycarbonyl)amino)butanoate** (S)-84a



(S)-84a was prepared by stirring benzaldehyde (**81**, 1.26 mL, 12.4 mmol, 1.05 equiv.) with ethyl (S)-3-aminobutanoate (**82**, 1.8 g, 11.8 mmol, 1 equiv.) for 24 h in 30 mL ethanol. Upon cooling to 0 °C, NaBH<sub>4</sub> (450 mg, 11.8 mmol, 1 equiv.) was added slowly in portions. When gas evolution stopped, the cooling bath was removed and the reaction stirred for another 2 h. Excess NaBH<sub>4</sub> was quenched by dropwise addition of water, and the Ethanol was removed under reduced pressure. The remains were dissolved in DCM (50 mL), and the solution washed with water (2x10 mL) and brine (1x10 mL). The organic phase was dried with MgSO<sub>4</sub> and filtered. NEt<sub>3</sub> (1.8 mL, 13 mmol, 1.1 equiv.) was added, then Boc<sub>2</sub>O (2.84 g, 13 mmol, 1.1 equiv) in portions. Upon stirring for 16 h at ambient temperature, the reaction mixture was washed with 1M HCl<sub>(aq)</sub> (2x15 mL), saturated NaHCO<sub>3(aq)</sub> (1x15 mL) solution and brine (1x10 mL). The organic phase was dried with MgSO<sub>4</sub>, filtered and the solvent removed under reduced pressure. Purification by column chromatography (hexanes:EtOAc 5:1, R<sub>f</sub> = 0.55) yielded 2.54 g (7.9 mmol, 67 %) clear viscous oil.

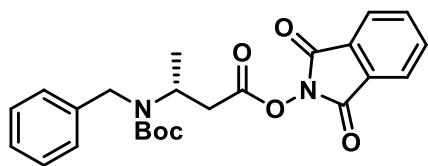
**3-(benzyl(*tert*-butoxycarbonyl)amino)butanoic acid** (S)-85a



(S)-85a was prepared from ester (S)-84a (2.23 g, 6.95 mmol, 1 equiv.) and potassium hydroxide (460 mg, 8.2 mmol, 1.2 equiv.), which was dissolved in 10 mL H<sub>2</sub>O and slowly added to a solution of the ester in 50 mL EtOH. After 3 h vigorous stirring the mixture was acidified and extracted with 3x25 mL EtOAc. The organic phases were dried with MgSO<sub>4</sub> and

the solvent evaporated under reduced pressure. The product was obtained as 1.91 g of clear viscous oil, which was used in the next step without further purification.

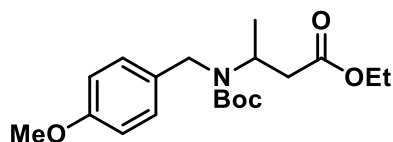
### 1,3-dioxoisindolin-2-yl (*S*)-3-(benzyl(*tert*-butoxycarbonyl)amino)butanoate (*S*)-86a



Compound (*S*)-**86a** was prepared from acid (*S*)-**85a** (1.87 g, 6.4 mmol, 1 equiv.), *N*-hydroxyphthalimide (1.25 g, 7.7 mmol, 1.2 equiv.), and DCC (1.6 g, 7.7 mmol, 1.2 equiv.) by stirring in 50 mL dry DCM over night. After reaction completion, the mixture was cooled to 0 °C and precipitated DCU was filtered off. Column chromatography (hexanes:EtOAc = 3:1 to 1:1) and recrystallization from EtOH gave an offwhite solid (1.73 g, 3.95 mmol, 39% over three steps). Analytical data was identical with **rac-86a**.

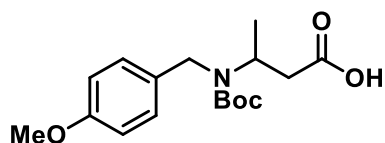
Optical rotation (DCM)  $[\alpha]_D^{20} = 31.7$  ( $c = 1.0$ , 589 nm)

### Ethyl 3-((*tert*-butoxycarbonyl)(4-methoxybenzyl)amino)butanoate **84b**



**84b** was prepared by stirring 4-methoxybenzylamine (1.5 mL, 11.5 mmol, 1 equiv.) with ethyl crotonate (1.42 mL, 27 mmol, 1 equiv.) for 4 d without additional solvent at ambient temperature. Afterwards, the reaction mixture was diluted with 40 mL DCM and  $\text{NEt}_3$  was added (2.3 mL, 17 mmol, 1.5 equiv.). Upon cooling to 0 °C,  $\text{Boc}_2\text{O}$  (3.27 g, 15 mmol, 1.3 equiv.) was added in portions. The reaction mixture was stirred for 16 h at ambient temperature, then washed with 1M  $\text{HCl}_{(\text{aq})}$  (2x20 mL), saturated  $\text{NaHCO}_{3(\text{aq})}$  (1x15 mL) solution and brine (1x15 mL). The organic phase was dried with  $\text{MgSO}_4$ , filtered and the solvent removed under reduced pressure. Purification by column chromatography (hexanes:EtOAc = 5:1,  $R_f = 0.50$ ) yielded 3.15 g clear viscous oil, which was used in the next step without further purification.

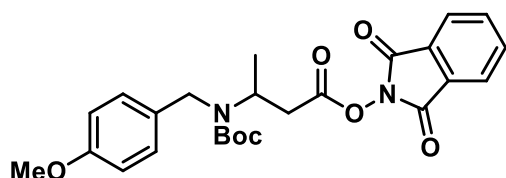
### 3-((*tert*-butoxycarbonyl)(4-methoxybenzyl)amino)butanoic acid **85b**



**85b** was prepared from ester **84b** (2.23 g, 6.95 mmol, 1 equiv.) and potassium hydroxide (460 mg, 8.2 mmol, 1.2 equiv.) which was dissolved in 10 mL  $\text{H}_2\text{O}$  and slowly added to a solution of the ester in 100 mL EtOH. After 3 h vigorous stirring the mixture was acidified

and extracted with 3x25 mL EtOAc. The organic phases were dried with MgSO<sub>4</sub> and the solvent evaporated under reduced pressure. The product was obtained as 2.7 g clear viscous oil, which was used in the next step without further purification.

**1,3-dioxoisindolin-2-yl 3-((*tert*-butoxycarbonyl)(4-methoxybenzyl)amino)butanoate**  
**86b**



Compound **86b** was prepared from acid **85b** (3.6 g, 11 mmol, 1 equiv.), *N*-hydroxyphthalimide (2.4 g, 11.6 mmol, 1.05 equiv.), and DCC (1.9 g, 11.6 mmol, 1.05 equiv.) by stirring in 100 mL dry DCM over night. After reaction completion, the mixture was cooled to 0 °C and precipitated DCU was filtered off. Column chromatography (hexanes:EtOAc = 4:1 to 2:1) gave a clear viscous oil (3.34 g, 7.76 mol, 51% over three steps).

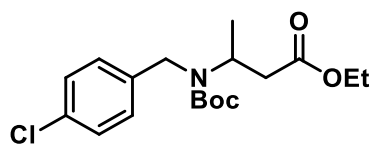
**R<sub>f</sub>** (hexanes:EtOAc = 2:1) = 0.26.

**IR** (neat): 2964, 2918, 1795, 1742, 1685, 1612, 1512, 1467, 1364, 1243, 1161, 1028, 970, 876, 831 cm<sup>-1</sup>.

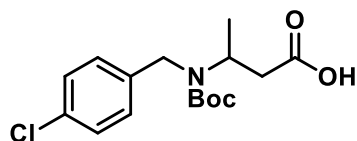
**<sup>1</sup>H NMR** (400 MHz, CDCl<sub>3</sub>): δ 7.86 (dd, *J* = 5.5, 3.1 Hz, 2H), 7.77 (dd, *J* = 5.5, 3.1 Hz, 2H), 7.21 (d, *J* = 7.8 Hz, 2H), 6.84 (d, *J* = 8.6 Hz, 2H), 4.63 (bs, 1H), 4.22 (bm, 2H), 3.78 (s, 3H), 3.07 (bd, 1H), 2.77 (bs, 1H), 1.49 (s, 9H), 1.27 (d, *J* = 4.6 Hz, 3H).

**<sup>13</sup>C NMR** (101 MHz, CDCl<sub>3</sub>): δ 167.9, 167.8(2 C), 161.9(2 C), 158.9(2 C), 134.9(2 C), 131.2(2 C), 128.9, 128.7, 124.0(2 C), 113.9, 80.3, 77.4, 55.3, 50.7, 49.6, 28.6(3 C), 18.5.

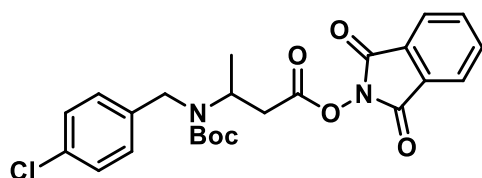
**HRMS** (ESI-EIC): *m/z* calculated for C<sub>25</sub>H<sub>28</sub>N<sub>2</sub>O<sub>7</sub> [M+H<sup>+</sup>]: 469.1974, found 469.1976.

**Ethyl 3-((*tert*-butoxycarbonyl)(4-chlorobenzyl)amino)butanoate 84c**

**84c** was prepared by stirring 4-chlorobenzylamine (1.5 mL, 9.2 mmol, 1 equiv.) with ethyl crotonate (1.15 mL, 9.2 mmol, 1 equiv.) for 3 d without additional solvent at ambient temperature. Afterwards, the reaction mixture was diluted with 30 mL DCM and  $\text{NEt}_3$  was added (1.9 mL, 13.5 mmol, 1.5 equiv.). Upon cooling to 0 °C,  $\text{Boc}_2\text{O}$  (2.8 g, 12.9 mmol, 1.4 equiv.) was added in portions. The reaction mixture was stirred for 16 h at ambient temperature, then washed with 1M  $\text{HCl}_{(\text{aq})}$  (2x10 mL), saturated  $\text{NaHCO}_{3(\text{aq})}$  (1x10 mL) solution and brine (1x10 mL). The organic phase was dried with  $\text{MgSO}_4$ , filtered and the solvent removed under reduced pressure. Purification by column chromatography (hexanes:EtOAc = 5:1,  $R_f$  = 0.5) yielded 2.52 g clear viscous oil, which was used in the next step without further purification.

**3-((*tert*-butoxycarbonyl)(4-chlorobenzyl)amino)butanoic acid 85c**

Compound **85c** was prepared from ester **84c** (2.39 g, 7.31 mmol, 1 equiv) and potassium hydroxide (620 mg, 11 mmol, 1.5 equiv.) which was dissolved in 10 mL  $\text{H}_2\text{O}$  and slowly added to a solution of the ester in 100 mL EtOH. After 3 h vigorous stirring the mixture was acidified and extracted with 3x25 mL EtOAc. The organic phases were dried with  $\text{MgSO}_4$  and the solvent evaporated under reduced pressure. The product was obtained as 2.09 g clear viscous oil, which was used in the next step without further purification.

**1,3-dioxoisindolin-2-yl 3-((*tert*-butoxycarbonyl)(4-chlorobenzyl)amino)butanoate 86c**

Compound **86c** was prepared from acid **85c** (1.9 g, 5.8 mmol, 1 equiv.), *N*-hydroxyphthalimide (1.00 g, 6.1 mmol, 1.05 equiv.), and DCC (1.95 g, 9.4 mmol, 1.05 equiv.) by stirring in 100 mL dry DCM over night. After reaction completion, the mixture was cooled to 0 °C and precipitated DCU was filtered off. Column chromatography

(hexanes:EtOAc = 4:1 to 1:1) and recrystallization from EtOH gave of viscous oil (1.60 g, 3.4 mmol, 46% over three steps).

**IR** (neat): 2926, 2851, 1739, 1624, 1579, 1450, 1311, 1076, 942, 843  $\text{cm}^{-1}$ .

**$^1\text{H}$  NMR** (300 MHz,  $\text{CDCl}_3$ ):  $\delta$  7.89 (dd,  $J = 5.5, 3.1$  Hz, 2H), 7.79 (dd,  $J = 5.5, 3.1$  Hz, 2H), 7.29 (d,  $J = 8.4$  Hz, 2H), 7.22 (d,  $J = 7.1$  Hz, 2H), 4.61 (s, 1H), 4.25 (bm, 2H), 3.11 (bd, 1H), 2.80 (s, 1H), 1.62 – 1.38 (bm, 9H), 1.32 – 1.23 (bm, 3H).

**$^{13}\text{C}$  NMR** (75 MHz,  $\text{CDCl}_3$ ):  $\delta$  167.7, 161.8, 134.9, 134.8, 128.9, 128.5, 127.7, 127.2, 124.1, 123.9, 77.3, 58.4, 50.6, 49.9, 28.5, 18.4.

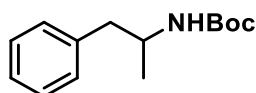
**HRMS** (ESI-EIC)  $m/z$  calculated for  $\text{C}_{24}\text{H}_{25}\text{ClN}_2\text{O}_6$  [ $\text{M}+\text{H}^+$ ]: 473.1479 found 473.1480.

### 3.6.4 Synthesis of Boc-amphetamines

#### General procedure **GP1**

A Schlenk tube with a magnetic stir bar was charged with a *N*-acyloxyphthalimide **1** (1 mmol, 1 equiv.) and the photocatalyst  $[\text{Ir}(\text{dtbbpy})(\text{ppy})_2]\text{PF}_6$  (10  $\mu\text{mol}$ , 1 mol%) in 10 ml acetonitrile/water (40/1, v/v) mixture (0.1 M concentration). The solution was degassed using three freeze-pump-thaw cycles and closed with a Teflon-sealed inlet for a glass rod, through which irradiation with a 455 nm high power LED took place. The photochemical reaction was stirred at room temperature and monitored by TLC analysis. After completion the solvent was removed under reduced pressure. The residue was purified by flash silica gel column chromatography or by extraction. For this the solvent was evaporated, the residue dissolved in EtOAc and extracted with 1 M HCl (3 x). The water phase was basified with KOH and extracted with dichloromethane (3 x). The side product phthalimide (hexanes:EtOAc = 2:1;  $R_f$  = 0.51) could be isolated in > 95% yield.

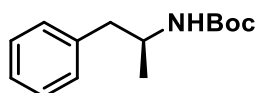
#### *tert*-butyl (1-phenylpropan-2-yl)carbamate ( $\pm$ )-**67a**



Compound ( $\pm$ )-**67a** was prepared from ( $\pm$ )-**86a** (460.0 mg, 1.05 mmol) and  $[\text{Ir}(\text{dtbbpy})(\text{ppy})_2]\text{PF}_6$  9.1 mg, 10.0  $\mu\text{mol}$ , 1 mol%) following **GP1**. Yield 133.3 mg (0.567 mmol, 54%) white solid.

Analytical data match to the reported data.<sup>100</sup>

#### (*S*)-*tert*-butyl (1-phenylpropan-2-yl)carbamate (*S*)-**67a**



Compound (*S*)-**85a** was prepared from (*S*)-**86a** (429.2 mg, 0.98 mmol) and  $[\text{Ir}(\text{dtbbpy})(\text{ppy})_2]\text{PF}_6$  (9.2 mg, 10.1  $\mu\text{mol}$ , 1.1 mol%) following **GP1**. Yields 119.8 mg (0.509 mmol, 52%) white solid.

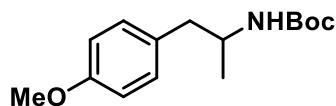
$R_f$  (hexanes:EtOAc = 19:1) = 0.17.

**Optical rotation** (DCM)  $[\alpha]_D^{20} = 12.7$  ( $c = 1.0$ , DCM, 589 nm). Enantioselectivity was determined via HPLC in comparison with **rac-67a** (Chiralpak AS-H, 4.6x250 mm, 10  $\mu\text{m}$ , n<sup>o</sup>Heptane/<sup>i</sup>PrOH 99:1, r.t., 14.01 min.), ee > 99:1.



**<sup>1</sup>H and <sup>13</sup>C NMR spectra** were identical with **rac-67a** and in accordance with the literature.<sup>100</sup>

**tert-butyl (1-(4-methoxyphenyl)propan-2-yl)carbamate 67b**



Compound **67b** was prepared from **86b** (478.3 mg, 1.02 mmol) and [Ir(dtbbpy)(ppy)<sub>2</sub>]<sub>2</sub>PF<sub>6</sub> (9.5 mg, 10.4 μmol, 1 mol%) following **GP1**. Yield 121.5 mg (0.45 mmol, 45%), white solid.

**R<sub>f</sub>** (hexanes:EtOAc = 19:1) = 0.15.

**m.p.:** 78.5-79.5 °C.

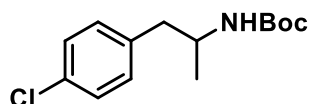
**IR** (neat): 3361, 2972, 2923, 1682, 1519, 1454, 1367, 1248, 1165, 1089, 1029, 890 cm<sup>-1</sup>.

**<sup>1</sup>H NMR** (400 MHz, CDCl<sub>3</sub>): δ 7.08 (d, J = 8.5 Hz, 2H), 6.82 (d, J = 8.6 Hz, 2H), 4.40 (s, 1H), 3.84 (s, 1H), 3.77 (s, 3H), 2.76 (dd, J = 13.4, 5.4 Hz, 1H), 2.59 (dd, J = 13.5, 7.4 Hz, 1H), 1.42 (s, 9H), 1.06 (d, J = 6.7 Hz, 3H).

**<sup>13</sup>C NMR** (101 MHz, CDCl<sub>3</sub>): δ 158.3, 155.4, 130.6(2 C), 130.4(2 C), 113.9, 79.2, 77.4, 55.4, 42.2, 28.6(3 C), 20.3.

**HRMS** (ESI-EIC): m/z calculated for C<sub>14</sub>H<sub>22</sub>NO<sub>2</sub> [M+H<sup>+</sup>]: 266.1751, found 266.1750.

**tert-butyl (1-(4-chlorophenyl)propan-2-yl)carbamate 68c**



Compound **68c** was prepared from **86c** (435 mg, 0.993 mmol) and [Ir(dtbbpy)(ppy)<sub>2</sub>]<sub>2</sub>PF<sub>6</sub> (9.2 mg, 10.1 μmol, 1.0 mol%) following **GP1**. Yield 80 mg (0.30 mmol, 30%), beige solid.

**R<sub>f</sub>** (hexanes:EtOAc = 19:1) = 0.17.

**m.p.:** 88-89 °C.

**IR** (neat): 3383, 2968, 1681, 1507, 1443, 1367, 1246, 1168, 1059, 814 cm<sup>-1</sup>.

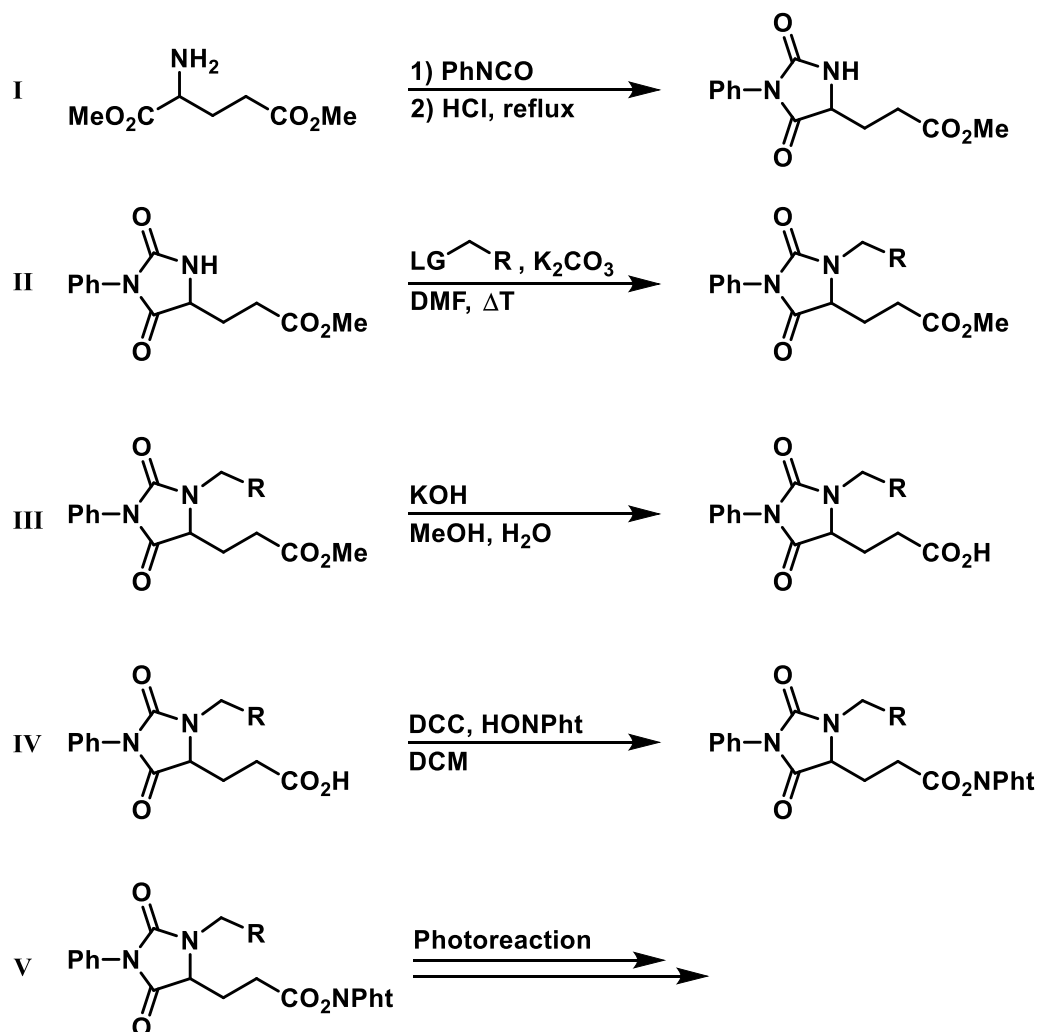
**<sup>1</sup>H NMR** (400 MHz, CDCl<sub>3</sub>): δ 7.21 (d, J = 7.7 Hz, 2H), 7.06 (d, J = 7.3 Hz, 2H), 4.34 (s, 1H), 3.82 (s, 1H), 2.75 (bd, J = 8.4 Hz, 1H), 2.59 (dd, J = 12.0, 7.3 Hz, 1H), 1.37 (s, 9H), 1.03 (d, J = 6.0 Hz, 3H).

**<sup>13</sup>C NMR** (101 MHz, CDCl<sub>3</sub>): δ 155.27, 136.9, 132.2, 130.9(2 C), 128.5(2 C), 79.4, 47.5, 42.5, 28.5(3 C), 20.2.

**HRMS** (ESI-EIC): m/z calculated for C<sub>14</sub>H<sub>20</sub>ClNONa [M+Na<sup>+</sup>]: 292.1075, found 292.1074.

### 3.6.5 Synthesis of Hydantoin

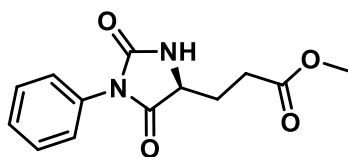
Suitable starting material for Photoreaction **V** was synthesized in four steps. In step **I**, glutamic acid was protected as phenyl hydantoin by stirring with phenyl isocyanate and then refluxing the strongly acidified solution. Next, the system for intramolecular cyclization was installed in step **II** under basic conditions, using either mesitylated propargylic alcohol or dimethylallyl bromide as coupling partner (Scheme 39).



Scheme 39: Schematic representation of the synthesis of hydantoin derivatives for photochemical decarboxylation.

Subsequently the methyl ester was cleaved under basic conditions (step **III**), and the resulting acid transformed to the desired *N*-acyloxyphthalimide without purification (step **IV**).

**Methyl (S)-3-(2,5-dioxo-1-phenylimidazolidin-4-yl)propanoate S1**



Compound **S1** was synthesized following the literature procedure<sup>96</sup> by dissolving dimethylglutamate hydrochloride (7 g, 33.2 mmol, 1 equiv.) in 100 mL MeCN, followed by addition of NEt<sub>3</sub> (5 mL, 36.5 mmol, 1.1 equiv.). Upon vigorous stirring for 15 min., the white precipitate was filtrated off and washed with 50 mL MeCN. The colourless liquid was collected and phenyl isocyanate (3.5 mL, 34.8 mmol, 1.05 equiv.) was added slowly over the course of three minutes. The now yellowish solution was stirred at room temperature for 3 h, and then the solvent was removed under reduced pressure. Next, the residue was dissolved in 100 mL MeOH, then 75 mL 6M HCl were added and the mixture refluxed for 1 h. The majority of the MeOH component of the solution was evaporated under reduced pressure and the remaining aqueous solution extracted (3 x 100 mL EtOAc). Upon drying over MgSO<sub>4</sub> the solution was filtrated, evaporated under reduced pressure and the residue recrystallized from EtOH to give the product (6.39 g, 24.2 mmol, 73%) as white crystalline compound.

**IR** (neat): 3267, 3056, 2951, 1699, 1648, 1593, 1495, 1442, 1313, 1230, 1172, 895, 752 cm<sup>-1</sup>.

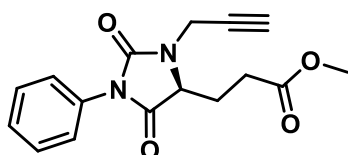
**<sup>1</sup>H NMR** (400 MHz, CDCl<sub>3</sub>): δ 7.50 – 7.44 (m, 2H), 7.41 – 7.37 (m, 3H), 6.26 (s, 1H), 4.26 (ddd, *J* = 6.5, 5.2, 1.4 Hz, 1H), 3.71 (s, 3H), 2.56 (t, *J* = 7.0 Hz, 2H), 2.31 (ddd, *J* = 14.1, 7.2, 5.2 Hz, 1H), 2.20 – 2.11 (m, 1H).

**<sup>13</sup>C NMR** (101 MHz, CDCl<sub>3</sub>): δ 177.9, 173.2, 172.3, 156.1, 131.3, 129.2, 129.1, 128.6, 128.3, 126.3, 126.1, 56.3, 52.1, 29.5, 27.0.

**HRMS** (ESI-EIC): *m/z* calculated for C<sub>13</sub>H<sub>15</sub>N<sub>2</sub>O<sub>4</sub> [M+H<sup>+</sup>]: 263.1026, found 263.1026.

Analytical data match the reported data.<sup>101</sup>

**Methyl (S)-3-(2,5-dioxo-1-phenyl-3-(prop-2-yn-1-yl)imidazolidin-4-yl)propanoate S2**



Compound **S2** was synthesized by suspending **S1** (1.5 g, 5.7 mmol, 1 equiv.), methylsulfonylated propargylic alcohol (0.91 mL, 6.9 mmol, 1.2 equiv.) and potassium carbonate (2.36g, 17.1 mmol, 3 equiv.) in a round bottom flask equipped with a reflux condenser in 50 mL DMF and stirring the resulting mixture at 80 °C for 5 h. Subsequently,

100 mL H<sub>2</sub>O were added and the mixture extracted with 3 x 30 mL cooled EtOAc. The organic phases were combined and washed with brine (3 x 20 mL). Upon drying with MgSO<sub>4</sub> and filtration the solvent was evaporated under reduced pressure. The crude product was purified by column chromatography (hexanes:EtOAc = 1:3) to give the product as colourless solid (2.9 mmol, 0.87 g, 51%).

**R<sub>f</sub>** (hexanes:EtOAc = 3:1) = 0.3.

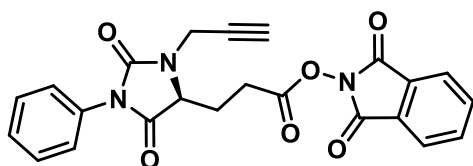
**IR** (neat): 3250, 2983, 1812, 1732, 1444, 1354, 1262, 1154, 1095, 991, 893, 850 cm<sup>-1</sup>.

**<sup>1</sup>H NMR** (400 MHz, CDCl<sub>3</sub>): δ 7.50 – 7.34 (m, 5H), 4.64 (dd, *J* = 17.9, 2.6 Hz, 1H), 4.40 (dd, *J* = 6.1, 3.5 Hz, 1H), 3.95 (dd, *J* = 17.9, 2.5 Hz, 1H), 3.68 (s, 3H), 2.52 – 2.25 (m, 5H).

**<sup>13</sup>C NMR** (101 MHz, CDCl<sub>3</sub>): δ 172.8, 171.0, 155.2, 131.5, 129.2, 128.5, 126.1, 76.6, 74.0, 57.9, 52.1, 31.1, 28.3, 24.0.

**HRMS** (ESI-EIC): *m/z* calculated for C<sub>16</sub>H<sub>17</sub>N<sub>2</sub>O<sub>4</sub> [M+H<sup>+</sup>]: 301.1183, found 301.1186.

**1,3-dioxoisindolin-2-yl (S)-3-(2,5-dioxo-1-phenyl-3-(prop-2-yn-1-yl)imidazolidin-4-yl)propanoate** **109**



Compound **109** was synthesized from **S2** in two steps. First, the methyl ester of compound **S2** (790.2 mg, 2.6 mmol) was hydrolyzed by stirring with KOH (180 mg, 3.2 mmol, 1.2 equiv.) in a MeOH/H<sub>2</sub>O mixture (20 mL, 2/1). Upon completion the aqueous mixture was acidified to pH ~3 using 1M HCl and subsequently extracted with 3 x 20 mL EtOAc. The organic fractions were combined and dried over MgSO<sub>4</sub> and the solvent evaporated under reduced pressure. Consequently the crude product was used in the next step without further purification, calculating the required reagents according to theoretical 100% yield. Therefore, the residue was dissolved in 20 mL DCM and *N*-hydroxyphthalimide (524 mg, 3.2 mmol, 1.2 equiv.) and DCC (665 mg, 3.2 mmol, 1.2 equiv.) were added. The solution was stirred over night, cooled to 0 °C, and the white precipitate (consisting mainly DCU) removed by filtration. Upon extraction (2 x 0.5M HCl, 1 x brine) the solution was dried over MgSO<sub>4</sub> and the solvent removed under reduced pressure. Column chromatography (hexanes:EtOAc = 2:1) yielded the product as colourless solid (1.72 g, 3.98 mmol, 66% over two steps).

**R<sub>f</sub>** (hexanes:EtOAc = 1:1) = 0.4.

**IR** (neat): 3282, 3142, 3056, 2928, 1673, 1437, 1310, 1254, 1203, 1107, 1013, 963, 912 cm<sup>-1</sup>.

**<sup>1</sup>H NMR** (300 MHz, CDCl<sub>3</sub>): δ 7.90 – 7.84 (m, 2H), 7.81 – 7.76 (m, 2H), 7.49 – 7.34 (m, 5H), 4.57 (dd, *J* = 18.0, 2.5 Hz, 1H), 4.43 (dd, *J* = 6.5, 3.7 Hz, 1H), 4.08 (dd, *J* = 18.0, 2.5 Hz, 1H), 3.01 – 2.79 (m, 2H), 2.62 – 2.50 (m, 1H), 2.49 – 2.34 (m, 2H).

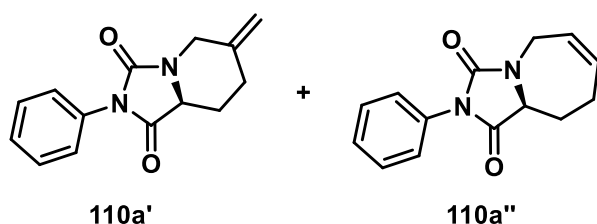
**<sup>13</sup>C NMR** (75 MHz, CDCl<sub>3</sub>): δ 170.6, 168.6, 161.7, 155.0, 134.9, 131.3, 129.2, 128.8, 128.4, 126.0, 124.1, 76.5, 74.3, 57.8, 31.3, 25.6, 23.8.

**HRMS** (ESI-EIC): *m/z* calculated for C<sub>23</sub>H<sub>18</sub>N<sub>3</sub>O<sub>6</sub> [M+H<sup>+</sup>]: 432.1190, found 432.1193.

**(S)-6-methylene-2-phenyltetrahydroimidazo[1,5-a]pyridine-1,3(2H,5H)-dione** **110a'**

and

**(S)-2-phenyl-5,8,9,9a-tetrahydro-1H-imidazo[1,5-a]azepine-1,3(2H)-dione** **110a''**



Compound **109a** (301 mg, 0.7 mmol, 1 equiv.), [Ir(dtbbpy)ppy<sub>2</sub>]<sup>+</sup>PF<sub>6</sub><sup>-</sup> (6.4 mg, 0.07 mmol, 1 mol%) and DIPEA (130 μL, 0.75 mmol, 1.05 equiv.) were dissolved in 4 mL MeCN and set under nitrogen atmosphere by application of 3 x freeze-pump-thaw technique in a Schlenk tube. The Schlenk tube was closed with a Teflon-sealed inlet for a glass rod, through which irradiation with a 455 nm high power LED took place. The solution was subsequently irradiated for 2.5 h until all starting material was consumed as judged by TLC, whereupon the irradiation was stopped and the solvent evaporated under reduced pressure. The residue was purified by column chromatography (hexanes:EtOAc = 5:1 to 1:1) and the inseparable product mixture was obtained as colourless crystals (ratio **110a'** to **110a''** = 1:2.4, 123.6 mg, 0.51 mmol, 73%). Further attempts to separate the two regioisomers by crystallization were unsuccessful.

**<sup>1</sup>H NMR** (400 MHz, CDCl<sub>3</sub>): δ 7.49 – 7.32 (m, 16H), 5.89 – 5.77 (m, 1H), 5.72 (dddd, *J* = 9.7, 4.3, 2.3, 1.1 Hz, 1H), 5.00 (q, *J* = 1.6 Hz, 2H), 4.93 (q, *J* = 1.6 Hz, 2H), 4.71 – 4.57 (m, 3H), 4.36 – 4.25 (m, 1H), 4.06 (dd, *J* = 12.0, 4.1 Hz, 2H), 3.71 (dt, *J* = 17.6, 2.3 Hz, 1H), 3.60 (dq, *J* = 14.4, 1.6 Hz, 2H), 2.61 (dt, *J* = 14.0, 2.8 Hz, 2H), 2.46 – 2.15 (m, 9H), 1.68 – 1.55 (m, 3H).

**<sup>13</sup>C NMR** (101 MHz, CDCl<sub>3</sub>): δ 172.0, 171.4, 155.1, 153.3, 139.6, 131.8, 131.7, 131.0, 129.0, 128.1, 128.0, 127.0, 126.0, 126.0, 112.2, 61.5, 56.8, 45.3, 40.9, 31.3, 29.6, 28.9, 24.1.

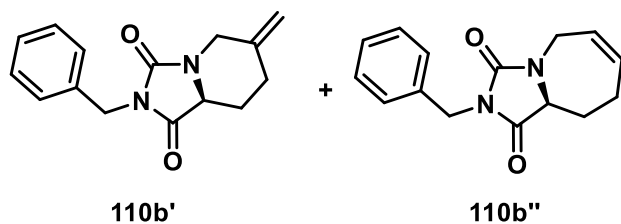
**HRMS** (ESI-EIC): *m/z* calculated for C<sub>14</sub>H<sub>15</sub>N<sub>2</sub>O<sub>2</sub> [M+H<sup>+</sup>]: 243.1128, found 243.1128.

*Same molecular formula and mass for 110a' and 110a''.*

(S)-2-benzyl-6-methylenetetrahydroimidazo[1,5-a]pyridine-1,3(2H,5H)-dione **110b'**

and

(S)-2-benzyl-5,8,9,9a-tetrahydro-1H-imidazo[1,5-a]azepine-1,3(2H)-dione **110b''**



Compound **109b** (334 mg, 0.75 mmol, 1 equiv.), [Ir(dtbbpy)ppy<sub>2</sub>]<sub>2</sub>PF<sub>6</sub> (7.5 mg, 0.08 mmol, 1mol%) and DIPEA (150 μL, 0.86 mmol, 1.15 equiv.) were dissolved in 4 mL MeCN and set under nitrogen atmosphere by application of 3 x freeze-pump-thaw technique in a Schlenk tube. The Schlenk tube was closed with a Teflon-sealed inlet for a glass rod, through which irradiation with a 455 nm high power LED took place. The solution was subsequently irradiated for 2.5 h until all starting material was consumed as judged by TLC, whereupon the irradiation was stopped and the solvent evaporated under reduced pressure. The residue was purified by column chromatography (hexanes:EtOAc = 5:1 to 1:1) and the product obtained as colourless crystals (ratio **110b'** to **110b''** = 1:1.9, 133.9 mg, 0.52 mmol, 70%).

<sup>1</sup>H NMR (400 MHz, CDCl<sub>3</sub>): δ 7.38 (ddd, *J* = 7.8, 3.6, 1.5 Hz, 6H), 7.34 – 7.27 (m, 8H), 5.72 (dd, *J* = 5.1, 2.6 Hz, 1H), 5.68 – 5.60 (m, 1H), 4.93 (d, *J* = 1.8 Hz, 2H), 4.86 (d, *J* = 1.8 Hz, 2H), 4.66 (s, 2H), 4.64 (s, 4H), 4.58 – 4.50 (m, 3H), 4.11 (dd, *J* = 5.8, 4.1 Hz, 1H), 3.88 (dd, *J* = 12.0, 3.9 Hz, 2H), 3.61 (dt, *J* = 17.8, 2.2 Hz, 1H), 3.50 (dd, *J* = 14.5, 1.7 Hz, 2H), 2.57 – 2.48 (m, 2H), 2.27 (tdd, *J* = 13.8, 7.7, 2.9 Hz, 5H), 2.18 – 1.94 (m, 3H), 1.47 – 1.34 (m, 2H).

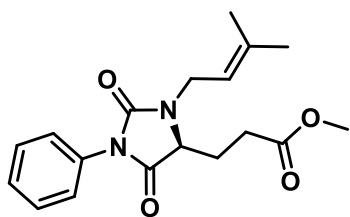
<sup>13</sup>C NMR (101 MHz, CDCl<sub>3</sub>): δ 172.8, 172.3, 156.1, 154.3, 139.8, 136.3, 136.2, 131.0, 128.7, 128.6, 128.6, 127.9, 127.0, 112.1, 61.7, 57.1, 45.1, 42.6, 42.4, 40.9, 31.3, 29.4, 28.7, 24.0.

HRMS (ESI-EIC): *m/z* calculated for C<sub>15</sub>H<sub>17</sub>N<sub>2</sub>O<sub>2</sub> [M+H<sup>+</sup>]: 257.1285, found 257.1289.

*Same molecular formula for 110b' and 110b''.*

**Methyl (S)-3-(3-(3-methylbut-2-en-1-yl)-2,5-dioxo-1-phenylimidazolidin-4-yl)propanoate**

**S3**



Compound **S3** was synthesized by suspending **S1** (1.5 g, 5.7 mmol, 1 equiv.), 3,3-dimethylallyl bromide (95% purity, 1.48 mL, 12.2 mmol, 2.1 equiv.) and potassium carbonate (2.3 g, 17.1 mmol, 3 equiv.) in a round bottom flask equipped with a reflux condenser in 50 mL DMF and stirring the resulting mixture at 80 °C for 5 h. Subsequently, 100 mL H<sub>2</sub>O were added and the mixture extracted with 3 x 30 mL cooled EtOAc. The organic phases were combined and washed with brine (3 x 20 mL). Upon drying with MgSO<sub>4</sub> and filtration the solvent was evaporated under reduced pressure. The crude product was purified by column chromatography (hexanes:EtOAc = ), yielding the desired compound as colourless solid (1.0 g, 3.05 mmol, 54%)

**R<sub>f</sub>** (hexanes:EtOAc = 4:1) = 0.35.

**IR** (neat): 3267, 3056, 2951, 2856, 1699, 1648, 1593, 1544, 1495, 1442, 1313, 1230, 1172, 983, 895, 810, 752 cm<sup>-1</sup>.

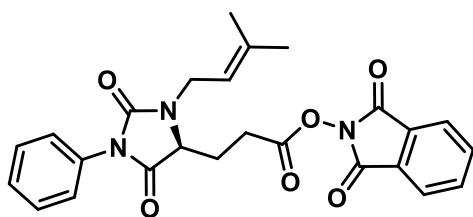
**<sup>1</sup>H NMR** (300 MHz, CDCl<sub>3</sub>): δ 7.49 – 7.32 (m, 5H), 5.25 – 5.16 (m, 1H), 4.34 (ddt, *J* = 15.4, 6.2, 1.1 Hz, 1H), 4.16 (dd, *J* = 6.3, 3.1 Hz, 1H), 3.75 (dd, *J* = 15.3, 8.4 Hz, 1H), 3.68 (s, 3H), 2.44 (td, *J* = 7.5, 1.4 Hz, 2H), 2.40 – 2.29 (m, 1H), 2.24 – 2.11 (m, 1H), 1.83 – 1.69 (m, 6H).

**<sup>13</sup>C NMR** (75 MHz, CDCl<sub>3</sub>): δ 172.7, 171.4, 155.2, 131.6, 131.5, 129.2, 129.1, 128.5, 128.2, 126.1, 119.8, 57.6, 52.0, 43.7, 28.0, 24.0.

**HRMS** (ESI-EIC): *m/z* calculated for C<sub>18</sub>H<sub>22</sub>N<sub>2</sub>O<sub>4</sub> [M+H<sup>+</sup>]: 331.1658, found 331.1654.

**1,3-dioxoisindolin-2-yl**  
**phenylimidazolidin-4-yl)propanoate**

**(S)-3-(3-(3-methylbut-2-en-1-yl)-2,5-dioxo-1-**  
**111**



Compound **111** was synthesized from **S3** in two steps. First, the methyl ester of compound **S3** (850 mg, 2.57 mmol, 1 equiv.) was hydrolyzed by stirring with KOH (152 mg, 2.7 mmol, 1.05 equiv.) in a MeOH/H<sub>2</sub>O mixture (2/1, 20 mL). Upon completion the aqueous mixture

was acidified to pH ~3 using 1M HCl and subsequently extracted with 3 x 20 mL EtOAc. The organic fractions were combined and dried over MgSO<sub>4</sub> and the solvent evaporated under reduced pressure. Consequently the crude product was used in the next step without further purification, calculating the required reagents according to theoretical 100% yield. Therefore, the residue was dissolved in 20 mL DCM and *N*-hydroxyphthalimide (445.3 mg, 2.73 mmol, 1.05 equiv.) and DCC (608.2 mg, 2.95 mmol, 1.15 equiv.) were added. The solution was stirred over night, cooled to 0 °C, and the white precipitate removed by filtration. Upon extraction (2 x 0.5M HCl, 1 x brine) the solution was dried over MgSO<sub>4</sub> and the solvent removed under reduced pressure. Column chromatography (hexanes:EtOAc = ) yielded the product as colourless solid (746 mg, 1.62 mmol, 63%).

**R<sub>f</sub>** (hexanes:EtOAc = 3:1) = 0.15.

**IR** (neat): 3059, 2978, 1689, 1419, 1319, 1249, 1183, 1106, 959, 794 cm<sup>-1</sup>.

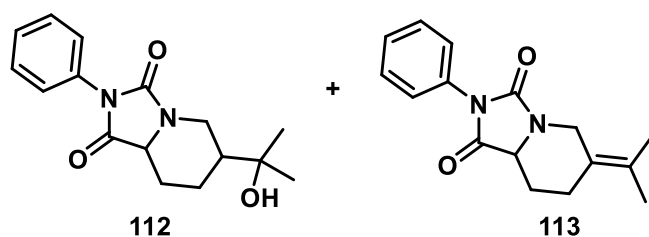
**<sup>1</sup>H NMR** (400 MHz, CDCl<sub>3</sub>): δ 7.89 (dd, *J* = 5.5, 3.1 Hz, 2H), 7.80 (dd, *J* = 5.5, 3.1 Hz, 2H), 7.49 – 7.33 (m, 5H), 5.24 (tdd, *J* = 6.6, 2.9, 1.4 Hz, 1H), 4.39 – 4.30 (m, 1H), 4.22 (dd, *J* = 7.2, 3.4 Hz, 1H), 3.85 (dd, *J* = 15.3, 8.1 Hz, 1H), 2.94 – 2.82 (m, 2H), 2.51 (dddd, *J* = 14.5, 8.6, 7.4, 3.4 Hz, 1H), 2.30 – 2.20 (m, 1H), 1.76 (t, *J* = 1.5 Hz, 6H).

**<sup>13</sup>C NMR** (101 MHz, CDCl<sub>3</sub>): δ 171.2, 168.7, 161.8, 155.2, 139.0, 134.9, 131.7, 129.1, 128.9, 128.2, 126.0, 124.1, 117.6, 57.4, 39.2, 25.8, 25.5, 24.2, 18.1.

**HRMS** (ESI-EIC): *m/z* calculated for C<sub>25</sub>H<sub>23</sub>N<sub>3</sub>O<sub>6</sub>Na [M+Na<sup>+</sup>]: 484.1479, found 484.1485.

**6-(2-hydroxypropan-2-yl)-2-phenyltetrahydroimidazo[1,5-a]pyridine-1,3(2H,5H)-dione**  
**112** and

**2-phenyl-6-(propan-2-ylidene)tetrahydroimidazo[1,5-a]pyridine-1,3(2H,5H)-dione**  
**113**



Compound **111** (180.0 mg, 0.4 mmol, 1 equiv.), *fac*-[Ir] (6.7 mg, 0.01 mmol, 2.5 mol%) and H<sub>2</sub>O (90 μL, 5 mmol, 12.5 equiv.) were dissolved in 6 mL MeCN and set under nitrogen atmosphere by application of 3 x freeze-pump-thaw technique in a Schlenk tube. The Schlenk tube was closed with a Teflon-sealed inlet for a glass rod, through which irradiation with a 455 nm high power LED took place. The solution was subsequently irradiated for 22 h until all starting material was consumed as judged by TLC, whereupon the irradiation was stopped



and the solvent evaporated under reduced pressure. The residue was purified by column chromatography (hexanes:EtOAc = 10:1 to 1:1) and the product obtained as colourless crystals (81 mg, yield not calculated).

**R<sub>f</sub>** (hexanes:EtOAc = 3:1) = 0.4.

**<sup>1</sup>H NMR** (400 MHz, CDCl<sub>3</sub>): δ 7.53 – 7.30 (m, 5H), 4.65 (s, 0H), 4.19 (dd, *J* = 7.0, 3.3 Hz, 1H), 3.81 (dt, *J* = 15.4, 8.1 Hz, 1H), 3.39 (d, *J* = 10.9 Hz, 1H), 3.13 (dt, *J* = 14.3, 7.2 Hz, 1H), 2.54 (h, *J* = 10.4, 9.5 Hz, 2H), 2.39 (dtd, *J* = 15.2, 7.7, 3.2 Hz, 1H), 2.15 (dq, *J* = 14.5, 7.1 Hz, 1H), 1.92 (d, *J* = 12.3 Hz, 1H), 1.76 – 1.56 (m, 2H), 1.51 (q, *J* = 7.4 Hz, 2H), 1.34 (q, *J* = 12.1 Hz, 1H), 1.22 – 1.07 (m, 1H), 0.97 (d, *J* = 6.4 Hz, 6H).

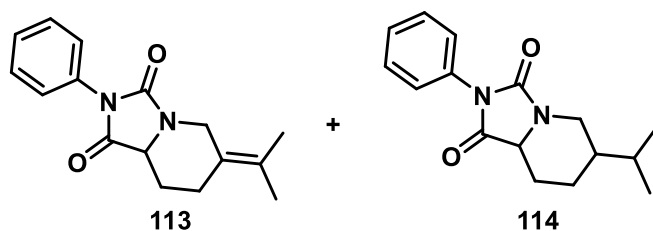
**<sup>13</sup>C NMR** (101 MHz, CDCl<sub>3</sub>): δ 176.1, 171.6, 155.2, 131.7, 129.1, 128.3, 126.1, 57.5, 49.5, 39.3, 36.4, 33.8, 27.9, 26.0, 25.6, 25.0, 24.1, 22.7, 22.3.

**LRMS** for **112** (APCI-EIC): *m/z* calculated for C<sub>16</sub>H<sub>21</sub>N<sub>2</sub>O<sub>3</sub> [M+H<sup>+</sup>]: 289.1552, found 289.1081.

#### **6-isopropyl-2-phenyltetrahydroimidazo[1,5-a]pyridine-1,3(2H,5H)-dione** **114**

and

#### **2-phenyl-6-(propan-2-ylidene)tetrahydroimidazo[1,5-a]pyridine-1,3(2H,5H)-dione** **113**



Compound **111** (183.1 mg, 0.4 mmol, 1 equiv.), [Ir(dtbbpy)ppy<sub>2</sub>]PF<sub>6</sub> (4.4 mg, 4.8 μmol, 1.2 mol%) and DIPEA (73 μL, 0.42 mmol, 1.05 equiv.) were dissolved in 6 mL MeCN and set under nitrogen atmosphere by application of 3 x freeze-pump-thaw technique in a Schlenk tube. The Schlenk tube was closed with a Teflon-sealed inlet for a glass rod, through which irradiation with a 455 nm high power LED took place. The solution was subsequently irradiated for 1.5 h until all starting material was consumed as judged by TLC, whereupon the irradiation was stopped and the solvent evaporated under reduced pressure. The residue was purified by column chromatography (hexanes:EtOAc = 5:1 to 1:1) and the product obtained as colourless crystals (85 mg, yield not calculated).

**R<sub>f</sub>** (hexanes:EtOAc = 3:1) = 0.4.

**<sup>1</sup>H NMR** (300 MHz, CDCl<sub>3</sub>): δ 7.51 – 7.31 (m, 6H), 4.87 (p, *J* = 1.5 Hz, 0H), 4.79 (p, *J* = 0.9 Hz, 1H), 4.30 (tdd, *J* = 12.6, 4.4, 1.8 Hz, 1H), 3.90 (ddd, *J* = 16.1, 11.9, 4.2 Hz, 1H), 2.74 (dd,

$J = 13.2, 11.5$  Hz, 0H), 2.60 (dd,  $J = 13.2, 11.1$  Hz, 1H), 2.42 – 2.29 (m, 1H), 2.19 – 2.02 (m, 2H), 1.78 (t,  $J = 1.1$  Hz, 2H), 1.59 – 1.43 (m, 2H), 1.35 – 1.22 (m, 1H), 0.96 (dd,  $J = 6.8, 1.4$  Hz, 4H).

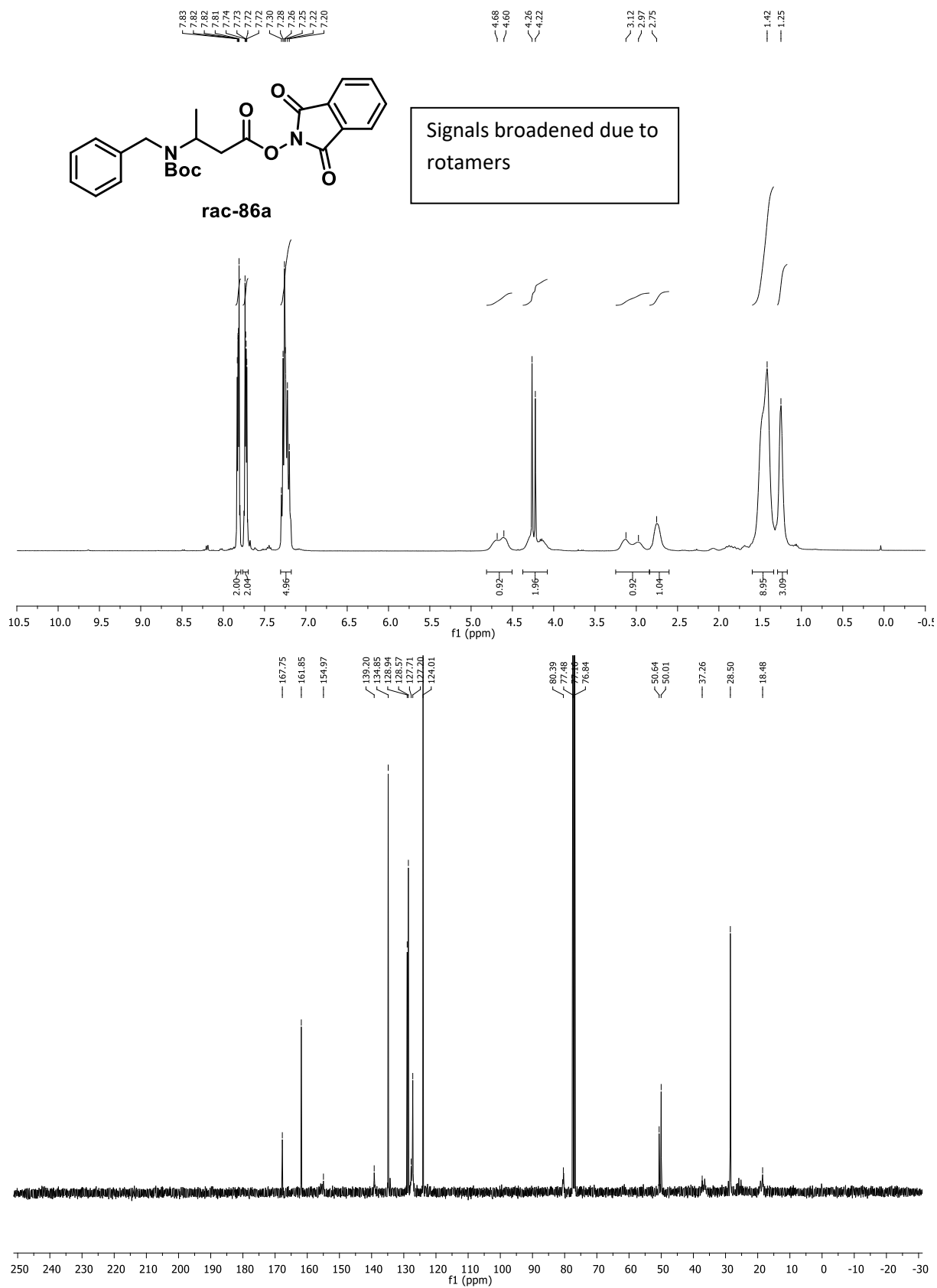
$^{13}\text{C NMR}$  (75 MHz,  $\text{CDCl}_3$ ):  $\delta$  172.0, 171.8, 153.6, 145.2, 134.3, 131.9, 129.1, 129.1, 128.1, 128.0, 126.1, 123.6, 111.3, 57.3, 57.1, 43.7, 43.2, 42.9, 42.4, 30.9, 28.3, 28.0, 27.8, 26.8, 21.5, 19.97.

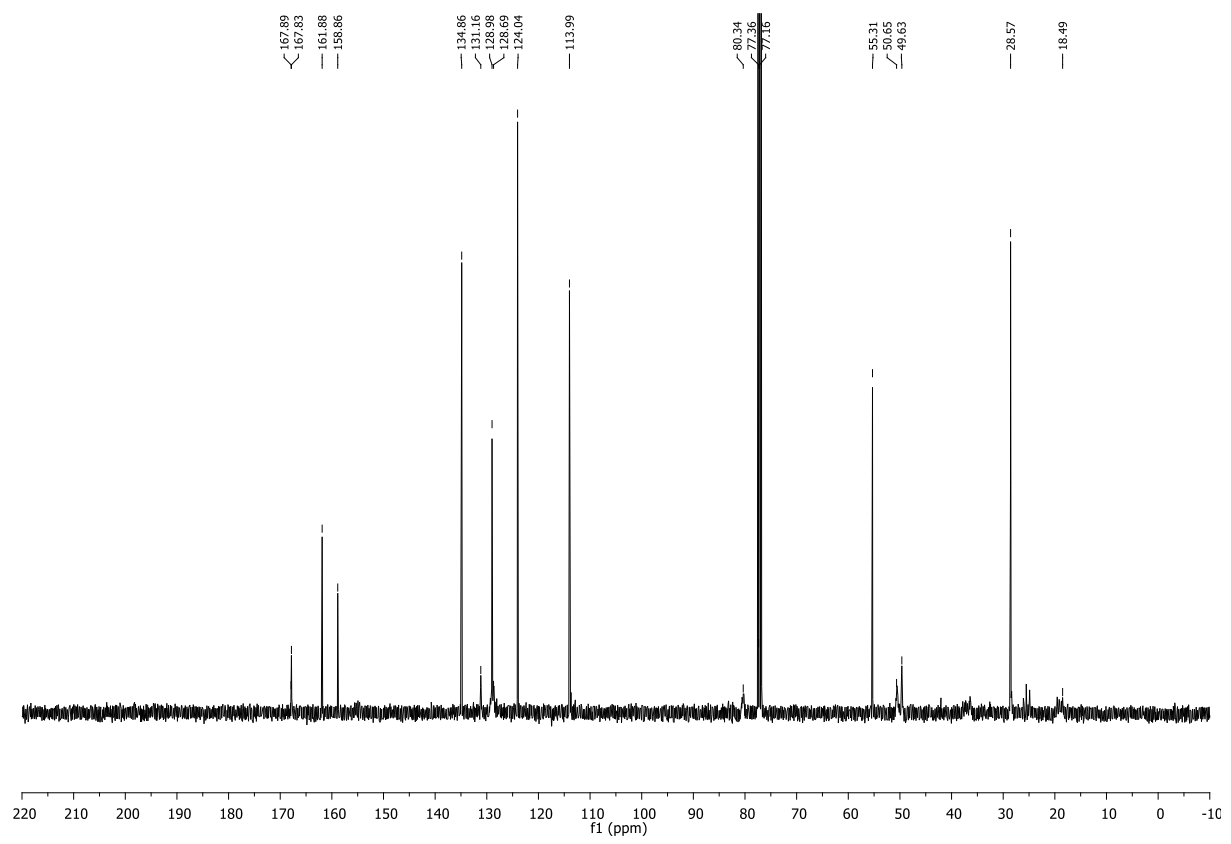
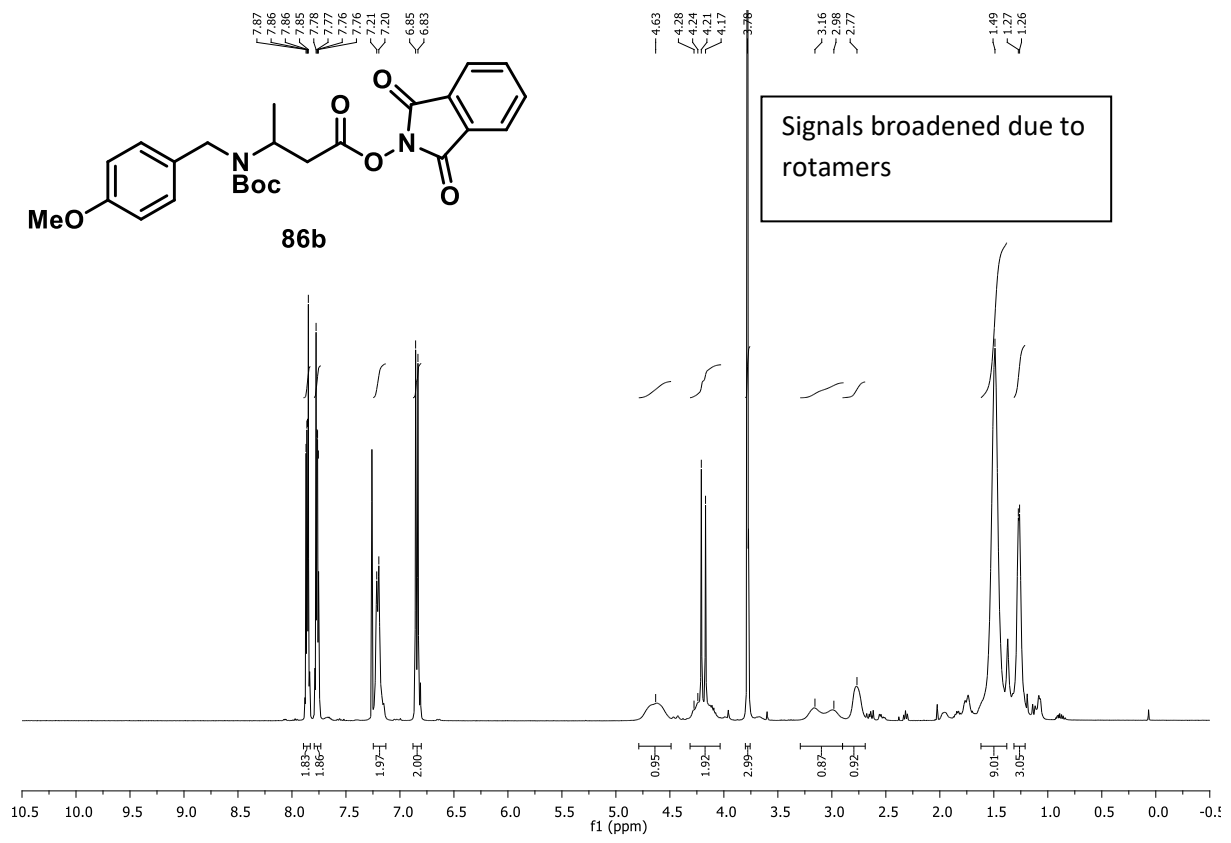
**HRMS** for **113** (ESI-EIC):  $m/z$  calculated for  $\text{C}_{16}\text{H}_{19}\text{N}_2\text{O}_2$   $[\text{M}+\text{H}^+]$ : 271.1447, found 271.1445.

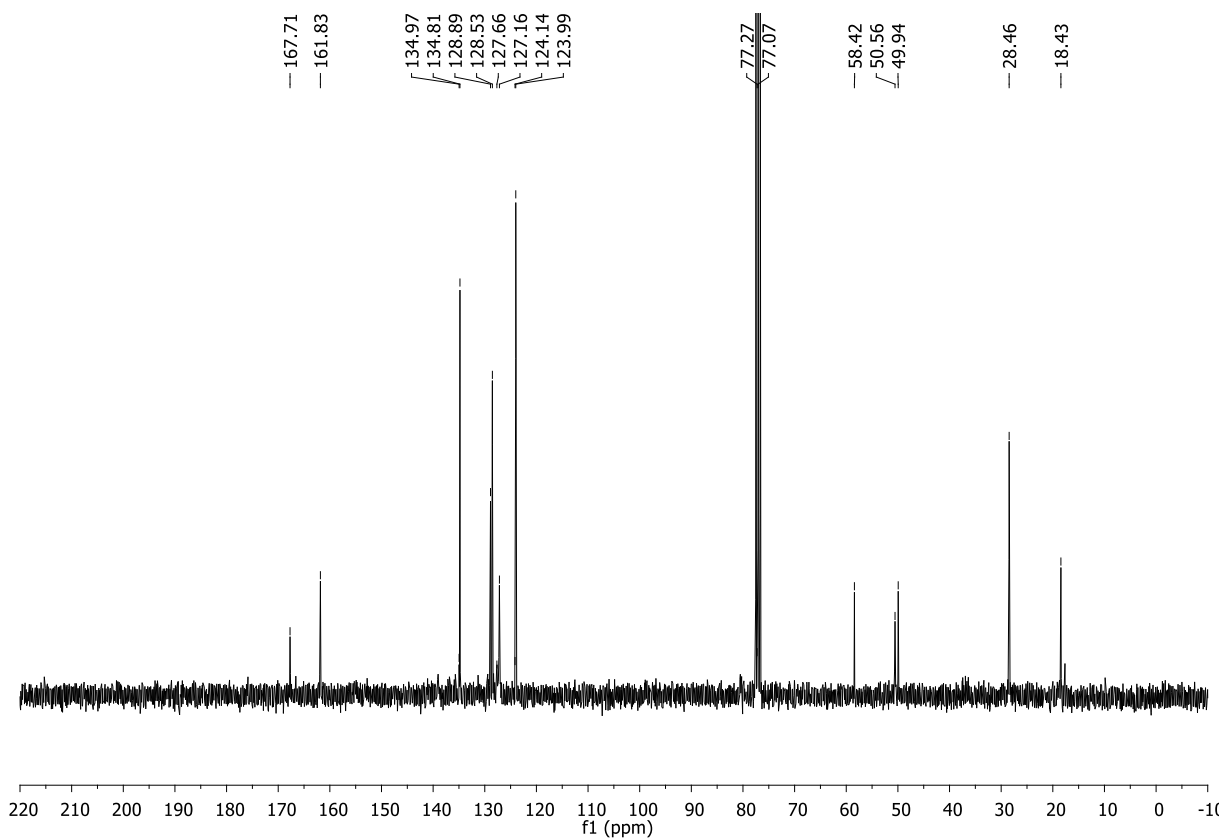
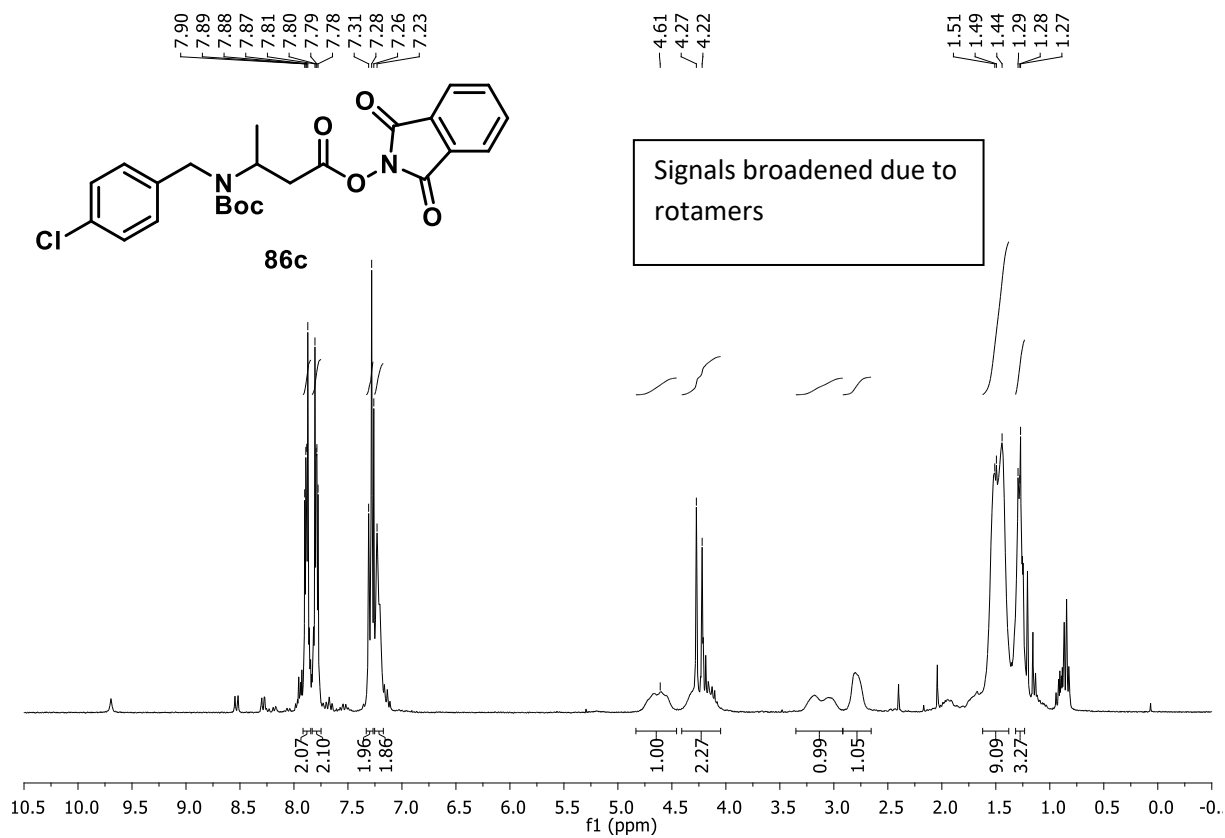
**HRMS** for **114** (ESI-EIC):  $m/z$  calculated for  $\text{C}_{16}\text{H}_{21}\text{N}_2\text{O}_2$   $[\text{M}+\text{H}^+]$ : 273.1598, found 273.1597.

### 3.6.6 Spectra

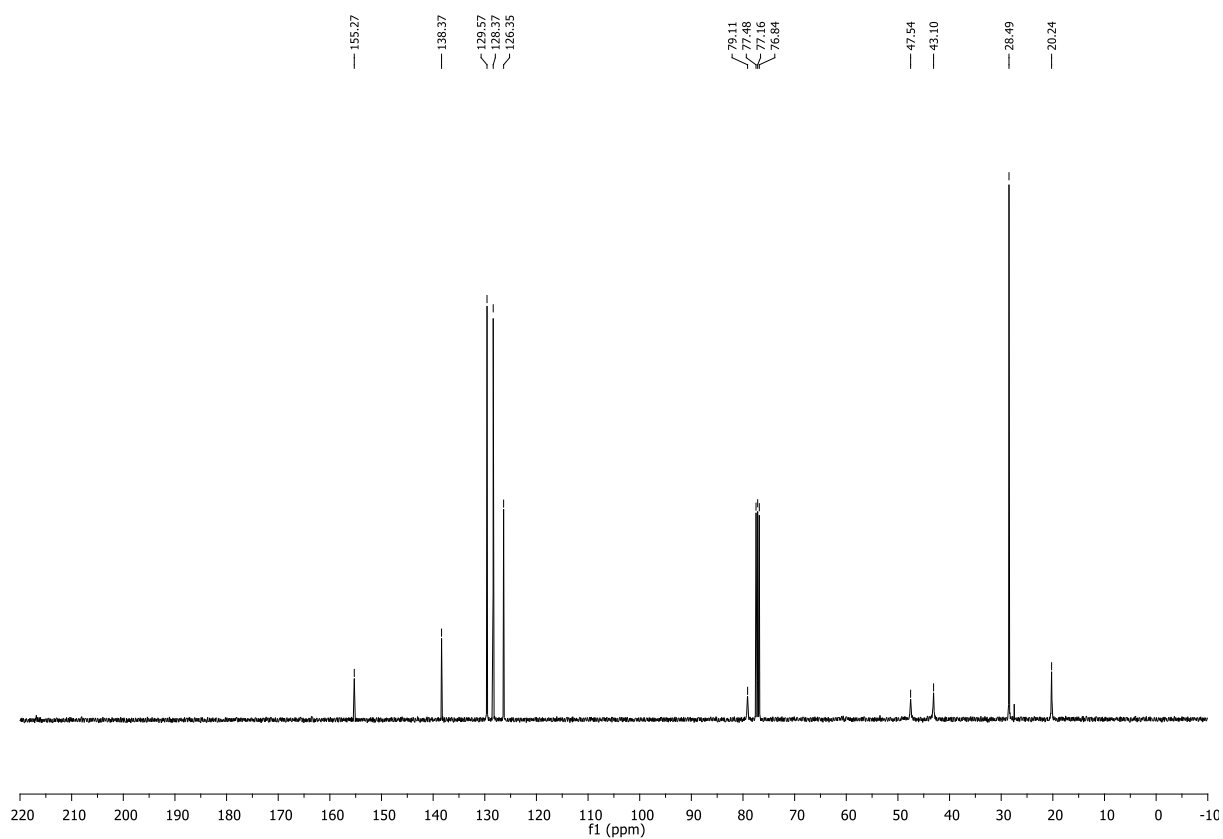
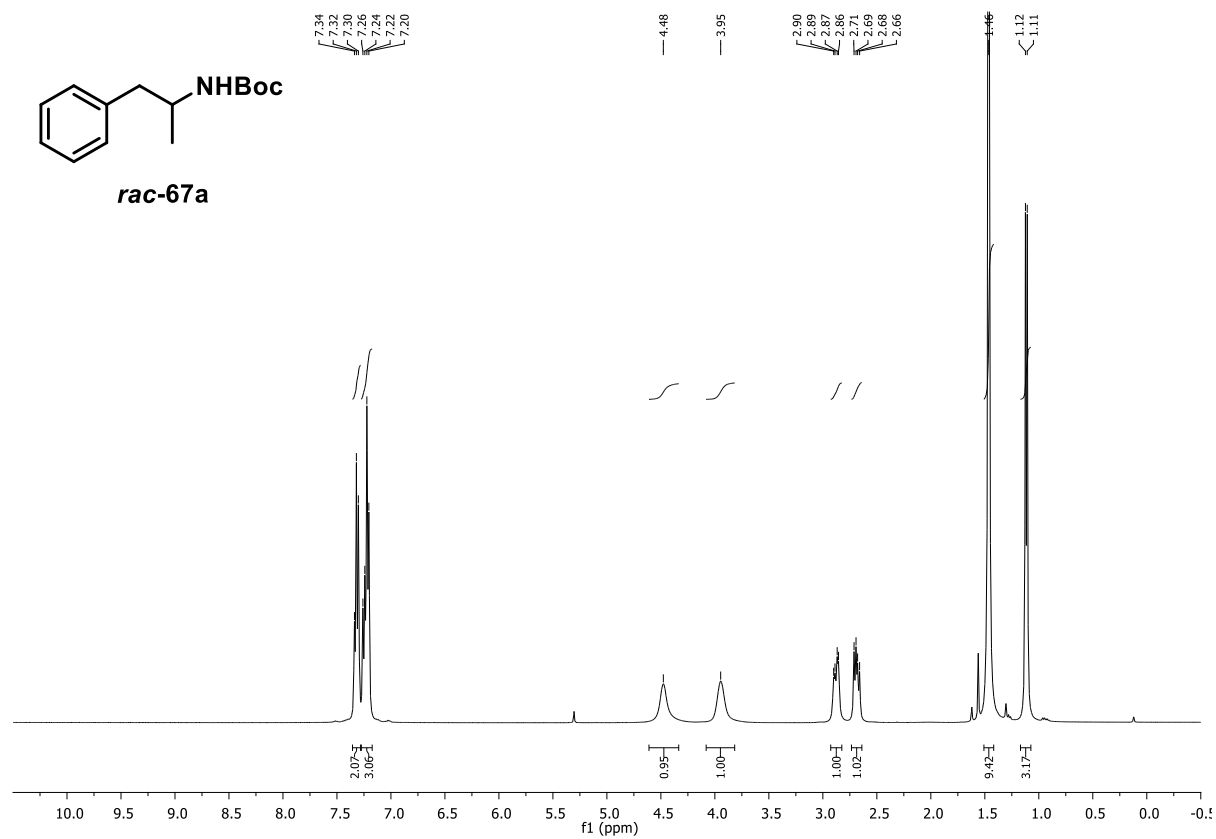
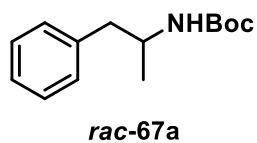
#### *N*-Acyloxyphthalimides for amphetamine synthesis

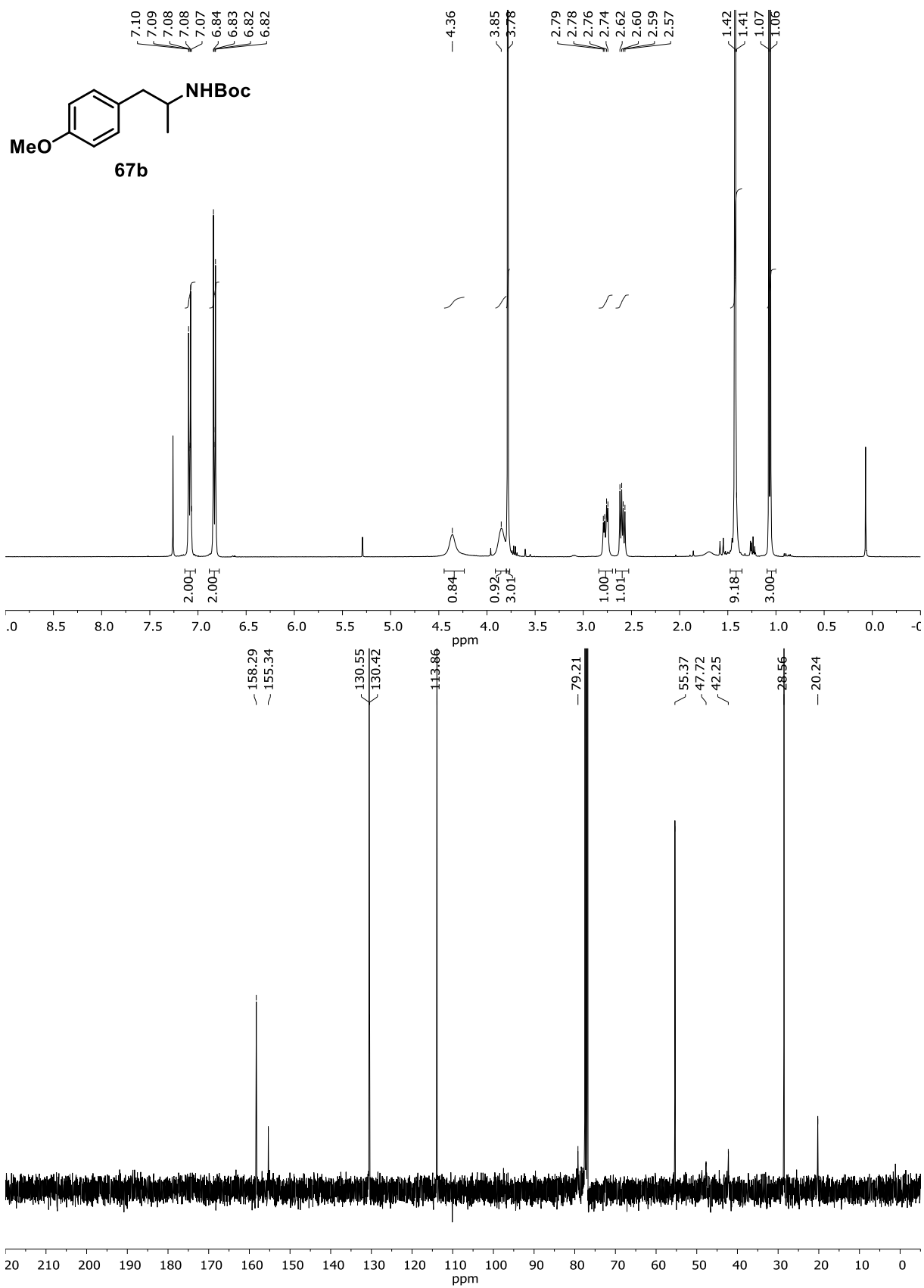


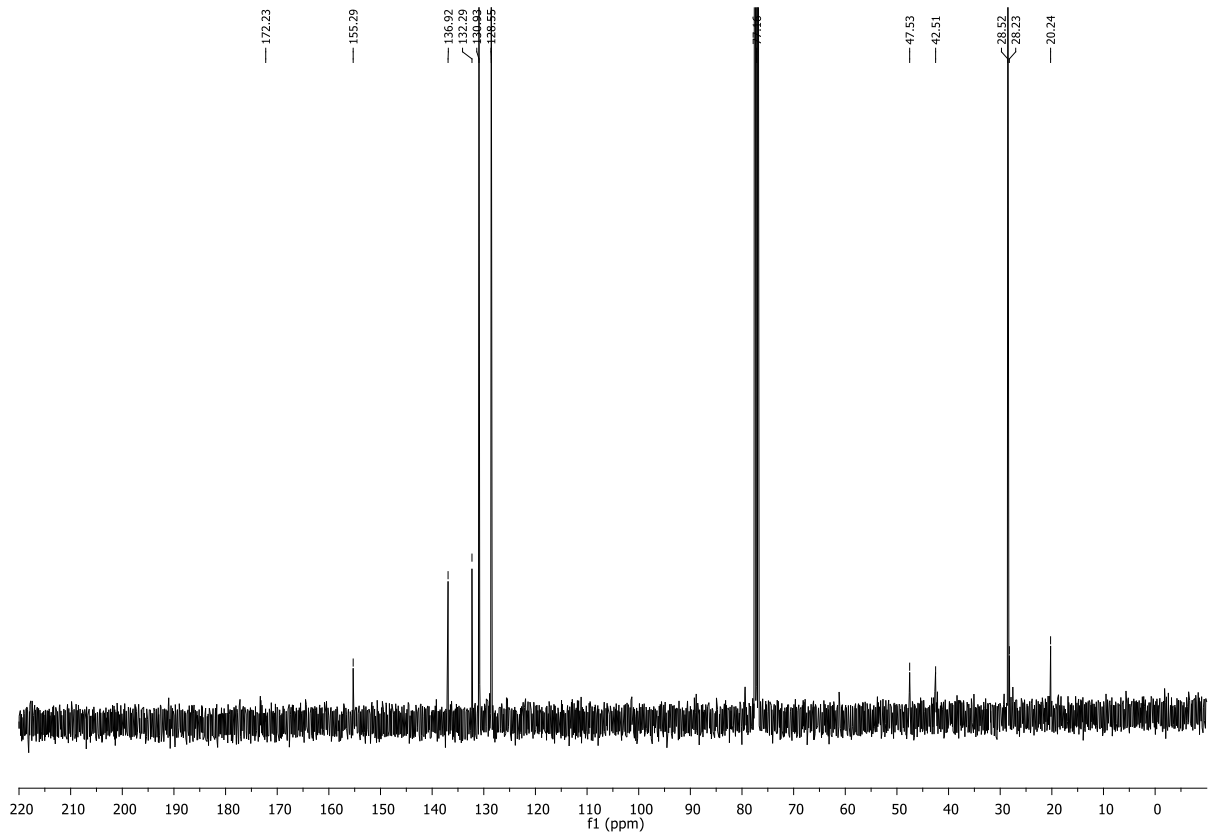
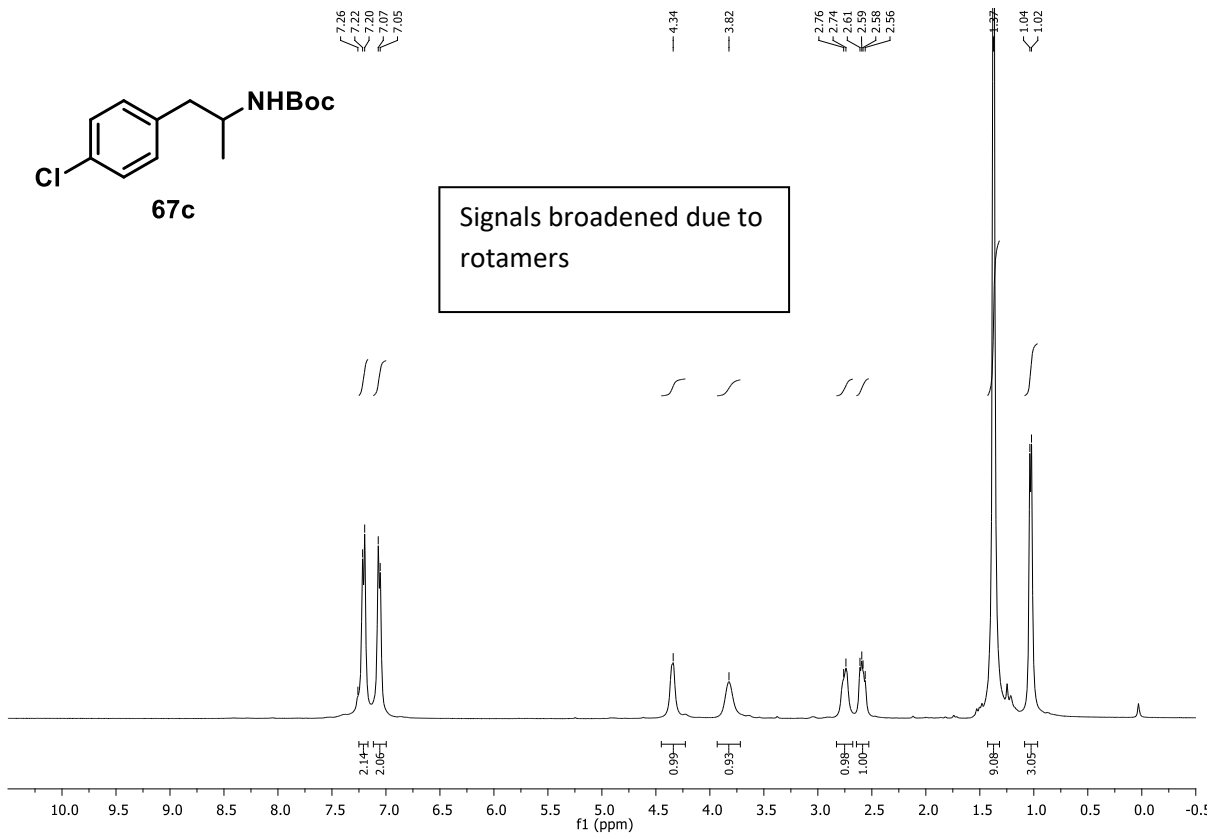




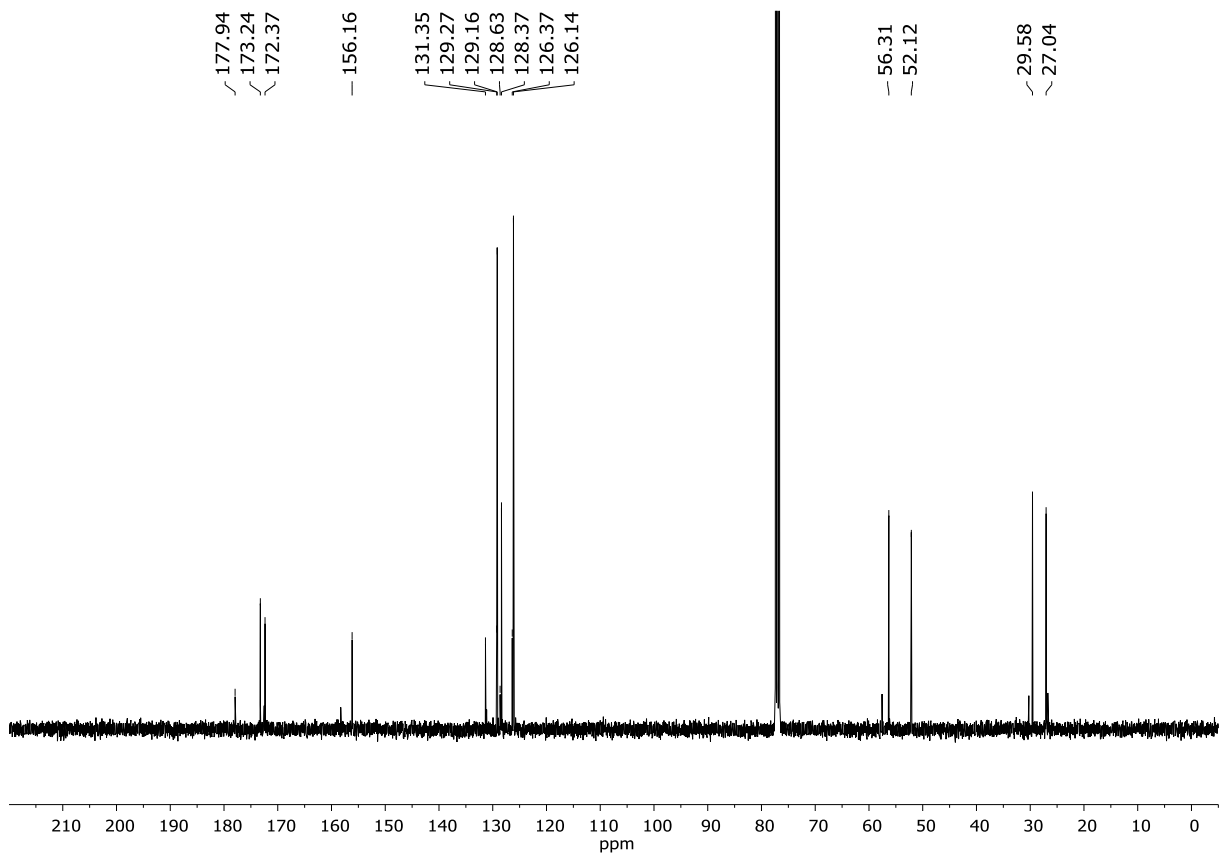
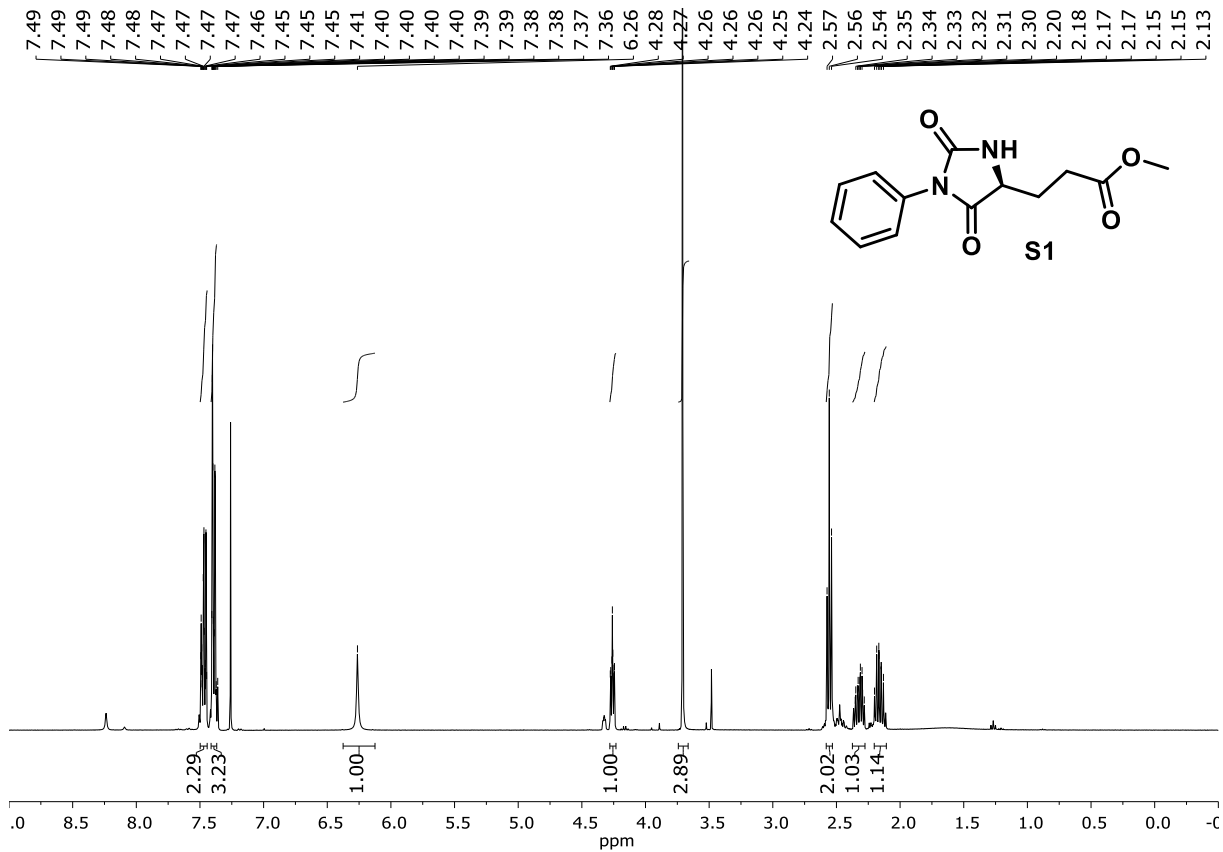
Boc-amphetamines

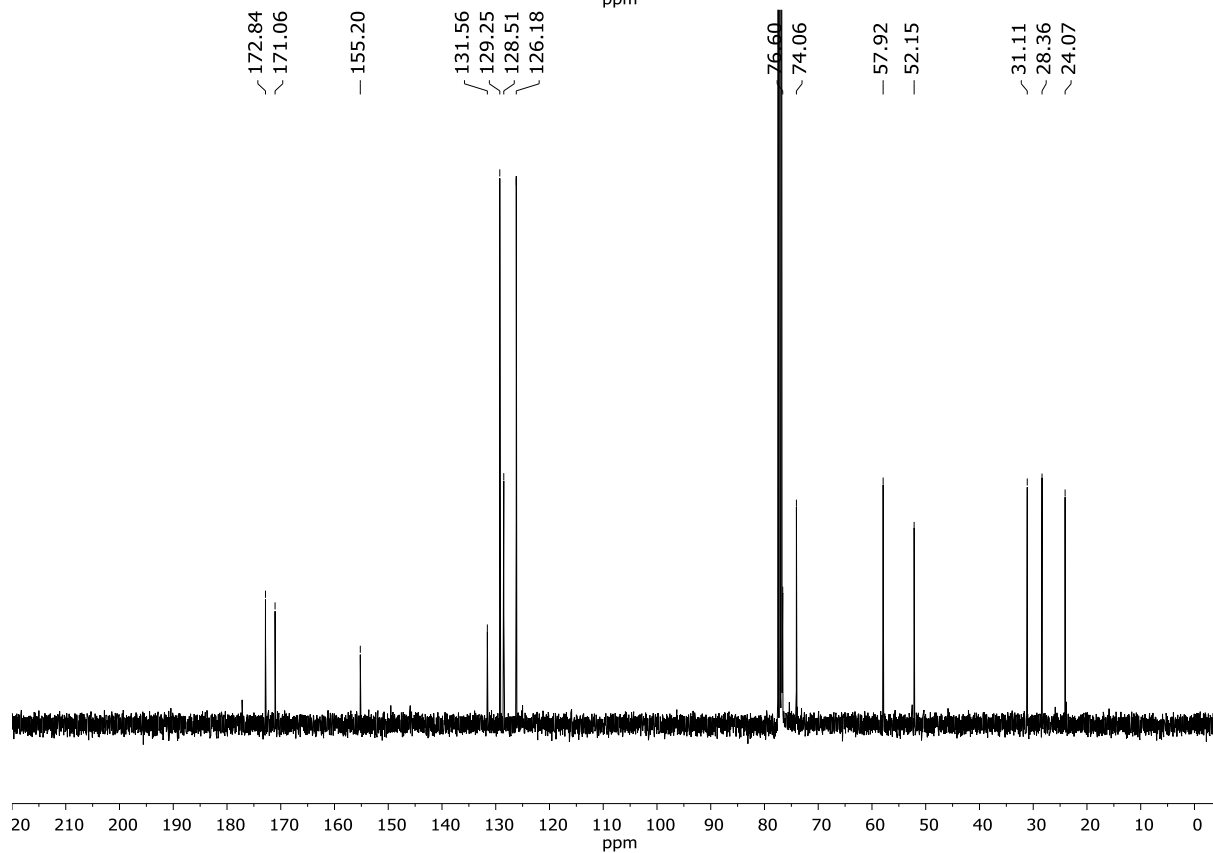
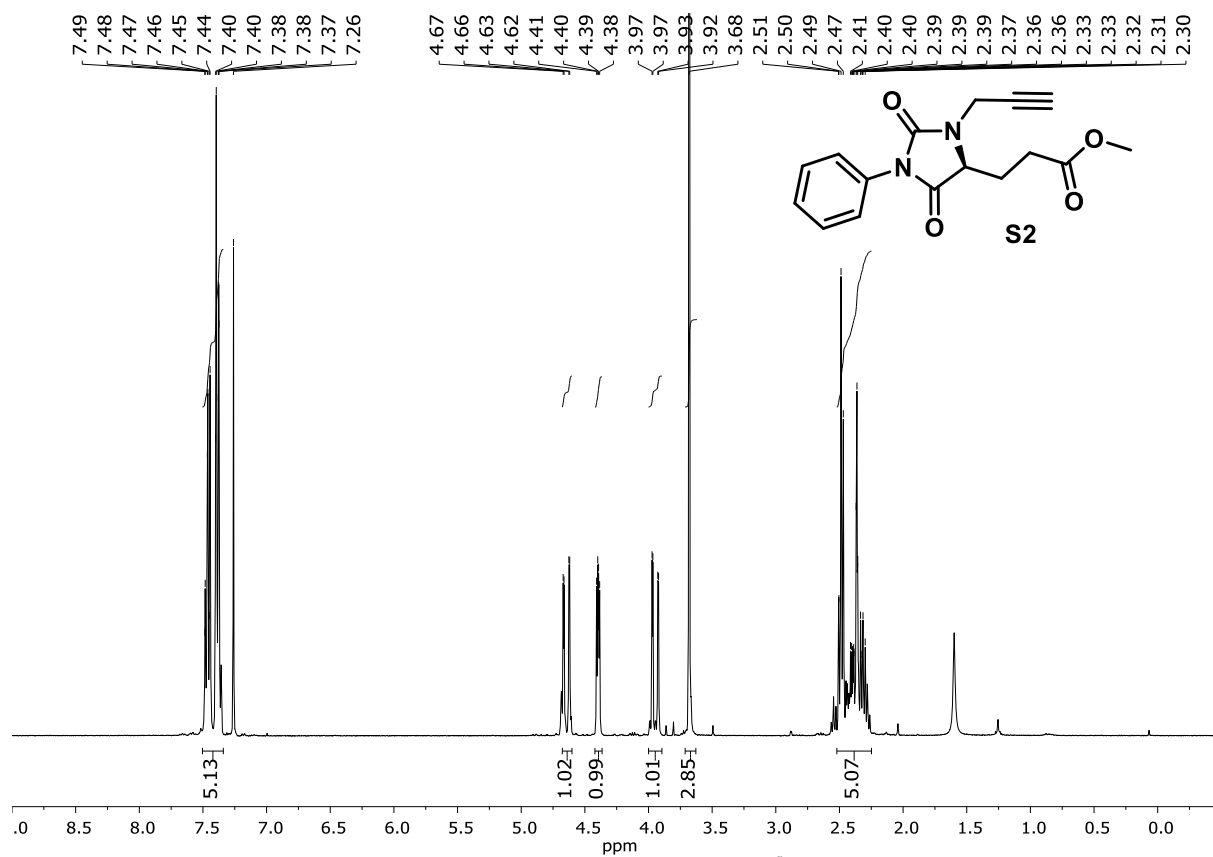


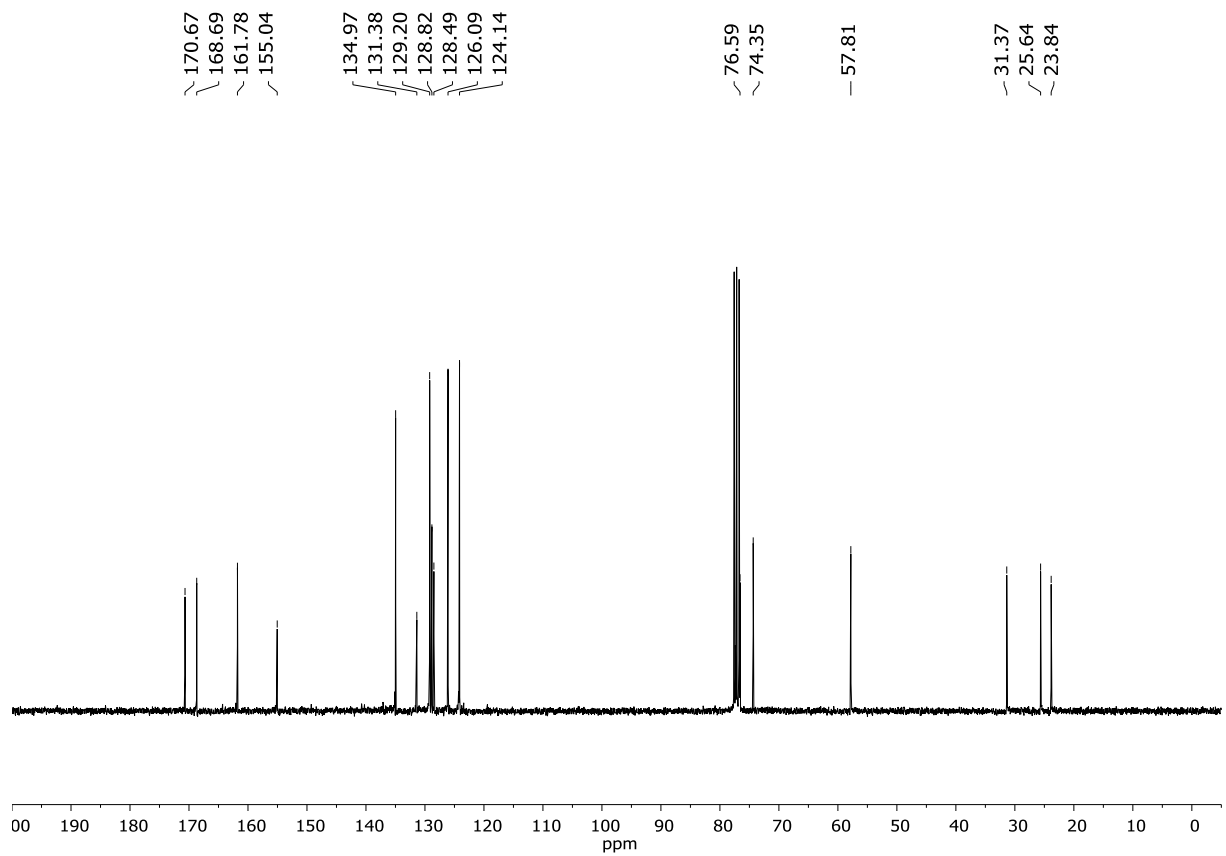
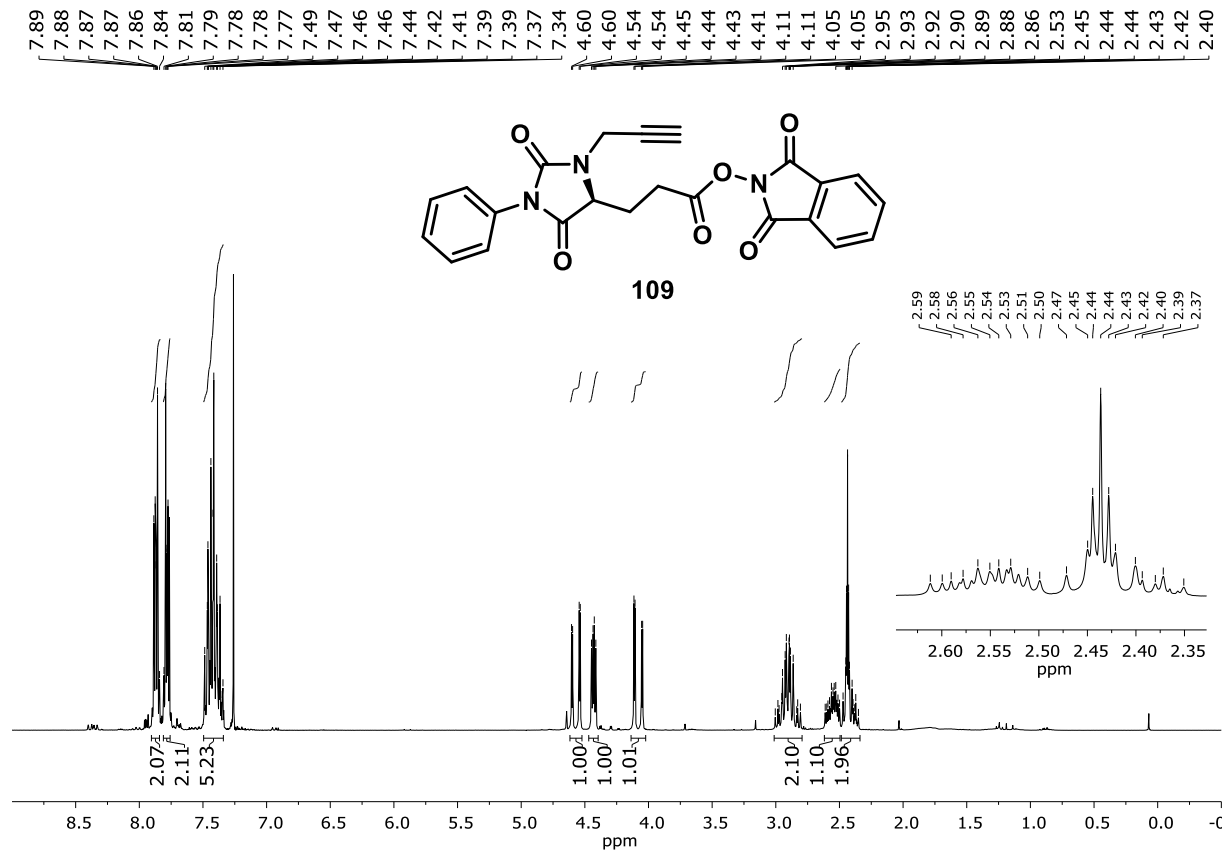


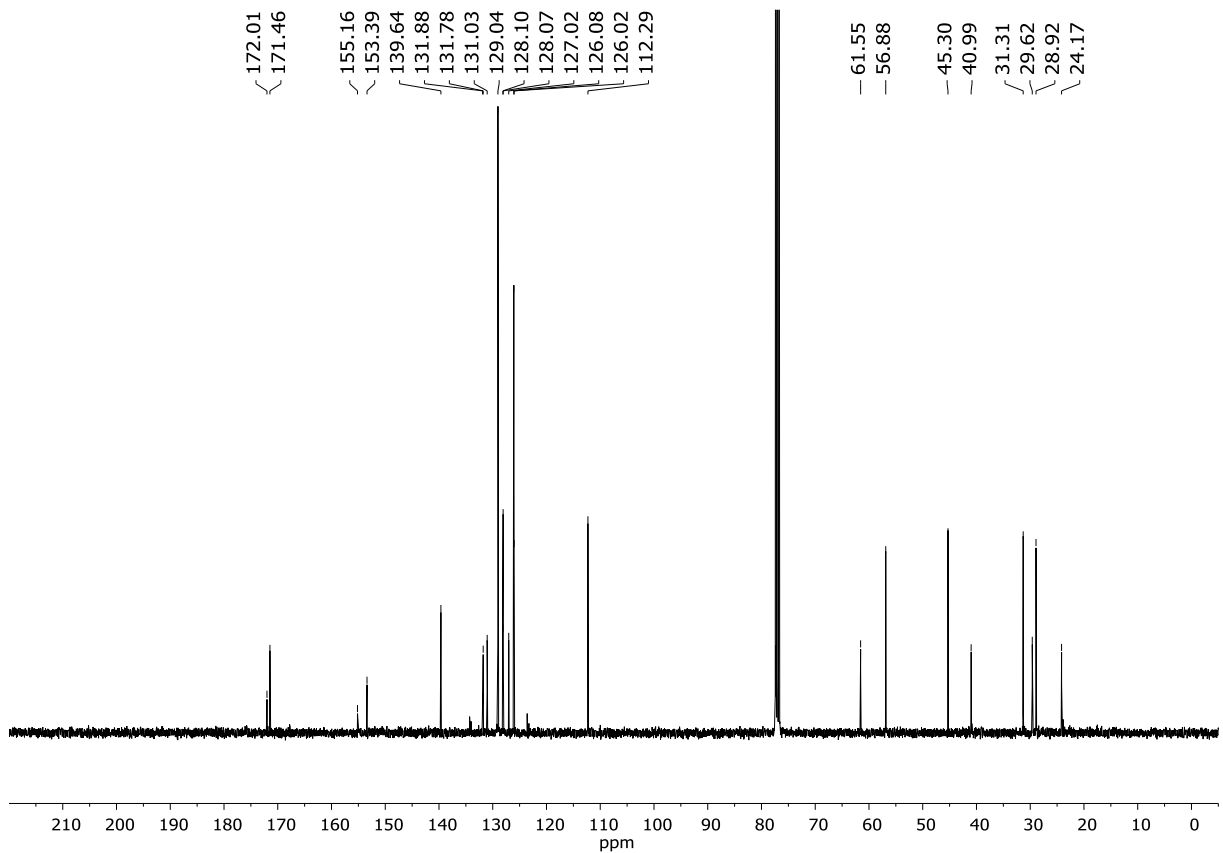
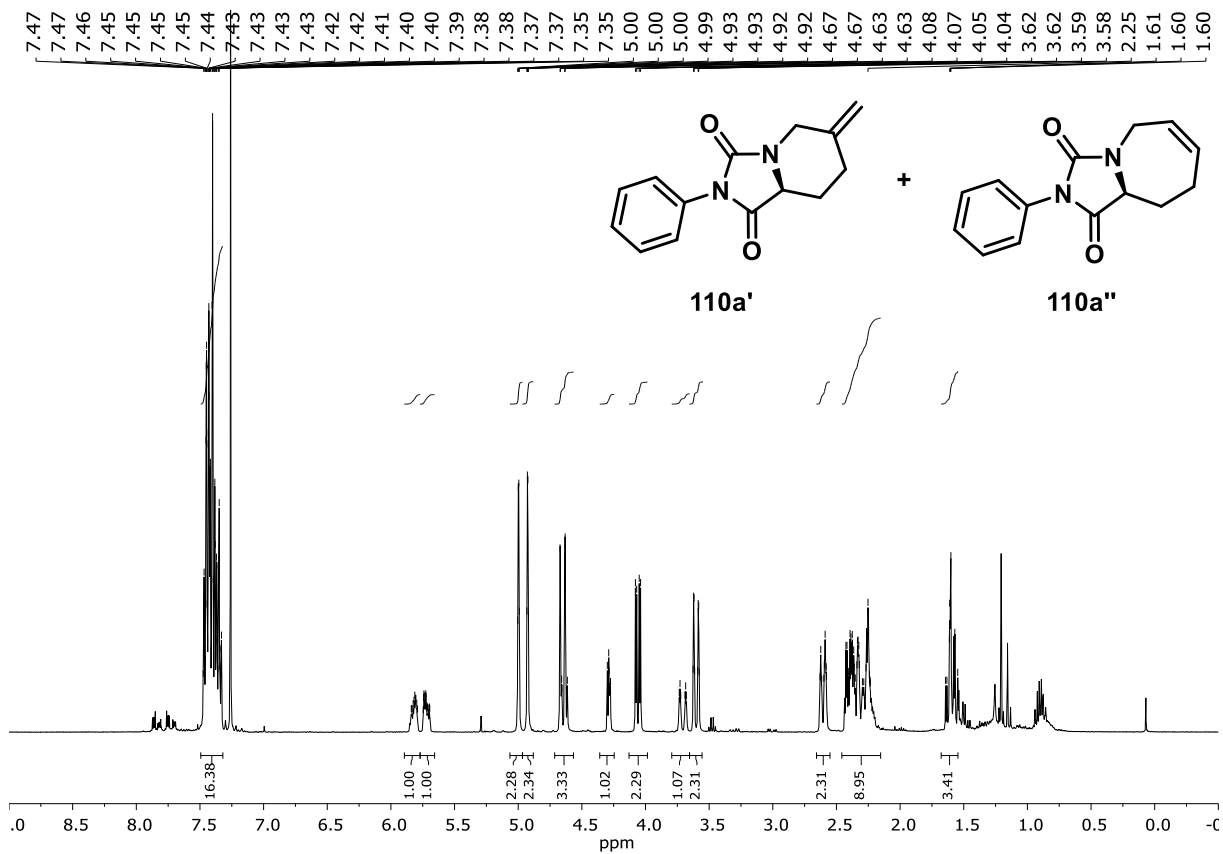


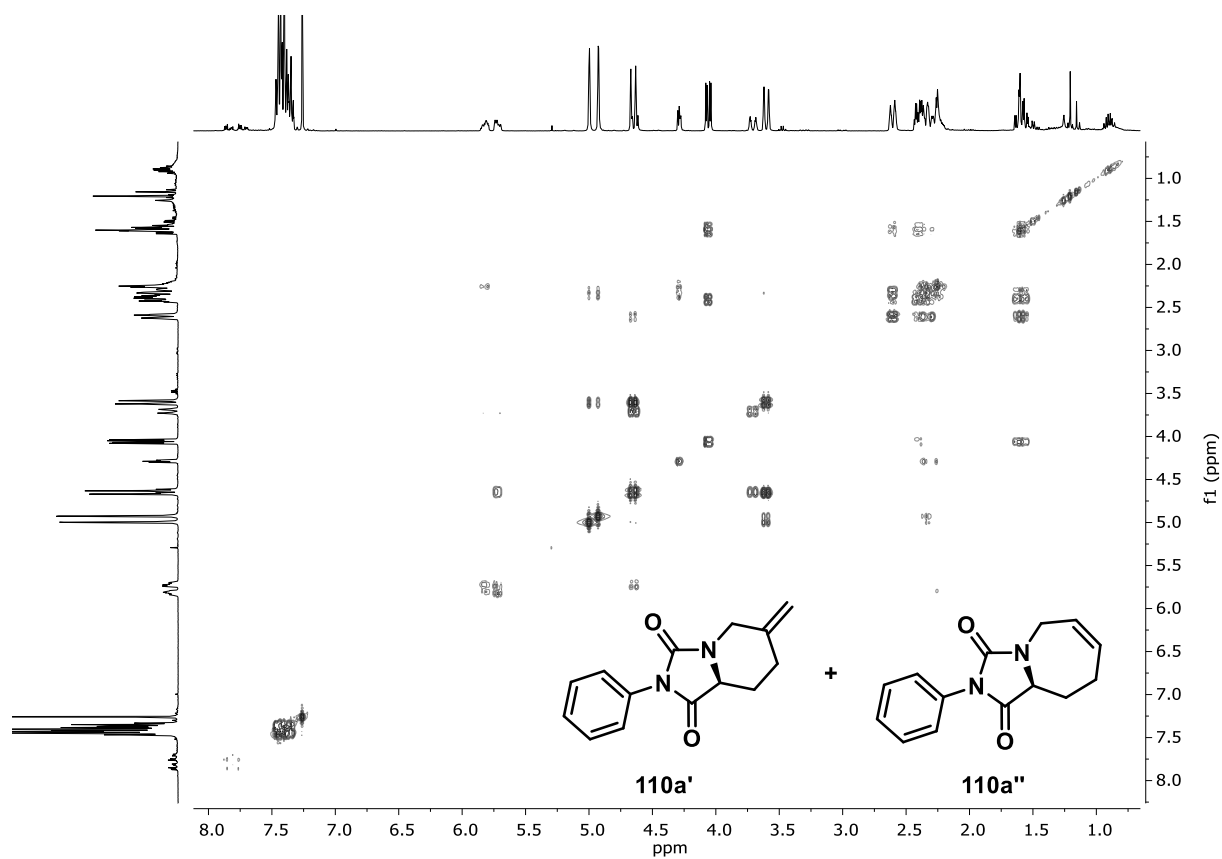


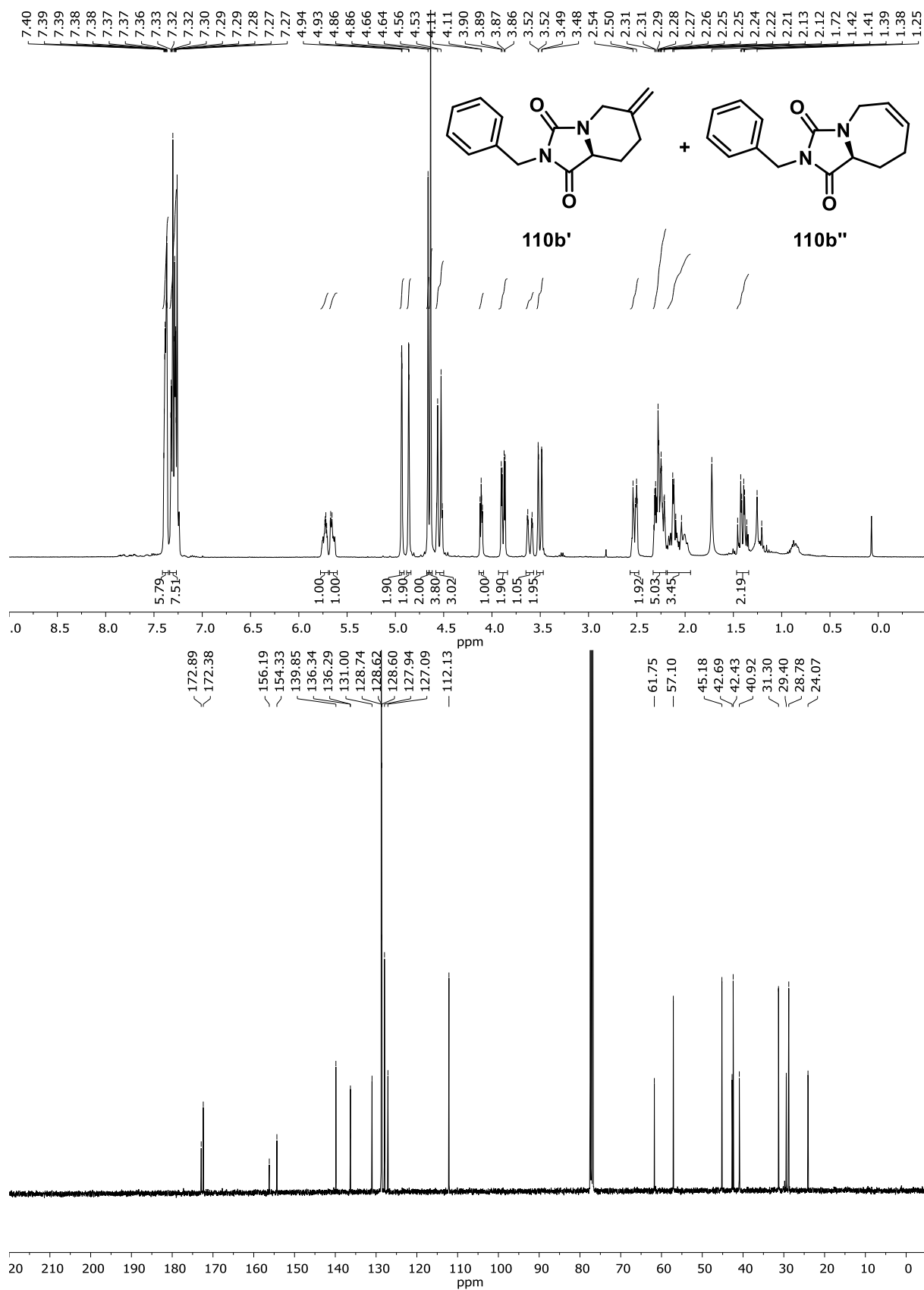


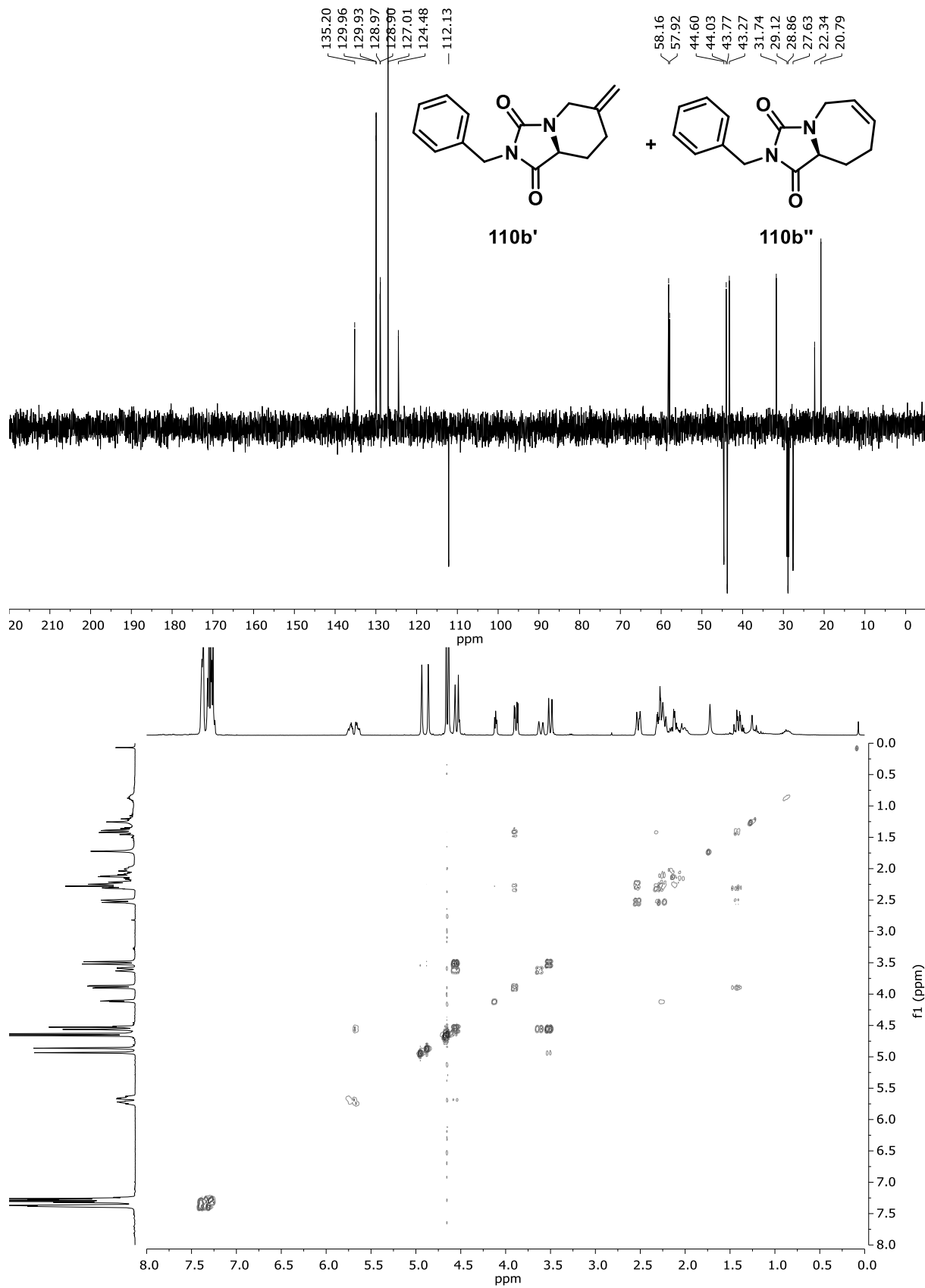


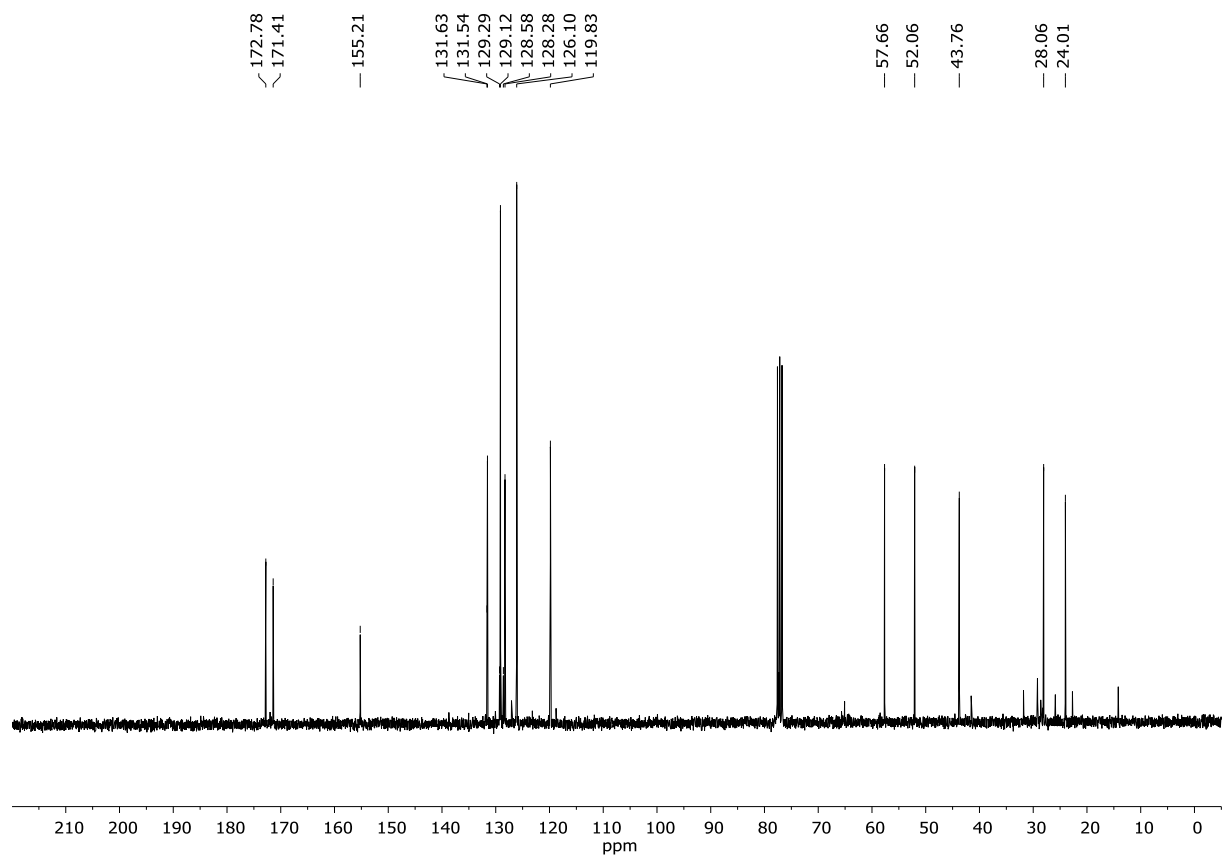
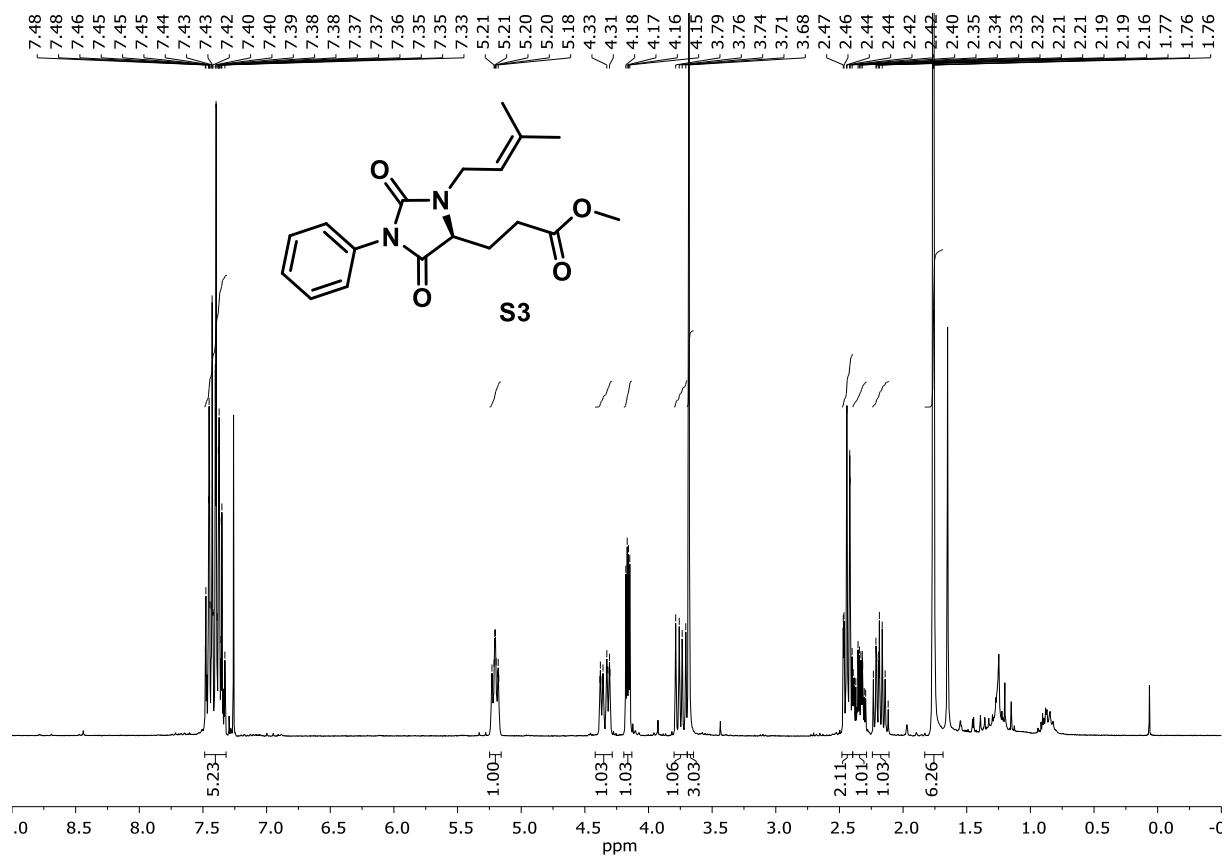




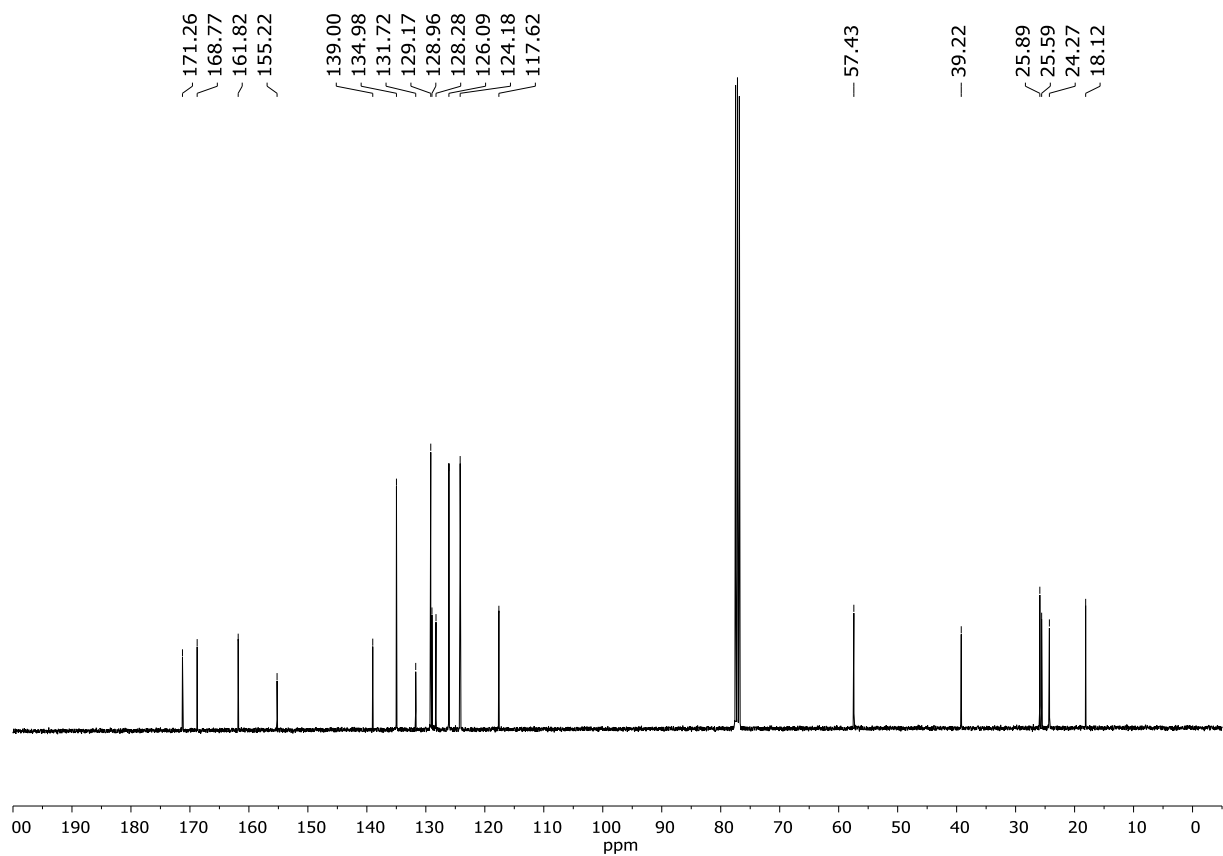
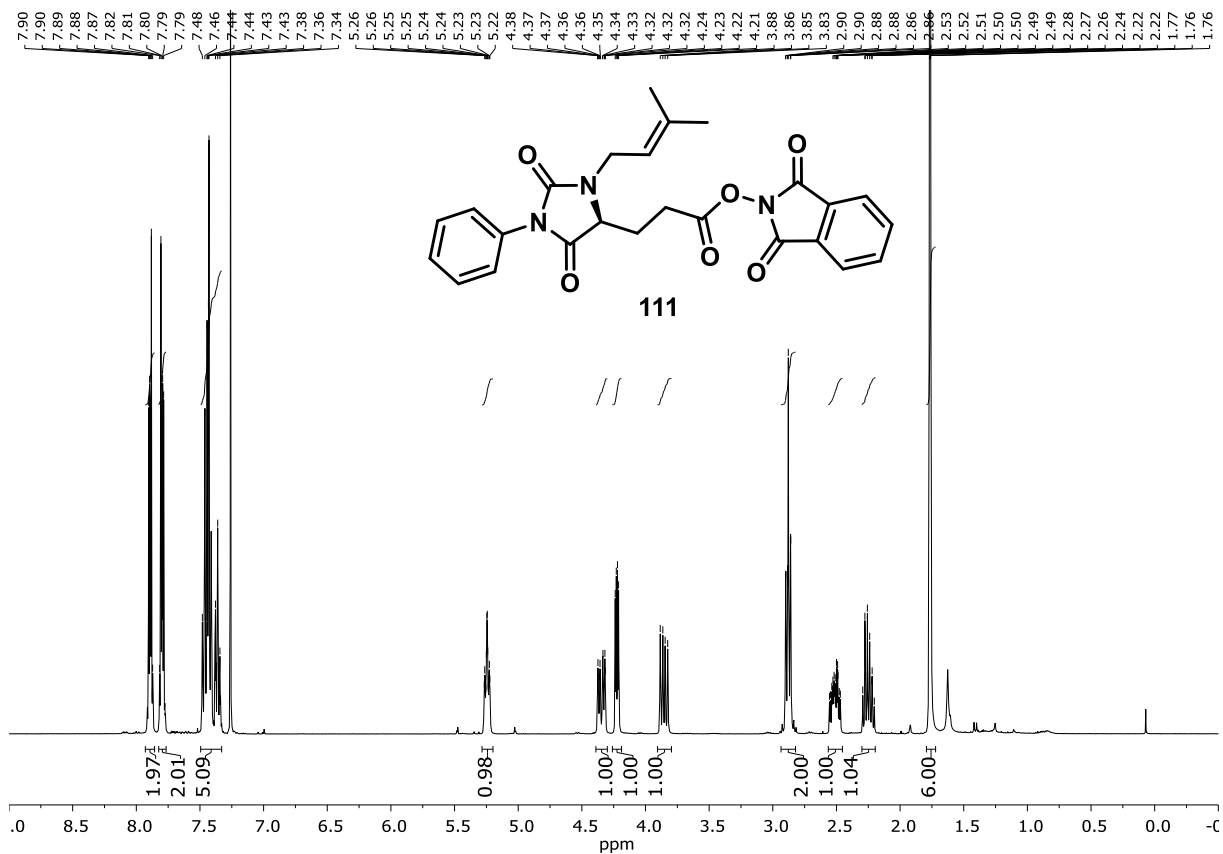


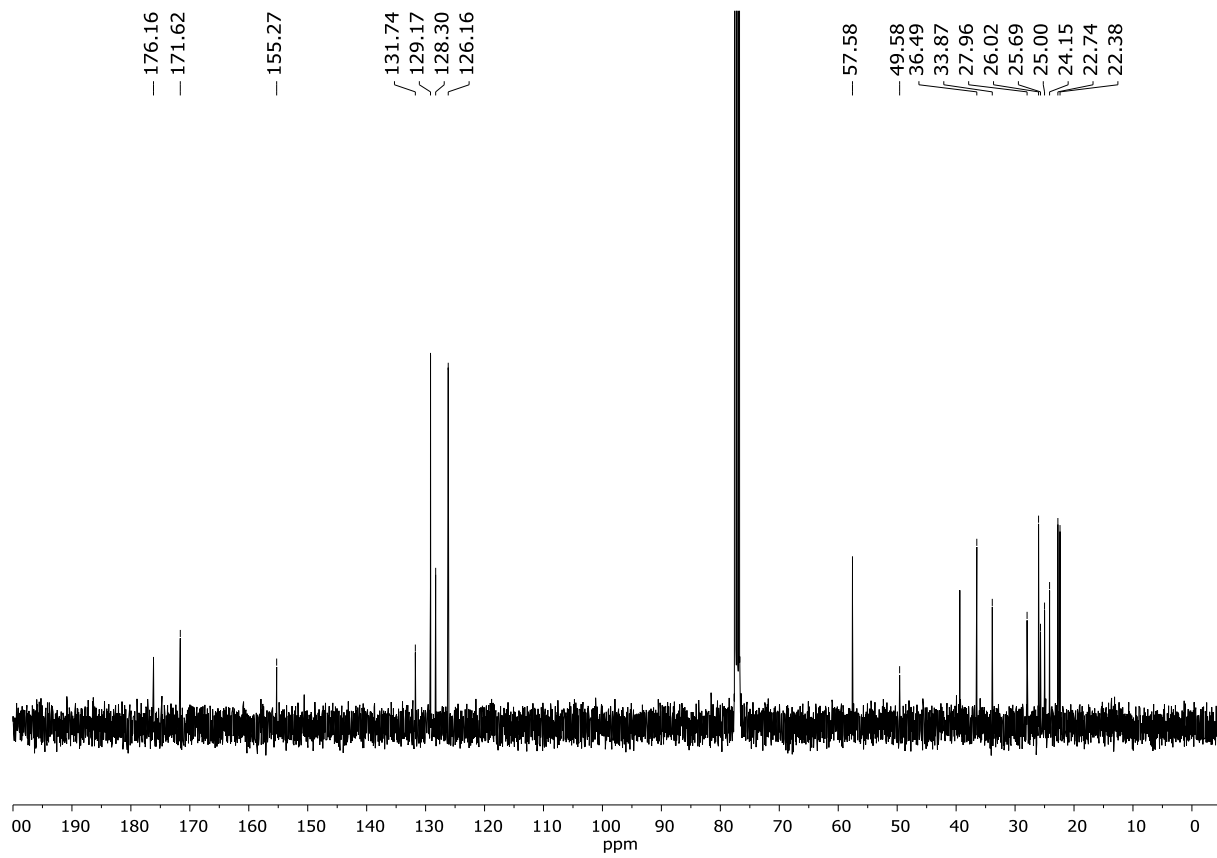
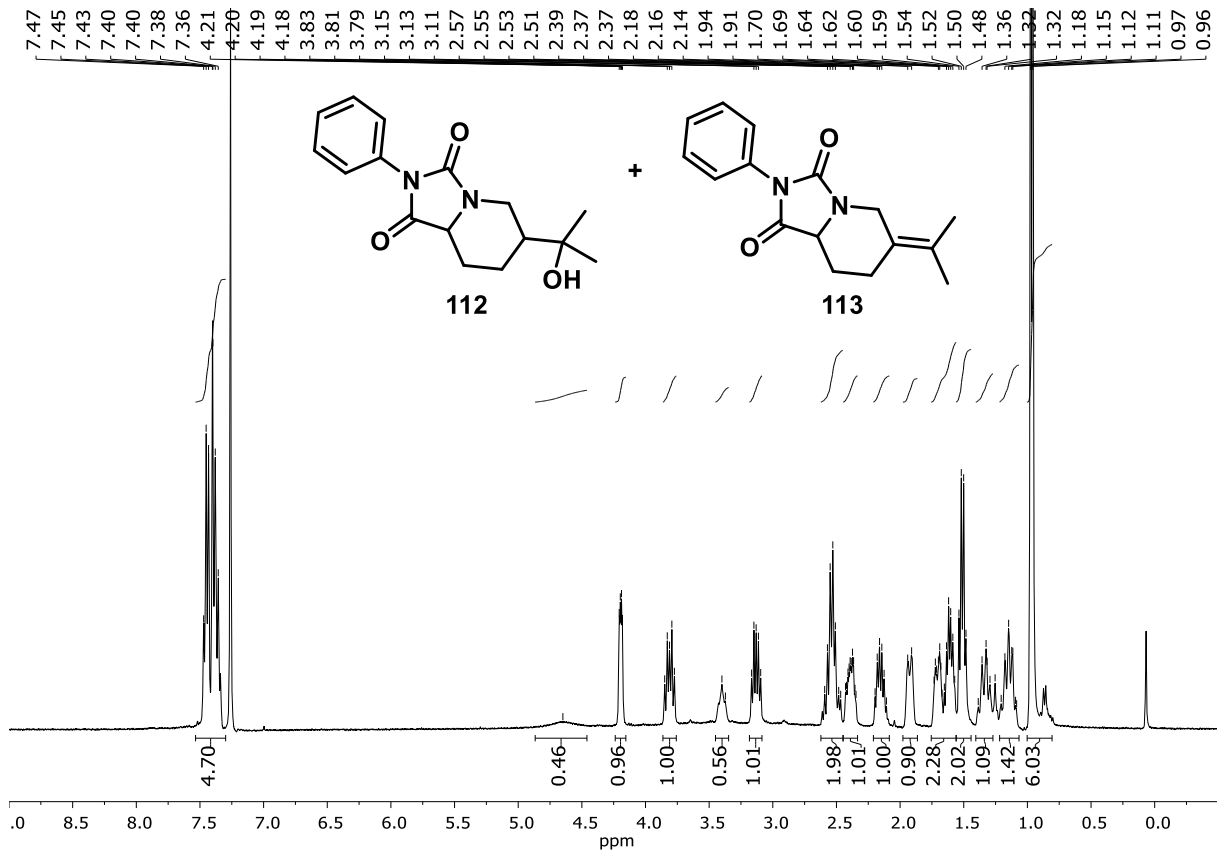


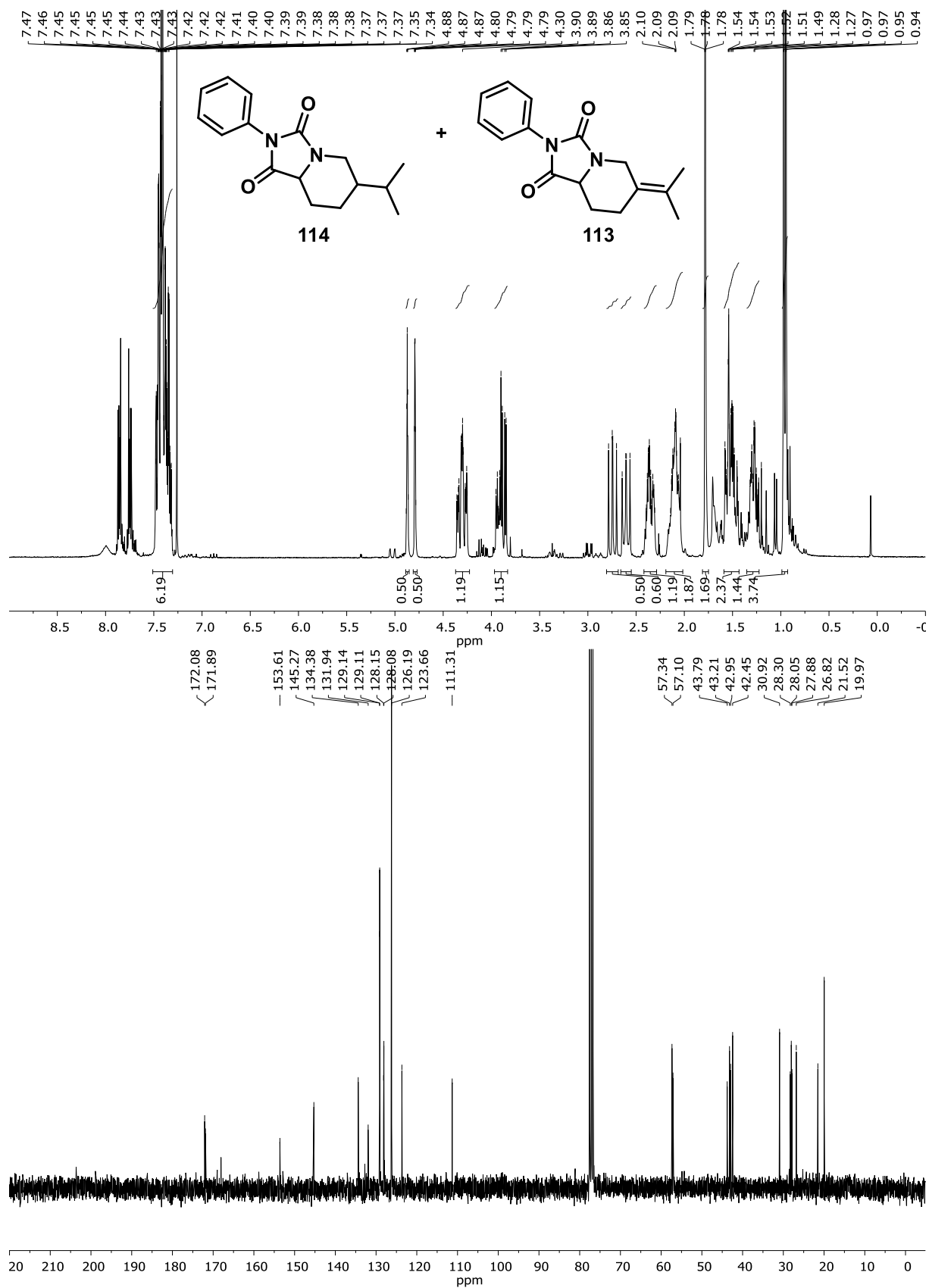


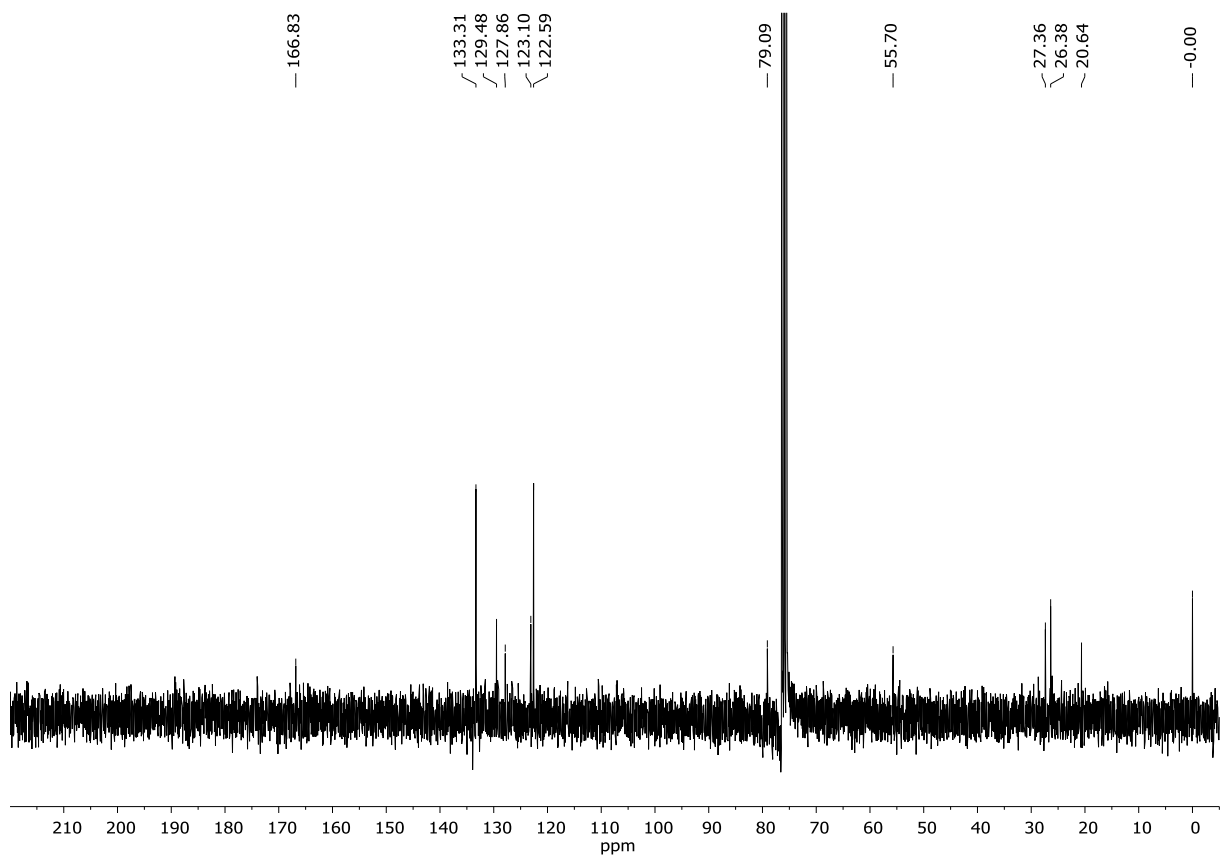
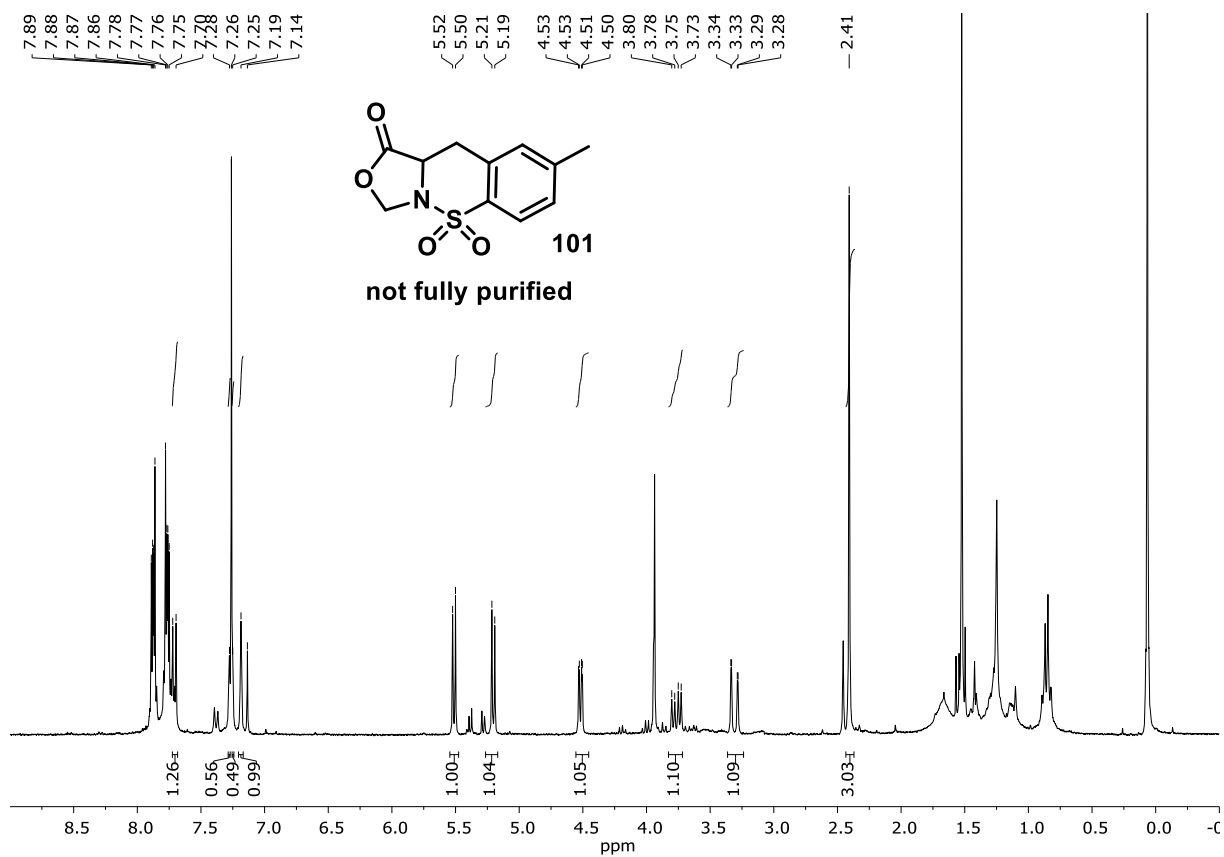












### 3.7 Literature

1. Shaw, M. H.; Twilton, J.; MacMillan, D. W. C., Photoredox Catalysis in Organic Chemistry. *J. Org. Chem.* **2016**, *81*, 6898-6926.
2. T. Koike; Akita, M., Visible-Light-Induced Photoredox Catalysis: An Easy Access to Green Radical Chemistry. *Synlett* **2013**, *24*, 2492-2505.
3. Marzo, L.; Pagire, S. K.; Reiser, O.; König, B., Visible-Light Photocatalysis: Does It Make a Difference in Organic Synthesis? *Angew. Chem. Int. Ed.* **2018**, *57*, 10034-10072.
4. Yoon, T. P.; Ischay, M. A.; Du, J., Visible light photocatalysis as a greener approach to photochemical synthesis. *Nat. Chem.* **2010**, *2*, 527-532.
5. D. M. Schultz; Yoon, T. P., Solar Synthesis: Prospects in Visible Light Photocatalysis. *Science* **2014**, *343*, 985-993.
6. Zeitler, K., Photoredox catalysis with visible light. *Angew. Chem. Int. Ed.* **2009**, *48*, 9785-9789.
7. Romero, N. A.; Nicewicz, D. A., Organic Photoredox Catalysis. *Chem. Rev.* **2016**, *116*, 10075-10166.
8. Ciamician, G., The Photochemistry of the Future. *Science* **1912**, *36*, 385-394.
9. Noyes, W. A.; Kassel, L. S., A Review of Photochemistry. *Chem. Rev.* **1926**, *3*, 199-225.
10. Leermakers, P. A.; Vesley, G. F., Organic Photochemistry and the Excited State. *J. Chem. Edu.* **1964**, *41*, 535-541.
11. Fukuzumi, S.; Ohkubo, K., Organic synthetic transformations using organic dyes as photoredox catalysts. *Org. Biomol. Chem.* **2014**, *12*, 6059-6071.
12. Prier, C. K.; Rankic, D. A.; MacMillan, D. W. C., Visible Light Photoredox Catalysis with Transition Metal Complexes: Applications in Organic Synthesis. *Chem. Rev.* **2013**, *113*, 5322-5363.
13. Xiao, J., Merging Organocatalysis with Transition Metal Catalysis: Highly Stereoselective  $\alpha$ -Alkylation of Aldehydes. *Organic Letters* **2012**, *14*, 1716-1719.
14. Lerch, S.; Unkel, L.-N.; Brasholz, M., Tandem Organocatalysis and Photocatalysis: An Anthraquinone-Catalyzed Indole-C3-Alkylation/Photooxidation/1,2-Shift Sequence. *Angew. Chem. Int. Ed.* **2014**, *53*, 1-6.
15. Prier, C. K.; MacMillan, D. W. C., Dual Photoredox Catalysis: The Merger of Photoredox Catalysis with Other Catalytic Activation Modes. In *Visible Light Photocatalysis in Organic Chemistry*, First ed.; Wiley-VCH Verlag GmbH & Co. KGaA: Weinheim, 2018; pp 299-333.
16. Skubi, K. L.; Blum, T. R.; Yoon, T. P., Dual Catalysis Strategies in Photochemical Synthesis. *Chem. Rev.* **2016**, *116*, 10035-10074.
17. Liu, Y.-Y.; Liu, J.; Lu, L.-Q.; Xiao, W.-J., Organocatalysis Combined with Photocatalysis. *Top. Curr. Chem.* **2019**, *377*, 36-51.
18. Zhou, Q.-Q.; Zou, Y.-Q.; Lu, L.-Q.; Xiao, W.-J., Visible-Light-Induced Organic Photochemical Reactions through Energy-Transfer Pathways. *Angew. Chem. Int. Ed.* **2019**, *58*, 1586-1604.
19. Strieth-Kalthoff, F.; Glorius, F., Triplet Energy Transfer Photocatalysis: Unlocking the Next Level. *Chem* **2020**, *6*, 1888-1903.
20. Roth, H. G.; Romero, N. A.; Nicewicz, D. A., Experimental and Calculated Electrochemical Potentials of Common Organic Molecules for Applications to single-Electron Redox Chemistry. *Synlett* **2016**, *27*, 714-723.
21. Verschueren, R. H.; DeBorggraeve, W. M., Electrochemistry and Photoredox Catalysis: A Comparative Evaluation in Organic Synthesis. *Molecules* **2019**, *24*, 2122-2160.
22. Fox, M. A.; Dulay, M. T., Heterogeneous Photocatalysis. *Chem. Rev.* **1993**, *93*, 341-357.
23. Tucker, J. W.; Stephenson, C. R. J., Shining Light on Photoredox Catalysis: Theory and Synthetic Applications. *J. Org. Chem.* **2012**, *77*, 1617-1622.

24. Juris, A.; Balzani, V., Characterization of the Excited State Properties of Some New Photosensitizers of the Ruthenium (Polypyridine) Family. *Helvetica Chimica Acta* **1981**, *64*, 2175-2182.
25. Kalyanasundaram, K., Photophysics, Photochemistry and Solar Energy Conversion with Tris(bipyridyl)Ruthenium(II) and its Analogues. *Coordination Chemistry Reviews* **1982**, *46*, 159-244.
26. Flamigni, L.; Barbieri, A.; Sabatini, C.; Ventura, B.; Barigelletti, F., Photochemistry and Photophysics of Coordination Compounds: Iridium. *Topics in Current Chemistry* **2007**, *281*, 143-203.
27. Hossein, A.; Bhattacharyya, A.; Reiser, O., Copper's rapid ascent in visible-light photoredox catalysis. *Science* **2019**, *364*, 450-462.
28. Shan, A. Y.; Ghazi, T. I. M.; Rashid, S. A., Immobilisation of titanium dioxide onto supporting materials in heterogeneous photocatalysis: A review. *Applied Catalysis A: General* **2010**, *389*, 1-8.
29. Fujishima, A.; Zhang, X., Titanium dioxide photocatalysis: present situation and future approaches. *C. R. Chimie* **2006**, *9*, 750-760.
30. Fu, M.-C.; Shang, R.; Zhao, B.; Wang, B.; Fu, Y., Photocatalytic decarboxylative alkynations mediated by triphenylphosphine and sodium iodide. *Science* **2019**, *363*, 1429-1434.
31. Pellegrin, Y.; Odobel, F., Sacrificial electron donor reagents for solar fuel production. *C. R. Chim.* **2015**, *20*, 283-295.
32. Williams, J. D.; Kappe, C. O., Recent advances toward sustainable flow photochemistry. *Curr. Opin. Green Sustain. Chem.* **2020**, *25*, 100351.
33. Sambigiato, C.; Noel, T., Flow Photochemistry: Shine Some Light on Those Tubes. *Trends Chem.* **2019**, *2*, 92-106.
34. Knowles, J. P.; Elliott, L. D.; Brooker-Milburn, K. I., Flow photochemistry: Old light through new windows. *Beilstein J. Org. Chem.* **2012**, *8*, 2025-2052.
35. Cambie, D.; Bottecchia, C.; Straathof, N. J. W.; Hessel, V.; Noel, T., Applications of Continuous-Flow Photochemistry in Organic Synthesis, Material Science, and Water Treatment. *Chem. Rev.* **2016**, *116*, 10276-10341.
36. Triemer, S.; Gilmore, K.; Vu, G. T.; Seeberger, P. H.; Seidl-Morgenstern, A., Literally Green Chemical Synthesis of Artemisinin from Plant Extracts. *Angew. Chem. Int. Ed.* **2018**, *57*, 5525-5528.
37. Hone, C. A.; Kappe, C. O., The Use of Molecular Oxygen for Liquid Phase Aerobic Oxidations in Continuous FLOW. *Top. Curr. Chem.* **2019**, *2*, 377-421.
38. Krebs, H. A.; Johnson, W. A., Metabolism of ketonic acids in animal tissues. *Biochem J* **1937**, *31*, 645-660.
39. Kharaka, Y. K.; Carothers, W. W.; Rosenbauer, R. J., Thermal decarboxylation of acetic acid: implications for origin of natural gas. *Geochimica et Cosmochimica Acta* **1983**, *47*, 397-402.
40. Klocke, E.; Matzeit, A.; Gockeln, M.; Schäfer, H. J., Influences on the selectivity of the Kolbe versus the Non-Kolbe Electrolysis in the Anodic Decarboxylation of Carboxylic Acids. *Chem. Ber.* **1993**, *126*, 1623-1630.
41. Wang, P.; Chen, X.; Peng, X.; Guo, J.; Zai, J.; Luo, X., Catalyst-Free Decarboxylation of Carboxylic Acids and Deoxygenation of Alcohols by Electro-induced Radical Formation. *Chem. Eur. J.* **2019**, *26*, 3226-3230.
42. Dzik, W. I.; Lange, P. P.; Gooßen, L. J., Carboxylates as sources of carbon nucleophiles and electrophiles: comparison of decarboxylative and decarbonylative pathways. *Chem. Sci.* **2012**, *3*, 2671-2678.
43. Davidson, R. S.; Harrison, K.; Steiner, P. R., The Photosensitized Decarboxylation of Carboxylic Acids by Aromatic Ketones. *J. Chem. Soc. C.* **1971**, 3480-3482.

44. Schwarz, J.; König, B., Decarboxylative reactions with and without light - a comparison. *Green Chem.* **2018**, *20*, 323-361.
45. Barton, D. H. R.; Crich, D.; Motherwell, W. B., New and improved methods for the radical decarboxylation of acids. *J. Chem. Soc. Chem. Commun.* **1983**, 939-941.
46. Barton, D. H. R.; Bridon, D.; Zard, S. Z., The Invention of Radical Reactions. Part 18. Decarboxylative Radical Addition to Arsenic, Antimony and Phenylsulfides-A Novel Synthesis of Noralcohols from Carboxylic Acids. *Tetrahedron* **1989**, *45*, 2615-2626.
47. Zard, S. Z., Xanthates and Related Derivatives as Radical Precursors. *Encyclopedia of Radicals in Chemistry, Biology and Materials* **2012**, 1-32.
48. Rodriguez-Tzompanzi, V.; Quintero, L.; Tepox-Luna, D. M.; Cruz-Gregorio, S.; Sartillo-Piscul, F., Blue light photoredox decarboxylation and tin-free Barton-McCombie reactions in the stereoselective synthesis of (+)-muscarine. *Tet. Let.* **2019**, *60*, 423-426.
49. Okada, K.; Okamoto, K.; Oda, M., A New and Practical Method of Decarboxylation: Photosensitized Decarboxylation of *N*-Acylxyphthalimides via Electron-Transfer Mechanism. *J. Am. Chem. Soc.* **1988**, *110*, 8736-8738.
50. Schnermann, M. J.; Overma, L. E., A Concise Synthesis of (-)-Aplyvioline Facilitated by a Strategic Tertiary Radical Conjugate Addition *Angew. Chem. Int. Ed.* **2012**, *51*, 9576-9580.
51. Chu, L.; Ohta, C.; Zuo, Z.; MacMillan, D. W. C., Carboxylic acids as a Traceless Activation Group for Conjugate Additions: A Three-Step Synthesis of Pregabalin. *J. Am. Chem. Soc.* **2014**, *136*, 10886-10889.
52. Le, C.; MacMillan, D. W. C., Fragment Couplings via CO<sub>2</sub>-Extrusion-Recombination: Expansion of a classic Bond-Forming Strategy via Metallophotoredox. *J. Am. Chem. Soc.* **2015**, *137*, 11938-11941.
53. Ventra, S.; Petronijevic, F. R.; MacMillan, D. W. C., Decarboxylative Fluorination of Aliphatic Carboxylic Acids via Photoredox Catalysis. *J. Am. Chem. Soc.* **2015**, *137*, 5654-5657.
54. Jia, J.; Lefebvre, Q.; Rueping, M., Reductive coupling of imines with redox-active esters by visible light photoredox organocatalysis. *Org. Chem. Front.* **2020**, *7*, 602-608.
55. Kachkovskiy, G.; Faderl, C.; Reiser, O., Visible Light-Mediated Synthesis of (Spiro)annelated Furans. *Adv. Synth. Catal.* **2013**, *355*, 2240-2248.
56. Warren, L. A.; Smiles, S., The rearrangement of 2-naphthol-1-sulphone. *J. Chem. Soc.* **1931**, 2207-2211.
57. Gilmore, K.; Mohamed, R. K.; Alabugin, I. V., The Baldwin rules: revised and extended. *WIREs Comput. Mol. Sci.* **2016**, *6*, 487-514.
58. Kong, W.; Fuentes, N.; Garcia-Dominguez, A.; Merino, E.; Nevado, C., Stereoselective synthesis of highly functionalized indanes and dibenzocycloheptadienes through complex radical cascade reactions. *Angew. Chem. Int. Ed.* **2015**, *54*, 2487-2491.
59. Mutai, K.; Kobayashi, K., Photoinduced Intramolecular Aromatic Substitution (the Photo-Smiles Rearrangement) in Amino Ethers. *Bull. Chem. Soc. Jpn.* **1980**, *54*, 462-265.
60. Lawson, C. A.; Dominey, A. P.; Williams, G. D.; Murphy, J. A., Visible Light-Mediated Smiles Rearrangements and Annulations of Non-Activated Aromatics. *Chem. Commun.* **2020**, *Advance Article*.
61. Henderson, A. R. P.; Kosowan, J. R.; Wood, T. E., The Truce-Smiles rearrangement and related reactions: a review. *Can. J. Chem.* **2017**, *95*, 483-504.
62. Whalley, D.; Dong, H.; Greaney, M., Alkene Carboarylation through Catalyst-Free, Visible Light-Mediated Smiles Rearrangement. *Chem. Eur. J.* **2018**, *25*, 1927-1930.
63. Fuentes, N.; Kong, W.; Fernandez-Sanchez, L.; Merino, E.; Nevado, C., Cyclization Cascades via *N*-Amidyl Radicals toward Highly Funtionalized Heterocyclic Scaffolds. *J. Am. Chem. Soc.* **2015**, *137*, 964-973.
64. Douglas, J. J.; Albright, H.; Sevrin, M. J.; Cole, K. P.; Stephenson, C. R. J., A Visible-Light-Mediated Radical Smiles Rearrangement and its Application to the Synthesis of a Difluoro-Substituted Spirocyclic ORL-1 Antagonist. *Angew. Chem. Int. Ed.* **2015**, *54*, 14898-14902.

65. Faderl, C. Photoinduced Decarboxylation of *N*-Acylphthalimides. Universität Regensburg, Regensburg, 2017.
66. Tyrkkö, E.; Andersson, M.; Kronstrand, R., The Toxicology of New Psychoactive Substances: Synthetic Cathinones and Phenylethylamines. *Therapeutic Drug Monitoring* **2016**, *38*, 190-216.
67. Kohls, P.; Jadhav, D.; Pandey, G.; Reiser, O., Visible Light Redox Catalysis: Generation and Addition of *N*-Aryltetrahydroisoquinoline-Derived  $\alpha$ -Amino Radicals to Michael Acceptors. *Org. Let.* **2012**, *14*, 672-675.
68. Kraus, G. A.; Wu, Y., 1,5- and 1,9-Hydrogen Atom Abstractions. Photochemical Strategies for radical Cyclizations. *J. Am. Chem. Soc.* **1992**, *114*, 8705-8707.
69. Millan-Ortiz, A.; Lopez-Valdez, G.; Cortez-Guzman, F.; Miranda, L. D., A novel carbamoyl radical based dearomatizing spiroacylation process. *Chem. Commun.* **2015**, *51*, 8345-8348.
70. Palframan, M. J.; Tchabanenko, K.; Robertson, J., Aryl pyrrolidinones via radical 1,4-aryl migration and 5-endo-trig cyclisation of *N*-(2-bromoallyl)arylcarboxamides. *Tet. Let.* **2006**, *47*, 8423-8425.
71. Tlahuexet-Aca, A.; Garza-Sanchez, R. A.; Glorius, F., Multicomponent Oxyalkylation of Styrenes Enabled by Hydrogen-Bond-Assisted Photoinduced Electron Transfer. *Angew. Chem. Int. Ed.* **2017**, *56*, 1-5.
72. Dalence-Guzman, M. F.; Berglund, M.; Skogvall, S.; Sterner, O., SAR studies of capsazepinoid bronchodilators. Part 1: The importance of the catechol moiety and aspects of the B-ring structure. *Bioorg. Med. Chem.* **2008**, 2499-2512.
73. Kistner, K.; Siklosi, N.; Babes, A.; Khalil, M.; Selescu, T.; Zimmermann, K.; Wirtz, S.; Becker, C.; Neurath, M. F.; Reeh, P. W.; Engel, M. A., Systemic desensitization through TRPA1 channels by capsazepine and mustard oil - a novel strategy against inflammation and pain. *Sci. Rep.* **2016**, *6*, 28621.
74. Ledermüller, K.; Schütz, M., Local CC2 response method based on the Laplace transform: Analytic energy gradients for ground and excited states. *Int. J. Chem. Phys.* **2014**, *140*, 164113.
75. Wang, S.-F.; Chuang, C.-P.; Lee, J.-H.; Liu, S.-T., Sodium p-toluenesulfinate/copper(II) acetate in free radical reactions. *Tetrahedron* **1999**, *55*, 2273-2288.
76. Heal, D. J.; Smith, S. L.; Gosden, J.; Nutt, D. J., Amphetamine, past and present - a pharmacological and clinical perspective. *J. Psychopharmacol.* **2013**, *27*, 479-496.
77. Young, R. C.; Meyer, T. J.; Whitten, D. G., Electron transfer quenching of excited states of metal complexes. *J. Am. Chem. Soc.* **1976**, *98*, 286-287.
78. Fröhlich, P. M.; Gantt, D.; Paramasigamini, V., Fluorescence Quenching of Indoles by *N,N*-Dimethylformamide. *Photochem. Photobiol.* **1977**, *26*, 639-642.
79. Schöllkopf, U.; Hinrichs, R.; Lonsky, R., Asymmetric Synthesis of Cyclic  $\alpha$ -Amino Acids by the Bislactim Ether Method. *Angew. Chem. Int. Ed.* **1987**, *26*, 143-145.
80. Seebach, D.; Gees, T.; Schuler, F., Preparation of  $\alpha$ -branched phenylalanines and of 1,1-disubstituted ethylenediamines via chiral imidazolidinones and oxazolidinones of glycine - preparative and mechanistic aspects. *Liebigs Annalen der Chemie* **1993**, *7*, 785-799.
81. Brouillette, W. J.; G. B. Brown; T. M. DeLorey; S. S. Shirali; Grunewald, G. L., Anticonvulsant Activities of Phenyl-Substituted Bicyclic 2,4-Oxazolidinediones and Monocyclic Models. Comparison with Binding to the Neuronal Voltage-Dependent Sodium Channel. *J. Med. Chem.* **1988**, 2218-2221.
82. Aurelio, L.; Box, J. S.; Brownlee, R. T. C.; Hughes, A. B.; Sleebs, M. M., An efficient Synthesis of *N*-Methyl Amino Acids by Way of Intermediate 5-Oxazolidinones. *J. Org. Chem.* **2003**, *68*, 2652-2667.
83. Barton, D. H. R.; Herve, Y.; Potier, P.; Thierry, J., Manipulation of the Carbonyl Groups of  $\alpha$ -Amino Acids and Peptides Using Radical Chemistry Based on Esters of *N*-Hydroxy-2-Thiopyridone. *Tetrahedron* **1988**, *44*, 5479-5486.



84. Lombardino, J. G.; Wiseman, E. H.; McLamore, W. M., Synthesis and Antiinflammatory Activity of Some 3-Carboxamides of 2-Alkyl-4-hydroxy-2H-1,2-benzothiazine 1,1-Dioxide. *J. Med. Chem.* **1971**, *14*, 1171-1175.
85. Ottonello, L.; Dapino, P.; Scirocco, M. C.; Balbi, A.; Bevilacqua, M.; Dallegri, F., Sulphonamides as anti-inflammatory agents: old drugs for new therapeutic strategies in neutrophilic inflammation? *Clinical Science* **1995**, *88*, 331-336.
86. Fontan, P. A.; Amura, C. R.; Sordelli, D. O., Treatment with non-steroidal anti-inflammatory agent delays the growth of spontaneous pulmonary metastases of a mammary adenocarcinoma of non-detected immunogenicity. *Br. J. Cancer* **1992**, *66*, 800-804.
87. Lian, M.; Li, Z.; Cai, Y.; Meng, Q.; Gao, Z., Enantioselective Photooxygenation of  $\beta$ -Keto Esters by Chiral Phase Transfer Catalysis using Molecular Oxygen. *Chem. Asian J.* **2012**, *7*, 2019-2023.
88. Koh, M. L.; Jolliffe, K. A.; Perrier, S., Hierarchical Assembly of Branched Supramolecular Polymers from (Cyclic Peptide)-Polymer Conjugates. *Biomacromolecules* **2014**, *15*, 4002-4011.
89. Eichinger, C. Immobilization of Photocatalysts on Solid Support and Photochemical Decarboxylations. Universität Regensburg, Regensburg, 2020.
90. Navarova, H.; Bemsdorff, F.; Döring, A.-C.; Zeier, H., Pipecolic Acid, an Endogeneous Mediator of Defense Amplification and Priming, Is a Critical Regulator of Inducible Plant Immunity. *The Plant Cell* **2012**, *24*, 5123-5141.
91. Bernsdorff, F.; Döring, A.-C.; Gruner, K.; Schuck, S.; Bräutigam, A.; Zeier, J., Pipecolic acid orchestrates plant systematic acquired resistance and defense priming via acid-dependent and -independent pathways. *Plant Cell* **2016**, *28*, 102-129.
92. Xu, J.; Jin, Z.; Chi, Y. R., Organocatalytic Enantioselective  $\gamma$ -Aminoalkylation of Unsaturated Ester: Access to Pipecolic Acid Derivatives. *Organic Letters* **2013**, *15*, 5028-5031.
93. Kadouri-Puchot, C.; Comese, S., Recent advances in asymmetric synthesis of pipecolic acid and derivatives. *Amino Acids* **2005**, *29*, 101-130.
94. Kaneko, H.; Ikawa, T.; Yamamoto, Y.; Arulmozhiraja, S.; Tokiwa, H.; Akai, S., 3-(Triflyloxy)benzynes Enable the Regiocontrolled Cycloaddition of Cyclic Ureas to Synthesize 1,4-Benzodiazepine derivatives. *Synlett* **2018**, *29*, 943-948.
95. Kistner, K.; Siklosi, N.; Babes, A.; Khalil, M.; Selescu, T.; Zimmermann, K.; Wirtz, S.; Becker, C.; Neurath, M. F.; Reeh, P. W.; Engel, M. A., Systematic desensitization through TRPA1 channels by capsazepine and mustard oil. *Sci. Rep.* **2016**, 1-11.
96. Bischoff, A. J.; Nelson, B. M.; Niemeyer, Z. L.; Sigman, M. S.; Movassaghi, M., Quantitative Modeling of Bis(pyridine)silver(I) Permanganate Oxidation of Hydantoin Derivatives: Guidelines for Predicting the Site of Oxidation in Complex Substrates. *J. Am. Chem. Soc.* **2017**, *139*, 15539-15547.
97. Lickefett, H.; Krohn, K.; König, W. A.; Gehrcke, B.; Syltatk, C., Enantioseparation of 5-Monosubstituted Hydantoins by Capillary Gas Chromatography - Investigation of Chemical and Enzymatic Racemization. *Tetrahedron: Asymmetry* **1993**, *4*, 1129-1135.
98. Oyaizu, K.; Ohtani, Y.; Shiozawa, A.; Sugawara, K.; Saito, T.; Yuasa, M., Highly Stable Gold(III) Complex with a Hydantoin Ligand in Alkaline Media. *Inorg. Chem.* **2005**, *44*, 6915-6917.
99. Sprouse, S.; King, K. A.; Spellane, P. J.; Watts, R. J., Photophysical Effects of Metal-Carbon  $\sigma$ -Bonds in Ortho-Metalated Complexes of Ir(III) and Rh(III). *J. Am. Chem. Soc.* **1984**, *106*, 6647-6653.
100. Quagliato, D. A.; Andrae, P. M.; Matelan, E. M., Efficient Procedure for the Reduction of  $\alpha$ -Amino Acids to Enantiomerically Pure  $\alpha$ -Methylamines. *J. Org. Chem.* **2000**, *65*, 5037-5042.
101. Dieltiens, N.; Claeys, D. D.; Zhdankin, V. V.; Nemykin, V. N.; Allaert, B.; Verpoort, F.; Stevens, C. V., The Pyroglutamate Hydantoin Rearrangement. *Eur. J. Org. Chem.* **2006**, 2649-2660.

## 4. Visible Light Mediated Oxidative Ring Expansion of Cyclopropanes<sup>†</sup>

### 4.1 The Endoperoxide Moiety

Oxygen is by mass the most abundant element in earth's crust, mainly bound to metals and half-metals in their corresponding oxides. In such oxides it is almost exclusively found in its oxidation state –II. Furthermore oxygen constitutes approximately 20% of earth's atmosphere as diatomic molecule O<sub>2</sub>, taking on the oxidation state 0.<sup>102</sup> Life on earth, save some deep-sea organisms, is governed by this oxidizing atmosphere and revolves around cleaving and forming carbon-oxygen bonds, changing the oxygen's oxidation state from 0 to –II or *vice versa* in the process.<sup>103</sup> In the –I state it is only rarely encountered in isolable molecules, and mostly found in reactive intermediates. These highly reactive molecules are of particular interest for chemistry and some have found widespread attention even in popular science. The simplest peroxide, H<sub>2</sub>O<sub>2</sub> (**120**), has various applications, *e.g.* as disinfectant, bleach, and as part of rocket fuel, all due to its highly oxidizing effect.<sup>104</sup>



Figure 8: Hydrogen peroxide (left) and organic peroxide (right).

The general instability of hydrogen peroxide is tamed by replacing the hydrogen with suitable carbon residues, tuning the reactivity *via* electronic and steric effects (Figure 8). These organic peroxides show increased stability, but are still rarely found in nature. However, many of them exhibit pharmaceutical properties, which was also the case for the first ever isolated organic peroxide, ascaridole (**121**, Figure 9). It was purified in 1908 from goosefoot-oil<sup>105</sup> and synthesized in 1944 by Karl Ziegler and Günther Schenck.<sup>106</sup> In pure form it was found to explode only when heated above 130 °C, and was used as pharmaceutical for its anthelmintic properties.<sup>107</sup>

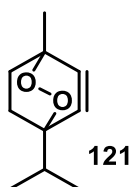


Figure 9: Ascaridole.

<sup>†</sup> Parts of this chapter are reproduced or adapted with permission from the Royal Society of Chemistry from Budde, S.; Goerdeler, F.; Floß, J.; Kreitmeier, P.; Hicks, E. F.; Moscovitz, O.; Seeberger, P. H.; Davies, H. M. L.; Reiser, O., *Visible-light mediated oxidative ring expansion of anellated cyclopropanes to fused endoperoxides with antimalarial activity*. *Org. Chem. Front.* **2020**, *7*, 1789-1795.

Ascaridole is, as most naturally occurring peroxides, a cyclic molecule, where the peroxide is part of at least one of the cycles.

More complex organic peroxides, such as the compound artesunate (**122**), display astounding selectivity in a pharmaceutical context, delivering their oxidative power only to certain sites in the body (Figure 10). This combination of selectivity and reactivity makes artesunate (**122**) the most effective treatment for Malaria, a disease caused by *Plasmodium* parasites and transferred by *Anopheles* mosquitos, affecting approximately 200 million humans every year.<sup>108</sup>

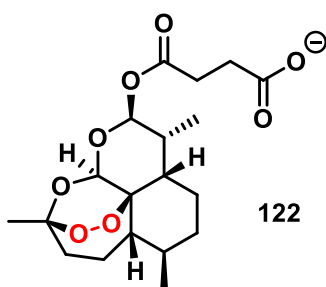


Figure 10: Artesunate.

Cyclic peroxides such as artesunate have been the target of synthetic research for decades, but their synthesis from scratch is challenging. While using natural precursors is a very effective approach for the large-scale synthesis of artesunate<sup>36, 109</sup>, the achievable variety of derivatives is restricted to a certain degree by the structural diversity of the natural precursors.<sup>110</sup>

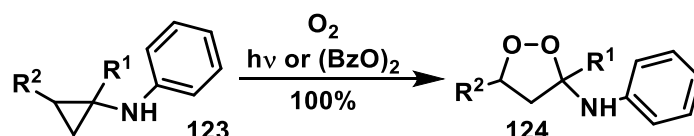
Synthetically, a number of methods are available to introduce a peroxide bridge as it is found in artesunate, and a few reviews on the topic are available.<sup>111-113</sup> Often comparably harsh conditions, *e.g.* highly reactive reagents or UV-light, are required, making them unsuitable in the synthesis of complex molecules because of incompatibility with functional groups.

The structural peculiarity, that diatomic oxygen molecule exists as diradical with two unpaired electrons, points the way to the most commonly used synthetic routes to organic peroxides, in which latent or manifest diradicals serve as precursors. This is where cyclopropanes come into play.

In the cyclopropane molecule, the bond angles between the three carbons are bent to 60° from the 109.5° in a strain-free tetraeder.<sup>114</sup> This distortion stores about 27 kcal/mol of energy, making cyclopropane ring-opening or ring expansion an energetically favorable process. Cyclopropanes undergo rapid ring-opening when a radical centre is generated in  $\alpha$ -position to the three-membered ring.<sup>115</sup> This observed behavior is exploited in the application of cyclopropylmethyl substituents as radical clocks in the elucidation of mechanisms. Not only

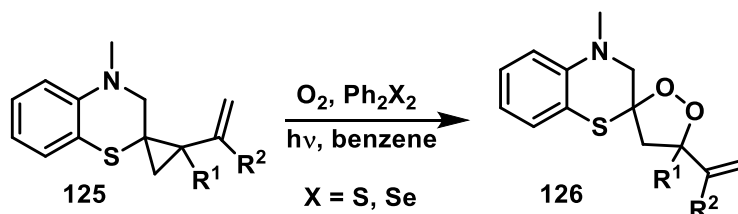
information on the type of the reaction – radical or non-radical – but also information on the rate constant of the reaction in question can be obtained, due to the known rate-constant of the ring opening of cyclopropylmethyl radical. Adding to their attractiveness as synthetic precursors is the relative ease of their synthesis, as numerous routes, including chiral ones, are available *e.g.* <sup>116-119</sup>, which lays the foundation for a broad application. Cyclopropane is a latent diradical, making it a well-paired reaction partner for the oxygen molecule and one of the favorite precursors for peroxide-containing molecules.

For example, Wimalasena *et al.* converted aminocyclopropanes **123** to the corresponding cyclic peroxides **124** in up to quantitative yields (Scheme 40).<sup>120</sup> This strategy was based on the one-electron oxidation of the amine moiety adjacent to the cyclopropane, leading to a radical-cation, triggering the opening of the cyclopropane. UV-light or a traditional radical starter, in this case benzoylperoxide, could initiate the reaction.



Scheme 40: Ring expansion of aminocyclopropanes demonstrated by Wimalasena *et al.*<sup>120</sup>.

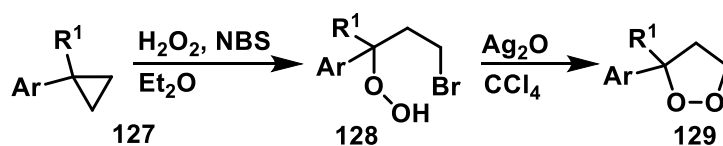
A related and widely studied class of molecules, vinylcyclopropanes<sup>121-123</sup>, can also act as precursor for the formation of cyclic peroxides. This strategy was used by Kataoka *et al.* for the synthesis of complex benzothiazine derivatives **126**, comprising a spiro-dioxolane as shown below (Scheme 41).<sup>124</sup> The derivatives were then further examined for potentially interesting pharmaceutical applications. The opening of the cyclopropane (**125**) is triggered by the addition of a radical to the double bond. Said radical was generated *in situ* from diphenyldiselenide or diphenylsulfide *via* homolysis of the respective compound by irradiation of visible light.



Scheme 41: Synthesis of a peroxide from a vinylcyclopropane.<sup>124</sup>

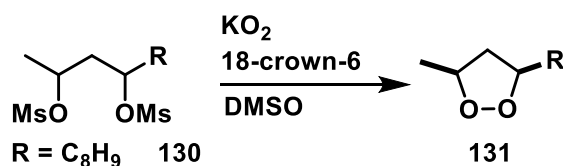
Starting from cyclopropanes, but trading a completely different path *via* a hydroperoxide compound is also possible. Rodriguez *et al.* described a strategy which does not rely on the generation of a radical adjacent to the cyclopropyl moiety, but the cyclopropane (**127**) scaffold is opened directly (Scheme 42). This introduces a hydroperoxide and a bromide

moiety (**128**), and in the next step silver oxide is used to eliminate HBr, forming a 1,2-dioxolane (**129**).<sup>125</sup>



Scheme 42: Stepwise synthesis of 1,2-dioxolane from a cyclopropyl precursor.<sup>125</sup>

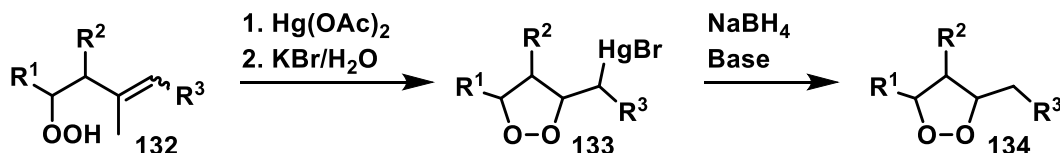
Formally the second step of the above shown reaction constitutes an intramolecular substitution, which in combination with an initial addition was also the essential step in the preparation of cyclic organic peroxides **131** from potassium superoxide (Scheme 43). The superoxide anion was used for the purpose of constructing a peroxide bridge as early as 1975 by E. J. Corey *et al.*<sup>126-127</sup>, who searched for synthetic routes towards compounds mimicking prostaglandin endoperoxides, which are biologically interesting molecules in humans<sup>128</sup>. In contrast to the examples described above for cyclopropyl-containing molecules, this strategy does not rely on the involvement of radicals.



Scheme 43: Superoxide as oxygen nucleophile.

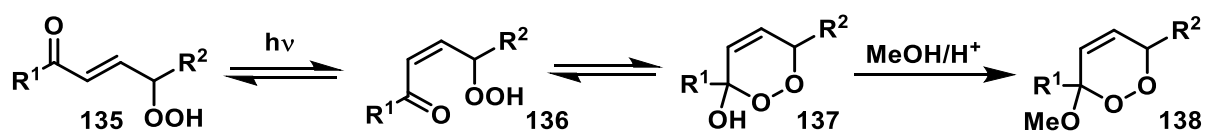
The yields obtained were only around 40%, presumably due to the highly reactive superoxide undergoing side reactions.

Also a formal intramolecular addition is shown in the example depicted below (Scheme 44), where mercury acetate was applied to facilitate the cyclization of a hydroperoxide (**132**) to a neighboring double bond.<sup>129</sup>



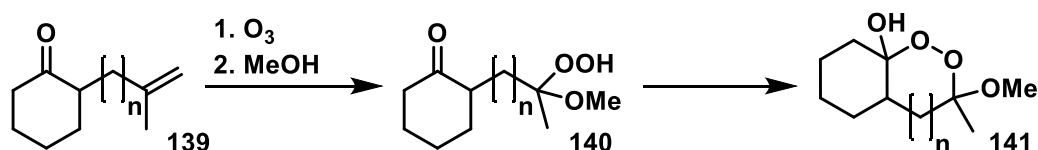
Scheme 44: Mercury(II) facilitating an intramolecular addition of a hydroperoxide.

In a comparable way hydroperoxides can form *intramolecular* ketals with carbonyl groups, which leads to endoperoxides with the special feature, that one of the adjacent carbons is directly connected to another oxygen containing functionality (Scheme 45).



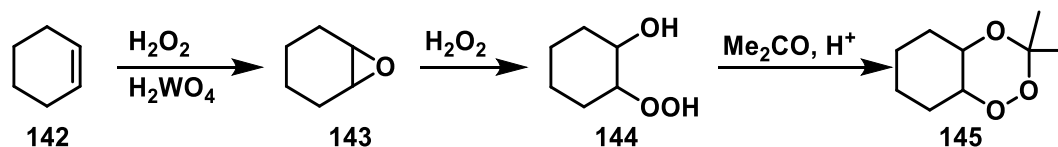
Scheme 45: Intramolecular perketalization under photochemical conditions reported by Dussault *et al.*<sup>130</sup>

Similarly, Nojima *et al.* developed a strategy involving ozonolysis of a double bond (Scheme 46), forming a hydroperoxyketal (**140**). This cyclizes with another carbonyl functionality, forming a cyclic endoperoxide consisting of two perketals (**141**).<sup>131</sup>



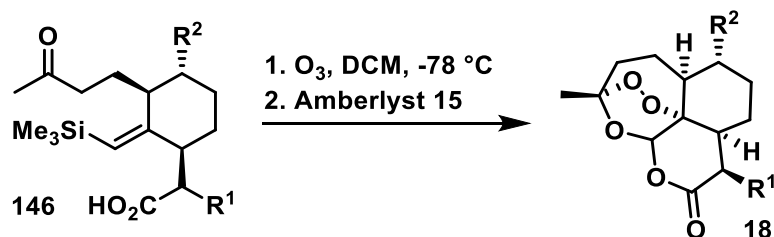
Scheme 46: Ozonolysis and consecutive ketalization leading to a peroxide formed by two perketals.

Also *intermolecular* ketalization is possible, as shown by the example reported by Payne *et al.* (Scheme 47).<sup>132</sup> Here, an epoxide (**143**) is opened using hydrogen peroxide and then an external ketone, *e.g.* acetone, is added to form the perketal, in this case a 1,2,4-trioxane (**145**).



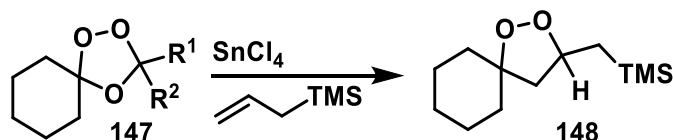
Scheme 47: Synthesis of an endoperoxide *via* intermolecular peroxyketal formation.

The structural motif of such a 1,2,4-trioxane is also found in the antimalarial drug artemisinin (**18**) and was therefore target of various synthetic approaches, described in several reviews.<sup>133-134</sup> Using the ozonolysis and ketalization strategy described above, artemisinin derivatives are accessible. In the example below (Scheme 48), the precursor only incorporates the carbon cycle; all the oxygen-containing rings are formed by ozonolysis and consecutive acid workup with an ion exchange resin, Amberlyst 15.<sup>135</sup>



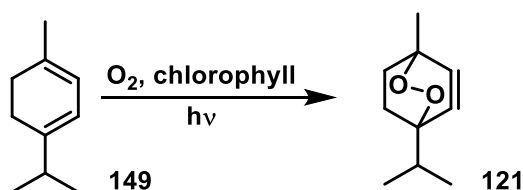
Scheme 48: Ozonolysis as the key step to artemisinin derivatives.

A different workup of ozonides can also be employed to directly form endoperoxides, which do not incorporate a perketal. Tin- or titanium chloride facilitate transformations such as the example shown below (Scheme 49), where an additional coupling partner is incorporated into the molecule, while selectively removing the oxygen in –II state from the ozonide.<sup>136-137</sup>



Scheme 49: Tin chloride facilitates the coupling of an ozonide with allyltrimethylsilane, forming an endoperoxide.

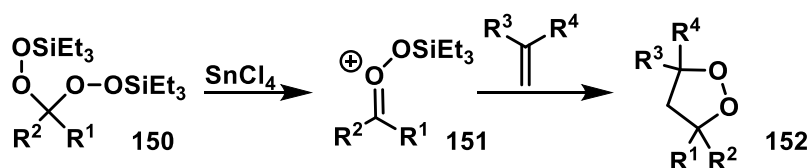
Strategies for the synthesis of cyclic peroxides under circumvention of hydroperoxide-containing intermediates include the [4+2]-cycloaddition of singlet oxygen to a 1,3-diene, which for example was used for the first synthesis of the abovementioned ascaridole (**121**) from  $\alpha$ -terpinene (**149**) using chlorophyll as catalyst under photocatalytic conditions (Scheme 50).<sup>106</sup>



Scheme 50: Synthesis of ascaridole presented by Schenk and Ziegler 1944.<sup>106</sup>

The Diels-Alder like [4+2] cycloaddition of singlet oxygen offers the advantage of high atom economy, as all atoms of the precursors are found in the product, and only a catalyst is needed for the formation of singlet oxygen, potentially from ambient air. While the operationally simple reaction setup speaks for itself, the requirements on the starting material are comparably high, as the two double bonds need to be in the right conformation, and side reactions such as a [2+2] cycloaddition or the Schenck-ene reaction are possible. However, the nature of the double bond may vary, *e.g.* enol-double bonds<sup>138</sup> work well, and most commonly cyclic substrates, which keep the two double bonds in the required conformation, are employed.

Apart from [4+2] cycloadditions, also a [3+2] cycloaddition route can lead to endoperoxides.

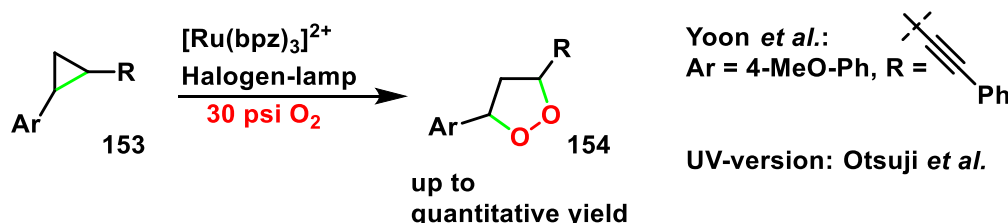


Scheme 51: Strategy for the synthesis reported by Woerpel *et al.* in 2005.<sup>139</sup>

Peroxyketals (**150**) were used as precursors for reactive peroxy-carbenium ions (**151**), which can undergo a [3+2] reaction, forming endoperoxides **152** with terminal alkenes (Scheme 51).<sup>139</sup> This strategy requires a Lewis acid such as tin- or titanium tetrachloride.

In conclusion, endoperoxides are accessible *via* a reasonable variety of synthetic routes, including cycloadditions, reactions of hydroperoxides and their respective ketals, UV and visible light mediated reactions.

The re-discovery of visible-light mediated reactions since the early 2000's led to great progress in that specific area of chemistry, as its advantages over UV-mediated and also traditional synthetic strategies are numerous. While reports about the use of visible light in conjunction with transition metal complexes<sup>140</sup> as an advance from the UV-version<sup>141</sup> for the synthesis of endoperoxides exist (Scheme 52), its full potential in this regard is still to be discovered.



Scheme 52: Visible light mediated photooxygenation of cyclopropanes reported by Yoon *et al.*.<sup>140</sup>

So far, great yields were achieved with substrates exhibiting a limited degree of structural complexity, namely cyclopropanes with electron rich aromatic substituents. Steps towards an increased applicability of the visible light mediated photooxygenation of cyclopropanes for the synthesis of biologically active and pharmaceutically relevant drugs, such as artemisinin, need to be undertaken and were the aim of this work.

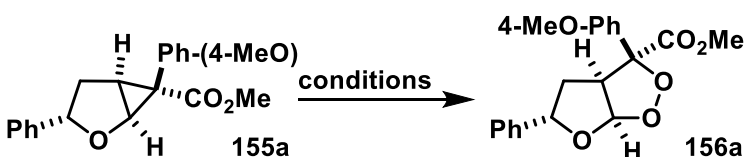


## 4.2 Preliminary Studies

Cyclopropanated five-membered heterocycles, *i.e.* substituted furan derivatives, are a precursor often used by the Reiser group.<sup>142-144</sup> Their advantages include comparably easy gram-scale synthesis from inexpensive raw materials *via* rhodium-catalyzed cyclopropanation, resulting in a great accessible structural diversity. Additionally, the cyclopropane system generated exhibits a favorable donor-acceptor substitution pattern.<sup>119, 142, 145-146</sup> Visible light mediated photooxygenation of the cyclopropyl group<sup>140</sup> (Table 6) would lead to compounds similar to those reported by Xu *et al.*<sup>147</sup>, who employed a [2+3]-cycloaddition strategy (based on Woerpel *et al.*<sup>139</sup>, compare also Scheme 51). The promising antimalarial activity found in biological tests of these molecules increased our interest and, together with the abovementioned background, were the foundation for the preliminary studies.

Following the precedent set by Yoon *et al.*, calling for the employment of [Ru(bpz)<sub>3</sub>](PF<sub>6</sub>)<sub>2</sub> ( $E^*_{1/2} = +1.4$  V *vs.* SCE<sup>140</sup>), only decomposition of the starting material **155a** ( $E_{(M/M^+)}: +1.40$  V *vs.* SCE) was observed.

Table 6: Initial testing.



#	catalyst	solvent	yield
1 <sup>1)</sup>	[Ru(bpz) <sub>3</sub> ](PF <sub>6</sub> ) <sub>2</sub> ( <b>2</b> )	MeNO <sub>2</sub> /toluene	decomp.
2	[MesAcr]ClO <sub>4</sub> ( <b>9</b> )	MeCN	15%, d.r. 3:1

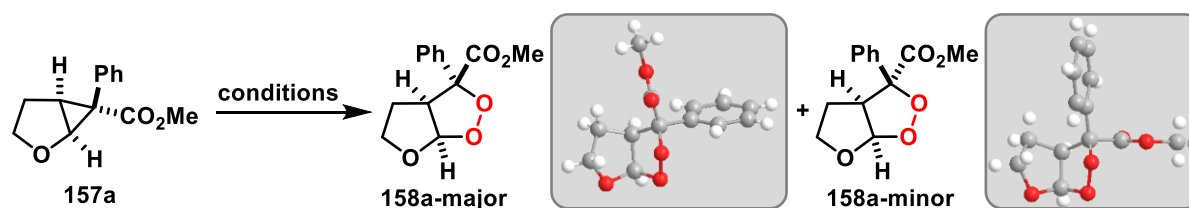
Irradiation with LED (455 nm) for 30 min under oxygen atmosphere (balloon); 0.1 M solution **155a** in respective solvent.

But as a reaction was definitely taking place, other catalysts were tested. Irradiation in presence of the highly oxidizing 9-mesityl-10-methyl-acridinium perchlorate (Fukuzumi's Catalyst **9**;  $E^*_{1/2} = +2.06$  V *vs.* SCE)<sup>148</sup> under O<sub>2</sub>-atmosphere in MeCN as solvent led to the formation of the two endoperoxides **156a-major** and **156a-minor** (d.r. 3:1, entry 2). Albeit complete conversion of the starting material **155a** was reached within 30 min, **156a** was observed only in a low yield of 15%, while copious amounts of polymeric byproduct precipitated from the reaction mixture. presumably not only the catalyst was an issue, but also substrate **155a** was too reactive, causing the formation of undesired byproducts.<sup>149</sup>

### 4.3 Optimization

Instead of substrate **155a**, comprising an electron rich aromatic substituent, a simpler starting material was chosen. Cyclopropanated dihydrofuran **157** is accessible *via* visible light mediated cyclopropanation followed by Rh-catalyzed reduction using commercially available furan and methyl phenyldiazoacetate (Table 7; compare also Scheme 53, *vide infra*). It exhibits a donor-acceptor substitution pattern on the cyclopropyl moiety, but does not have additional substituents which might undergo reactions under the highly oxidizing conditions. Furthermore, the electron-rich 4-MeO-Ph substituent was exchanged for an electronically neutral functionality. This should be adequate to the high oxidizing power of Fukuzumi's catalyst, which was successfully used in the oxidation of unsubstituted aryl groups<sup>11</sup>, and also broaden the limitations discovered in the known literature.

Table 7: Conditions Screening.



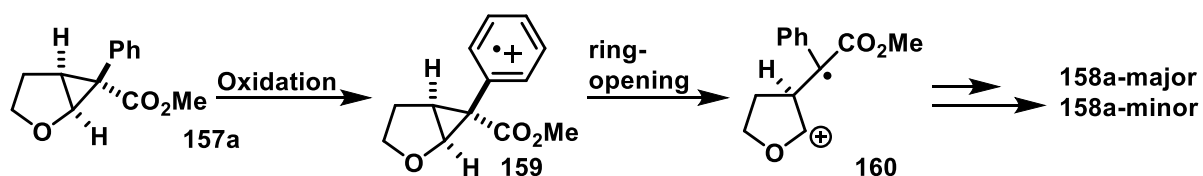
#	catalyst	substrate	solvent	yield
1 <sup>1)</sup>	[Ru(bpz) <sub>3</sub> ](PF <sub>6</sub> ) <sub>2</sub>	157a	MeNO <sub>2</sub> /tol	-
2 <sup>2)</sup>	Ir[dF(CF <sub>3</sub> )ppy] <sub>2</sub> (dtbpy)PF <sub>6</sub>	157a	MeCN	<5%
3	[MesAcr]ClO <sub>4</sub>	157a	MeCN	47%, d.r. 4:1 <sup>5</sup>
4	[MesAcr]ClO <sub>4</sub>	157a	CHCl <sub>3</sub>	6% d.r. 1:1
5	[MesAcr]ClO <sub>4</sub>	157a	HFIP	10% d.r. 1:1
6 <sup>3)</sup>	[MesAcr]ClO <sub>4</sub>	157a	MeCN	49%, d.r. 4:1
7 <sup>4)</sup>	[Ru(bpy) <sub>3</sub> ]Cl <sub>2</sub>	157a	MeCN	-
8	Rose Bengal	157a	MeCN	-
9	no catalyst	157a	MeCN	-
10	[MesAcr]ClO <sub>4</sub> , no light	157a	MeCN	-
11	[MesAcr]ClO <sub>4</sub> , no O <sub>2</sub>	157a	MeCN	-

NMR-Yields determined using 1,4-diacetylbenzene as internal standard. Reaction conditions: 10 mol% catalyst, 0.2 mmol substrate, 2 mL solvent, blue LED (455 nm), O<sub>2</sub>-Balloon, 16 h, r.t.. <sup>1)</sup>0.5 mol% catalyst, 0.2 mmol substrate, 2 mL MeNO<sub>2</sub>/toluene 1:1, 30 psi O<sub>2</sub>, 16h, r.t.. <sup>2)</sup>2 mol% catalyst; <sup>3)</sup> 30 psi O<sub>2</sub>, 10 h. <sup>4)</sup> 5 mol% Catalyst. <sup>5)</sup> Combined isolated yield of separated diastereomers.

While transition metal catalysts failed to produce the product in relevant quantity under the tested conditions, employing Fukuzumi's catalyst **9** gave rise to the diastereomers **158-major** and **158-minor**, which were separated by column chromatography and characterized by X-ray crystallography. Notably, the orientation of the phenyl and ester group was reversed for the major diastereomer compared to the starting material. A short screening for optimum conditions showed that the reaction is strongly dependent on the solvent (entries 3-5), with acetonitrile giving the best yield and diastereomeric ratio. While the yield was by and large constant, the reaction time decreased when instead of air (ambient pressure, 20 h) an O<sub>2</sub>-balloon (16 h, entry 3) or oxygen overpressure (30 psi, 10 h, entry 6) were applied. Control experiments using the known singlet-oxygen producing catalysts [Ru(bpy)<sub>3</sub>]<sup>2+</sup> or Rose Bengal

(entries 9 & 10) did not facilitate the reaction, revealing that a mechanism not solely dependent on singlet oxygen is operative. Furthermore it was shown that light, oxygen, as well as catalyst were necessary for the reaction to proceed (entries 9-11).

As a working hypothesis, the catalyst was suspected to oxidize the aryl substituent, generating a radical cation adjacent to the cyclopropane (**159**), therefore triggering its opening (Scheme 53). This would separate the radical site from the cationic site (**160**), but both stabilized by the heteroatom adjacent to the furane ring and the aryl moiety, respectively. This would lead to free rotation at the radical site, which might explain the formation of the two observed diastereomers.

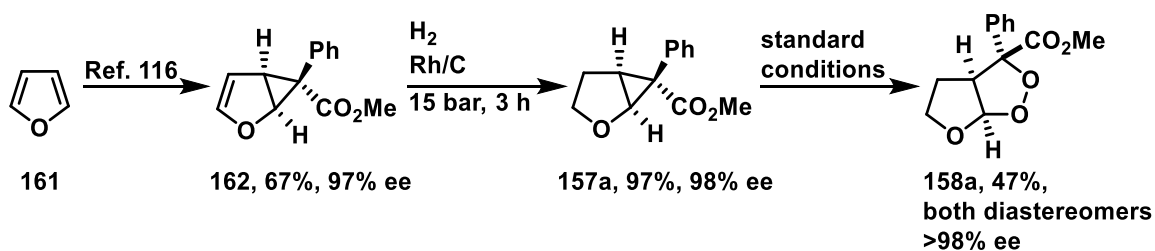


Scheme 53: Working hypothesis on the initial mechanistic steps of the reaction.

With this mechanistic picture in mind, the limitations of the reaction were to be explored by choosing appropriate substrates.

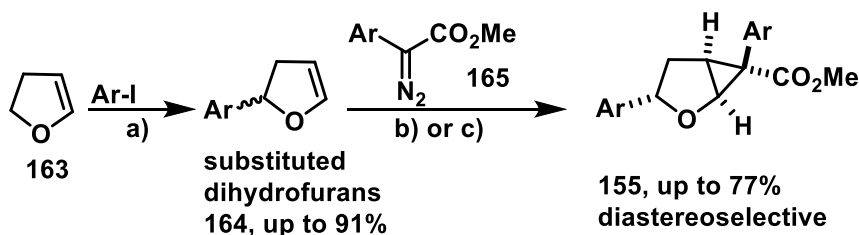
## 4.4 Substrate Scope

Before performing variations on the substrate scope, enantiomerically enriched (-)-**157** was synthesized by carrying out an enantioselective cyclopropanation of furan **161** using a chiral rhodium catalyst (Scheme 54). After several recrystallizations the desired enantiomeric excess of >99% was achieved, and upon hydrogenation the appropriate substrate (-)-**157a** for the peroxidation was isolated. Applying the standard conditions, the corresponding (-)-**158a** was formed without erosion of enantiopurity.



Scheme 54: Synthesis of enantiomerically enriched peroxide.

Since endoperoxides with the core structure of **158a**, comprising a 5-aryl substituent on the furan core, are reported to have especially promising anti-malarial activity<sup>147</sup>, the focus was shifted to substrates with such substituents (**155**). This particular substitution pattern is accessible *via* Heck-arylation of 2,3-dihydrofuran **163**<sup>150</sup> followed by cyclopropanation with 2-aryl 2-diazoacetates **165** (Scheme 55).<sup>118</sup> The Heck arylation leads to a racemate (**164**), while the consecutive cyclopropanation proceeds with complete diastereoselectivity (**155**).



a) 5-10 mol% Pd(OAc)<sub>2</sub>, <sup>n</sup>Bu<sub>4</sub>NCl, KOAc, molecular sieves, DMF, 24 h.

b) h<sub>v</sub>455 nm, DCM, 24 h.

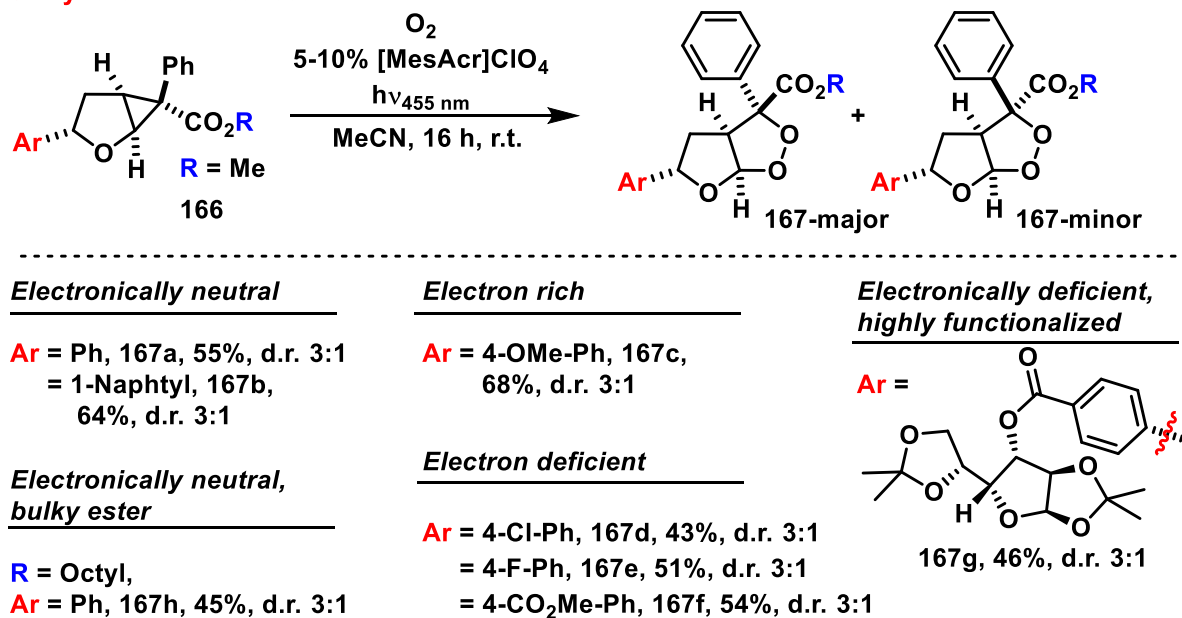
c) 0.8 mol% Rh<sub>2</sub>(OAc)<sub>4</sub>, DCM, 3 h.

Scheme 55: Synthesis of 5-aryl substituted substrates.

For the latter either the traditional transition metal catalyzed pathway using Rh<sub>2</sub>(OAc)<sub>4</sub> was applied, or the recently reported, visible light driven process<sup>118</sup> which allows for an environmentally friendly, metal free approach. Both conditions gave cyclopropanes **155** in 32 - 77% yield with complete diastereoselectivity, in which the cyclopropanation occurs opposite of the aryl moiety and the ester group orients on the convex side of the bicycle.

Substrates containing electron rich, electron deficient, bulky and highly functionalized 5-aryl substituents were successfully synthesized (**166a-g**) and consecutively subjected to the optimized conditions to convert them to their respective endoperoxides **167a-g** (Scheme 56).

#### 5-Arylfuran Derivatives



Scheme 56: Variations on the 5-aryl substituent.

By and large the yields were constant in the range of 50%, and therefore comparable to the unsubstituted furan derivative. This leads to the conclusion that the nature of the 5-aryl substituent does not have a significant impact and no interference occurs with the mechanism operative in this reaction. A crystal structure was obtained for the minor diastereomer of compound **167e** (Figure 11).

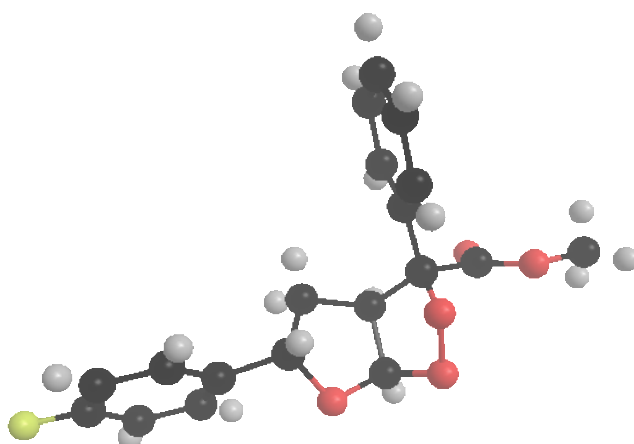
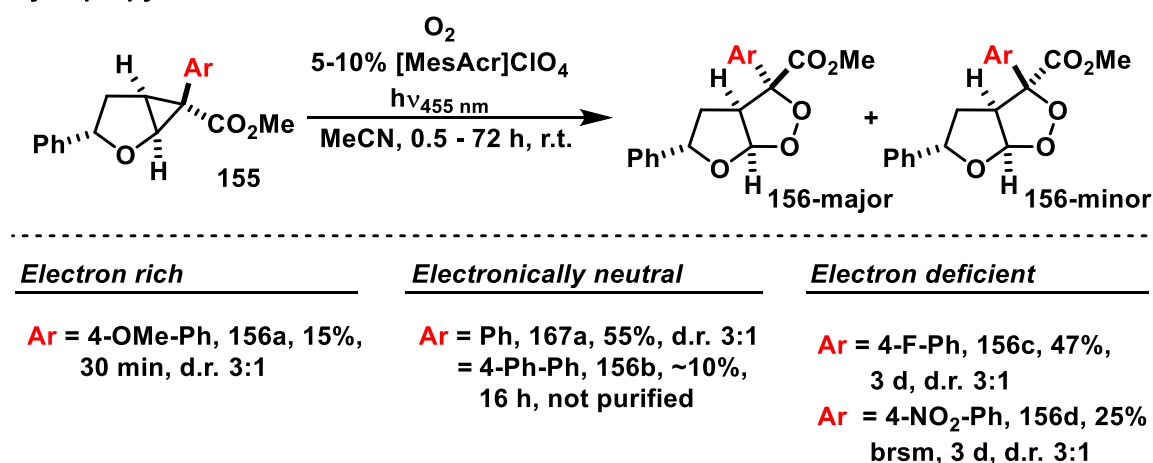


Figure 11: crystal structure of the minor diastereomer of compound **167e**.

Next, the influence of variations on the Aryl group adjacent to the cyclopropane was explored (Scheme 57). Changes on this position were expected to significantly alter the reaction

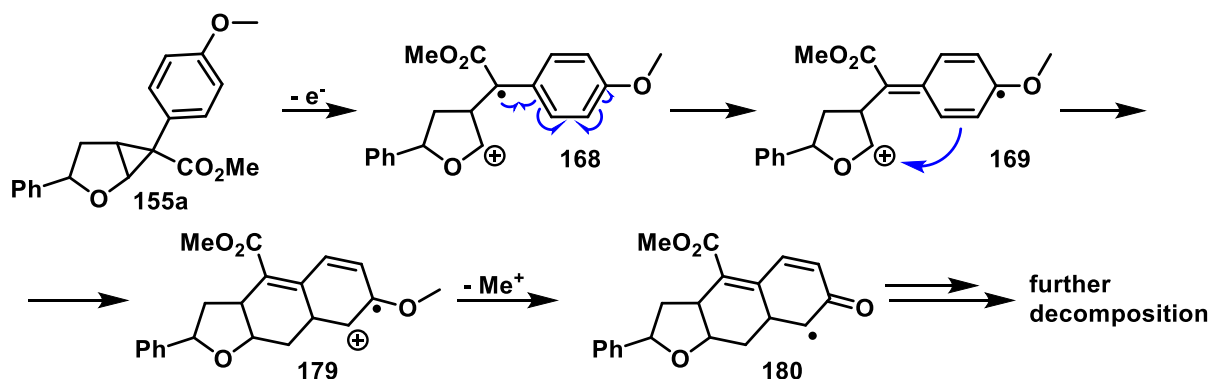
outcome, as in the diarylcyclopropane literature models, mostly electron rich 4-OMe substituted substrates were used and were found to deliver distinctly higher yields than the unsubstituted or electron deficient derivatives. In order to test this, the 5-phenyl substituted dihydrofuran was cyclopropanated with different aryldiazoacetates. The corresponding electron rich (4-OMe, **155a**), bulky (4-Ph, **155b**) and electron deficient (4-F, **155c**, and 4-NO<sub>2</sub>, **155d**) substrates were subjected to the standard reaction conditions, with greatly deviating results.

#### Cyclopropyl-Ar Derivatives



Scheme 57: Variations on the cyclopropyl-aryl group.

The electron rich compound **155a** had already been tested in the beginning of the project, as it is the closest analogue to the reported literature examples, and was thought to be oxidized easiest because of its low reduction potential. As described earlier (Table 6, *vide supra*), it underwent rapid conversion, and the starting material was consumed after only 30 min. During the reaction, a white precipitate formed, which was separated by filtration. It was found to be hardly dissolvable in any tested solvent, and NMR analysis showed broad peaks, indicating a polymeric substance of unknown constitution. Column chromatography of the filtrate gave very little of the desired peroxide compound. The short reaction time is in accordance with the literature and the mechanistic proposal, as electron rich substrates are easier oxidized by the catalyst. However, due to the higher complexity of the substrate in comparison with the diarylcyclopropanes reported in literature, there are more pathways available, leading to side-reactions. One possible pathway, involving a cyclization to the aryl ring, is shown below (Scheme 58).



Scheme 58: Possible decomposition steps in the electron rich substrate **155a**.

While the reaction with the electron rich substrate could lead to some interesting molecules, unfortunately it did not lead to a productive outcome.

However, with the successful transformation of the highly electron deficient 4-NO<sub>2</sub>-Ph substituted substrate **155d** an unexpected outcome was observed (Figure 12), as there is no evidence that such an electron deficient phenyl group can be oxidized by Fukuzumi's catalyst **9**.<sup>20</sup> As crystal structures from both the starting material as well as the product are available, there is no doubt that this transformation took place. This leads to the hypothesis that the heteroatom of the furan-ring may also be oxidized by the catalyst, which ultimately leads to the same result as the oxidation on the aryl substituent of the cyclopropyl group; the hypothetical mechanism is discussed in the respective section (See chapter 4.7).

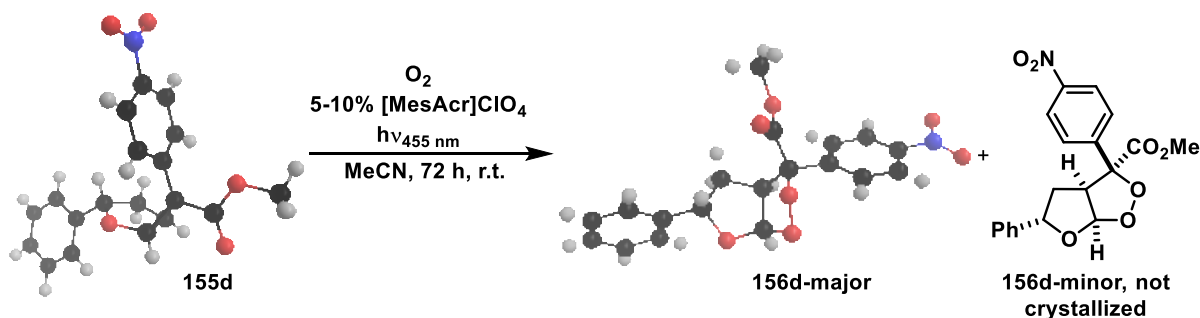


Figure 12: Transformation of the electron deficient substrate, depicted with the available crystal structures.

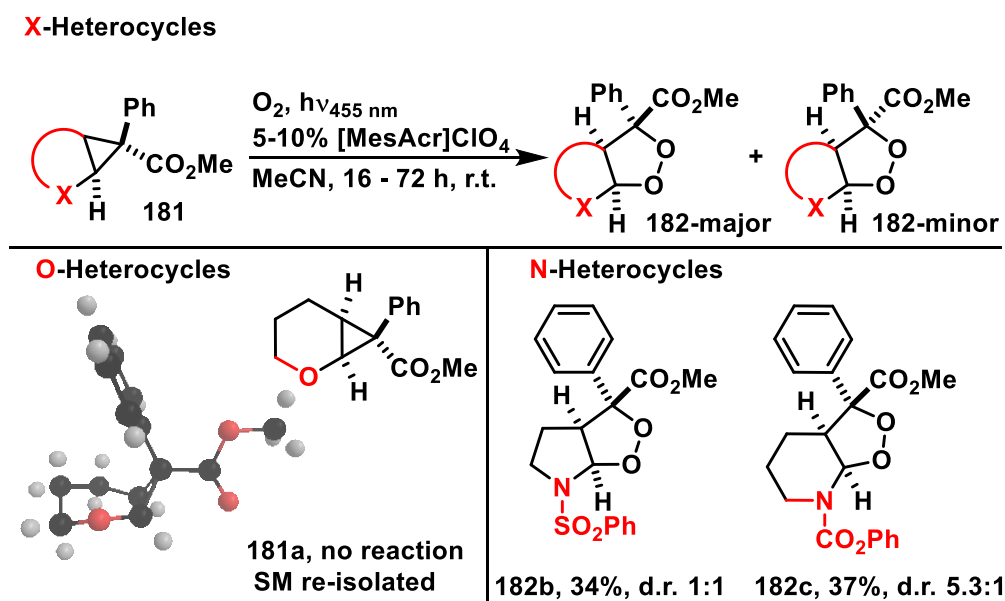
Not only electronically different substituents were tested, but also the sterically more demanding yet electronically neutral 4-Ph substituent was introduced (**155b**). With this, a low yield (10%) of a product exhibiting the characteristic <sup>1</sup>H-NMR signals for the peroxide moiety was isolated (**156b**), but could not be purified to a sufficient degree. No other distinct reaction products were identified, instead a similar precipitate as in the case of the electron rich substrate **155a** was observed.

After all, changes on the aryl substituent of the cyclopropyl moiety had huge impact on the outcome of the reaction, which was expected as this moiety plays a crucial role in the



transformation from a mechanistic point of view. While giving interesting clues towards the possible mechanism, all of the changes were detrimental to the yield.

Consecutively, the limitations of the variations of the heterocycle were to be investigated (Scheme 59). First, instead of the five-membered furan substrate, the next larger ring size, a six-membered pyran derivative **181a** was subjected to the transformation. However, the reaction was still not completed after three days of irradiation. After removal of the solvent, the crude NMR revealed that indeed very little conversion had taken place. Most of the starting material was intact, which was quite astounding given the high reactivity of the oxygen species which are produced under these conditions, and the redox potential of **181a** being in range of the catalyst. To exclude experimental error, the reaction was carefully repeated, with the same outcome. It seemed that the small steric change had a huge impact on the substrate's reactivity. This was an important riddle to solve and will be discussed in further detail in chapter 4.7 but the underlying issue here is thought to be the reversibility of the oxidation and the cyclopropane ring opening, which may proceed less likely in the six-membered pyran derivative.

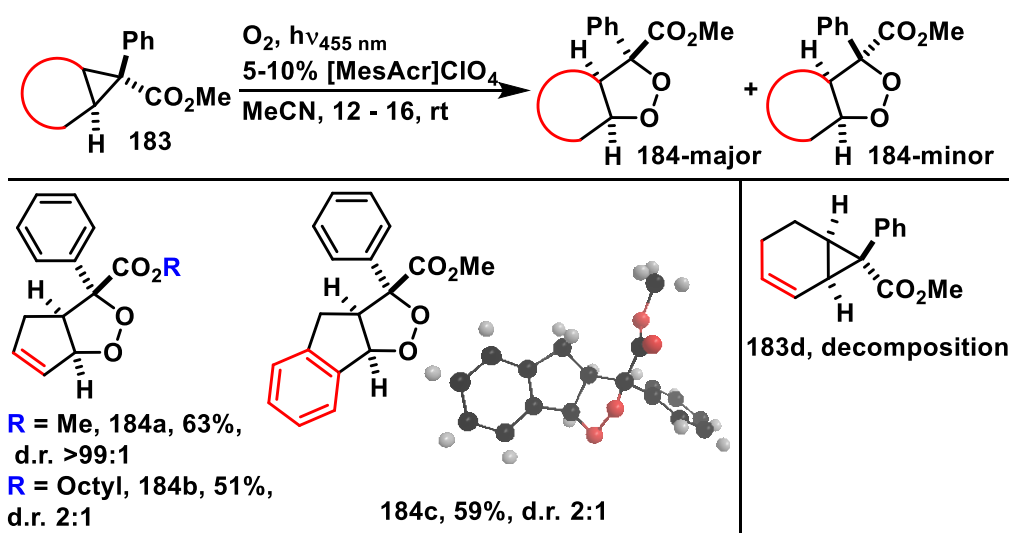


Scheme 59: Variations on the heterocycle.

While the switch from five- to six-membered oxygen-heterocycles did radically change the outcome, the analogous variation was possible with nitrogen containing heterocycles derived from pyrrolidine (**182b**) and piperidine (**182c**, Scheme 59). With these two substrates, the yield was generally lower than with the model substrate **157**, but in a comparable range. This may be because of the  $sp^2$ -hybridization of the nitrogen centre, which leads to planarization and represents a key difference to the pyran-derived substrate.

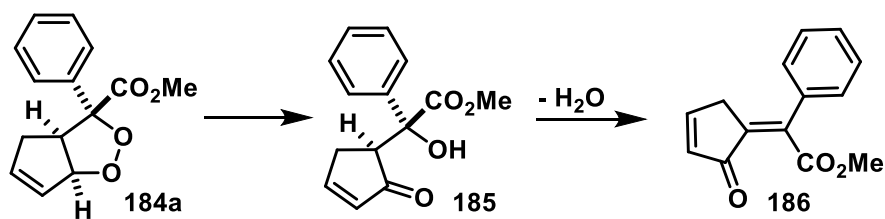
Delighted with the results for the nitrogen-cycle, we asked if  $sp^2$ -hybridized carbocycles may also be suitable substrates for the peroxidation (Scheme 60). The starting materials were accessed *via* cyclopropanation of cyclopentadiene, indene and cyclohexadiene. In case of cyclopentadiene this required the use of large excess of the diene substrate, as it was possible to cyclopropanate this substrate twice.<sup>151</sup>

### Carbocycles



Scheme 60: Transformations of carbocycles.

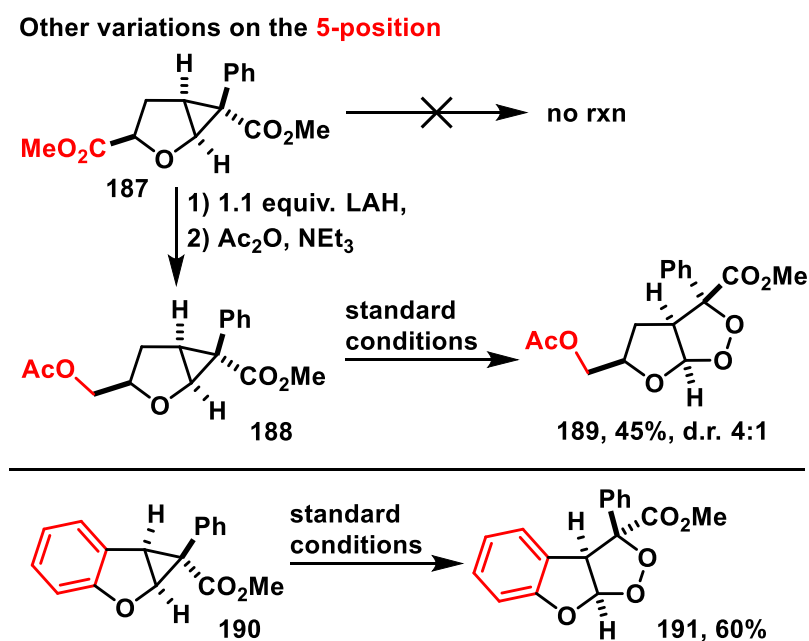
To our delight, the peroxidation proceeded well for the two five-membered rings, with the indene product **184c** being confirmed by X-ray crystallography. Two different esters were synthesized for the cyclopentadiene-derived substrate, and while both were successfully transformed, the small methyl ester **183a** did only give rise to one diastereomer, the larger octyl ester **183b** gave two diastereomers as expected based on the previous observations. For the first case, it can be hypothesized, that both diastereomers may undergo follow-up reactions, but the minor diastereomer undergoes further transformations more readily, leading to its consumption, and therefore only one diastereomer is observed. While it is possible that this reaction may be selective, it is very unlikely, as for the larger ester, this behaviour is not observed. However, the reasons for this behaviour were not further explored so far. Furthermore it must be noted, that the reproduction of the reaction of substrate **183a** was difficult, and for the peroxide, ring-opening of the oxygen bridge was observed to varying degrees (Scheme 61).



Scheme 61: One possible route of degradation for peroxide **184a**.

This spontaneous opening of the peroxide-bridge was observed to a significant degree only in the carbocycles, while in the other peroxides, a base was required to trigger the first step. The second step, *i.e.* the elimination of water, yielding product **186**, was only found in the carbocycles, presumably because of the formation of a larger conjugated system.

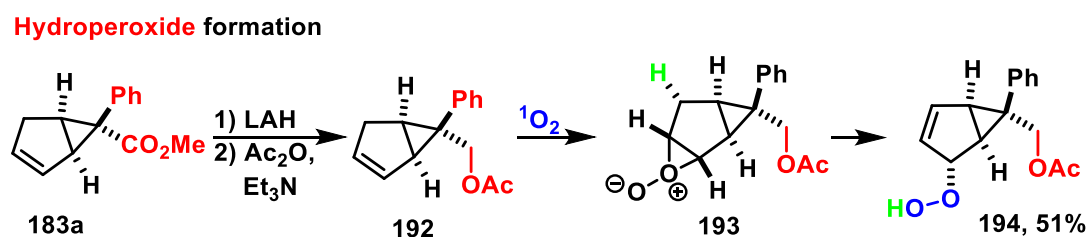
Other variations included non-aryl substituents on the 5-position (Scheme 62). Here an ester (**187**) and a  $\text{CH}_2\text{OAc}$ -group (**188**) derived from the ester by reduction and protection were tested. Compound **187** comprising an ester group did not show conversion under standard conditions, presumably because of the strong electron withdrawing effect of the ester, which would destabilize the intermediate. To confirm that, in this case, an electronic effect prohibits the reaction, and not a steric influence as with the pyran example discussed above, the ester on this position was reduced to an alcohol and consecutively acetate-protected (**188**). This compound was successfully transformed to peroxide **189**, giving a yield in the range of the unsubstituted furan compound.



Scheme 62: Variations on the 5-position other than aryl substituents.

A further variation on the 5-position was the introduction of an aromatic system, which is actually conjugated with the furan's oxygen. This case was investigated using benzofuran derived **190**. Transformation under standard conditions gave, presumably, the peroxide **191**. Judging from the NMR, the peroxide formed, albeit only one diastereomer was observed. However, mass spectrometry revealed only the mass of the starting compound, without the addition of di-oxygen. Consecutively testing its stability, compound **191** proved to be stable at 6 °C (stored in the refrigerator) for three months, without significant changes to the NMR. Sadly, the product was observed as an oily liquid, which did not crystallize, so no X-ray analysis could be performed. The formation of the peroxide is still supported by the NMR and therefore proposed – oxygen may be lost easily under HRMS-conditions. A possible explanation for the observation of only one diastereomer is the interaction of the two  $\pi$ -systems in the starting material, which may prevent the isomerisation of the ester and aryl group.

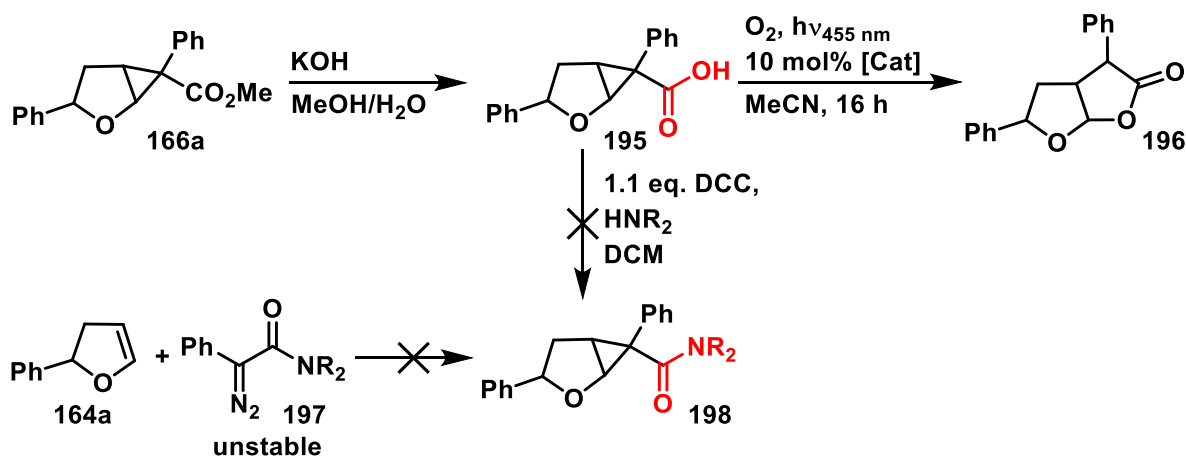
So far, the only successful variation on the cyclopropyl-ester was the exchange of methyl- to octyl-ester. This was done in order to make the resulting peroxides more lipophilic, which was found to have a favourable influence on the biological activity against malaria-plasmodia, discussed in the respective chapter. Another variation was tested on the cyclopentene-derived substrate **183a**, where a reduction of the ester was performed, and the resulting alcohol was acetate protected, giving rise to compound **192**. After the photoreaction under standard conditions, instead of a peroxide bridge, hydroperoxide formation with an intact cyclopropyl ring was observed (**194**). This may be explained by the reaction of the double bond in a Schenck-ene-type reaction (**193**, Scheme 63).



Scheme 63: Variations on the cyclopropyl-ester group.

This example shows that the ester itself, with its electron withdrawing effect, is required for the reaction to produce a peroxide bridge. A possible variation of the ester, which does not completely change its electronic effects, is an amide. Two routes to amide **198** are possible, but unfortunately could not be achieved so far (Scheme 64). The synthesis from scratch, using a phenyldiazoamide **197**, is impossible, as the required diazo compound is not stable and

undergoes intramolecular reactions in the presence of the Rh-catalyst. Likewise, no functioning protocol could be developed to make the amide from the free acid **195**, which is obtained upon ester hydrolysis after cyclopropanation. None of the desired products was observed after applying a standard coupling procedure featuring DCC. The free acid also did not undergo the photoreaction to the desired endoperoxide, instead, among decomposition products, furo[2,3-b]furan **196** was observed, arising from intramolecular cyclization.<sup>143</sup>



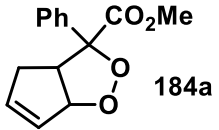
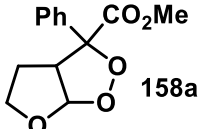
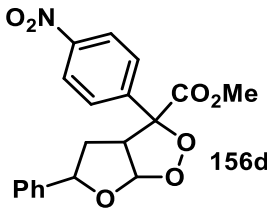
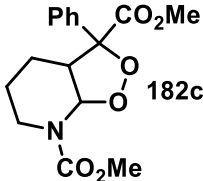
Scheme 64: Attempted variations on the cyclopropyl-ester.

After all, a reasonable variety of derivatives was synthesized, showing overall good to medium yields in the endoperoxide-formation, and laying a good foundation for the biological tests.

## 4.5 Stability of the Endoperoxides

Apart from the biological tests and the cyclovoltammetry data discussed at the beginning of this chapter (and further in the chapter “Mechanistic Studies”), also data on the stability of the endoperoxides was gathered by subjecting them to thermal analysis (Table 8). Peroxides and especially endoperoxides are regarded as prone to spontaneous decomposition, and handling them safely, especially in view of a gram-scale experiment producing a significant amount of potentially explosive substance, required additional data. Thermal analysis allows for the determination of decomposition temperatures.

Table 8: Decomposition temperatures.

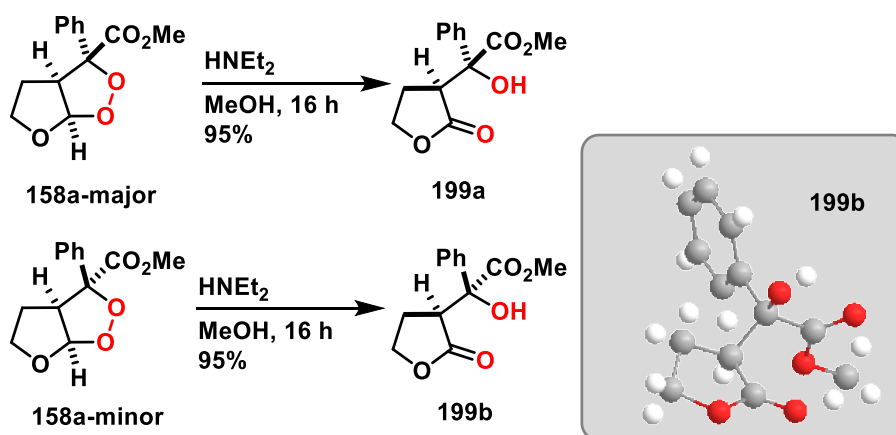
#	compound	decomposition temperature as determined by thermal analysis
1	 184a	189 °C
2	 158a	212 °C
3	 156d	290 °C
4	 182c	303 °C

Experimental details see SI.

To our delight, spontaneous decomposition did not turn out to be an issue with the compounds synthesized during this work, which all show astounding thermal stability. The lowest measured decomposition temperature was observed for the carbocyclic compound **184a** at 189 °C, indicating that the compounds are presumably safe to handle in view of possible explosive characteristics.

## 4.6 Transformations of the Endoperoxides

While the endoperoxides were comparably stable against thermal decomposition, they readily undergo transformations in basic media. As literature shows, endoperoxides undergo a variety of reactions<sup>152</sup>, among them the opening of their peroxide bridge under basic conditions, or even when simply stirred in protic solvents such as methanol.<sup>147</sup> When peroxide **158a-major** was stirred in methanol with catalytic amounts of diethylamide, the below shown lactone **199a** was formed (Scheme 65).

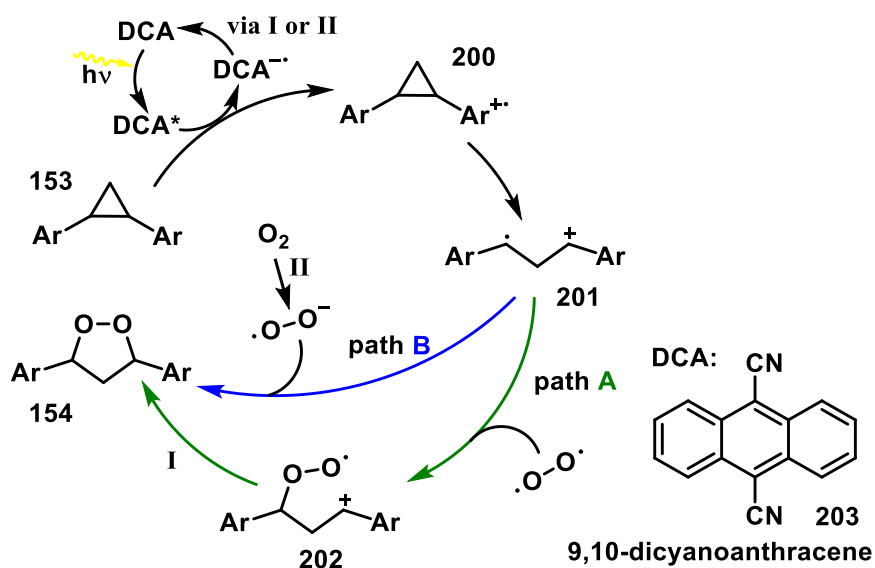


Scheme 65: Opening of the peroxide moiety under basic conditions.

The reaction proceeded under complete stereocontrol, meaning that both diastereomers opened to their respective lactone under conservation of the stereoinformation at the quaternary carbon. This is supported by the obtained X-ray structure of lactone **199b** derived from **158a-minor**. While the obtained compounds had been unknown and so far no direct application is known, the lactones comprise several vectors for further transformations and accessible under full stereocontrol.

## 4.7 Mechanistic Studies

The photochemical peroxidation of diarylcyclopropanes was first discovered in the 1980s and the mechanism was consecutively studied with the means available at the time.<sup>141, 153</sup> The catalyst used was dicyanoanthracene (DCA **203**), in conjunction with 405 nm light generated by a high-pressure mercury lamp with a  $\text{NH}_3\text{-CuSO}_4$  solution as optical filter. Otsuji *et al.* performed a number of key experiments investigating the mechanism, most importantly showing that the reaction was distinctly different from common dye-sensitized oxygenation<sup>154</sup>, as the reaction is not triggered by the formation of singlet-oxygen *via* energy-transfer (ET), but rather oxidation of the substrate by the catalyst. The proposed mechanism (Scheme 66) starts with the irradiation of the catalyst **203**, bringing it to its excited form. Upon encounter with a diarylcyclopropane (**153**), a single-electron transfer (SET) takes place, and the substrate is oxidized to the radical cation (**200**), with the initial site of the oxidation being one of the aryl groups. This triggers a fast ring opening, separating the site of radical and cation (**201**).



Scheme 66: Mechanism as proposed by Otsuji *et al.*<sup>141</sup>

From there, two different pathways may lead to the endoperoxide. Path A has triplet oxygen attached at the radical site (**202**), followed by the reduction of the cation by the DCA-anion (I), regenerating the catalyst and finally completing the ring expansion.

Path B requires the DCA-anion to reduce oxygen to the superoxide radical anion (II), which then combines with the said radical-cation, leading to the endoperoxide.



Otsuji reported acetonitrile being the best solvent and the yield dropping when less polar solvents were used.<sup>155</sup> However, using aromatic hydrocarbons such as phenanthrene as additives was found to significantly accelerate the reaction, but leading to opening of the endoperoxide and consecutive further oxidation on less electron rich diarylcyclopropanes (*i.e.* none of the two aryl groups being *p*-OMe substituted).

Furthermore the effect of inorganic salts on the reaction had been examined, showing a benign effect of  $BF_4^-$  and  $ClO_4^-$  anions, significantly accelerating the reaction.<sup>156</sup> The effect of the perchlorate on the reaction was also shown to be dependent on the counter-cation, with the magnesium-salt giving the best results and up to 10-times faster reaction compared to saltless conditions. Otsuji *et al.* suspected the added salts to suppress electron back-transfer after the initial oxidation, therefore inhibiting the back-reaction, by interacting with the ionic radicals (**201-203**) generated.

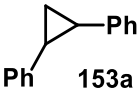
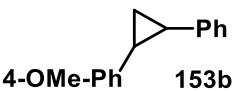
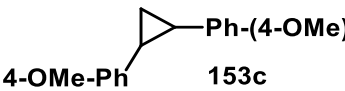
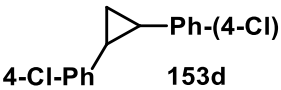
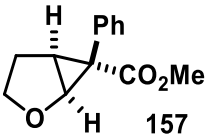
Yoon *et al.* in 2014 used a transition-metal based catalyst, namely  $[Ru(bpz)_3](PF_6)_2$  (**2**), in conjunction with a 23 W fluorescent light bulb to facilitate the transformation on substrates very similar to the ones reported by Otsuji.<sup>140</sup> Mostly electron rich diarylcyclopropanes were converted in excellent yields, and the mechanism proposed does not deviate from Otsuji's.

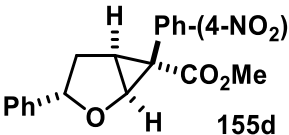
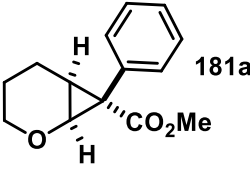
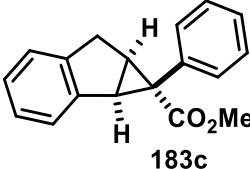
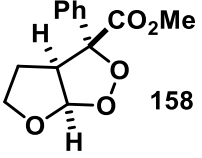
As the reaction described in this work significantly expands the substrate scope, facilitating the conversion of structurally complex arylcyclopropanes, even comprising very electron deficient aryl-substituents, the mechanism required additional investigation.

First, the reaction was shown to be dependent on both light and catalyst (Table 7). Furthermore, it was shown that the catalyst used by Yoon *et al.*,  $[Ru(bpz)_3](PF_6)_2$  (**2**), did not lead to product formation, even with the electron rich substrate **155a**. This showed that Fukuzumi's catalyst must exhibit unique properties, which were found to be the appropriate oxidation potential. Conveniently, the  $[MesAcr]^+$  catalyst comes with  $BF_4^-$  or  $ClO_4^-$  counterions (because they are stable towards oxidation, compared to *e.g.*  $Cl^-$ ), which were shown by Otsuji to have a benign influence on the reaction. The salt effect was also observed, when  $[Ir]$ , which did not facilitate the oxygenation on its own, led to complete conversion of the starting material with  $Mg(ClO_4)_2$  as an additive. However, no peroxide formation, but rather decomposition was observed in this case. Using common singlet-oxygen producing catalysts, such as  $[Ru(bpy)_3]^{2+}$  or Rose Bengal, was also ineffective, reproducing the initial finding of Otsuji, that singlet-oxygen itself was not sufficient for the photooxygenation.

More physicochemical data was therefore gathered, first of which the reduction potentials of several substrates and the catalysts were measured, which are shown in Table 9 in comparison to selected examples of the previously discussed diarylcyclopropane compounds.

Table 9 Comparison of electrochemical data for several selected compounds.

#	Compound	$E_{(M/M^+)} \text{ vs. SCE [V]}$	Comment
1	[Ru(bpz) <sub>3</sub> ](PF <sub>6</sub> ) <sub>2</sub> ( <b>2</b> )	1.4 <sup>a)</sup>	Yoon's catalyst. Most substrates presented herein not in range.
2	DCE ( <b>203</b> )	1.285 <sup>b)</sup>	Otsuji's catalyst. Most substrates presented herein not in range.
3	 <b>153a</b>	1.09 <sup>b)</sup>	Decomposition, no dioxolanes isolated, neither under Otsuji's nor Yoon's conditions.
4	 <b>153b</b>	0.795 <sup>b)</sup>	Up to 99% <sup>a), b)</sup>
5	 <b>153c</b>	0.505 <sup>b)</sup>	Up to 99% <sup>a), b)</sup>
6	 <b>153d</b>	0.102 <sup>b)</sup>	No dioxolanes isolated under Otsuji's conditions, Yoon not tested.
7	[MesAcr]ClO <sub>4</sub> ( <b>9</b> )	2.07 <sup>c)</sup>	Fukuzumi's catalyst. Substrates presented in this work in oxidation range
8	Ir[dF(CF <sub>3</sub> )ppy] <sub>2</sub> (dtbbpy)PF <sub>6</sub> ( <b>5</b> )	1.69	No reaction under standard conditions. Some conversion with Mg(ClO <sub>4</sub> ) <sub>2</sub> as additive.
9	 <b>157</b>	1.95	Model substrate

10	 155d	Two peaks: 1.84 2.21	Highly electron deficient aryl group on cyclopropane; Origin of second, lower oxidation peak unknown.
11	 181a	2.00	Unreactive albeit in range of catalyst's oxidation potential.
12	 183c	1.87	Successful conversion
13	 158	2.83	Product of model substrate. Ox.-potential far higher than substrate's.

a)Ref.<sup>140</sup>, b)Ref.<sup>141</sup>, c)Ref.<sup>148</sup>. Reduction potential converted from Ag/Ag<sup>+</sup>-electrode to SCE by subtracting 45 mV.

The diarylcyclopropanes **153** used in the literature precedents exhibit clearly lower oxidation potentials than the donor-acceptor-substituted cyclopropanes employed in this work. Only the oxidation potential of Fukuzumi's catalyst (**9**) is high enough to enable a SET to these substrates, making the literature conditions incompatible with them. However, not only electronic properties matter: The case of the unreactive cyclopropanated pyran substrate **181a** shows that while the substrate may be oxidized by the catalyst, there are also steric requirements to enable a successful cyclopropane ring opening. It must be suspected that this substrate is actually oxidized but undergoes back-reaction more efficiently than any irreversible transformation, leading to conversion of the radical cation. In hindsight, the addition of Mg(ClO<sub>4</sub>)<sub>2</sub> might have been an interesting experiment for this substrate.

Further insight in the mechanism may be gained by quenching experiments, which are used to evaluate the interaction of the catalyst with the substrate. For a given catalyst concentration different amounts of quencher, *i.e.* substrate, are added and the fluorescence intensity (Figure 13) as well as the fluorescence lifetime (Figure 14) of the catalyst are observed (for details, see experimental part). Catalyst [MesAcr]ClO<sub>4</sub> and substrate **157** were used.

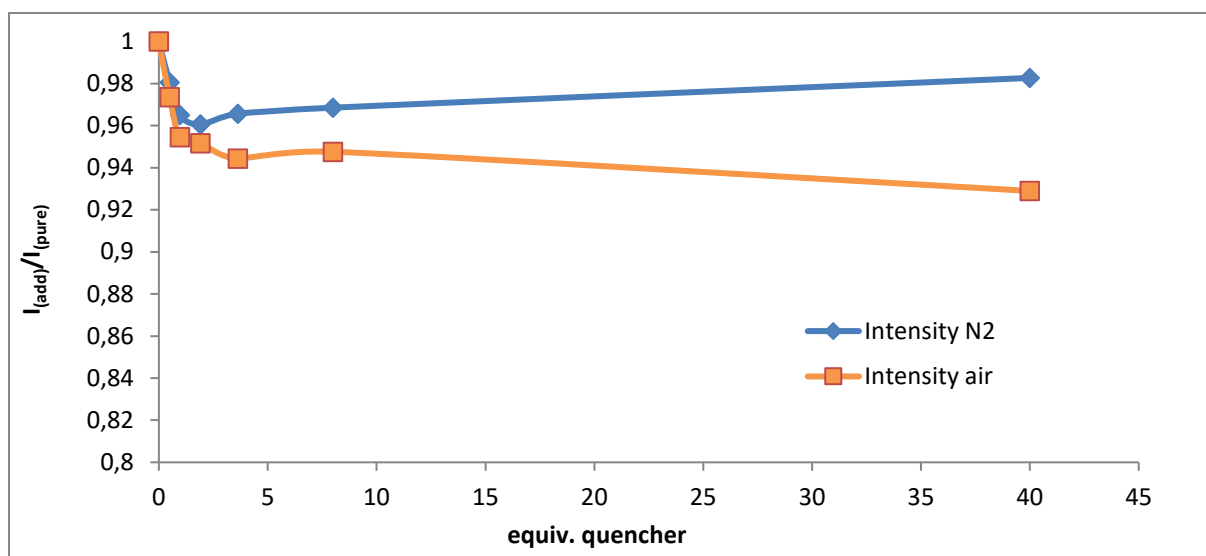


Figure 13: Fluorescence intensity quenching.

The fluorescence intensity after addition of the quencher is shown relative to the blank intensity of the catalyst and plotted against the equivalents of quencher added. It can be seen, that the fluorescence intensity drops until about five equivalents of quencher are added, showing a positive interaction between substrate and catalyst, and then stays relatively constant upon further addition, indicating a saturation of the catalyst. The interaction was examined both under air and under degassed conditions, as oxygen may influence the interaction. This is clearly true, as the overall intensity under oxygen is higher than under degassed conditions (see experimental part), but the relative quenching effect is very similar. However, the quenching effect itself is quite small, as the intensity does not decrease more than 8% of its original value. Plotting the interaction in a Stern-Volmer-style was inconclusive and did not allow the distinction of dynamic and static quenching.

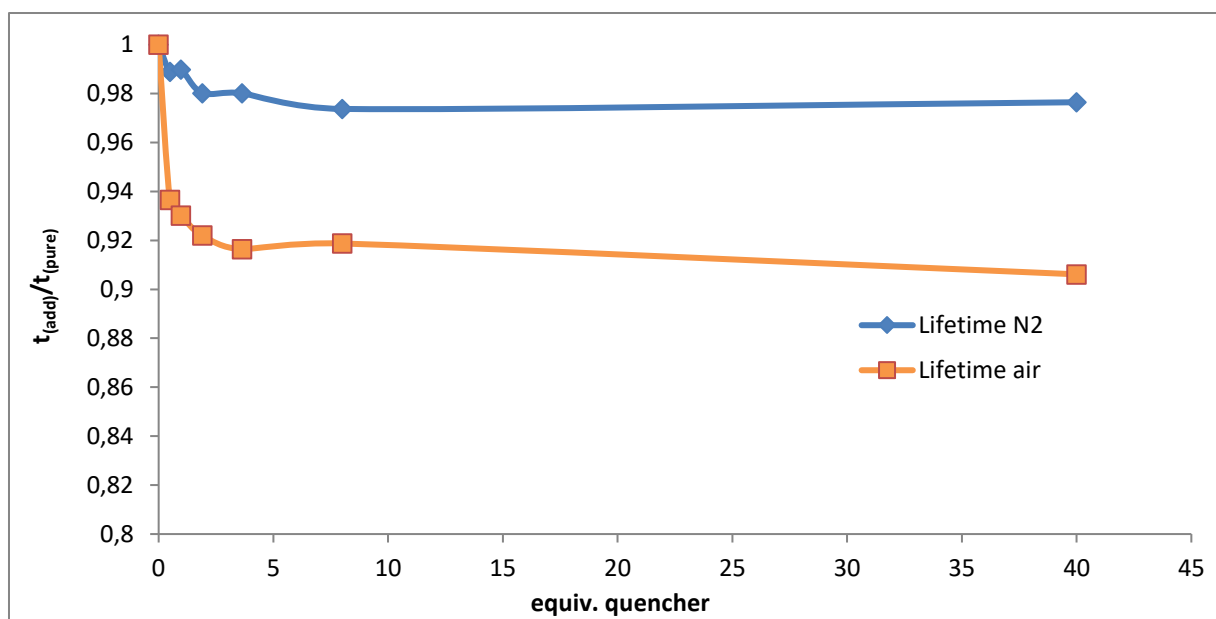


Figure 14: Fluorescence lifetime quenching.

The analogous plot of the lifetime-quenching shows similar tendencies, but a greater impact of oxygen atmosphere, which is expected as the catalyst can react with oxygen itself.

As the quenching was clearly detectable, but rather small, a collaboration with Dr. Roger Jan Kutta from the group of Prof. Patrick Nürnbergger was initiated to investigate further spectroscopic studies on the system. Because a reversible color change from yellow to orange was observed when it was irradiated with blue light, indene substrate **183c** was chosen for time-resolved and stationary UV/vis studies on the photocatalytic system. These experiments were performed by Dr. Jan Roger Kutta and Svenja Wortmann at the University of Regensburg.

First, a spectrum of the components of the reaction was measured in MeCN, then the reaction mixture (substrate concentration 100 mM) was illuminated using a blue LED ( $\lambda = 450$  nm), leading to a change in the spectrum at around 300 nm. When the illumination was stopped, the additional contribution decayed with an approximate lifetime of 500 s and resulted in a spectrum showing additional contributions, indicating conversion (Figure 15).

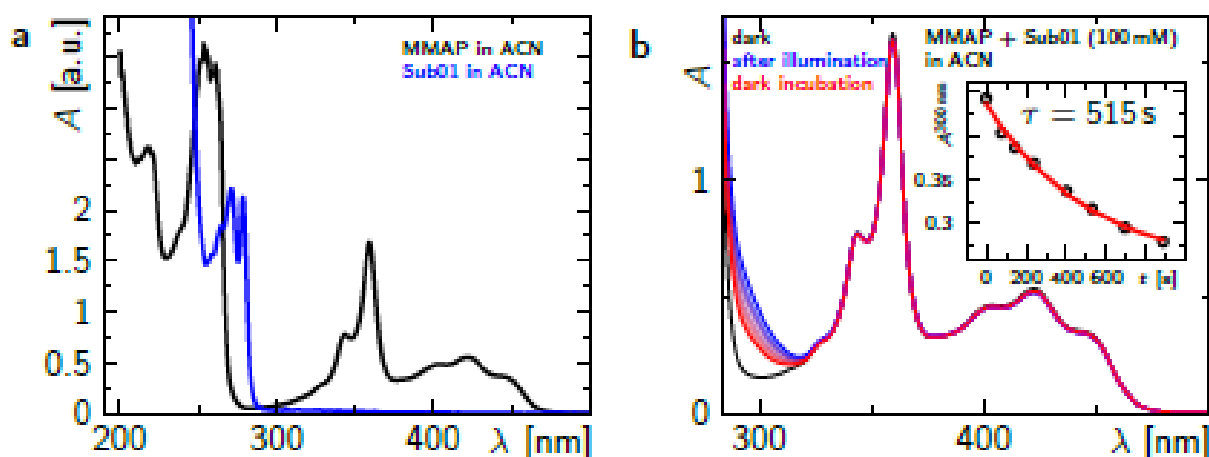


Figure 15

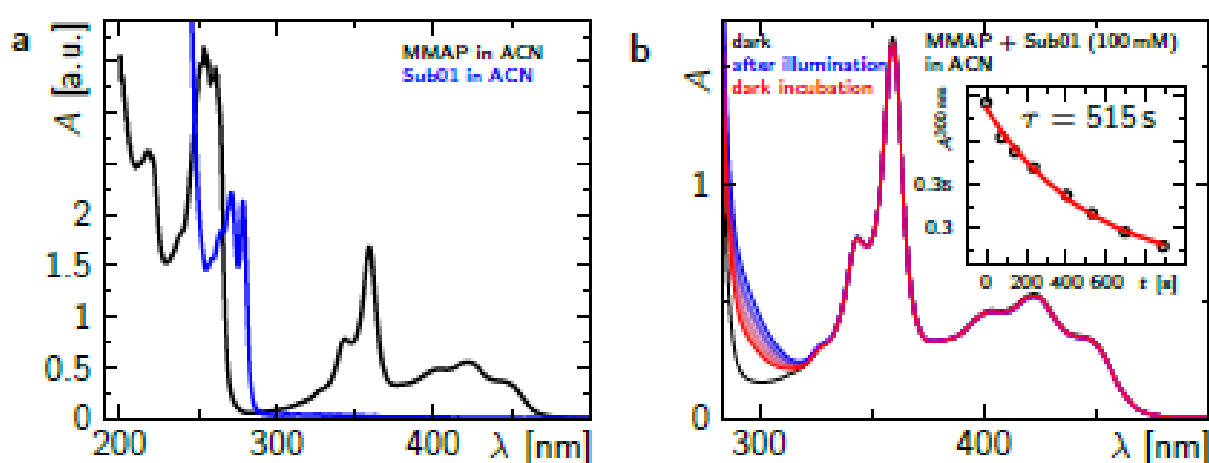


Figure 15: a: stationary absorption of [MesAcr]ClO<sub>4</sub> and **183c** in MeCN; b: Sequence spectra of the system [MesAcr]ClO<sub>4</sub> and **183c** in MeCN after illumination with 450 nm light and incubation in the dark. Figures taken from report by R. J. Kutta.

Consecutively, the time-resolved UV/vis absorption and emission spectra of the catalyst were measured, giving further insight into its behaviour (see experimental part), before the catalyst was examined in presence of the substrate (100 mM), giving the spectra shown below (Figure 16).

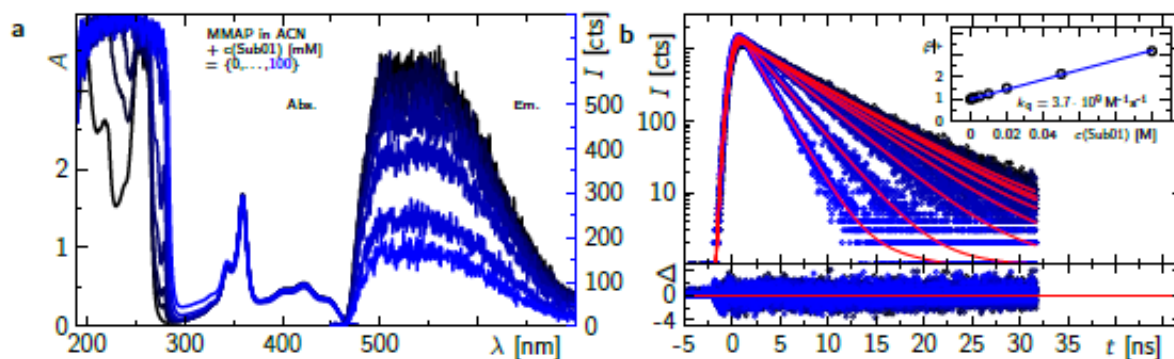


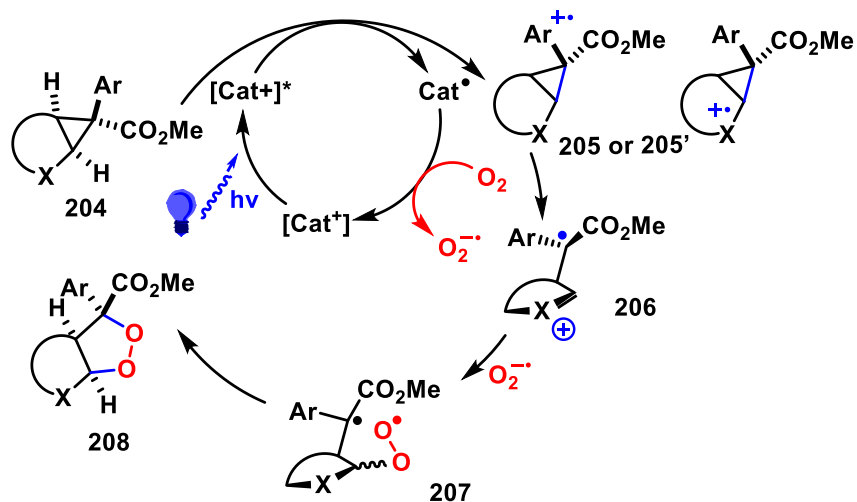
Figure 16: Quenching of the excited singlet state of [MesAcr]ClO<sub>4</sub> by substrate **183c** in oxygen-saturated MeCN. Figures taken from report by R. J. Kutta. a: stationary absorption and emission spectra in dependence on the

substrate-concentration as indicated. b: Time-resolved emission after exciting at 443 nm and detecting at 490 nm ( $\Delta t_{\text{IRF}} \sim 1$  ns) in dependence of the substrate concentration as indicated. The red lines represent exponential fits, the inset shows the Stern-Volmer plot.

In the presence of the substrate the lifetime of the charge-transfer state  $^1S_{1,CT}^*$  was notably reduced while the lifetime of the locally excited state  $^1S_{1,LE}^*$  was not altered, leading to the conclusion that the reaction between the substrate and the  $^1S_{1,CT}^*$  species of [MesAcr]ClO<sub>4</sub> leads to singlet-born radical pairs, which recombine faster than they are formed. Such recombination behaviour is often observed for excited singlet state reactions and can be analyzed *via* a Stern-Volmer analysis, shown in the right spectrum of Figure 16b. Comparison of the calculated bimolecular reaction rate of  $3.7 \times 10^9 \text{ M}^{-1}\text{s}^{-1}$  to the theoretical totally diffusion controlled reaction rate of  $1.86 \times 10^{10} \text{ M}^{-1}\text{s}^{-1}$  shows that approximately 20% of encounters lead to a reaction.

Further spectroscopic experiments on this matter are currently underway, continuing the cooperation.

Taking these findings into account, a mechanism similar to the literature precedent was proposed (Scheme 67). First, a one-electron oxidation takes place on the aryl group adjacent to the cyclopropyl group, forming a cationic radical **205**. The dependence on a sufficiently highly oxidizing catalyst such as [MesAcr]<sup>+</sup> indicates that the first step is indeed a single electron transfer (SET) from the substrate to the catalyst to give rise to **205** *via* oxidation of the arene moiety<sup>11</sup> or to **205'** *via* oxidation of the heteroatom/double bond.<sup>157</sup> Ring opening to **206** results in the separation of the radical and cationic centre, the former being stabilized due to the synergistic push-pull interaction between the ester and the arene group, while the latter profits from mesomeric conjugation with the neighbouring heteroatom or  $\pi$ -system.



Scheme 67: Mechanistic proposal.

**206** is then trapped by superoxide radical anion<sup>155, 158</sup> leading to diradical **207**, which then collapses in a productive manner to the product **208** provided that attack of  $O_2^{\bullet-}$  has taken place *syn* to the neighbouring group.

The striking difference in reactivity between furan (**157**) and pyran (**181a**) ring systems required further investigation, as the oxidation potentials of both the five- and six-membered ring systems were in the range of the catalyst, but only the five-membered analogue was converted, while the six-membered didn't show any significant conversion even after 3 days of irradiation. Therefore, calculations on a B3LYP/6-31G level were used to obtain information on the HOMO-Orbitals (Figure 17).

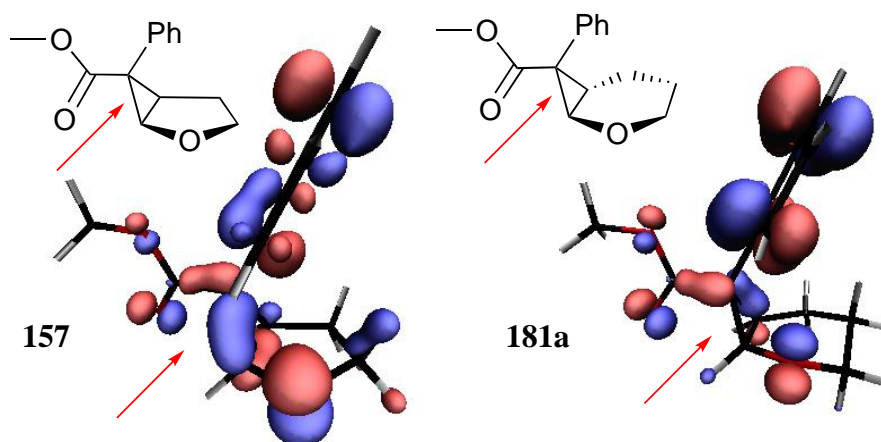


Figure 17: Representation of the HOMO-orbitals of furan and pyran derivatives calculated with GAMESS<sup>159-160</sup> on B3LYP/6-31G level, visualized with VMD<sup>161</sup>.

Both molecule's HOMO-orbitals show electron density localized over the phenyl ring, where the initial oxidation is likely to occur, and over the oxygen of their respective heterocycle. However, there is a significant difference on the *exo*-bond of the cyclopropane, where in the furan derivative this bond is activated, as there is strong electron density observed in this region, while in the pyran derivative this activation is completely missing.

Arguably, the orbitals shown are the orbitals of the unoxidized molecule in its ground state, so one could point out that the orbitals will most certainly change upon oxidation. MM2-simulation was therefore used to obtain further information on the behaviour of the substrate upon oxidation.



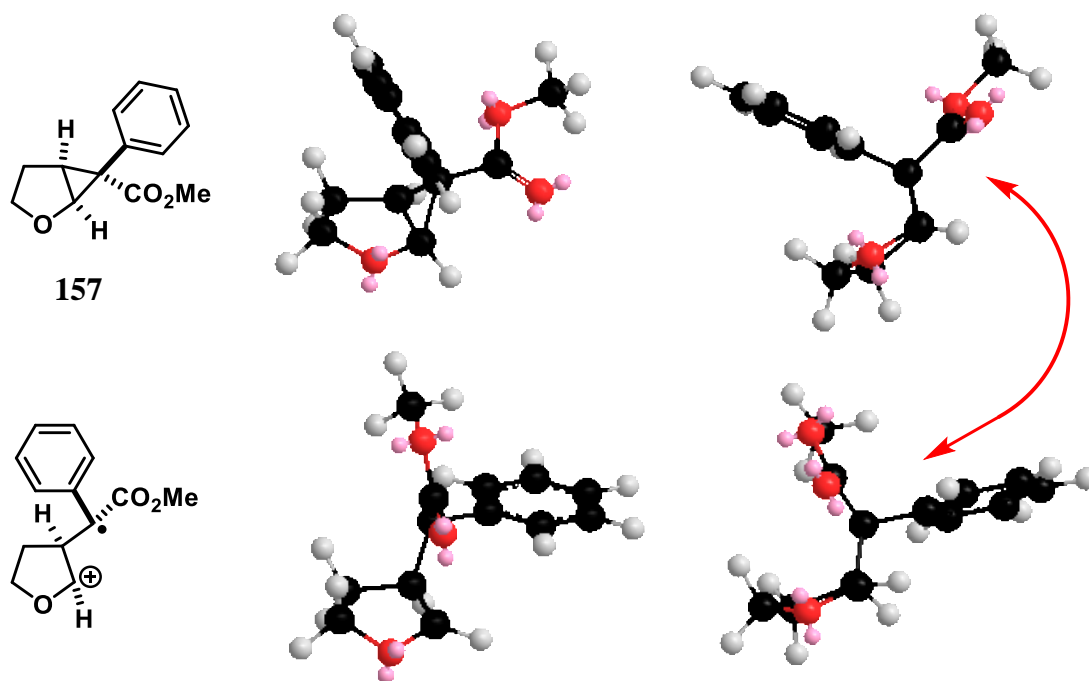


Figure 18: MM2-representaion of the furan model substrate before and after oxidation.

The furan model substrate shows inversion of configuration, as ester and phenyl-group switch places (Figure 18). This corresponds to the observed configuration of the major diastereomer in the peroxide product, where for the major the configuration has switched and in the minor the initial configuration is conserved.

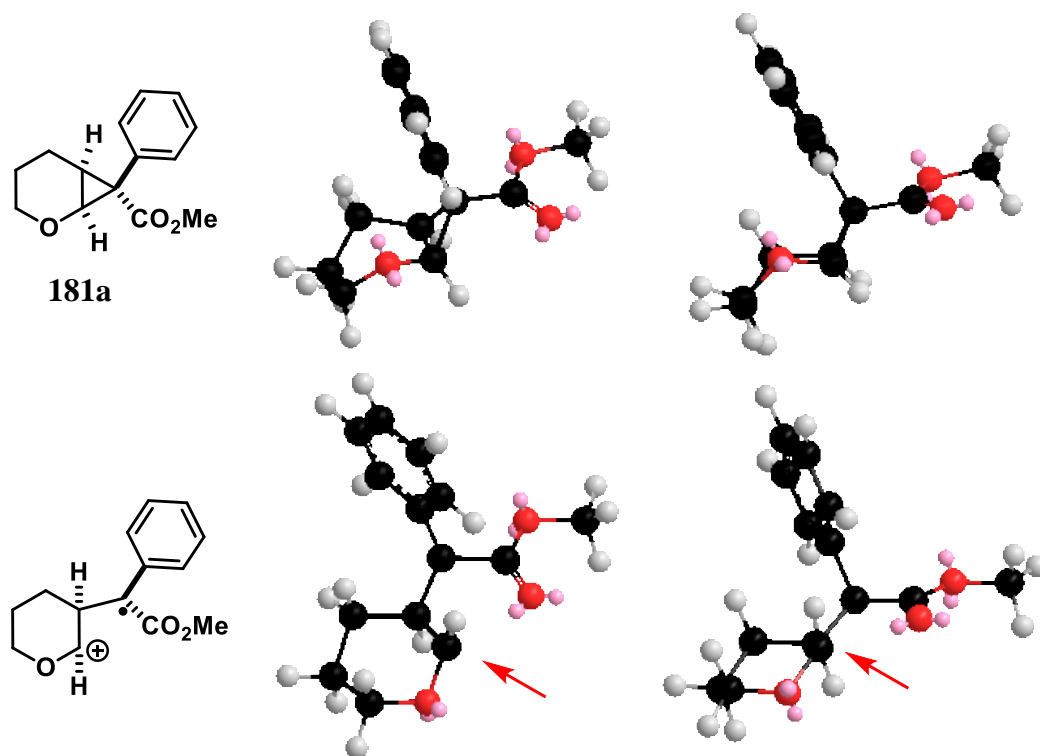


Figure 19: MM2-Representation of the pyran derivative before and after oxidation.

For the pyran derivative, the MM2-representation does not show a similar change of configuration for ester and phenyl group (Figure 19). However, the position of the proton marked with a red arrow is significantly altered in comparison to its counterpart on the furan derivative. It is suspected, that such an orientation would block the reaction with the oxygen species from one side, which prevents a successful progress of the reaction, but rather leads to back-reaction.

While in the literature precedents for the oxygenation of diarylcyclopropanes electron withdrawing substituents were not tolerated, the conditions identified in this work were even able to transform the *para*-nitrophenyl-derivative, albeit very slowly and with low yields. As an oxidation of such electron deficient aromatic systems can be considered impossible for Fukuzumi's catalyst, the question where the initial oxidation would take place was elucidated by B3LYP/6-31G level calculations of the HOMO-orbital (Figure 20).

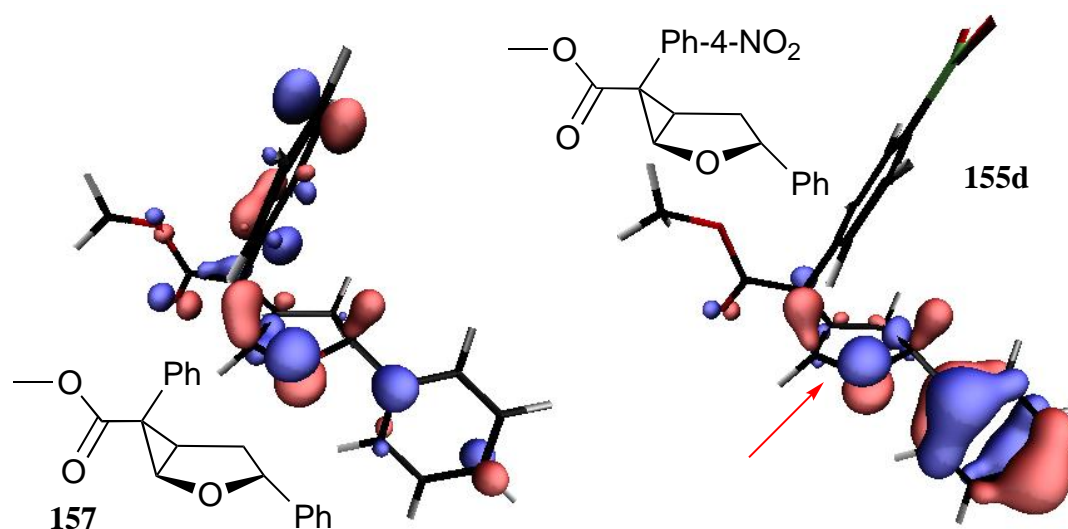


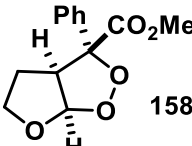
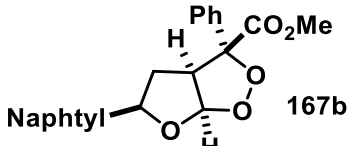
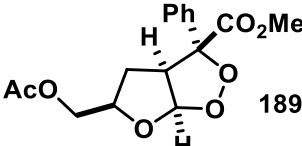
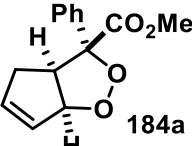
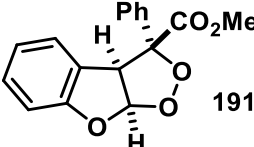
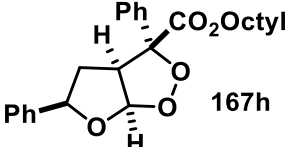
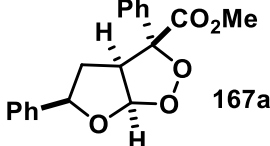
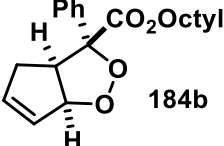
Figure 20: Representation of the HOMO-Orbitals of substrates **155d** and **157** calculated with GAMESS<sup>159-160</sup> on B3LYP/6-31G level, visualized with VMD<sup>161</sup>.

As expected, the HOMO-Orbital does not extend over this electron deficient group (Figure 20, right), but does include the heteroatom of the five-membered ring (red arrow). As oxidation of this ether-oxygen may lead to the same intermediate (Scheme 67, **205'**) we hypothesize this process to allow for the observed slow conversion of compound **155d** to the corresponding peroxide. Oxidation of the heteroatom may be an alternative pathway to the oxidation of the aryl moiety for similar substrates, *e.g.* for compound **155c**. For more depictions of HOMO-orbitals of selected substrates see experimental section.

## 4.8 Biological Tests

The endoperoxide scaffold is of high biological interest, as it is presumed to cause the anti-malarial properties of drugs such as artesunate. Malaria is a disease caused by *Plasmodium* parasites, transmitted by *Anopheles* mosquitoes, which thrive in warm climate and are therefore expanding due to the climate change. While artesunate exhibits superior effectiveness against Malaria, there is a growing resistance against artemisinin and its derivatives, which increases the demand for new drugs<sup>162</sup>. Encouraged by the promising results for bicyclic peroxides containing a furan moiety reported by Xu *et al.*<sup>147</sup>, a selection of endoperoxide containing compounds obtained in this study was tested against *Plasmodium Falciparum* to assess their biological activity. The testings took place at the Max Planck Institute of colloids and interfaces in Berlin at the work group of Prof. Seeberger, mainly by Felix Goerdeler (Table 10).<sup>149</sup>

Table 10: Biological activity against *P. falciparum* in vitro.

#	compound	IC50	#	compound	IC50
1	 <b>158</b>	>100	5	 <b>167b</b>	40
2	 <b>189</b>	>100	6	 <b>184a</b>	19
3	 <b>191</b>	80	7	 <b>167h</b>	14
4	 <b>167a</b>	60	8	 <b>184b</b>	2.5

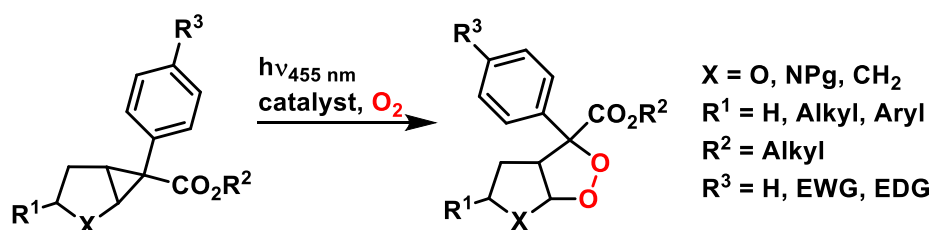
IC50 [ $\mu\text{mol}$ ]. For procedure, see experimental section.

The model compound **158** displayed no activity ( $\text{IC}_{50} > 100 \mu\text{mol}$ ) in the tested concentration range, while for the closest literature compound, which comprises a methyl group instead of an ester, an  $\text{IC}_{50}$  value of  $7 \mu\text{mol}$  is reported.<sup>147</sup> The  $\text{IC}_{50}$  improved from  $60 \mu\text{mol}$  for phenyl-substituted compound **167a** (entry 4) to  $40 \mu\text{mol}$  for naphthyl-substituted **167b** (entry 5), demonstrating an increase of activity with increasing lipophilicity. Notably, carbocyclic

compound **184a** was superior by far, which therefore was focus of our interest. To counter the detrimental effect of the methyl ester`s polarity, it was exchanged for an octyl ester, thereby increasing its lipophilicity. This led to a further improvement in both the phenyl substituted (entry 7, **167h**, compared to entry 4, **167a**) as well as the carbocyclic compound (entry 8, **184b**, compared to entry 6, **184a**) with the latter exhibiting a promising IC<sub>50</sub> in the low micromolar range. This led to attempts to transform the ester moiety into an ether or other, less polar moieties, which have not been completed successfully within the range of this thesis. However, further research to increase the lipophilicity of the products may lead to more active compounds, while using the advantages of flow-photochemistry<sup>37</sup> may help to increase the so far mediocre yield.

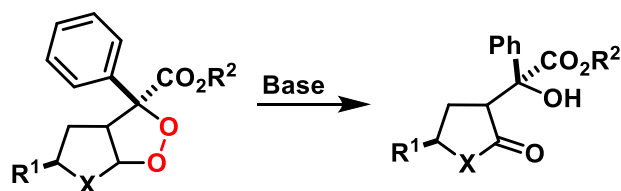
## 4.9 Conclusions

In conclusion the visible light mediated photooxygenation of arylcyclopropanes was expanded to structurally complex fused hetero- and carbocycles by using the highly oxidizing, low-cost organic dye [MesAc]ClO<sub>4</sub> (**9**) instead of transition metal catalysts (Scheme 68).



Scheme 68: Synthesis of various endoperoxides from cyclopropanated carbo- and heterocycles *via* visible light mediated photooxygenation.

While the stereocenter at the benzyl position isomerizes during the oxygenation, the orientation of the other stereocenters in the tested molecules was not altered. This allows for the introduction of chirality, which is especially interesting considering the possible transformation of the peroxides to butyrolactones under basic conditions in high yield. Also, similar structures would be available from the various heterocycles that were successfully transformed to endoperoxides (Scheme 69).



Scheme 69: Possibly accessible structures by treatment of endoperoxides described in this work with base.

Given the encouraging IC<sub>50</sub> values of **167h** and **184b**, which were found to be in the low micromolar range, and the identification of the polarity of the endoperoxides as key structural property influencing the determined activity, the foundation to further research on this compound class was laid.

## 4.10 Experimental Section Endoperoxides

### 4.10.1 General Information

#### Solvents and Chemicals

All commercially available compounds were used as received. Anhydrous solvents were prepared by established laboratory procedures. Ethyl acetate, hexanes (40/60) and DCM were distilled prior to use in chromatography. [MesAc]ClO<sub>4</sub> and [Ir(dtbbpy)ppy<sub>2</sub>]PF<sub>6</sub> were prepared according to the literature.<sup>163-164</sup>

2-Aryl-2-diazoacetates were prepared according to the literature from aryl acetates and tosylazide<sup>119</sup>.

#### Light source in photoreactions

For irradiation, CREE XLamp XP-E D5-15 or OSLOON SSL 80 LED ( $\lambda = 450\text{-}465$  nm, maximum at 455 nm) light emitting diodes were employed.

#### NMR spectroscopy

<sup>1</sup>H, <sup>13</sup>C, <sup>19</sup>F and 2D spectra were recorded on BRUKER Avance 300 or BRUKER Avance III 400 “Nanobay” spectrometers. The spectra were recorded in CDCl<sub>3</sub> unless otherwise specified. The <sup>1</sup>H-NMR chemical shifts are reported as  $\delta$  in parts per million (ppm) relative to the signal of CHCl<sub>3</sub> at 7.26 ppm. Coupling constants *J* are given in Hertz (Hz), with following indications for the multiplicity of the signals: s = singlet, d = doublet, t = triplet, q = quartet, quint = quintet, sept = septet, m = multiplet; to indicate broad signals, the letter b is used in front of the multiplicity indication (*e.g.* bs = broad singlet).

The chemical shifts for <sup>13</sup>C-NMR are reported as  $\delta$  in parts per million (ppm) relative to the center line of CDCl<sub>3</sub> at 77.0 ppm.

#### Chromatography

For column chromatography silica gel 60 (Merck, 0.040-0.063 mm particle size) was used. Thin layer chromatography (TLC) was performed on silica gel 60 F254 coated aluminum sheets (Merck) and visualized with UV and vanillin (2.5 g vanillin, 425 mL EtOH, 50 mL conc. AcOH, 25 mL conc. H<sub>2</sub>SO<sub>4</sub>) or KMnO<sub>4</sub> (1 g KMnO<sub>4</sub>, 2 g Na<sub>2</sub>CO<sub>3</sub>, 100 mL H<sub>2</sub>O) stain.

#### Further analytics

**Melting points** were determined on an OptiMelt MPA 100

**FT-IR spectroscopy** was carried out on an Agilent Technologies Cary 680 FTIR machine with diamond single reflection accessory.

**Mass spectroscopy** was carried out by the Central Analytical Laboratory of the University of Regensburg on Jeol AccuTOF GCX, Agilent Q-TOF 6540 UHD or ThermoQuest Finnigan TSQ 7000 systems.

**X-ray crystallography** was performed on Agilent Technologies SuperNova, Single source at offset/far, Atlas diffractometer or a GV1000, TitanS2 diffractometer at  $T = 123$  K during data collection. The structures were solved with the **ShelXT**<sup>165</sup> structure solution using **Olex2**<sup>166</sup> as the graphical interface. The model was refined with version 2018/3 of **ShelXL**<sup>165</sup> using Least Squares minimization.

**Cyclic voltammetry** was measured on an Autolab PGSTAT 302N setup at 20°C in MeCN containing  $\text{Bu}_4\text{NBF}_4$  as supporting electrolyte. The electrochemical cell consisted of a glassy carbon working electrode, a platinum wire as counterelectrode and a silver wire as reference electrode. The solvent was degassed by  $\text{N}_2$  sparging prior to the measurements, and the redox potentials were referenced against ferrocene as internal standard. The values were then calculated and reported in reference to SCE electrode.

**Optical Rotation** was measured using an Anton Paar MCP500 Polarimeter at 589 nm in the specified solvent.

**Calorimetry** was measured on a Perkin Elmer TGA 7 under synthetic air atmosphere.

**Chiral HPLC** was carried out on a Varian 920-LC with Chiralpak AS-H, Phenomenex Lux Cellulose-1 or 2 as chiral stationary phase (as specified), using mixtures of  $n$ -heptane and  $i$ -PrOH as eluent.

**Fluorescence intensity** was measured with a Horiba Scientific FluoroMax4 Spectrofluorometer.

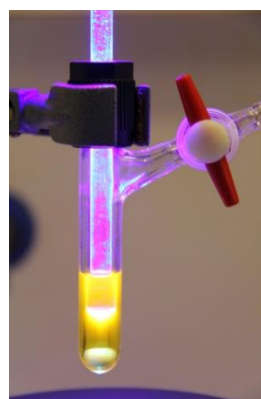
**Fluorescence lifetime** was measured with a Horiba DeltaPro Fluorescence Lifetime System equipped with a 370 nm Deltadiode DD-370.

## Setup

Pre-assembly:

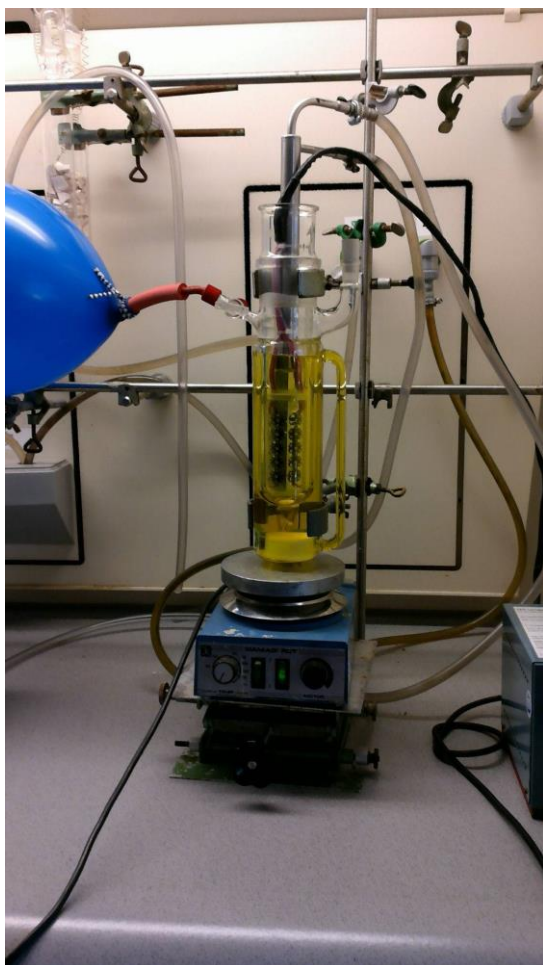


In operation:





Large scale (15 mmol) setup – immersion well reactor:





#### 4.10.2 Biological Testing

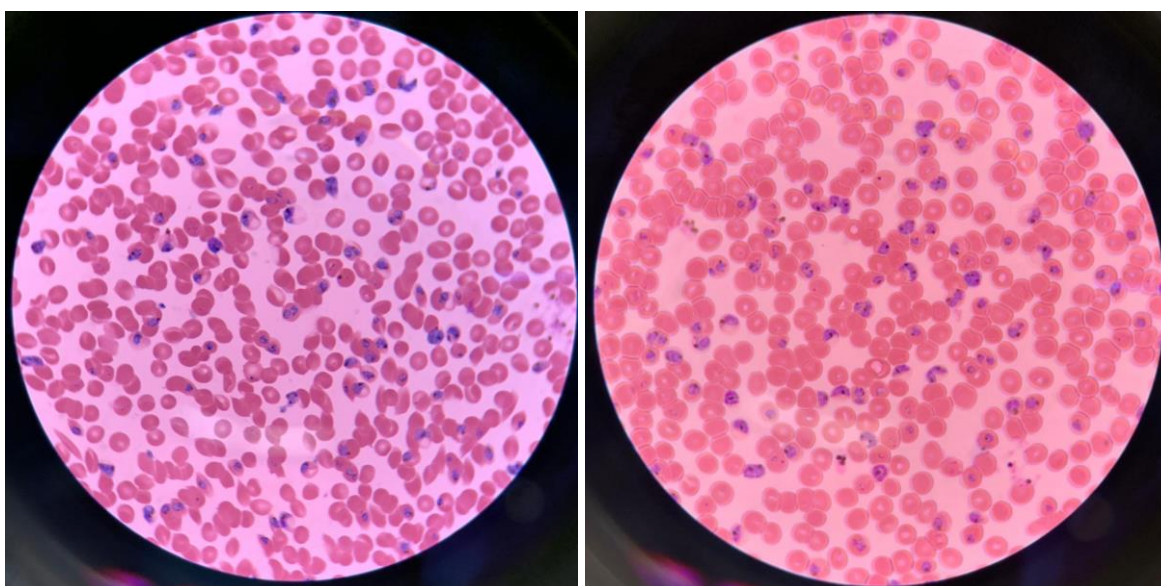
The anti-malarial activity was evaluated at the Max Planck Institute of Colloids and Interfaces, Berlin, following the protocol from Dery *et al.*<sup>167</sup>

Synchronized *Plasmodium falciparum* parasites were cultivated at 1% hematocrit as described by Radfar *et al.*<sup>168</sup> Parasitemia was determined by blood smears. Therefore, a small sample of medium was spread on a glass slide, fixed with methanol for 30 s and then stained with Giemsa staining solution (6%) for 15 min. Prior to the experiment, infected erythrocytes were diluted to 1% parasitemia and resuspended to 4% hematocrit.

The samples were then weighed in (1-3 mg), dissolved in DMSO and a dilution series covering an appropriate range of concentrations was created. In a 96 well plate, 50  $\mu$ L of drug solution were mixed with 50  $\mu$ L of *Plasmodium* culture in triplicates for each concentration. In addition, three wells with 0.5% DMSO (negative control) and three wells with 8  $\mu$ M artemisinin (positive control) were included.

The cultures were kept at 37 °C for 96 h, corresponding to two lifecycles of the parasites, and subsequently frozen. After adding 100  $\mu$ L of lysis buffer (20 mM Tris (pH 7.5), 5 mM EDTA, 0.008% (W/V) saponin, and 0.08% (V/V) Triton X-100, 1x SYBR Green-1) to each well, the plate was incubated in the dark for 3 h. SYBR Green-1 intercalates with the nucleic acids from *Plasmodium* and its fluorescence intensity is thus proportional to the amount of parasites in culture. After the incubation time, the SYBR Green-1 fluorescence was measured at 528 nm and plotted vs. log(c). The plot was fitted with the dose-response function using Origin (originlab, Version 2018.b) and the IC50 determined using the software's Derived Parameters feature.

Dose-response function:  $y = A_1 + \frac{A_2 - A_1}{1 + 10^{(\log x^0 - x)p}}$



Red blood cells (red-ish) and *Plasmodium* parasites (blue-ish).

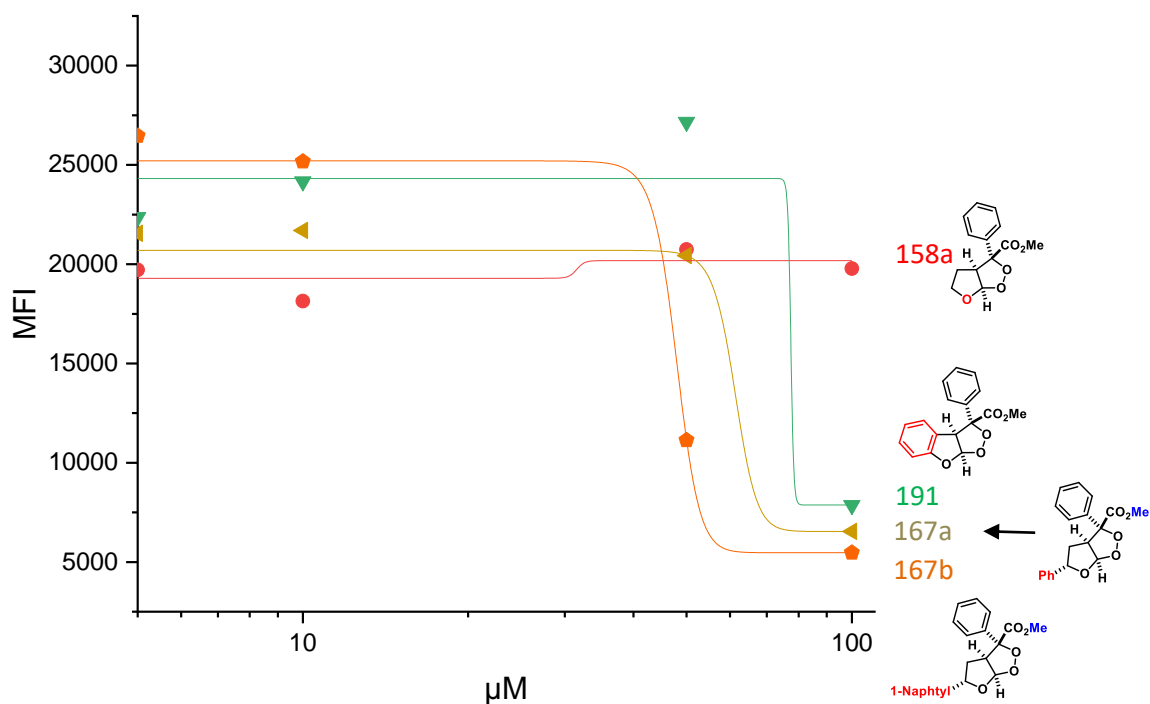


Figure 21: Mean fluorescence intensity (MFI in arbitrary units) plotted vs. concentration [c in  $\mu\text{M}$  ] of tested substances, first series.

The first series of tests was performed with more data points under  $1 \mu\text{M}$  concentration, as it was estimated that the compounds were in the range of the literature compounds reported by Xu *et al.*<sup>147</sup> However, the first series of compounds turned out to have  $\text{IC}_{50}$  values between 10 and  $100 \mu\text{M}$ , leading to the data points being too far apart to make accurate calculations for  $\text{IC}_{50}$  values (*vide supra*). The test could have been repeated for precise determination of these values, which was omitted as the  $\text{IC}_{50}$  values found for the first series were not in an interesting range (around  $1 \mu\text{M}$ ) to save valuable resources. Nevertheless, a trend was visible, as the least polar compound **167b** was the most active, while the most polar compound **158a** was virtually inactive. Therefore, two more series of less polar compounds were prepared and tested (*vide infra*) with data points chosen in a more appropriate range. The trend continued, as the introduction of non-polar groups (octyl-instead of methyl ester) lead to lower  $\text{IC}_{50}$  values.

Table 11: Experimental values to Figure 22.

	A1		A2		Log <sub>x</sub> 0		p		span		Statistics	
		$\sigma_{x^-}$		$\sigma_{x^-}$	$\text{IC}_{50}$	$\sigma_{x^-}$	V	$\sigma_{x^-}$		$\sigma_{x^-}$	$\chi^2$	$r^2$
189	-1646967	*)	21345	4157	931	746253	-0.004	0.06702	1668313	*)	2200410	0.698
184a	4274	391	20963	800	18,95	1,4257	-0.217	0.26268	16688	892	614177	0.990
167h	4697	393	23828	1968	15,19	1,85673	-0.068	0.01686	19130	2073	556136	0.989

1. \*) 1.26786E10;

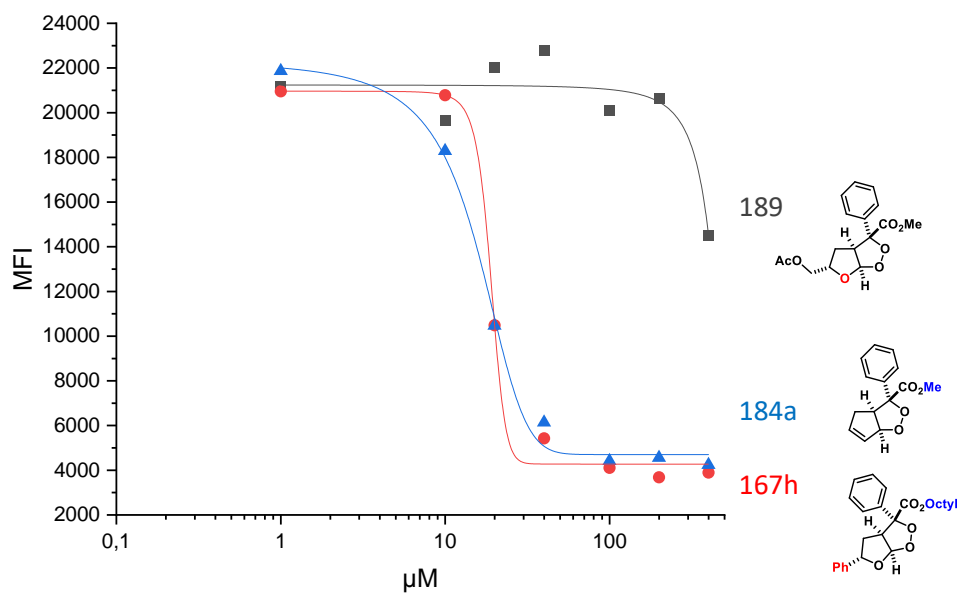


Figure 22: Mean fluorescence intensity (MFI in arbitrary units) plotted vs. concentration [c in  $\mu\text{M}$ ] of tested substances, series two.

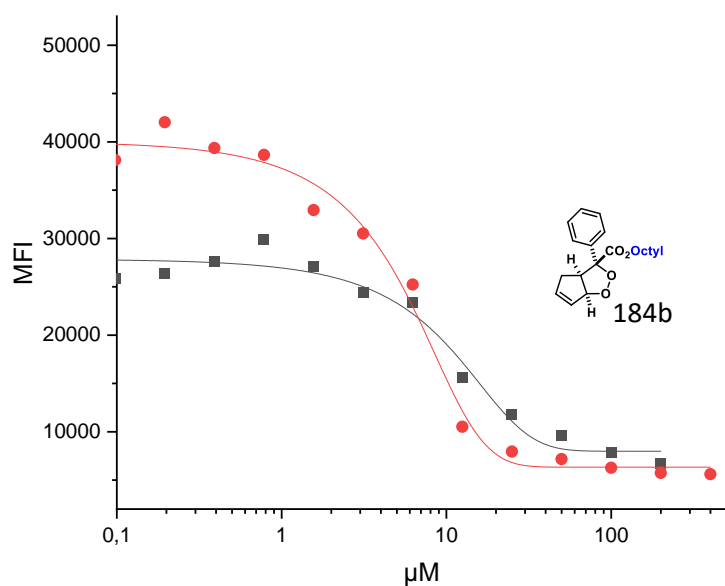


Figure 23: Mean fluorescence intensity (MFI in arbitrary units) plotted vs. concentration [c in  $\mu\text{M}$ ] of tested substances, series three.

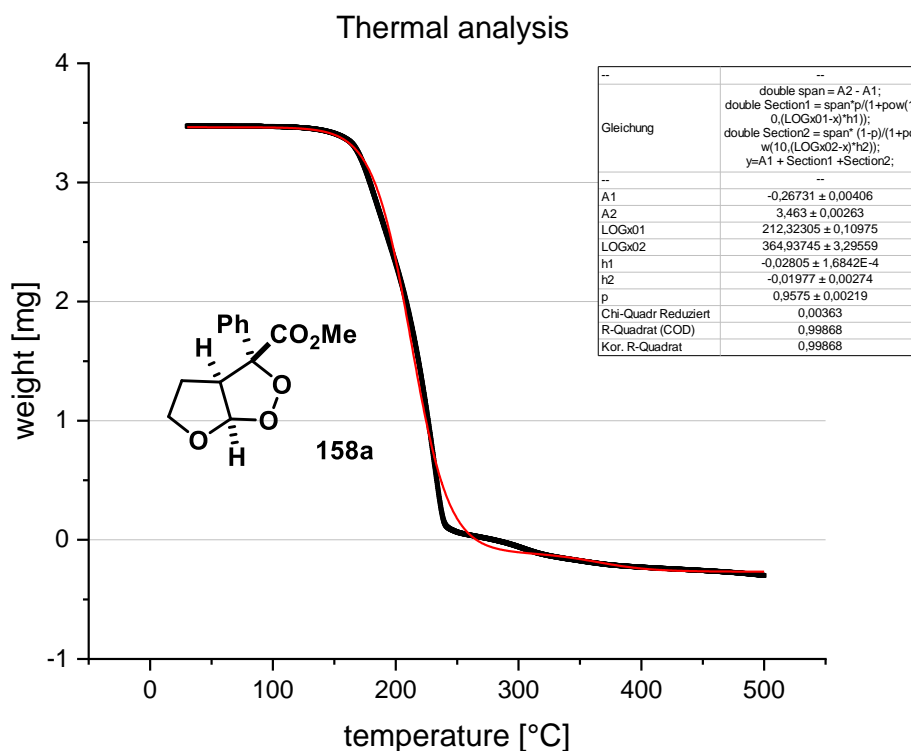
Table 12: Experimental values to Figure 23.

	A1		A2		Log <sub>x</sub> 0		p		span		Statistics	
		$\sigma_{x^-}$		$\sigma_{x^-}$	IC50	$\sigma_{x^-}$	V	$\sigma_{x^-}$		$\sigma_{x^-}$	$\chi^2$	$r^2$
184b <sub>1</sub>	7974	1020	43082	26831	2.55	14.97	-0.0452	0.0242	35107	27172	2200410	0.698
184b <sub>2</sub>	6322	831	61512	22828	2.17	4.22	-0.0898	0.0288	55189	23040	614177	0.990

### 4.10.3. Thermogravimetric Analysis

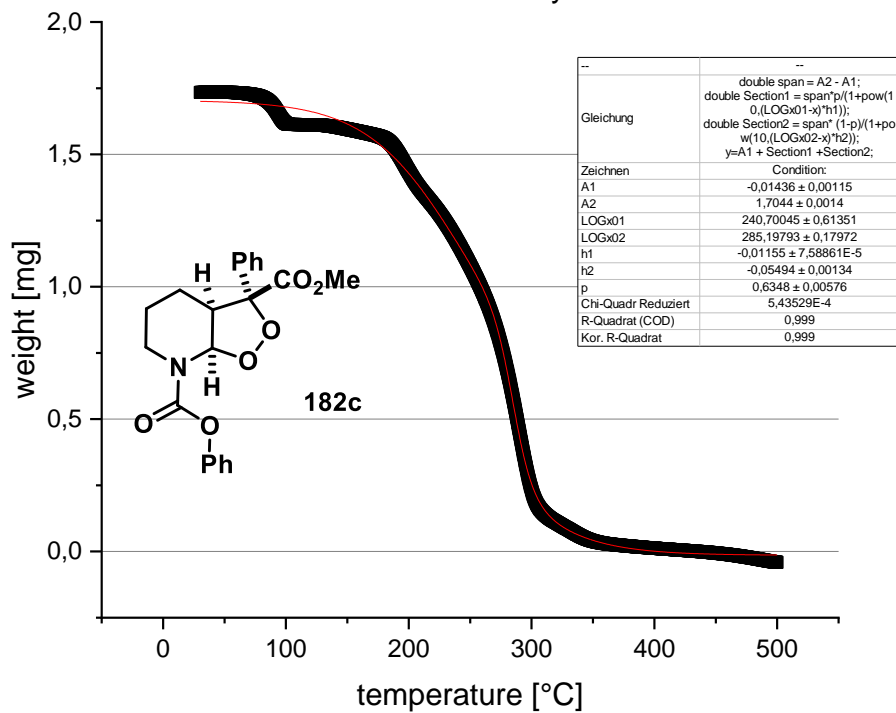
In order to determine the stability of the endoperoxides, thermogravimetric analysis (TGA) was performed on compound **158a**.

The compounds were weighed in under an atmosphere of synthetic air and heated from 30 °C to 500 °C at a rate of 10 °C/min while continuously measuring the sample weight. The weight was plotted against the temperature as shown below (**black**). The sigmoid curve (**red**) was fitted with the software program *Origin 2019b* from OriginLab. The minimum of the first derivative of said fit corresponds to the decomposition of the compound.



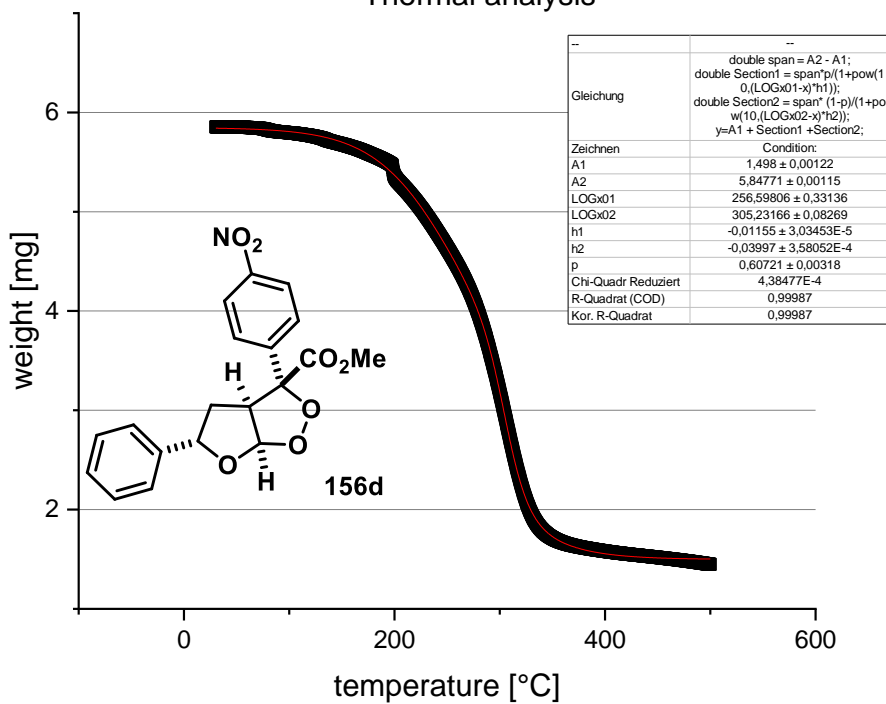
Decomposition temperature: 212 °C.

### Thermal analysis

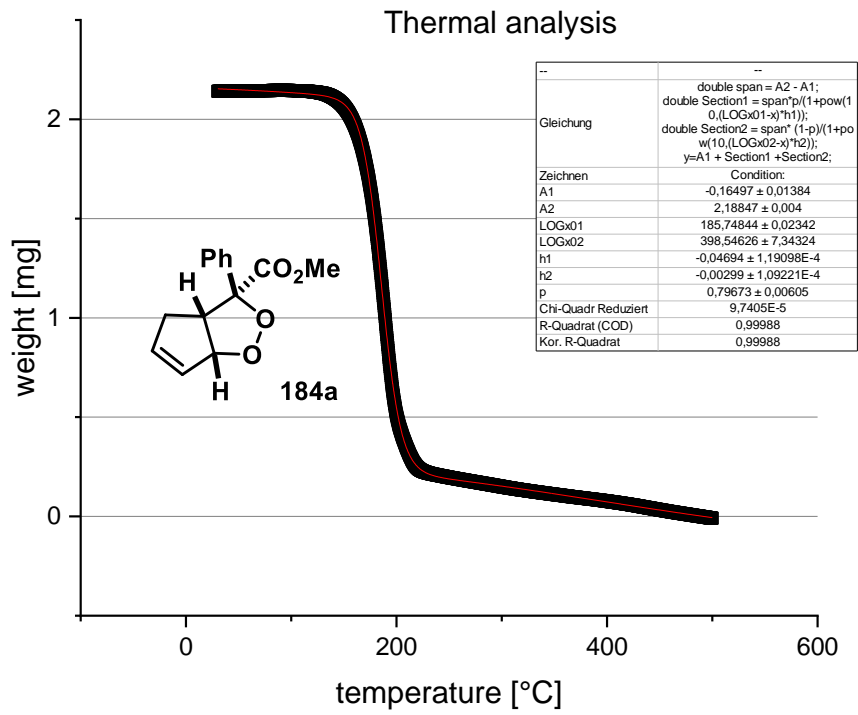


Decomposition at 290 °C; presumably loss of residual water at 93 °C.

### Thermal analysis



Decomposition at 303 °C.



Decomposition at 189 °C.

#### 4.10.4. Cyclovoltammetry

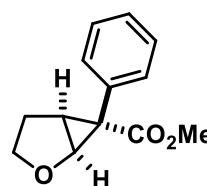
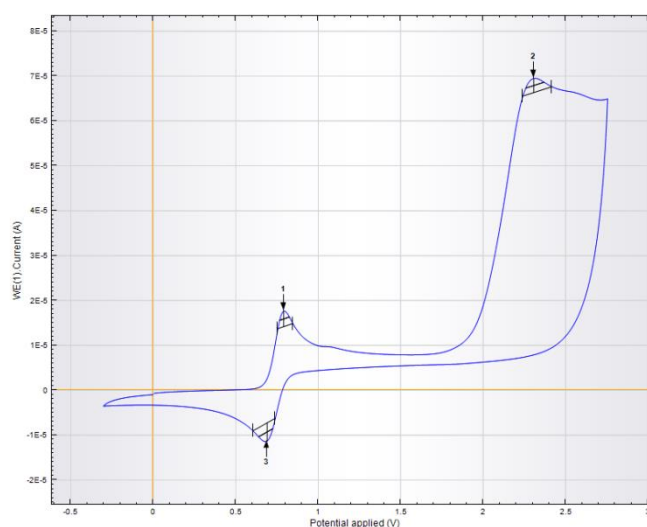
Cyclic voltammetry was used to determine the oxidation potential of some substrates and compared with the literature value<sup>148</sup> for [MesAcr]<sup>+</sup> of +2.07 V in the oxidative cycle. Ferrocene was used as internal standard (peaks are marked in *italics*), the potential vs. SCE is then calculated as follows:<sup>169</sup>

$$E_{1/2}[V] = E_S[V] - E_F[V] + C$$

( $E_{1/2}[V]$ : Redox potential vs. SCE;  $E_S[V]$ : Measured redox potential of the analyte;  $E_F[V]$ :

Measured redox potential of ferrocene; Correction factor  $C := + 0.38$  V)

#### Rac-methyl-6-phenyl-2-oxabicyclo[3.1.0]hexane-6-carboxylate **157a**



#### Index Peak position

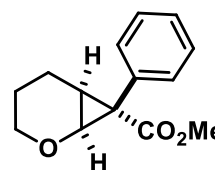
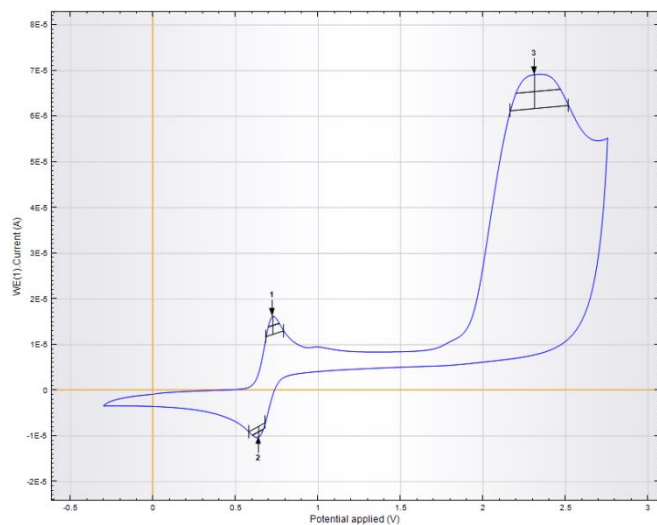
1 0.79056

2 2.3062

3 0.68985

$E_{(M/M^+)}$ : 1.95 V vs. SCE

#### Methyl 7-phenyl-2-oxabicyclo[4.1.0]heptane-7-carboxylate **181a**



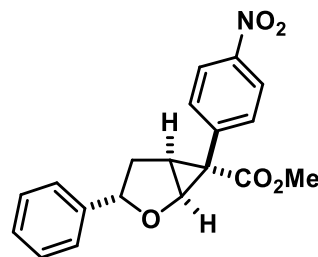
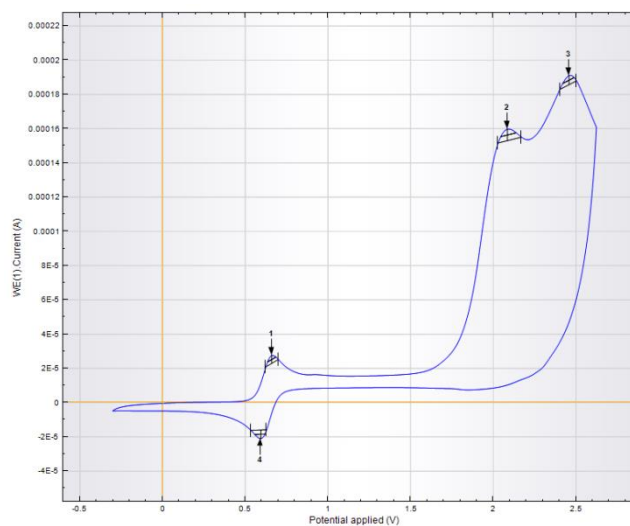
#### Index Peak position

1 0.7251

2 0.6395

3 2.3112

$E_{(M/M^+)}$ : 2.00 V vs. SCE

**Index Peak position**

1 0.65964

2 2.0847

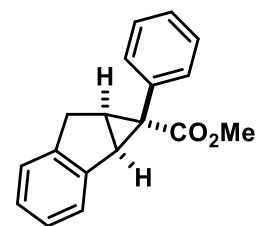
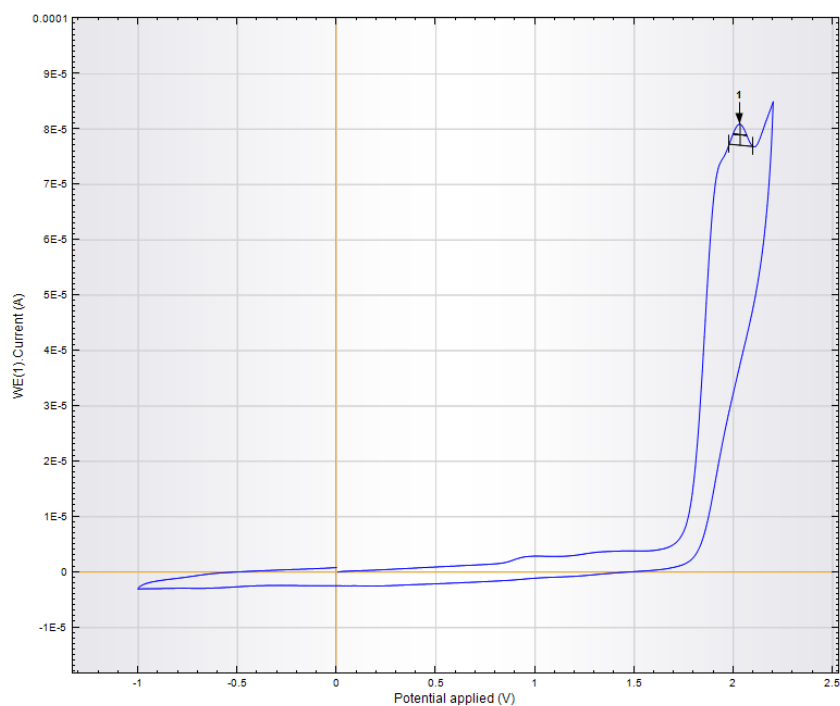
3 2.4573

4 0.59418

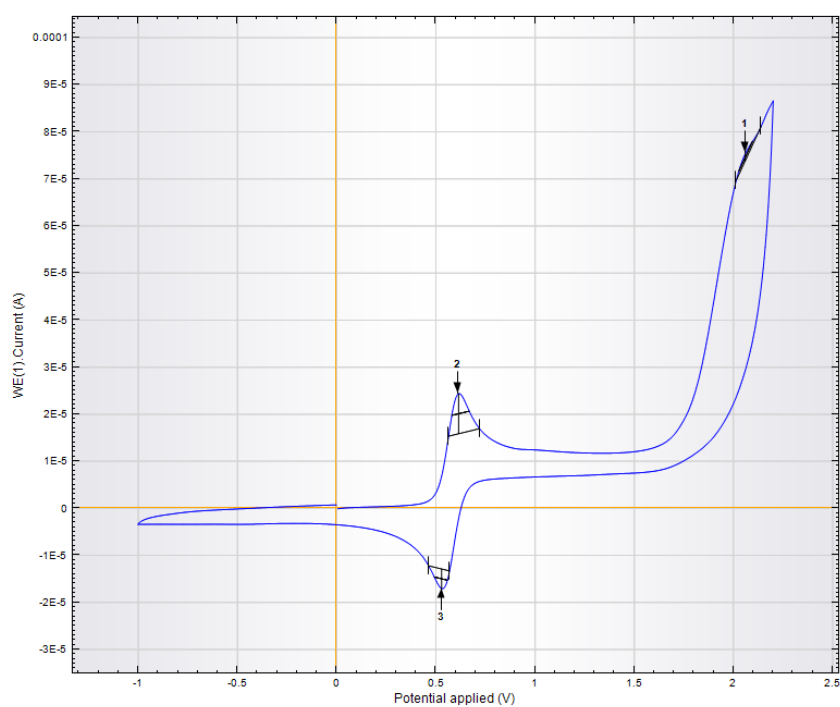
$E_{(M/M^+)}$ : 1.84 V vs. SCE for peak 2;

$E_{(M/M^+)}$ : 2.21 V vs. SCE for peak 3



**Index Peak position**

1 2.0343

**Index Peak position**

1 2.0595

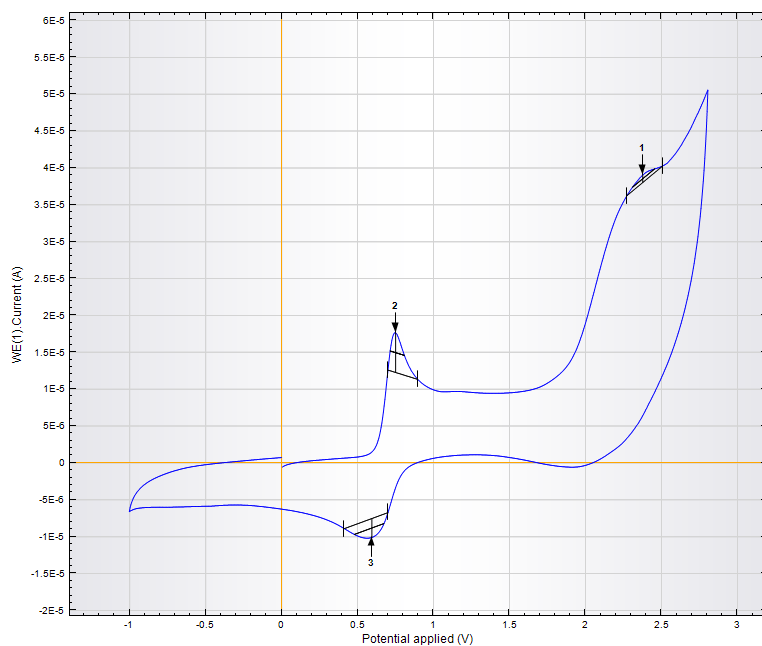
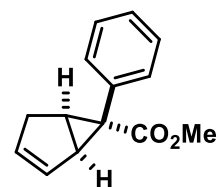
2 0.61432

3 0.52872

 $E_{(M/M^+)}$ : 1.87 V vs. SCE

### Methyl 6-phenylbicyclo[3.1.0]hex-2-ene-6-carboxylate

183a



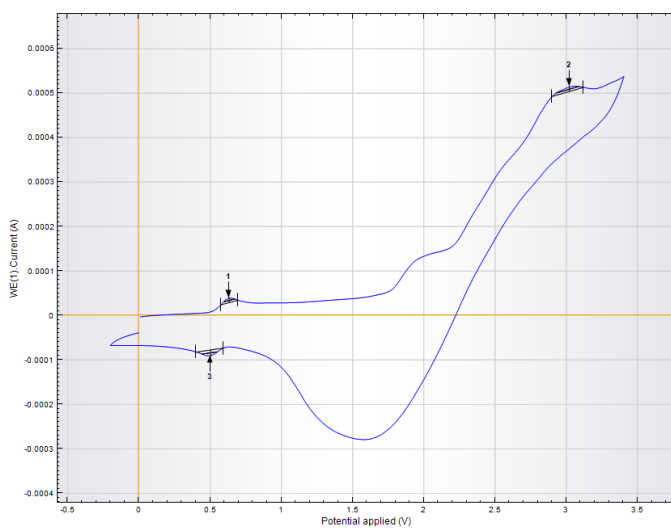
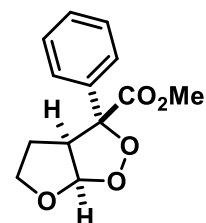
#### Index Peak position

1	2.3767
2	0.75027
3	0.59418

$E_{(M/M^+)}$ : 2.08 V vs. SCE

### Methyl 3-phenyltetrahydro-3H-furo[2,3-c][1,2]dioxole-3-carboxylate

158a



#### Index Peak position

1	0.63446
2	3.0212
3	0.50354

$E_{(M/M^+)}$ : 2.83 V vs. SCE

#### 4.10.5. Fluorescence Quenching

Fluorescence intensity and lifetime quenching can give indications about the interaction of catalyst and substrate. Therefore, the intensity and lifetime of the fluorescence of the catalyst [MesAcr]ClO<sub>4</sub> were measured in the respective solvent. Then substrate **157a** was added successively, and the development of intensity and lifetime analyzed (see tables 13 and 14 below and figures 24 and 25).

Table 13: Measurements under air

probe	pure	25 $\mu$ L	50 $\mu$ L	100 $\mu$ L	200 $\mu$ L	500 $\mu$ L	substpure
Intensity [au]	1878380	1828803	1792953	1787610	1773803	1779917	1744917
Lifetime [ns]	6,473319	6,062533	6,020994	5,968409	5,931989	5,947243	5,865632
Chi <sup>2</sup>	1,153671	1,135958	1,18721	1,171837	1,147781	1,11271	1,1853
added vol. [L]	0	0,000025	0,00005	0,0001	0,0002	0,0005	n.A
total vol. [L]	0,002	0,002025	0,00205	0,0021	0,0022	0,0025	n.A
n <sub>(cat)</sub> [mmol]	0,00016	0,000162	0,000164	0,000168	0,000176	0,0002	n.A
n <sub>(qu)</sub> [mmol]	0	8E-05	0,00016	0,00032	0,00064	0,001601	n.A
n <sub>(qu)</sub> /n <sub>(cat)</sub>	0	0,49381	0,975576	1,904696	3,636237	7,999721	40
I <sub>(qu)</sub> /I <sub>(pure)</sub>	1	0,973607	0,954521	0,951676	0,944326	0,947581	0,928948
t <sub>(add)</sub> /t <sub>(pure)</sub>	1	0,936542	0,930125	0,922001	0,916375	0,918732	0,906124
[I <sub>(pure)</sub> /i <sub>(add)</sub> ]-1	0	0,027109	0,047646	0,050777	0,058956	0,055319	0,076487

Excitation at 440 nm, emission measured between 450 and 600 nm, intensity at maximum is reported.

Table 14: Measurements under nitrogen

probe	pure	25 $\mu$ L	50 $\mu$ L	100 $\mu$ L	200 $\mu$ L	500 $\mu$ L	substpure
Intensity [au]	1322897	1297073	1276573	1270797	1277430	1281240	1299920
Lifetime [ns]	7,789377	7,702887	7,710023	7,635077	7,634908	7,584592	7,605927
Chi <sup>2</sup>	1,057809	1,063876	1,0761	1,076137	1,12047	1,100293	1,144738
added vol. [L]	0	0,000025	0,00005	0,0001	0,0002	0,0005	n.A
total vol. [L]	0,002	0,002025	0,00205	0,0021	0,0022	0,0025	n.A
n <sub>(cat)</sub> [mmol]	0,00016	0,000162	0,000164	0,000168	0,000176	0,0002	n.A
n <sub>(qu)</sub> [mmol]	0	8E-05	0,00016	0,00032	0,00064	0,001601	n.A
n <sub>(qu)</sub> /n <sub>(cat)</sub>	0	0,49381	0,975576	1,904696	3,636237	7,999721	40
I <sub>(add)</sub> /I <sub>(pure)</sub>	1	0,98048	0,964983	0,960617	0,965631	0,968511	0,982632
t <sub>(qu)</sub> /t <sub>(pure)</sub>	1	0,988896	0,989813	0,980191	0,980169	0,97371	0,976449
[I <sub>(pure)</sub> /i <sub>(add)</sub> ]-1	0	0,019909	0,036287	0,040998	0,035592	0,032513	0,017675

Excitation at 440 nm, emission measured between 450 and 600 nm, intensity at maximum is reported.

The starting intensity of pure catalyst solution is lower by approx. 20% under air compared to under nitrogen atmosphere.

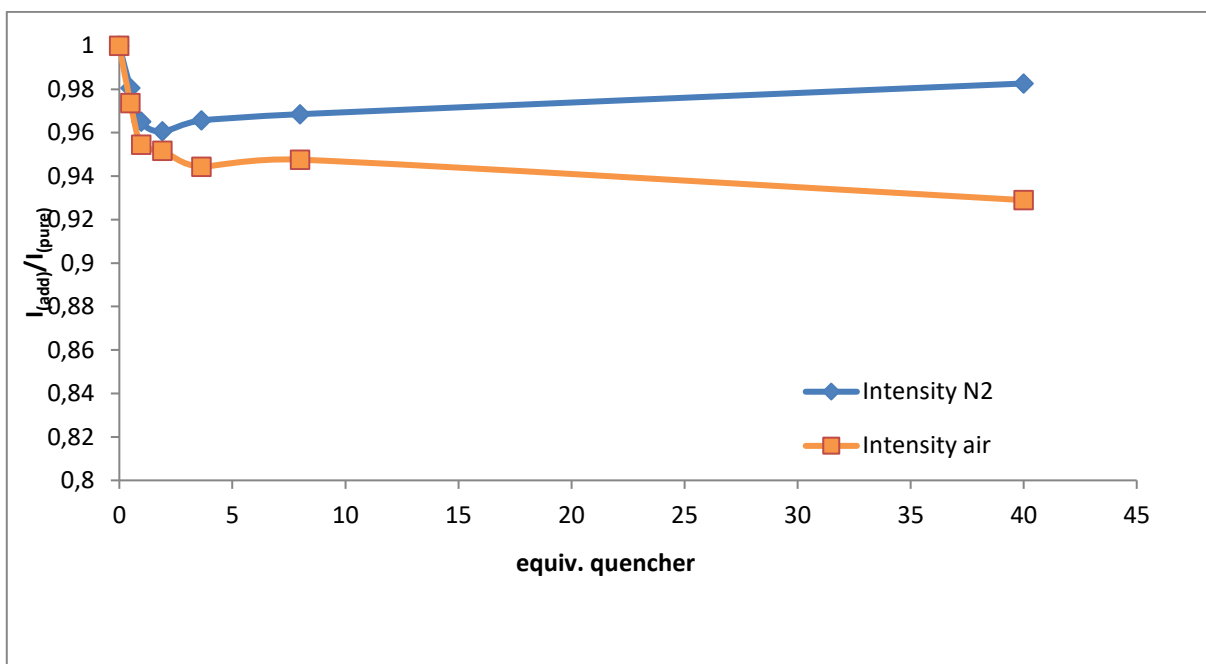


Figure 24: Fluorescence intensity quenching of substrate **157a** .

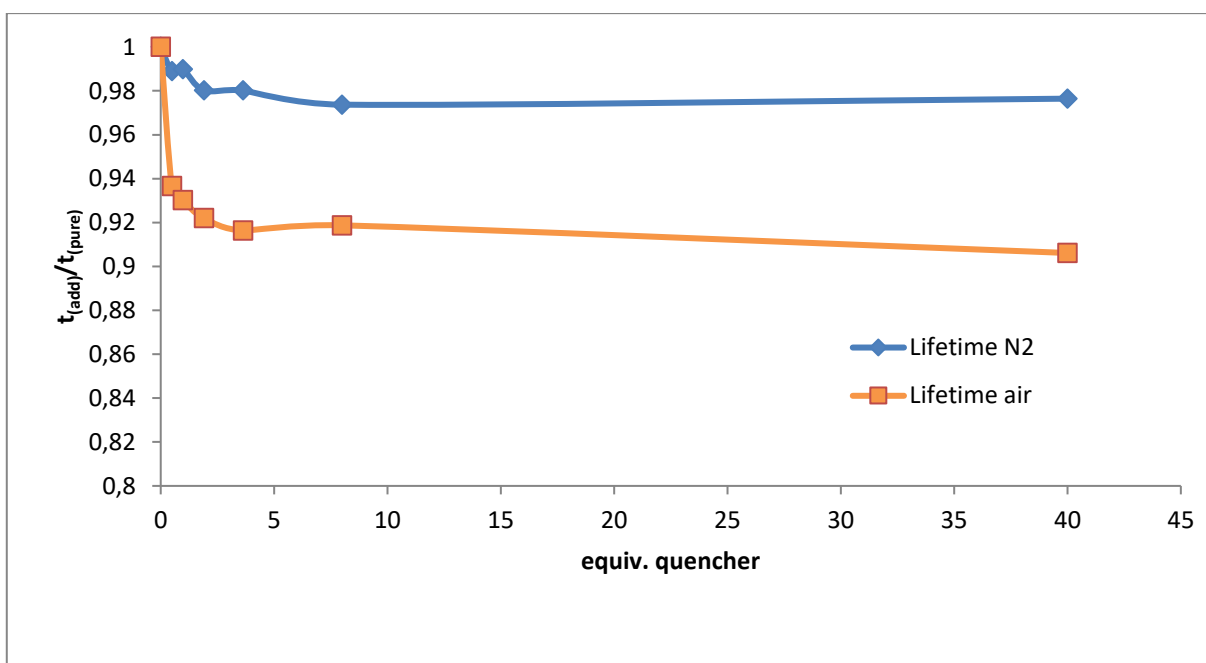
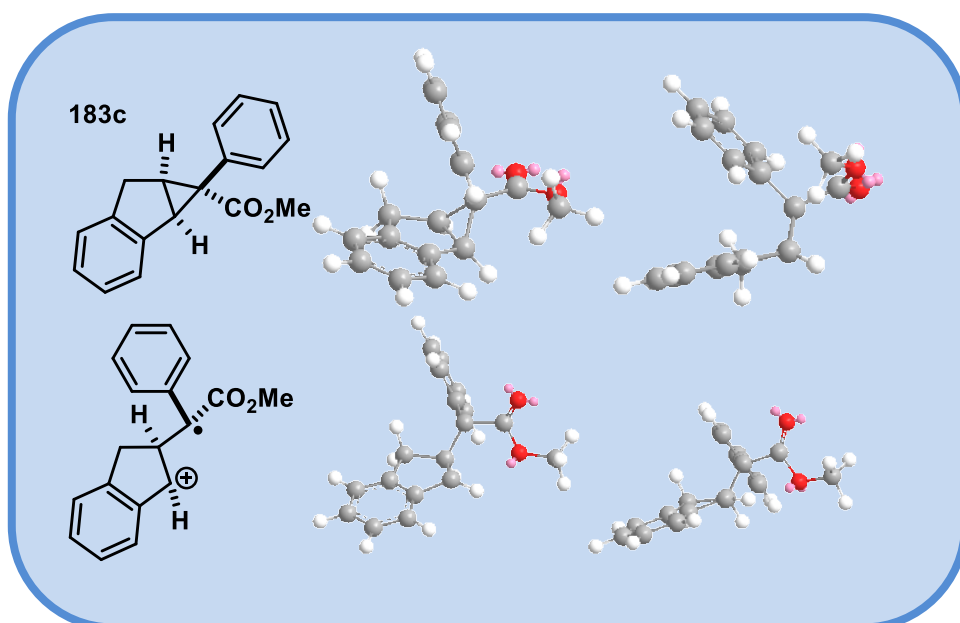
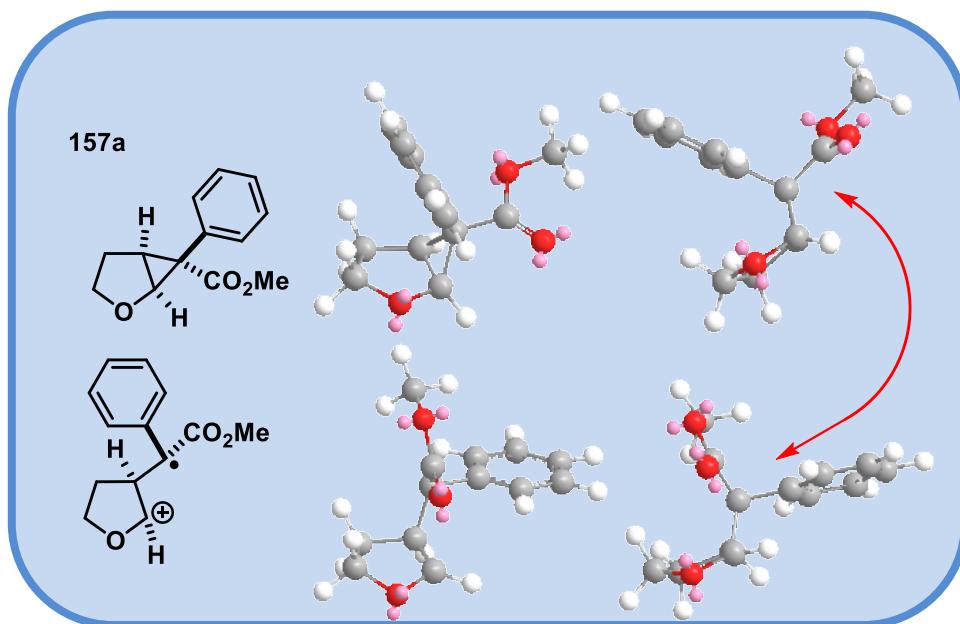


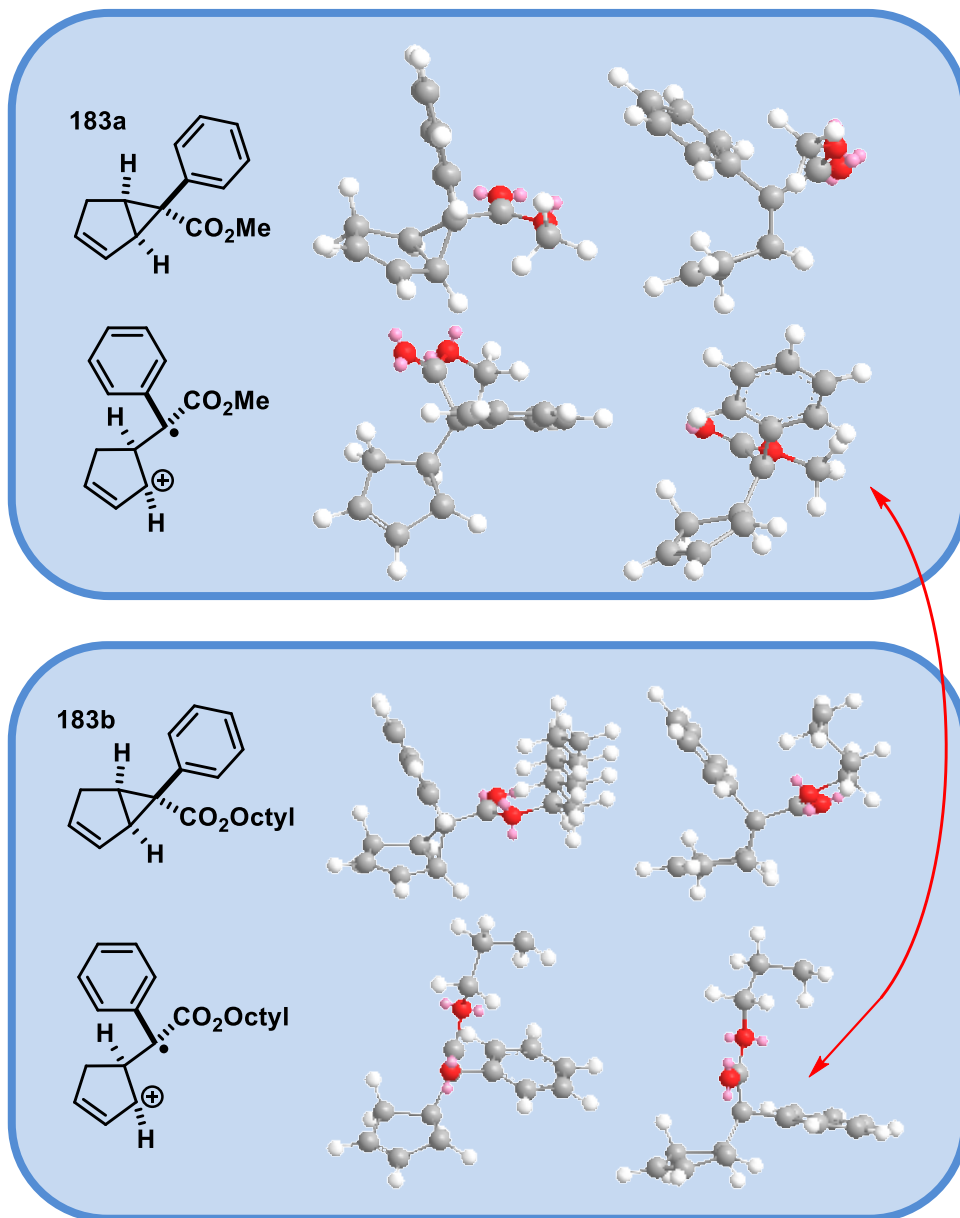
Figure 25: Fluorescence lifetime quenching of substrate **157a**.

A stronger quenching is observed under air than under nitrogen atmosphere, but both show similar behavior. Overall quenching is low but significant, indicating that there is interaction between the catalyst and the substrate.

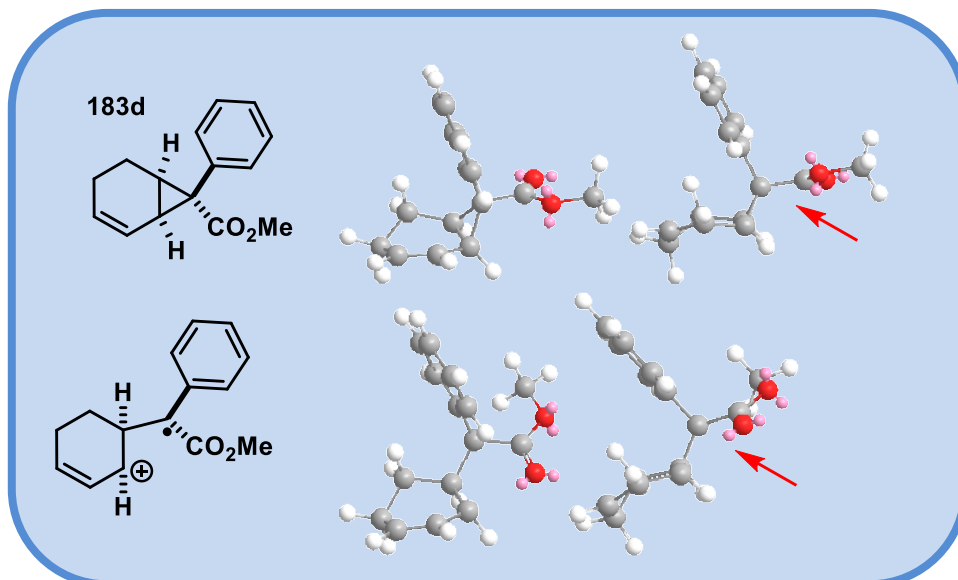
#### 4.10.6. MM2 Minimization: Structure Analysis

MM2 Structure Minimization was done using Chem3D Version 17.1.0.105 on the structures shown on the right. The minimized structures are shown from two different angles, and important features are marked with a red arrow and commented below the corresponding figure.

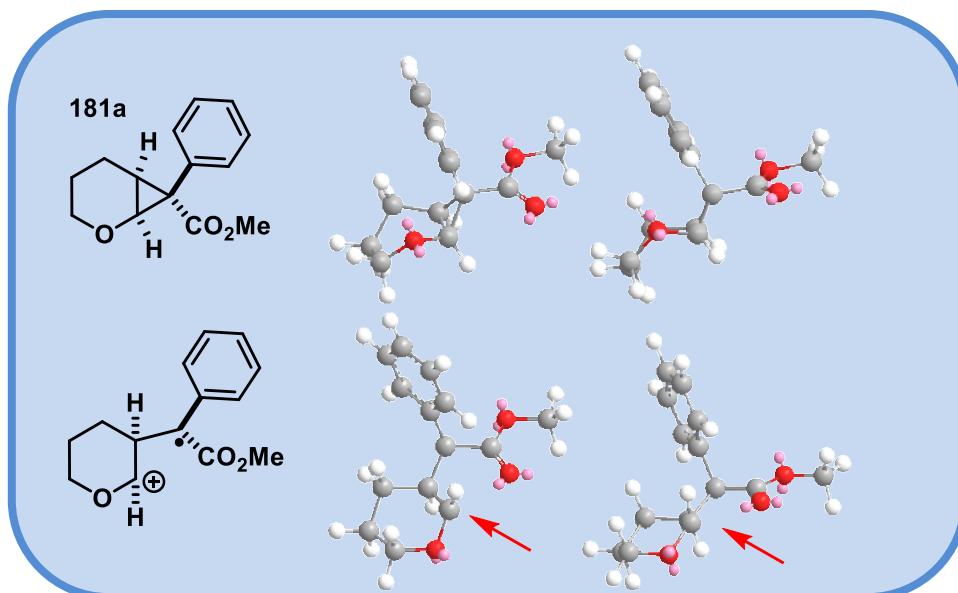




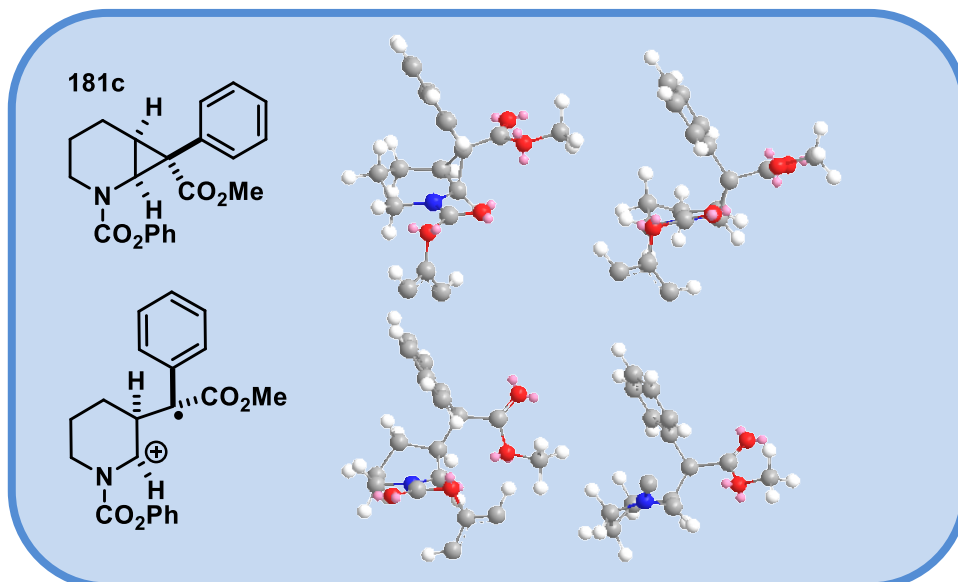
Parts of the octyl group are omitted in the depiction for clarity; the octyl ester has a great impact on the orientation in the oxidized form, which is also observed in the actual diastereomeric outcome of the reactions.



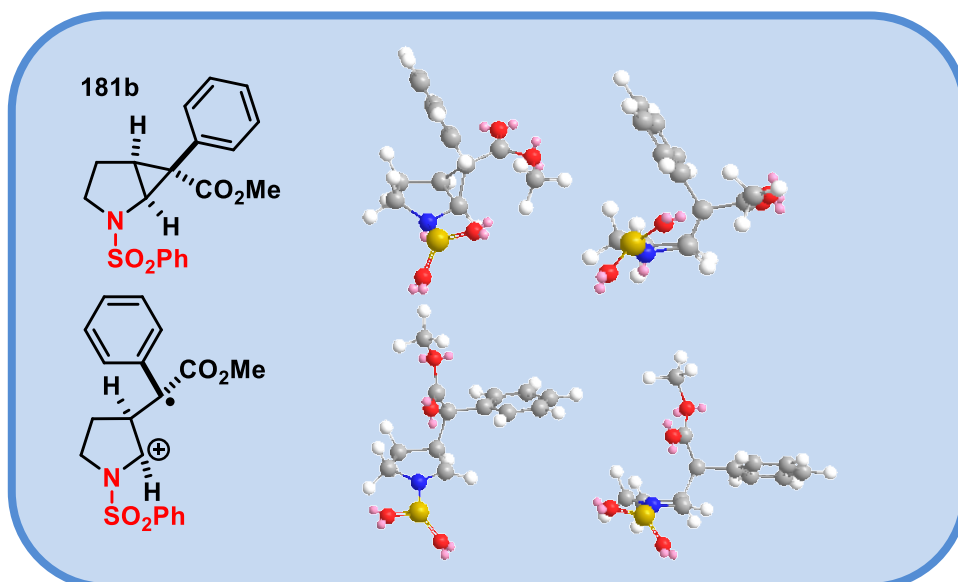
As there are other reactions (*e.g.* Schenck-ene) possible, this substrate seems to readily react under the conditions but not in the desired way, leading to the observed decomposition.



The proton marked has an unusual orientation compared to all other structures, especially to the piperidin-derived shown below, which might explain that this substrate did not undergo a reaction.



Parts of the protecting group are omitted for clarity; In contrast to the pyran derivative (above), the oxidized structures appears to be less bent.



Parts of the protection group are omitted for clarity. The orientation of the ester changes analogously as for the furan derivative.



#### 4.10.7. Gamess Optimization and Orbital Simulation

Gamess<sup>159-160</sup> (General Atomic and Molecular Electronic Structure System, Version 2019.R1.P1.mkl) was used to assess the Highest Occupied Molecular Orbital (HOMO) of selected compounds in search of possible explanations for observed differences in reactivity (*vide infra*). More information on the program 'Gamess' is available at <https://www.msg.chem.iastate.edu/GAMESS/>. The input file for Gamess was partially prepared using 'Avogadro' (Version 1.2.0, [www.avogadro.cc/](http://www.avogadro.cc/)) and further modified with the input given below. Avogadro and VMD<sup>161</sup> (Visual Molecular Dynamics, Version 1.9.3 <https://www.ks.uiuc.edu/Research/vmd/>) were used to visualize the results, the latter one to produce the pictures shown below.

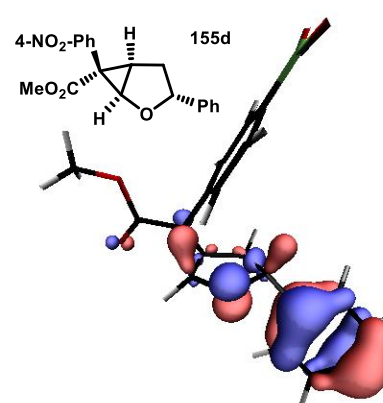
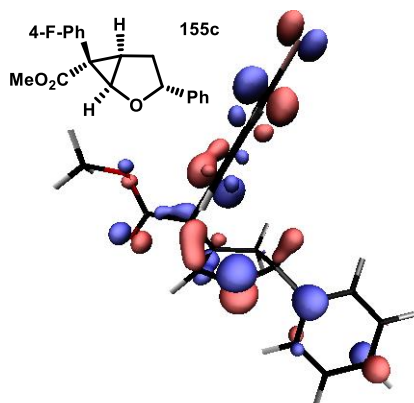
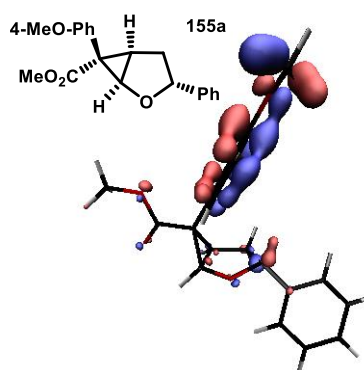
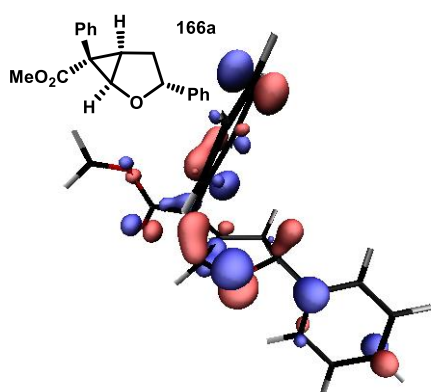
##### Gamess input command:

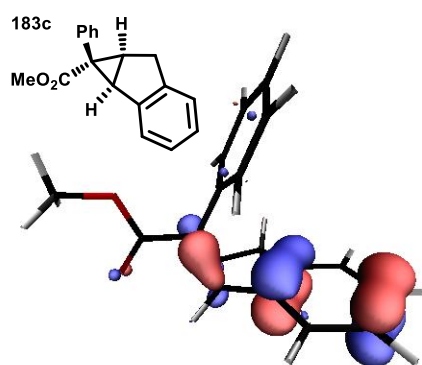
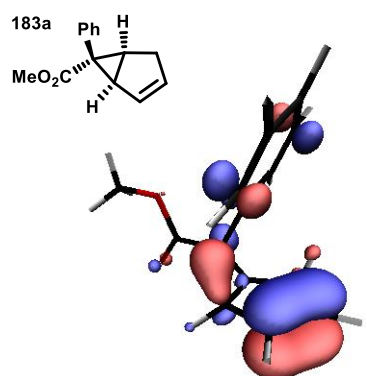
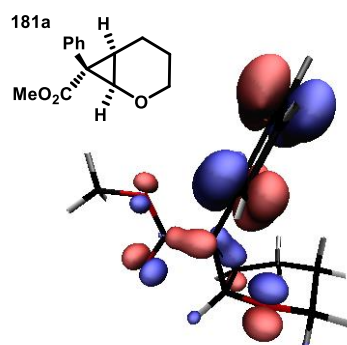
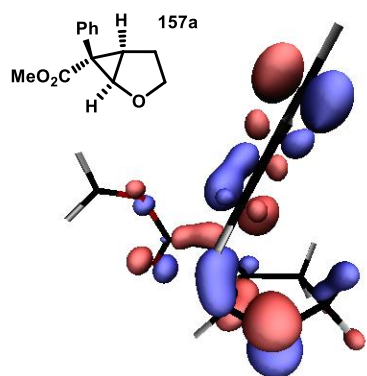
```
$BASIS GBASIS=N31 NGAUSS=6 $END
```

```
$CONTRL SCFTYP=RHF RUNTYP=OPTIMIZE DFTTYP=B3LYP $END
```

```
$STATPT OPTTOL=0.0001 NSTEP=250 $END
```

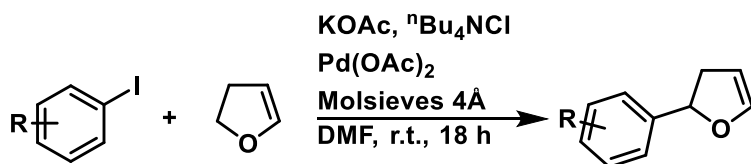
```
$SYSTEM MWORDS=300 $END
```





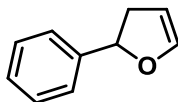
#### 4.10.8. Synthesis of Starting Materials

General Procedure 2 (GP2) for the synthesis of 2-aryl-2,3-dihydrofurans



Following the literature procedure<sup>150</sup>, a 100 mL round bottom flask was equipped with a magnetic stirbar and charged with KOAc (2.2 equiv.), <sup>n</sup>Bu<sub>4</sub>NCl (2.5 equiv.) and crushed 4 Å Molsieves (approx. a teaspoon per 5 mL DMF) which all was thoroughly stirred in DMF (1 mL per mmol of Ar-I). Then iodobenzene (1 equiv.), 2,3-dihydrofuran (5-10 equiv.) and Pd(OAc)<sub>2</sub> (5 mol%) were added successively in this order. The reaction mixture turned dark black within 10 min, and was further stirred for 18 h (overnight) at room temperature. For work-up, Et<sub>2</sub>O (approx. 10 mL per mmol Ar-I) was added and the resulting mixture filtered over a plug of celite. The filtrate was then washed twice with water and once with brine, dried over MgSO<sub>4</sub>, filtrated and evaporated under reduced pressure. Purification of the crude by column chromatography yielded the pure product, which was then used in the next step.

#### 2-phenyl-2,3-dihydrofuran 164a



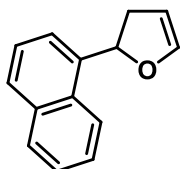
Following **GP2**, KOAc (1.08 g, 11 mmol, 2.2 equiv.), <sup>n</sup>Bu<sub>4</sub>NCl (3.50 g, 12.5 mmol, 2.5 equiv.) and a spoonful of crushed Molsieves 4 Å were suspended in 5 mL DMF. Then iodobenzene (1.02 g, 1.86 mL) and 2,3-dihydrofuran (3.5 mL, 45 mmol, 9 equiv.) was added. At last, Pd(OAc)<sub>2</sub> (56 mg, 0.25 mmol, 5 mol%) was added, and the reaction was stirred over night. After workup, the crude product was further purified by column chromatography (hexanes:EtOAc = 19:1), yielding a colorless clear oil. (663 mg, 4.54 mmol, 91%);

**R<sub>f</sub>** (hexanes:EtOAc = 9:1) = 0.62; purple with vanillin.

**<sup>1</sup>H NMR** (300 MHz, CDCl<sub>3</sub>): δ 7.41 – 7.28 (m, 5H), 6.46 (q, *J* = 2.4 Hz, 1H), 5.52 (dd, *J* = 10.7, 8.4 Hz, 1H), 4.97 (q, *J* = 2.6 Hz, 1H), 3.09 (ddt, *J* = 15.4, 10.7, 2.4 Hz, 1H), 2.62 (ddt, *J* = 15.2, 8.4, 2.4 Hz, 1H).

**LR-MS** (EI-MS): *m/z* calc. for C<sub>10</sub>H<sub>10</sub>O [M<sup>+</sup>] 146.0731, found 146.0719.

Analytical data is in accordance with the literature.<sup>150</sup>

**2-(naphthalene-1-yl)-2,3-dihydrofuran****164b**

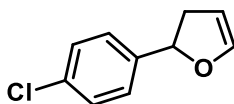
Following **GP2**, KOAc (1.1 g, 11 mmol, 2.2 equiv.), <sup>n</sup>Bu<sub>4</sub>NCl (3.47 g, 12.5 mmol, 2.5 equiv.) and a spoonful of crushed Molsieves 4 Å were suspended in 5 mL DMF. Then 1-iodonaphthalene (1.27 g, 5 mmol, 1 equiv.), and 2,3-dihydrofuran (3.5 mL, 45 mmol, 9 equiv.) were added. At last, Pd(OAc)<sub>2</sub> (56 mg, 0.25 mmol, 5 mol%) was added, and the reaction was stirred over night. After workup the crude product was further purified by column chromatography (hexanes:EtOAc = 19:1), yielding a colorless clear oil. (848 mg, 4.33 mmol, 86%);

**R<sub>f</sub>** (hexanes:EtOAc = 9:1) = 0.55; brown with vanillin.

**<sup>1</sup>H NMR** (300 MHz, CDCl<sub>3</sub>): δ 7.95 – 7.88 (m, 2H), 7.81 (bd, *J* = 8.2 Hz, 1H), 7.61 (bdt, *J* = 7.1 Hz, 1H), 7.55 – 7.47 (m, 3H), 6.59 (q, *J* = 2.4 Hz, 1H), 6.19 (dd, *J* = 11.0, 8.4 Hz, 1H), 5.04 (q, *J* = 2.6 Hz, 1H), 3.30 (ddt, *J* = 15.1, 11.0, 2.4 Hz, 1H), 2.67 (ddt, *J* = 15.1, 8.4, 2.4 Hz, 1H).

**LR-MS** (EI-MS): *m/z* calc. for C<sub>10</sub>H<sub>10</sub>O [*M*<sup>+</sup>] 196.0888, found 196.0886.

Analytical data is in accordance with the literature.<sup>150</sup>

**2-(4-chlorophenyl)-2,3-dihydrofuran****164c**

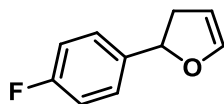
Following **GP2**, KOAc (1.1 g, 11 mmol, 2.2 equiv.), <sup>n</sup>Bu<sub>4</sub>NCl (3.5 g, 12.5 mmol, 2.5 equiv.) and a spoonful of crushed Molsieves 4 Å were suspended in 5 mL DMF. Then 4-chloriodobenzene (1.20 g, 5 mmol, 1 equiv.), and 2,3-dihydrofuran (3.5 mL, 45 mmol, 9 equiv.) were added. At last, Pd(OAc)<sub>2</sub> (56 mg, 0.25 mmol, 5 mol%) was added, and the reaction was stirred over night. After workup the crude product was further purified by column chromatography (hexanes:EtOAc = 19:1), yielding a colorless clear oil. (741 mg, 4.12 mmol, 86%);

**R<sub>f</sub>** (hexanes:EtOAc = 9:1) = 0.72; bright purple with vanillin.

**<sup>1</sup>H NMR** (300 MHz, CDCl<sub>3</sub>): δ 7.35 – 7.27 (m, 4H), 6.44 (q, *J* = 2.4 Hz, 1H), 5.49 (dd, *J* = 10.8, 8.2 Hz, 1H), 4.96 (q, *J* = 2.6 Hz, 1H), 3.08 (ddt, *J* = 15.3, 10.8, 2.4 Hz, 1H), 2.55 (ddt, *J* = 15.3, 8.2, 2.4 Hz, 1H).

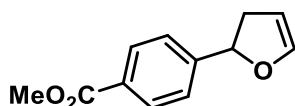
**LR-MS** (EI-MS): *m/z* calc. for C<sub>10</sub>H<sub>10</sub>O [*M*<sup>+</sup>] 180.0342, found 180.0337.

Analytical data is in accordance with the literature<sup>170</sup>.

**2-(4-fluorophenyl)-2,3-dihydrofuran****164d**

Following **GP2**, KOAc (1.04 g, 11 mmol, 2.2 equiv.),  ${}^n\text{Bu}_4\text{NCl}$  (3.3 g, 12 mmol, 2.5 equiv.) and a spoonful of crushed Molsieves 4 Å were suspended in 7 mL DMF. Then 1-fluoroiodobenzene (1.06 g, 4.8 mmol, 1 equiv.), and 2,3-dihydrofuran (3.5 mL, 45 mmol, 10 equiv.) were added. At last,  $\text{Pd}(\text{OAc})_2$  (50 mg, 0.22 mmol, 5 mol%) was added, and the reaction was stirred over night. The crude product isolated after workup as yellowish oil (607 mg, 3.7 mmol, 77%), was used in the next step without further purification.

Analytical data is in accordance with the literature.<sup>171</sup>

**Methyl-4-(2,3-dihydrofuran-2-yl)benzoate****164e**

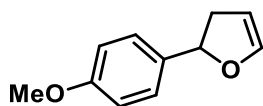
Following **GP2**, KOAc (860 mg, 8.8 mmol, 2.2 equiv.),  ${}^n\text{Bu}_4\text{NCl}$  (2.78 g, 10 mmol, 2.5 equiv.) and a spoonful of crushed Molsieves 4 Å were suspended in 5 mL DMF. Then methyl 4-iodobenzoate (1.05 g, 4 mmol, 1 equiv.), and 2,3-dihydrofuran (2.7 mL, 34 mmol, 8.5 equiv.) were added. At last,  $\text{Pd}(\text{OAc})_2$  (45 mg, 0.2 mmol, 5 mol%) was added, and the reaction was stirred over night. After workup the crude product was further purified by column chromatography (hexanes:EtOAc = 99:1 to 19:1), yielding a colorless clear oil. (709 mg, 3.48 mmol, 87%);

$R_f$  (hexanes:EtOAc = 9:1) = 0.6; brownish with vanillin.

${}^1\text{H NMR}$  (300 MHz,  $\text{CDCl}_3$ ):  $\delta$  8.03 (d,  $J$  = 8.5 Hz, 2H), 7.42 (d,  $J$  = 8.1 Hz, 2H), 6.47 (q,  $J$  = 2.4 Hz, 1H), 5.56 (dd,  $J$  = 10.8, 8.2 Hz, 1H), 4.96 (q,  $J$  = 2.5 Hz, 1H), 3.91 (s, 3H), 3.12 (ddt,  $J$  = 15.5, 10.9, 2.4 Hz, 1H), 2.56 (ddt,  $J$  = 15.2, 8.2, 2.4 Hz, 1H).

**LR-MS** (EI-MS):  $m/z$  calc. for  $\text{C}_{12}\text{H}_{12}\text{O}_3$  [ $\text{M}^+$ ] 204.0786, found 204.0790.

Analytical data is in accordance with the literature<sup>172</sup>.



Following **GP2**, KOAc (1.1 g, 11 mmol, 2.2 equiv.),  ${}^n\text{Bu}_4\text{NCl}$  (3.5 g, 12.5 mmol, 2.5 equiv.) and a spoonful of crushed Molsieves 4 Å were suspended in 5 mL DMF. Then 4-iodoanisole (1.17 g, 5 mmol, 1 equiv.), and 2,3 dihydrofuran (3.5 mL, 45 mmol, 9 equiv.) were added. At last,  $\text{Pd}(\text{OAc})_2$  (56 mg, 0.25 mmol, 5 mol%) was added, and the reaction was stirred over night. After workup the crude product was further purified by column chromatography (hexanes:EtOAc = 19:1), yielding a colorless clear oil. (751 mg, 4.27 mmol, 86%);

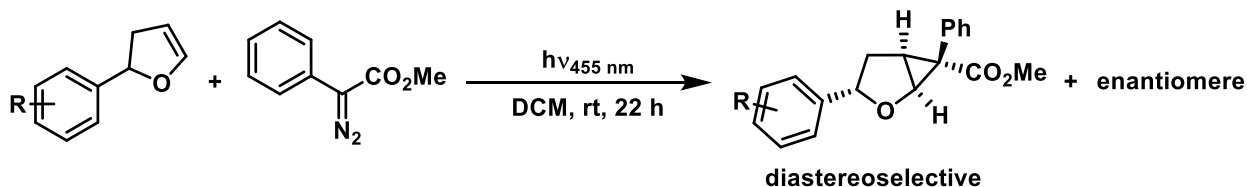
$R_f$  (hexanes:EtOAc = 9:1) = 0.57; dark brown with vanillin.

${}^1\text{H NMR}$  (300 MHz,  $\text{CDCl}_3$ ):  $\delta$  7.42 – 7.26 (m, 3H), 6.97 – 6.79 (m, 2H), 6.43 (q,  $J$  = 2.4 Hz, 1H), 5.47 (dd,  $J$  = 10.6, 8.5 Hz, 1H), 4.96 (q,  $J$  = 2.5 Hz, 1H), 3.81 (s, 3H), 3.04 (ddt,  $J$  = 15.3, 10.6, 2.4 Hz, 1H), 2.61 (ddt,  $J$  = 15.2, 8.5, 2.4 Hz, 1H).

**LR-MS** (EI-MS):  $m/z$  calc. for  $\text{C}_{10}\text{H}_{10}\text{O}$  [ $\text{M}^+$ ] 176.0837, found 176.0836.

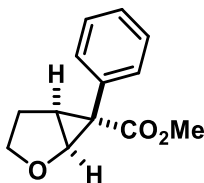
Analytical data is in accordance with the literature<sup>150</sup>.

### General Procedure 3 (**GP3**) for the photochemical cyclopropanation



Modifying the literature procedure<sup>118</sup> aryl 2,3-dihydrofuran (1 equiv.) and methyl 2-phenyl-2-diazoacetate (1.5 equiv.) were dissolved in dry DCM (approx. 6 mL per mmol dihydrofuran) in a schlenk tube equipped with a glass rod (see 4.10.1 for setup details). The mixture was degassed either by bubbling  $\text{N}_2$  for 3 min or 3 freeze-pump-thaw cycles. After 24 h of blue light irradiation, the solvent was evaporated under reduced pressure and the crude mixture purified by column chromatography.

**Methyl (1*S*\*,5*S*\*,6*R*\*)-6-phenyl-2-oxabicyclo[3.1.0]hexane-6-carboxylate (±)-157a**



Following **GP3** 2,3-dihydrofuran (1.0 mL, 14 mmol, 3 equiv.) was reacted with methyl 2-phenyl-2-diazoacetate (790 mg, 4.5 mmol, 1 equiv.) for 22 h in 20 mL DCM. The crude product was purified by column chromatography (Hexanes:EtOAc = 9:1) to yield 821 mg (3.77 mmol, 83%) of a viscous colorless oil (at room temperature) which solidified in the fridge to an amorphous substance.

**R<sub>f</sub>** (hexanes:EtOAc = 4:1) = 0.35; greenish with vanillin.

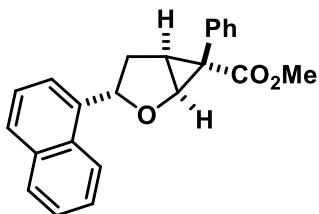
**IR (neat):** 3050, 2952, 2902, 1701, 1434, 1312, 1243, 1117, 1068, 1027, 943, 901, 859 cm<sup>-1</sup>.

**<sup>1</sup>H NMR** (300 MHz, CDCl<sub>3</sub>): δ 7.43 – 7.28 (m, 5H), 4.50 (d, *J* = 5.7 Hz, 1H), 3.77 (ddd, *J* = 10.1, 8.4, 3.6 Hz, 1H), 3.56 (s, 3H), 2.65 (t, *J* = 5.7 Hz, 1H), 2.43 – 2.31 (m, 1H), 2.30 – 2.16 (m, 1H), 1.90 – 1.79 (m, 1H).

**<sup>13</sup>C NMR** (75 MHz, CDCl<sub>3</sub>): δ 172.0, 132.2, 131.5, 128.5, 127.6, 70.2, 70.1, 52.4, 38.1, 32.5, 26.3.

**HR-MS** (EI-MS): *m/z* calc. for C<sub>13</sub>H<sub>14</sub>O<sub>3</sub> [M<sup>+</sup>] 218.09375, found 218.09385.

**Methyl 3-(naphthalene-1-yl)-6-phenyl-2-oxabicyclo[3.1.0]hexane-6-carboxylate 166b**



According to **GP3**, compound **164b** (503 mg, 2.56 mmol, 1 equiv.) and methyl 2-phenyl-2-diazoacetate (590 mg, 3.3 mmol, 1.3 equiv.) were reacted for 22 h in 15 mL DCM. Column chromatography (hexanes:EtOAc = 9:1) yielded a colorless oil which solidified in the fridge (598 mg, 1.73 mmol, 68%).

**R<sub>f</sub>** (hexanes:EtOAc = 9:1) = 0.4; light brown with vanillin.

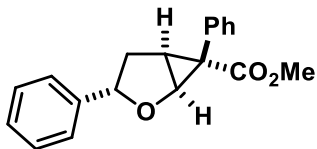
**IR (neat):** 3059, 2952, 1726, 1693, 1429, 1366, 1329, 1249, 1222, 1156, 1124, 1100, 1012, 989, 969, 880, 855, 773 cm<sup>-1</sup>.

**<sup>1</sup>H NMR** (400 MHz, CDCl<sub>3</sub>): δ 7.80 (d, *J* = 9.0 Hz, 1H), 7.71 (d, *J* = 8.2 Hz, 1H), 7.50 (m, 5H), 7.45 – 7.36 (m, 5H), 7.32 (m, 1H), 4.89 (d, *J* = 5.8 Hz, 1H), 4.25 (t, *J* = 8.3 Hz, 1H), 3.64 (s, 3H), 2.81 (t, *J* = 5.8 Hz, 1H), 2.55 (dd, *J* = 13.4, 8.3 Hz, 1H), 2.24 (ddd, *J* = 13.4, 8.3, 6.0 Hz, 1H).

$^{13}\text{C}$  NMR (101 MHz,  $\text{CDCl}_3$ ):  $\delta$  172.2, 137.6, 133.9, 132.5, 131.8, 129.7, 128.8, 128.1, 127.9, 126.0, 125.6, 125.5, 123.1, 122.3, 81.0, 70.1, 52.5, 37.7, 34.8, 32.4.

HR-MS (EI-MS):  $m/z$  calc. for  $\text{C}_{23}\text{H}_{20}\text{O}_3$  [ $\text{M}^+$ ] 344.14070, found 344.13983.

**Methyl (1*R*,3*R*,5*R*,6*S*)-3,6-diphenyl-2-oxabicyclo[3.1.0]hexane-6-carboxylate** **167a**



According to **GP3**, compound **164a** (506 mg, 3.47 mmol, 1 equiv.) and methyl 2-phenyl-2-diazoacetate (790 mg, 4.5 mmol, 1.3 equiv.) were reacted for 22 h in 20 mL DCM. Column chromatography (hexanes:EtOAc = 9:1) yielded a colorless crystalline solid (737 mg, 2.50 mmol, 72%).

$R_f$  (hexanes:EtOAc = 9:1) = 0.25; light brown with vanillin.

**m.p.:** 94 °C.

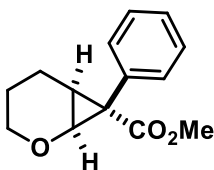
**IR (neat):** 3052, 2938, 2907, 2880, 1700, 1600, 1435, 1248, 1114, 1068, 1002, 946, 863  $\text{cm}^{-1}$ .

$^1\text{H}$  NMR (400 MHz,  $\text{CDCl}_3$ ):  $\delta$  7.40 (m, 5H), 7.22 (m, 3H), 7.08 (m, 2H), 4.75 (d,  $J = 5.8$  Hz, 1H), 3.60 (s+t overlap, 4H), 3.54 (s, 1H), 2.73 (t,  $J = 6.0$  Hz, 1H), 2.35 (dd,  $J = 13.4, 8.3$  Hz, 1H), 2.16 (ddd,  $J = 13.4, 8.3, 6.0$  Hz, 1H).

$^{13}\text{C}$  NMR (75 MHz,  $\text{CDCl}_3$ ):  $\delta$  172.2, 142.2, 132.4, 131.7, 128.7, 128.6, 128.4, 128.0, 127.7, 127.6, 125.5, 83.0, 70.2, 52.5, 37.6, 35.7, 32.3.

HR-MS (EI-MS):  $m/z$  calc. for  $\text{C}_{19}\text{H}_{18}\text{O}_3$  [ $\text{M}^+$ ] 294.12505, found 294.12494.

**Methyl 7-phenyl-2-oxabicyclo[4.1.0]heptane-7-carboxylate** **181a**



Following **GP3**, 3,4-dihydro-2*H*-pyran (2 g, 10 mmol, 1 equiv.) and methyl 2-phenyl-2-diazoacetate (2.6 g, 15 mmol, 1.5 equiv.) were reacted. Column chromatography (hexanes:EtOAc = 9:1) yielded a colorless crystalline solid (360 mg, 1.55 mmol, 88%).

$R_f$  (hexanes:EtOAc 4:1) = 0.33; light brown with vanillin.

**m.p.:** 110-113 °C.

**IR (neat):** 3063, 2989, 2949, 2856, 1701, 1433, 1390, 1342, 1248, 1202, 1081, 1061, 972, 904  $\text{cm}^{-1}$ .



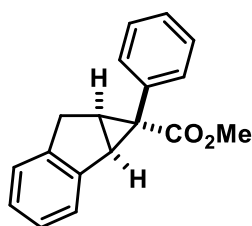
<sup>1</sup>H NMR (400 MHz, CDCl<sub>3</sub>): δ 7.38 – 7.28 (m, 5H), 4.21 (d, *J* = 7.5 Hz, 1H), 3.55 (s, 3H), 3.44 – 3.38 (m, 1H), 3.30 (ddd, *J* = 12.6, 10.7, 2.1 Hz, 1H), 2.16 (td, *J* = 7.3, 1.1 Hz, 1H), 2.01 (ddt, *J* = 14.2, 11.4, 7.0 Hz, 1H), 1.91 – 1.84 (m, 1H), 1.07 – 0.98 (m, 1H), 0.37 – 0.23 (m, 1H).

<sup>13</sup>C NMR (101 MHz, CDCl<sub>3</sub>): δ 173.7, 133.2, 132.5, 128.0, 127.0, 64.5, 62.1, 52.3, 34.8, 25.3, 21.1, 17.4.

HR-MS (EI-MS): *m/z* calc. for C<sub>14</sub>H<sub>16</sub>O<sub>3</sub> [M<sup>+</sup>] 232.10940, found 232.10881.

**Methyl (1*S*\*,1*aR*\*,6*aR*\*)-1-phenyl-1,1*a*,6,6*a*-tetrahydrocyclopropa[*a*]indene-1-carboxylate**

**183c**



According to **GP3**, indene (2.1 g, 18 mmol, 10 equiv.) and methyl 2-phenyl-2-diazoacetate (330 mg, 1.9 mmol, 1 equiv.) were reacted for 18 h in 6 mL DCM. Column chromatography (hexanes:EtOAc = 19:1 to 9:1) yielded a colorless crystalline solid (460 mg, 1.74 mmol, 91%).

*R<sub>f</sub>* (hexanes:EtOAc = 9:1) = 0.4; light brown with vanillin.

*m.p.*: 125 °C.

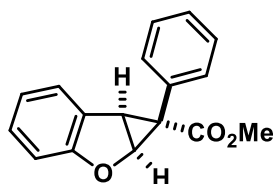
IR (neat): 3046, 2951, 2915, 2839, 1708, 1494, 1432, 1314, 1245, 1218, 1158, 1052, 942, 867 cm<sup>-1</sup>.

<sup>1</sup>H NMR (300 MHz, CDCl<sub>3</sub>): δ 7.40 (d, *J* = 7.5 Hz, 1H), 7.13 – 7.00 (m, 4H), 6.99 – 6.84 (m, 3H), 6.72 (d, *J* = 7.5 Hz, 1H), 3.63 (s, 3H), 3.47 (d, *J* = 6.8 Hz, 1H), 3.23 (dd, *J* = 17.9, 6.7 Hz, 1H), 2.87 (t, *J* = 7.0 Hz, 1H), 2.75 (d, *J* = 17.9 Hz, 1H).

<sup>13</sup>C NMR (75 MHz, CDCl<sub>3</sub>): δ 174.0, 143.0, 141.4, 132.2, 132.1, 127.3, 126.5, 126.3, 126.1, 125.0, 124.1, 52.5, 40.7, 38.2, 33.2, 32.1.

HR-MS (EI-MS): *m/z* calc. for C<sub>18</sub>H<sub>16</sub>O<sub>3</sub> [M<sup>+</sup>] 264.1144, found 264.1148.

**Methyl 1-phenyl-1*a*,6*b*-dihydro-1*H*-cyclopropa[*b*]benzofuran-1-carboxylate** **190**



Following **GP3**, benzo[*b*]furan (1.2 g, 10 mmol, 3 equiv.) and methyl 2-phenyl-2-diazoacetate (602 mg, 3.4 mmol, 1 equiv.) were reacted. Column chromatography (hexanes:EtOAc = 19:1) yielded colorless crystalline solid (683 mg, 2.56 mmol, 76%).

**R<sub>f</sub>** (hexanes:EtOAc = 9:1) = 0.4; bright red with vanillin.

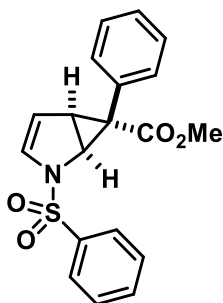
**<sup>1</sup>H NMR** (300 MHz, CDCl<sub>3</sub>): δ 7.35 (dd, *J* = 7.4, 1.5 Hz, 1H), 7.08 (s, 5H), 6.94 – 6.87 (td, *J* = 7.4, 1.3 Hz, 1H), 6.80 (td, *J* = 7.4, 1.1 Hz, 1H), 6.46 (dq, *J* = 8.1, 0.7 Hz, 1H), 5.36 (d, *J* = 5.5 Hz, 1H), 3.79 (dd, *J* = 5.5, 0.5 Hz, 1H), 3.67 (s, 3H).

**<sup>13</sup>C NMR** (75 MHz, CDCl<sub>3</sub>): δ 173.3, 159.4, 132.5, 129.5, 128.0, 127.5, 127.1, 126.4, 125.0, 121.1, 109.6, 70.4, 52.7, 37.4, 30.9.

**LR-MS** (EI-MS): *m/z* calc. for C<sub>17</sub>H<sub>14</sub>O<sub>3</sub> [M<sup>+</sup>] 266.0943, found 266.0937.

Analytical data is in accordance with the literature.<sup>119</sup>

### Methyl 6-phenyl-2-(phenylsulfonyl)-2-azabicyclo[3.1.0]hex-3-ene-6-carboxylate S3



1-(phenylsulfonyl)-1*H*-pyrrole (1.6 g, 7.7 mmol, 2 equiv.) and Rh<sub>2</sub>(OAc)<sub>4</sub> were dissolved in 10 mL DCM and a solution of methyl 2-phenyl-2-diazoacetate (0.76 g, 3.8 mmol, 1 equiv.) in 5 mL DCM was added via a syringe pump over the course of 2 h. After completion of the reaction the solvent was removed and column chromatography (hexanes:EtOAc = 9:1) yielded a colorless crystalline solid (562 mg, 1.58 mmol, 41%), which was used in the next step without additional purification.

**R<sub>f</sub>** (hexanes:EtOAc = 7:1) = 0.3; light brown with vanillin.

**m.p.:** 118-120 °C.

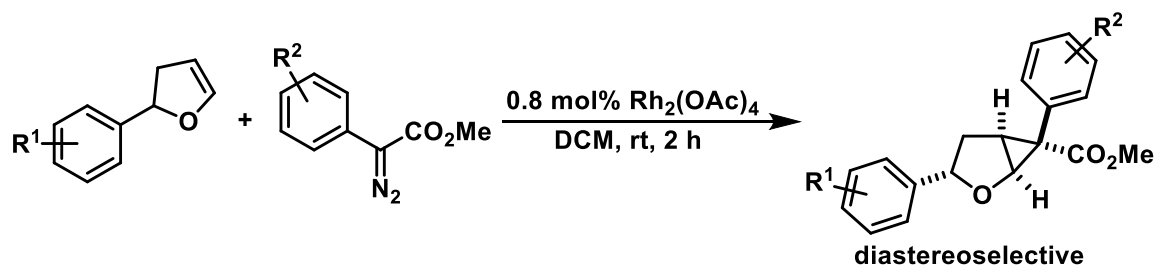
**IR** (neat): 3123, 2874, 2933, 2810, 2758, 1700, 1413, 1364, 1297, 1152, 1014, 831, 760 cm<sup>-1</sup>.

**<sup>1</sup>H NMR** (400 MHz, CDCl<sub>3</sub>): δ 7.84 (d, *J* = 7.7 Hz, 2H), 7.62 (t, *J* = 7.6 Hz, 1H), 7.54 (t, *J* = 7.6 Hz, 2H), 7.25 (q, *J* = 4.9 Hz, 5H), 5.97 (d, *J* = 3.4 Hz, 1H), 5.31 (t, *J* = 3.1 Hz, 1H), 4.60 (dd, *J* = 6.6, 1.4 Hz, 1H), 3.57 (s, 3H), 3.17 (dd, *J* = 6.6, 2.4 Hz, 1H).

**<sup>13</sup>C NMR** (101 MHz, CDCl<sub>3</sub>): δ 173.3, 137.7, 133.3, 132.3, 130.6, 130.2, 129.3, 127.7, 127.3, 127.0, 111.4, 77.4, 77.1, 76.8, 52.6, 51.9, 38.5, 28.0.

**HR-MS** (ESI-TOF): *m/z* calc. for C<sub>19</sub>H<sub>18</sub>NO<sub>4</sub>S [M+H<sup>+</sup>] 356.0951, found 356.0954.

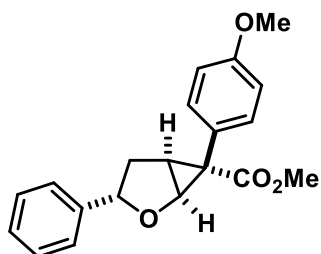
*General Procedure 4 (GP4) for the Rh<sub>2</sub>(OAc)<sub>4</sub> Catalyzed Cyclopropanation of Phenyl-2,3-dihydrofurans*



In a modification of commonly employed Rh-catalyzed cyclopropanations <sup>e.g. 119</sup>, a solution of 2-phenyl-2,3-dihydrofuran (1 equiv.) and Rh<sub>2</sub>(OAc)<sub>4</sub> (0.08 mol%) in dry DCM (approx. 5 mL per mmol furan) in an 100 mL round bottom flask was degassed by bubbling N<sub>2</sub> for 3 min. The flask was then equipped with a rubber septum and a nitrogen balloon. In a separate flask, the methyl 2-aryl-2-diazoacetate (approx. 1.3 equiv.) was dissolved in dry DCM and the solution also degassed via N<sub>2</sub>-bubbling for 3 min. This solution was then drawn up into a syringe and added to the solution of substrate and catalyst *via* a syringe pump over the course of 2-4 h. The resulting solution was stirred for further 2 h, then the solvent was removed under reduced pressure and the resulting crude purified by column chromatography.

**Methyl (1S\*,3S\*,5S\*,6R\*)-6-(4-methoxy)-3-phenyl-2-oxabicyclo[3.1.0]hexane-6-carboxylate**

**155a**



Following **GP4**, compound **164a** (562 mg, 3.86 mmol, 1.2 equiv.) and methyl 2-(4-methoxyphenyl)-2-diazoacetate (711 mg, 3.22 mmol, 1 equiv.) were reacted. Column chromatography (hexanes:EtOAc = 9:1 to 7:1) yielded a colorless crystalline solid (554 mg, 1.70 mmol, 53%).

**R<sub>f</sub>** (hexanes:EtOAc = 9:1) = 0.18; yellow with vanillin.

**m.p.:** 98-100 °C.

**IR** (neat): 3000, 2956, 2943, 2908, 2841, 1695, 1613, 1513, 1248, 1174, 1109, 1074, 1036, 862 cm<sup>-1</sup>.

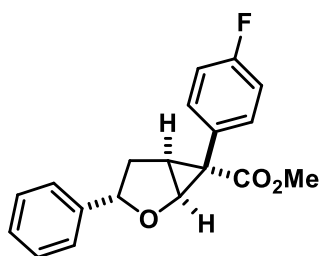
**<sup>1</sup>H NMR** (400 MHz, CDCl<sub>3</sub>): δ 7.36 – 7.29 (m, 2H), 7.29 – 7.16 (m, 3H), 7.11 (d, *J* = 7.0 Hz, 2H), 6.96 (d, *J* = 8.8 Hz, 2H), 4.74 (d, *J* = 5.8 Hz, 1H), 3.85 (s, 3H), 3.68 (t, *J* = 8.3 Hz, 1H),

3.60 (s, 3H), 2.71 (t,  $J = 5.9$  Hz, 1H), 2.34 (dd,  $J = 13.3, 8.4$  Hz, 1H), 2.16 (ddd,  $J = 13.5, 8.2, 6.1$  Hz, 1H).

$^{13}\text{C}$  NMR (101 MHz,  $\text{CDCl}_3$ ):  $\delta$  172.5, 159.1, 142.4, 132.8, 128.4, 127.5, 125.5, 124.4, 114.2, 83.1, 70.2, 55.3, 52.4, 36.9, 35.7, 32.3.

HR-MS (EI-MS):  $m/z$  calc. for  $\text{C}_{20}\text{H}_{21}\text{O}_4$   $[\text{M}+\text{H}^+]^+$  325.1439, found 325.1434.

Methyl (1*S*\*,3*S*\*,5*S*\*,6*R*\*)-6-(4-fluorophenyl)-3-phenyl-2-oxabicyclo[3.1.0]hexane-6-carboxylate **155c**



Following **GP4**, compound **164a** (226 mg, 1.55 mmol, 1.3 equiv.) and methyl 2-(4-fluorophenyl)-2-diazoacetate (230 mg, 1.18 mmol, 1 equiv.) were reacted. Column chromatography (hexanes:EtOAc = 19:1 to 9:1) yielded a yellowish crystalline solid (132 mg, 0.42 mmol, 36%).

$R_f$  (hexanes:EtOAc = 9:1) = 0.22; brown with vanillin.

**m.p.:** 112-114 °C.

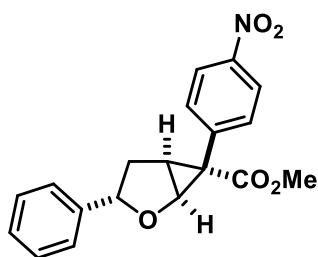
**IR** (neat): 3063, 2999, 2954, 2907, 2839, 1697, 1513, 1436, 1246, 1175, 1110, 1072, 1036, 862  $\text{cm}^{-1}$ .

$^1\text{H}$  NMR (400 MHz,  $\text{CDCl}_3$ ):  $\delta$  7.39 (m, 2H), 7.30 – 7.19 (m, 3H), 7.16 – 7.08 (m, 4H), 4.76 (d,  $J = 5.8$  Hz, 1H), 3.66 (t,  $J = 8.3$  Hz, 1H), 3.61 (s, 3H), 2.75 (t,  $J = 5.8$  Hz, 1H), 2.33 (dd,  $J = 13.5, 8.4$  Hz, 1H), 2.19 (ddd,  $J = 13.5, 8.4, 6.0$  Hz, 1H).

$^{13}\text{C}$  NMR (101 MHz,  $\text{CDCl}_3$ ):  $\delta$  171.9, 162.4 (d), 142.1, 133.4 (d), 128.4, 128.3 (d), 127.6, 125.5, 115.8 (d), 83.2, 70.1, 52.4, 37.0, 35.6, 32.3.

HR-MS (EI-MS):  $m/z$  calc. for  $\text{C}_{19}\text{H}_{17}\text{O}_3\text{F}$   $[\text{M}^+]$  312.11562, found 312.11497.

**Methyl (1*S*\*,3*S*\*,5*S*\*,6*R*\*)-6-(4-nitrophenyl)-3-phenyl-2-oxabicyclo[3.1.0]hexane-6-carboxylate** **155d**



Following **GP4**, compound **164a** (340 mg, 0.84 mmol, 1.2 equiv.) and methyl 2-(4-nitrophenyl)-2-diazoacetate (156 mg, 0.71 mmol, 1 equiv.) were reacted. Column chromatography (hexanes:EtOAc = 9:1 to 7:1) yielded a colorless crystalline solid (76 mg, 0.22 mmol, 32%).

The reaction was performed twice to obtain enough material for the follow-up reaction.

**R<sub>f</sub>** (hexanes:EtOAc = 9:1) = 0.18; yellow with vanillin.

**m.p.:** 181 °C.

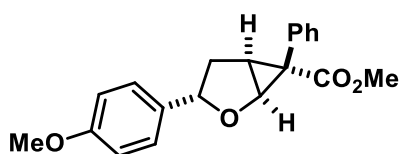
**IR** (neat): 3063, 2963, 2363, 1709, 1598, 1512, 1446, 1349, 1248, 1176, 1111, 1065, 943, 869 cm<sup>-1</sup>.

**<sup>1</sup>H NMR** (400 MHz, CDCl<sub>3</sub>): δ 8.29 (d, *J* = 8.8 Hz, 2H), 7.60 (d, *J* = 8.8 Hz, 2H), 7.25 (m, 3H), 7.11 – 7.07 (m, 2H), 4.82 (d, *J* = 5.7 Hz, 1H), 3.65 (t, *J* = 8.2 Hz, 1H), 3.61 (s, 3H), 2.84 (t, *J* = 5.7 Hz, 1H), 2.36 – 2.21 (m, 2H).

**<sup>13</sup>C NMR** (101 MHz, CDCl<sub>3</sub>): δ 170.7, 147.5, 141.6, 140.2, 132.8, 128.5, 127.8, 125.3, 123.8, 83.3, 70.0, 52.6, 37.5, 35.4, 32.7.

**HR-MS** (EI-MS): *m/z* calc. for C<sub>19</sub>H<sub>17</sub>NO<sub>5</sub> [M<sup>+</sup>] 339.11012, found 339.10954.

**Methyl (1*S*\*,3*S*\*,5*S*\*,6*R*\*)-3-(4-Methoxyphenyl)-6-phenyl-2-oxabicyclo[3.1.0]hexane-6-carboxylate** **166c**



Following **GP4**, compound **164f** (573 mg, 3.26 mmol, 1 equiv.) and methyl 2-phenyl-2-diazoacetate (695 mg, 3.95 mmol, 1.2 equiv.) were reacted. Column chromatography (hexanes:EtOAc = 9:1) yielded a colorless solid (855 mg, 2.64 mmol, 81%).

**R<sub>f</sub>** (hexanes:EtOAc = 9:1) = 0.25; brown with vanillin.

**m.p.:** 101-103 °C.

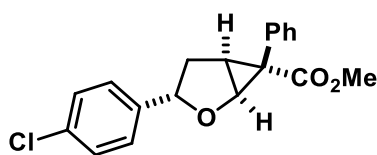
**IR** (neat): 3061, 2999, 2934, 1695, 1612, 1512, 1436, 1246, 1174, 1110, 1074, 1036, 1007, 862, 706 cm<sup>-1</sup>.

<sup>1</sup>H NMR (400 MHz, CDCl<sub>3</sub>): δ 7.41 (m, 5H), 7.01 (d, *J* = 8.7 Hz, 2H), 6.78 (d, *J* = 8.7 Hz, 2H), 4.73 (d, *J* = 5.8 Hz, 1H), 3.75 (s, 3H), 3.60 (s, 3H), 3.55 (t, *J* = 8.2 Hz, 1H), 2.74 (t, *J* = 5.8 Hz, 1H), 2.31 (dd, *J* = 13.4, 8.2 Hz, 1H), 2.16 (ddd, *J* = 13.7, 8.3, 6.1 Hz, 1H).

<sup>13</sup>C NMR (101 MHz, CDCl<sub>3</sub>): δ 172.2, 159.1, 134.2, 132.5, 131.7, 128.7, 127.7, 127.0, 113.8, 82.8, 70.0, 55.3, 52.4, 37.6, 35.6, 32.3.

HR-MS (EI-MS): *m/z* calc. for C<sub>20</sub>H<sub>20</sub>O<sub>4</sub> [M<sup>+</sup>] 324.13695, found 324.13606.

Methyl (1*S*\*,3*S*\*,5*S*\*,6*R*\*)-3-(4-chlorophenyl)-6-phenyl-2-oxabicyclo[3.1.0]hexane-6-carboxylate **166d**



Following **GP4**, compound **164c** (732 mg, 4.1 mmol, 1 equiv.) and methyl 2-phenyl-2-diazoacetate (1.07 g, 6.1 mmol, 1.5 equiv.) were reacted. Column chromatography (hexanes:EtOAc = 19:1 to 7:1) yielded a colorless oil which solidified in the fridge (598 mg, 3.13 mmol, 77%).

*R<sub>f</sub>* (hexanes:EtOAc = 4:1) = 0.42; light brown with vanillin.

*m.p.*: 162-164 °C

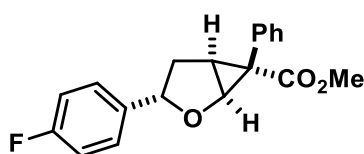
IR (neat): 3060, 2935, 1700, 1492, 1435, 1329, 1246, 1178, 1112, 1072, 1003, 944, 863, 831 cm<sup>-1</sup>.

<sup>1</sup>H NMR (400 MHz, CDCl<sub>3</sub>): δ 7.45 – 7.37 (m, 5H), 7.21 (d, *J* = 8.5 Hz, 2H), 7.02 (d, *J* = 8.5 Hz, 2H), 4.75 (d, *J* = 5.8 Hz, 1H), 3.60 (s, 3H), 3.56 (t, *J* = 8.3 Hz, 1H), 2.73 (t, *J* = 5.8 Hz, 1H), 2.35 (dd, *J* = 13.4, 8.3 Hz, 1H), 2.10 (ddd, *J* = 13.4, 8.3, 6.1 Hz, 1H).

<sup>13</sup>C NMR (101 MHz, CDCl<sub>3</sub>): δ 172.1, 140.8, 133.2, 132.3, 131.7, 128.7, 128.5, 127.8, 126.9, 82.3, 70.1, 52.5, 37.6, 35.8, 32.1.

HR-MS (EI-MS): *m/z* calc. for C<sub>19</sub>H<sub>17</sub>O<sub>3</sub>Cl [M<sup>+</sup>] 328.0860, found 328.0864.

Methyl (1*S*\*,3*S*\*,5*S*\*,6*R*\*)-3-(4-fluorophenyl)-6-phenyl-2-oxabicyclo[3.1.0]hexane-6-carboxylate **166e**



Following **GP4**, compound **164d** (607 mg, 3.7 mmol, 1 equiv.) and methyl 2-phenyl-2-diazoacetate (930 mg, 5.3 mmol, 1.3 equiv.) were reacted to form an orange

solution. Column chromatography (hexanes:EtOAc = 9:1) yielded a colorless crystalline solid (595 mg, 1.91 mmol, 52%).

**R<sub>f</sub>** (hexanes:EtOAc = 4:1) = 0.37; light brown with vanillin.

**m.p.:** 151-153 °C.

**IR** (neat): 3060, 2923, 1700, 1600, 1509, 1450, 1330, 1248, 1182, 1114, 1071, 1002, 944, 836 cm<sup>-1</sup>.

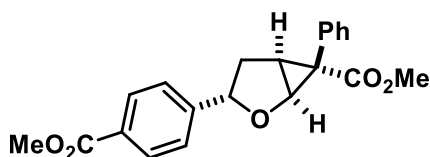
**<sup>1</sup>H NMR** (400 MHz, CDCl<sub>3</sub>) δ 7.40 (m, 5H), 7.05 (m, 2H), 6.93 (m, 2H), 4.75 (d, *J* = 5.8 Hz, 1H), 3.60 (s, 3H), 3.57 (t, *J* = 8.3 Hz, 1H), 2.74 (t, *J* = 5.8 Hz, 1H), 2.34 (dd, *J* = 13.4, 8.3 Hz, 1H), 2.16 – 2.09 (m, 1H).

**<sup>13</sup>C NMR** (101 MHz, CDCl<sub>3</sub>): δ 172.1, 163.4, 161.0, 137.9 (d), 132.4, 131.7, 128.7, 127.8, 127.3 (d), 115.2 (d), 82.4, 70.0, 52.5, 37.6, 35.8, 32.1. Doublets observed due to coupling with fluorine

**<sup>19</sup>F NMR** (282 MHz, CDCl<sub>3</sub>) δ -114.56 (tt, *J* = 8.6, 5.4 Hz).

**HR-MS** (EI-MS): *m/z* calc. for C<sub>19</sub>H<sub>17</sub>O<sub>3</sub>F [M<sup>+</sup>] 312.11562, found 312.11559.

**Methyl (1*S*\*,3*S*\*,5*S*\*,6*R*\*)-3-(4-(methoxycarbonyl)phenyl)-6-phenyl-2-oxabicyclo[3.1.0]hexane-6-carboxylate 166f**



Following **GP4**, compound **164e** (633 mg, 3.1 mmol, 1 equiv.) and methyl 2-phenyl-2-diazoacetate (810 mg, 4.6 mmol, 1.5 equiv.) were reacted. Column chromatography (hexanes:EtOAc = 19:1 to 9:1) yielded a colorless crystalline solid (847 mg, 2.4 mmol, 77%).

**R<sub>f</sub>** (hexanes:EtOAc = 4:1) = 0.25; brown with vanillin.

**m.p.:** 130 °C.

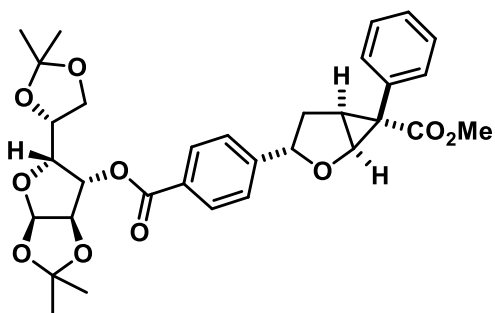
**IR** (neat): 3035, 2951, 2909, 1711, 1612, 1496, 1433, 1275, 1239, 1106, 1068, 947, 857 cm<sup>-1</sup>.

**<sup>1</sup>H NMR** (400 MHz, CDCl<sub>3</sub>): δ 7.92 (d, *J* = 8.4 Hz, 2H), 7.45 – 7.36 (m, 5H), 7.15 (d, *J* = 8.4 Hz, 2H), 4.78 (d, *J* = 5.8 Hz, 1H), 3.87 (s, 3H), 3.65 (t, *J* = 8.3 Hz, 1H), 3.59 (s, 3H), 2.73 (t, *J* = 5.8 Hz, 1H), 2.39 (dd, *J* = 13.3, 8.3 Hz, 1H), 2.12 (ddd, *J* = 13.3, 8.3, 6.1 Hz, 1H).

**<sup>13</sup>C NMR** (101 MHz, CDCl<sub>3</sub>): δ 172.0, 166.8, 147.4, 132.2, 131.6, 129.8, 129.3, 128.7, 127.8, 125.2, 82.4, 70.2, 52.5, 52.1, 37.7, 35.7, 32.0.

**HR-MS** (APCI-MS): *m/z* calc. for C<sub>21</sub>H<sub>21</sub>O<sub>5</sub> [M+H]<sup>+</sup> 353.1384, found 353.1386.

**Methyl (1*R*,3*R*,5*R*,6*S*)-3-(4-((((3*aR*,5*R*,6*S*,6*aR*)-5-((*R*)-2,2-dimethyl-1,3-dioxolan-4-yl)-2,2-dimethyltetrahydrofuro[2,3-*d*][1,3]dioxol-6-yl)oxy)carbonyl)phenyl)-6-phenyl-2-oxabicyclo[3.1.0]hexane-6-carboxylate** **166g**



Following **GP4**, the corresponding dihydrofuran derivative (410 mg, 0.95 mmol, 1 equiv.) and methyl 2-phenyl-2-diazoacetate (190 mg, 1.05 mmol, 1.1 equiv.) were reacted. Column chromatography (hexanes:EtOAc = 4:1 to 3:1) yielded a colorless oil (220 mg, 0.38 mmol, 40%).

**R<sub>f</sub>** (hexanes:EtOAc = 4:1) = 0.2; brown with vanillin.

**IR** (neat): 2956, 2906, 2840, 1740, 1713, 1612, 1516, 1368, 1219, 1177, 1030, 910, 835, 800 cm<sup>-1</sup>.

**<sup>1</sup>H NMR** (400 MHz, CDCl<sub>3</sub>-*d*): δ 7.89 (d, *J* = 8.3 Hz, 2H), 7.44 – 7.37 (m, 5H), 7.16 (d, *J* = 8.3 Hz, 2H), 5.92 (d, *J* = 3.7 Hz, 1H), 5.48 – 5.45 (m, 1H), 4.77 (d, *J* = 5.7 Hz, 1H), 4.60 (d, *J* = 3.7 Hz, 1H), 4.33 – 4.28 (m, 2H), 4.11 – 4.03 (m, 2H), 3.65 (t, *J* = 8.3 Hz, 1H), 3.59 (s, 3H), 2.73 (t, *J* = 5.8 Hz, 1H), 2.40 (dd, *J* = 13.3, 8.5 Hz, 1H), 2.10 (ddd, *J* = 13.8, 8.1, 6.2 Hz, 1H), 1.54 (s, 3H), 1.39 (s, 3H), 1.30 (s, 3H), 1.23 (s, 3H).

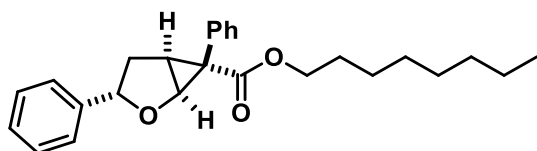
**<sup>13</sup>C NMR** (101 MHz, CDCl<sub>3</sub>): δ 171.9, 164.9, 148.1, 132.2, 131.6, 129.9, 128.8, 128.6, 127.8, 125.4, 125.3, 112.4, 109.4, 105.2, 83.4, 82.3, 82.3, 80.0, 72.6, 70.2, 67.3, 52.5, 37.7, 35.7, 31.9, 26.9, 26.8, 26.3, 25.2.

**HR-MS** (ESI-MS): *m/z* calc. for C<sub>32</sub>H<sub>36</sub>O<sub>10</sub>Na [M+Na<sup>+</sup>]<sup>+</sup> 603.2199, found 603.2201.

**Optical rotation** (DCM): [*a*]<sub>D</sub><sup>20</sup> = 81.1°



**Octyl (1*S*\*,3*S*\*,5*S*\*,6*R*\*)-3,6-diphenyl-2-oxabicyclo[3.1.0]hexane-6-carboxylate 167h**



Following **GP4**, compound **164a** (830 mg, 3.03 mmol, 1 equiv.) and octyl 2-phenyl-2-diazoacetate (891 mg, 6.1 mmol, 2 equiv.) were reacted. After reaction completion the crude was purified *via* column chromatography (hexanes:EtOAc = 99:1), yielding a colorless oil (841 mg, 2.14 mmol, 70%).

**R<sub>f</sub>** (hexanes:EtOAc = 9:1) = 0.6; light brown with vanillin.

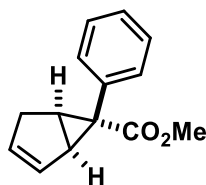
**IR** (neat): 3060, 2925, 2855, 1705, 1449, 1330, 1242, 1177, 1156, 1110, 1065, 972, 751, 698 cm<sup>-1</sup>.

**<sup>1</sup>H NMR** (400 MHz, CDCl<sub>3</sub>): δ 7.42 – 7.33 (m, 5H), 7.22 (m, 3H), 7.09 (d, *J* = 7.1 Hz, 2H), 4.75 (d, *J* = 5.8 Hz, 1H), 3.99 (td, *J* = 6.5, 1.4 Hz, 2H), 3.64 (t, *J* = 8.3 Hz, 1H), 2.72 (t, *J* = 5.9 Hz, 1H), 2.36 (dd, *J* = 13.3, 8.3 Hz, 1H), 2.16 (ddd, *J* = 13.7, 8.2, 6.1 Hz, 1H), 1.49 (p, *J* = 6.4 Hz, 2H), 1.35 – 1.15 (m, 12H), 0.89 (t, *J* = 7.0 Hz, 3H).

**<sup>13</sup>C NMR** (101 MHz, CDCl<sub>3</sub>): δ 171.7, 142.3, 132.7, 131.6, 128.6, 128.4, 127.5, 127.5, 125.5, 82.9, 69.9, 65.2, 37.9, 35.8, 31.9, 31.8, 29.2, 29.1, 28.5, 25.8, 22.7, 14.2.

**HR-MS** (EI-MS): *m/z* calc. for C<sub>26</sub>H<sub>33</sub>O<sub>3</sub> [M+H]<sup>+</sup> 393.2424, found 393.2427.

**Methyl (1*S*\*,5*R*\*,6*S*\*)-6-phenylbicyclo[3.1.0]hex-2-ene-6-carboxylate 183a**



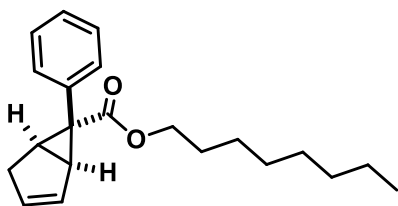
Following **GP4**, freshly distilled cyclopentadiene (1.8 mL, 21.3 mmol, 7 equiv.) and methyl 2-phenyl-2-diazoacetate (5.3 mL, 3.0 mmol, 1 equiv.) were reacted. Column chromatography (hexanes:EtOAc = 99:1 to 9:1) yielded a colorless crystalline solid (318 mg, 1.49 mmol, 49%).

**<sup>1</sup>H NMR** (400 MHz, CDCl<sub>3</sub>): δ 7.29 – 7.20 (m, 3H), 7.15 – 7.05 (m, 2H), 5.78 – 5.71 (m, 1H), 5.24 – 5.16 (m, 1H), 3.58 (s, 3H), 3.00 – 2.87 (m, 1H), 2.72 – 2.56 (m, 2H), 2.14 – 1.99 (m, 1H).

**<sup>13</sup>C NMR** (101 MHz, CDCl<sub>3</sub>): δ 174.5, 133.1, 133.0, 132.9, 129.7, 127.6, 126.8, 52.5, 40.9, 37.9, 34.2, 32.4.

Analysis was in accordance with the literature.<sup>173</sup>

### Octyl (1*S*\*,5*R*\*,6*S*\*)-6-phenylbicyclo[3.1.0]hex-2-ene-6-carboxylate 183b



Following **GP4**, freshly distilled cyclopentadiene (0.225 mL, 2.7 mmol, 5 equiv.) and octyl 2-Phenyl-2-diazoacetate (145 mg, 0.53 mmol, 1 equiv.) were reacted in presence of  $\text{Rh}_2(\text{OAc})_4$  (1.4 mg, 0.0032 mmol, 0.006 equiv.). Column chromatography (hexanes:EtOAc = 99:1 to 9:1) yielded a colorless oil (85.9 mg, 0.275 mmol, 52%).

$R_f$  (hexanes:EtOAc = 9:1) = 0.7.

**IR** (neat): 3061, 2925, 2855, 1708, 1456, 1226, 1222, 1156, 1072, 972, 950, 866, 746  $\text{cm}^{-1}$ .

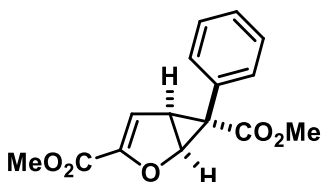
**$^1\text{H}$  NMR** (400 MHz  $\text{CDCl}_3$ ):  $\delta$  7.35 – 7.18 (m, 3H), 7.12 – 7.06 (m, 2H), 5.76 (dt,  $J = 5.4, 2.0$  Hz, 1H), 5.23 – 5.18 (m, 1H), 4.03 – 3.92 (m, 2H), 2.94 – 2.88 (m, 1H), 2.69 – 2.59 (m, 2H), 2.14 – 2.05 (m, 1H), 1.46 (p,  $J = 6.7$  Hz, 2H), 1.23 (m,  $J = 28.5, 8.5$  Hz, 10H), 0.88 (t,  $J = 7.0$  Hz, 3H).

**$^{13}\text{C}$  NMR** (101 MHz,  $\text{CDCl}_3$ ):  $\delta$  174.0, 132.9, 132.7, 129.8, 127.5, 126.6, 65.1, 41.6, 40.5, 38.2, 34.2, 32.1, 31.8, 29.2, 29.1, 28.6, 25.8, 22.7, 14.2.

Spectra are contaminated with octyl phenylacetate, integrals are corrected to account for that.

**HR-MS** (ESI-MS):  $m/z$  calc. for  $\text{C}_{21}\text{H}_{29}\text{O}_2$   $[\text{M}+\text{H}^+]^+$  313.2167, found 313.2162.

### Dimethyl (3*R*\*,5*S*\*,6*R*\*)-6-phenyl-2-oxabicyclo[3.1.0]hex-3-ene-3,6-dicarboxylate S4

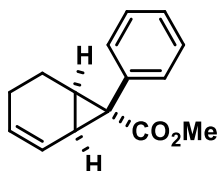


Following **GP4**, methyl 2-furoate (530  $\mu\text{L}$ , 5 mmol, 2 equiv.) and methyl 2-phenyl-2-diazoacetate (440 mg, 2.5 mmol, 2 equiv.) were reacted. Column chromatography (hexanes:EtOAc = 5:1) yielded a colorless crystalline solid (563 mg, 2.07 mmol, 88%).

**$^1\text{H}$  NMR** (400 MHz,  $\text{CDCl}_3$ ):  $\delta$  7.41 – 7.20 (m, 6H), 4.77 (dd,  $J = 10.5, 6.9$  Hz, 1H), 4.61 (d,  $J = 6.1$  Hz, 1H), 3.55 (s, 3H), 3.27 (s, 3H), 2.72 (ddd,  $J = 7.2, 6.1, 1.1$  Hz, 1H), 2.59 (ddd,  $J = 13.9, 10.5, 7.2$  Hz, 1H), 2.26 (ddd,  $J = 13.9, 6.9, 1.1$  Hz, 1H).

**$^{13}\text{C}$  NMR** (101 MHz,  $\text{CDCl}_3$ ):  $\delta$  173.1, 158.8, 148.8, 132.2, 129.5, 128.0, 127.7, 114.12, 71.1, 52.8, 52.0, 39.5, 28.5.

Analytical data is in accordance with the literature.<sup>119</sup>



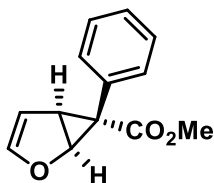
Following the literature procedure<sup>151</sup>, AgSbF<sub>6</sub> (179 mg, 0.52 mmol, 0.1 equiv.) was weighed into a flame dried Schlenk flask under N<sub>2</sub> atmosphere. The flask was wrapped in aluminum foil to exclude light and 10 mL dry DCM as well as Cyclohexadiene (2.4 mL, 25.2 mmol, 5 equiv.) were added. In a separate flask, methyl 2-phenyl-2-diazoacetate (970 mg, 5.5 mmol, 1 equiv.) was dissolved in 6 mL dry DCM and degassed by N<sub>2</sub> sparging, after which it was added to the cyclohexadiene-solution *via* a syringe pump over the course of 3 h. The solution was stirred for additional 1 h, then the solvent was removed under reduced pressure and the crude purified *via* column chromatography (hexanes:EtOAc = 19:1 to 9:1). The product was then recrystallized from Et<sub>2</sub>O to remove remaining cyclohexadiene to yield white crystals (415 mg 1.8 mmol, 33%).

**<sup>1</sup>H NMR** (400 MHz, CDCl<sub>3</sub>): δ 7.27 (d, *J* = 16.6 Hz, 5H), 6.03 (d, *J* = 9.4 Hz, 1H), 5.50 – 5.37 (m, 1H), 3.59 (s, 3H), 2.42 – 2.29 (m, 2H), 2.04 – 1.94 (m, 1H), 1.83 (m, 1H), 1.59 (dd, *J* = 15.7, 8.4 Hz, 1H), 0.47 (dt, *J* = 18.5, 9.8 Hz, 1H).

**<sup>13</sup>C NMR** (101 MHz, CDCl<sub>3</sub>): δ 174.0, 134.7, 131.7, 128.4, 127.7, 126.9, 122.7, 52.4, 40.3, 27.7, 25.6, 21.0, 16.8.

Analytical data is in accordance with the literature.<sup>151</sup>

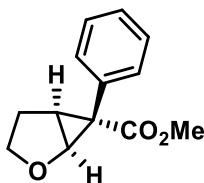
**Methyl (1*S*,5*S*,6*R*)-6-phenyl-2-oxabicyclo[3.1.0]hex-3-ene-6-carboxylate (-)-162**



In an modification of GP3 and following the literature procedure<sup>119</sup>, furan (150  $\mu$ L, 2 mmol, 2 equiv.) and methyl 2-phenyl-2-diazoacetate (176 mg, 1 mmol, 1 equiv.) were reacted in presence of  $\text{Rh}_2(\text{S-TCPTTL})_4$  (1.8 mg, 1  $\mu$ mol, 0.1 mol%) in dry hexanes (2 mL). After reaction completion, the solution was washed with 1M HCl, water and brine to remove the rhodium catalyst. Column chromatography (hexanes:EtOAc = 4:1) and repeated recrystallization from methanol afforded the product as white solid (145 mg, 0.67 mmol, 67%; 97% ee as determined by chiral HPLC).

Analytical data is in accordance with the literature.<sup>119</sup>

**Methyl (1*S*,5*S*,6*R*)-6-phenyl-2-oxabicyclo[3.1.0]hexane-6-carboxylate (-)-157**



In an uncovered vial, (-)-**162** (120 mg, 0.55 mmol, 1 equiv.) was dissolved in EtOAc (10 mL), and Rh/C (8.1 mg, 0.0039 mmol, 0.7 mol%) was added. The vial was then placed in an autoclave and after purging with  $\text{H}_2$  three times, the reaction was stirred under 30 bar  $\text{H}_2$  for 2 h. The crude product was purified by column chromatography (hexanes:EtOAc = 9:1) to yield a viscous clear oil which solidified in the fridge (116 mg, 0.53 mmol, 97%).

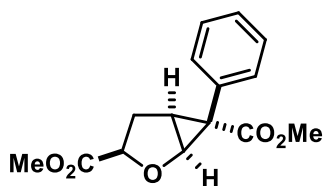
Analytical data is identical to ( $\pm$ )-**1a**.

**Optical** rotation:  $[\alpha]_D^{20} = -66.6^\circ$  in DCM.

Chiral HPLC chromatogram available; column: Phenomenex Lux Cellulose-1; eluent Heptane: *i*PrOH 99:1; Flow: 1 mL/min Retention time: 28.5, 29.6. Enantiomeric excess 98% ee.

**Dimethyl (1*S*\*,3*R*\*,5*S*\*,6*R*\*)-6-phenyl-2-oxabicyclo[3.1.0]hexane-3,6-dicarboxylate**

**187**



**S4** (531 mg, 1.94 mmol, 1 equiv.) was dissolved in 5 mL EtOAc. Pd/C (5% w/w Pd, 40 mg, 0.019 mmol Pd, 0.1 equiv.) was added, and the solution was stirred in an autoclave at 25 bar H<sub>2</sub> for 2h. Then the solution was filtrated, the solvent evaporated under reduced pressure and the crude purified by column chromatography (hexanes:EtOAc 9:1 to 5:1), yielding a colorless crystalline solid (523 mg, 1.89 mmol, 97%)

**R<sub>f</sub>** (hexanes:EtOAc = 4:1) = 0.36; reddish brown with vanillin.

**m.p.:** 140-142 °C.

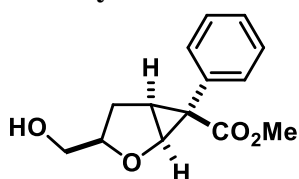
**IR** (neat): 3028, 2957, 2849, 1752, 1735, 1700, 1497, 1435, 1232, 1155, 1084, 1025, 956, 862 cm<sup>-1</sup>.

**<sup>1</sup>H NMR** (300 MHz, CDCl<sub>3</sub>): δ 7.38 – 7.22 (m, 5H), 4.77 (dd, *J* = 10.4, 6.9 Hz, 1H), 4.61 (d, *J* = 6.0 Hz, 1H), 3.55 (s, 3H), 3.26 (s, 3H), 2.72 (ddd, *J* = 7.1, 6.1, 1.0 Hz, 1H), 2.59 (ddd, *J* = 13.8, 10.4, 7.2 Hz, 1H), 2.26 (ddd, *J* = 13.9, 6.9, 1.0 Hz, 1H).

**<sup>13</sup>C NMR** (101 MHz, CDCl<sub>3</sub>): δ 171.7, 170.1, 133.3, 129.9, 128.2, 127.9, 83.6, 71.3, 52.5, 52.0, 41.2, 32.6, 29.0.

**HR-MS** (APCI-MS): *m/z* calc. for C<sub>15</sub>H<sub>17</sub>O<sub>5</sub> [M+H]<sup>+</sup> 277.1071, found 277.1074.

**Methyl (1*S*\*,3*R*\*,5*S*\*,6*R*\*)-3-(hydroxymethyl)-6-phenyl-2-oxabicyclo[3.1.0]hexane-6-carboxylate **S5****



**187** (1.01 g, 3.6 mmol, 1 equiv.) was dissolved in a mixture of 15 mL THF and 25 mL MeOH, and NaBH<sub>4</sub> (281 mg, 7.7 mmol, 2.1 equiv.) was slowly added in portions (gas evolution!). The reaction was stirred over night, then the solvents were evaporated and the crude subjected to column chromatography (hexanes:EtOAc = 2:1), yielding a colorless solid (554 mg, 2.23 mmol, 62%).

**R<sub>f</sub>** (hexanes:EtOAc = 2:1) = 0.23; yellow with vanillin.

**m.p.:** 118 °C.

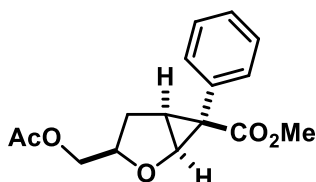
**IR** (neat): 3469, 3043, 2954, 1707, 1446, 1332, 1252, 1103, 1252, 1103, 1047, 1026, 960, 863  $\text{cm}^{-1}$ .

**$^1\text{H}$  NMR** (400 MHz,  $\text{CDCl}_3$ ):  $\delta$  7.46 – 7.32 (m, 3H), 7.28 – 7.22 (m, 2H), 4.56 – 4.45 (m, 2H), 3.57 (s, 3H), 3.03 (dd,  $J = 12.0, 3.1$  Hz, 1H), 2.72 (ddd,  $J = 7.8, 6.2, 1.8$  Hz, 1H), 2.43 (dd,  $J = 12.0, 6.1$  Hz, 1H), 2.20 (dt,  $J = 13.5, 7.9$  Hz, 1H), 1.60 (ddd,  $J = 13.6, 9.6, 1.9$  Hz, 1H), 0.93 (bs, 1H).

**$^{13}\text{C}$  NMR** (101 MHz,  $\text{CDCl}_3$ ):  $\delta$  171.7, 133.3, 131.4, 128.5, 127.9, 90.3, 69.5, 63.0, 52.3, 43.1, 33.2, 26.9.

**HR-MS** (ESI-MS):  $m/z$  calc. for  $\text{C}_{14}\text{H}_{17}\text{O}_4$   $[\text{M}+\text{H}^+]^+$  249.1121, found 249.1125.

**Methyl (1*S*\*,3*R*\*,5*S*\*,6*R*\*)-3-(acetoxymethyl)-6-phenyl-2-oxabicyclo[3.1.0]hexane-6-carboxylate 188**



**S5** (520 mg, 2.1 mmol, 1 equiv.) was dissolved in 10 mL DCM, and triethylamine (400  $\mu\text{L}$ , 2.9 mmol, 1.4 equiv) was added.  $\text{Ac}_2\text{O}$  was added (275  $\mu\text{L}$ , 2.7 mmol, 1.3 equiv.) and the resulting cloudy solution stirred for 3 h. Then the solution was washed with 0.5 M HCl,  $\text{NaHCO}_3$ (aq, sat), and brine. The organic phase was then dried over  $\text{MgSO}_4$  and the crude was purified by crystallization from DCM/ $\text{Et}_2\text{O}$ , yielding colorless crystals (504 mg, 1.74 mmol, 83%).

**R<sub>f</sub>** (hexanes:EtOAc = 4:1) = 0.38; bright yellow with vanillin.

**m.p.:** 114-116  $^\circ\text{C}$ .

**IR** (neat): 3043, 2966, 2910, 1745, 1700, 1437, 1372, 1249, 1229, 1072, 1043, 962, 858  $\text{cm}^{-1}$ .

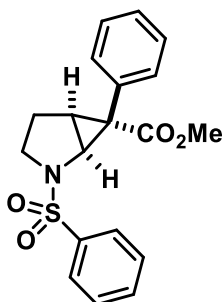
**$^1\text{H}$  NMR** (300 MHz,  $\text{CDCl}_3$ ):  $\delta$  7.45 – 7.27 (m, 3H), 7.22 (dd,  $J = 8.0, 1.5$  Hz, 2H), 4.65 – 4.46 (m, 2H), 3.54 (s, 3H), 3.31 (dd,  $J = 11.6, 3.5$  Hz, 1H), 2.69 (ddd,  $J = 7.6, 6.1, 1.6$  Hz, 1H), 2.58 (dd,  $J = 11.6, 8.4$  Hz, 1H), 2.33 (ddd,  $J = 13.6, 8.4, 7.7$  Hz, 1H), 1.92 (s, 3H), 1.44 (ddd,  $J = 13.6, 9.3, 1.6$  Hz, 1H).

**$^{13}\text{C}$  NMR** (75 MHz,  $\text{CDCl}_3$ ):  $\delta$  171.6, 170.4, 133.3, 130.9, 128.4, 127.9, 86.4, 70.6, 65.0, 52.3, 42.7, 32.6, 28.5, 20.7.

**HR-MS** (ESI-MS):  $m/z$  calc. for  $\text{C}_{16}\text{H}_{19}\text{O}_5$   $[\text{M}+\text{H}^+]^+$  291.1227, found 291.1231.

**Methyl (1*S*\*,5*S*\*,6*R*\*)-6-phenyl-2-(phenylsulfonyl)-2-azabicyclo[3.1.0]hexane-6-carboxylate**

**181b**



Compound **S3** (422 mg, 1.18 mmol, 1 equiv.) was dissolved in 10 mL EtOAc and hydrogenated in the presence of Rh/C (5 w/w% Rh, 30 mg, 0.006 mmol, 0.5 mol%) under 30 bar H<sub>2</sub> in an autoclave. After 3 h, the dispersion was filtrated and the crude mixture subjected to column chromatography (hexanes: EtOAc = 9:1 to 4:1), yielding the product (387 mg, 1.08 mmol, 92%) as colorless crystalline solid.

**R<sub>f</sub>** (hexanes:EtOAc = 4:1) = 0.33; brown with vanillin.

**m.p.:** 128-130 °C.

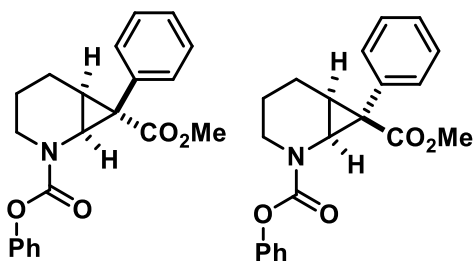
**IR** (neat): 3027, 2960, 2926, 1771, 1737, 1707, 1599, 1498, 1435, 1357, 1297, 1252, 1096, 954, 887, 820, 749, 671 cm<sup>-1</sup>.

**<sup>1</sup>H NMR** (300 MHz, CDCl<sub>3</sub>): δ 7.91 – 7.81 (m, 2H), 7.66 – 7.50 (m, 3H), 7.32 (s, 5H), 4.27 (d, *J* = 6.8 Hz, 1H), 3.58 (s, 3H), 3.26 – 3.14 (m, 1H), 2.48 (dd, *J* = 6.6, 5.7 Hz, 1H), 1.97 – 1.76 (m, 3H).

**<sup>13</sup>C NMR** (75 MHz, CDCl<sub>3</sub>): δ 171.83, 139.51, 132.88, 131.54, 131.26, 129.39, 128.74, 127.95, 127.00, 52.83, 51.84, 48.08, 37.27, 30.68, 25.09.

**HR-MS** (ESI-TOF): *m/z* calc. for C<sub>19</sub>H<sub>20</sub>NO<sub>4</sub>S [M+H<sup>+</sup>]<sup>+</sup> 358.1108, found 358.1110.

**7-methyl 2-phenyl 7-phenyl-2-azabicyclo[4.1.0]heptane-2,7-dicarboxylate 181c**



7-methyl 2-phenyl 7-phenyl-2-azabicyclo[4.1.0]hept-4-ene-2,7-dicarboxylate (500 mg, 1.43 mmol, 1 equiv.) was dissolved in 5 mL EtOAc, Rh/C (5% w/w Rh, 16 mg, 7.8 μmol, 0.5 mol%) was added and the vial placed in an autoclave. The solution was stirred under 25 bar H<sub>2</sub> for 1.5 h, then filtrated and the solvent was removed under reduced pressure. Column

chromatography (hexanes:EtOAc = 5:1) yields a white amorphous compound (403 mg, 1.15 mmol, 80%)

**R<sub>f</sub>** (hexanes:EtOAc = 4:1) = 0.32; faint grey with vanillin.

**m.p.:** 76-78 °C.

**IR** (neat): 3042, 2944, 2880, 1704, 1594, 1417, 1385, 1242, 1192, 1157, 1063, 965, 930, 801 cm<sup>-1</sup>.

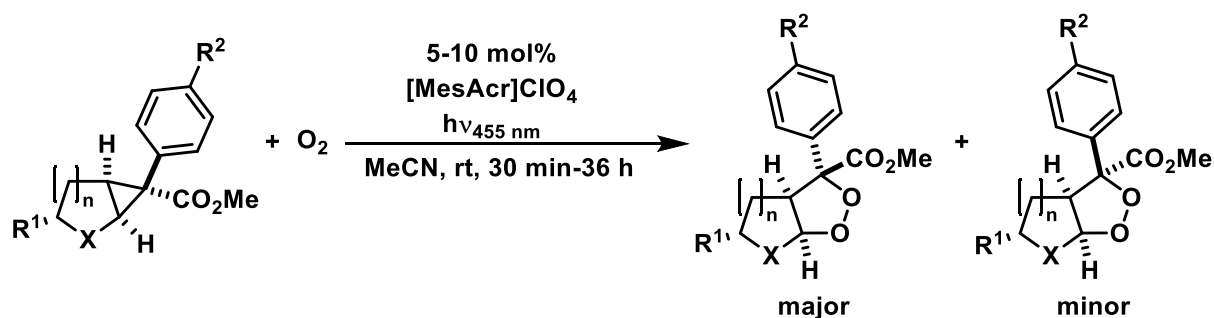
**<sup>1</sup>H NMR** (400 MHz, CDCl<sub>3</sub>): δ 7.47 – 7.30 (m, 7H), 7.30 – 7.12 (m, 3H), 3.94 (dd, *J* = 69.8, 9.3 Hz, 1H), 3.58 (d, *J* = 11.0 Hz, 3H), 3.35 (dd, *J* = 28.5, 14.5 Hz, 1H), 2.93 (dt, *J* = 53.6, 11.7 Hz, 1H), 2.44 (dt, *J* = 16.3, 7.9 Hz, 1H), 2.10 – 1.84 (m, 2H), 1.38 – 1.23 (m, 1H), 0.63 – 0.43 (m, 1H).

**<sup>13</sup>C NMR** (101 MHz, CDCl<sub>3</sub>): δ 173.6, 173.5, 155.6, 155.3, 151.4, 151.3, 133.2, 133.0, 131.8, 131.5, 129.5, 129.4, 128.7, 128.5, 127.6, 127.6, 125.6, 125.5, 121.8, 121.7, 52.7, 52.6, 42.5, 42.4, 42.0, 41.4, 35.0, 34.8, 24.9, 24.7, 21.1, 20.7, 18.6, 18.5.

**HR-MS** (ESI-MS): *m/z* calc. for C<sub>21</sub>H<sub>22</sub>NO<sub>4</sub> [M+H]<sup>+</sup> 352.1543, found 352.1551.



*General Procedure 5 (GP5) for the Visible Light Mediated Synthesis of Endoperoxides from Cyclopropanated Heterocycles.*

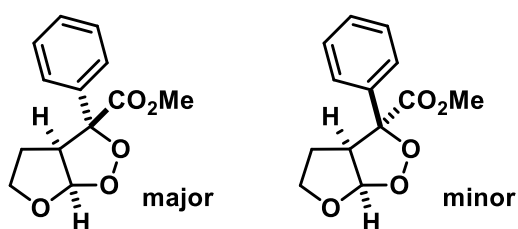


In an appropriate Schlenk-tube equipped with a magnetic stirbar, cyclopropanated heterocyclic starting material (1 equiv.) and catalyst  $[MesAc]ClO_4$  (0.05 – 0.1 equiv) were dissolved in dry MeCN (approximately 10 mL per mmol cyclopropane). An  $O_2$  filled rubber balloon was attached and the vigorously stirred solution was irradiated at room temperature with blue light (455 nm) *via* a glass rod sticking into the solution until complete conversion of starting material was observed as judged by TLC (30 min – 36 h). Then the solvent was evaporated under reduced pressure and the diastereomeric ratio was determined from the crude reaction mixture *via* NMR. Column chromatography (hexanes:EtOAc) was used for purification. See for pictures of the reaction setup

When the diastereomers were inseparable, the IR spectrum of the mixture is given and overlapping NMR-signals are marked.

**Methyl (3*S*\*,3*aS*\*,6*aR*\*)-3-phenyltetrahydro-3*H*-furo[2,3-*c*][1,2]dioxole-3-carboxylate and methyl (3*R*\*,3*aS*\*,6*aR*\*)-3-phenyltetrahydro-3*H*-furo[2,3-*c*][1,2]dioxole-3-carboxylate**

**158a**



Following **GP5**, compound ( $\pm$ )-**158a** (330 mg, 1.5 mmol, 1 equiv.) was dissolved in 15 mL MeCN and irradiated in the presence of  $[MesAc]ClO_4$  (30 mg, 0.075 mmol, 5 mol%) for 16 h. Column chromatography (hexanes:EtOAc = 8% to 20%) allowed separation of the diastereomers, each yielding a colorless crystalline solid; major: 140.9 mg, minor: 35.2 mg; total: 176.1 mg (0.71 mmol, 47%).

### 15 mmol scale

In a 200 mL water cooled circulating immersion-well photoreactor (pictures see General Information), 3.27 g (15.0 mmol) ( $\pm$ )-157a and 309 mg (0.75 mmol, 5 mol%) [MesAc]ClO<sub>4</sub> where dissolved in 200 mL MeCN and saturated with O<sub>2</sub> by bubbling oxygen through the solution for 10 min. An O<sub>2</sub> filled balloon was attached and the solution was irradiated for 15 h with 30 Oslon SSL 80 LED (maximum 455 nm). After evaporation of the solvent under reduced pressure the oily residue was purified by flash chromatography (hexanes:EtOAc = 10% to 20%). The diastereomers were separable by column chromatography, giving a combined yield of 1.46 g (5.83 mmol, 39%; Major diastereomer 1.19 g, Minor diastereomer 0.27 g)

### Major

**R<sub>f</sub>** (hexanes:EtOAc = 4:1) = 0.13; dark brown with vanillin.

**m.p.:** 110-112 °C.

**IR** (neat): 2956, 2896, 1732, 1493, 1449, 1368, 1251, 1193, 1083, 1020, 989, 925, 860, 727, 698 cm<sup>-1</sup>.

**<sup>1</sup>H NMR** (300 MHz, CDCl<sub>3</sub>):  $\delta$  7.70 – 7.62 (m, 2H), 7.45 – 7.30 (m, 3H), 5.74 (d,  $J$  = 5.0 Hz, 1H), 4.19 (ddd,  $J$  = 10.5, 8.4, 6.1 Hz, 1H), 4.03 (dtd,  $J$  = 11.0, 6.3, 5.4, 2.6 Hz, 2H), 3.74 (s, 3H), 2.27 (dddd,  $J$  = 13.7, 10.4, 9.4, 8.0 Hz, 1H), 2.15 – 2.04 (m, 1H).

**<sup>13</sup>C NMR** (75 MHz, CDCl<sub>3</sub>):  $\delta$  168.22, 137.97, 128.67, 128.49, 126.24, 108.26, 92.69, 69.28, 60.75, 53.01, 29.73.

### Minor

**R<sub>f</sub>** (hexanes:EtOAc 4:1) = 0.25; dark brown with vanillin.

**m.p.:** 123-125 °C.

**IR** (neat): 2990, 2958, 2899, 1739, 1494, 1449, 1370, 1311, 1271, 1240, 1205, 1064, 957, 931, 840, 810, 734, 696 cm<sup>-1</sup>.

**<sup>1</sup>H NMR** (300 MHz, CDCl<sub>3</sub>):  $\delta$  7.42 – 7.28 (m, 5H), 5.98 (dd,  $J$  = 5.1, 0.6 Hz, 1H), 4.49 (ddd,  $J$  = 9.7, 5.1, 2.0 Hz, 1H), 3.98 – 3.79 (m, 2H), 3.73 (s, 3H), 1.90 (dddd,  $J$  = 13.4, 10.9, 9.8, 8.4 Hz, 1H), 1.53 (m, 1H).

**<sup>13</sup>C NMR** (75 MHz, CDCl<sub>3</sub>):  $\delta$  172.40, 133.71, 129.00, 128.81, 125.47, 108.87, 92.40, 69.44, 57.79, 53.50, 27.60.

**HR-MS** (EI-MS):  $m/z$  calc. for C<sub>13</sub>H<sub>15</sub>O<sub>5</sub> [M+H]<sup>+</sup> 251.0914, found 251.0913.

**Crystals** suitable for X-ray analysis (minor: CCDC 1980425, major: CCDC 1980424) were obtained by recrystallization from DCM/Et<sub>2</sub>O.

**(-)-2a**

Analytical data is identical for (*S*)-isomers.

**Optical** rotation (*S*)-major:  $[\alpha]_D^{20} = -264.9^\circ$  in DCM.

**Optical** rotation (*S*)-minor:  $[\alpha]_D^{20} = -259.9^\circ$  in DCM.

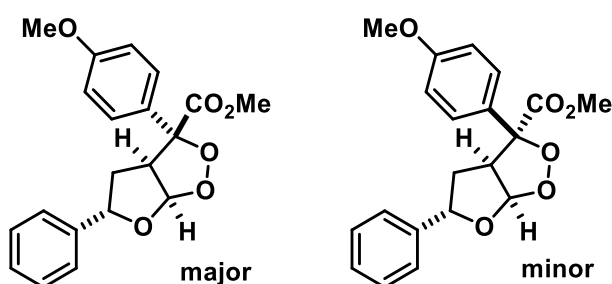
Chiral HPLC chromatogram available (see Chiral HPLC).

(*S*)-major: column: Chiralpak AS-H; eluent Heptane:<sup>i</sup>PrOH 95:5; Flow: 0.5 mL/min; Retention time [min]: 39.7, 55.3; enantiomeric excess >98% ee.

(*S*)-minor: column: Phenomenex-Lux Cellulose 1; eluent Heptane:<sup>i</sup>PrOH 99:1; Flow: 1 mL/min; Retention time [min]: 15.8, 50.8; enantiomeric excess >99% ee.

**Methyl (3*R*\*,3*aS*\*,5*S*\*,6*aR*\*)-3-(4-methoxyphenyl)-5-phenyltetrahydro-3*H*-furo[2,3-*c*][1,2]dioxole-3-carboxylate** and

**Methyl (3*S*\*,3*aS*\*,5*S*\*,6*aR*\*)-3-(4-methoxyphenyl)-5-phenyltetrahydro-3*H*-furo[2,3-*c*][1,2]dioxole-3-carboxylate** **156a**



Following **GP5**, compound **155a** (64.7 mg, 0.2 mmol, 1 equiv.) was dissolved in 2.5 mL MeCN and irradiated with blue light for 16 h in the presence of [MesAc]ClO<sub>4</sub> (6.3 mg, 0.015 mmol, 8 mol%). Column chromatography (hexanes:EtOAc = 19:1 to 9:1) yielded the major diastereomer as colorless crystalline solid, (8.5 mg, 0.022 mmol, 11.3%); The minor diastereomer could not be purified, the total yield was calculated based on the diastereomeric ratio of 3:1 determined from the crude NMR as 15%

**R<sub>f</sub>** (hexanes:EtOAc = 4:1) = 0.32; light brown with vanillin.

**m.p.**: 148 °C.

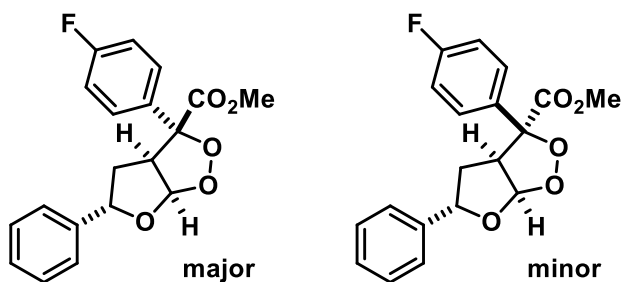
**IR** (neat): 3064, 2956, 2919, 2879, 2849, 1738, 1607, 1510, 1451, 1298, 1253, 1212, 1180, 1058, 1026, 992, 957, 932, 807, 771, 702 cm<sup>-1</sup>.

**<sup>1</sup>H NMR** (400 MHz, CDCl<sub>3</sub>): δ 7.60 (d, *J* = 8.9 Hz, 2H), 7.39 – 7.28 (m, 5H), 6.94 (d, *J* = 8.9 Hz, 2H), 5.96 (d, *J* = 5.1 Hz, 1H), 5.46 (dd, *J* = 10.6, 5.5 Hz, 1H), 4.15 (ddd, *J* = 9.6, 5.1, 1.7 Hz, 1H), 3.82 (s, 3H), 3.77 (s, 3H), 2.47 – 2.40 (m, 1H), 2.18 (dt, *J* = 13.9, 10.0 Hz, 1H).

**<sup>13</sup>C NMR** (101 MHz, CDCl<sub>3</sub>): δ 168.5, 159.9, 140.0, 129.9, 128.6, 128.2, 127.6, 126.0, 113.9, 108.1, 92.5, 81.8, 61.3, 55.4, 53.0, 38.2.

**HR-MS** (EI-MS): *m/z* calc. for C<sub>20</sub>H<sub>20</sub>NaO<sub>6</sub> [M+Na<sup>+</sup>]<sup>+</sup> 379.1152, found 379.1147.

Methyl (3*R*\*,3*aS*\*,5*S*\*,6*aR*\*)-3-(4-fluorophenyl)-5-phenyltetrahydro-3*H*-furo[2,3-  
 c][1,2]dioxole-3 carboxylate and  
 Methyl (3*S*\*,3*aS*\*,5*S*\*,6*aR*\*)-3-(4-fluorophenyl)-5-phenyltetrahydro-3*H*-furo[2,3-  
 c][1,2]dioxole-3-carboxylate **156c**



Following **GP5**, compound **155c** (99.5 mg, 0.3 mmol, 1 equiv.) was dissolved in 3 mL MeCN and irradiated with blue light for 70 h in the presence of [MesAcr]ClO<sub>4</sub> (9.6 mg, 0.023 mmol, 8 mol%). Column chromatography (hexanes:EtOAc = 19:1 to 9:1) yielded the major diastereomer as colorless crystalline solid, (36.4 mg, 0.11 mmol, 35%); The minor diastereomer could not be purified, the total yield was calculated based on the diastereomeric ratio of 3:1 determined from the crude NMR as 47%

**m.p.:** 124-126 °C.

**R<sub>f</sub>** (hexanes:EtOAc = 4:1) = 0.4; light brown with vanillin.

**IR** (neat): 3062, 2925, 2855, 1719, 1599 1495, 1450, 1379, 1359, 1228, 1129, 1068, 1021, 861 cm<sup>-1</sup>.

**<sup>1</sup>H NMR** (400 MHz, CDCl<sub>3</sub>): δ 7.70 (dd, *J* = 7.1, 1.5 Hz, 2H), 7.44 – 7.30 (m, 8H), 5.95 (d, *J* = 5.1 Hz, 1H), 5.47 (dd, *J* = 10.6, 5.5 Hz, 1H), 4.22 – 4.16 (m, 1H), 3.78 (s, 3H), 2.46 (ddd, *J* = 13.9, 5.6, 1.3 Hz, 1H), 2.20 (ddd, *J* = 13.9, 10.6, 9.6 Hz, 1H).

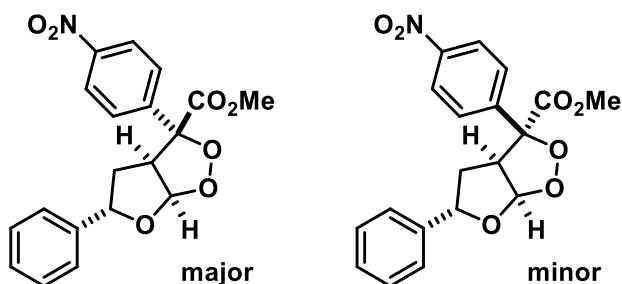
**<sup>13</sup>C NMR** (101 MHz, CDCl<sub>3</sub>): δ 178.5, 152.5, 140.0, 138.0, 128.8, 128.6, 128.6, 128.2, 126.3, 126.0, 108.1, 81.8, 61.4, 53.1, 38.2.

**<sup>19</sup>F NMR** (377 MHz, CDCl<sub>3</sub>): δ -115.58 (tt, *J* = 8.7, 5.4 Hz).

**HR-MS** (EI-MS): *m/z* calc. for C<sub>19</sub>H<sub>18</sub>FO<sub>5</sub> [M+H]<sup>+</sup> 345.1133, found 345.1134.

**Methyl (3*R*\*,3*aS*\*,5*S*\*,6*aR*\*)-3-(4-nitrophenyl)-5-phenyltetrahydro-3*H*-furo[2,3-*c*][1,2]dioxole-3-carboxylate** and

**Methyl (3*S*\*,3*aS*\*,5*S*\*,6*aR*\*)-3-(4-nitrophenyl)-5-phenyltetrahydro-3*H*-furo[2,3-*c*][1,2]dioxole-3-carboxylate** **156d**



Following **GP5**, compound **155d** (115 mg, 0.34 mmol, 1 equiv.) was dissolved in 4 mL MeCN and irradiated with blue light for 70 h in the presence of [MesAc]ClO<sub>4</sub> (13.5 mg, 0.03 mmol, 9 mol%). No significant further conversion was observed, so that the reaction was stopped albeit not all starting material was consumed. Column chromatography (hexanes:EtOAc = 19:1 to 7:1) allowed for recovery of 42.2 mg **155d** as starting material, which is 36% of the total starting material. Therefore the conversion was 64%. The major diastereomer was isolated as colorless crystalline solid, (15.1 mg, 0.04 mmol, 18.7% brsm, 12.2% total); as the minor diastereomer could not be purified, the total yield was calculated based on the diastereomeric ratio of 3:1 determined from the crude NMR as 25% brsm.

**R<sub>f</sub>** (hexanes:EtOAc = 4:1) = 0.18; dark brown with vanillin.

**m.p.**: 164-167 °C.

**IR** (neat): 3492, 3073, 3030, 2958, 2918, 2851, 1739, 1597, 1516, 1347, 1258, 1174, 1134, 1071, 983, 921, 852, 737, 697 cm<sup>-1</sup>.

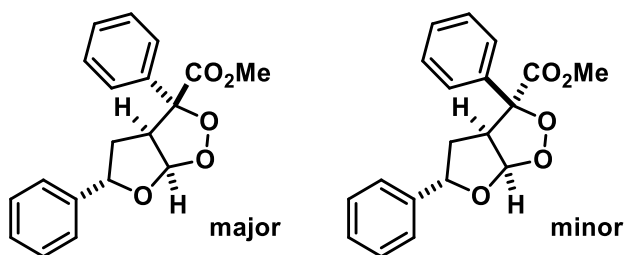
**<sup>1</sup>H NMR** (400 MHz, CDCl<sub>3</sub>): δ 8.29 – 8.24 (m, 2H), 7.93 – 7.87 (m, 2H), 7.40 – 7.30 (m, 5H), 5.95 (d, *J* = 5.0 Hz, 1H), 5.47 (dd, *J* = 10.8, 5.4 Hz, 1H), 4.15 (ddd, *J* = 9.4, 5.0, 1.5 Hz, 1H), 3.82 (s, 3H), 2.50 – 2.43 (m, 1H), 2.22 (ddd, *J* = 14.0, 10.8, 9.4 Hz, 1H).

**<sup>13</sup>C NMR** (101 MHz, CDCl<sub>3</sub>): δ 167.2, 148.2, 144.9, 139.5, 128.7, 128.4, 127.8, 126.0, 123.7, 107.8, 92.3, 82.0, 62.2, 53.5, 38.2.

**HR-MS** (EI-MS): *m/z* calc. for C<sub>19</sub>H<sub>18</sub>NO<sub>7</sub> [M+H]<sup>+</sup> 372.1078, found 372.1079.

**Crystals** suitable for X-ray analysis (major: CCDC 1980428) were obtained by recrystallization from DCM/Et<sub>2</sub>O.

Methyl (3*R*\*,3*aS*\*,5*S*\*,6*aR*\*)-3,5-diphenyltetrahydro-3*H*-furo[2,3-*c*][1,2]dioxole-3-carboxylate and Methyl (3*S*\*,3*aS*\*,5*S*\*,6*aR*\*)-3,5-diphenyltetrahydro-3*H*-furo[2,3-*c*][1,2]dioxole-3-carboxylate **167a**



Following **GP5**, compound **155a** (301 mg, 1.02 mmol, 1 equiv.) was dissolved in 10 mL MeCN and irradiated with blue light for 15 h in the presence of [MesAc]ClO<sub>4</sub> (40 mg, 0.097 mmol, 10 mol%). Crude NMR revealed a diastereomeric ratio of 2.6:1. Column chromatography (hexanes:EtOAc = 9:1) yielded the major diastereomer as white crystalline solid (132.7 mg, 0.405 mmol, 40%); The minor diastereomer could not be purified, the total yield was calculated based on the diastereomeric ratio determined as 55%;

**R<sub>f</sub>** (hexanes:EtOAc = 4:1) = 0.2.

**m.p.**: 100-102 °C.

**IR** (neat): 3033, 2958, 1701, 1603, 1461, 1326, 1260, 1239, 1153, 1114, 1085, 1032, 962, 937, 902, 879, 811 cm<sup>-1</sup>.

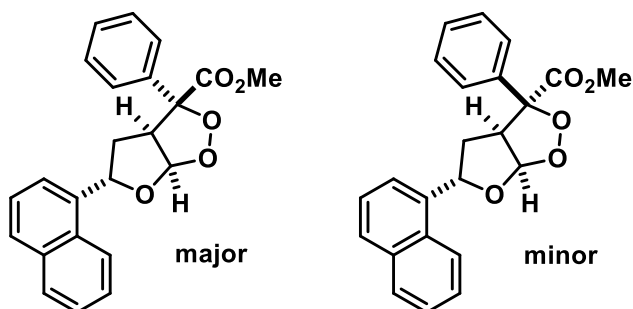
**<sup>1</sup>H NMR** (400 MHz, CDCl<sub>3</sub>): δ 7.72 – 7.66 (m, 2H), 7.45 – 7.31 (m, 8H), 5.95 (d, *J* = 5.1 Hz, 1H), 5.47 (dd, *J* = 10.6, 5.5 Hz, 1H), 4.19 (ddd, *J* = 9.5, 5.1, 1.7 Hz, 1H), 3.78 (s, 3H), 2.47 (ddd, *J* = 13.9, 5.5, 1.3 Hz, 1H), 2.20 (ddd, *J* = 13.9, 10.6, 9.5 Hz, 1H).

**<sup>13</sup>C NMR** (101 MHz, CDCl<sub>3</sub>): δ 168.2, 140.0, 138.0, 128.7, 128.6, 128.6, 128.2, 126.3, 126.0, 108.1, 92.7, 81.8, 61.4, 53.1, 38.2.

**HR-MS** (ESI-MS): *m/z* calc. for C<sub>19</sub>H<sub>19</sub>O<sub>5</sub> [M+H]<sup>+</sup> 327.1227, found 327.1229.

**Methyl (3*R*\*,3*aS*\*,5*S*\*,6*aR*\*)-5-(naphthalen-1-yl)-3-phenyltetrahydro-3*H*-furo[2,3-  
c][1,2]dioxole-3-carboxylate and**

**Methyl (3*S*\*,3*aS*\*,5*S*\*,6*aR*\*)-5-(naphthalen-1-yl)-3-phenyltetrahydro-3*H*-furo[2,3-  
c][1,2]dioxole-3-carboxylate** **167b**



Following **GP5**, compound **166b** (282 mg, 0.81 mmol, 1 equiv.) was dissolved in 8 mL MeCN and irradiated with blue light for 13 h in the presence of [MesAcr]ClO<sub>4</sub> (33 mg, 0.08 mmol, 10 mol%). Crude NMR revealed a diastereomeric ratio of 3:1. Column chromatography (hexanes:EtOAc = 3% to 10%) yielded a inseparable mixture of diastereomers as white crystalline solid (195 mg, 0.519 mmol, 64%);

**R<sub>f</sub>** (hexanes:EtOAc = 4:1) = 0.55.

**m.p.:** 80-82 °C.

**IR** (neat): 3064, 3030, 2951, 2844, 1738, 1594, 1441, 1321, 1239, 1196, 1142, 993, 955, 799 cm<sup>-1</sup>.

**Major** as assigned from 2D-NMR

**<sup>1</sup>H NMR** (400 MHz, CDCl<sub>3</sub>): δ 8.03 (d, *J* = 8.4 Hz, 2H), 7.69 (d, *J* = 7.1 Hz, 2H), 7.45 – 7.38 (m, 5H), 5.97 (d, *J* = 5.0 Hz, 1H), 5.52 (dd, *J* = 10.7, 5.6 Hz, 1H), 4.20 (ddd, *J* = 9.7, 5.1, 1.6 Hz, 1H), 3.92 (s, 3H), 3.79 (s, 3H), 2.54 – 2.47 (m, 1H), 2.15 (dt, *J* = 13.9, 10.7, 1H).

**<sup>13</sup>C NMR** (101 MHz, CDCl<sub>3</sub>): δ 168.1, 166.9, 145.2, 137.8, 130.0, 129.9, 128.8, 128.6, 126.3, 125.8, 108.1, 92.7, 81.3, 61.3, 53.2, 52.2, 38.2.

**Minor:** as assigned from 2D-NMR

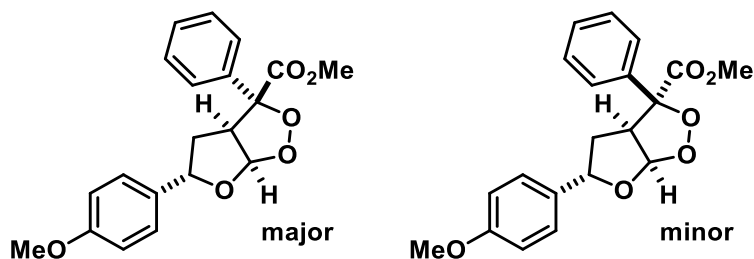
**<sup>1</sup>H NMR** (400 MHz, CDCl<sub>3</sub>): δ 7.96 (d, *J* = 8.3 Hz, 2H), 7.47 – 7.36 (m, 5H), 7.28 (d, *J* = 8.7 Hz, 2H), 6.20 (d, *J* = 5.1 Hz, 1H), 5.23 (dd, *J* = 10.8, 5.6 Hz, 1H), 4.66 (dd, *J* = 9.6, 5.2 Hz, 1H), 3.89 (s, 3H), 3.78 (s, 3H), 1.95 (dd, *J* = 13.5, 5.6 Hz, 1H), 1.81 (dt, *J* = 13.6, 10.0 Hz, 1H).

**<sup>13</sup>C NMR** (101 MHz, CDCl<sub>3</sub>): δ 172.2, 166.9, 145.3, 133.6, 129.8, 129.7, 129.2, 129.0, 125.6, 125.5, 108.7, 92.4, 81.3, 58.4, 53.6, 52.2, 36.1.

**HR-MS** (APCI-MS): *m/z* calc. for C<sub>23</sub>H<sub>24</sub>NO<sub>5</sub> [M+NH<sub>4</sub><sup>+</sup>]<sup>+</sup> 394.1654, found 394.1645.

**Methyl (3*R*\*,3*aS*\*,5*S*\*,6*aR*\*)-5-(4-Methoxyphenyl)-3-phenyltetrahydro-3*H*-furo[2,3-*c*][1,2]dioxole-3-carboxylate** and

**Methyl (3*S*\*,3*aS*\*,5*S*\*,6*aR*\*)-5-(4-Methoxyphenyl)-3-phenyltetrahydro-3*H*-furo[2,3-*c*][1,2]dioxole-3-carboxylate**



Following GP4, **11** (98 mg, 0.47 mmol, 1 equiv.) was dissolved in 3 mL MeCN and irradiated with blue light for 16 h in the presence of [MesAc]ClO<sub>4</sub> (10 mg, 0.024 mmol, 9 mol%). Crude NMR revealed a diastereomeric ratio of 3:1. Column chromatography (hexanes:EtOAc 5% to 10%) allowed for separation of the diastereomers, which were each isolated as clear crystalline material after removal of the solvent. Major: 85.4 mg, 0.24 mmol, 51%; Minor: 28.4 mg, 0.079 mmol, 17%); combined: 68%

#### Major

**R<sub>f</sub>** (hexanes:EtOAc 9:1) = 0.15. Light brown with vanillin.

**m.p.:** 145-147 °C

**IR** (neat): 2955, 2841, 1735, 1613, 1515, 1446, 1247, 1247, 1174, 1062, 1029, 985, 833, 736 cm<sup>-1</sup>.

**<sup>1</sup>H NMR** (400 MHz, CDCl<sub>3</sub>): δ 7.72 – 7.66 (m, 2H), 7.46 – 7.34 (m, 3H), 7.29 (d, *J* = 8.6 Hz, 2H), 6.89 (d, *J* = 8.7 Hz, 2H), 5.92 (d, *J* = 5.0 Hz, 1H), 5.42 (dd, *J* = 10.7, 5.4 Hz, 1H), 4.19 (ddd, *J* = 9.6, 5.1, 1.6 Hz, 1H), 3.81 (s, 3H), 3.77 (s, 3H), 2.46 – 2.36 (m, 1H), 2.25 – 2.14 (m, 1H).

**<sup>13</sup>C NMR** (101 MHz, CDCl<sub>3</sub>): δ 168.3, 159.6, 138.0, 131.8, 128.7, 128.5, 127.5, 126.3, 114.0, 107.9, 92.7, 81.6, 61.4, 55.4, 53.1, 38.1.

**HR-MS** (EI-MS): *m/z* calc. for C<sub>20</sub>H<sub>21</sub>O<sub>6</sub> [M+H]<sup>+</sup> 357.1333, found 357.1331.

#### Minor

**R<sub>f</sub>** (hexanes:EtOAc 9:1) = 0.08. Light brown with vanillin.

**m.p.:** 158-161 °C

**IR** (neat): 3034, 2958, 1701, 1603, 1461, 1436, 1260, 1239, 1153, 1086, 1032, 962 879, 811, 750 cm<sup>-1</sup>.

**<sup>1</sup>H NMR** (400 MHz, CDCl<sub>3</sub>): δ 7.71 (d, *J* = 7.3 Hz, 2H), 7.40 (dd, *J* = 14.8, 7.6 Hz, 5H), 6.92 (d, *J* = 8.6 Hz, 2H), 5.73 (d, *J* = 5.5 Hz, 1H), 4.99 (dd, *J* = 10.3, 5.7 Hz, 1H), 4.25 (td, *J* = 9.1, 5.6



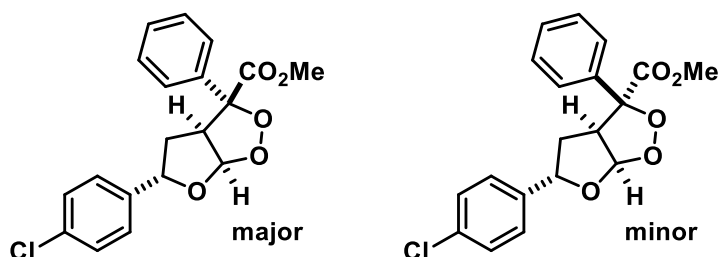
Hz, 1H), 3.82 (s, 3H), 3.66 (s, 3H), 2.70 (ddd,  $J = 12.6, 8.7, 5.7$  Hz, 1H), 2.01 (dt,  $J = 12.6, 9.9$  Hz, 1H).

$^{13}\text{C}$  NMR (101 MHz,  $\text{CDCl}_3$ ):  $\delta$  167.6, 159.6, 137.1, 132.3, 128.9, 128.7, 127.5, 126.1, 114.0, 108.2, 92.5, 82.7, 61.9, 55.4, 53.0, 38.1.

HR-MS (EI-MS):  $m/z$  calc. for  $\text{C}_{20}\text{H}_{21}\text{O}_6$   $[\text{M}+\text{H}^+]^+$  357.1333, found 357.1330.

**Methyl (3*R*\*,3*aS*\*,5*S*\*,6*aR*\*)-5-(4-chlorophenyl)-3-phenyltetrahydro-3*H*-furo[2,3-*c*][1,2]dioxole-3-carboxylate** and

**Methyl (3*S*\*,3*aS*\*,5*S*\*,6*aR*\*)-5-(4-chlorophenyl)-3-phenyltetrahydro-3*H*-furo[2,3-*c*][1,2]dioxole-3-carboxylate** **167d**



Following GP4, **166d** (337 mg, 1.0 mmol, 1 equiv.) was dissolved in 10 mL MeCN and irradiated with blue light for 16 h in the presence of  $[\text{MesAc}]\text{ClO}_4$  (39 mg, 0.09 mmol, 9 mol%). Crude NMR revealed a diastereomeric ratio of 1.7:1. Column chromatography (hexanes:EtOAc = 3% to 10%) yielded a inseparable mixture of diastereomers as white crystalline solid (159 mg, 0.44 mmol, 43%).

$R_f$  (hexanes:EtOAc 4:1) = 0.25. Light brown with vanillin.

**m.p.:** 62 °C

**Ir** (neat): 3069, 2952, 2899, 1727, 1600, 1493, 1448, 1252, 1120, 1061, 986, 969, 917, 756, 725  $\text{cm}^{-1}$ .

#### Major

$^1\text{H}$  NMR (400 MHz,  $\text{CDCl}_3$ )  $\delta$  7.68 (d,  $J = 7.3$  Hz, 2H), 7.45 – 7.27 (m, 7H), 5.94 (d,  $J = 5.0$  Hz, 1H), 5.43 (dd,  $J = 10.6, 5.4$  Hz, 1H), 4.19 (dd,  $J = 8.6, 4.9$  Hz, 1H), 3.78 (s, 3H), 2.46 (dd,  $J = 13.8, 5.0$  Hz, 1H), 2.13 (dt,  $J = 13.8, 10.2$  Hz, 1H),

#### Minor

$^1\text{H}$  NMR (400 MHz,  $\text{CDCl}_3$ )  $\delta$  7.45 – 7.27 (m, 7H), 7.15 (d,  $J = 8.3$  Hz, 2H), 6.17 (d,  $J = 5.0$  Hz, 1H), 5.15 (dd,  $J = 10.7, 5.6$  Hz, 1H), 4.65 (dd,  $J = 8.9, 5.3$  Hz, 1H), 3.78 (s, 3H), 1.91 (dd,  $J = 13.4, 5.4$  Hz, 1H), 1.79 (dt,  $J = 13.4, 10.2$  Hz, 1H).

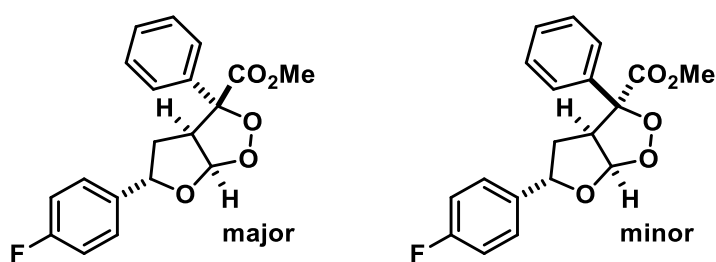
#### Mixture

$^{13}\text{C}$  NMR (101 MHz,  $\text{CDCl}_3$ )  $\delta$  172.3, 168.1, 138.7, 138.5, 137.8, 133.9, 133.6, 129.1, 129.0, 128.8, 128.6, 128.6, 127.4, 127.2, 126.3, 125.5, 108.6, 108.0, 92.6, 92.4, 81.2, 81.1, 61.3, 58.4, 53.6, 53.1, 38.3, 36.1.

HR-MS (EI-MS):  $m/z$  calc. for  $\text{C}_{19}\text{H}_{18}\text{ClO}_5$   $[\text{M}+\text{H}^+]^+$  361.0837, found 361.0837.

Methyl (3*R*\*,3*aS*\*,5*S*\*,6*aR*\*)-5-(4-fluorophenyl)-3-phenyltetrahydro-3*H*-furo[2,3-*c*][1,2]dioxole-3-carboxylate and

Methyl (3*S*\*,3*aS*\*,5*S*\*,6*aR*\*)-5-(4-fluorophenyl)-3-phenyltetrahydro-3*H*-furo[2,3-*c*][1,2]dioxole-3-carboxylate



Following **GP5**, **166e** (310 mg, 1.0 mmol, 1 equiv.) was dissolved in 15 mL MeCN and irradiated with blue light for 16 h in the presence of  $[\text{MesAcr}]\text{ClO}_4$  (40 mg, 0.1 mmol, 10 mol%). Crude NMR revealed a diastereomeric ratio of 3:1. Column chromatography (hexanes:EtOAc 3% to 10%) yielded an inseparable mixture of diastereomers as colorless crystalline solid (178 mg, 0.51 mmol, 51%).

$R_f$  (hexanes:EtOAc 4:1) = 0.25. Light brown with vanillin.

**m.p.:** 120-122 °C.

**Ir** (neat): 3073, 2953, 2910, 1732, 1603, 1511, 1446, 1274, 1221, 1071, 1003, 918, 836, 724  $\text{cm}^{-1}$ .

#### Major

$^1\text{H}$  NMR (300 MHz,  $\text{CDCl}_3$ )  $\delta$  7.72 – 7.66 (m, 2H), 7.46 – 7.29 (m, 5H), 7.09 – 6.93 (m, 2H), 5.94 (d,  $J = 5.0$  Hz, 1H), 5.44 (dd,  $J = 10.7, 5.4$  Hz, 1H), 4.20 (ddd,  $J = 9.5, 5.0, 1.6$  Hz, 1H), 3.77 (d,  $J = 1.7$  Hz, 3H), 2.45 (dddd,  $J = 14.0, 5.5, 1.6, 0.7$  Hz, 1H), 2.16 (ddd,  $J = 14.0, 10.8, 9.5$  Hz, 1H).

#### Minor

$^1\text{H}$  NMR (300 MHz,  $\text{CDCl}_3$ )  $\delta$  7.46 – 7.29 (m, 5H), 7.22 – 7.16 (m, 2H), 7.09 – 6.93 (m, 2H), 6.17 (d,  $J = 5.1$  Hz, 1H), 5.16 (dd,  $J = 10.5, 5.8$  Hz, 1H), 4.69 – 4.61 (m, 1H), 3.77 (d,  $J = 1.7$  Hz, 3H), 1.95 – 1.75 (m, 2H).

#### $^{13}\text{C}$ mixture:

$^{13}\text{C}$  NMR (75 MHz,  $\text{CDCl}_3$ )  $\delta$  169.1, 164.2, 160.9, 137.8, 135.7, 135.7, 135.6, 133.6, 129, 1, 128.9, 128.7, 128.5, 127.8, 127.7, 127.5, 126.2, 125.4, 115.6, 115.5, 115.3, 115.2, 108.5, 107.9, 92.6, 81.2, 61.3, 58.4, 53.6, 53.1, 38.3, 36.1

$^{19}\text{F}$  mixture:

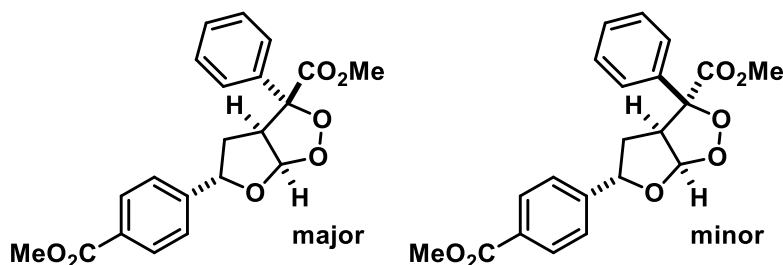
**19F** NMR (282 MHz,  $\text{CDCl}_3$ ):  $\delta$  -114.56 (tt,  $J = 8.6, 5.3$  Hz), -114.81 (tt,  $J = 8.7, 5.3$  Hz).

**HR-MS** (EI-MS):  $m/z$  calc. for  $\text{C}_{19}\text{H}_{18}\text{FO}_5$   $[\text{M}+\text{H}^+]^+$  345.1133, found 345.1131.

**Crystals** suitable for X-ray analysis (minor: CCDC 1980427) were obtained by recrystallization from DCM/ $\text{Et}_2\text{O}$ .

**Methyl (3*R*\*,3*aS*\*,5*S*\*,6*aR*\*)-5-(4-(methoxycarbonyl)phenyl)-3-phenyltetrahydro-3*H*-furo[2,3-*c*][1,2]dioxole-3-carboxylate** and

**Methyl (3*S*\*,3*aS*\*,5*S*\*,6*aR*\*)-5-(4-(methoxycarbonyl)phenyl)-3-phenyltetrahydro-3*H*-furo[2,3-*c*][1,2]dioxole-3-carboxylate** **167f**



Following **GP5**, compound **1g** (98 mg, 0.27 mmol, 1 equiv.) was dissolved in 3 mL MeCN and irradiated with blue light for 16 h in the presence of  $[\text{MesAc}]\text{ClO}_4$  (10 mg, 0.024 mmol, 9 mol%). Crude NMR revealed a diastereomeric ratio of 3:1. Column chromatography (hexanes: $\text{EtOAc} = 10\%$  to  $25\%$ ) allowed for separation of the diastereomers as white crystalline solids. Major: 42 mg, 0.11 mmol, 40.5%; Minor: 14 mg, 0.036 mmol, 13.5%); combined: 54%

Major

**R<sub>f</sub>** (hexanes: $\text{EtOAc} = 4:1$ ) = 0.2. Light brown with vanillin.

**m.p.:** 172 °C.

**IR** (neat): 2999, 2955, 2904, 1720, 1433, 1255, 1192, 1068, 1007, 919, 882, 851, 800, 768, 722  $\text{cm}^{-1}$ .

**$^1\text{H}$  NMR** (400 MHz,  $\text{CDCl}_3$ ):  $\delta$  8.03 (d,  $J = 8.4$  Hz, 2H), 7.69 (d,  $J = 7.1$  Hz, 2H), 7.45 – 7.38 (m, 5H), 5.97 (d,  $J = 5.0$  Hz, 1H), 5.52 (dd,  $J = 10.7, 5.6$  Hz, 1H), 4.20 (ddd,  $J = 9.7, 5.1, 1.6$  Hz, 1H), 3.92 (s, 3H), 3.79 (s, 3H), 2.54 – 2.47 (m, 1H), 2.15 (ddd,  $J = 13.9, 10.7, 9.5$  Hz, 1H).

**$^{13}\text{C}$  NMR** (101 MHz,  $\text{CDCl}_3$ ):  $\delta$  168.1, 166.9, 145.2, 137.8, 130.0, 129.9, 128.8, 128.6, 126.3, 125.8, 108.1, 92.7, 81.3, 61.3, 53.2, 52.2, 38.2.

**HR-MS** (EI-MS):  $m/z$  calc. for  $\text{C}_{21}\text{H}_{21}\text{O}_7$   $[\text{M}+\text{H}^+]^+$  385.1282, found 385.1284.

### Minor

**R<sub>f</sub>** (hexanes:EtOAc 4:1) = 0.18. Light brown with vanillin.

**m.p.:** 188 °C.

**IR** (neat): 2956, 2907, 2840, 1738, 1612, 1436, 1217, 1177, 1030, 976, 909, 882, 800, 763 cm<sup>-1</sup>.

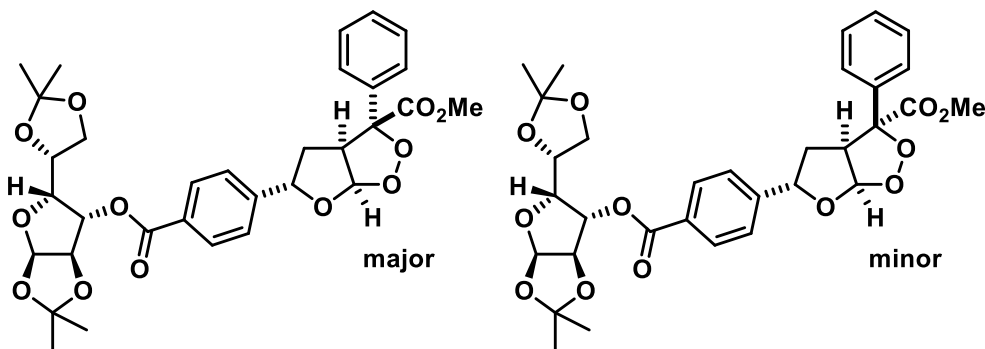
**<sup>1</sup>H NMR** (400 MHz, CDCl<sub>3</sub>): δ 7.96 (d, *J* = 8.3 Hz, 2H), 7.47 – 7.36 (m, 5H), 7.28 (d, *J* = 8.7 Hz, 2H), 6.20 (d, *J* = 5.1 Hz, 1H), 5.23 (dd, *J* = 10.8, 5.6 Hz, 1H), 4.66 (dd, *J* = 9.6, 5.2 Hz, 1H), 3.89 (s, 3H), 3.78 (s, 3H), 1.95 (dd, *J* = 13.5, 5.6 Hz, 1H), 1.81 (dt, *J* = 13.6, 10.0 Hz, 1H).

**<sup>13</sup>C NMR** (101 MHz, CDCl<sub>3</sub>): δ 172.2, 166.9, 145.3, 133.6, 129.8, 129.7, 129.2, 129.0, 125.6, 125.5, 108.7, 92.4, 81.3, 58.4, 53.6, 52.2, 36.1.

**HR-MS** (EI-MS): *m/z* calc. for C<sub>21</sub>H<sub>21</sub>O<sub>7</sub> [M+H]<sup>+</sup> 385.1282, found 385.1286.

**Methyl (3*R*\*,3*aS*\*,5*S*\*,6*aR*\*)-5-(4-(((3*aR*,5*R*,6*S*,6*aR*)-5-((*R*)-2,2-dimethyl-1,3-dioxolan-4-yl)-2,2-dimethyltetrahydrofuro[2,3-*d*][1,3]dioxol-6-yl)oxy)carbonyl)phenyl)-3-phenyltetrahydro-3*H*-furo[2,3-*c*][1,2]dioxole-3-carboxylate and Methyl**

**(3*S*\*,3*aS*\*,5*S*\*,6*aR*\*)-5-(4-(((3*aR*,5*R*,6*S*,6*aR*)-5-((*R*)-2,2-dimethyl-1,3-dioxolan-4-yl)-2,2-dimethyltetrahydrofuro[2,3-*d*][1,3]dioxol-6-yl)oxy)carbonyl)phenyl)-3-phenyltetrahydro-3*H*-furo[2,3-*c*][1,2]dioxole-3-carboxylate** **167g**



Following **GP5**, compound **166g** (174 mg, 0.30 mmol, 1 equiv.) was dissolved in 5 mL MeCN and irradiated with blue light for 20 h in the presence of [MesAcr]ClO<sub>4</sub> (10.3 mg, 0.025 mmol, 8 mol%). Due to the introduction of a chiral residue (Diacetone-D-glucose) this reaction can lead to four different diastereomers. A pair of two diastereomers was purified by column chromatography (hexanes:EtOAc = 10% to 50%), yielding a viscous clear oil (84 mg, 0.14 mmol, 46%). The material obtained showed a diastereomeric ratio for this pair of 3:1.

**R<sub>f</sub>** (hexanes:EtOAc = 2:1) = 0.2; dark brown with vanillin.

**IR** (neat): 3064, 3001, 2953, 2854, 1736, 1435, 1356, 1254, 1218, 1068, 1015, 949, 820 cm<sup>-1</sup>.

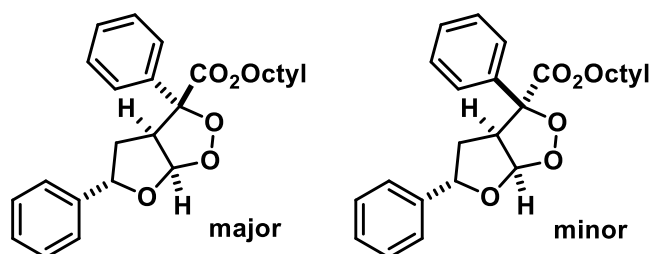
**<sup>1</sup>H NMR** (300 MHz, Chloroform-*d*): δ 8.04 – 7.99 (m, 6H), 7.93 (d, *J* = 8.2 Hz, 2H), 7.71 – 7.66 (m, 5H), 7.46 – 7.33 (m, 20H), 7.28 (d, *J* = 8.7 Hz, 2H), 6.20 (d, *J* = 5.2 Hz, 1H), 6.01 – 5.91 (m, 7H), 5.56 – 5.45 (m, 7H), 5.23 (dd, *J* = 10.8, 5.6 Hz, 1H), 4.70 – 4.58 (m, 5H), 4.41 – 4.28 (m,

9H), 4.20 (dd,  $J = 9.0, 5.0$  Hz, 3H), 4.14 – 4.04 (m, 8H), 3.80 – 3.76 (m, 11H), 2.50 (dd,  $J = 14.2, 5.6$  Hz, 2H), 2.20 – 2.07 (m, 3H), 1.95 (dd,  $J = 13.6, 5.7$  Hz, 1H), 1.78 (dt,  $J = 13.6, 9.8$  Hz, 1H), 1.55 (d,  $J = 4.0$  Hz, 12H), 1.40 (d,  $J = 5.6$  Hz, 12H), 1.31 (d,  $J = 4.6$  Hz, 12H), 1.25 (d,  $J = 7.3$  Hz, 12H).

$^{13}\text{C}$  NMR (75 MHz,  $\text{CDCl}_3$ ):  $\delta$  168.0, 164.8, 145.7, 137.6, 130.0, 129.8, 129.1, 128.7, 128.5, 126.1, 125.8, 125.3, 112.4, 109.4, 108.0, 105.1, 92.5, 92.2, 83.3, 81.0, 79.9, 72.5, 67.2, 61.1, 53.5, 53.1, 26.8, 26.7, 26.2, 25.2.

HR-MS (ESI-MS):  $m/z$  calc. for  $\text{C}_{32}\text{H}_{37}\text{O}_{12}$   $[\text{M}+\text{H}^+]^+$  613.2280, found 613.2279.

**Octyl (3*R*\*,3*aS*\*,5*S*\*,6*aR*\*)-3,5-diphenyltetrahydro-3*H*-furo[2,3-*c*][1,2]dioxole-3-carboxylate** and **Octyl (3*S*\*,3*aS*\*,5*S*\*,6*aR*\*)-3,5-diphenyltetrahydro-3*H*-furo[2,3-*c*][1,2]dioxole-3-carboxylate** **167h**



Following **GP5**, compound **167h** (475 mg, 1.21 mmol, 1 equiv.) was dissolved in 12 mL MeCN and irradiated with blue light for 15 h in the presence of  $[\text{MesAcr}]\text{ClO}_4$  (49 mg, 0.12 mmol, 10 mol%). Crude NMR revealed a diastereomeric ratio of 3:1. Column chromatography (hexanes:EtOAc = 99:1 to 9:1) yielded the major diastereomer as white solid (173 mg, 0.407 mmol, 34%) and a mixed fraction containing also the minor diastereomer (combined 232 mg, 0.547 mmol, 45%).

Major:

$R_f$  (hexanes:EtOAc = 9:1) = 0.7: Faint brown with vanillin.

**m.p.:** 153 °C.

**Ir** (neat): 2923, 2854, 1737, 1495, 1451, 1376, 1341, 1249, 1212, 1066, 1006, 917, 875, 782  $\text{cm}^{-1}$ .

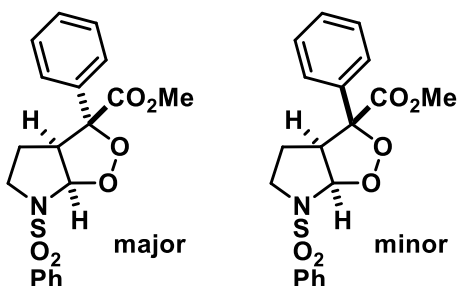
$^1\text{H}$  NMR (300 MHz,  $\text{CDCl}_3$ ):  $\delta$  7.70 (dd,  $J = 8.2, 1.4$  Hz, 2H), 7.45 – 7.32 (m, 8H), 5.96 (d,  $J = 5.1$  Hz, 1H), 5.48 (dd,  $J = 10.7, 5.5$  Hz, 1H), 4.25 – 4.07 (m, 3H), 2.57 – 2.42 (m, 1H), 2.19 (ddd,  $J = 13.9, 10.6, 9.5$  Hz, 1H), 1.67 – 1.57 (m, 2H), 1.22 (s, 10H), 0.87 (t,  $J = 6.8$  Hz, 3H).

$^{13}\text{C}$  NMR (75 MHz,  $\text{CDCl}_3$ ):  $\delta$  167.8, 140.0, 138.2, 128.7, 128.6, 128.5, 128.2, 126.3, 126.0, 108.0, 92.6, 81.9, 66.4, 61.3, 38.2, 31.8, 29.2, 29.1, 28.5, 25.8, 22.7, 14.2.

HR-MS (ESI-MS):  $m/z$  calc. for  $\text{C}_{26}\text{H}_{32}\text{O}_5$   $[\text{M}+\text{NH}_4^+]^+$  442.2593, found 442.2597.

**Methyl (3*R*\*,3*aS*\*,6*aR*\*)-3-phenyl-6-(phenylsulfonyl)hexahydro-[1,2]dioxolo[3,4-*b*]pyrrole-3-carboxylate** and

**Methyl (3*S*\*,3*aS*\*,6*aR*\*)-3-phenyl-6-(phenylsulfonyl)hexahydro-[1,2]dioxolo[3,4-*b*]pyrrole-3-carboxylate**      **182b**



Following **GP5**, compound **181b** (71.5 mg, 0.2 mmol, 1 equiv.) was dissolved in 10 mL MeCN and irradiated with blue light for 12 h in the presence of [MesAcr]ClO<sub>4</sub> (8.3 mg, 0.02 mmol, 10 mol%). Crude NMR revealed a diastereomeric ratio of 1:1, column chromatography (hexanes:EtOAc = 9:1 to 4:1) allowed for separation of the diastereomers, which were isolated as colorless viscous oils. Major: 13.5 mg, 0.034 mmol, 17% Minor: 13.2 mg, 0.034 mmol, 17%; combined: 26.7 mg, 0.068 mmol, 34%.

#### Major

**R<sub>f</sub>** (hexanes:EtOAc = 4:1) = 0.14.

**IR** (neat): 2944, 2840, 1707, 1584, 1453, 1412, 1274, 1237, 1121, 1006, 913, 853, 760 cm<sup>-1</sup>.

**<sup>1</sup>H NMR** (400 MHz, CDCl<sub>3</sub>): δ 7.94 – 7.89 (m, 2H), 7.63 – 7.51 (m, 5H), 7.43 – 7.35 (m, 3H), 6.00 (d, *J* = 5.9 Hz, 1H), 4.16 – 4.09 (m, 1H), 3.69 (s, 3H), 3.63 – 3.57 (m, 1H), 3.38 (td, *J* = 8.9, 7.1 Hz, 1H), 2.36 (dq, *J* = 13.7, 8.8 Hz, 1H), 2.09 (ddt, *J* = 13.9, 7.3, 3.9 Hz, 1H).

**<sup>13</sup>C NMR** (101 MHz, CDCl<sub>3</sub>): δ 167.6, 139.1, 137.4, 133.1, 129.2, 129.1, 128.9, 128.8, 128.6, 127.8, 126.1, 94.4, 92.7, 60.2, 53.1, 47.5, 28.4.

**HR-MS** (EI-MS): *m/z* calc. for C<sub>19</sub>H<sub>20</sub>NO<sub>6</sub>S [M+H]<sup>+</sup> 390.1011, found 390.1015.

#### Minor

**R<sub>f</sub>** (hexanes:EtOAc 4:1) = 0.17.

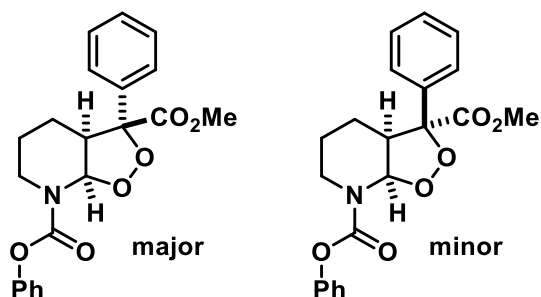
**<sup>1</sup>H NMR** (400 MHz, CDCl<sub>3</sub>): δ 7.97 (d, *J* = 7.7 Hz, 2H), 7.59 (dt, *J* = 26.4, 7.3 Hz, 3H), 7.37 – 7.31 (m, 3H), 7.20 – 7.13 (m, 2H), 6.25 (d, *J* = 5.9 Hz, 1H), 4.64 – 4.49 (m, 1H), 3.75 (s, 3H), 3.43 (t, *J* = 8.7 Hz, 1H), 3.08 – 2.99 (m, 1H), 2.04 – 1.89 (m, 1H), 1.50 (d, *J* = 6.7 Hz, 1H).

**<sup>13</sup>C NMR** (101 MHz, CDCl<sub>3</sub>): δ 167.6, 139.1, 137.4, 133.1, 129.2, 129.1, 128.9, 128.8, 128.6, 127.8, 126.1, 94.4, 92.7, 60.2, 53.1, 47.5, 28.4.

**HR-MS** (EI-MS): *m/z* calc. for C<sub>19</sub>H<sub>20</sub>NO<sub>6</sub>S [M+H]<sup>+</sup> 390.1011, found 390.1011.

**3-methyl 7-phenyl (3R\*,3aS\*,7aR\*)-3-phenyltetrahydro-3H-[1,2]dioxolo[3,4-b]pyridine-3,7(4H)-dicarboxylate** and

**3-methyl 7-phenyl (3S\*,3aS\*,7aR\*)-3-phenyltetrahydro-3H-[1,2]dioxolo[3,4-b]pyridine-3,7(4H)-dicarboxylate** **182c**



Following **GP5**, compound **181c** (154 mg, 0.44 mmol, 1 equiv.) was dissolved in 10 mL MeCN and irradiated with blue light for 15 h in the presence of [MesAc]ClO<sub>4</sub> (14 mg, 0.035 mmol, 8 mol%). Crude NMR revealed a diastereomeric ratio of 5.3:1. Column chromatography (hexanes:EtOAc = 9:1 to 2:1) yielded the major diastereomer as colourless crystalline solid, (52.7 mg, 0.137 mmol, 31%); The minor diastereomer could not be purified, the total yield was calculated based on the diastereomeric ratio determined from the crude NMR as 37%;

**R<sub>f</sub>** (hexanes:EtOAc = 9:1) = 0.1.

**m.p.**: 153 °C.

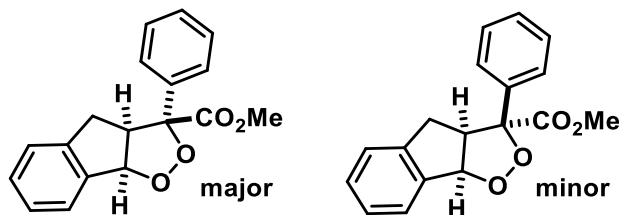
**IR** (neat): 2967, 1735, 1591, 1445, 1413, 1287, 1247, 1193, 1100, 1052, 960, 909, 793 cm<sup>-1</sup>.

**<sup>1</sup>H NMR** (400 MHz, CDCl<sub>3</sub>): δ 7.75 (d, *J* = 6.9 Hz, 2H), 7.46 – 7.29 (m, 6H), 7.18 (t, *J* = 7.3 Hz, 1H), 7.02 (s, 2H), 6.05 (d, *J* = 4.7 Hz, 1H), 4.17 – 4.03 (m, 1H), 3.75 (s, 3H), 3.34 – 3.08 (m, 2H), 2.25 – 2.15 (m, 1H), 1.99 – 1.80 (m, 2H), 1.60 (s, 1H); broadened signals due to rotamers.

**<sup>13</sup>C NMR** (101 MHz, CDCl<sub>3</sub>): δ 167.8, 150.9, 137.3, 129.3, 129.0, 128.8, 125.8, 125.7, 121.7, 92.2, 84.8, 52.9, 50.3, 40.2, 39.8, 22.1, 21.9.

**HR-MS** (APCI-MS): *m/z* calc. for C<sub>21</sub>H<sub>22</sub>NO<sub>6</sub> [M+H]<sup>+</sup> 384.1442, found 384.1443.

**Methyl (3R\*,3aR\*,8aR\*)-3-phenyl-3,3a,8,8a-tetrahydroindeno[2,1-c][1,2]dioxole-3-carboxylate** and **Methyl (3S\*,3aR\*,8aR\*)-3-phenyl-3,3a,8,8a-tetrahydroindeno[2,1-c][1,2]dioxole-3-carboxylate** **184c**



Following **GP5**, compound **183c** (132 mg, 0.5 mmol, 1 equiv.) was dissolved in 10 mL MeCN and irradiated with blue light for 10 h in the presence of [MesAc]ClO<sub>4</sub> (16.5 mg, 0.04 mmol,

8 mol%). Crude NMR revealed a diastereomeric ratio of 2.8:1. Column chromatography (hexanes:EtOAc = 19:1 to 7:1) yielded the major diastereomer as white crystalline solid, (63.7 mg, 0.21 mmol, 43.9%); The minor diastereomer could not be purified, the total yield was calculated based on the diastereomeric ratio determined from the crude NMR as 59%;

**m.p.:** 146-148 °C.

**IR** (neat): 30423062, 2920, 2855, 2342, 1739, 1461, 1445, 1335, 1236, 1064, 932, 815, 784  $\text{cm}^{-1}$ .

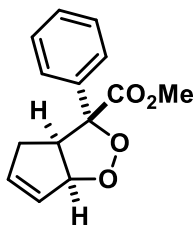
**$^1\text{H}$  NMR** (400 MHz,  $\text{CDCl}_3$ ):  $\delta$  7.77 (d,  $J = 7.4$  Hz, 2H), 7.47 – 7.32 (m, 5H), 7.26 (t,  $J = 6.8$  Hz, 2H), 5.58 (d,  $J = 6.9$  Hz, 1H), 4.40 (ddd,  $J = 9.0, 6.8, 5.3$  Hz, 1H), 3.72 (s, 3H), 3.43 (dd,  $J = 17.2, 9.1$  Hz, 1H), 3.22 (dd,  $J = 17.2, 5.1$  Hz, 1H).

**$^{13}\text{C}$  NMR** (101 MHz,  $\text{CDCl}_3$ ):  $\delta$  168.6, 143.2, 139.1, 138.4, 129.8, 128.5, 128.4, 127.4, 126.1, 125.9, 124.5, 92.9, 89.2, 60.3, 52.7, 35.7.

**HR-MS** (APCI-MS):  $m/z$  calc. for  $\text{C}_{18}\text{H}_{17}\text{O}_4$   $[\text{M}+\text{H}^+]^+$  297.1121, found 297.1123.

**Crystals** suitable for X-ray analysis (major: CDC 1980432) were obtained by recrystallization from DCM/ $\text{Et}_2\text{O}$ .

**Methyl (3*R*\*,3*aR*\*,6*aS*\*)-3-phenyl-3,3*a*,4,6*a*-tetrahydrocyclopenta[*c*][1,2]dioxole-3-carboxylate**      **184a**



Following **GP5**, compound **183a** (53 mg, 0.25 mmol, 1 equiv.) was dissolved in 3 mL MeCN and irradiated in the presence of  $[\text{MesAcr}]\text{ClO}_4$  (10.4 mg, 0.025 mmol, 10 mol%) for 13 h. Column chromatography (hexanes:EtOAc = 19:1) yielded an ochre crystalline solid (39.4 mg, 0.157 mmol, 63%); only one diastereomer was observed in the crude NMR.

**R<sub>f</sub>** (hexanes:EtOAc = 9:1) = 0.18; dark brown with vanillin.

**IR** (neat): 3064, 3001, 2953, 2854, 1736, 1435, 1356, 1254, 1218, 1068, 1015, 949, 820  $\text{cm}^{-1}$ .

**$^1\text{H}$  NMR** (400 MHz,  $\text{CDCl}_3$ ):  $\delta$  7.75 – 7.68 (m, 2H), 7.44 – 7.31 (m, 3H), 6.11 (dt,  $J = 6.0, 2.4$  Hz, 1H), 5.80 (dq,  $J = 5.7, 2.2$  Hz, 1H), 5.21 (dt,  $J = 7.1, 1.9$  Hz, 1H), 4.14 (ddd,  $J = 8.8, 7.1, 3.7$  Hz, 1H), 3.72 (s, 3H), 2.82 (ddt,  $J = 18.2, 8.7, 2.3$  Hz, 1H), 2.53 (ddq,  $J = 18.2, 4.3, 2.3$  Hz, 1H).

**$^{13}\text{C}$  NMR** (101 MHz,  $\text{CDCl}_3$ ):  $\delta$  168.9, 138.9, 137.2, 128.5, 128.4, 126.3, 93.1, 90.7, 57.8, 52.8, 36.9.

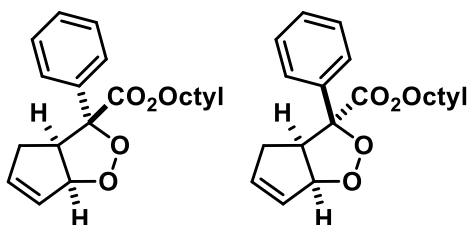
**HR-MS** (APCI-MS):  $m/z$  calc. for  $\text{C}_{14}\text{H}_{14}\text{NO}_4$   $[\text{M}+\text{H}^+]^+$  247.0970, found 247.0966.



As further undesired side reactions may occur, the reaction must not be run longer than until full consumption of starting material.

**Octyl (3*R*\*,3*aR*\*,6*aS*\*)-3-phenyl-3,3*a*,4,6*a*-tetrahydrocyclopenta[*c*][1,2]dioxole-3-carboxylate** and

**Octyl (3*S*\*,3*aR*\*,6*aS*\*)-3-phenyl-3,3*a*,4,6*a*-tetrahydrocyclopenta[*c*][1,2]dioxole-3-carboxylate** **184b**



Following **GP5**, compound **183b** (75 mg, 0.24 mmol, 1 equiv.) was dissolved in 2 mL MeCN and irradiated with blue light for 12 h in the presence of [MesAc]ClO<sub>4</sub> (8 mg, 0.02 mmol, 8 mol%). Column chromatography (hexanes:EtOAc = 19:1) yielded a colourless oil, (42.3 mg, 0.122 mmol, 51%); consisting of two inseparable diastereomers.

**R<sub>f</sub>** (hexanes:EtOAc = 19:1) = 0.2.

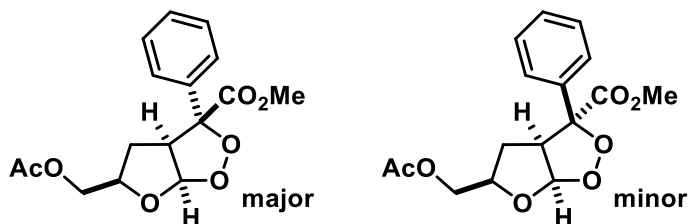
**IR** (neat): 2956, 2926, 1737, 1597, 1494, 1449, 1347, 1211, 1159, 1091, 1011, 965, 910, 814 cm<sup>-1</sup>.

**<sup>1</sup>H NMR** (300 MHz, CDCl<sub>3</sub>): δ 7.74 – 7.69 (m, 2H), 7.39 – 7.33 (m, 3H), 6.11 (dt, *J* = 5.0, 2.2 Hz, 1H), 5.83 – 5.77 (m, 1H), 5.19 (dt, *J* = 7.0, 1.8 Hz, 1H), 4.18 – 4.06 (m, 3H), 2.82 (ddt, *J* = 18.0, 8.7, 2.2 Hz, 1H), 2.55 (ddt, *J* = 15.8, 3.9, 1.9 Hz, 1H), 1.55 (m, 2H), 1.32 – 1.16 (m, 10H), 0.88 (t, *J* = 6.8 Hz, 3H).

**<sup>13</sup>C NMR** (75 MHz, CDCl<sub>3</sub>): δ 170.3, 139.0, 137.1, 128.3, 127.5, 126.2, 92.9, 90.6, 65.9, 57.3, 36.8, 31.7, 29.1, 29.0, 28.3, 25.6, 22.6, 14.1.

**HR-MS** (ESI-MS): *m/z* calc. for C<sub>21</sub>H<sub>29</sub>O<sub>4</sub> [M+H]<sup>+</sup> 345.2060, found 345.2064.

**Methyl (3*R*\*,3*aS*\*,5*R*\*,6*aR*\*)-5-(acetoxymethyl)-3-phenyltetrahydro-3*H*-furo[2,3-*c*][1,2]dioxole-3-carboxylate and methyl (3*S*\*,3*aS*\*,5*R*\*,6*aR*\*)-5-(acetoxymethyl)-3-phenyltetrahydro-3*H*-furo[2,3-*c*][1,2]dioxole-3-carboxylate** 189



Following **GP5**, compound **188** (252 mg, 0.87 mmol, 1 equiv.) was dissolved in 10 mL MeCN and irradiated with blue light for 16 h in the presence of [MesAc]ClO<sub>4</sub> (28.5 mg, 0.07 mmol, 8 mol%). Column chromatography (hexanes:EtOAc = 9:1 to 4:1) yielded the major diastereomer as colorless oil (100.9 mg, 0.313 mmol, 36%); The minor diastereomer could not be purified, the total yield was calculated based on the diastereomeric ratio of 4:1 determined from the crude-NMR as 45%.

**R<sub>f</sub>** (hexanes:EtOAc 4:1) = 0.35.

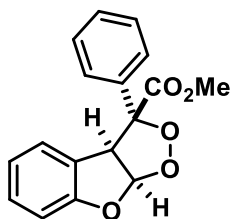
**IR** (neat): 3048, 2955, 2074, 1735, 1491, 1448, 1249, 1216, 1078, 1008, 917, 875, 824 cm<sup>-1</sup>.

**<sup>1</sup>H NMR** (400 MHz, CDCl<sub>3</sub>): δ 7.72 – 7.62 (m, 2H), 7.47 – 7.30 (m, 3H), 5.69 (d, *J* = 5.5 Hz, 1H), 4.42 – 4.30 (m, 2H), 4.26 (dd, *J* = 10.6, 6.3 Hz, 1H), 4.15 (ddd, *J* = 9.8, 7.3, 5.5 Hz, 1H), 3.73 (s, 3H), 2.50 (ddd, *J* = 13.4, 9.8, 6.7 Hz, 1H), 2.12 (s, 3H), 1.84 (dt, *J* = 13.4, 7.4 Hz, 1H).

**<sup>13</sup>C NMR** (101 MHz, CDCl<sub>3</sub>): δ 171.69, 170.49, 133.34, 130.92, 128.40, 127.90, 86.45, 70.69, 65.03, 52.39, 42.75, 32.66, 28.50, 20.77.

**HR-MS** (APCI-MS): *m/z* calc. for C<sub>16</sub>H<sub>19</sub>O<sub>7</sub> [M+H]<sup>+</sup> 323.1125, found 323.1131.

**Methyl (3*S*\*,3*aS*\*,8*aS*\*)-3-phenyl-3*a*,8*a*-dihydro-3*H*-[1,2]dioxolo[3,4-*b*]benzofuran-3-carboxylate** 191



Following **GP5**, compound **190** (133 mg, 0.5 mmol, 1 equiv.) was dissolved in 5 mL MeCN and irradiated in the presence of [MesAc]ClO<sub>4</sub> (20.2 mg, 0.49 mmol, 10 mol%) for 2 h. Crude NMR showed only one diastereomer. Column chromatography (hexanes:EtOAc = 9:1) yielded colorless oil (89 mg, 0.3 mmol, 60%).

**R<sub>f</sub>** (hexanes: EtOAc = 4:1) = 0.58; bright red with vanillin.

**IR** (neat): 3029, 2952, 2843, 1734, 1637, 1606, 1484, 1452, 1230, 1170, 1112, 1034, 973, 936, 798, 729, 753, 694  $\text{cm}^{-1}$ .

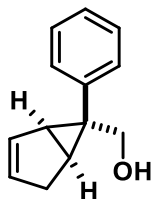
**$^1\text{H}$  NMR** (400 MHz,  $\text{CDCl}_3$ ):  $\delta$  7.58 (d,  $J = 6.9$  Hz, 2H), 7.39 – 7.30 (m, 3H), 7.17 (td,  $J = 7.7$ , 1.6 Hz, 1H), 7.06 – 7.00 (m, 2H), 6.89 (td,  $J = 7.4$ , 1.1 Hz, 1H), 6.64 (d,  $J = 9.8$  Hz, 1H), 6.29 (d,  $J = 9.8$  Hz, 1H), 3.76 (s, 3H).

**$^{13}\text{C}$  NMR** (101 MHz,  $\text{CDCl}_3$ ):  $\delta$  171.3, 152.0, 140.1, 130.0, 128.6, 128.6, 126.9, 126.1, 125.2, 124.1, 121.9, 120.6, 116.7, 81.6, 53.1.

**HR-MS** (ESI-MS):  $m/z$  calc. for  $\text{C}_{17}\text{H}_{15}\text{O}_3$   $[(\text{M}-\text{O}_2)+\text{H}^+]^+$  267.1021, found 267.1019. *Note:* For this peroxide, no applied method would allow for detection of the actual peroxide, instead it seems to rapidly lose  $\text{O}_2$  upon ionization. However, the substance was kept for 3 months at 4–6  $^\circ\text{C}$  and showed no signs of decomposition.

#### 4.10.9. Synthesis of Hydroperoxides

##### ((1*R*\*,5*S*\*,6*R*\*)-6-phenylbicyclo[3.1.0]hex-2-en-6-yl)methanol S6



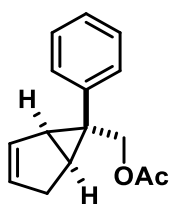
Compound **183a** (108.4 mg, 0.5 mmol, 1 equiv.) was reduced to the alcohol by stirring it in 10 mL MeOH and slowly adding NaBH<sub>4</sub> (45.9 mg, 1.2 mmol, 2.4 equiv.) to the solution. When the gas evolution ceased, stirring was continued for 3 h, then water was added dropwise to quench the remaining NaBH<sub>4</sub>. The reaction mixture was acidified using 1M HCl<sub>aq</sub> and then extracted with EtOAc. The organic phases were combined and dried over MgSO<sub>4</sub>, filtered over a plug of silica and used in the next step without further purification, yielding 80.4 mg (0.43 mmol, 86%) of clear viscous oil.

**<sup>1</sup>H NMR** (400 MHz, CDCl<sub>3</sub>): δ 7.29 (t, *J* = 7.2 Hz, 2H), 7.20 (dd, *J* = 19.2, 7.8 Hz, 3H), 5.76 – 5.67 (m, 1H), 5.11 (dq, *J* = 5.5, 2.1 Hz, 1H), 3.65 (dd, *J* = 11.1, 4.0 Hz, 1H), 3.43 (dd, *J* = 11.2, 5.2 Hz, 1H), 2.55 (dd, *J* = 18.4, 7.5 Hz, 1H), 2.31 (dt, *J* = 5.4, 2.2 Hz, 1H), 2.04 (dq, *J* = 18.4, 3.3 Hz, 1H), 1.96 – 1.88 (m, 1H), 1.39 (s, 1H).

**<sup>13</sup>C NMR** (75 MHz, CDCl<sub>3</sub>): δ 136.5, 132.2, 130.9, 130.7, 128.1, 126.6, 71.4, 39.1, 35.1, 33.1, 26.6.

**HR-MS** (EI-MS): *m/z* calc. for C<sub>13</sub>H<sub>14</sub>O [M<sup>+</sup>]<sup>+</sup> 186.1039, found 186.1036.

##### ((1*S*\*,5*R*\*,6*R*\*)-6-phenylbicyclo[3.1.0]hex-2-en-6-yl)methyl acetate 192



Compound **S6** (70.0 mg, 0.37 mmol, 1 equiv.) was dissolved in DCM and acetic anhydride (50 μL, 0.49 mmol, 1.3 equiv.) was added. The reaction was cooled to 0°C using an ice-bath, and NEt<sub>3</sub> (70 μL, 0.49 mmol, 1.3 equiv.) was added slowly. After stirring for 2 h, the mixture was quenched by adding water, and consecutively washed with water, NaHCO<sub>3aq, sat</sub> and 1M HCl. Upon drying over MgSO<sub>4</sub> the solvent was removed and the crude further purified by column chromatography, yielding 80.9 mg clear viscous oil (0.35 mmol, 96%).

**R<sub>f</sub>** (hexanes:EtOAc = 9:1) = 0.4.

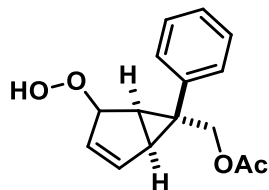
**IR** (neat): 3057, 3026, 2903, 2837, 1736, 1602, 1496, 1445, 1361, 1223, 1027, 957, 767 cm<sup>-1</sup>.

$^1\text{H NMR}$  (300 MHz,  $\text{CDCl}_3$ ):  $\delta$  7.26 (s, 5H), 5.71 (dq,  $J = 5.6, 2.2$  Hz, 1H), 5.12 (dtd,  $J = 5.6, 2.2, 1.2$  Hz, 1H), 4.10 (d,  $J = 11.2$  Hz, 1H), 3.98 (d,  $J = 11.2$  Hz, 1H), 2.61 – 2.49 (m, 1H), 2.39 – 2.34 (m, 1H), 2.09 – 1.95 (m, 5H).

$^{13}\text{C NMR}$  (75 MHz,  $\text{CDCl}_3$ ):  $\delta$  171.2, 136.3, 132.2, 131.2, 130.4, 127.8, 126.5, 72.3, 35.5, 35.4, 33.2, 27.0, 21.1.

**HR-MS** (EI-MS):  $m/z$  calc. for  $\text{C}_{15}\text{H}_{16}\text{O}_2$  [ $\text{M}^+$ ] $^+$  228.1144, found 228.1147.

**((1*S*\*,5*R*\*,6*R*\*)-4-hydroperoxy-6-phenylbicyclo[3.1.0]hex-2-en-6-yl)methyl acetate **194****



Following **GP5**, compound **192** (73 mg, 0.32 mmol, 1 equiv.) was dissolved in MeCN and [MesAc]ClO<sub>4</sub> (12.3 mg, 0.03 mmol, 0.1 equiv.) was added. The reaction was irradiated with a 455 nm LED and progress monitored by TLC. The reaction was terminated after 3 h and the mixture directly subjected to column chromatography. Hydroperoxide **194** was obtained as 52.6 mg beige solid (0.20 mmol, 63%).

$R_f$  (hexanes:EtOAc = 7:1) = 0.2.

**m.p.**: decomposes upon heating above 80 °C. Compound turns dark brown.

**IR**(neat): 3400, 3061, 2925, 2855, 1710, 1602, 1495, 1455, 1379, 1222, 1157, 972, 759, 723, 699  $\text{cm}^{-1}$ .

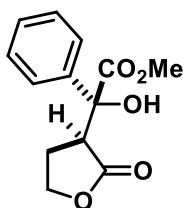
$^1\text{H NMR}$  (400 MHz,  $\text{CDCl}_3$ )  $\delta$  8.15 (s, 1H), 7.29 – 7.08 (m, 5H), 6.17 (d,  $J = 5.5$  Hz, 1H), 5.26 (d,  $J = 5.5$  Hz, 1H), 4.55 (s, 1H), 4.18 (d,  $J = 11.3$  Hz, 1H), 4.05 (d,  $J = 11.3$  Hz, 1H), 2.51 (dt,  $J = 5.1, 2.4$  Hz, 1H), 2.42 (d,  $J = 5.7$  Hz, 1H), 2.01 (s, 3H).

$^{13}\text{C NMR}$  (101 MHz,  $\text{CDCl}_3$ ):  $\delta$  171.0, 138.6, 135.0, 131.7, 127.9, 127.7, 126.9, 88.6, 70.8, 42.5, 33.6, 32.0, 20.9.

**HR-MS** (APCI-MS):  $m/z$  calc. for  $\text{C}_{15}\text{H}_{17}\text{O}_4$  [ $\text{M}+\text{H}^+$ ] $^+$  261.1121, found 261.1121.

#### 4.10.10. Synthesis of Butyrolactones from Endoperoxides

##### Methyl (*R*\*)-2-hydroxy-2-((*S*\*)-2-oxotetrahydrofuran-3-yl)-2-phenylacetate **199a**



**158a-major** (48.9 mg, 0.19 mmol, 1 equiv.) was dissolved in 5 mL MeOH and HNEt<sub>2</sub> (20  $\mu$ L, 0.19 mmol, 1 equiv.) was added while stirring. The reaction was stirred over night for 16 h and the solvent evaporated under reduced pressure. Column chromatography (hexanes:EtOAc 1:1) yielded the product was white very viscous oil (46.4 mg, 18.5  $\mu$ mol, 95%).

**R<sub>f</sub>** (hexanes:EtOAc 1:1) = 0.2.

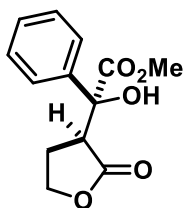
**IR** (neat): 3524, 3064, 3004, 2952, 1766, 1722, 1449, 1427, 1375, 1254, 1132, 1077, 1027, 968 cm<sup>-1</sup>.

**<sup>1</sup>H NMR** (400 MHz, CDCl<sub>3</sub>):  $\delta$  7.60 – 7.49 (m, 2H), 7.45 – 7.29 (m, 3H), 4.60 – 4.35 (m, 2H), 4.20 (q, *J* = 8.2 Hz, 1H), 3.82 (s, 3H), 3.32 (t, *J* = 9.3 Hz, 1H), 2.45 (dq, *J* = 12.7, 8.8 Hz, 1H), 2.20 (dddd, *J* = 12.8, 9.5, 7.6, 4.0 Hz, 1H).

**<sup>13</sup>C NMR** (75 MHz, CDCl<sub>3</sub>):  $\delta$  176.2, 173.4, 138.6, 128.5 (2C), 125.4, 79.4, 66.7, 53.6, 48.0, 25.6.

**HR-MS** (APCI-MS): *m/z* calc. for C<sub>13</sub>H<sub>15</sub>O<sub>5</sub> [M+H]<sup>+</sup> 251.0914, found 251.0916.

##### Methyl (*S*\*)-2-hydroxy-2-((*S*\*)-2-oxotetrahydrofuran-3-yl)-2-phenylacetate **199b**



**158a-minor** (33.8 mg, 0.13 mmol, 1 equiv.) was dissolved in 5 mL MeOH and HNEt<sub>2</sub> (15  $\mu$ L, 0.14 mmol, 1.1 equiv.) was added while stirring. The reaction was stirred over night for 16 h and the solvent evaporated under reduced pressure. Column chromatography (hexanes:EtOAc = 1:1) yielded the product was white amorphous solid (32.1 mg, 12.8  $\mu$ mol, 95%).

**R<sub>f</sub>** (hexanes:EtOAc = 1:1) = 0.2.

**m.p.:** 130-133 °C.

**IR** (neat): 3482, 2962, 2925, 2856, 2360, 1765, 1719, 1497, 1449, 1224, 1256, 1180, 1143, 1111, 1021, 932, 895, 842 cm<sup>-1</sup>.

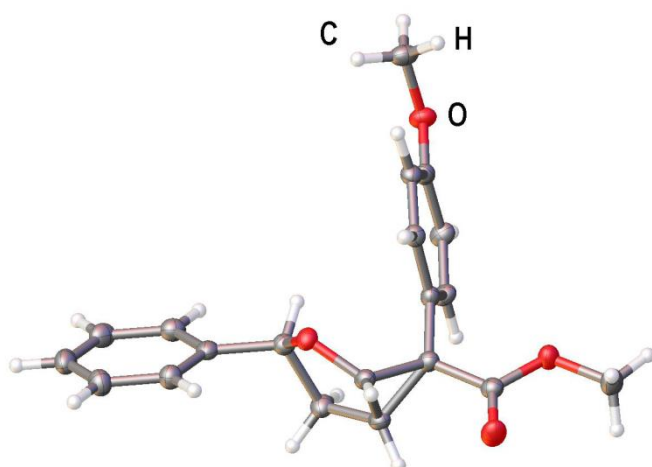
**<sup>1</sup>H NMR** (400 MHz, CDCl<sub>3</sub>): δ 7.62 (d, *J* = 7.6 Hz, 2H), 7.36 (dt, *J* = 15.7, 7.1 Hz, 3H), 4.34 (td, *J* = 8.9, 3.1 Hz, 1H), 4.17 (q, *J* = 8.9 Hz, 1H), 4.13 (s, 1H), 3.87 (s, 3H), 3.77 (t, *J* = 9.7 Hz, 1H), 2.25 – 2.13 (m, 1H), 2.05 – 1.96 (m, 1H).

**<sup>13</sup>C NMR** (101 MHz, CDCl<sub>3</sub>): δ 175.98, 174.02, 139.18, 128.71, 128.43, 125.86, 77.29, 66.93, 53.98, 48.48, 23.84.

**HR-MS** (APCI-MS): *m/z* calc. for C<sub>13</sub>H<sub>15</sub>O<sub>5</sub> [M+H<sup>+</sup>]<sup>+</sup> 251.0914, found 251.0916.

**Crystals** suitable for X-ray analysis (CDC 1980429) were obtained by recrystallization from DCM/Et<sub>2</sub>O.

#### 4.10.11. Crystal Structures

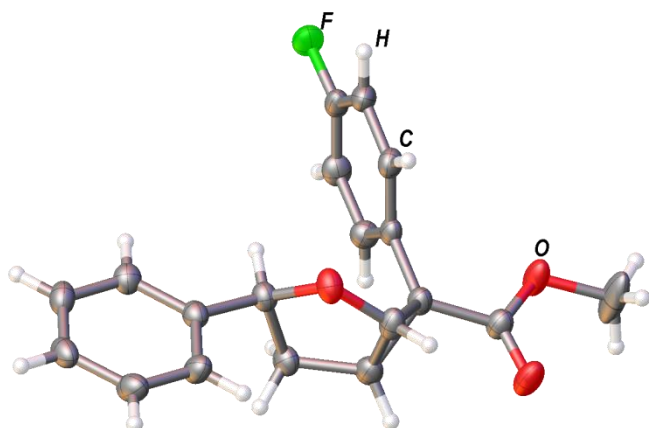


**Experimental:** Single clear colourless prism-shaped crystals of **155a** were obtained by recrystallisation from DCM/Et<sub>2</sub>O/pentane. A suitable crystal (0.27×0.20×0.17) was selected and mounted on a MITIGEN holder with inert oil on a SuperNova, Single source at offset/far, Atlas diffractometer. The crystal was kept at  $T = 123.00(10)$  K during data collection. Using **Olex2**<sup>166</sup>, the structure was solved with the **ShelXT**<sup>165</sup> structure solution program, using the Intrinsic Phasing solution method. The model was refined with **ShelXL**<sup>165</sup> using Least Squares minimisation.

**Crystal Data.** C<sub>20</sub>H<sub>20</sub>O<sub>4</sub>,  $M_r = 324.36$ , triclinic, P-1 (No. 2),  $a = 12.0615(2)$  Å,  $b = 14.8226(3)$  Å,  $c = 15.1286(3)$  Å,  $\alpha = 67.799(2)^\circ$ ,  $\beta = 81.5530(10)^\circ$ ,  $\gamma = 87.6980(10)^\circ$ ,  $V = 2476.70(9)$  Å<sup>3</sup>,  $T = 123.00(10)$  K,  $Z = 6$ ,  $Z' = 3$ ,  $\mu(\text{CuK}\alpha) = 0.733$ , 54132 reflections measured, 9938 unique ( $R_{int} = 0.0236$ ) which were used in all calculations. The final  $wR_2$  was 0.0833 (all data) and  $R_1$  was 0.0319 ( $I > 2(I)$ ).

Compound	155a
Formula	C <sub>20</sub> H <sub>20</sub> O <sub>4</sub>
$D_{calc.}/\text{g cm}^{-3}$	1.305
$\mu/\text{mm}^{-1}$	0.733
Formula Weight	324.36
Colour	clear colourless
Shape	prism
Max Size/mm	0.27
Mid Size/mm	0.20
Min Size/mm	0.17
$T/\text{K}$	123.00(10)
Crystal System	triclinic
Space Group	P-1
$a/\text{Å}$	12.0615(2)
$b/\text{Å}$	14.8226(3)
$c/\text{Å}$	15.1286(3)
$\alpha/^\circ$	67.799(2)
$\beta/^\circ$	81.5530(10)
$\gamma/^\circ$	87.6980(10)
$V/\text{Å}^3$	2476.70(9)
$Z$	6
$Z'$	3
$\theta_{min}/^\circ$	3.579
$\theta_{max}/^\circ$	74.375
Measured Refl.	54132
Independent Refl.	9938
Reflections Used	9298
$R_{int}$	0.0236
Parameters	889
Restraints	0
Largest Peak	0.256
Deepest Hole	-0.188
GooF	1.039
$wR_2$ (all data)	0.0833
$wR_2$	0.0816
$R_1$ (all data)	0.0341
$R_1$	0.0319

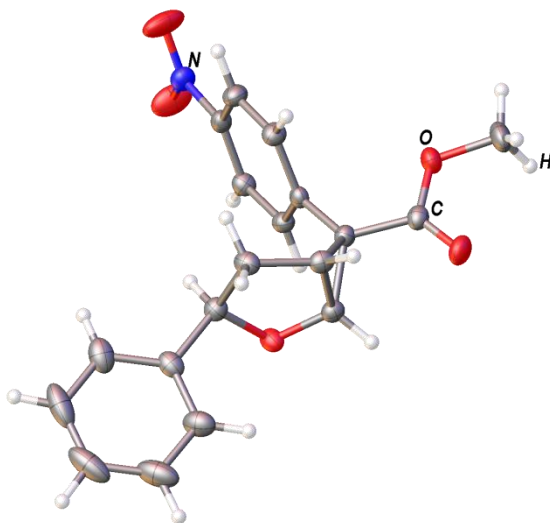




**Experimental:** Single clear colourless irregular-shaped crystals of **155c** were obtained by recrystallisation from diethyl ether. A suitable crystal  $0.29 \times 0.16 \times 0.09$  mm<sup>3</sup> was selected and mounted on a MITIGEN holder oil on an SuperNova, Single source at offset/far, Atlas diffractometer. The crystal was kept at a steady  $T = 123.01(10)$  K during data collection. The structure was solved with the **ShelXT**<sup>165</sup> structure solution program using the Intrinsic Phasing solution method and by using **Olex2**<sup>166</sup> as the graphical interface. The model was refined with version 2016/6 of **ShelXL**<sup>165</sup> using Least Squares minimisation.

**Crystal Data.** C<sub>19</sub>H<sub>17</sub>FO<sub>3</sub>,  $M_r = 312.32$ , monoclinic,  $P2_1/c$  (No. 14),  $a = 7.79512(16)$  Å,  $b = 9.30322(20)$  Å,  $c = 21.9617(5)$  Å,  $\beta = 98.048(2)^\circ$ ,  $\alpha = \gamma = 90^\circ$ ,  $V = 1576.97(6)$  Å<sup>3</sup>,  $T = 123.01(10)$  K,  $Z = 4$ ,  $Z' = 1$ ,  $\mu(\text{CuK}\alpha) = 0.794$ , 21337 reflections measured, 3301 unique ( $R_{int} = 0.0253$ ) which were used in all calculations. The final  $wR_2$  was 0.1087 (all data) and  $R_1$  was 0.0396 ( $I > 2(I)$ ).

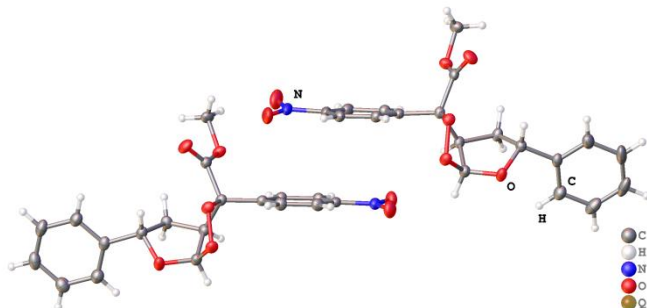
Compound	155c
Formula	C <sub>19</sub> H <sub>17</sub> FO <sub>3</sub>
$D_{calc.}/\text{g cm}^{-3}$	1.316
$\mu/\text{mm}^{-1}$	0.794
Formula Weight	312.32
Colour	clear colourless
Shape	irregular
Size/mm <sup>3</sup>	$0.29 \times 0.16 \times 0.09$
$T/\text{K}$	123.01(10)
Crystal System	monoclinic
Space Group	$P2_1/c$
$a/\text{Å}$	7.79512(16)
$b/\text{Å}$	9.30322(20)
$c/\text{Å}$	21.9617(5)
$\alpha/^\circ$	90
$\beta/^\circ$	98.048(2)
$\gamma/^\circ$	90
$V/\text{Å}^3$	1576.97(6)
$Z$	4
$Z'$	1
Wavelength/Å	1.54184
Radiation type	CuK $\alpha$
$\theta_{min}/^\circ$	4.066
$\theta_{max}/^\circ$	76.658
Measured Refl.	21337
Independent Refl.	3301
Reflections with $I > 2(I)$	2924
$R_{int}$	0.0253
Parameters	209
Restraints	0
Largest Peak	0.297
Deepest Hole	-0.248
GooF	1.033
$wR_2$ (all data)	0.1087
$wR_2$	0.1046
$R_1$ (all data)	0.0447
$R_1$	0.0396
Creation Method	
Solution	Olex2 1.2-alpha
Refinement	(compiled 2018.07.26 svn.r3523 for OlexSys, GUI svn.r5532)



**Experimental:** Single clear colourless prism-shaped crystals of **155d** were obtained by recrystallisation from DCM/Et<sub>2</sub>O/pentane. A suitable crystal 0.26×0.18×0.12 mm<sup>3</sup> was selected and mounted on a MITIGEN holder oil on an SuperNova, Single source at offset/far, Atlas diffractometer. The crystal was kept at a steady  $T = 123.01(10)$  K during data collection. The structure was solved with the **ShelXT**<sup>165</sup> structure solution program using the Intrinsic Phasing solution methods solution method and by using **Olex2**<sup>166</sup> as the graphical interface. The model was refined with version 2018/3 of **ShelXL**<sup>165</sup> using Least Squares minimisation.

**Crystal Data.** C<sub>19</sub>H<sub>17</sub>NO<sub>5</sub>,  $M_r = 339.33$ , monoclinic,  $P2_1/c$  (No. 14),  $a = 13.7013(3)$  Å,  $b = 11.6692(2)$  Å,  $c = 10.4671(2)$  Å,  $\beta = 104.314(2)^\circ$ ,  $\alpha = \gamma = 90^\circ$ ,  $V = 1621.55(7)$  Å<sup>3</sup>,  $T = 123.01(10)$  K,  $Z = 4$ ,  $Z' = 1$ ,  $\mu(\text{CuK}\alpha) = 0.842$ , 17252 reflections measured, 3245 unique ( $R_{int} = 0.0210$ ) which were used in all calculations. The final  $wR_2$  was 0.0894 (all data) and  $R_1$  was 0.0342 ( $I > 2(I)$ ).

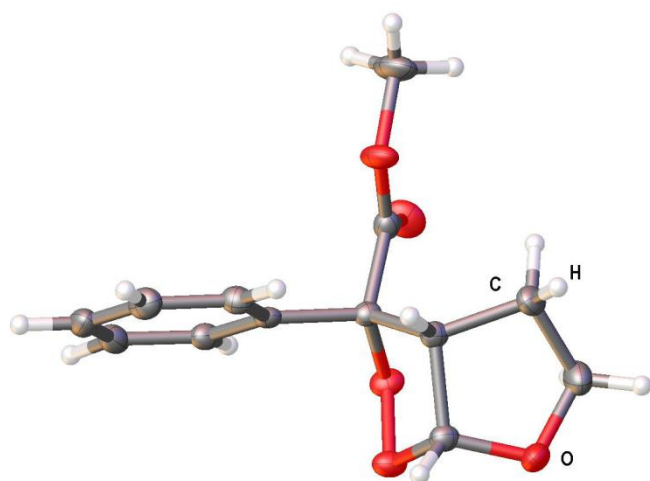
Compound	155d
Formula	C <sub>19</sub> H <sub>17</sub> NO <sub>5</sub>
$D_{calc.}/\text{g cm}^{-3}$	1.390
$\mu/\text{mm}^{-1}$	0.842
Formula Weight	339.33
Colour	clear colourless
Shape	prism
Size/mm <sup>3</sup>	0.26×0.18×0.12
$T/\text{K}$	123.01(10)
Crystal System	monoclinic
Space Group	$P2_1/c$
$a/\text{Å}$	13.7013(3)
$b/\text{Å}$	11.6692(2)
$c/\text{Å}$	10.4671(2)
$\alpha/^\circ$	90
$\beta/^\circ$	104.314(2)
$\gamma/^\circ$	90
$V/\text{Å}^3$	1621.55(7)
$Z$	4
$Z'$	1
Wavelength/Å	1.54184
Radiation type	CuK $\alpha$
$\Theta_{min}/^\circ$	5.046
$\Theta_{max}/^\circ$	74.257
Measured Refl.	17252
Independent Refl.	3245
Reflections with $I > 2(I)$	2910
$R_{int}$	0.0210
Parameters	294
Restraints	0
Largest Peak	0.234
Deepest Hole	-0.232
GooF	1.054
$wR_2$ (all data)	0.0894
$wR_2$	0.0861
$R_1$ (all data)	0.0380
$R_1$	0.0342
Creation Method	
Solution	Olex2 1.2-alpha
Refinement	(compiled 2018.07.26 svn.r3523 for OlexSys, GUI svn.r5532)



**Experimental:** Single clear colourless prism-shaped crystals of **156d** were obtained by recrystallisation from DCM/Et<sub>2</sub>O/pentane. A suitable crystal 0.20×0.17×0.13 mm<sup>3</sup> was selected and mounted on a MITIGEN holder oil on an SuperNova, Single source at offset/far, Atlas diffractometer. The crystal was kept at a steady  $T = 123.00(10)$  K during data collection. The structure was solved with the **ShelXT**<sup>165</sup> structure solution program using the Intrinsic Phasing solution method and by using **Olex2**<sup>166</sup> as the graphical interface. The model was refined with version 2018/3 of **ShelXL**<sup>165</sup> using Least Squares minimisation.

**Crystal Data.** C<sub>38</sub>H<sub>34</sub>N<sub>2</sub>O<sub>14</sub>,  $M_r = 742.67$ , monoclinic,  $P2_1$  (No. 4),  $a = 6.99870(10)$  Å,  $b = 12.21330(10)$  Å,  $c = 19.7453(2)$  Å,  $\beta = 91.0500(10)^\circ$ ,  $\alpha = \gamma = 90^\circ$ ,  $V = 1687.49(3)$  Å<sup>3</sup>,  $T = 123.00(10)$  K,  $Z = 2$ ,  $Z' = 1$ ,  $\mu(\text{CuK}\alpha) = 0.953$ , 29386 reflections measured, 7073 unique ( $R_{int} = 0.0242$ ) which were used in all calculations. The final  $wR_2$  was 0.0645 (all data) and  $R_1$  was 0.0256 ( $I > 2(I)$ ).

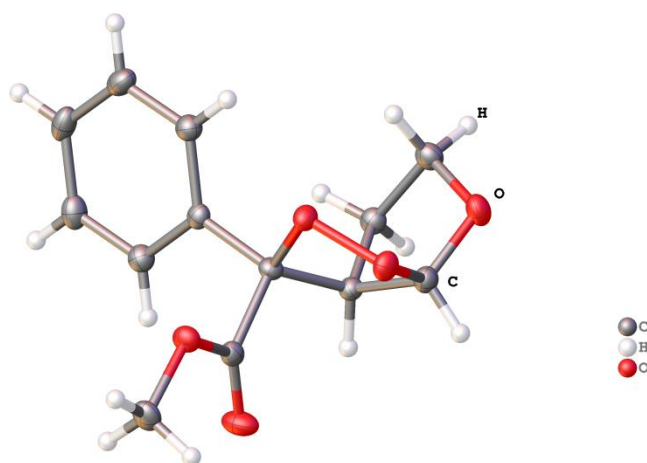
Compound	156d
Formula	C <sub>38</sub> H <sub>34</sub> N <sub>2</sub> O <sub>14</sub>
$D_{calc.}/\text{g cm}^{-3}$	1.462
$\mu/\text{mm}^{-1}$	0.953
Formula Weight	742.67
Colour	clear colourless
Shape	prism
Size/mm <sup>3</sup>	0.20×0.17×0.13
$T/\text{K}$	123.00(10)
Crystal System	monoclinic
Flack Parameter	-0.04(4)
Hooft Parameter	0.03(3)
Space Group	$P2_1$
$a/\text{Å}$	6.99870(10)
$b/\text{Å}$	12.21330(10)
$c/\text{Å}$	19.7453(2)
$\alpha/^\circ$	90
$\beta/^\circ$	91.0500(10)
$\gamma/^\circ$	90
$V/\text{Å}^3$	1687.49(3)
$Z$	2
$Z'$	1
Wavelength/Å	1.54184
Radiation type	CuK $\alpha$
$\theta_{min}/^\circ$	4.257
$\theta_{max}/^\circ$	76.375
Measured Refl.	29386
Independent Refl.	7073
Reflections with $I > 2(I)$	6895
$R_{int}$	0.0242
Parameters	489
Restraints	1
Largest Peak	0.203
Deepest Hole	-0.183
GooF	1.047
$wR_2$ (all data)	0.0645
$wR_2$	0.0636
$R_1$ (all data)	0.0266
$R_1$	0.0256



**Experimental:** Single clear colourless prism-shaped crystals of **158a-major** were obtained by recrystallisation from DCM/Et<sub>2</sub>O/pentane. A suitable crystal 0.22×0.12×0.09 mm<sup>3</sup> was selected and mounted on a MITIGEN holder with inert oil on an GV1000, TitanS2 diffractometer. The crystal was kept at a steady  $T = 123.01(10)$  K during data collection. The structure was solved with the **ShelXT**<sup>165</sup> structure solution program using the Intrinsic Phasing solution method and by using **Olex2**<sup>166</sup> as the graphical interface. The model was refined with version 2016/6 of **ShelXL**<sup>165</sup> using Least Squares minimisation.

**Crystal Data.** C<sub>13</sub>H<sub>14</sub>O<sub>5</sub>,  $M_r = 250.24$ , orthorhombic,  $P2_12_12_1$  (No. 19),  $a = 7.94950(10)$  Å,  $b = 9.83780(10)$  Å,  $c = 15.6228(2)$  Å,  $\alpha = \beta = \gamma = 90^\circ$ ,  $V = 1221.79(3)$  Å<sup>3</sup>,  $T = 123.01(10)$  K,  $Z = 4$ ,  $Z' = 1$ ,  $\mu(\text{CuK}\alpha) = 0.883$ , 13755 reflections measured, 2441 unique ( $R_{int} = 0.0401$ ) which were used in all calculations. The final  $wR_2$  was 0.0863 (all data) and  $R_1$  was 0.0326 ( $I > 2(I)$ ).

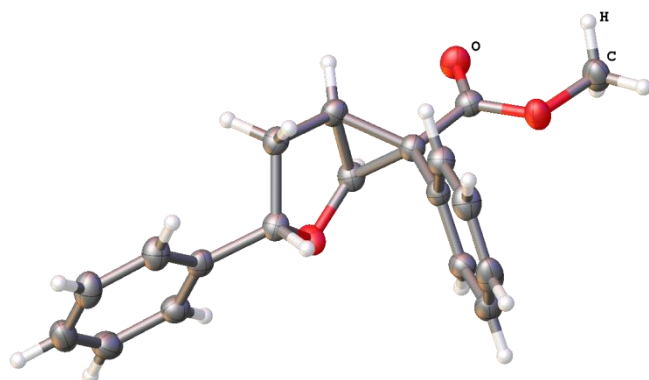
Compound	158a-major
Formula	C <sub>13</sub> H <sub>14</sub> O <sub>5</sub>
$D_{calc}/\text{g cm}^{-3}$	1.360
$\mu/\text{mm}^{-1}$	0.883
Formula Weight	250.24
Colour	clear colourless
Shape	prism
Size/mm <sup>3</sup>	0.22×0.12×0.09
$T/\text{K}$	123.01(10)
Crystal System	orthorhombic
Flack Parameter	-0.06(6)
Hooft Parameter	-0.04(6)
Space Group	$P2_12_12_1$
$a/\text{Å}$	7.94950(10)
$b/\text{Å}$	9.83780(10)
$c/\text{Å}$	15.6228(2)
$\alpha/^\circ$	90
$\beta/^\circ$	90
$\gamma/^\circ$	90
$V/\text{Å}^3$	1221.79(3)
$Z$	4
$Z'$	1
Wavelength/Å	1.54184
Radiation type	CuK $\alpha$
$\theta_{min}/^\circ$	5.314
$\theta_{max}/^\circ$	73.372
Measured Refl.	13755
Independent Refl.	2441
Reflections with $I > 2(I)$	2391
$R_{int}$	0.0401
Parameters	208
Restraints	0
Largest Peak	0.360
Deepest Hole	-0.289
GooF	1.042
$wR_2$ (all data)	0.0863
$wR_2$	0.0856
$R_1$ (all data)	0.0333
$R_1$	0.0326



**Experimental:** Single clear colourless prism-shaped crystals of **158a-minor** were obtained by recrystallisation from DCM/Et<sub>2</sub>O/pentane. A suitable crystal 0.19×0.14×0.10 mm<sup>3</sup> was selected and mounted on a MITIGEN holder oil on an SuperNova, Single source at offset/far, Atlas diffractometer. The crystal was kept at a steady  $T = 123.00(10)$  K during data collection. The structure was solved with the **ShelXT**<sup>165</sup> structure solution program using the Intrinsic Phasing solution method and by using **Olex2**<sup>166</sup> as the graphical interface. The model was refined with version 2018/3 of **ShelXL**<sup>165</sup> using Least Squares minimisation.

**Crystal Data.** C<sub>13</sub>H<sub>14</sub>O<sub>5</sub>,  $M_r = 250.24$ , monoclinic,  $P2_1/c$  (No. 14),  $a = 8.4209(2)$  Å,  $b = 11.6353(2)$  Å,  $c = 12.1410(2)$  Å,  $\beta = 105.937(2)^\circ$ ,  $\alpha = \gamma = 90^\circ$ ,  $V = 1143.85(4)$  Å<sup>3</sup>,  $T = 123.00(10)$  K,  $Z = 4$ ,  $Z' = 1$ ,  $\mu(\text{CuK}\alpha) = 0.943$ , 13754 reflections measured, 2380 unique ( $R_{int} = 0.0234$ ) which were used in all calculations. The final  $wR_2$  was 0.0856 (all data) and  $R_1$  was 0.0330 ( $I > 2(I)$ ).

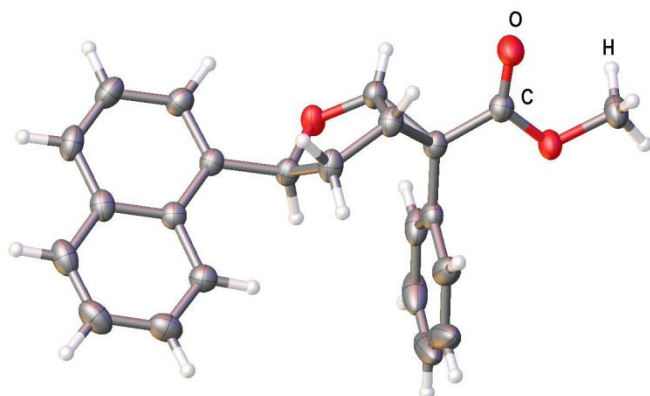
Compound	158a-minor
Formula	C <sub>13</sub> H <sub>14</sub> O <sub>5</sub>
$D_{calc.}/\text{g cm}^{-3}$	1.453
$\mu/\text{mm}^{-1}$	0.943
Formula Weight	250.24
Colour	clear colourless
Shape	prism
Size/mm <sup>3</sup>	0.19×0.14×0.10
$T/\text{K}$	123.00(10)
Crystal System	monoclinic
Space Group	$P2_1/c$
$a/\text{Å}$	8.4209(2)
$b/\text{Å}$	11.6353(2)
$c/\text{Å}$	12.1410(2)
$\alpha/^\circ$	90
$\beta/^\circ$	105.937(2)
$\gamma/^\circ$	90
$V/\text{Å}^3$	1143.85(4)
$Z$	4
$Z'$	1
Wavelength/Å	1.54184
Radiation type	CuK $\alpha$
$\theta_{min}/^\circ$	5.368
$\theta_{max}/^\circ$	76.165
Measured Refl.	13754
Independent Refl.	2380
Reflections with $I > 2(I)$	2231
$R_{int}$	0.0234
Parameters	164
Restraints	0
Largest Peak	0.326
Deepest Hole	-0.217
GooF	1.034
$wR_2$ (all data)	0.0856
$wR_2$	0.0838
$R_1$ (all data)	0.0350
$R_1$	0.0330



**Experimental:** Single clear colourless prism-shaped crystals of **155a** were obtained by recrystallisation from DCM/Et<sub>2</sub>O/pentane. A suitable crystal 0.28×0.17×0.14 mm<sup>3</sup> was selected and mounted on a MITIGEN holder oil on an SuperNova, Single source at offset/far, Atlas diffractometer. The crystal was kept at a steady  $T = 123.01(10)$  K during data collection. The structure was solved with the **ShelXT**<sup>165</sup> structure solution program using the Intrinsic Phasing solution method and by using **Olex2**<sup>166</sup> as the graphical interface. The model was refined with version 2016/6 of **ShelXL**<sup>165</sup> using Least Squares minimisation.

**Crystal Data.** C<sub>19</sub>H<sub>18</sub>O<sub>3</sub>,  $M_r = 294.33$ , monoclinic,  $P2_1/c$  (No. 14),  $a = 11.8626(2)$  Å,  $b = 9.88239(17)$  Å,  $c = 13.0212(2)$  Å,  $\beta = 101.0990(16)^\circ$ ,  $\alpha = \gamma = 90^\circ$ ,  $V = 1497.93(4)$  Å<sup>3</sup>,  $T = 123.01(10)$  K,  $Z = 4$ ,  $Z' = 1$ ,  $\mu(\text{CuK}\alpha) = 0.703$ , 16352 reflections measured, 3028 unique ( $R_{int} = 0.0248$ ) which were used in all calculations. The final  $wR_2$  was 0.1009 (all data) and  $R_1$  was 0.0384 ( $I > 2(I)$ ).

Compound	155a
Formula	C <sub>19</sub> H <sub>18</sub> O <sub>3</sub>
$D_{calc.}/\text{g cm}^{-3}$	1.305
$\mu/\text{mm}^{-1}$	0.703
Formula Weight	294.33
Colour	clear colourless
Shape	prism
Size/mm <sup>3</sup>	0.28×0.17×0.14
$T/\text{K}$	123.01(10)
Crystal System	monoclinic
Space Group	$P2_1/c$
$a/\text{Å}$	11.8626(2)
$b/\text{Å}$	9.88239(17)
$c/\text{Å}$	13.0212(2)
$\alpha/^\circ$	90
$\beta/^\circ$	101.0990(16)
$\gamma/^\circ$	90
$V/\text{Å}^3$	1497.93(4)
$Z$	4
$Z'$	1
Wavelength/Å	1.54184
Radiation type	CuK $\alpha$
$\theta_{min}/^\circ$	3.797
$\theta_{max}/^\circ$	74.536
Measured Refl.	16352
Independent Refl.	3028
Reflections with $I > 2(I)$	2801
$R_{int}$	0.0248
Parameters	200
Restraints	0
Largest Peak	0.196
Deepest Hole	-0.197
GooF	1.049
$wR_2$ (all data)	0.1009
$wR_2$	0.0979
$R_1$ (all data)	0.0414
$R_1$	0.0384
Creation Method	
Solution	Olex2 1.2-alpha
Refinement	(compiled 2018.07.26 svn.r3523 for OlexSys, GUI svn.r5532)

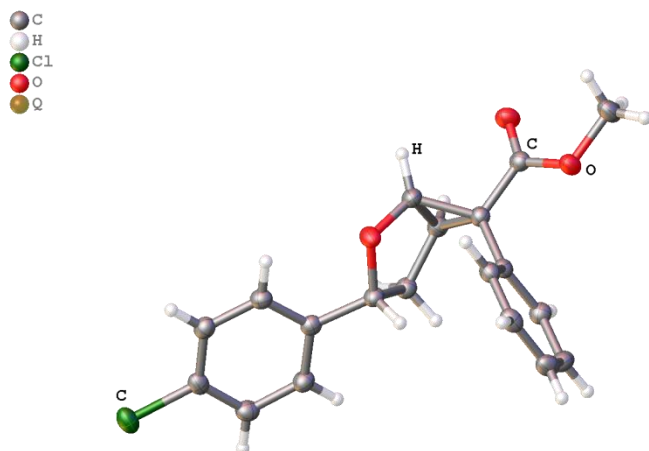


**Experimental.** Single clear colourless prism-shaped crystals of **166b** were obtained by recrystallisation from DCM/Et<sub>2</sub>O/pentane. A suitable crystal (0.21×0.16×0.13) was selected and mounted on a MITIGEN holder with inert oil on a GV1000, TitanS2 diffractometer. The crystal was kept at  $T = 122.94(19)$  K during data collection. Using **Olex2**<sup>166</sup>, the structure was solved with the **ShelXT**<sup>165</sup> structure solution program, using the Intrinsic Phasing solution method. The model was refined with ShelXL<sup>165</sup> using Least Squares minimisation.

**Crystal Data.** C<sub>23</sub>H<sub>20</sub>O<sub>3</sub>,  $M_r = 344.39$ , monoclinic, P2<sub>1</sub>/c (No. 14),  $a = 18.55810(10)$  Å,  $b = 16.75580(10)$  Å,  $c = 18.73840(10)$  Å,  $\beta = 113.1090(10)^\circ$ ,  $\alpha = \gamma = 90^\circ$ ,  $V = 5359.27(6)$  Å<sup>3</sup>,  $T = 122.94(19)$  K,  $Z = 12$ ,  $Z' = 3$ ,  $\mu(\text{CuK}\alpha) = 0.670$ , 87373 reflections measured, 10748 unique ( $R_{int} = 0.0397$ ) which were used in all calculations. The final  $wR_2$  was 0.1111 (all data) and  $R_1$  was 0.0428 ( $I > 2(I)$ ).

Compound	166b
Formula	C <sub>23</sub> H <sub>20</sub> O <sub>3</sub>
$D_{calc}/\text{g cm}^{-3}$	1.280
$\mu/\text{mm}^{-1}$	0.670
Formula Weight	344.39
Colour	clear colourless
Shape	prism
Max Size/mm	0.21
Mid Size/mm	0.16
Min Size/mm	0.13
$T/\text{K}$	122.94(19)
Crystal System	monoclinic
Space Group	P2 <sub>1</sub> /c
$a/\text{Å}$	18.55810(10)
$b/\text{Å}$	16.75580(10)
$c/\text{Å}$	18.73840(10)
$\alpha/^\circ$	90
$\beta/^\circ$	113.1090(10)
$\gamma/^\circ$	90
$V/\text{Å}^3$	5359.27(6)
$Z$	12
$Z'$	3
$\theta_{min}/^\circ$	3.679
$\theta_{max}/^\circ$	73.457
Measured Refl.	87373
Independent Refl.	10748
Reflections Used	10057
$R_{int}$	0.0397
Parameters	943
Restraints	0
Largest Peak	0.137
Deepest Hole	-0.300
GooF	1.062
$wR_2$ (all data)	0.1111
$wR_2$	0.1088
$R_1$ (all data)	0.0451
$R_1$	0.0428



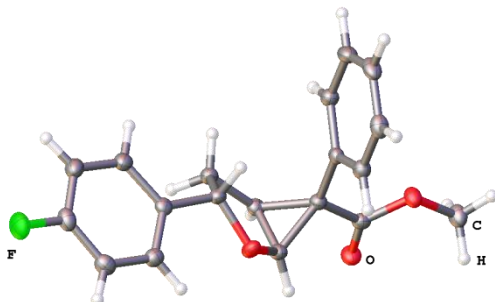


**Experimental:** Single clear colourless prism-shaped crystals of **166d** were obtained by recrystallization from DCM/Et<sub>2</sub>O/pentane. A suitable crystal 0.21×0.18×0.07 mm<sup>3</sup> was selected and mounted on a MITIGEN holder oil on an SuperNova, Single source at offset/far, Atlas diffractometer. The crystal was kept at a steady  $T = 123.00(10)$  K during data collection. The structure was solved with the **ShelXT**<sup>165</sup> structure solution program using the Intrinsic Phasing solution method and by using **Olex2**<sup>166</sup> as the graphical interface. The model was refined with version 2018/3 of **ShelXL**<sup>165</sup> using Least Squares minimisation.

**Crystal Data.** C<sub>19</sub>H<sub>17</sub>ClO<sub>3</sub>,  $M_r = 328.77$ , monoclinic,  $P2_1/c$  (No. 14),  $a = 11.6388(3)$  Å,  $b = 10.4822(2)$  Å,  $c = 13.0337(3)$  Å,  $\beta = 99.515(2)^\circ$ ,  $\alpha = \gamma = 90^\circ$ ,  $V = 1568.24(6)$  Å<sup>3</sup>,  $T = 123.00(10)$  K,  $Z = 4$ ,  $Z' = 1$ ,  $\mu(\text{CuK}\alpha) = 2.263$ , 17244 reflections measured, 3156 unique ( $R_{int} =$

Compound	166d		
0.0247)			
which	Formula	C <sub>19</sub> H <sub>17</sub> ClO <sub>3</sub>	
were	$D_{calc.}/\text{g cm}^{-3}$	1.393	
used in	$\mu/\text{mm}^{-1}$	2.263	
all	Formula Weight	328.77	
calculati	Colour	clear colourless	
ons. The	Shape	prism	
final	Size/mm <sup>3</sup>	0.21×0.18×0.07	
was	$T/\text{K}$	123.00(10)	
0.0814	$wR_2$	Crystal System	monoclinic
(all data)	Space Group	$P2_1/c$	
and $R_1$	$a/\text{Å}$	11.6388(3)	
was	$b/\text{Å}$	10.4822(2)	
0.0302 (I	$c/\text{Å}$	13.0337(3)	
> 2(I)).	$\alpha/^\circ$	90	
	$\beta/^\circ$	99.515(2)	
	$\gamma/^\circ$	90	
	$V/\text{Å}^3$	1568.24(6)	
	$Z$	4	
	$Z'$	1	
	Wavelength/Å	1.54184	
	Radiation type	CuK $\alpha$	
	$\Theta_{min}/^\circ$	3.851	
	$\Theta_{max}/^\circ$	74.159	
	Measured Refl.	17244	
	Independent Refl.	3156	
	Reflections with $I > 2(I)$	3000	
	$R_{int}$	0.0247	
	Parameters	209	
	Restraints	0	
	Largest Peak	0.298	
	Deepest Hole	-0.255	
	GooF	1.032	
	$wR_2$ (all data)	0.0814	
	$wR_2$	0.0800	
	$R_1$ (all data)	0.0317	
	$R_1$	0.0302	
	Creation Method		
	Solution	Olex2 1.2-alpha	
	Refinement	(compiled	
		2018.07.26	
		svn.r3523 for	
		OlexSys, GUI	
		svn.r5532)	

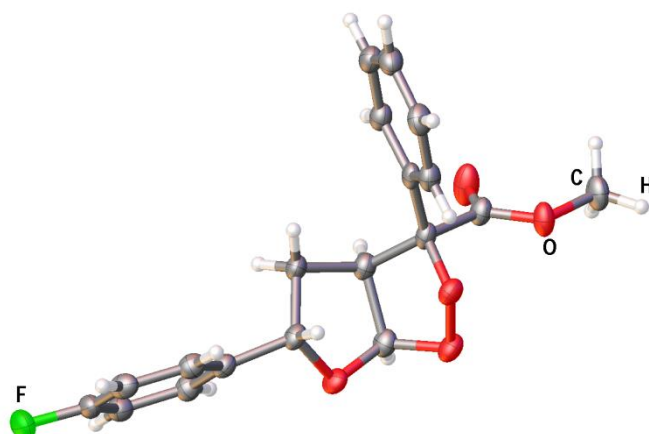




**Experimental:** Single clear colourless prism-shaped crystals of **166e** were obtained by recrystallisation from DCM/Et<sub>2</sub>O/pentane. A suitable crystal 0.27×0.15×0.09 mm<sup>3</sup> was selected and mounted on a MITIGEN holder with inert oil on an SuperNova, Single source at offset/far, Atlas diffractometer. The crystal was kept at a steady  $T = 123.01(10)$  K during data collection. The structure was solved with the **ShelXT**<sup>165</sup> structure solution program using the Intrinsic Phasing solution method and by using **Olex2**<sup>166</sup> as the graphical interface. The model was refined with version 2018/3 of **ShelXL**<sup>165</sup> using Least Squares minimisation.

**Crystal Data.** C<sub>19</sub>H<sub>17</sub>FO<sub>3</sub>,  $M_r = 312.32$ , monoclinic,  $P2_1/c$  (No. 14),  $a = 11.6831(2)$  Å,  $b = 10.0186(2)$  Å,  $c = 13.0076(2)$  Å,  $\beta = 100.573(2)^\circ$ ,  $\alpha = \gamma = 90^\circ$ ,  $V = 1496.67(5)$  Å<sup>3</sup>,  $T = 123.01(10)$  K,  $Z = 4$ ,  $Z' = 1$ ,  $\mu(\text{Cu } K\alpha) = 0.836$ , 16695 reflections measured, 3096 unique ( $R_{int} = 0.0206$ ) which were used in all calculations. The final  $wR_2$  was 0.0868 (all data) and  $R_1$  was 0.0321 ( $I > 2(I)$ ).

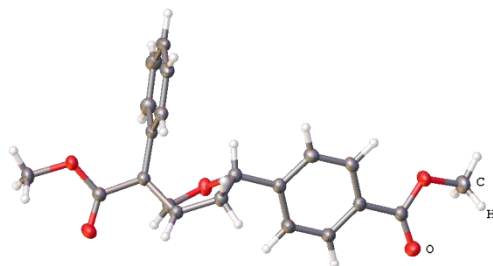
Compound	166e
Formula	C <sub>19</sub> H <sub>17</sub> FO <sub>3</sub>
$D_{calc.}/\text{g cm}^{-3}$	1.386
$\mu/\text{mm}^{-1}$	0.836
Formula Weight	312.32
Colour	clear colourless
Shape	prism
Size/mm <sup>3</sup>	0.27×0.15×0.09
$T/\text{K}$	123.01(10)
Crystal System	monoclinic
Space Group	$P2_1/c$
$a/\text{Å}$	11.6831(2)
$b/\text{Å}$	10.0186(2)
$c/\text{Å}$	13.0076(2)
$\alpha/^\circ$	90
$\beta/^\circ$	100.573(2)
$\gamma/^\circ$	90
$V/\text{Å}^3$	1496.67(5)
$Z$	4
$Z'$	1
Wavelength/Å	1.54184
Radiation type	Cu $K\alpha$
$\theta_{min}/^\circ$	3.849
$\theta_{max}/^\circ$	76.251
Measured Refl.	16695
Independent Refl.	3096
Reflections with $I > 2(I)$	2872
$R_{int}$	0.0206
Parameters	276
Restraints	0
Largest Peak	0.298
Deepest Hole	-0.185
Goof	1.060
$wR_2$ (all data)	0.0868
$wR_2$	0.0845
$R_1$ (all data)	0.0344
$R_1$	0.0321



**Experimental:** Single clear colourless prism-shaped crystals of **167e** were obtained by recrystallisation from DCM/Et<sub>2</sub>O/Pentane. A suitable crystal 0.12×0.08×0.08 mm<sup>3</sup> was selected and mounted on a MITIGEN holder oil on an GV1000, TitanS2 diffractometer. The crystal was kept at a steady  $T = 122.96(15)$  K during data collection. The structure was solved with the **ShelXT**<sup>165</sup> structure solution program using the Intrinsic Phasing solution method and by using **Olex2**<sup>166</sup> as the graphical interface. The model was refined with version 2018/3 of **ShelXL**<sup>165</sup> using Least Squares minimisation.

**Crystal Data.** C<sub>19</sub>H<sub>17</sub>FO<sub>5</sub>,  $M_r = 344.32$ , monoclinic,  $P2_1/c$  (No. 14),  $a = 12.8902(4)$  Å,  $b = 10.7066(3)$  Å,  $c = 11.7428(3)$  Å,  $\beta = 101.317(3)^\circ$ ,  $\alpha = \gamma = 90^\circ$ ,  $V = 1589.12(8)$  Å<sup>3</sup>,  $T = 122.96(15)$  K,  $Z = 4$ ,  $Z' = 1$ ,  $\mu(\text{CuK}\alpha) = 0.941$ , 19261 reflections measured, 3217 unique ( $R_{int} = 0.0358$ ) which were used in all calculations. The final  $wR_2$  was 0.1125 (all data) and  $R_1$  was 0.0414 ( $I > 2(I)$ )

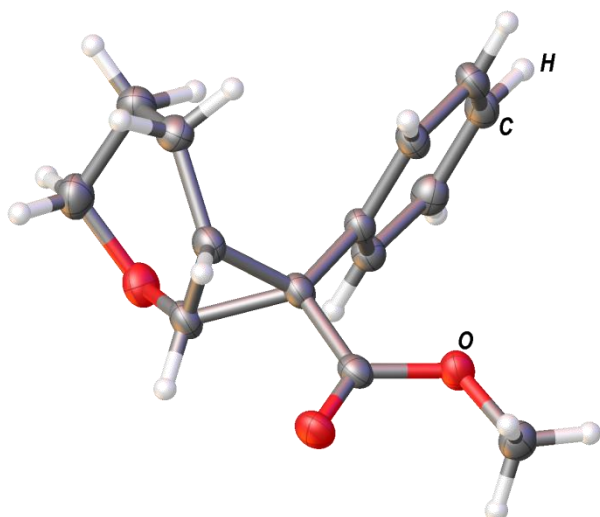
Compound	167e
Formula	C <sub>19</sub> H <sub>17</sub> FO <sub>5</sub>
$D_{calc.}/\text{g cm}^{-3}$	1.439
$\mu/\text{mm}^{-1}$	0.941
Formula Weight	344.32
Colour	clear colourless
Shape	prism
Size/mm <sup>3</sup>	0.12×0.08×0.08
$T/\text{K}$	122.96(15)
Crystal System	monoclinic
Space Group	$P2_1/c$
$a/\text{Å}$	12.8902(4)
$b/\text{Å}$	10.7066(3)
$c/\text{Å}$	11.7428(3)
$\alpha/^\circ$	90
$\beta/^\circ$	101.317(3)
$\gamma/^\circ$	90
$V/\text{Å}^3$	1589.12(8)
$Z$	4
$Z'$	1
Wavelength/Å	1.54184
Radiation type	CuK $\alpha$
$\theta_{min}/^\circ$	3.497
$\theta_{max}/^\circ$	73.919
Measured Refl.	19261
Independent Refl.	3217
Reflections with $I > 2(I)$	2934
$R_{int}$	0.0358
Parameters	227
Restraints	0
Largest Peak	0.201
Deepest Hole	-0.285
GooF	1.037
$wR_2$ (all data)	0.1125
$wR_2$	0.1092
$R_1$ (all data)	0.0445
$R_1$	0.0414
Creation Method	
Solution	Olex2 1.3-dev
Refinement	(compiled 2019.03.18 svn.r3573 for OlexSys, GUI svn.r5689) #



**Experimental:** Single clear colourless prism-shaped crystals of **167f** were obtained by recrystallisation from DCM/Et<sub>2</sub>O/pentane. A suitable crystal 0.16×0.13×0.08 mm<sup>3</sup> was selected and mounted on a suitable support on an SuperNova, Single source at offset/far, Atlas diffractometer. The crystal was kept at a steady  $T = 123.00(10)$  K during data collection. The structure was solved with the **ShelXT**<sup>165</sup> structure solution program using the Intrinsic Phasing solution method and by using **Olex2**<sup>166</sup> as the graphical interface. The model was refined with version 2018/3 of **ShelXL**<sup>165</sup> using Least Squares minimisation.

**Crystal Data.** C<sub>21</sub>H<sub>20</sub>O<sub>5</sub>,  $M_r = 352.37$ , triclinic,  $P-1$  (No. 2),  $a = 5.9347(2)$  Å,  $b = 12.1303(3)$  Å,  $c = 12.1467(3)$  Å,  $\alpha = 89.852(2)^\circ$ ,  $\beta = 87.791(2)^\circ$ ,  $\gamma = 89.479(2)^\circ$ ,  $V = 873.75(4)$  Å<sup>3</sup>,  $T = 123.00(10)$  K,  $Z = 2$ ,  $Z' = 1$ ,  $\mu(\text{Cu } K\alpha) = 0.783$ , 19644 reflections measured, 3528 unique ( $R_{int} = 0.0281$ ) which were used in all calculations. The final  $wR_2$  was 0.0946 (all data) and  $R_1$  was 0.0356 ( $I > 2(I)$ ).

Compound	167f
Formula	C <sub>21</sub> H <sub>20</sub> O <sub>5</sub>
$D_{calc.}/\text{g cm}^{-3}$	1.339
$\mu/\text{mm}^{-1}$	0.783
Formula Weight	352.37
Colour	clear colourless
Shape	prism
Size/mm <sup>3</sup>	0.16×0.13×0.08
$T/\text{K}$	123.00(10)
Crystal System	triclinic
Space Group	$P-1$
$a/\text{Å}$	5.9347(2)
$b/\text{Å}$	12.1303(3)
$c/\text{Å}$	12.1467(3)
$\alpha/^\circ$	89.852(2)
$\beta/^\circ$	87.791(2)
$\gamma/^\circ$	89.479(2)
$V/\text{Å}^3$	873.75(4)
$Z$	2
$Z'$	1
Wavelength/Å	1.54184
Radiation type	Cu $K\alpha$
$\theta_{min}/^\circ$	3.642
$\theta_{max}/^\circ$	74.576
Measured Refl.	19644
Independent Refl.	3528
Reflections with $I > 2(I)$	3186
$R_{int}$	0.0281
Parameters	316
Restraints	0
Largest Peak	0.282
Deepest Hole	-0.217
Goof	1.032
$wR_2$ (all data)	0.0946
$wR_2$	0.0913
$R_1$ (all data)	0.0395
$R_1$	0.0356

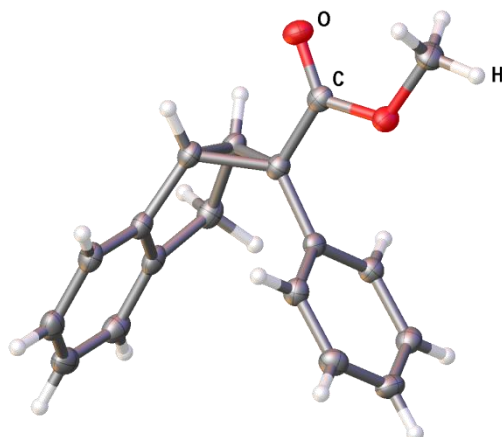


**Experimental:** Single clear colourless prism-shaped crystals of **181a** were obtained by recrystallisation from DCM/Et<sub>2</sub>O. A suitable crystal 0.26×0.14×0.12 mm<sup>3</sup> was selected and mounted on a MITIGEN holder oil on an SuperNova, Single source at offset/far, Atlas diffractometer. The crystal was kept at a steady  $T = 123.01(10)$  K during data collection. The structure was solved with the **ShelXT**<sup>165</sup> structure solution program using the Intrinsic Phasing solution method and by using **Olex2**<sup>166</sup> as the graphical interface. The model was refined with version 2016/6 of **ShelXL**<sup>165</sup> using Least Squares minimisation.

**Crystal Data.** C<sub>14</sub>H<sub>16</sub>O<sub>3</sub>,  $M_r = 232.27$ , orthorhombic, *Pbca* (No. 61),  $a = 8.00279(16)$  Å,  $b = 16.9635(4)$  Å,  $c = 17.0457(4)$  Å,  $\alpha = \beta = \gamma = 90^\circ$ ,  $V = 2314.04(9)$  Å<sup>3</sup>,  $T = 123.01(10)$  K,  $Z = 8$ ,  $Z' = 1$ ,  $\mu(\text{CuK}\alpha) = 0.754$ , 14494 reflections measured, 2395 unique ( $R_{int} = 0.0360$ ) which were used in all calculations. The final  $wR_2$  was 0.1107

(all data) and  $R_1$  was 0.0411 ( $I > 2(I)$ ).

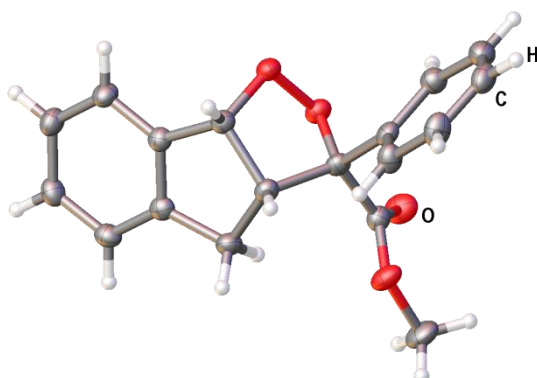
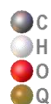
Compound	181a
Formula	C <sub>14</sub> H <sub>16</sub> O <sub>3</sub>
$D_{calc}/\text{g cm}^{-3}$	1.333
$\mu/\text{mm}^{-1}$	0.754
Formula Weight	232.27
Colour	clear colourless
Shape	prism
Size/mm <sup>3</sup>	0.26×0.14×0.12
$T/\text{K}$	123.01(10)
Crystal System	orthorhombic
Space Group	<i>Pbca</i>
$a/\text{Å}$	8.00279(16)
$b/\text{Å}$	16.9635(4)
$c/\text{Å}$	17.0457(4)
$\alpha/^\circ$	90
$\beta/^\circ$	90
$\gamma/^\circ$	90
$V/\text{Å}^3$	2314.04(9)
$Z$	8
$Z'$	1
Wavelength/Å	1.54184
Radiation type	CuK $\alpha$
$\theta_{min}/^\circ$	5.190
$\theta_{max}/^\circ$	76.316
Measured Refl.	14494
Independent Refl.	2395
Reflections with $I > 2(I)$	2101
$R_{int}$	0.0360
Parameters	155
Restraints	0
Largest Peak	0.265
Deepest Hole	-0.195
GooF	1.034
$wR_2$ (all data)	0.1107
$wR_2$	0.1054
$R_1$ (all data)	0.0475
$R_1$	0.0411



**Experimental:** Single clear colourless prism-shaped crystals of **183c** were obtained by recrystallisation from DCM/Et<sub>2</sub>O/pentane. A suitable crystal 0.19×0.17×0.09 mm<sup>3</sup> was selected and mounted on a MITIGEN holder oil on an SuperNova, Single source at offset/far, Atlas diffractometer. The crystal was kept at a steady  $T = 123.01(10)$  K during data collection. The structure was solved with the ShelXT 2018/3<sup>165</sup> structure solution program using the Intrinsic Phasing solution method and by using **Olex2**<sup>166</sup> as the graphical interface. The model was refined with version 2018/3 of ShelXL 2018/3<sup>165</sup> using Least Squares minimisation.

**Crystal Data.** C<sub>18</sub>H<sub>16</sub>O<sub>2</sub>,  $M_r = 264.31$ , monoclinic,  $P2_1/c$  (No. 14),  $a = 11.7253(2)$  Å,  $b = 16.1027(3)$  Å,  $c = 7.43946(14)$  Å,  $\beta = 104.833(2)^\circ$ ,  $\alpha = \gamma = 90^\circ$ ,  $V = 1357.83(5)$  Å<sup>3</sup>,  $T = 123.01(10)$  K,  $Z = 4$ ,  $Z' = 1$ ,  $\mu(\text{Cu } K\alpha) = 0.659$ , 17407 reflections measured, 2716 unique ( $R_{int} = 0.0213$ ) which were used in all calculations. The final  $wR_2$  was 0.0888 (all data) and  $R_1$  was 0.0342 ( $I > 2(I)$ ).

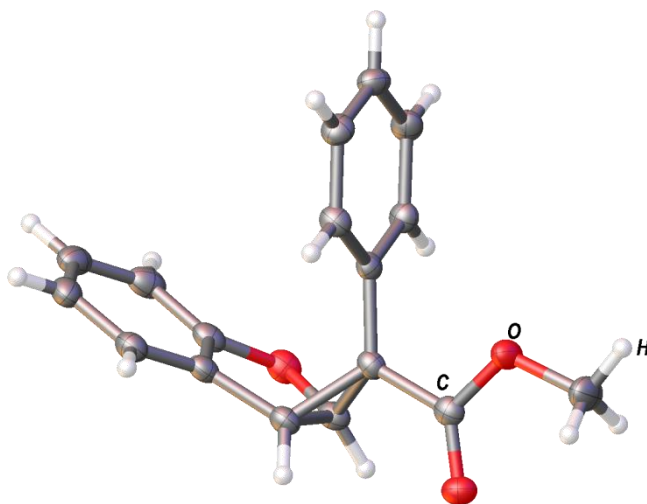
Compound	183c
Formula	C <sub>18</sub> H <sub>16</sub> O <sub>2</sub>
$D_{calc.}/\text{g cm}^{-3}$	1.293
$\mu/\text{mm}^{-1}$	0.659
Formula Weight	264.31
Colour	clear colourless
Shape	prism
Size/mm <sup>3</sup>	0.19×0.17×0.09
$T/\text{K}$	123.01(10)
Crystal System	monoclinic
Space Group	$P2_1/c$
$a/\text{Å}$	11.7253(2)
$b/\text{Å}$	16.1027(3)
$c/\text{Å}$	7.43946(14)
$\alpha/^\circ$	90
$\beta/^\circ$	104.833(2)
$\gamma/^\circ$	90
$V/\text{Å}^3$	1357.83(5)
$Z$	4
$Z'$	1
Wavelength/Å	1.54184
Radiation type	Cu $K\alpha$
$\theta_{min}/^\circ$	3.900
$\theta_{max}/^\circ$	73.929
Measured Refl.	17407
Independent Refl.	2716
Reflections with $I > 2(I)$	2547
$R_{int}$	0.0213
Parameters	190
Restraints	0
Largest Peak	0.236
Deepest Hole	-0.176
GooF	1.039
$wR_2$ (all data)	0.0888
$wR_2$	0.0872
$R_1$ (all data)	0.0360
$R_1$	0.0342



**Experimental:** Single clear dark colourless prism-shaped crystals of **184c** were obtained by recrystallisation from DCM/Et<sub>2</sub>O/pentane. A suitable crystal 0.26×0.15×0.13 mm<sup>3</sup> was selected and mounted on a MITIGEN holder oil on an GV1000, TitanS2 diffractometer. The crystal was kept at a steady  $T = 123.01(10)$  K during data collection. The structure was solved with the ShelXT 2018/3<sup>165</sup> structure solution program using the Intrinsic Phasing solution method and by using Olex2<sup>166</sup> as the graphical interface. The model was refined with version 2018/3 of ShelXL 2018/3<sup>165</sup> using Least Squares minimisation.

**Crystal Data.** C<sub>18</sub>H<sub>16</sub>O<sub>4</sub>,  $M_r = 296.31$ , monoclinic,  $P2_1/c$  (No. 14),  $a = 13.2541(3)$  Å,  $b = 6.14070(12)$  Å,  $c = 18.1087(4)$  Å,  $\beta = 104.293(2)^\circ$ ,  $\alpha = \gamma = 90^\circ$ ,  $V = 1428.23(5)$  Å<sup>3</sup>,  $T = 123.01(10)$  K,  $Z = 4$ ,  $Z' = 1$ ,  $\mu(\text{Cu K}) = 0.578$ , 14871 reflections measured, 2838 unique ( $R_{int} = 0.0282$ ) which were used in all calculations. The final  $wR_2$  was 0.0908 (all data) and  $R_1$  was 0.0353 ( $I > 2(I)$ ).

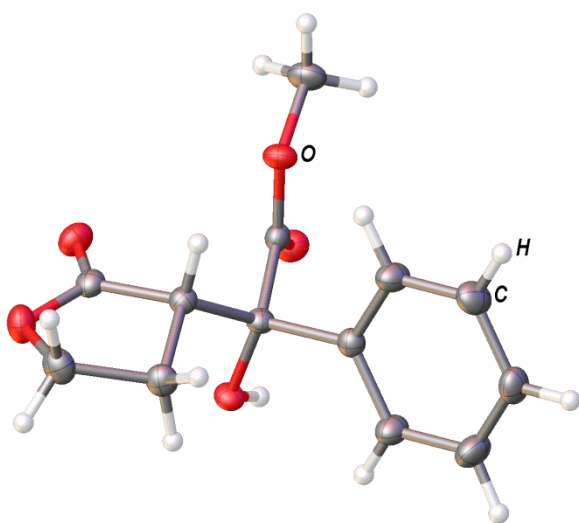
Compound	184c
Formula	C <sub>18</sub> H <sub>16</sub> O <sub>4</sub>
$D_{calc.}/\text{g cm}^{-3}$	1.378
$\mu/\text{mm}^{-1}$	0.578
Formula Weight	296.31
Colour	clear dark colourless
Shape	prism
Size/mm <sup>3</sup>	0.26×0.15×0.13
$T/\text{K}$	123.01(10)
Crystal System	monoclinic
Space Group	$P2_1/c$
$a/\text{Å}$	13.2541(3)
$b/\text{Å}$	6.14070(12)
$c/\text{Å}$	18.1087(4)
$\alpha/^\circ$	90
$\beta/^\circ$	104.293(2)
$\gamma/^\circ$	90
$V/\text{Å}^3$	1428.23(5)
$Z$	4
$Z'$	1
Wavelength/Å	1.39222
Radiation type	Cu K
$\theta_{min}/^\circ$	3.107
$\theta_{max}/^\circ$	59.969
Measured Refl.	14871
Independent Refl.	2838
Reflections with $I > 2(I)$	2467
$R_{int}$	0.0282
Parameters	208
Restraints	0
Largest Peak	0.294
Deepest Hole	-0.220
GooF	1.034
$wR_2$ (all data)	0.0908
$wR_2$	0.0860
$R_1$ (all data)	0.0415
$R_1$	0.0353



**Experimental:** Single clear colourless prism-shaped crystals of **190** were obtained by recrystallisation from DCM/Et<sub>2</sub>O/pentane. A suitable crystal 0.20×0.14×0.07 mm<sup>3</sup> was selected and mounted on a MITIGEN holder oil on an SuperNova, Single source at offset/far, Atlas diffractometer. The crystal was kept at a steady  $T = 123.00(10)$  K during data collection. The structure was solved with the **ShelXT**<sup>165</sup> structure solution program using the Intrinsic Phasing solution method and by using **Olex2**<sup>166</sup> as the graphical interface. The model was refined with version 2016/6 of **ShelXL**<sup>165</sup> using Least Squares minimisation.

**Crystal Data.** C<sub>17</sub>H<sub>14</sub>O<sub>3</sub>,  $M_r = 266.28$ , monoclinic,  $P2_1/c$  (No. 14),  $a = 11.5255(2)$  Å,  $b = 15.7925(2)$  Å,  $c = 7.67337(16)$  Å,  $\beta = 106.926(2)^\circ$ ,  $\alpha = \gamma = 90^\circ$ ,  $V = 1336.18(4)$  Å<sup>3</sup>,  $T = 123.00(10)$  K,  $Z = 4$ ,  $Z' = 1$ ,  $\mu(\text{CuK}\alpha) = 0.733$ , 27148 reflections measured, 2692 unique ( $R_{int} = 0.0361$ ) which were used in all calculations. The final  $wR_2$  was 0.0888 (all data) and  $R_1$  was 0.0336 ( $I > 2(I)$ ).

Compound	190
Formula	C <sub>17</sub> H <sub>14</sub> O <sub>3</sub>
$D_{calc.}/\text{g cm}^{-3}$	1.324
$\mu/\text{mm}^{-1}$	0.733
Formula Weight	266.28
Colour	clear colourless
Shape	prism
Size/mm <sup>3</sup>	0.20×0.14×0.07
$T/\text{K}$	123.00(10)
Crystal System	monoclinic
Space Group	$P2_1/c$
$a/\text{Å}$	11.5255(2)
$b/\text{Å}$	15.7925(2)
$c/\text{Å}$	7.67337(16)
$\alpha/^\circ$	90
$\beta/^\circ$	106.926(2)
$\gamma/^\circ$	90
$V/\text{Å}^3$	1336.18(4)
$Z$	4
$Z'$	1
Wavelength/Å	1.54184
Radiation type	CuK $\alpha$
$\theta_{min}/^\circ$	4.009
$\theta_{max}/^\circ$	73.791
Measured Refl.	27148
Independent Refl.	2692
Reflections with $I > 2(I)$	2389
$R_{int}$	0.0361
Parameters	182
Restraints	0
Largest Peak	0.192
Deepest Hole	-0.238
GooF	1.042
$wR_2$ (all data)	0.0888
$wR_2$	0.0852
$R_1$ (all data)	0.0384
$R_1$	0.0336



**Experimental:** Single clear colourless prism crystals of **199a** were used as supplied. A suitable crystal with dimensions  $0.16 \times 0.10 \times 0.06 \text{ mm}^3$  was selected and mounted on a Lindemann tube oil on a SuperNova, Single source at offset/far, Atlas diffractometer. The crystal was kept at a steady  $T = 123.01(10) \text{ K}$  during data collection. The structure was solved with the **ShelXT** 2018/3<sup>165</sup> solution program using dual methods methods and by using **Olex**<sup>166</sup> as the graphical interface. The model was refined with **ShelXL** 2018/3<sup>165</sup> using full matrix least squares minimisation on  $F^2$ .

**Crystal Data.**  $\text{C}_{13}\text{H}_{14}\text{O}_5$ ,  $M_r = 250.24$ , monoclinic,  $P2_1/c$  (No. 14),  $a = 9.4933(2) \text{ \AA}$ ,  $b = 8.4381(2) \text{ \AA}$ ,  $c = 15.4728(3) \text{ \AA}$ ,  $\beta = 97.573(2)^\circ$ ,  $\alpha = \gamma = 90^\circ$ ,  $V = 1228.64(5) \text{ \AA}^3$ ,  $T = 123.01(10) \text{ K}$ ,  $Z = 4$ ,  $Z' = 1$ ,  $\mu(\text{Cu } K\alpha) = 0.878$ , 13027 reflections measured, 2463 unique ( $R_{int} = 0.0187$ ) which were used in all calculations. The final  $wR_2$  was 0.0802 (all data) and  $R_1$  was 0.0302 ( $I > 2(I)$ ).

Compound	199a
Formula	$\text{C}_{13}\text{H}_{14}\text{O}_5$
$D_{calc.} / \text{g cm}^{-3}$	1.353
$\mu / \text{mm}^{-1}$	0.878
Formula Weight	250.24
Colour	clear colourless
Shape	prism
Size/ $\text{mm}^3$	$0.16 \times 0.10 \times 0.06$
$T / \text{K}$	123.01(10)
Crystal System	monoclinic
Space Group	$P2_1/c$
$a / \text{Å}$	9.4933(2)
$b / \text{Å}$	8.4381(2)
$c / \text{Å}$	15.4728(3)
$\alpha / ^\circ$	90
$\beta / ^\circ$	97.573(2)
$\gamma / ^\circ$	90
$V / \text{Å}^3$	1228.64(5)
$Z$	4
$Z'$	1
Wavelength/ $\text{Å}$	1.54184
Radiation type	Cu $K\alpha$
$\theta_{min} / ^\circ$	4.699
$\theta_{max} / ^\circ$	73.835
Measured Refl's.	13027
Ind't Refl's	2463
Refl's with $I > 2(I)$	2283
$R_{int}$	0.0187
Parameters	219
Restraints	0
Largest Peak	0.313
Deepest Hole	-0.207
GooF	1.057
$wR_2$ (all data)	0.0802
$wR_2$	0.0783
$R_1$ (all data)	0.0324
$R_1$	0.0302

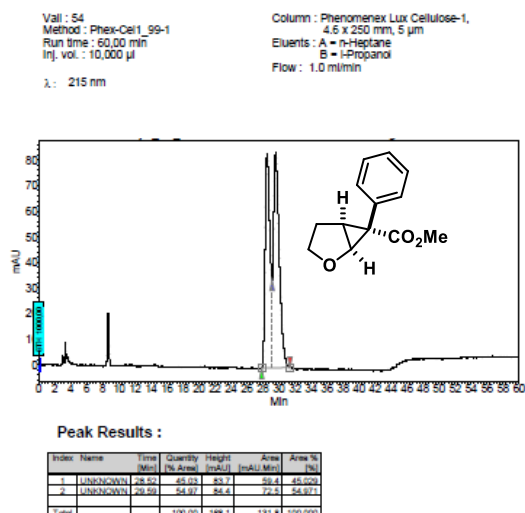


#### 4.10.12. Chiral HPLC

HPLC chromatograms are shown below.

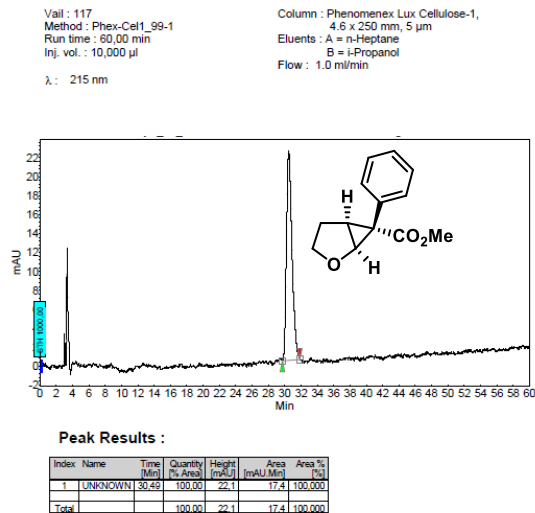
(±)-157a

(±)-methyl 6-phenyl-2-oxabicyclo[3.1.0]hexane-6-carboxylate



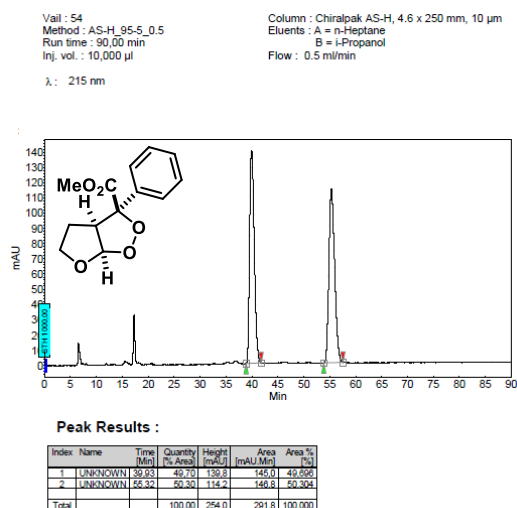
(-)-157

(-)-methyl (1*S*,5*S*,6*R*)-6-phenyl-2-oxabicyclo[3.1.0]hexane-6-carboxylate



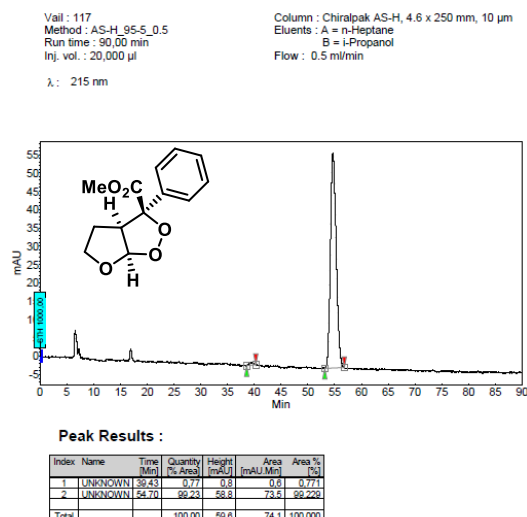
(±)-158a-major

(±)-methyl 3-phenyltetrahydro-3*H*-furo[2,3-*c*][1,2]dioxole-3-carboxylate



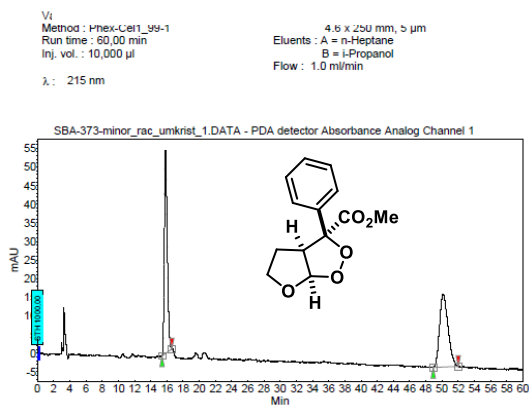
(-)-158a-major

(-)-methyl (3*R*,3*aS*,6*aR*)-3-phenyltetrahydro-3*H*-furo[2,3-*c*][1,2]dioxole-3-carboxylate



### (±)-158a-minor

### (±)-Methyl 3-phenyltetrahydro-3H-furo[2,3-c][1,2]dioxole-3-carboxylate

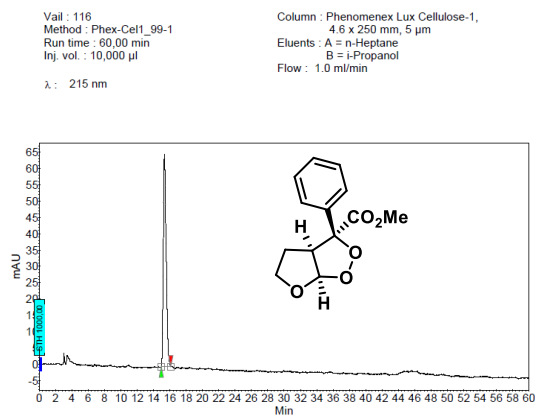


#### Peak Results :

Index	Name	Time (Min)	Quantity (% Area)	Height (mAU)	Area (mAU Min)	Area % (%)
1	UNKNOWN	15.32	49.14	55.8	23.1	49.132
2	UNKNOWN	50.15	50.88	19.8	24.9	50.865
Total			100.00	74.2	47.1	100.000

### (-)-158a-minor

### Methyl (3S,3aS,6aR)-3-phenyltetrahydro-3H-furo[2,3-c][1,2]dioxole-3-carboxylate

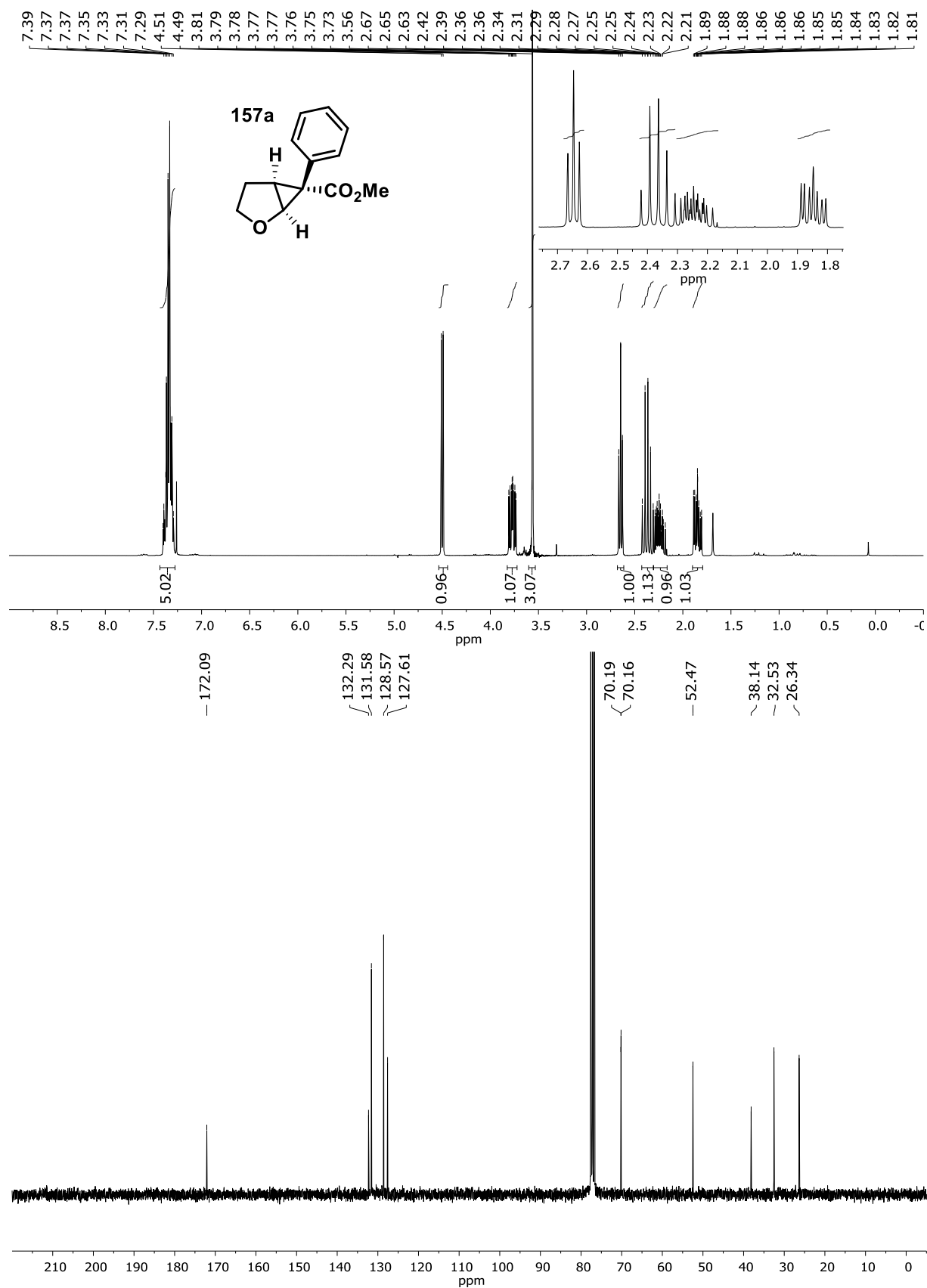


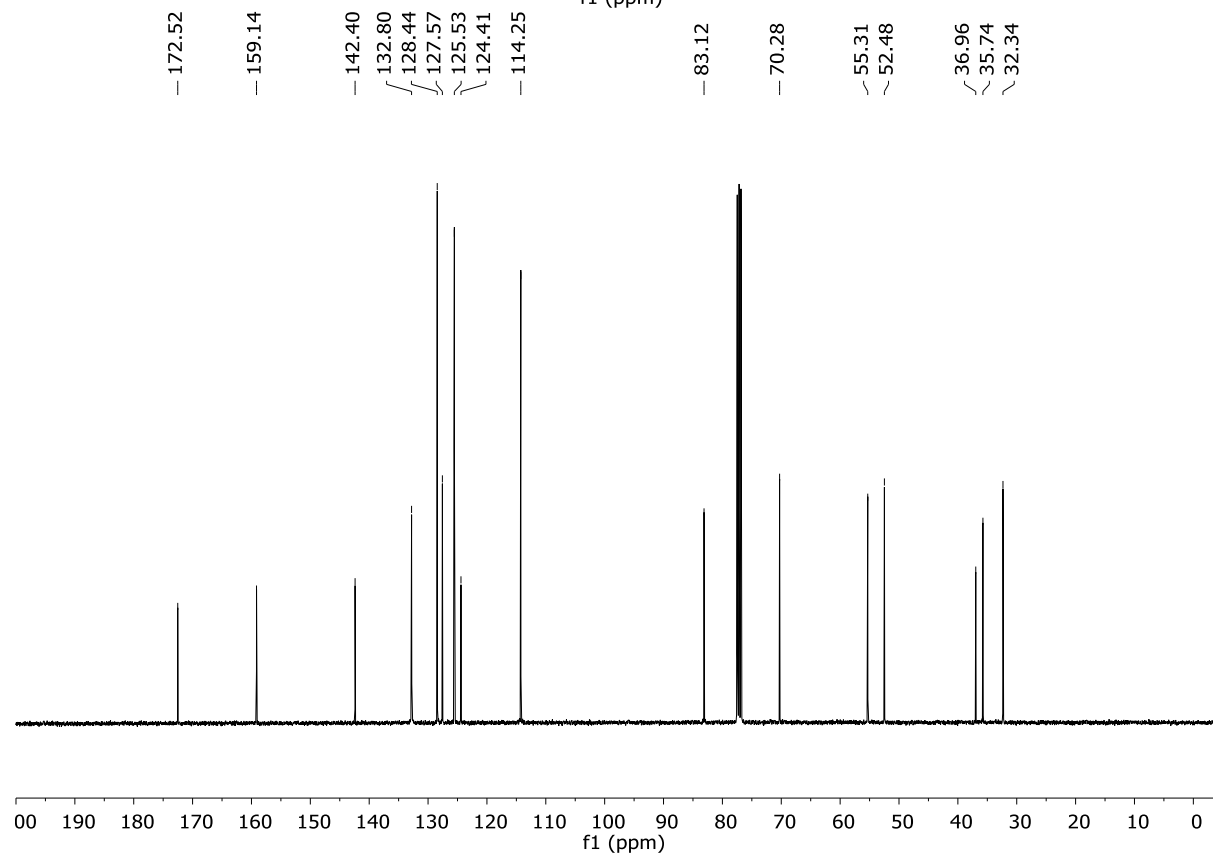
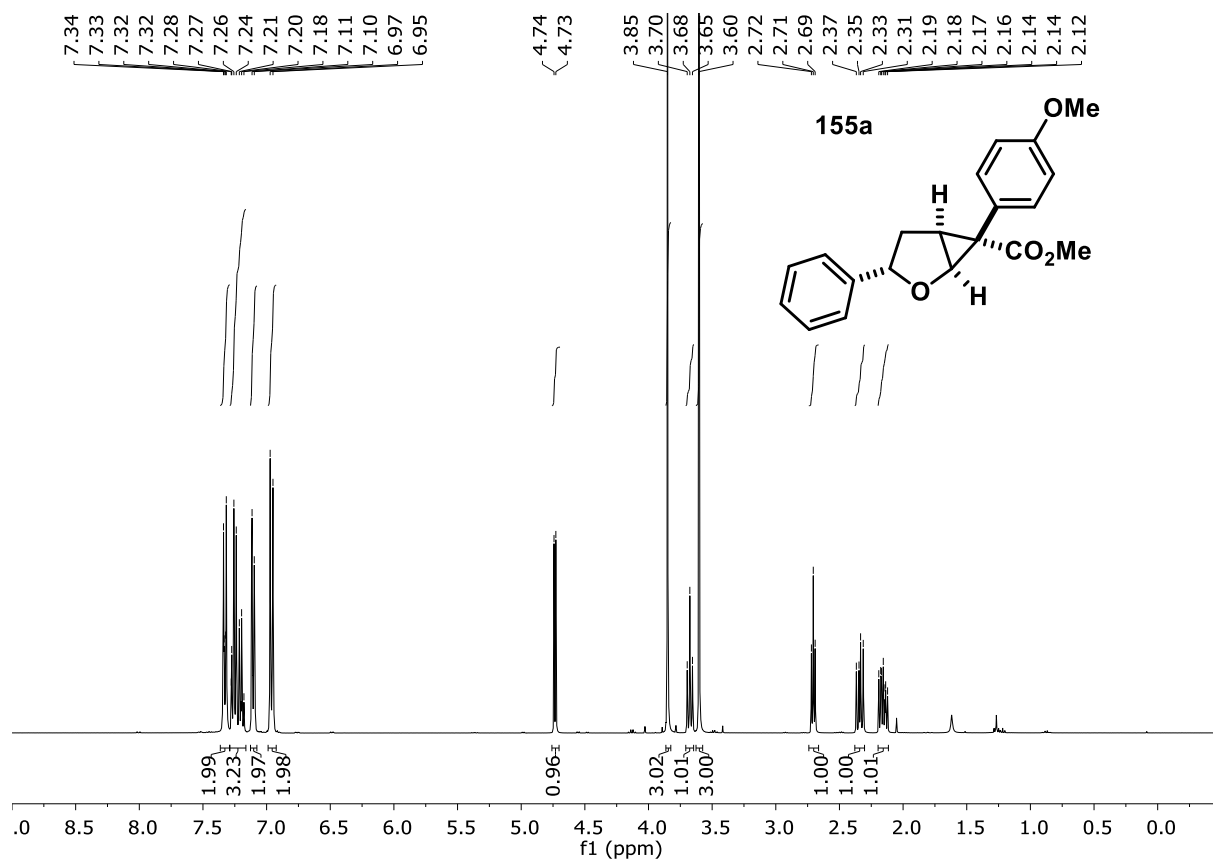
#### Peak Results :

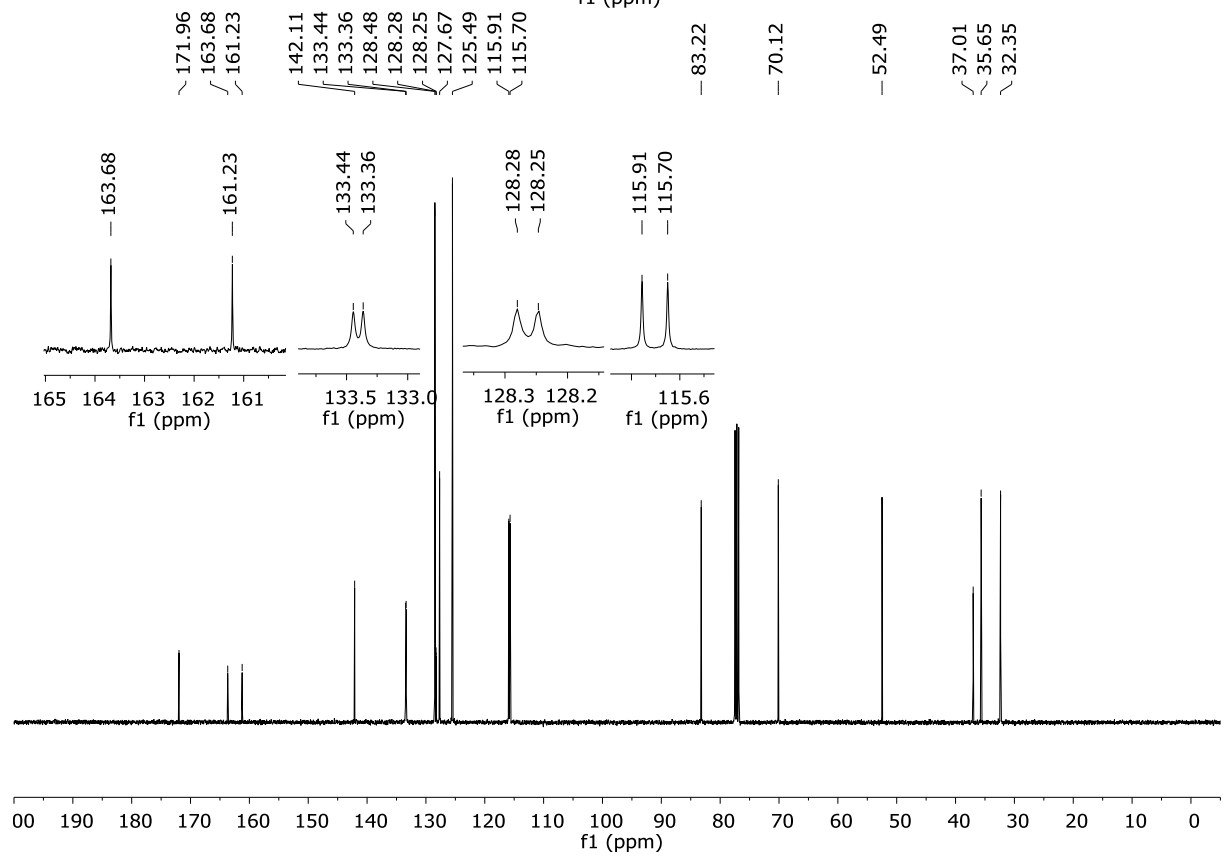
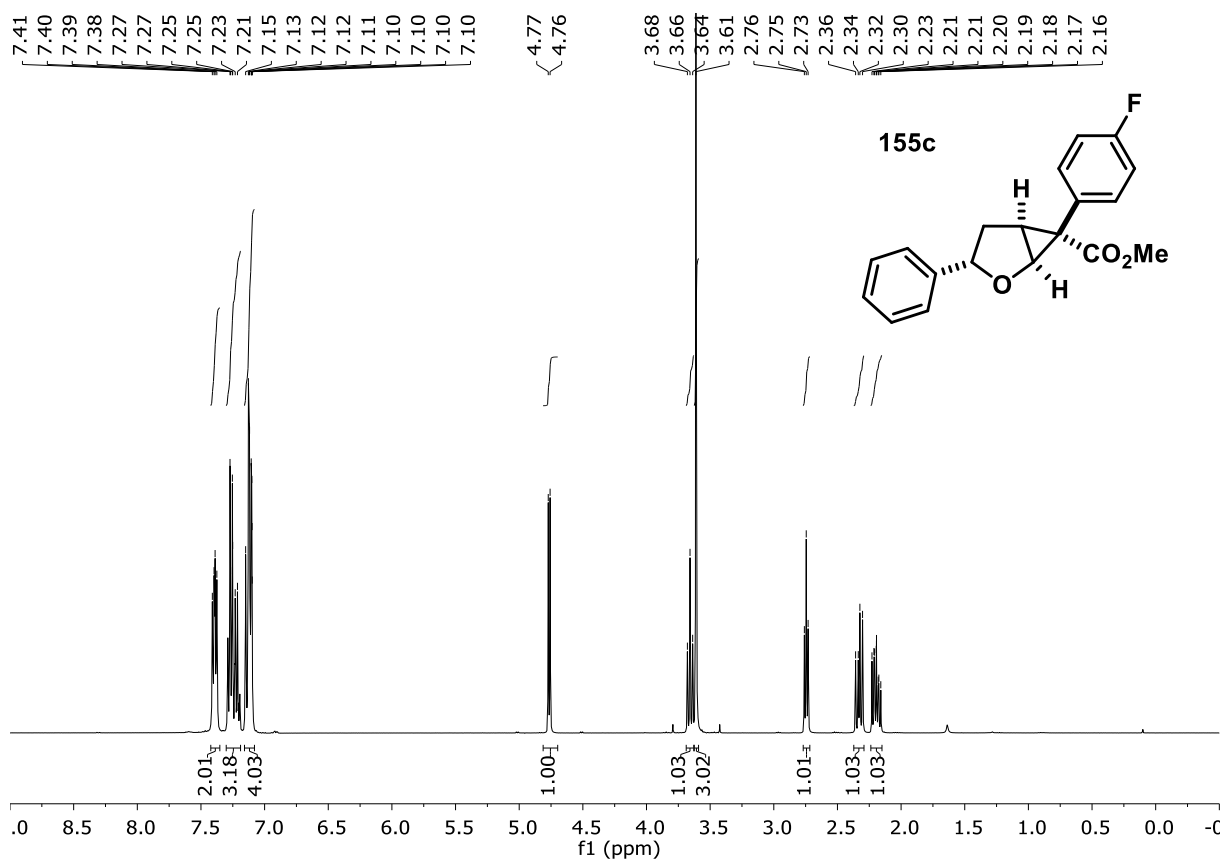
Index	Name	Time (Min)	Quantity (% Area)	Height (mAU)	Area (mAU Min)	Area % (%)
1	UNKNOWN	15.32	100.00	65.1	26.9	100.000
Total			100.00	65.1	26.9	100.000

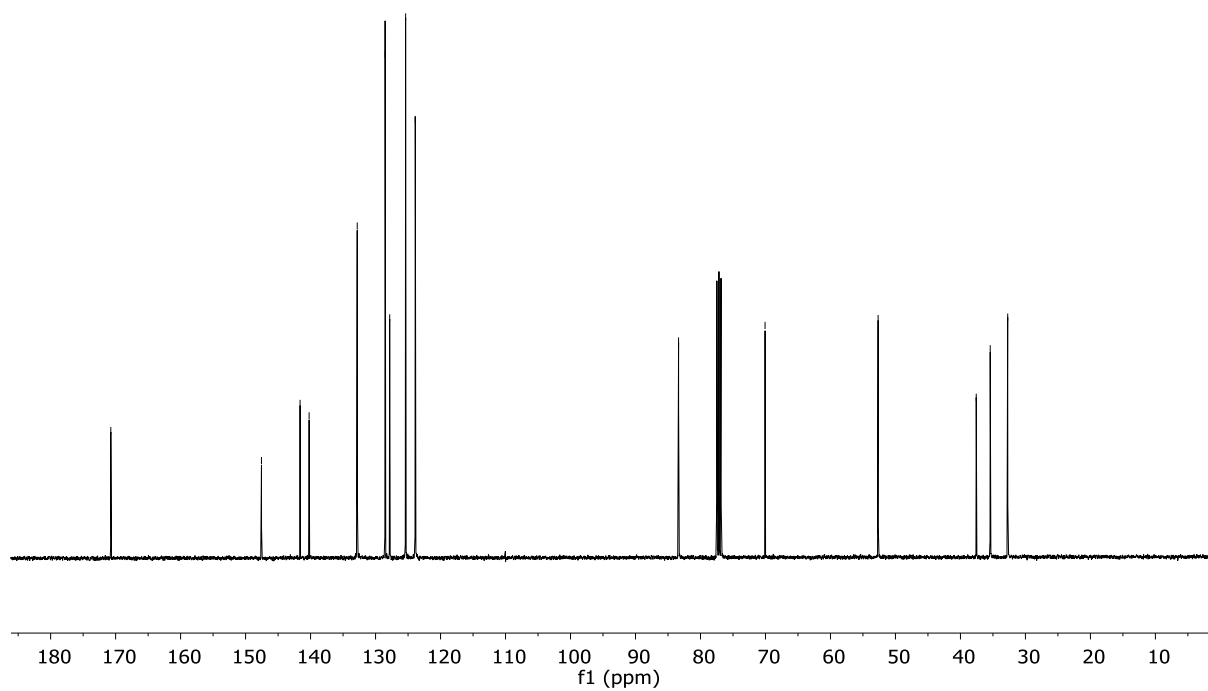
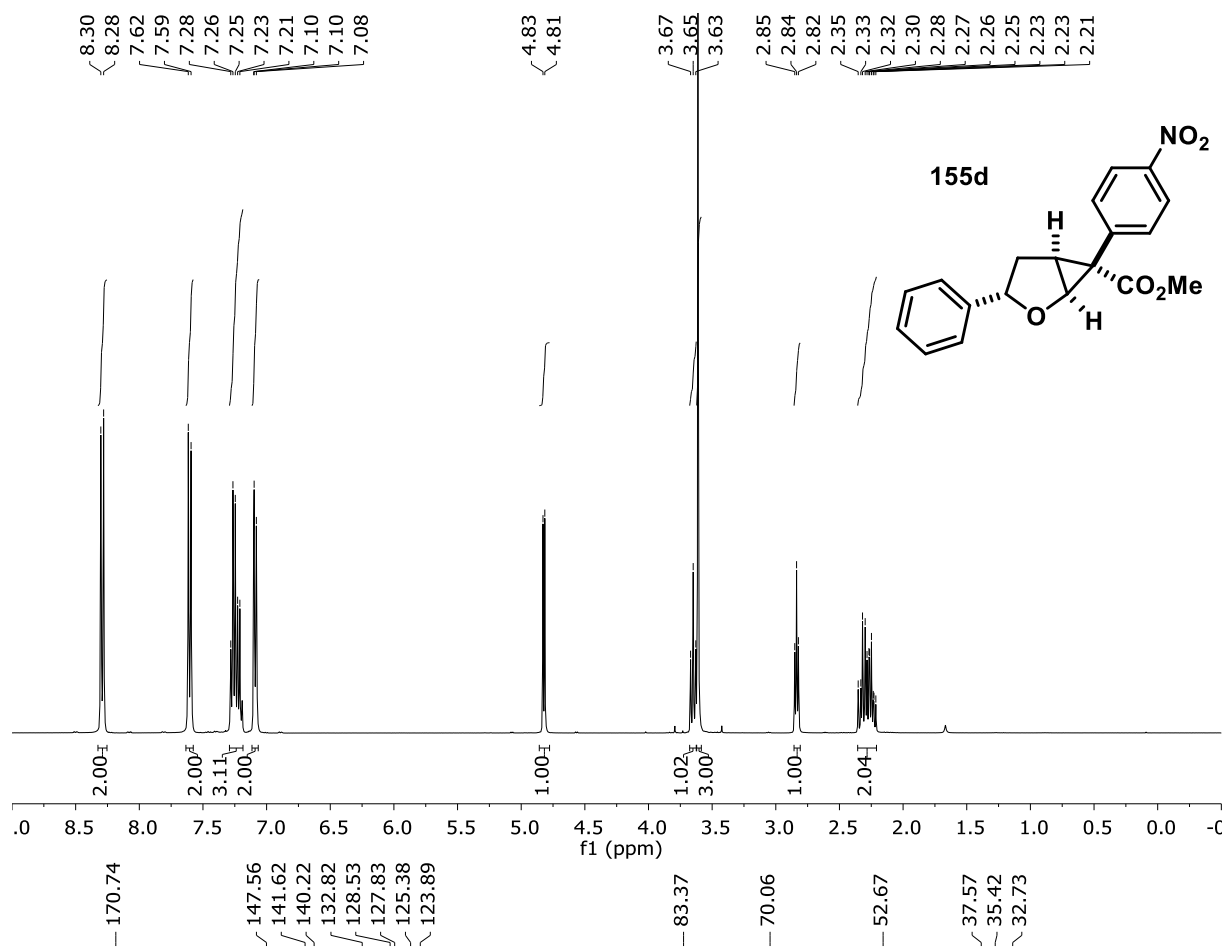
### 4.10.13. NMR Spectra

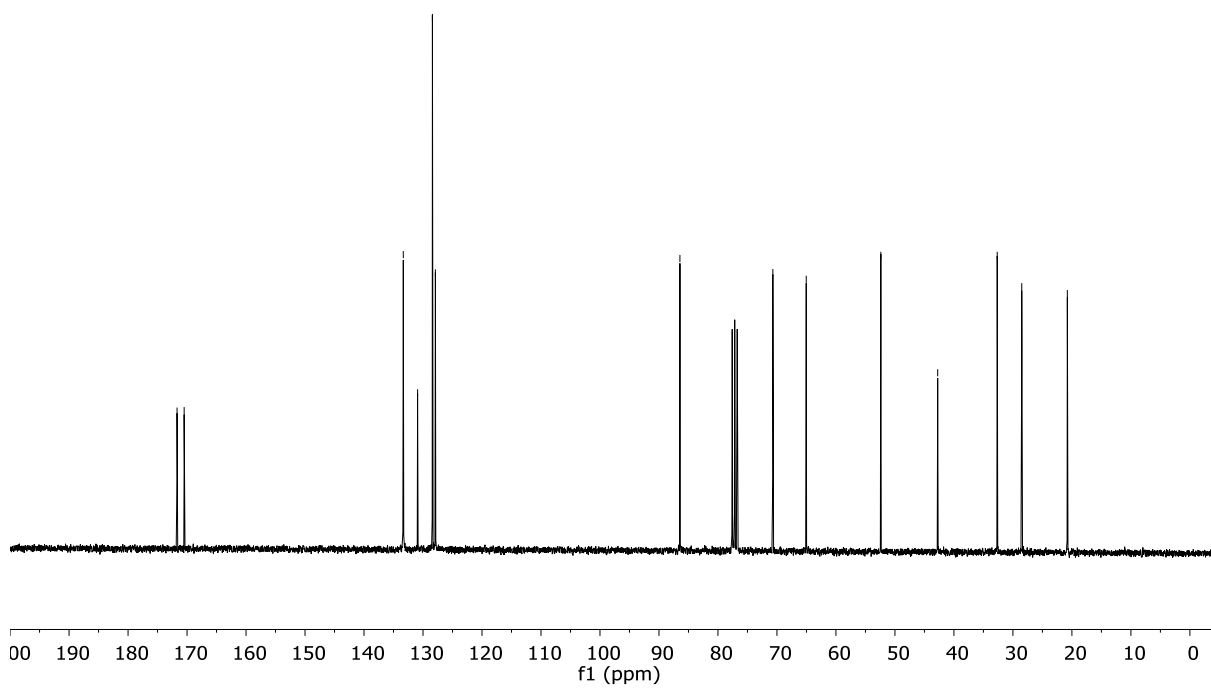
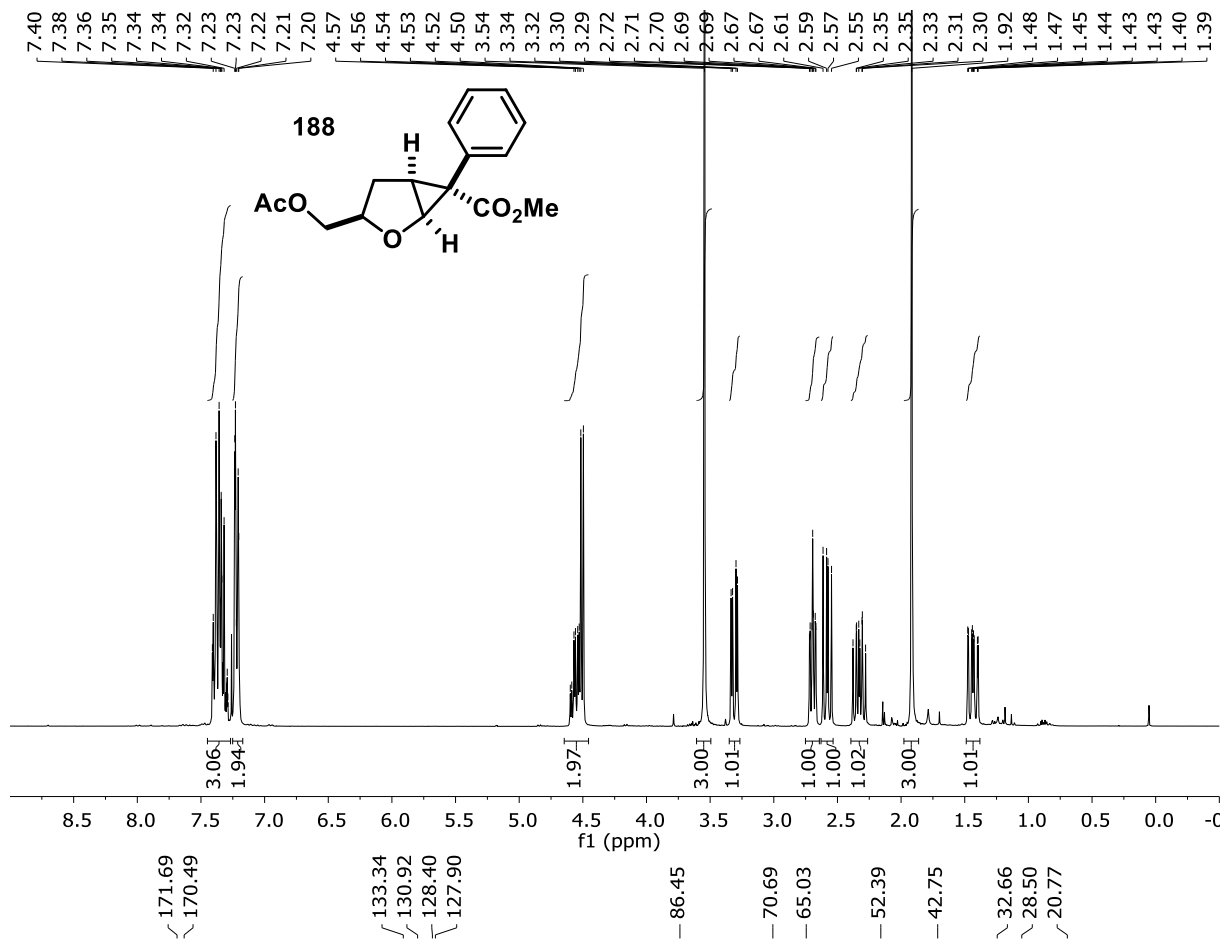
#### Starting Materials 1

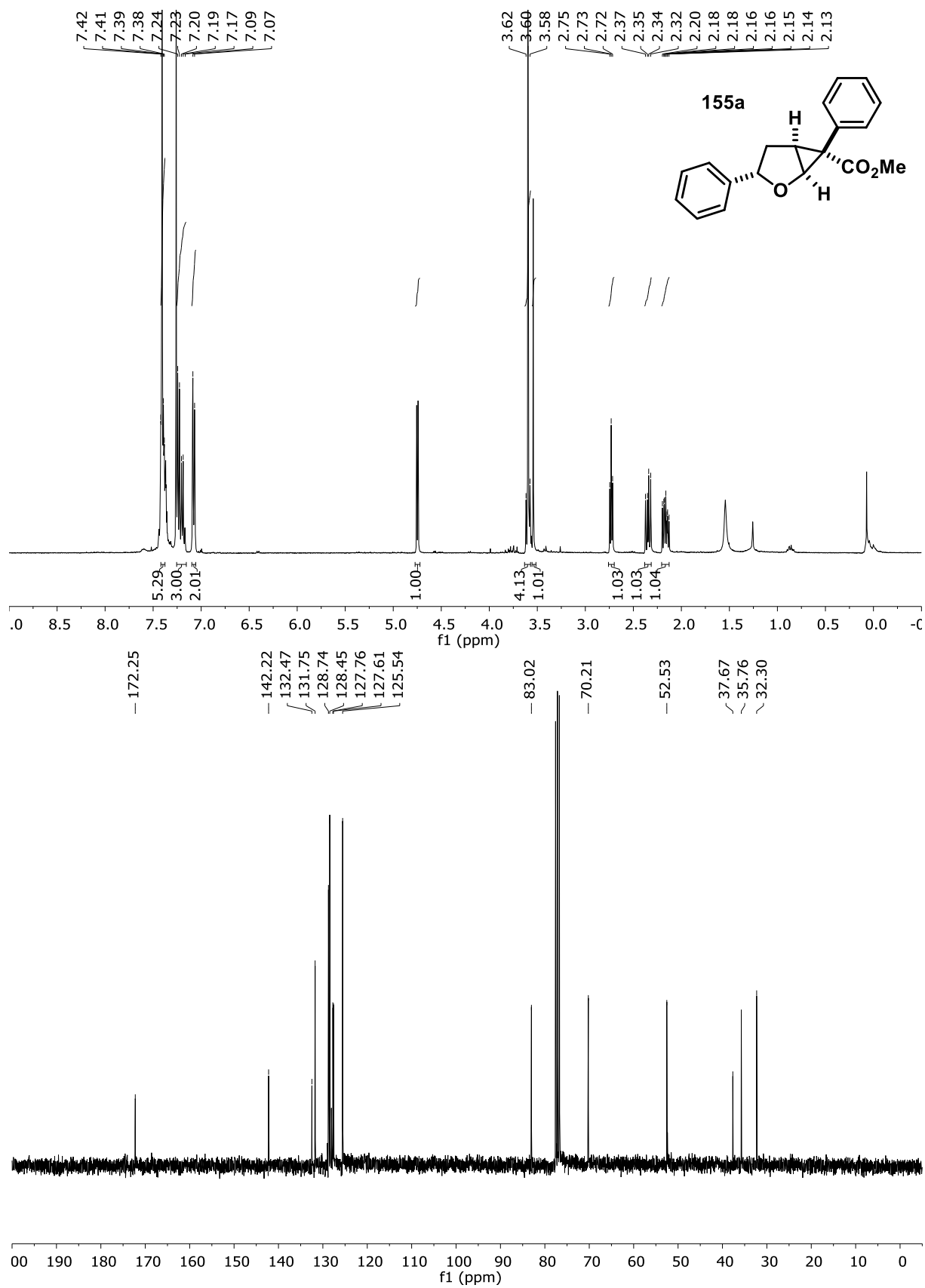




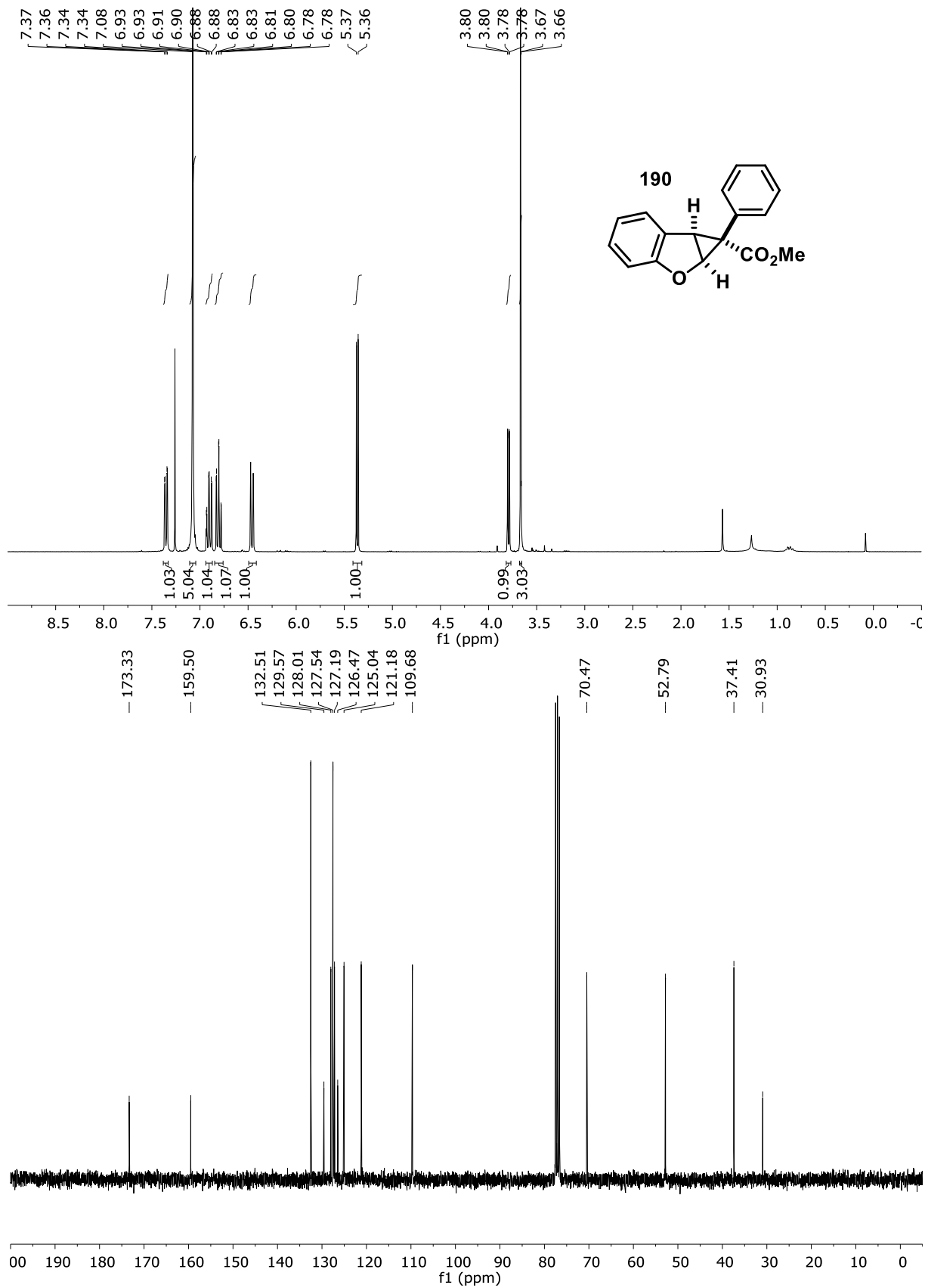


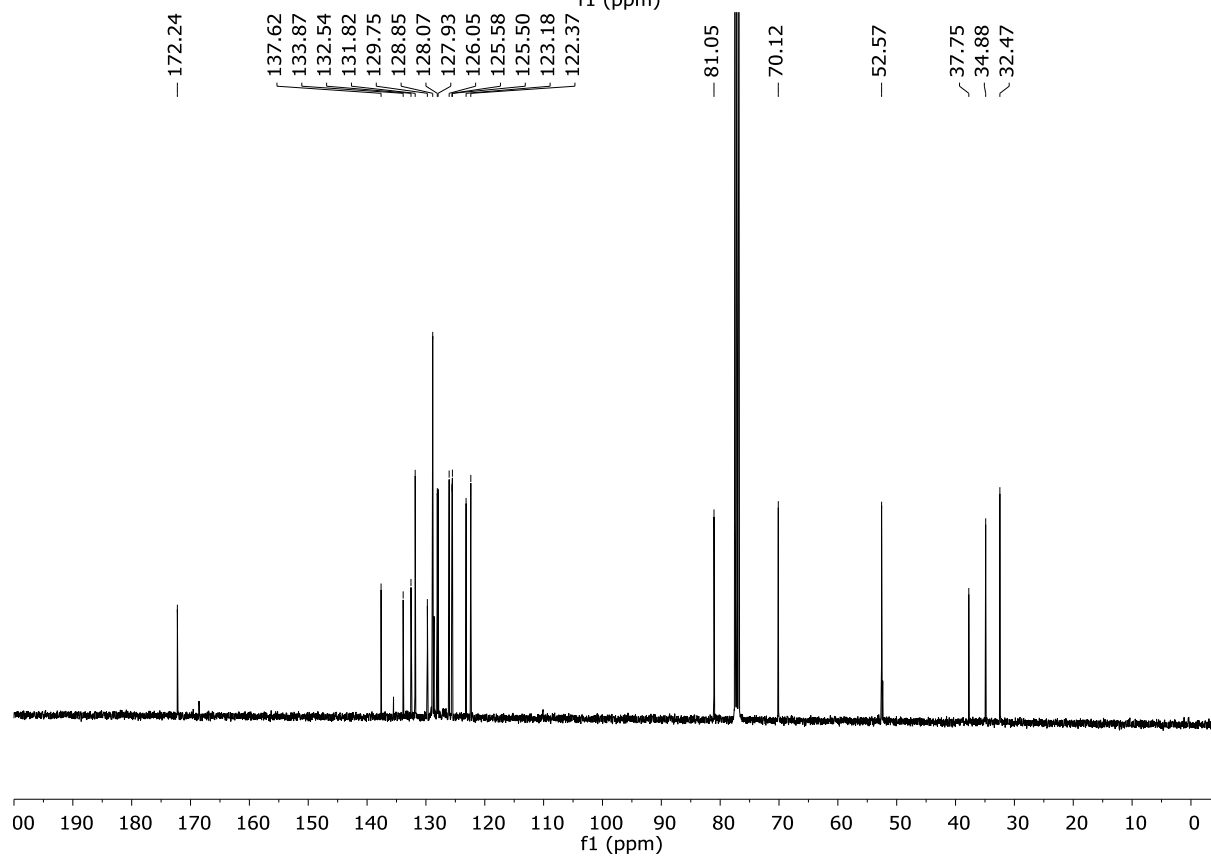
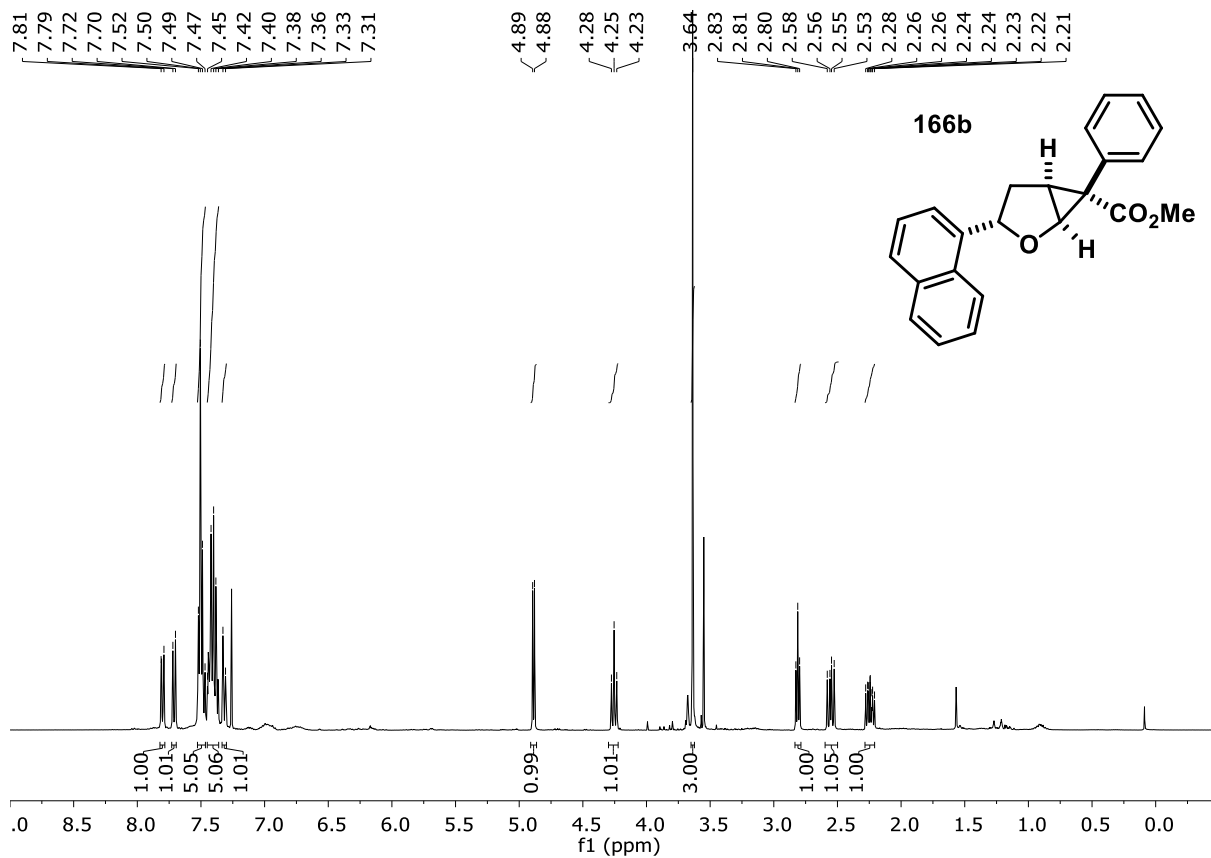


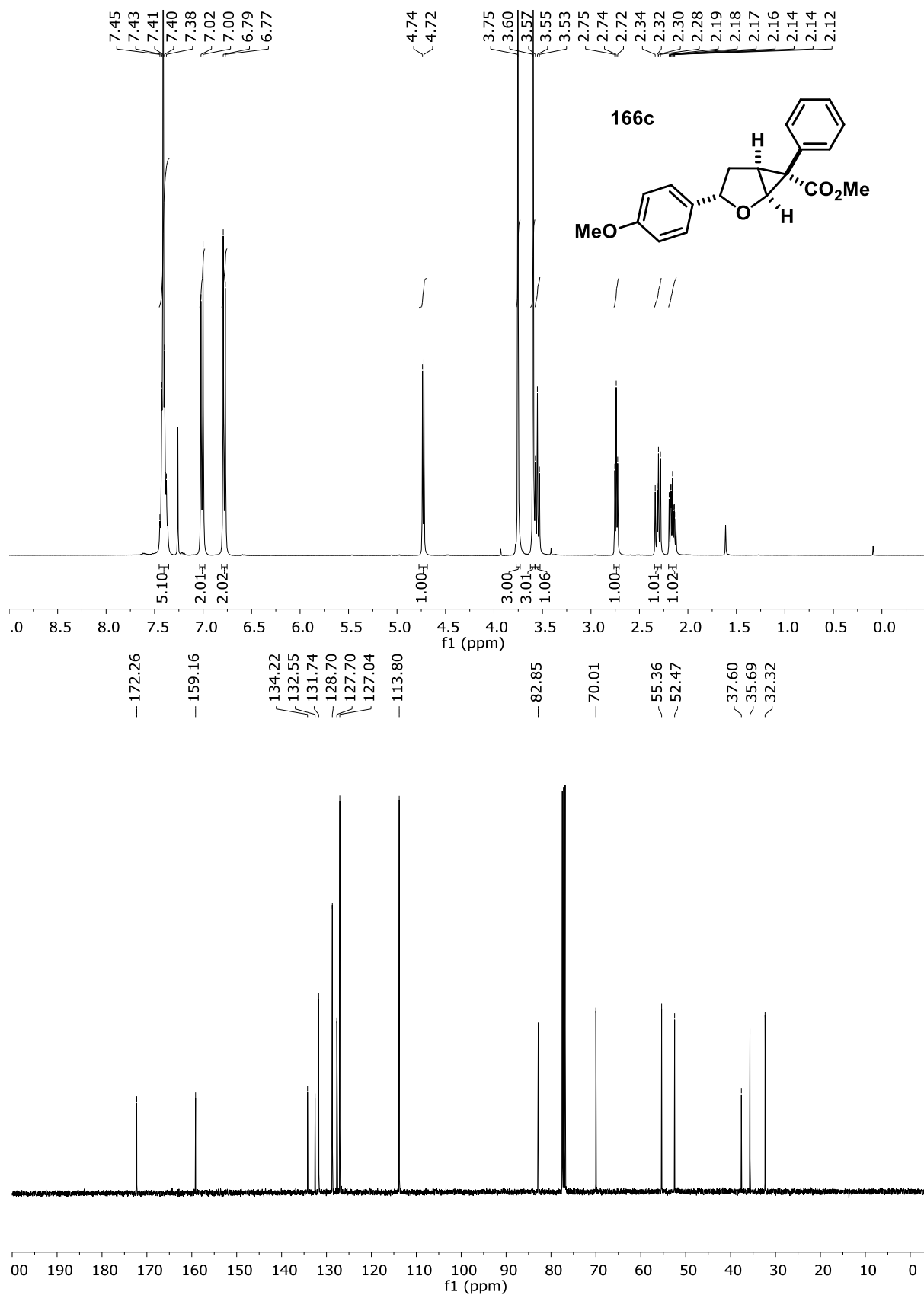


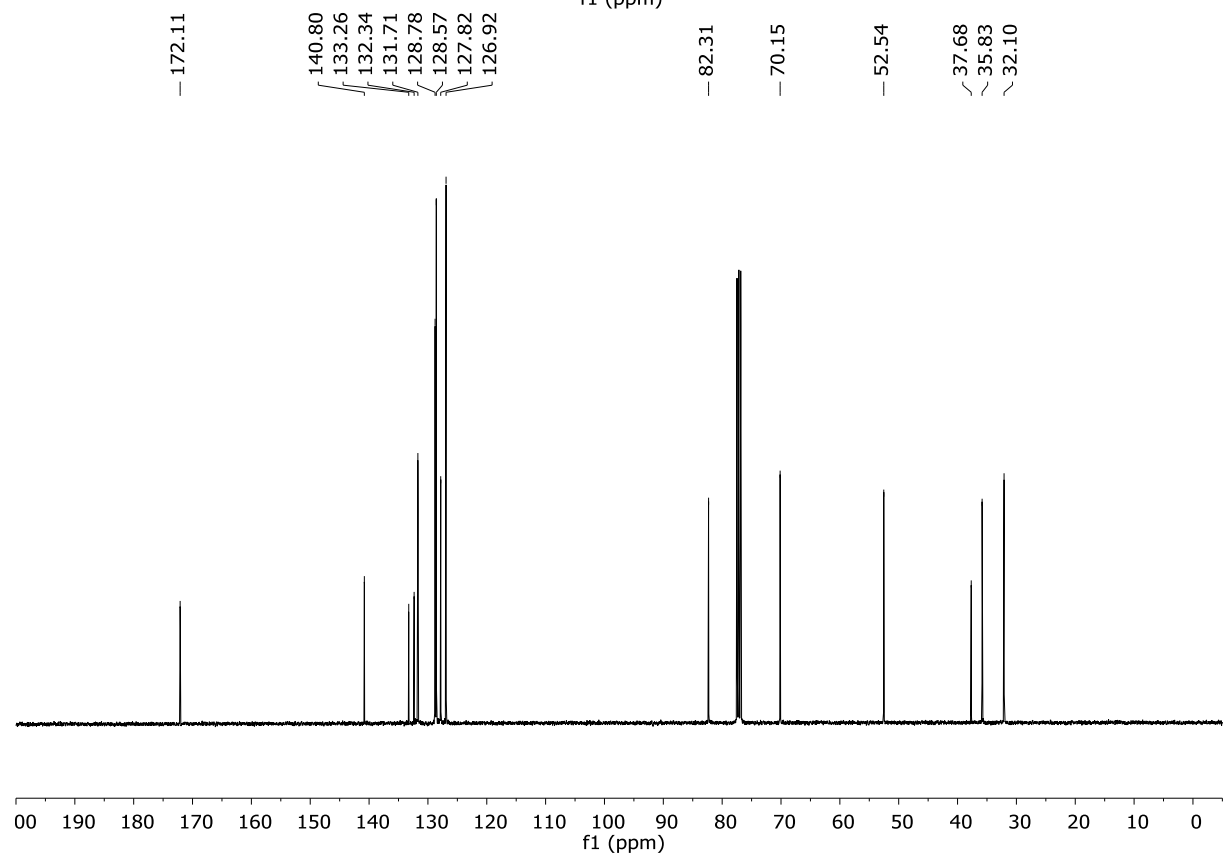
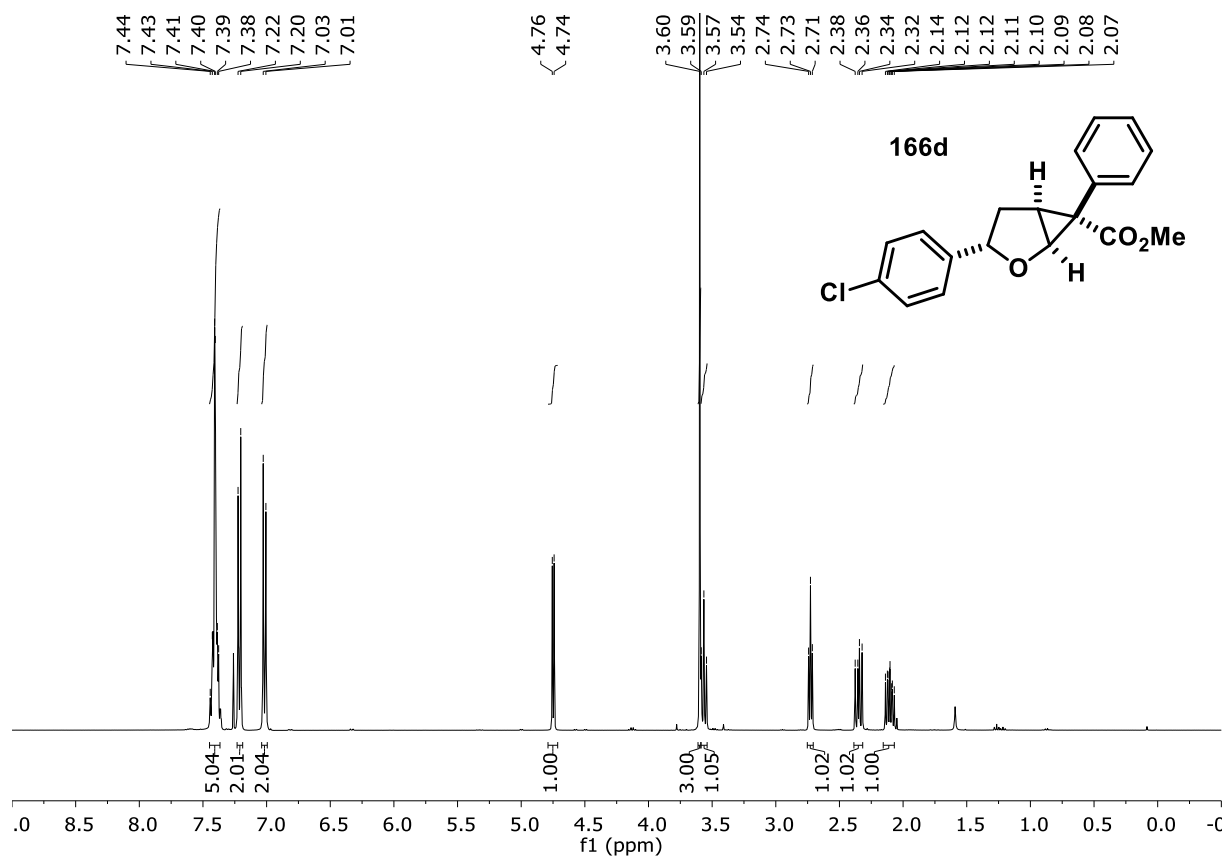


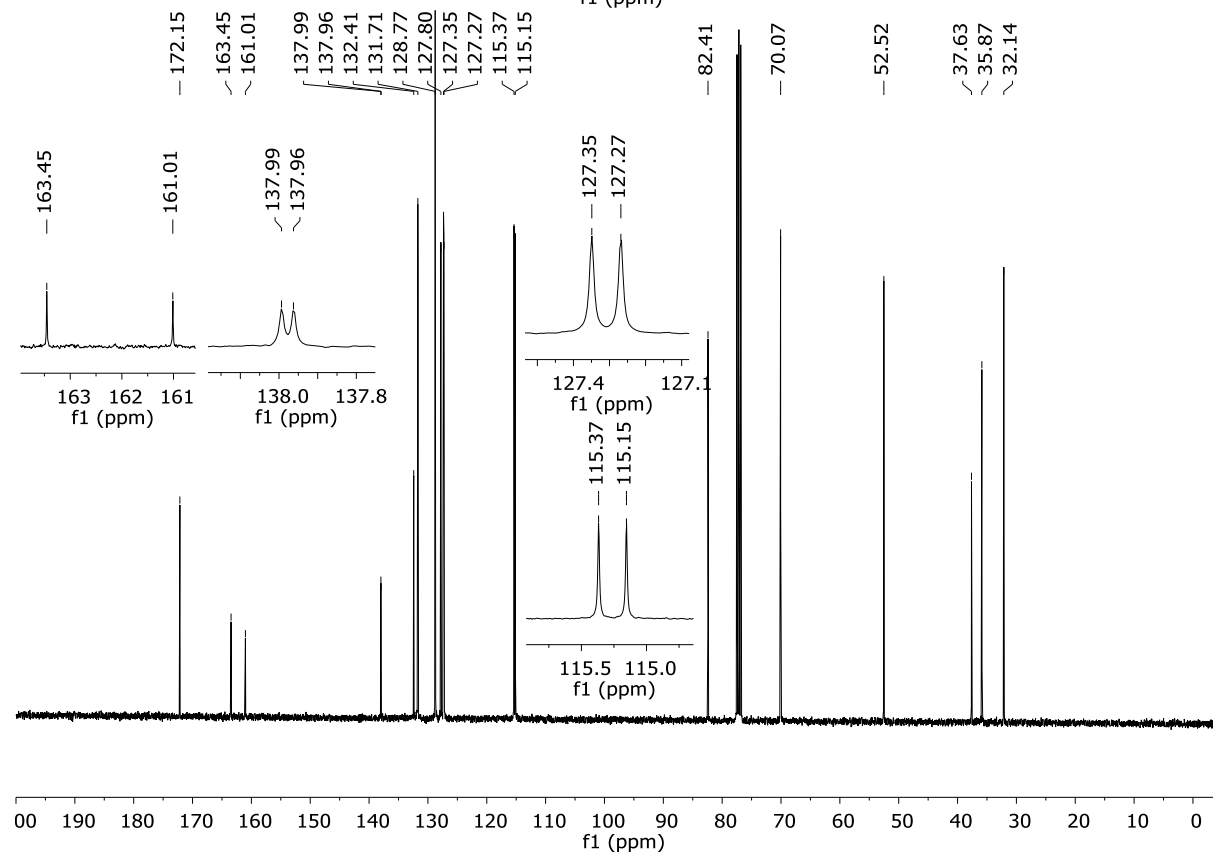
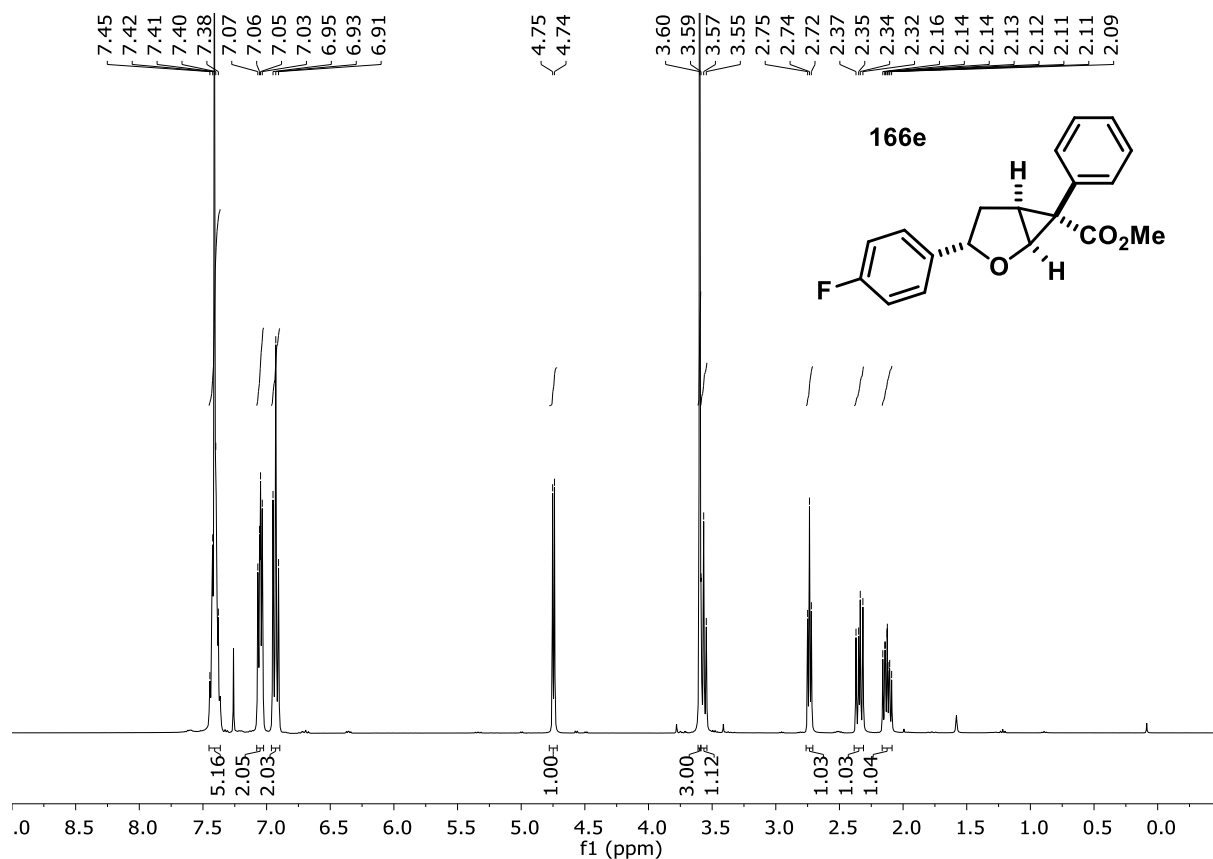


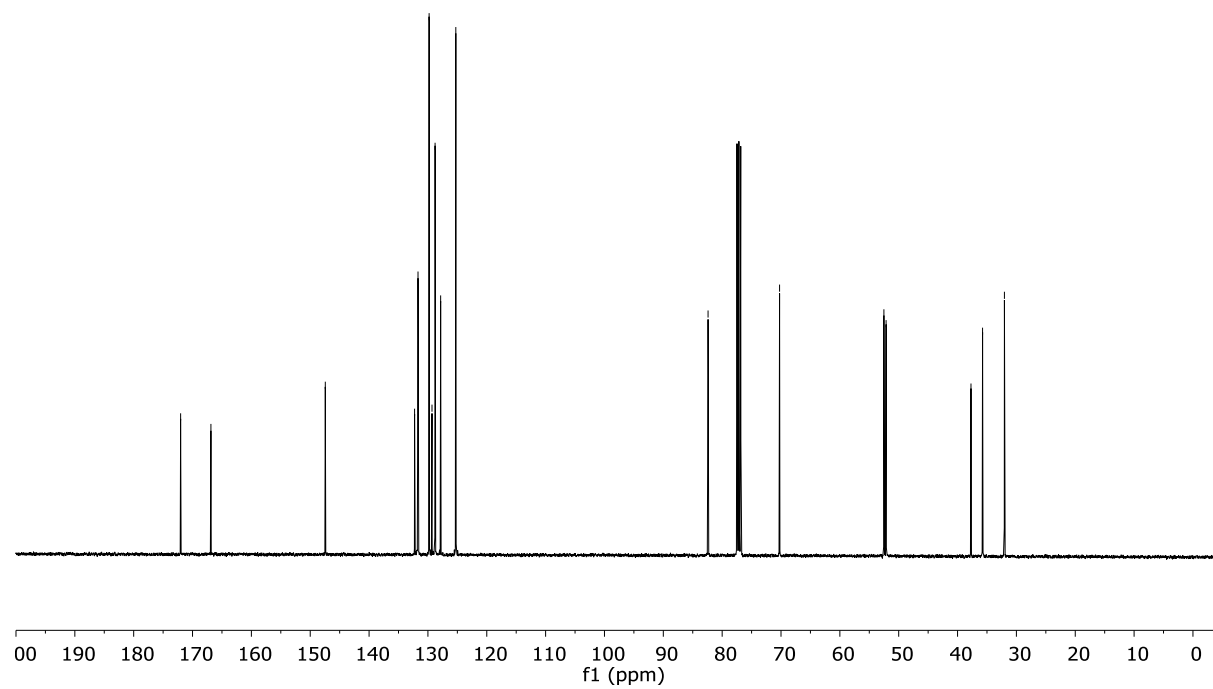
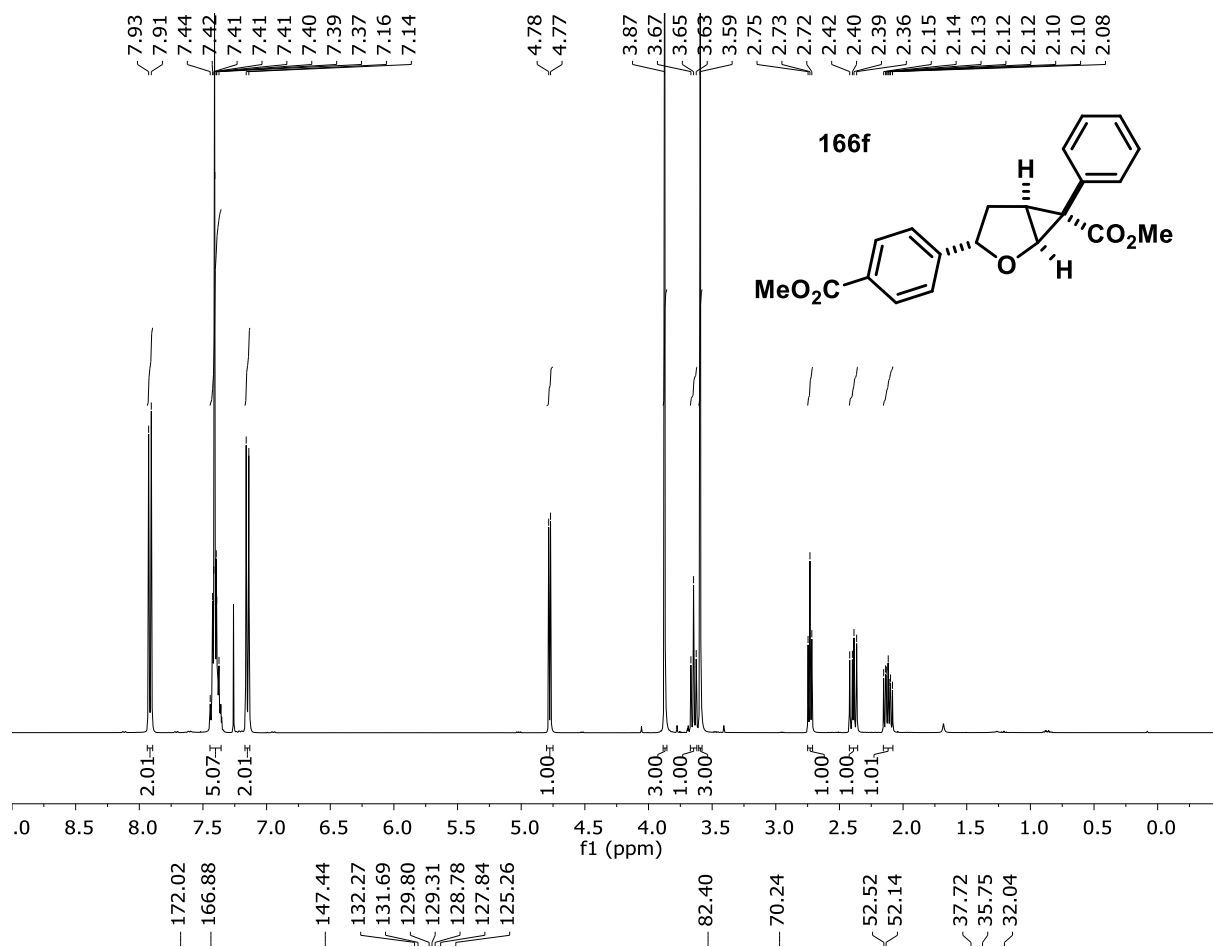


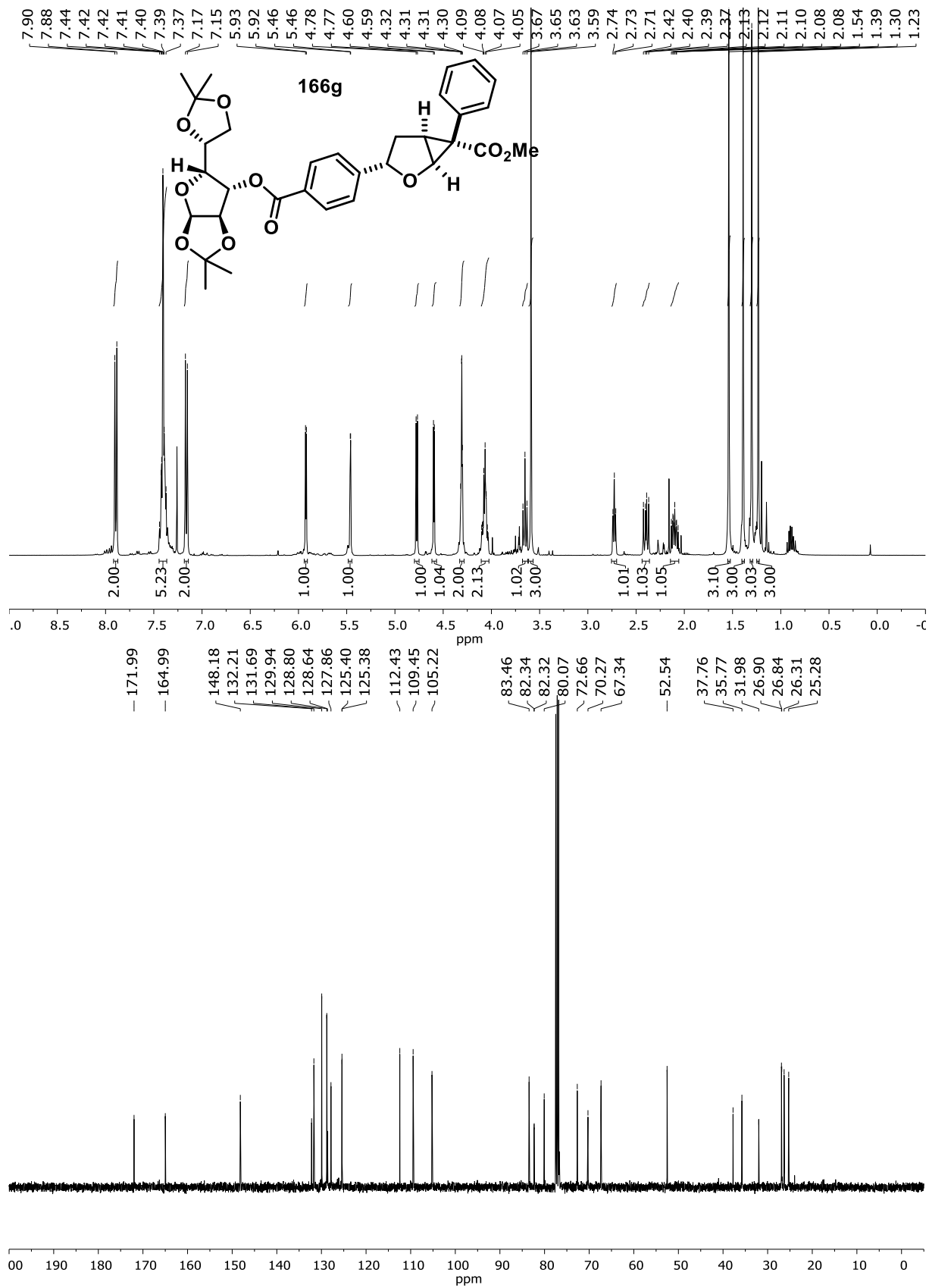


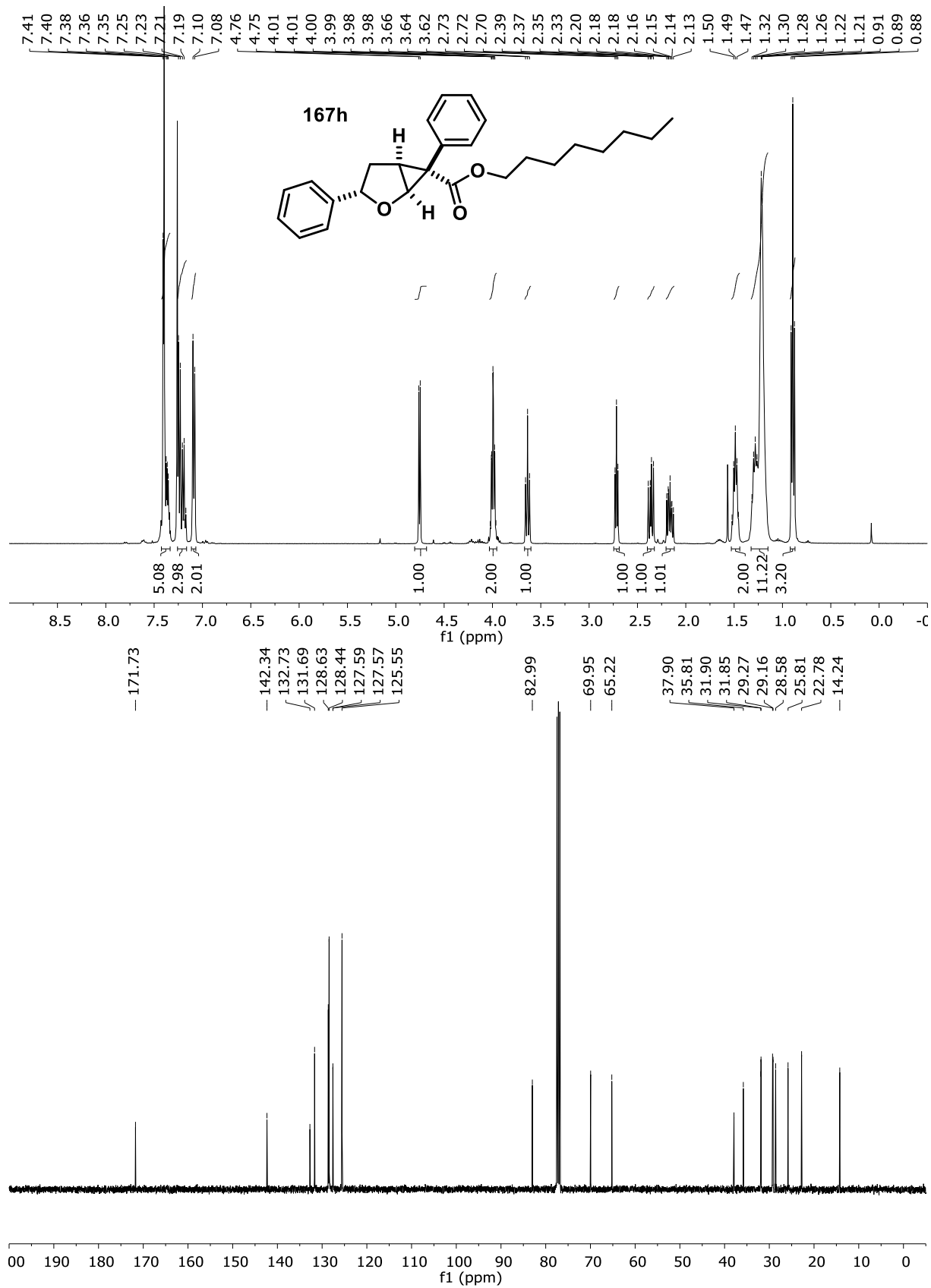




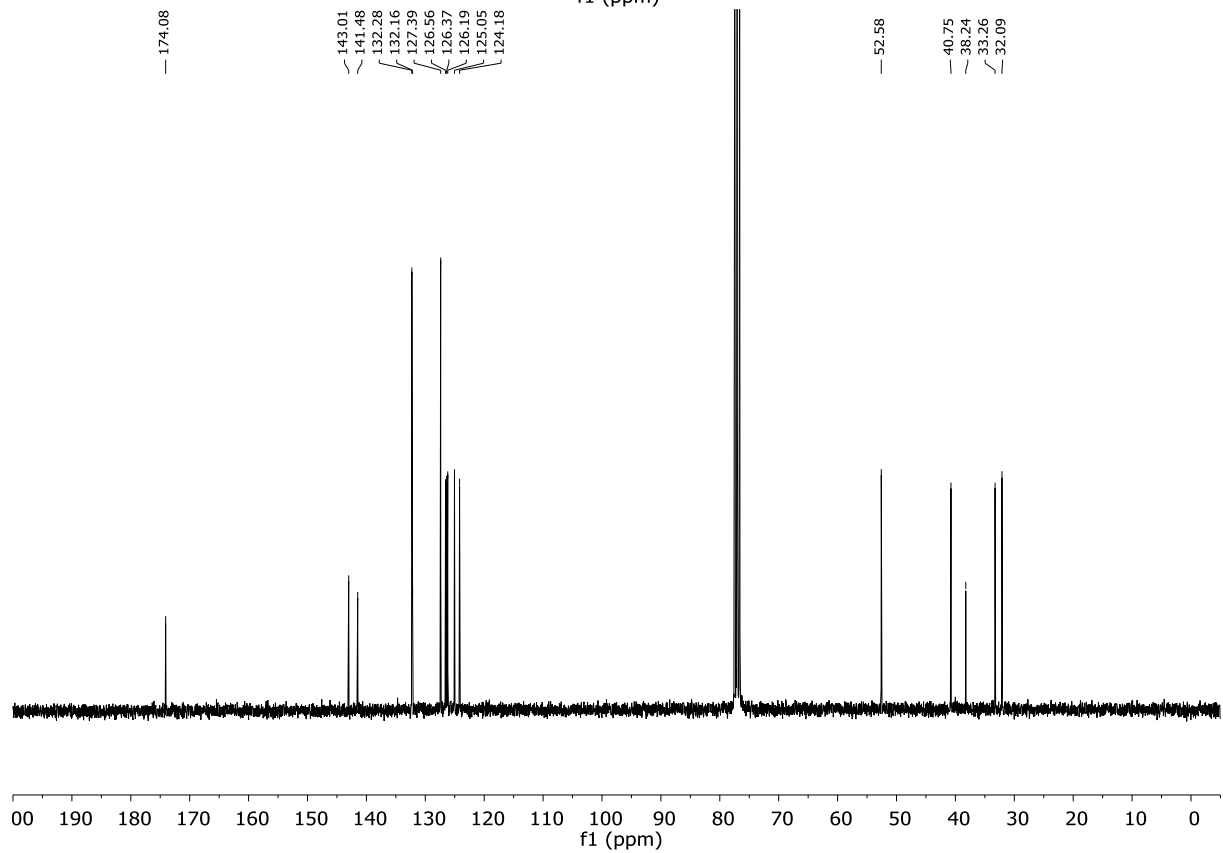
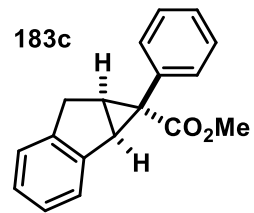
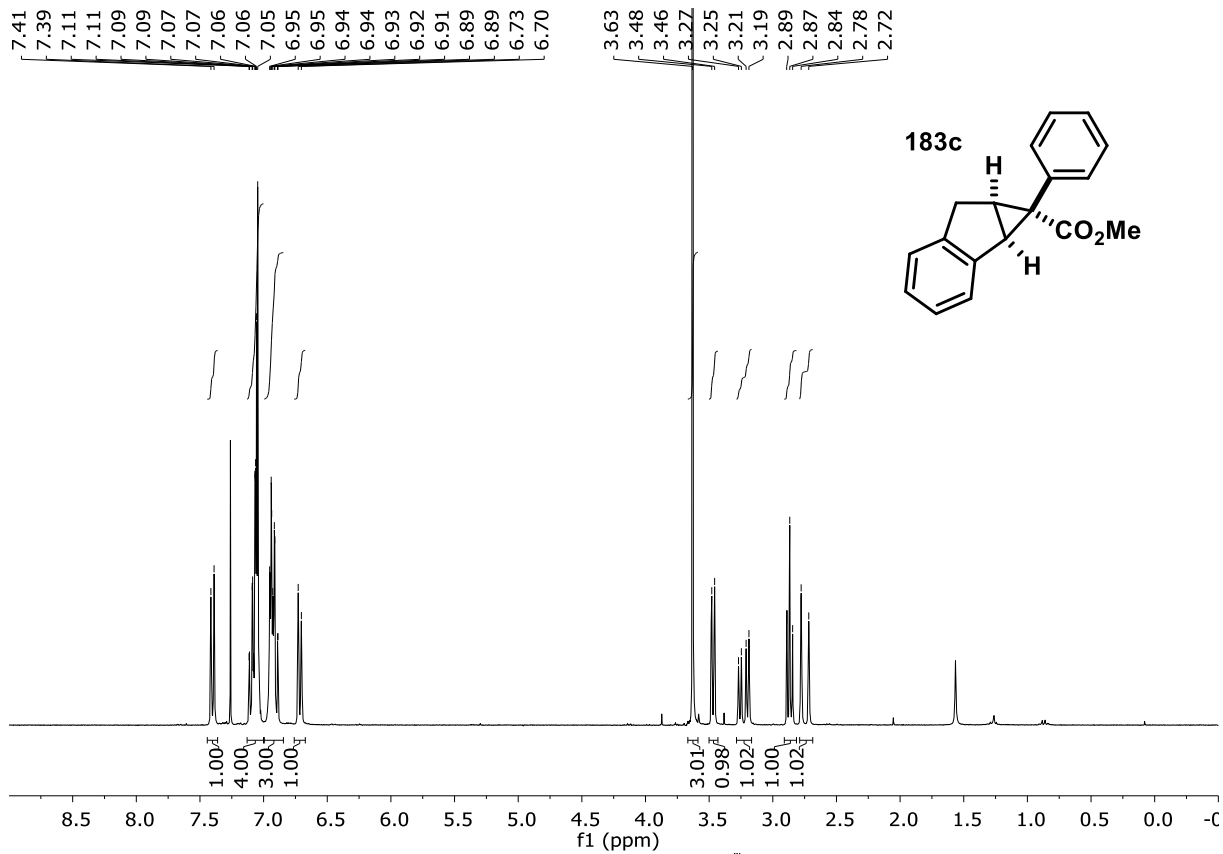


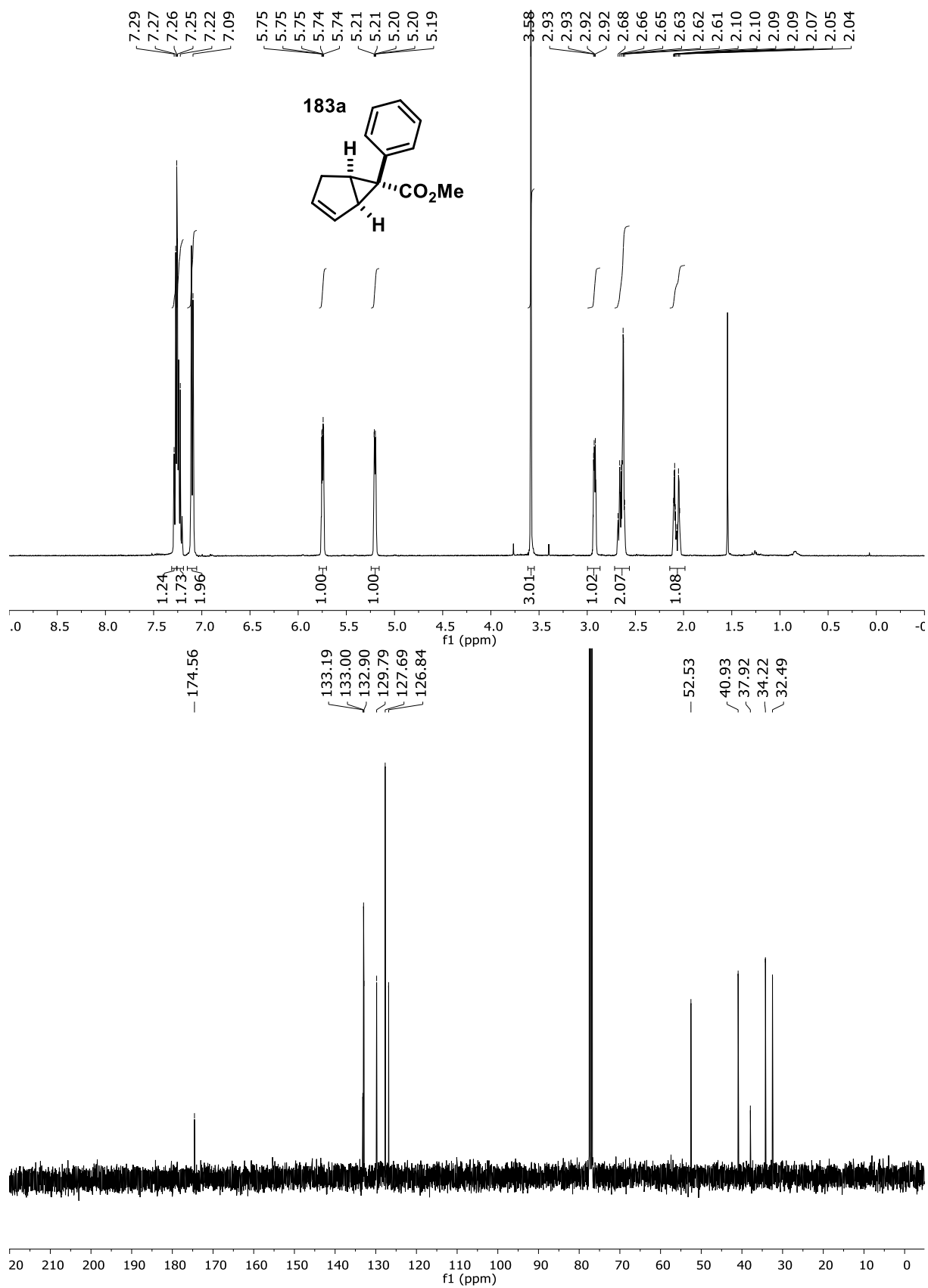


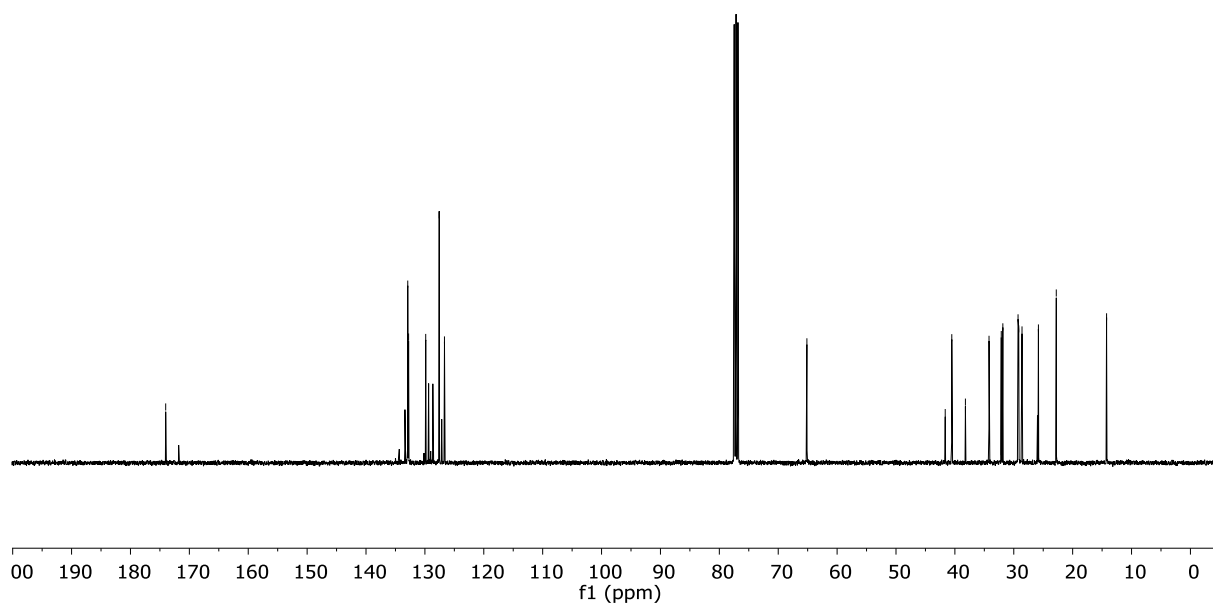
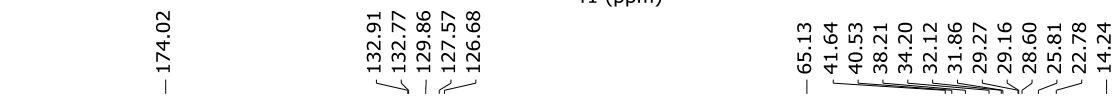
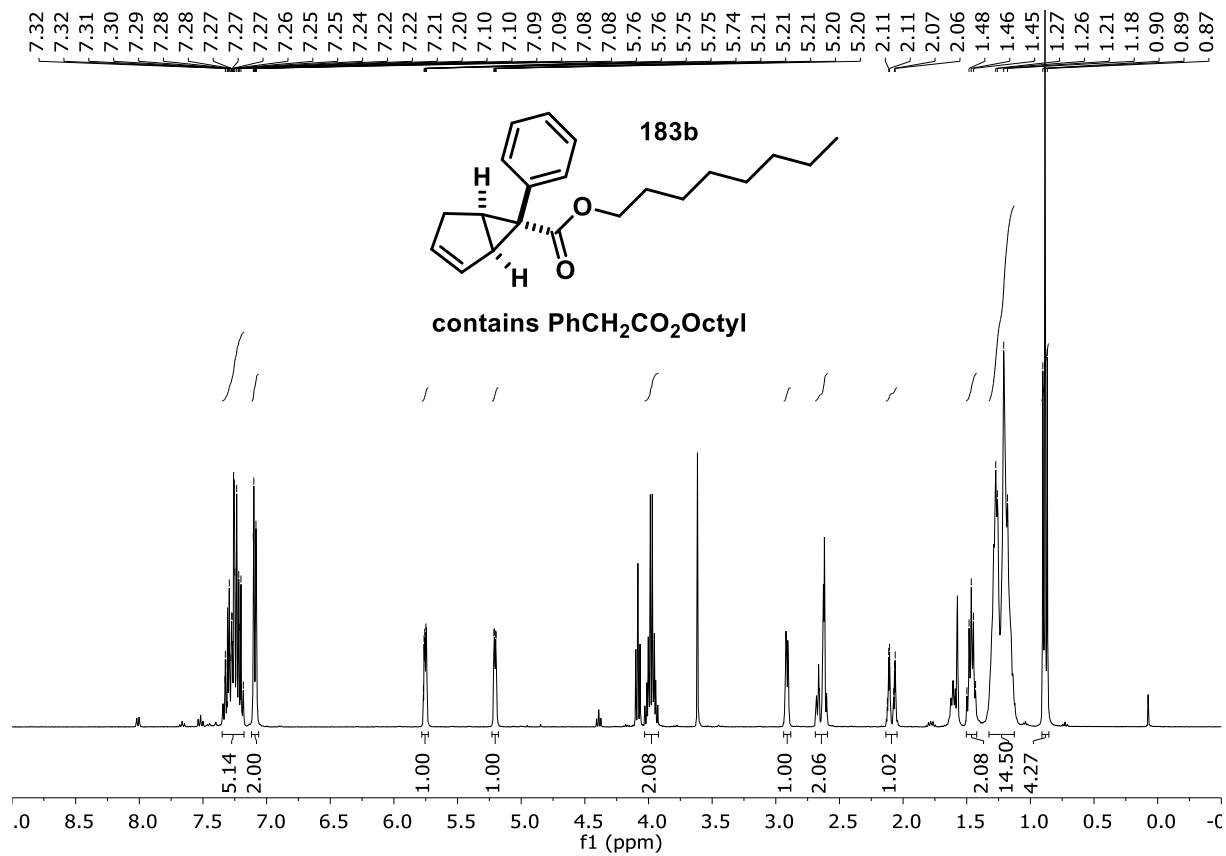


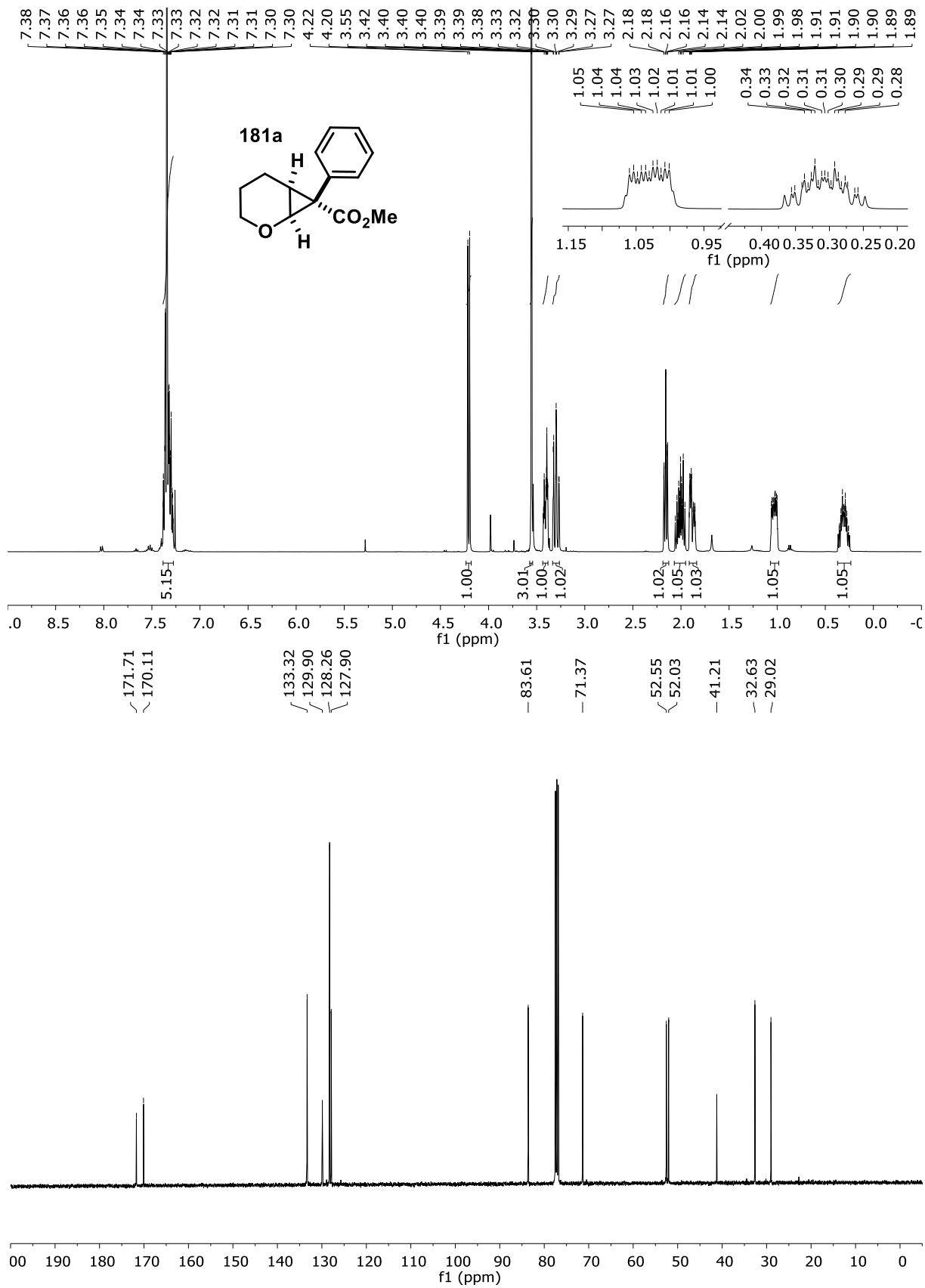


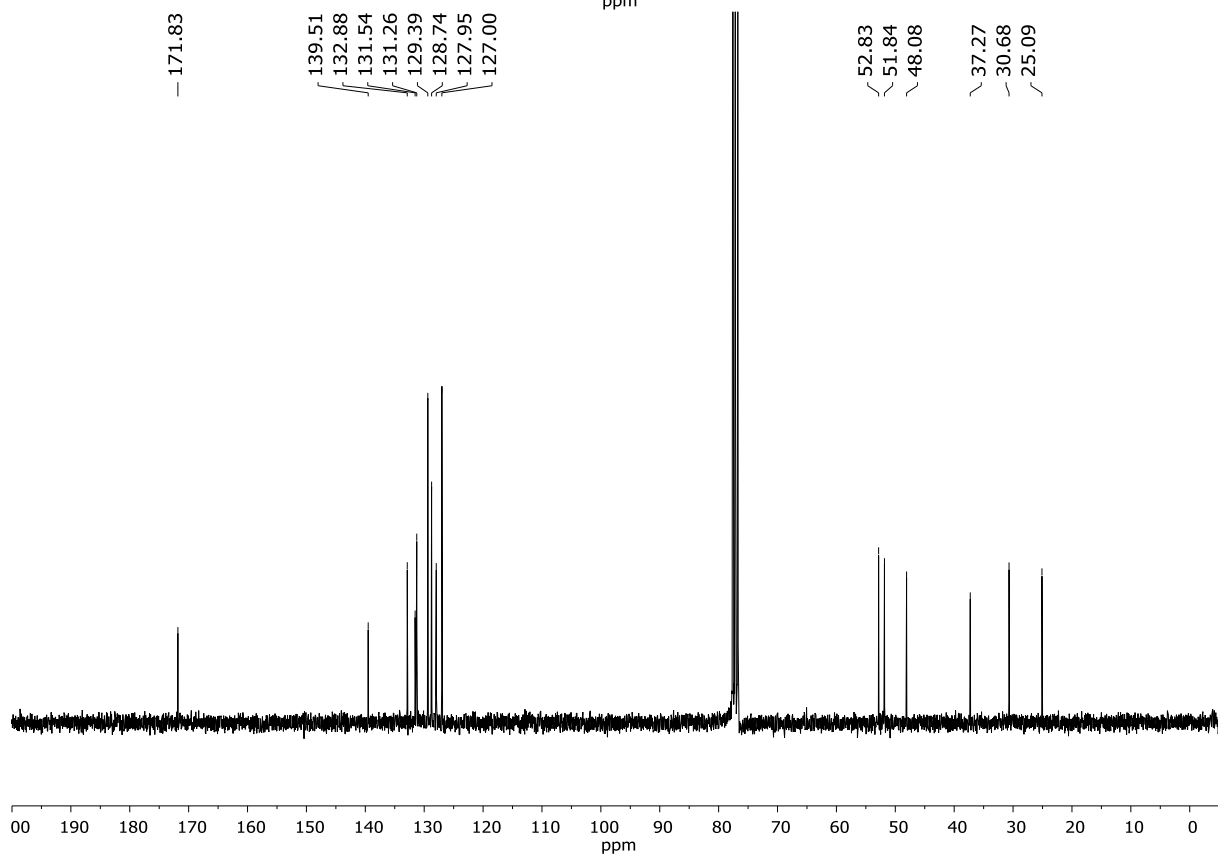
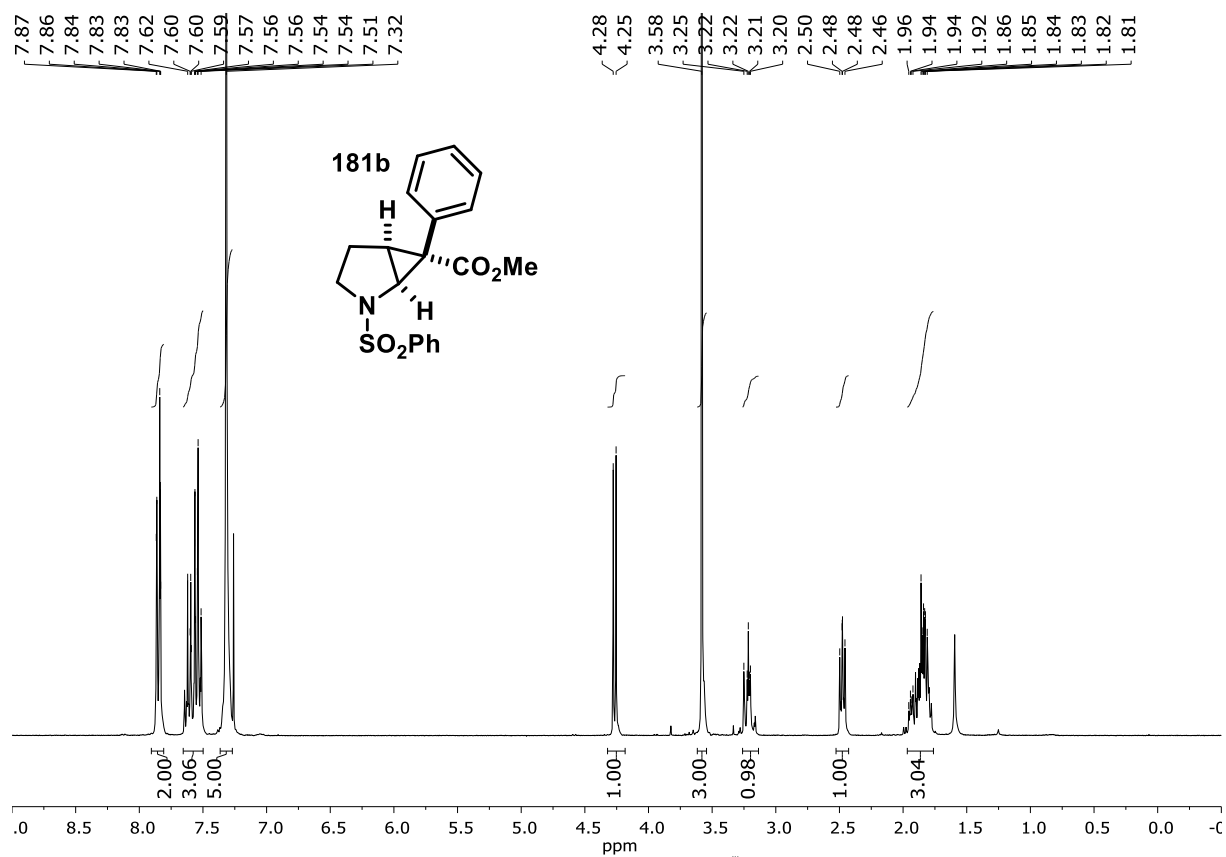


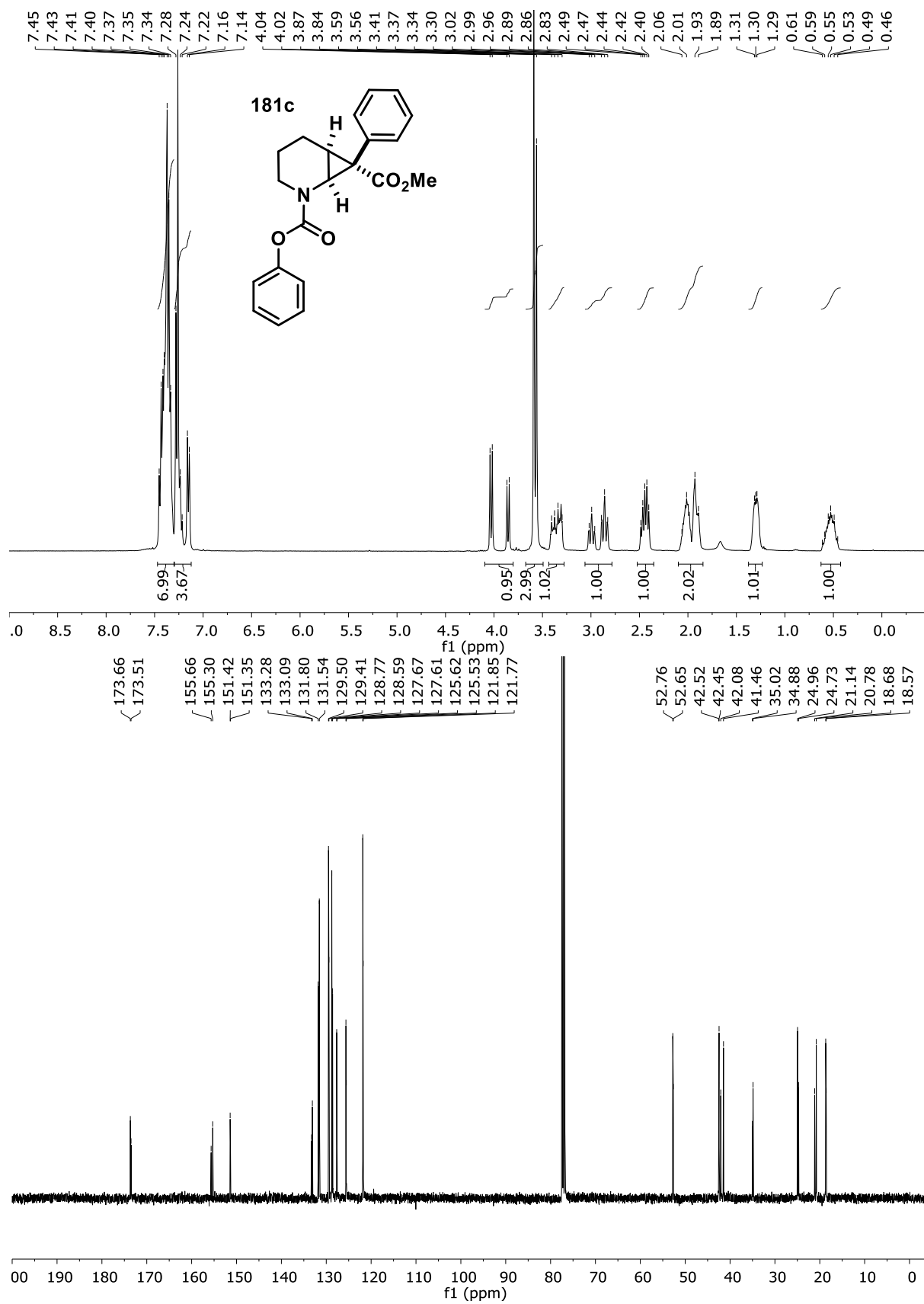


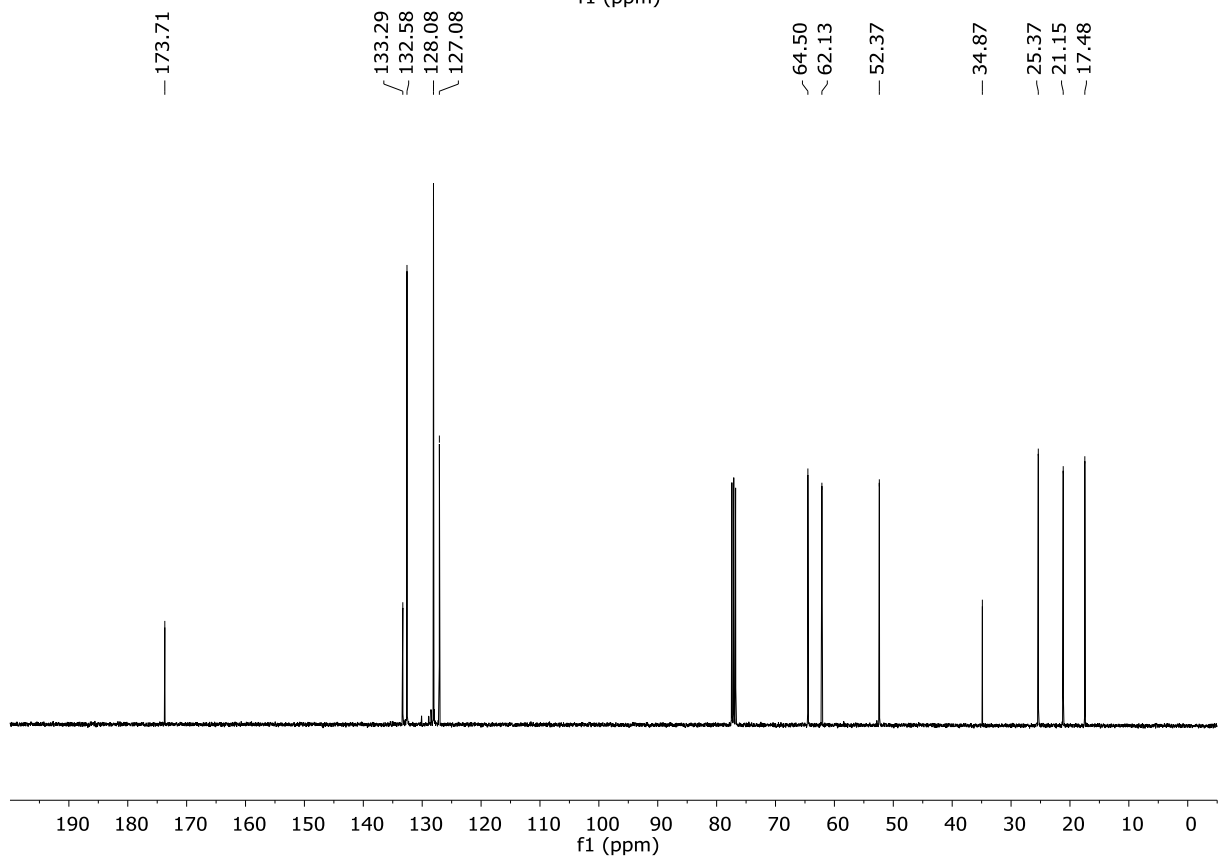
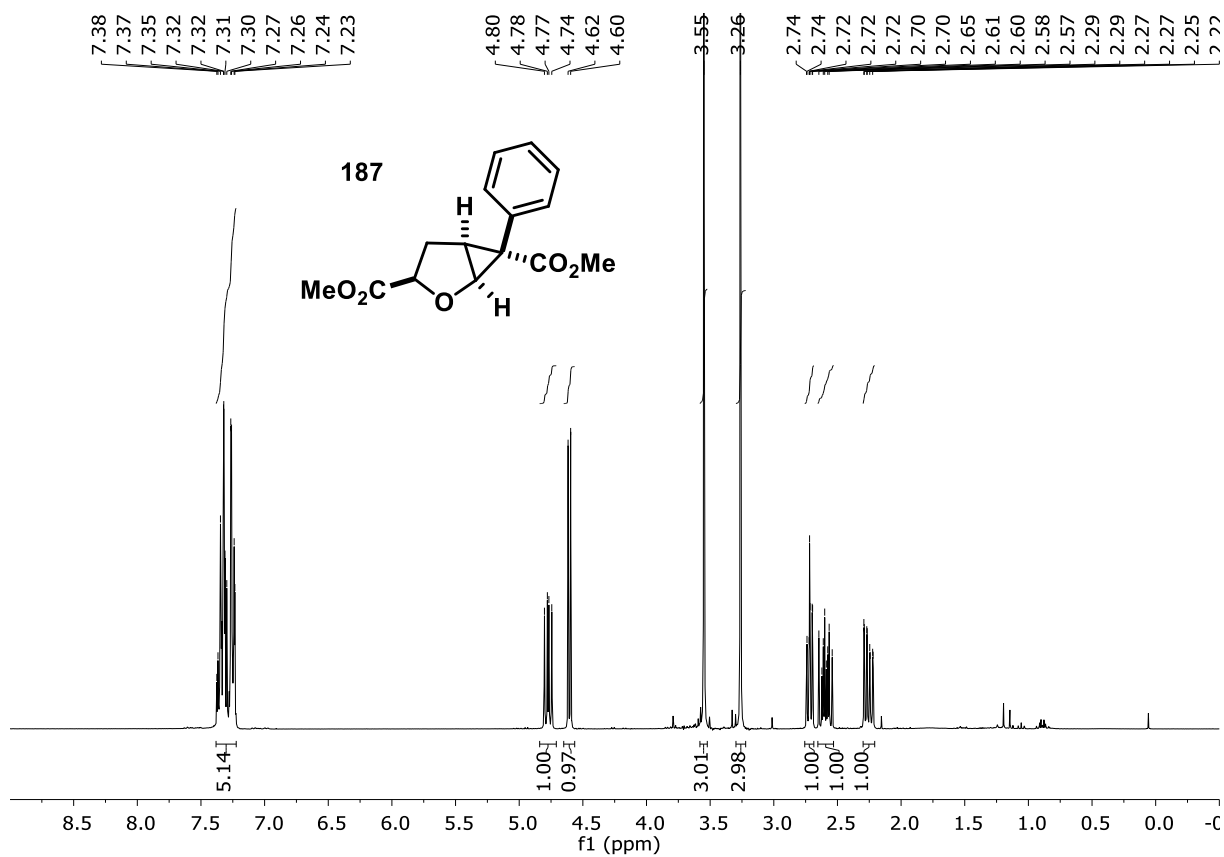


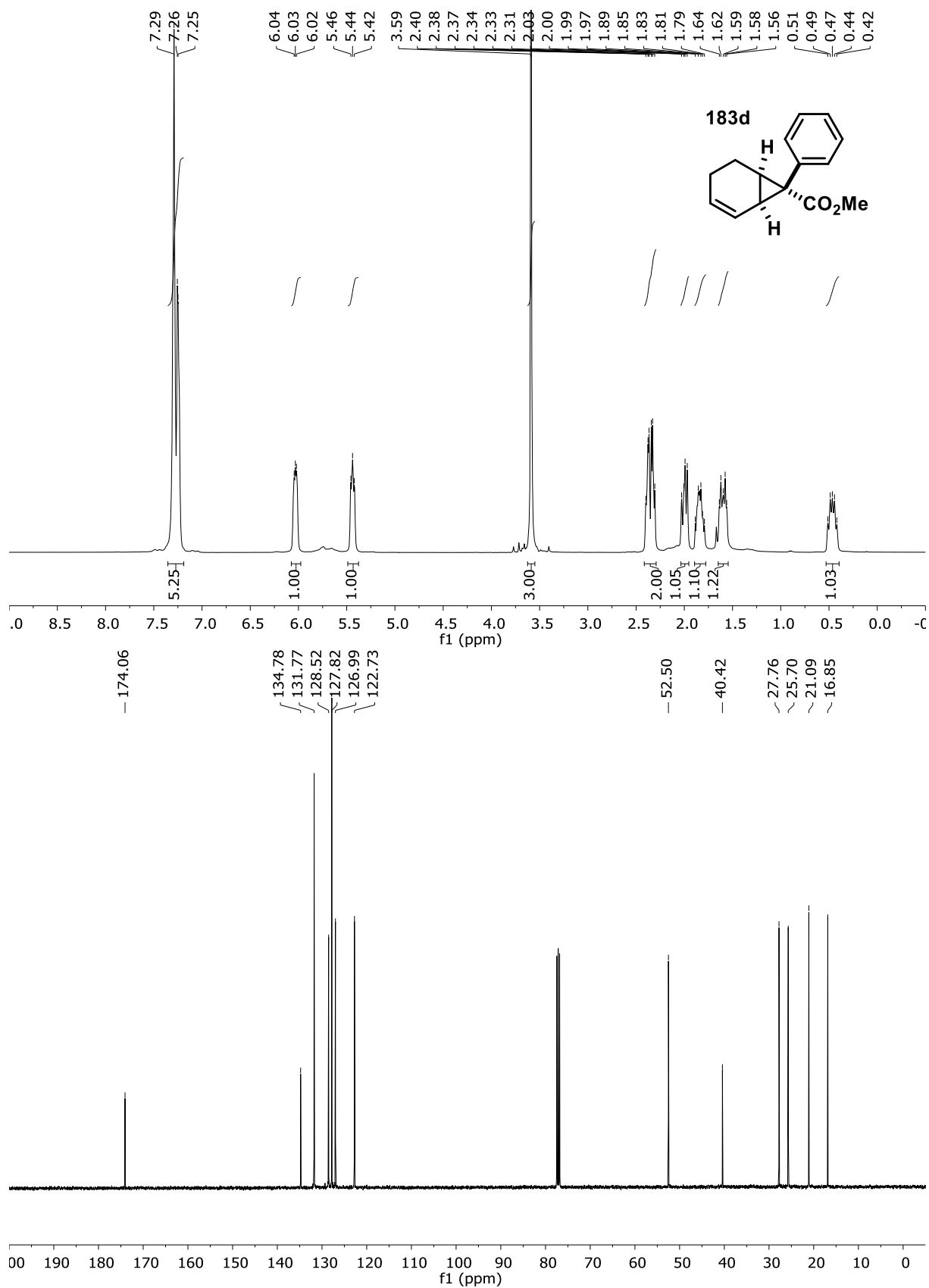








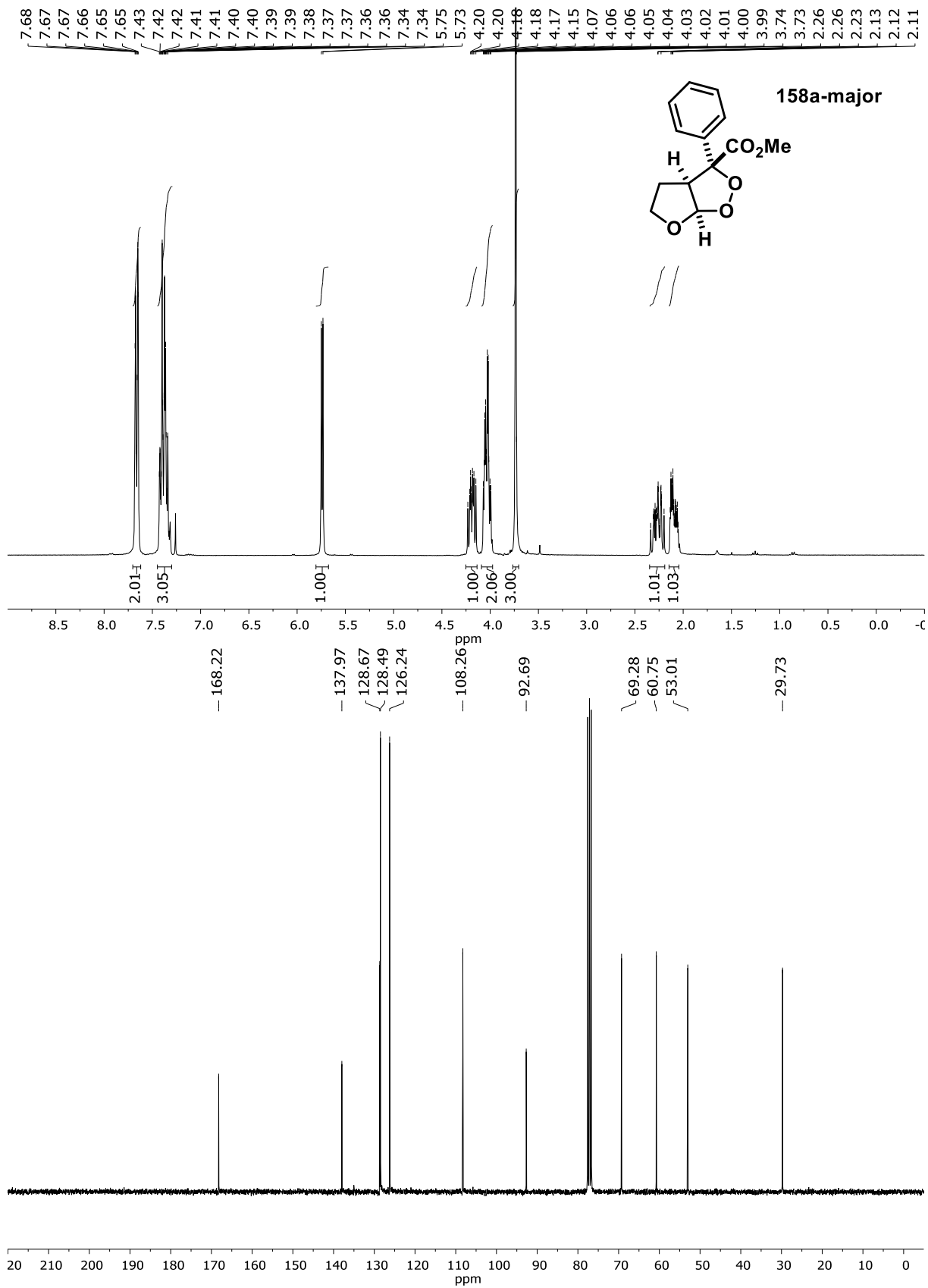


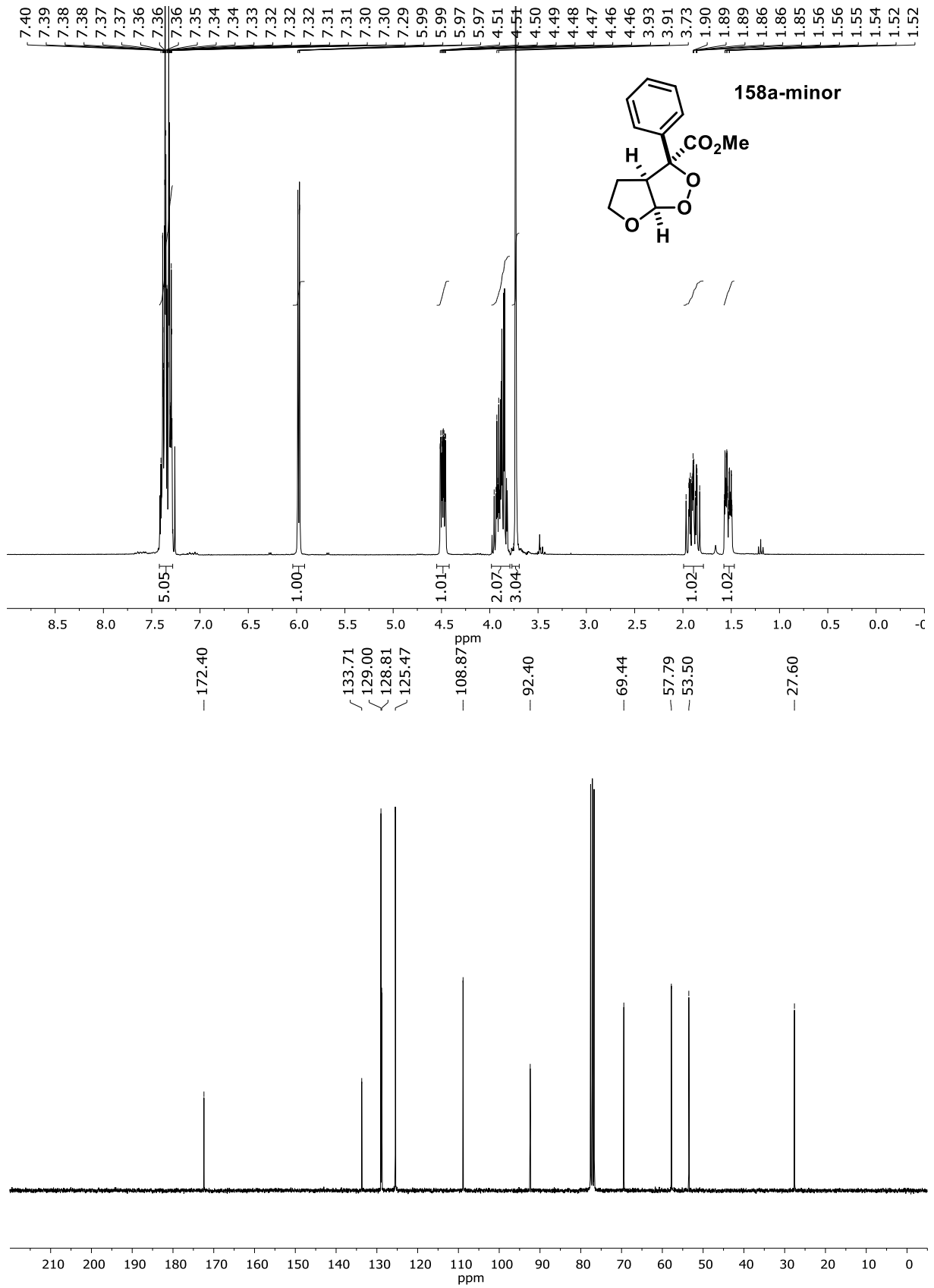


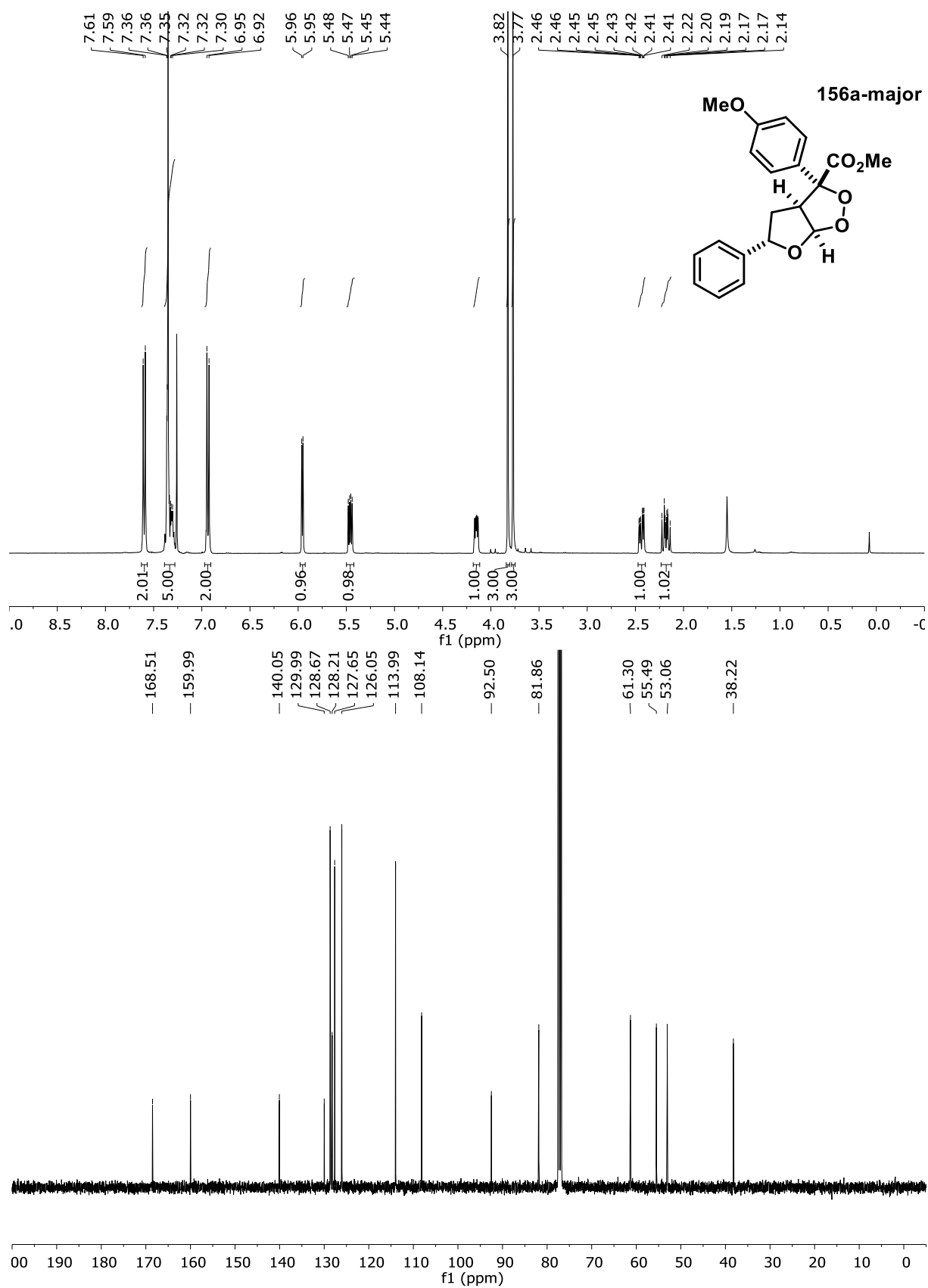


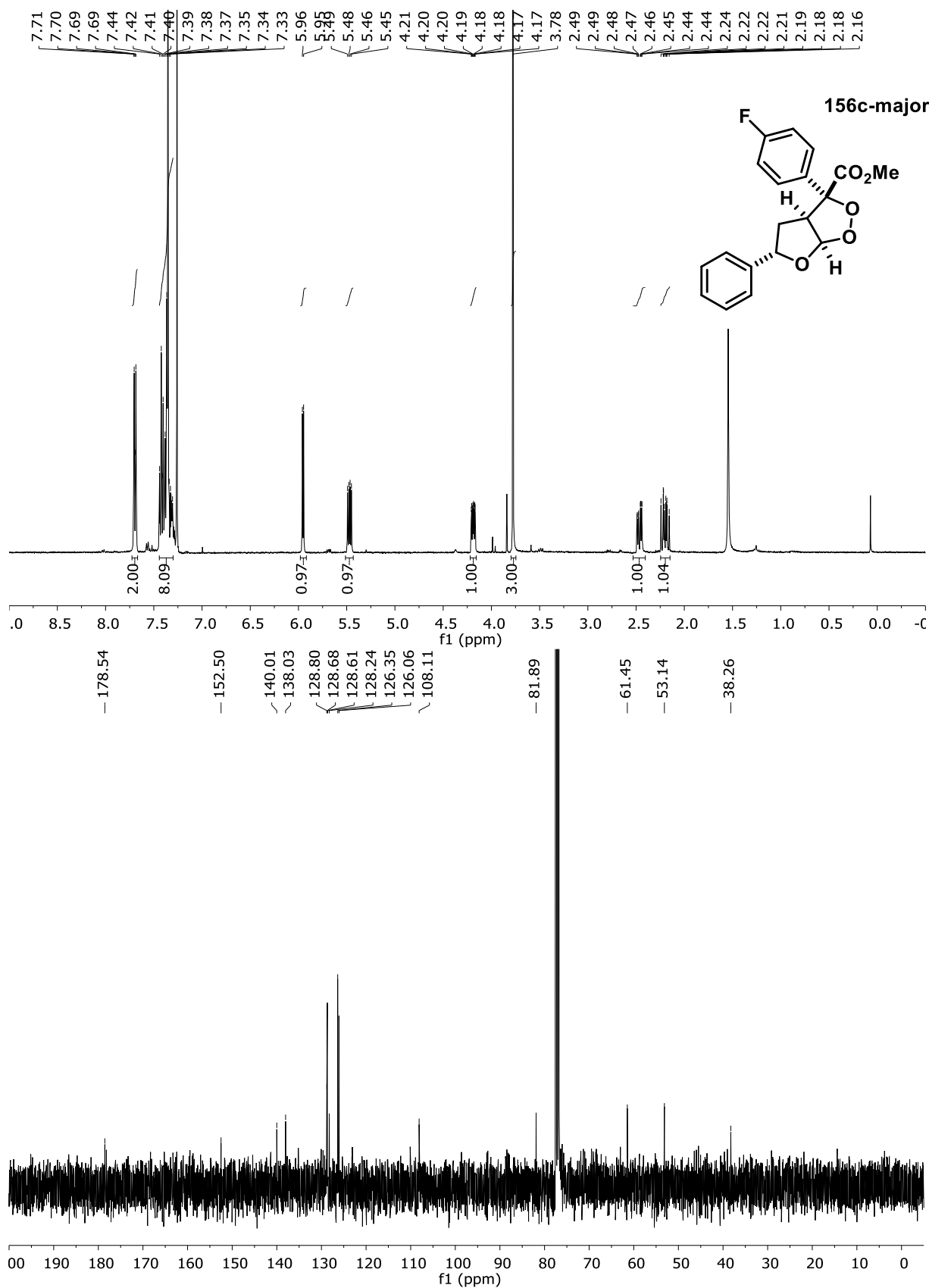


Peroxides 2

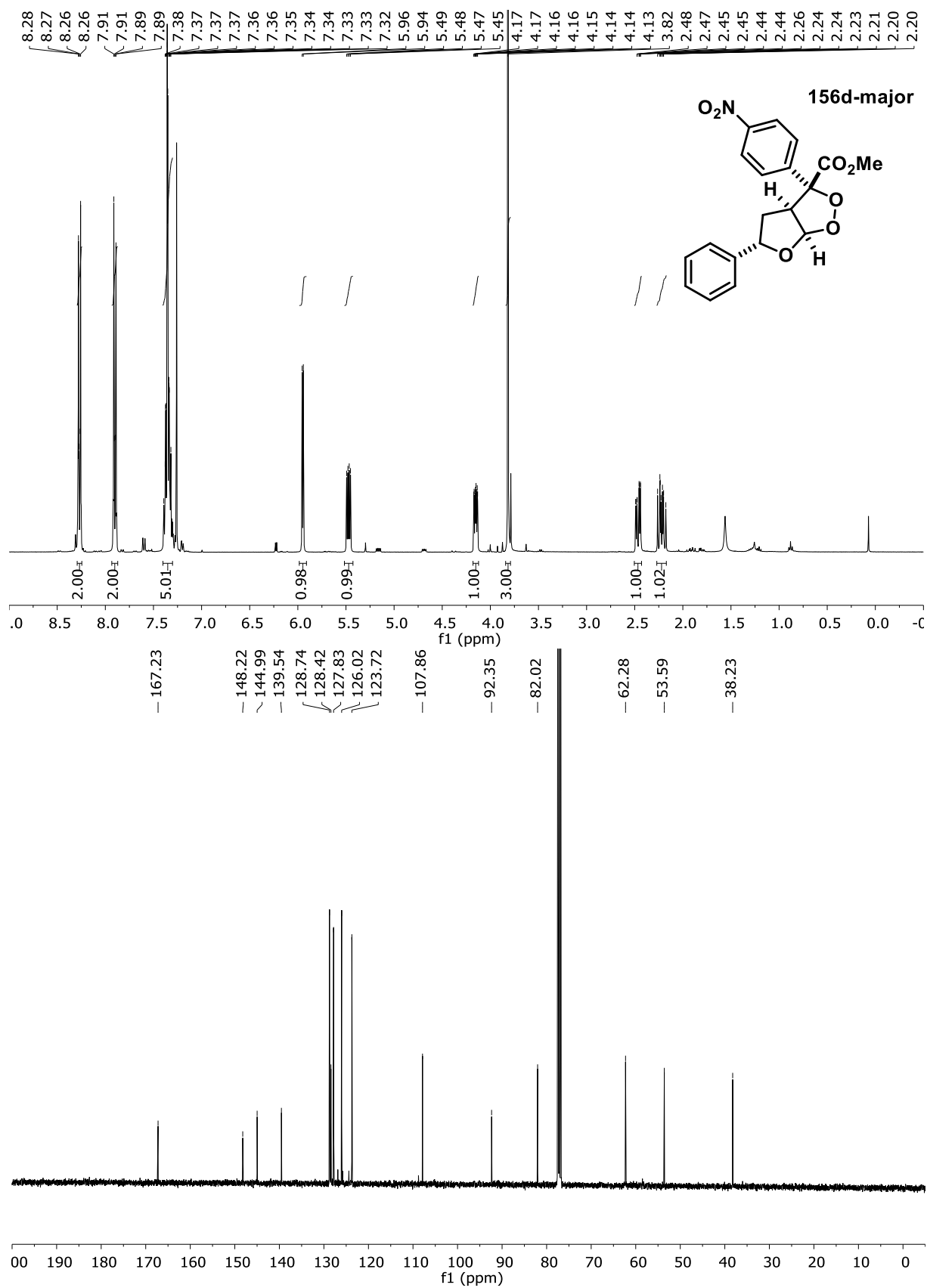


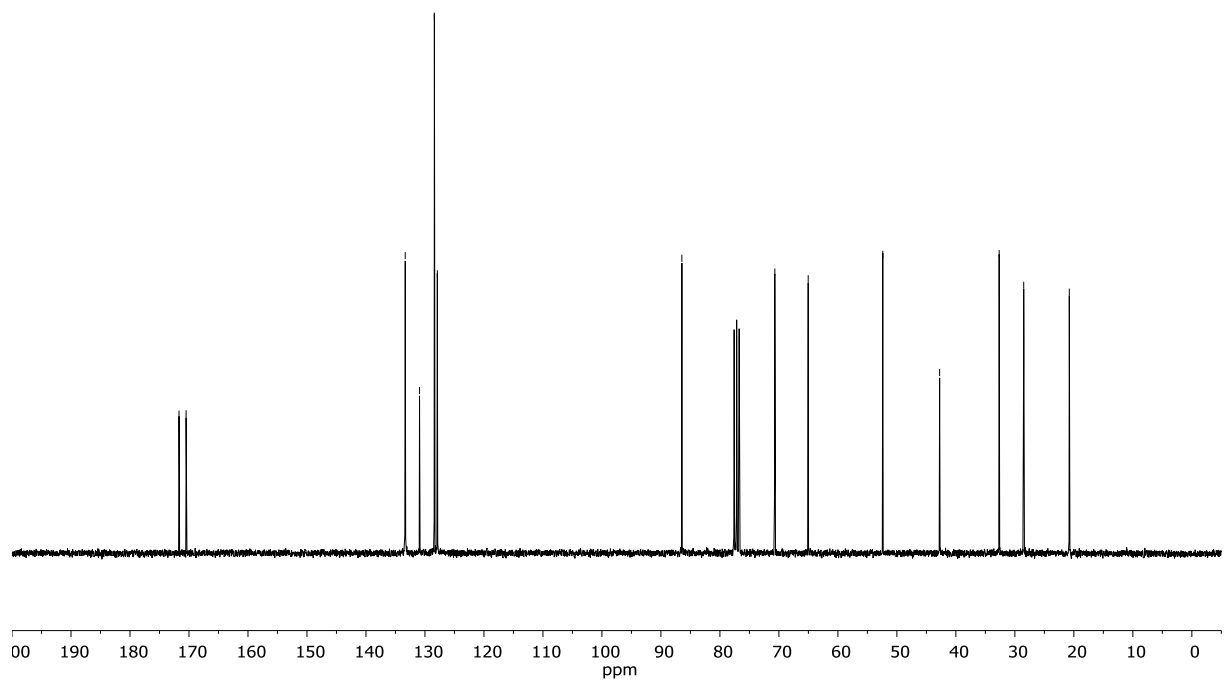
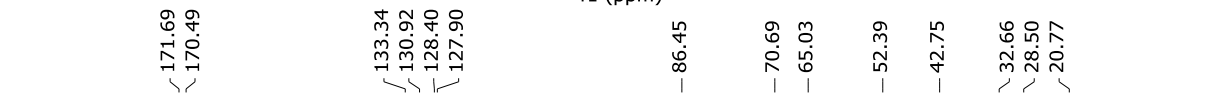
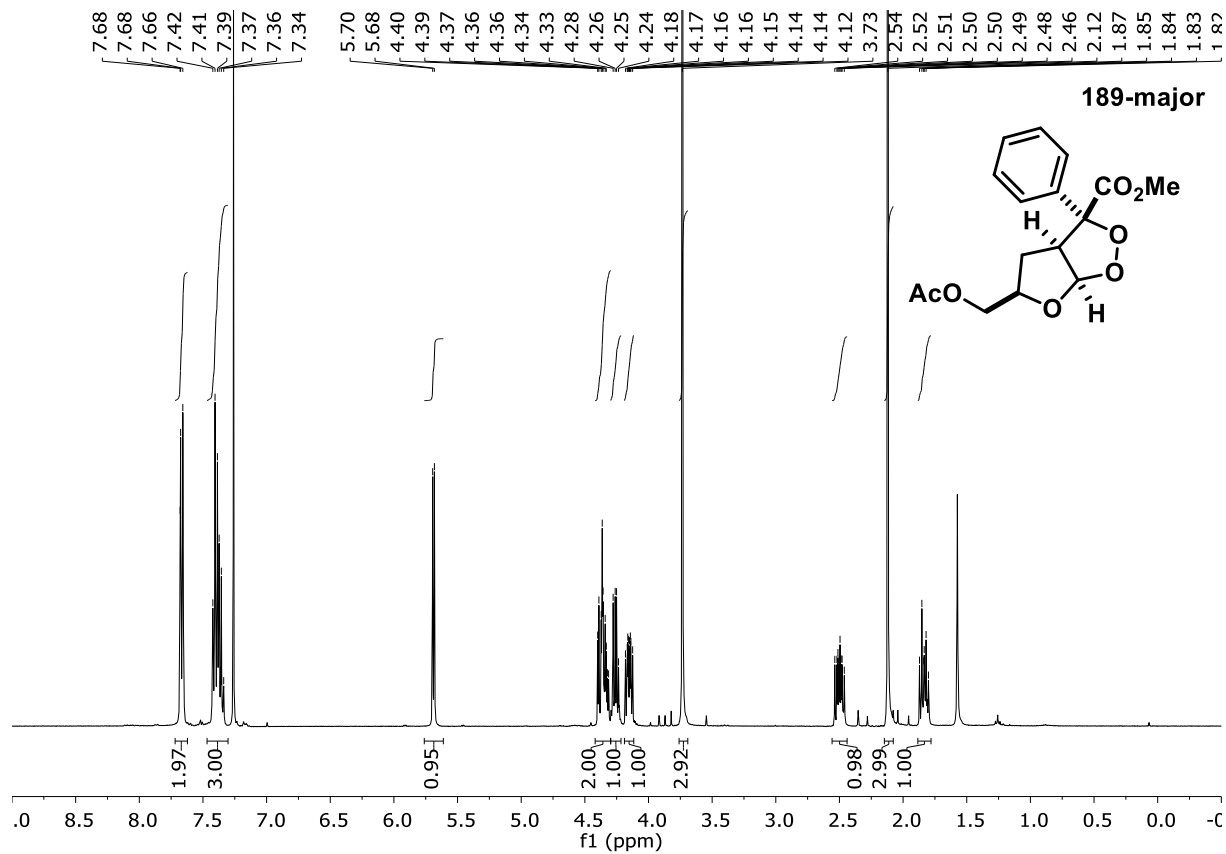




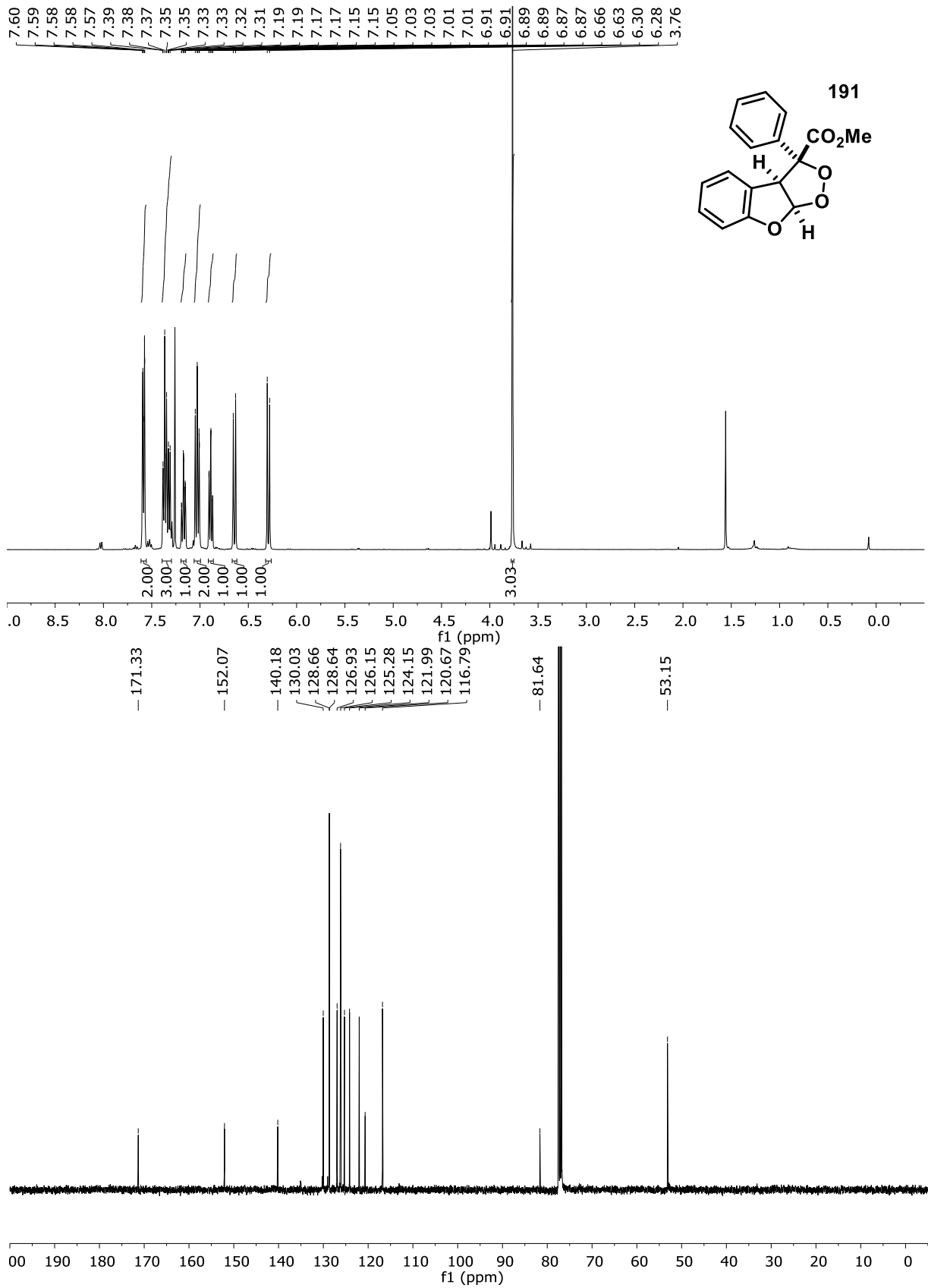


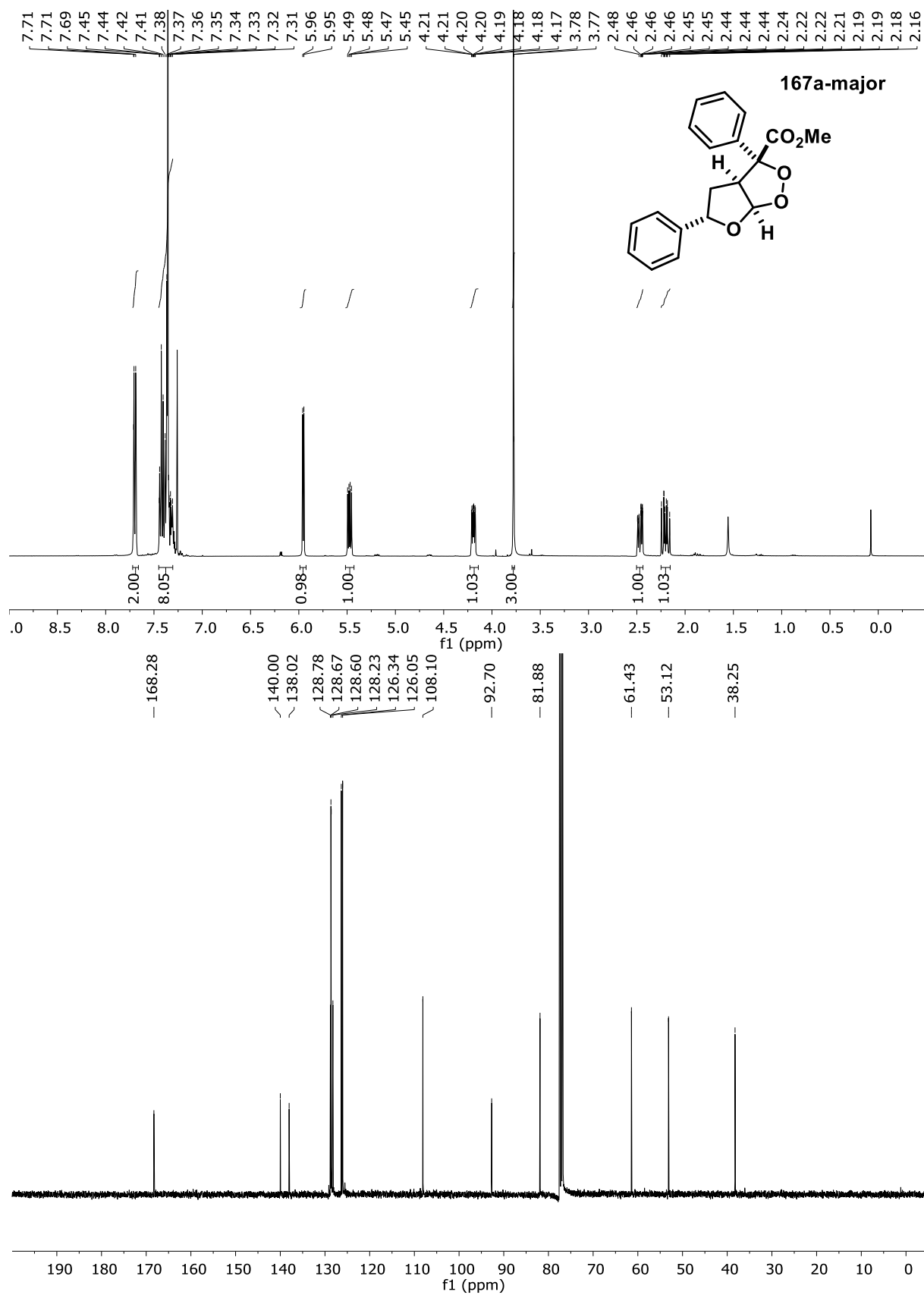


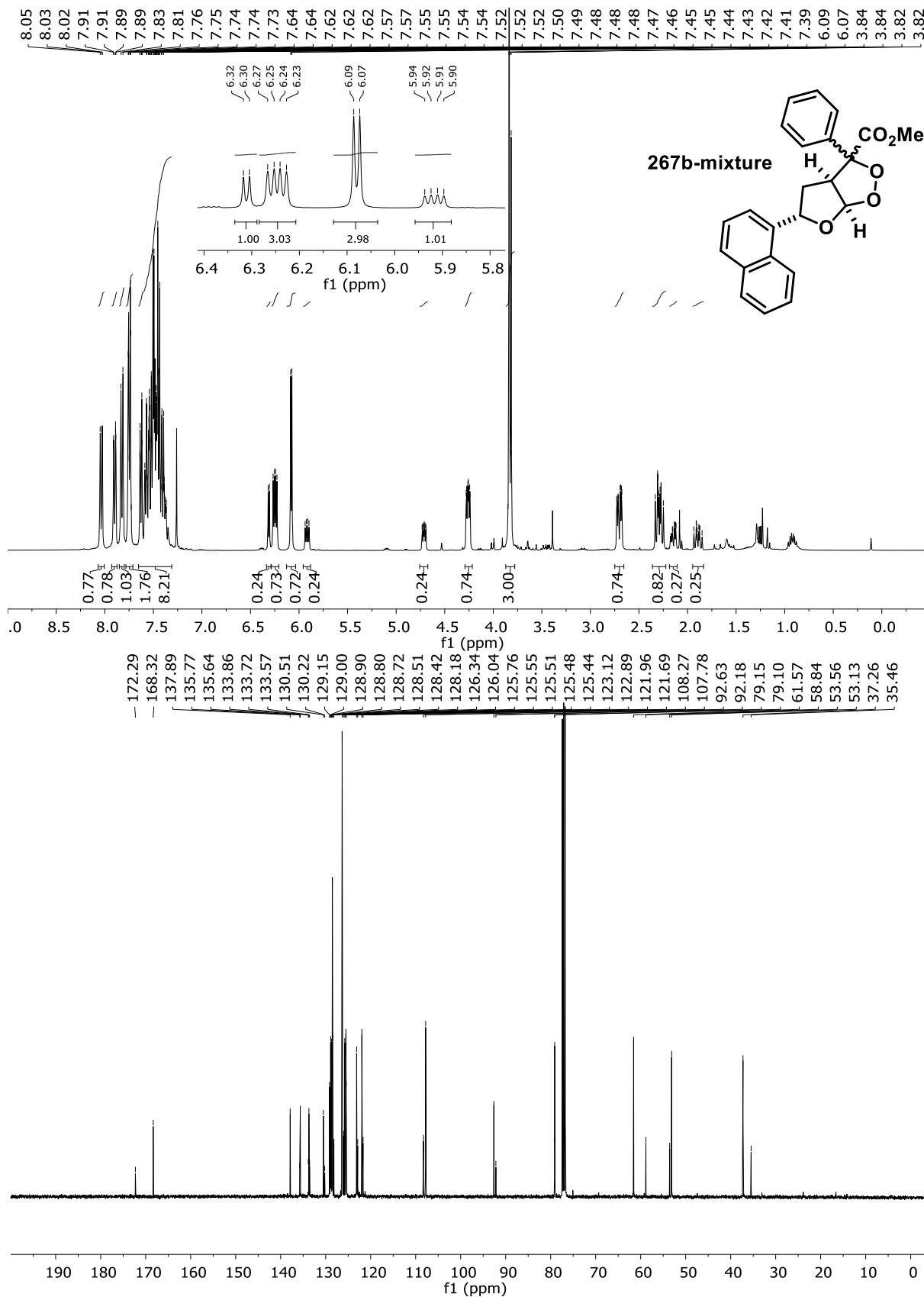




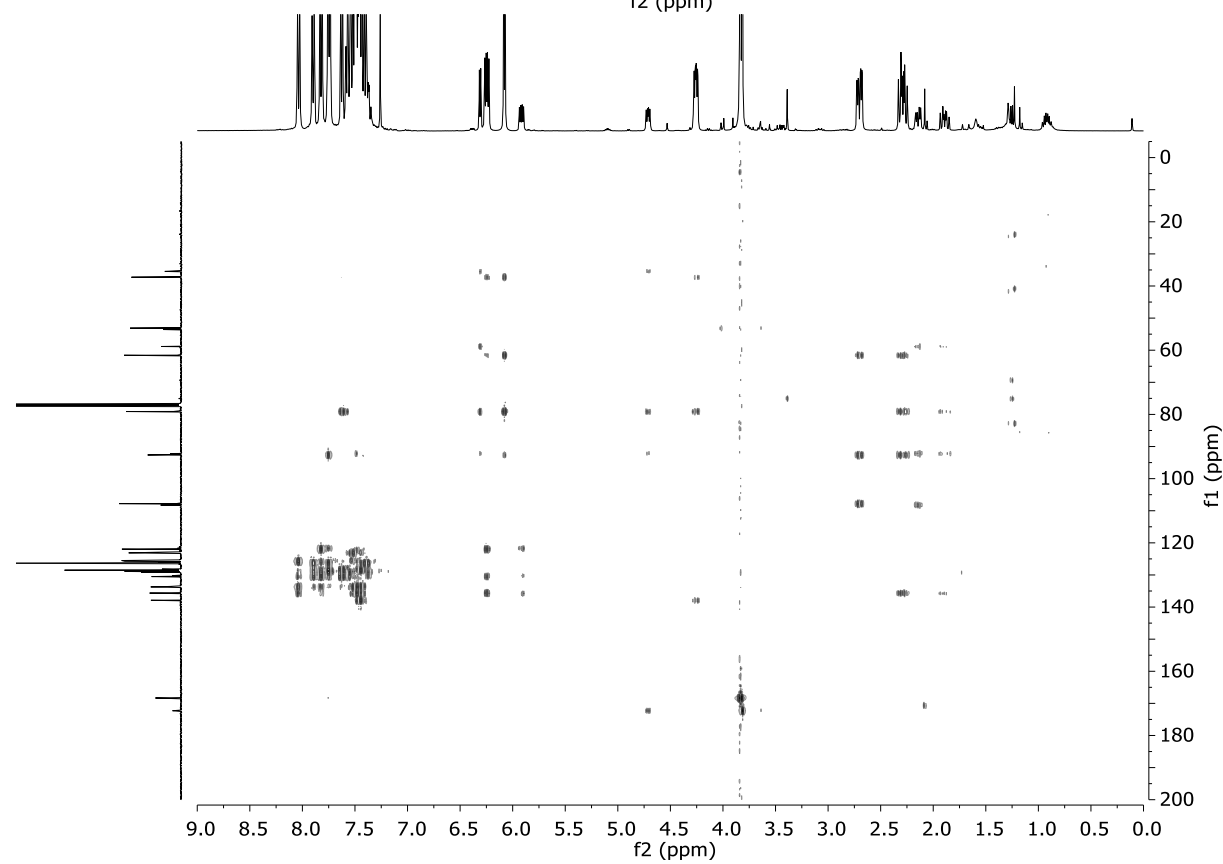
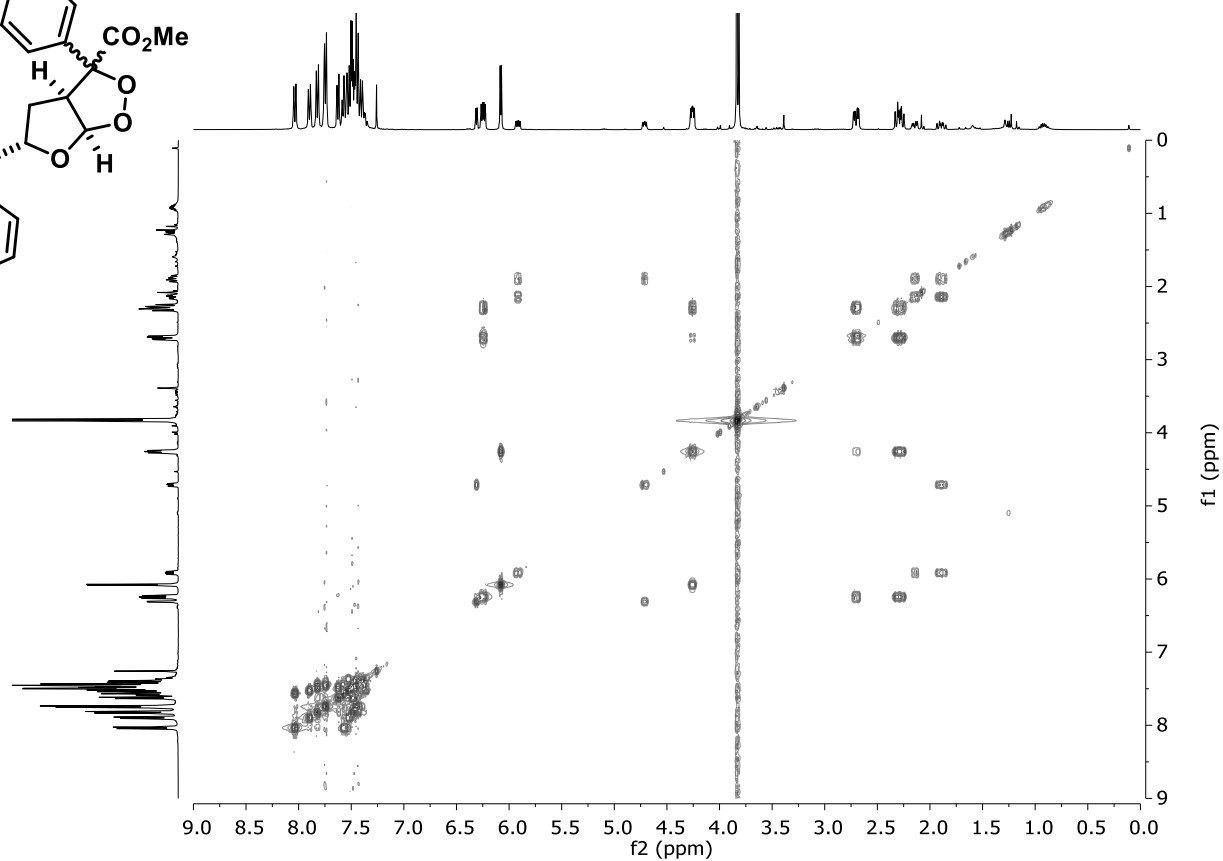
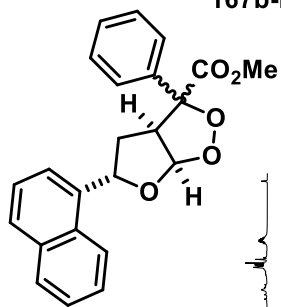


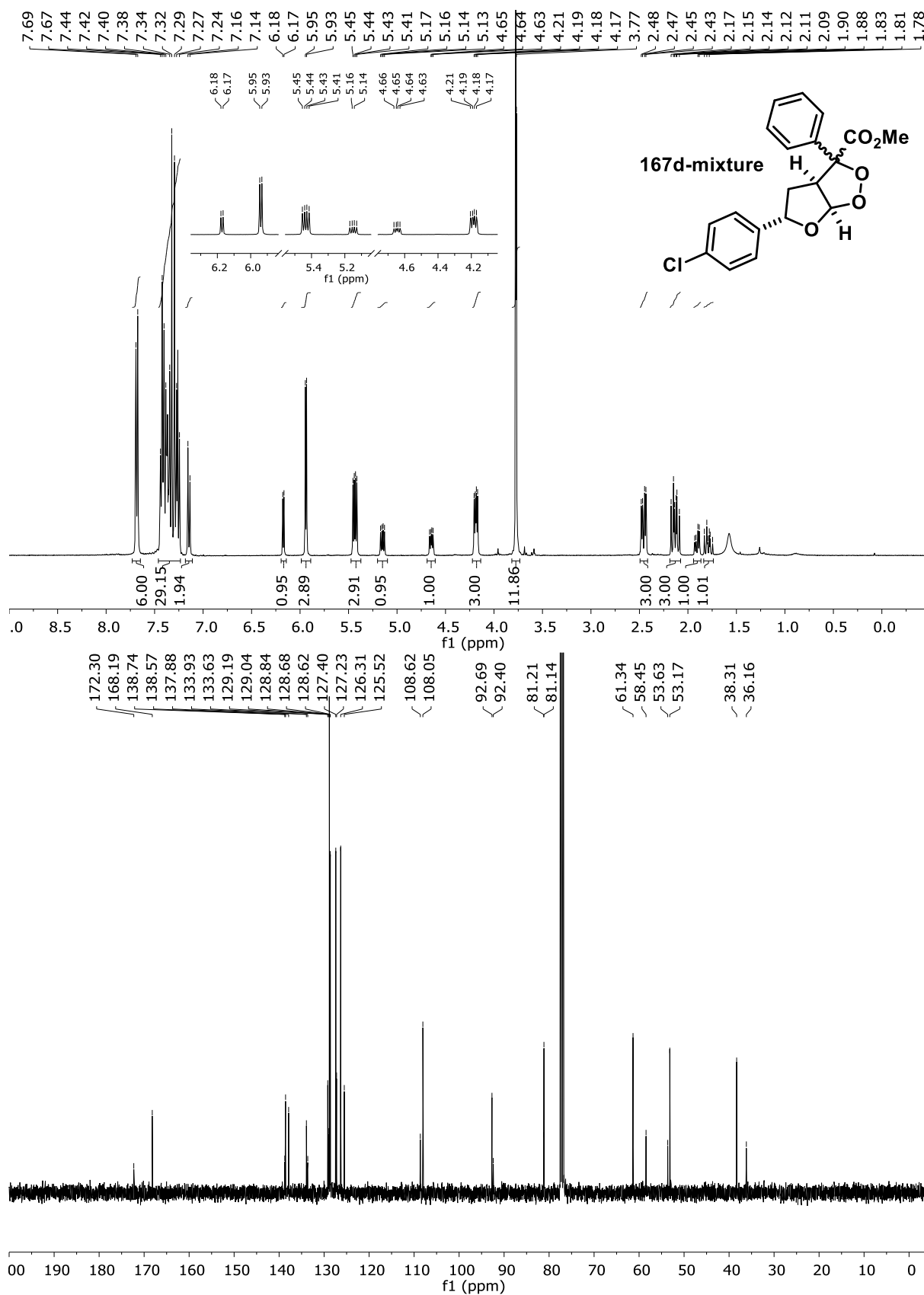


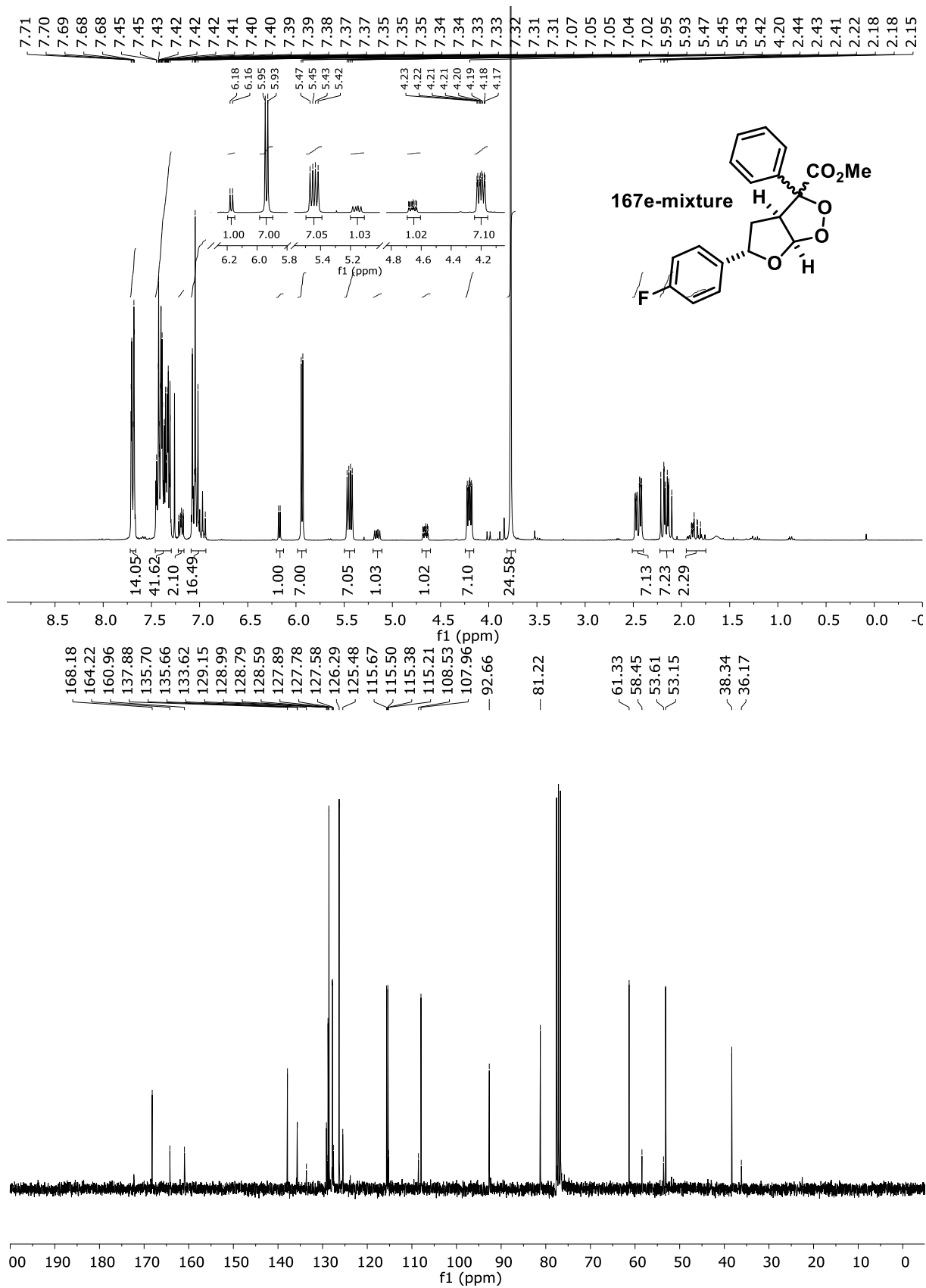




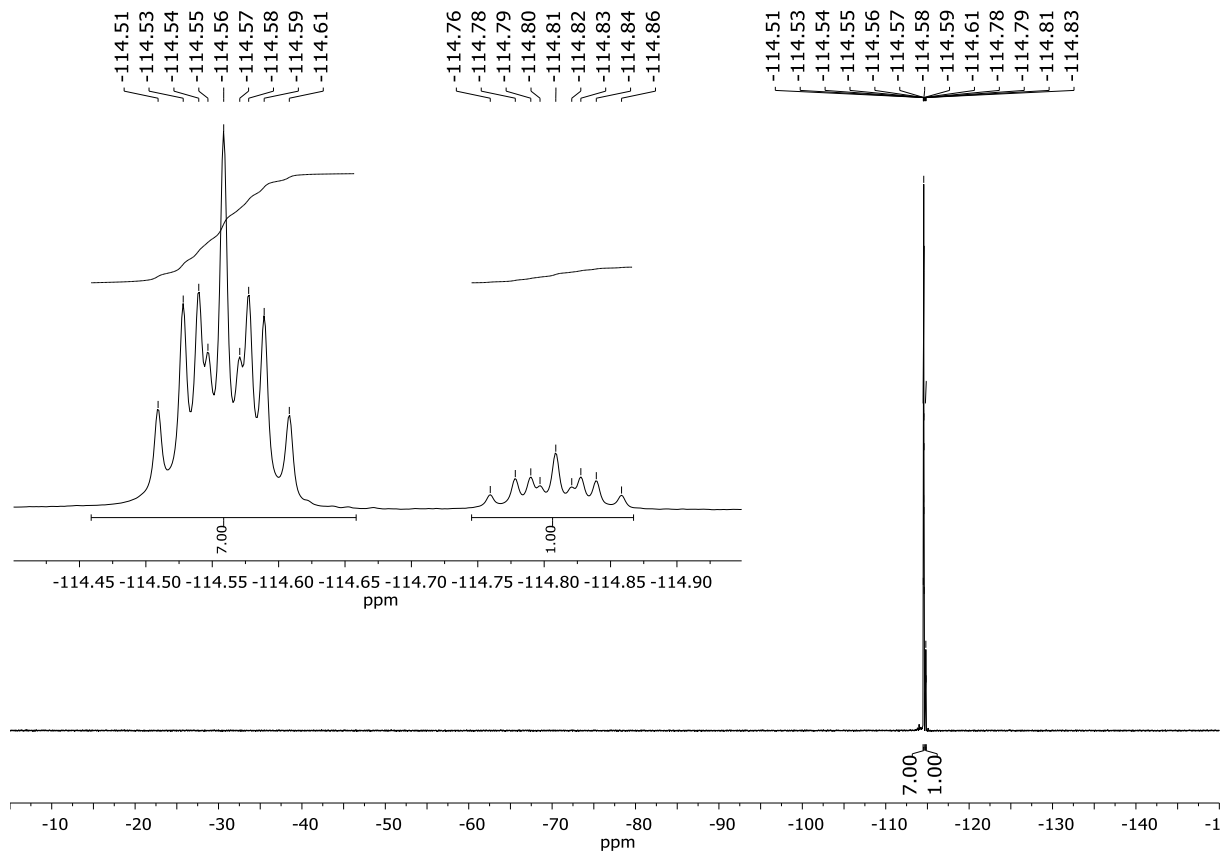
167b-mixture



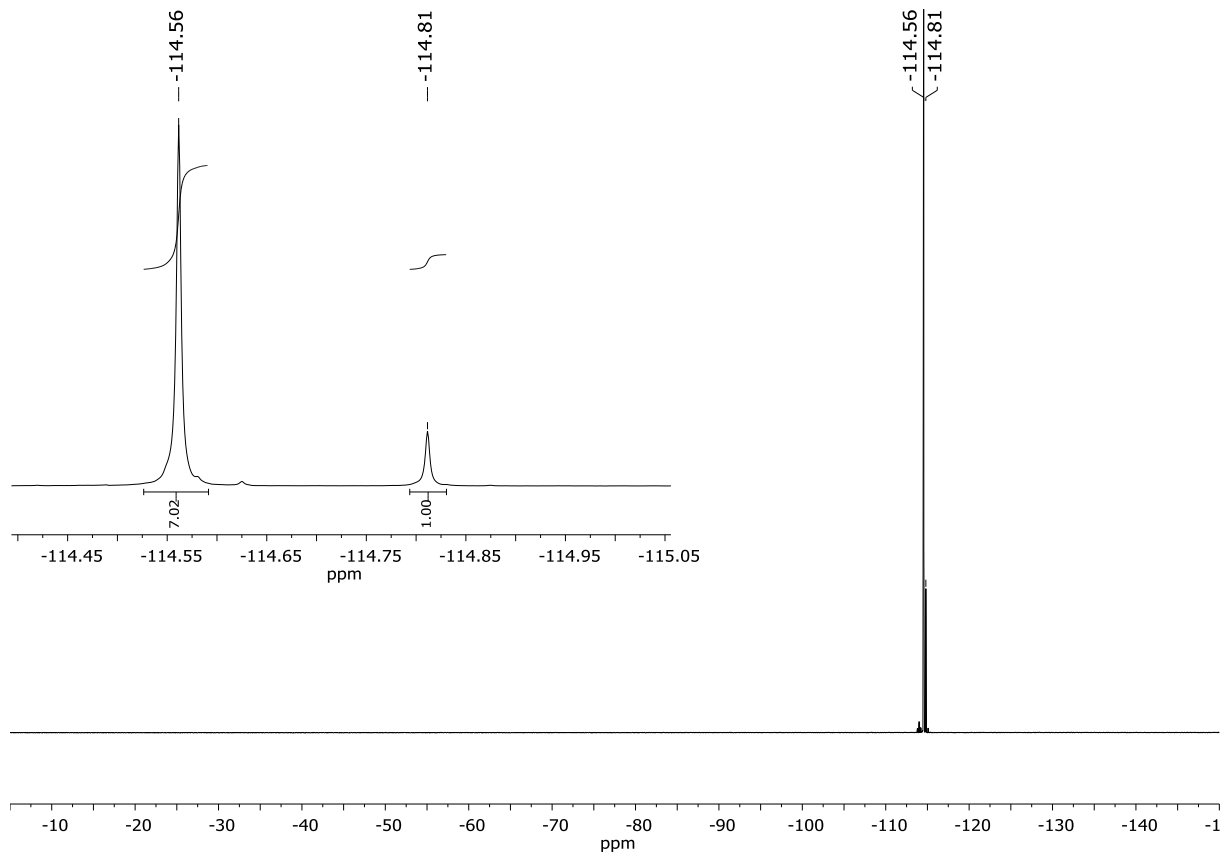


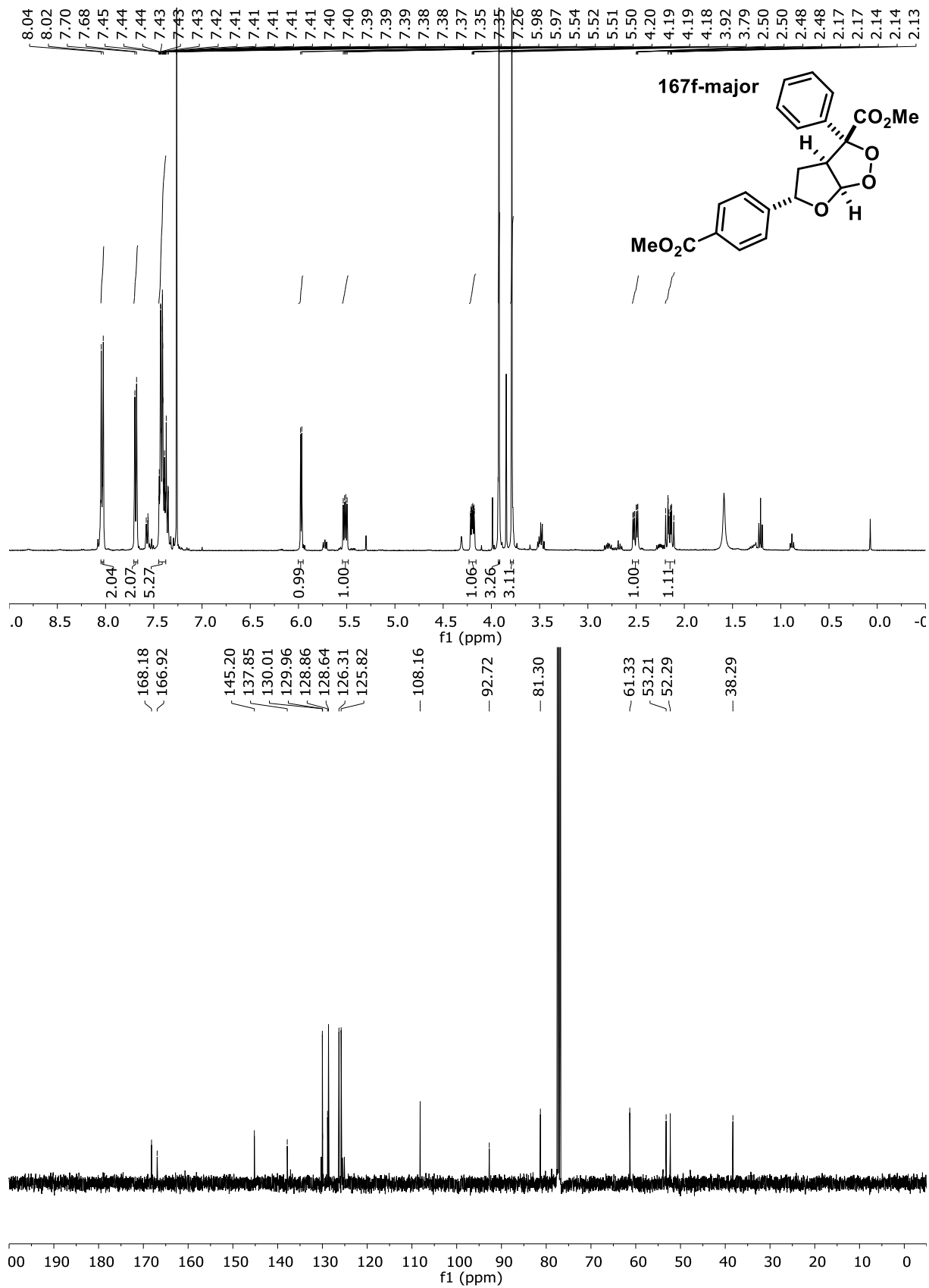


167e-mixture <sup>19</sup>F

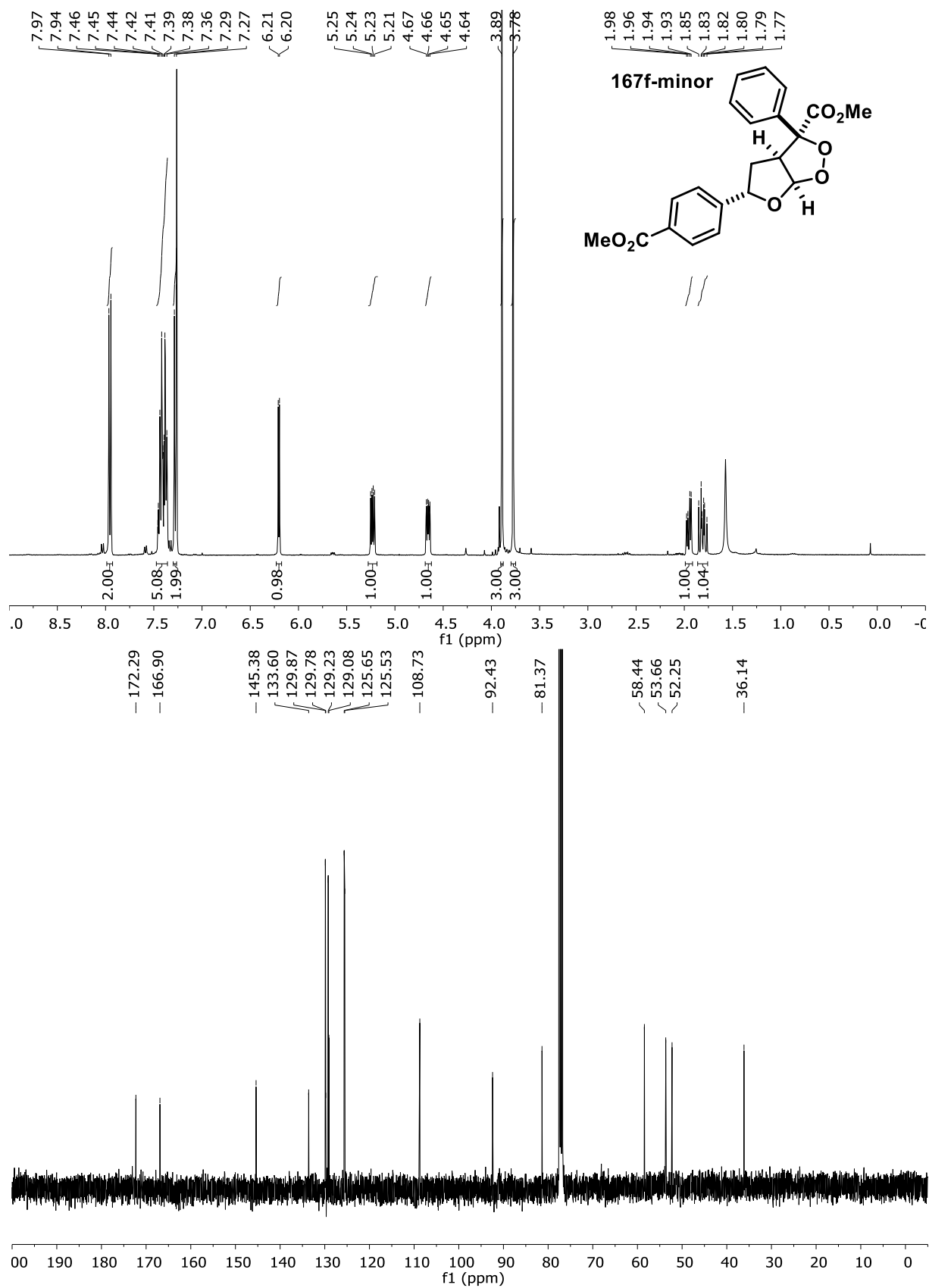


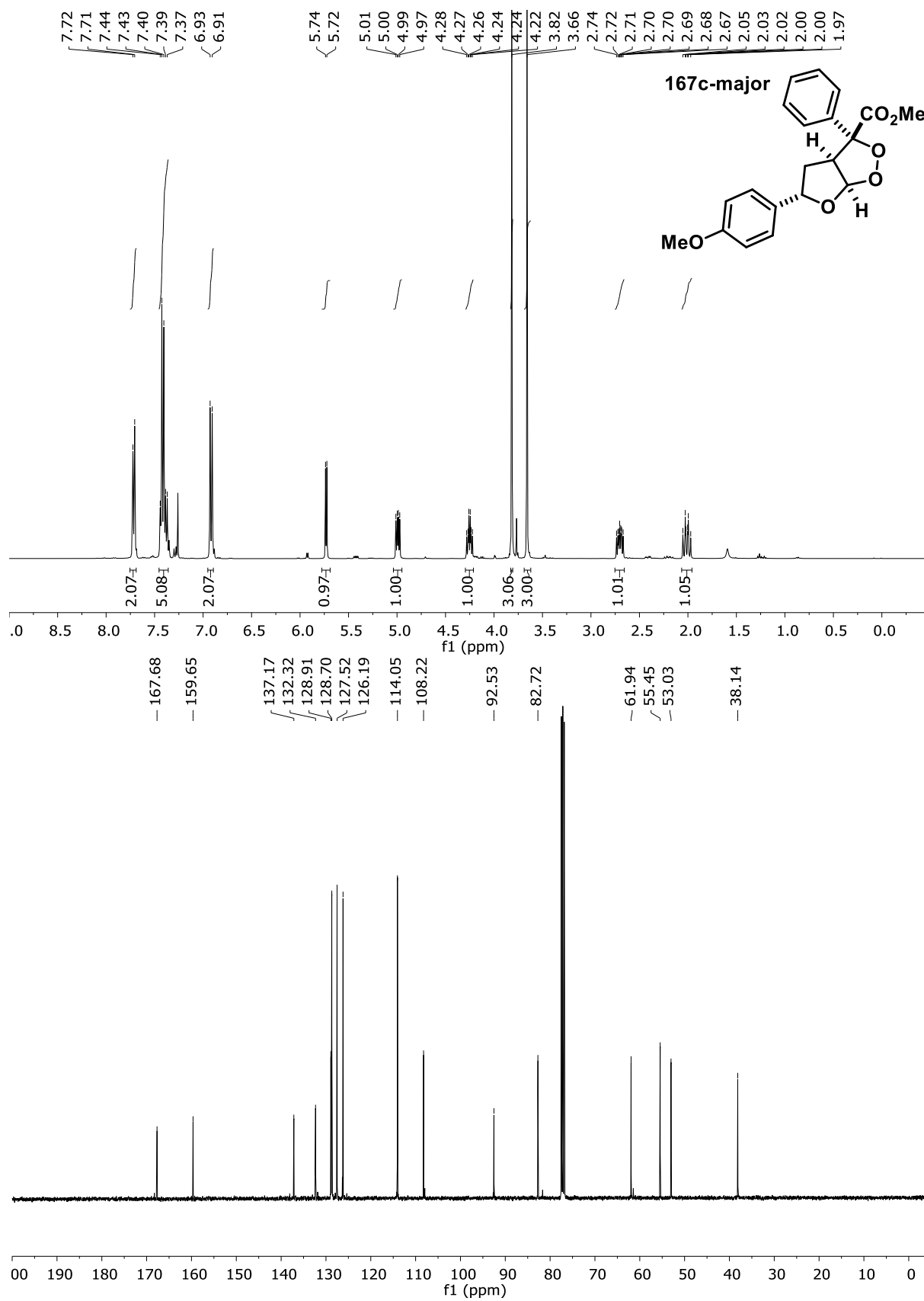
167e-mixture <sup>19</sup>F-CPD

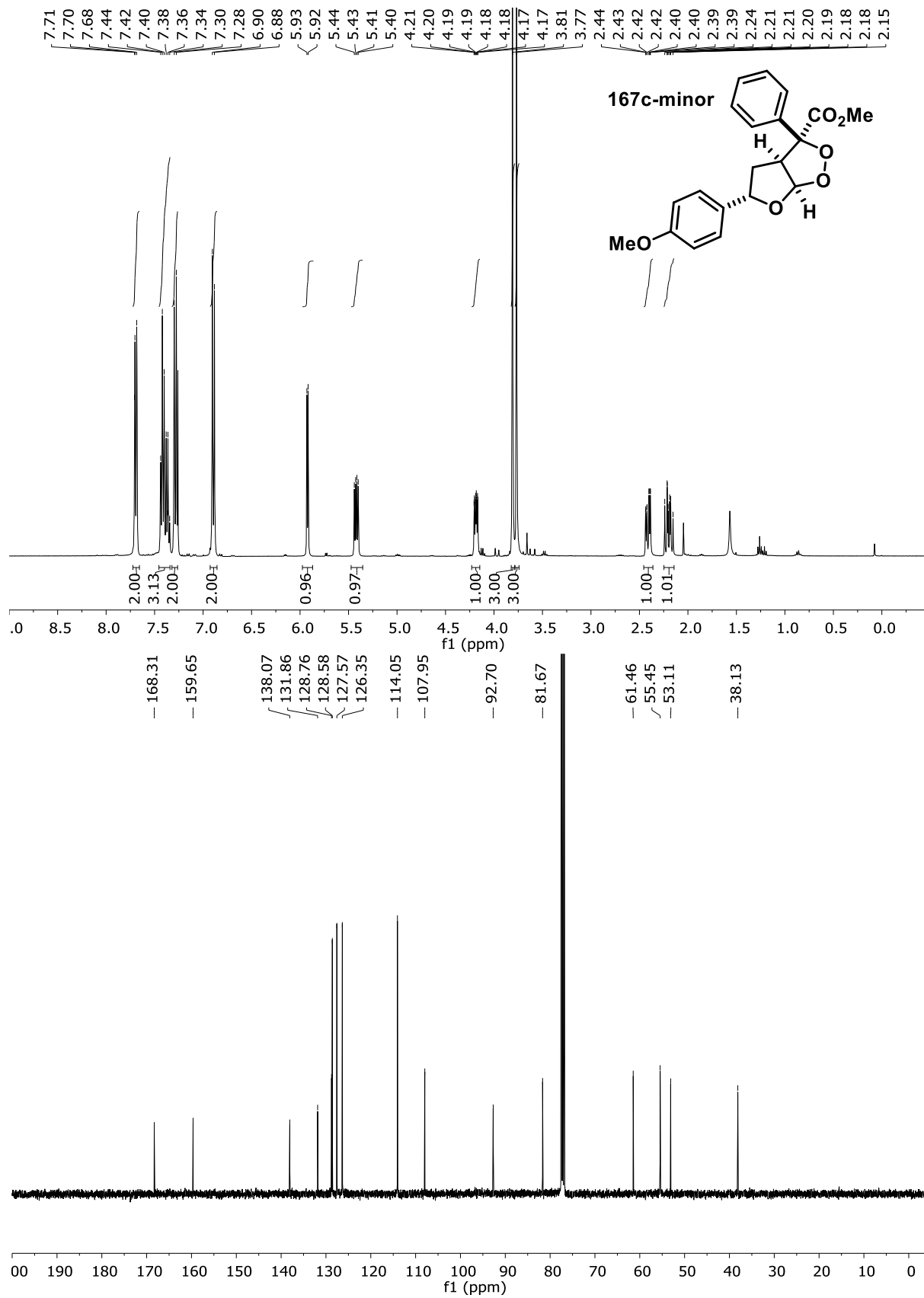


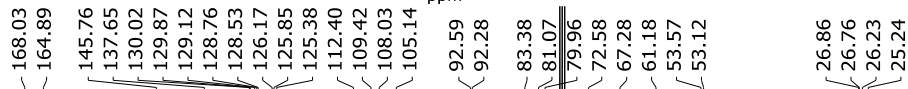
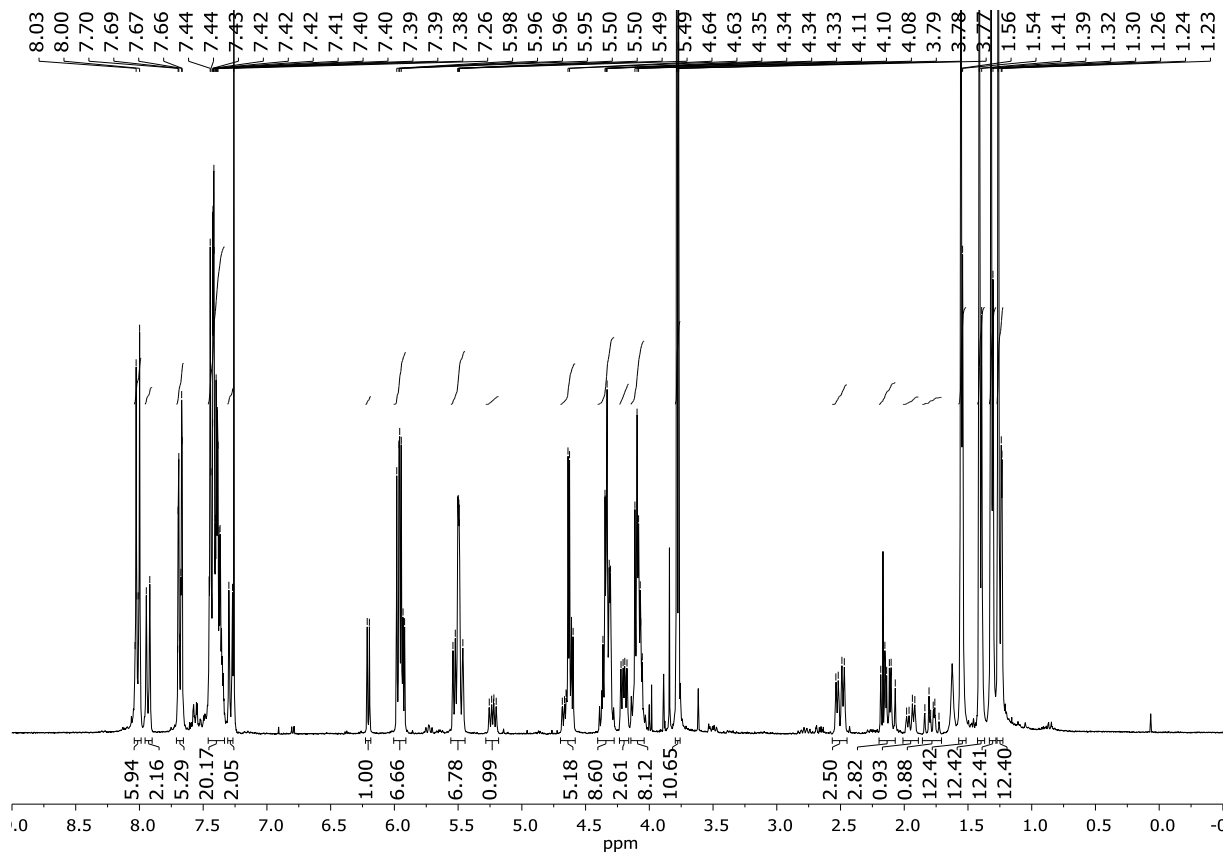




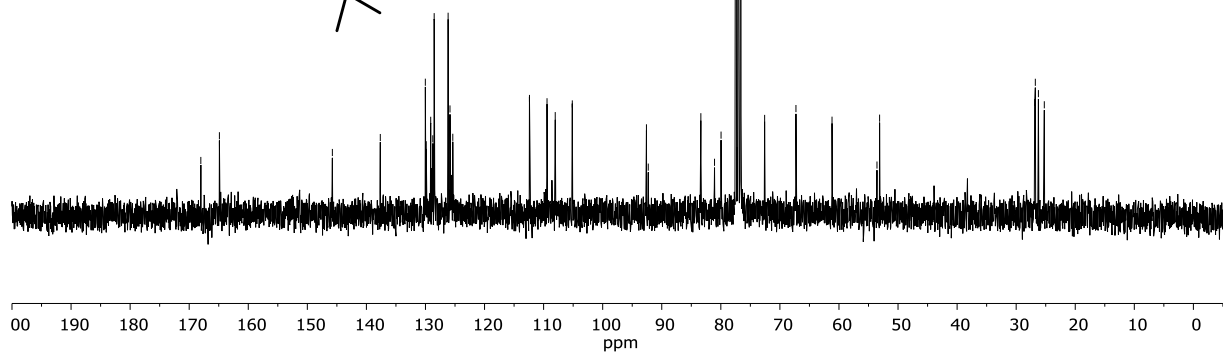
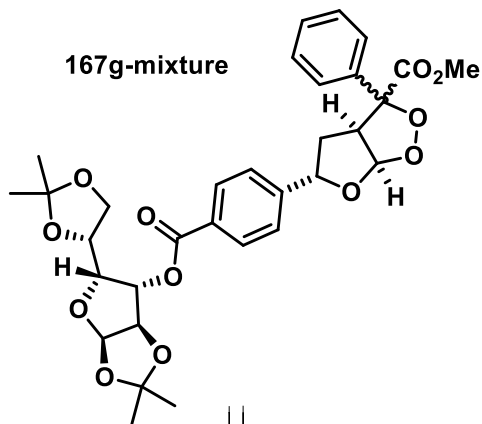


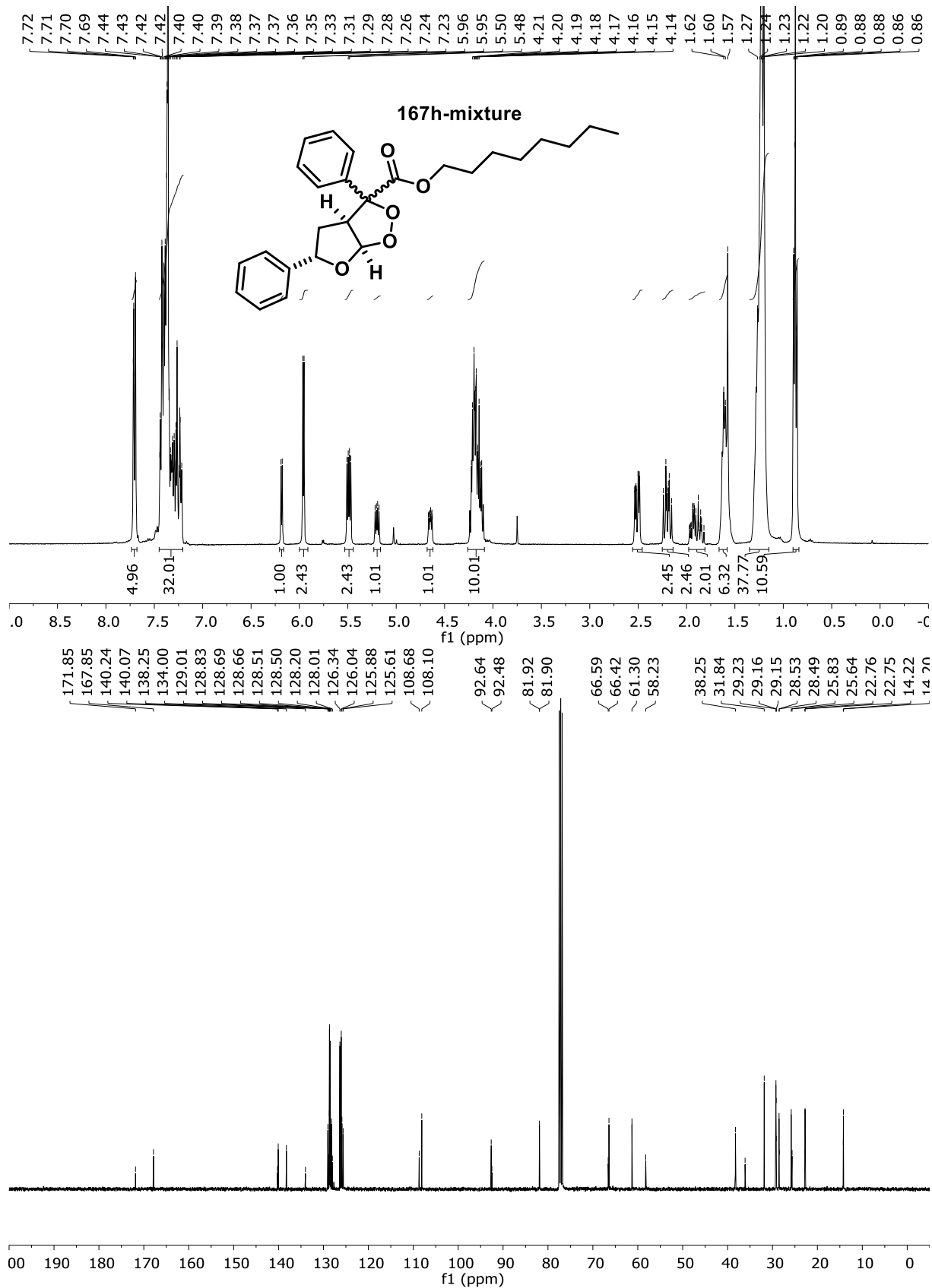


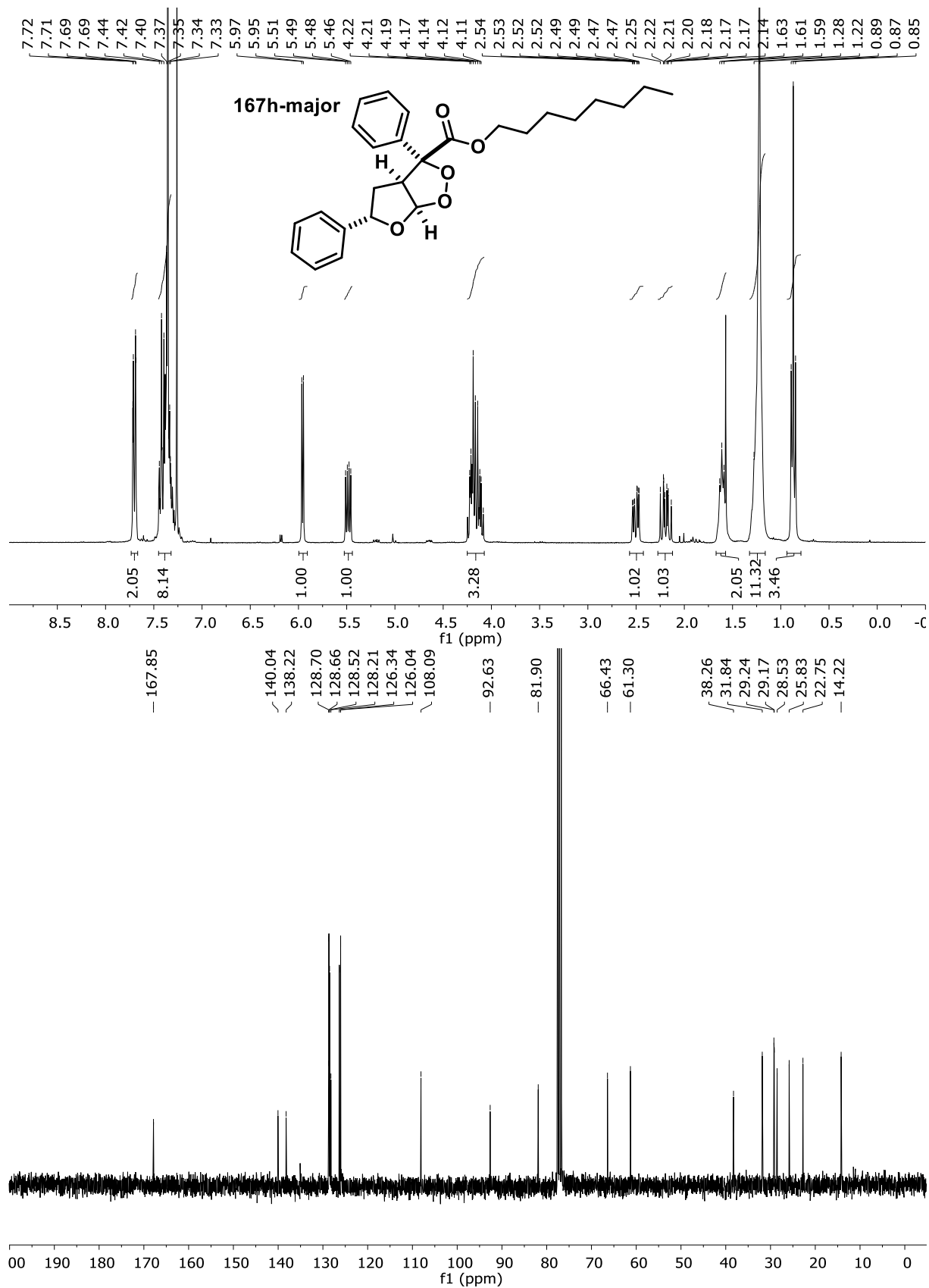


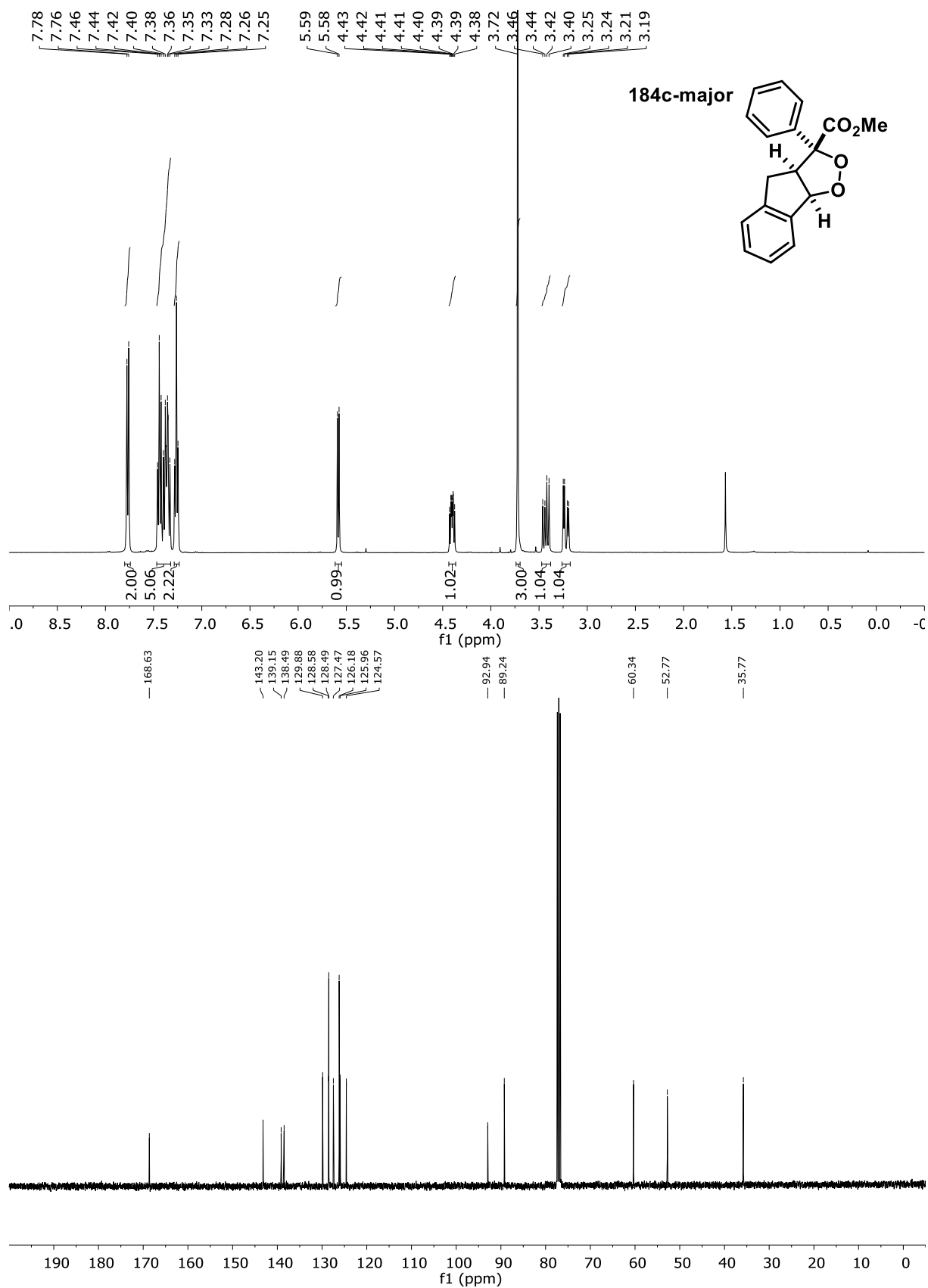


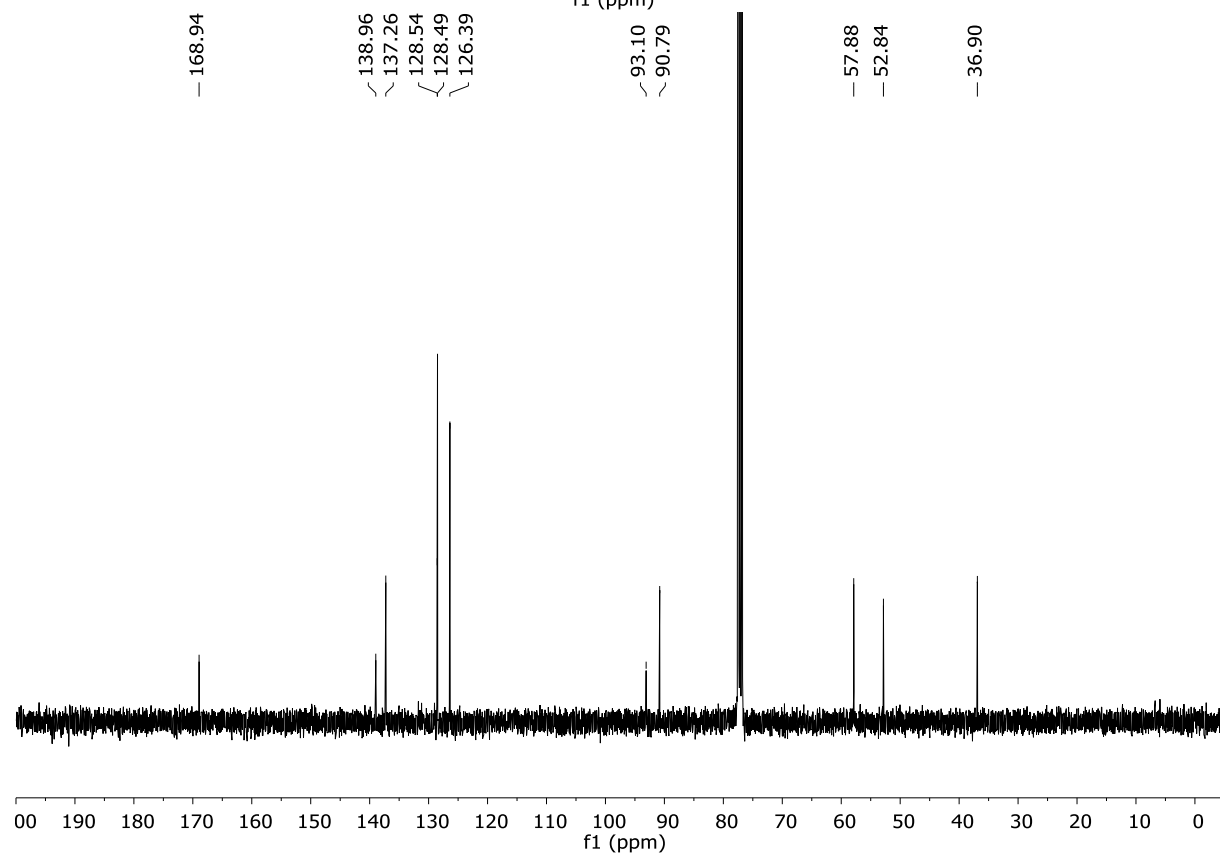
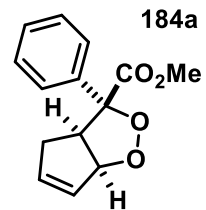
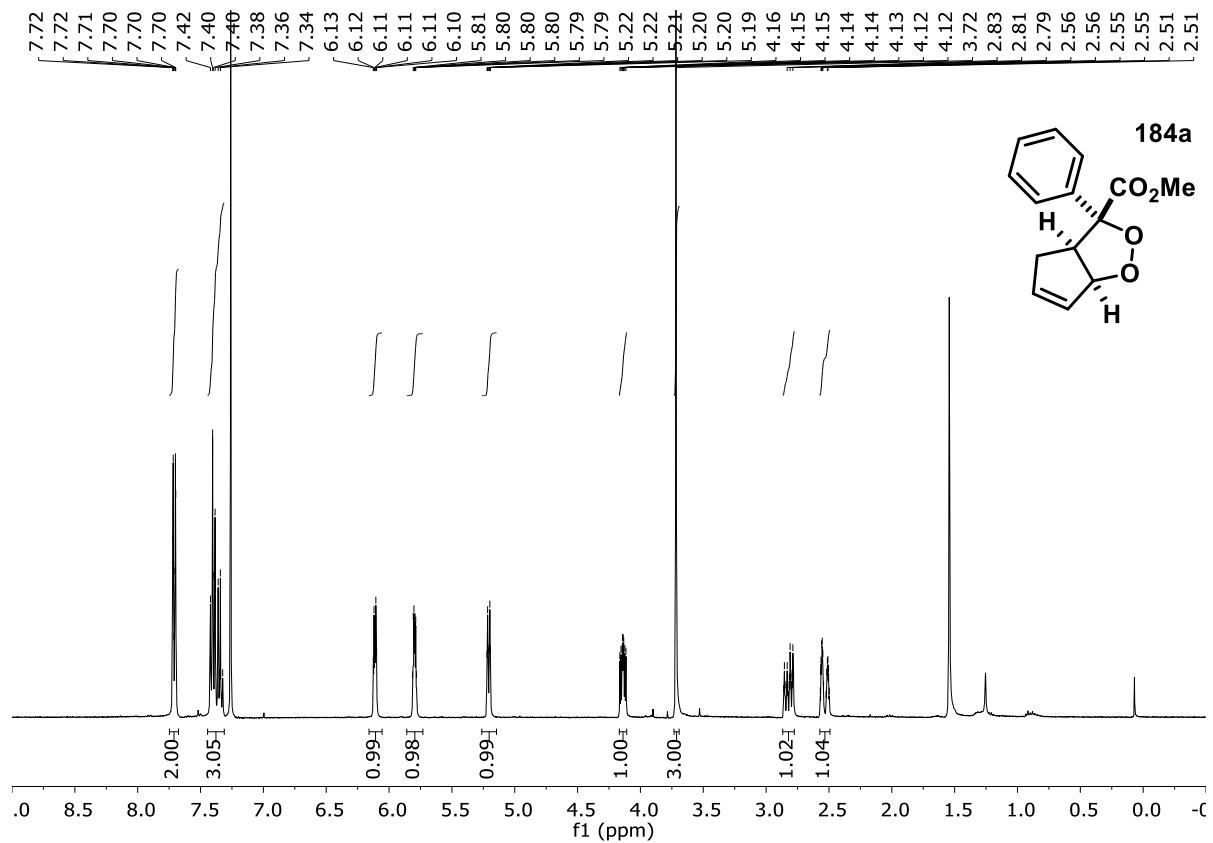
167g-mixture



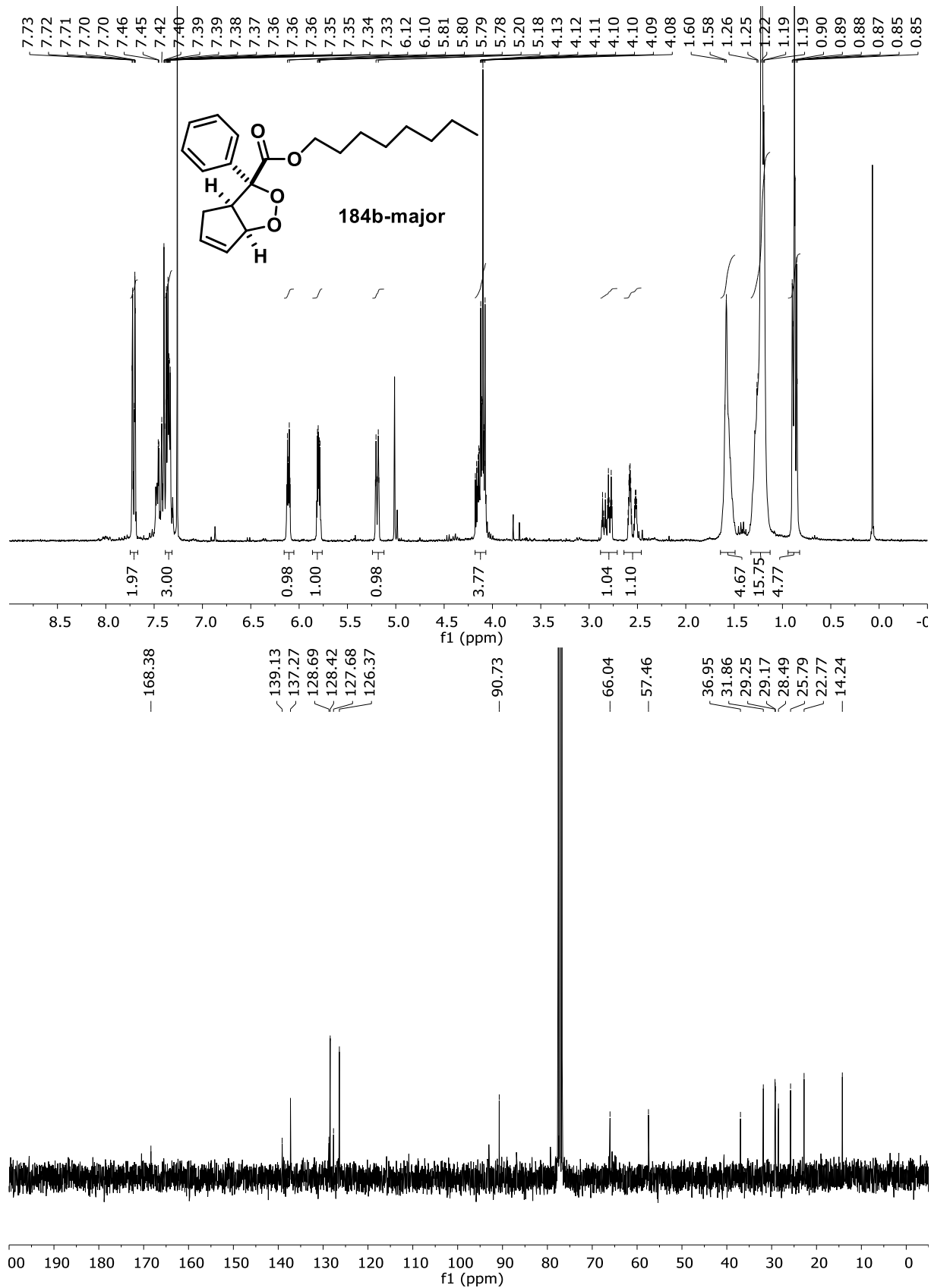


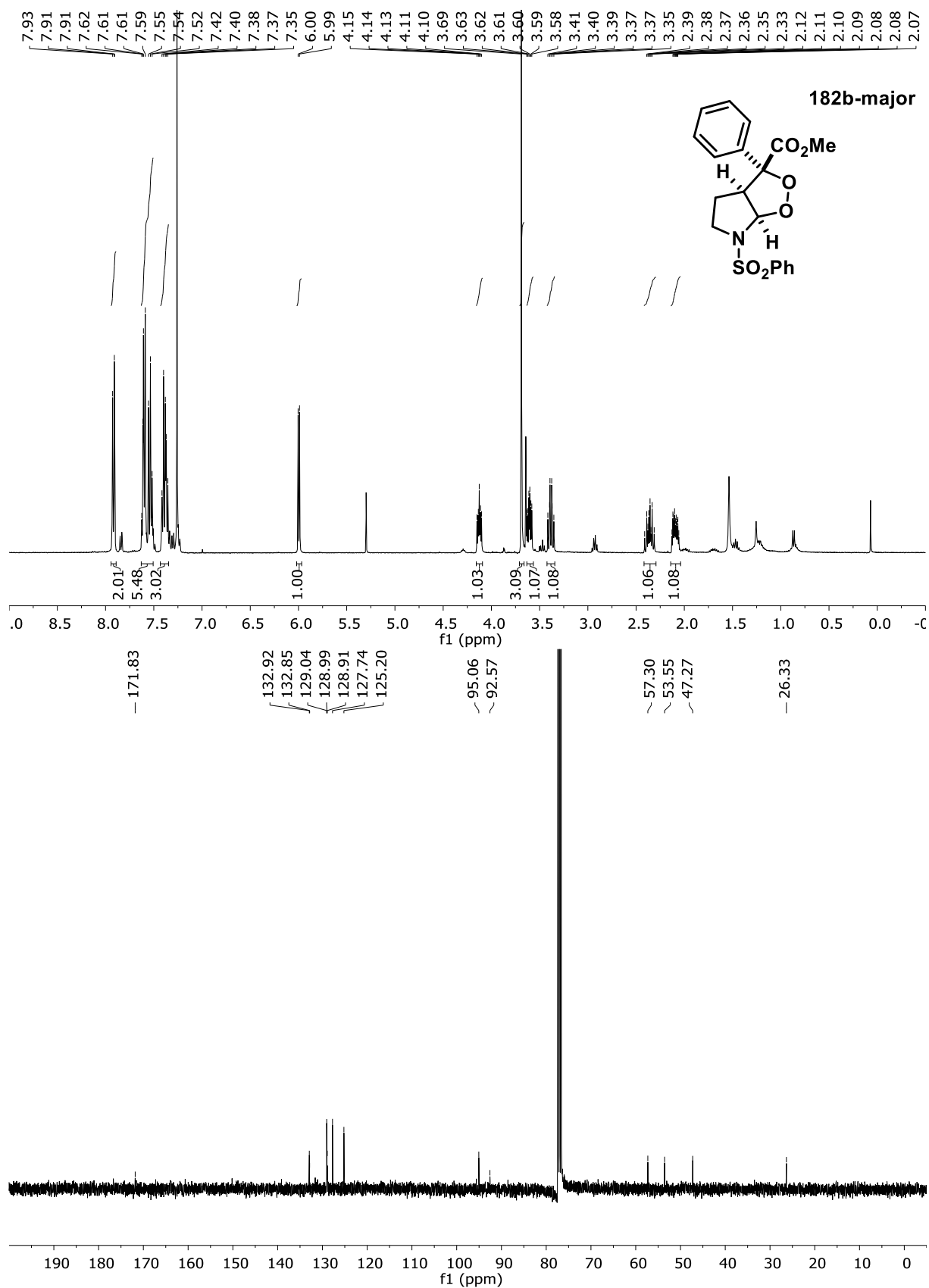


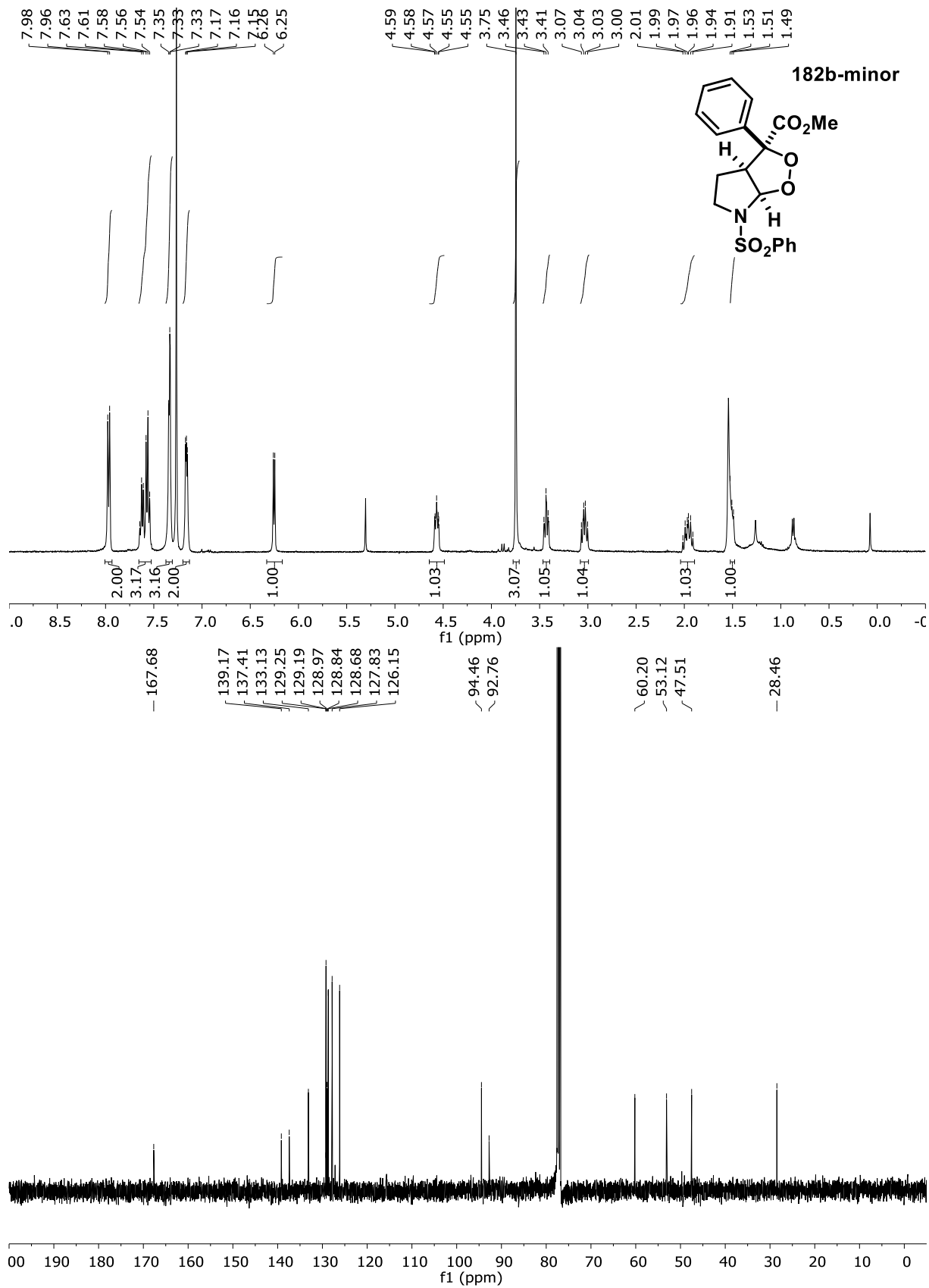


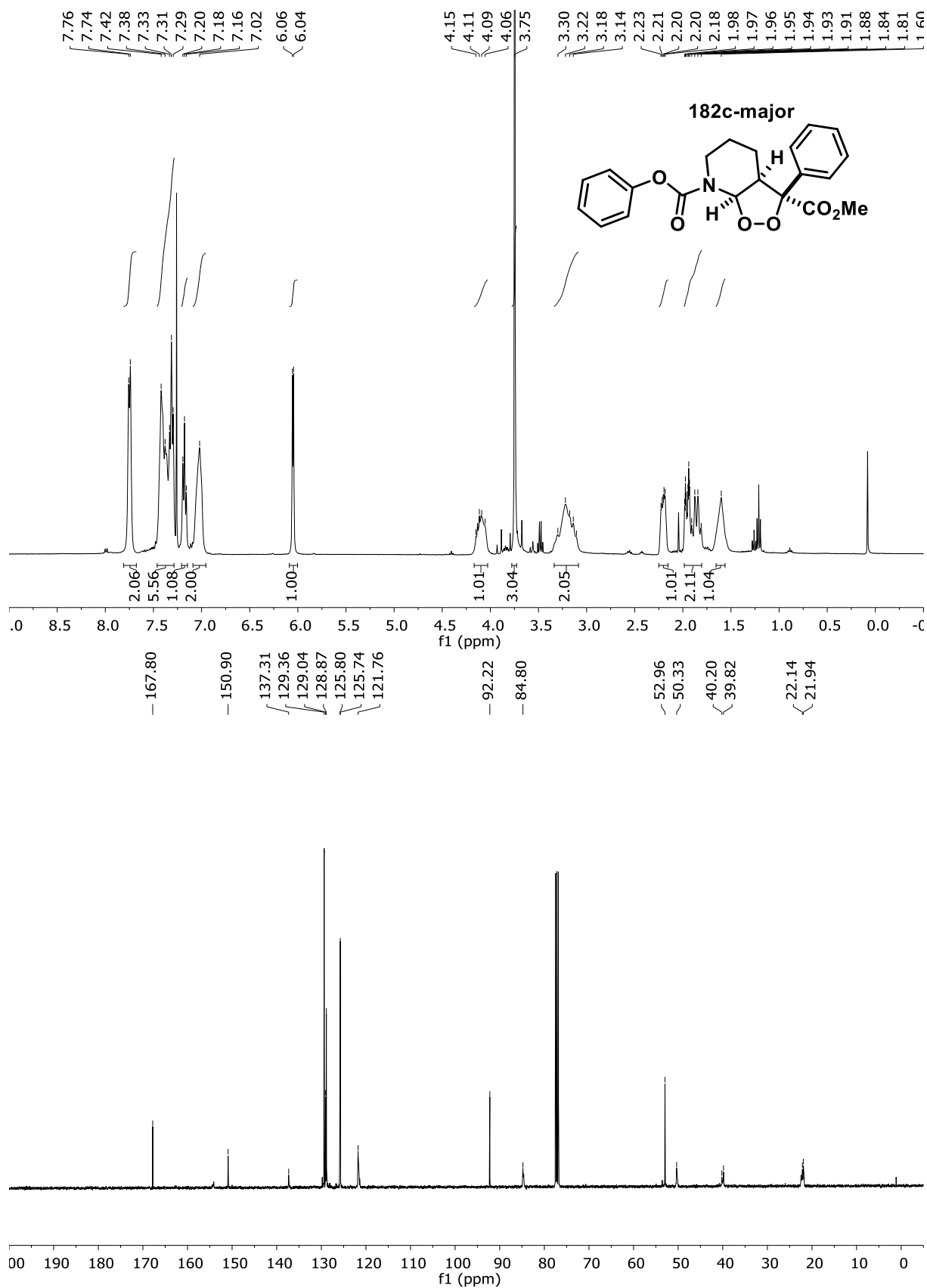




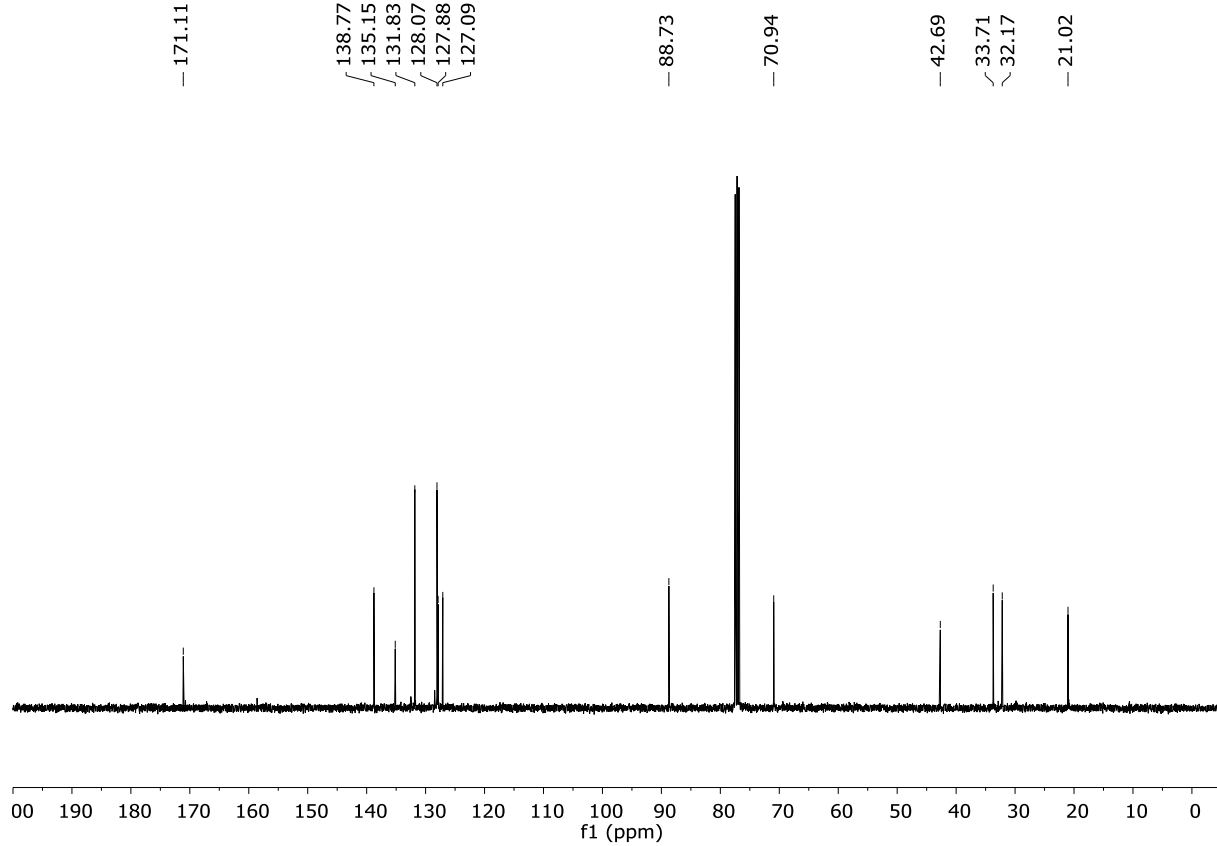
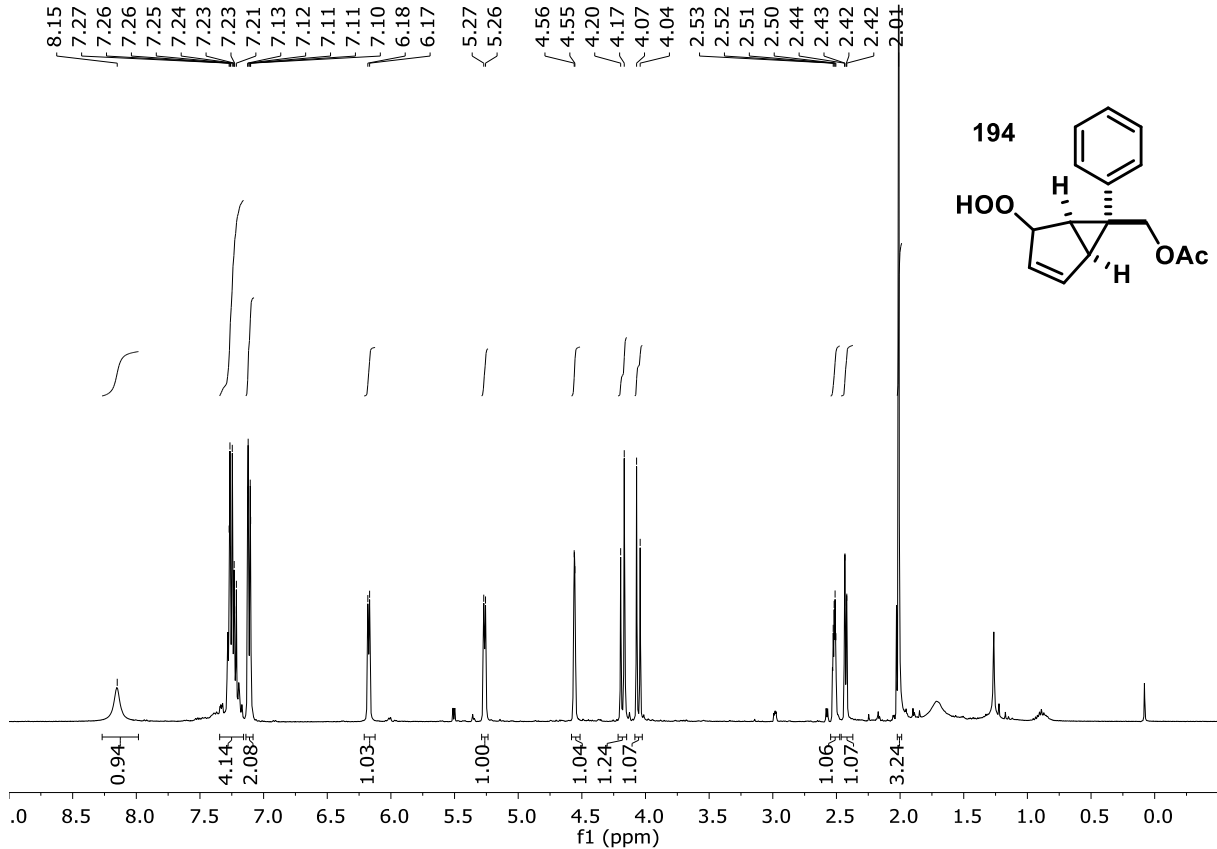


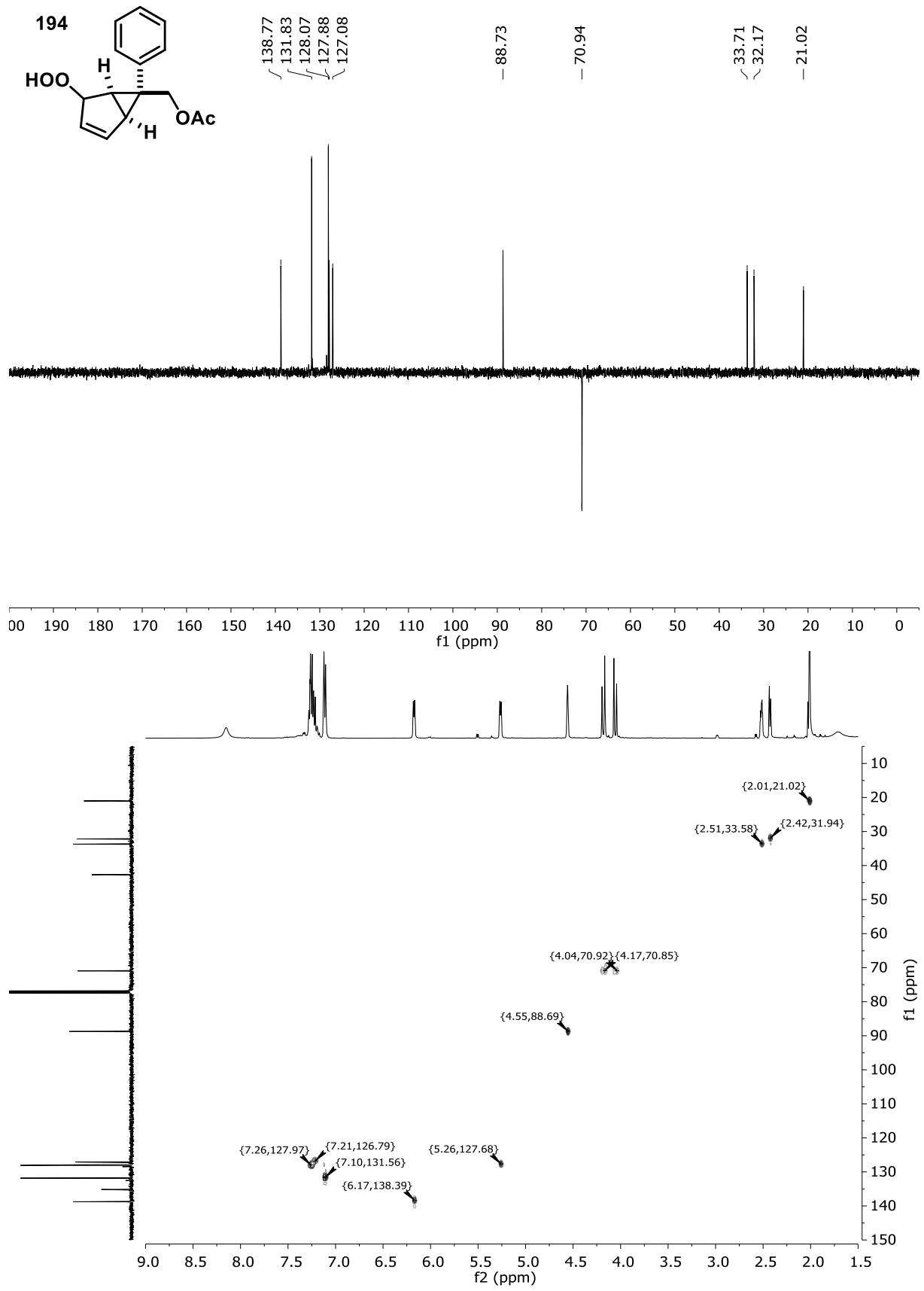


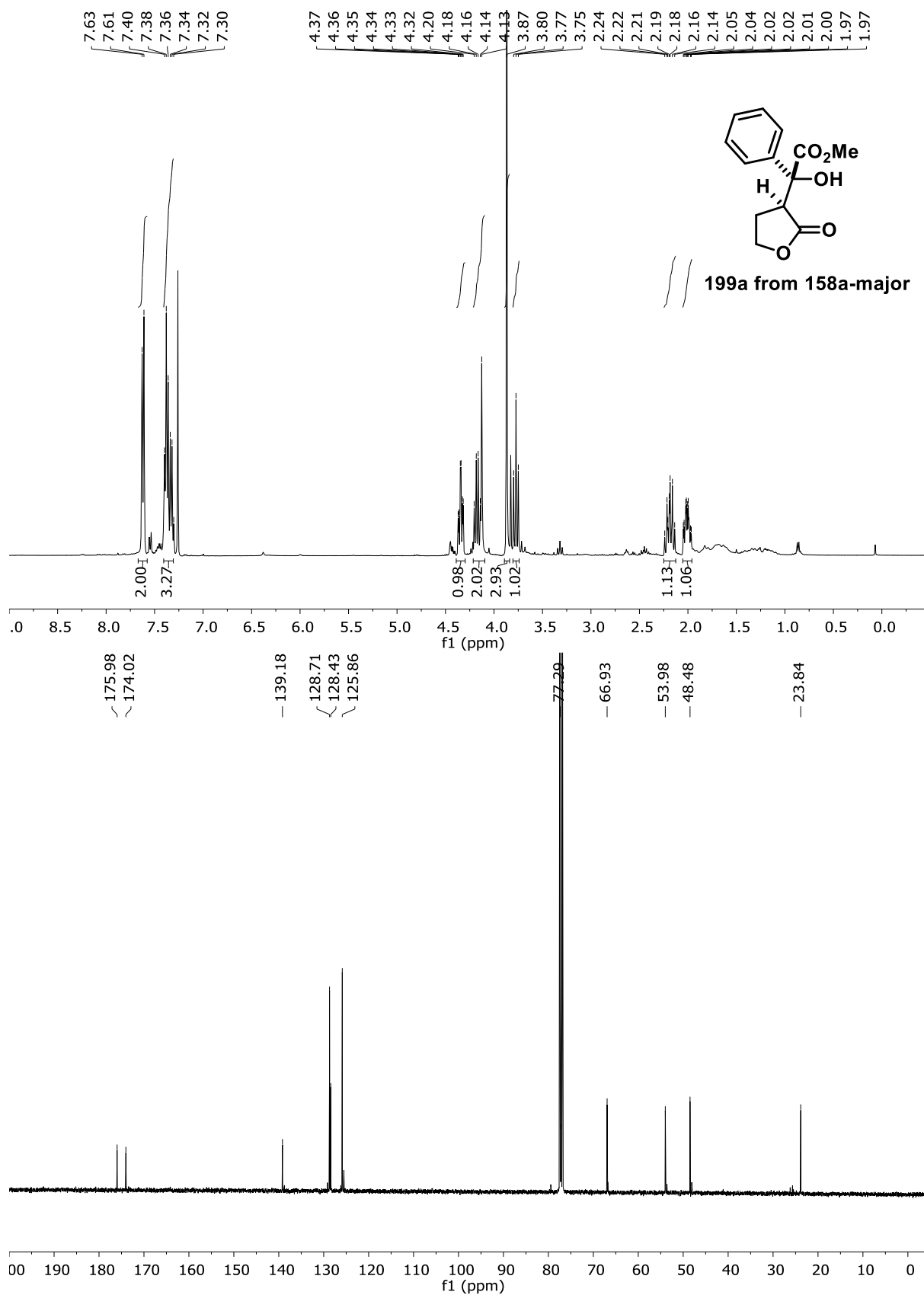


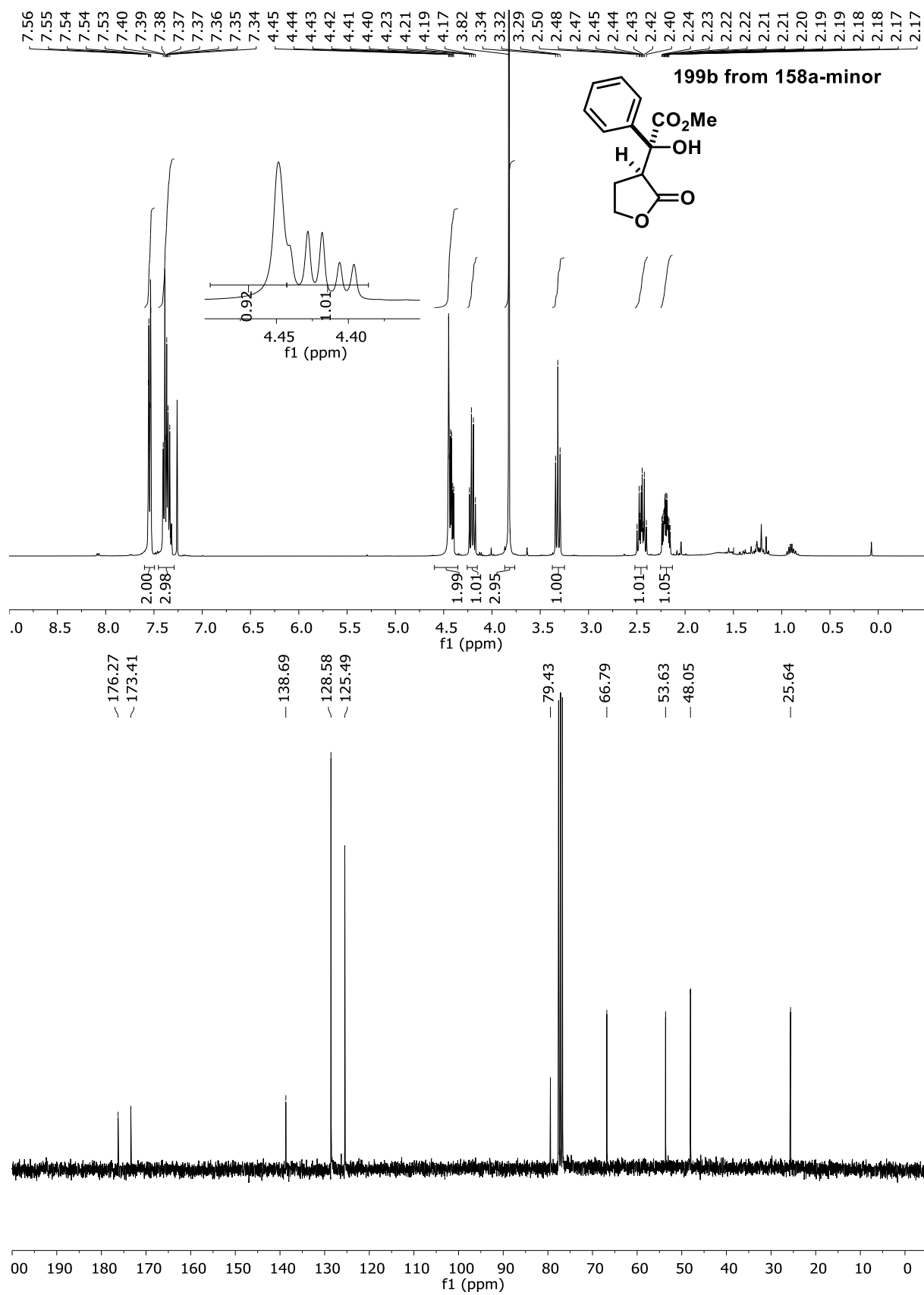


Others

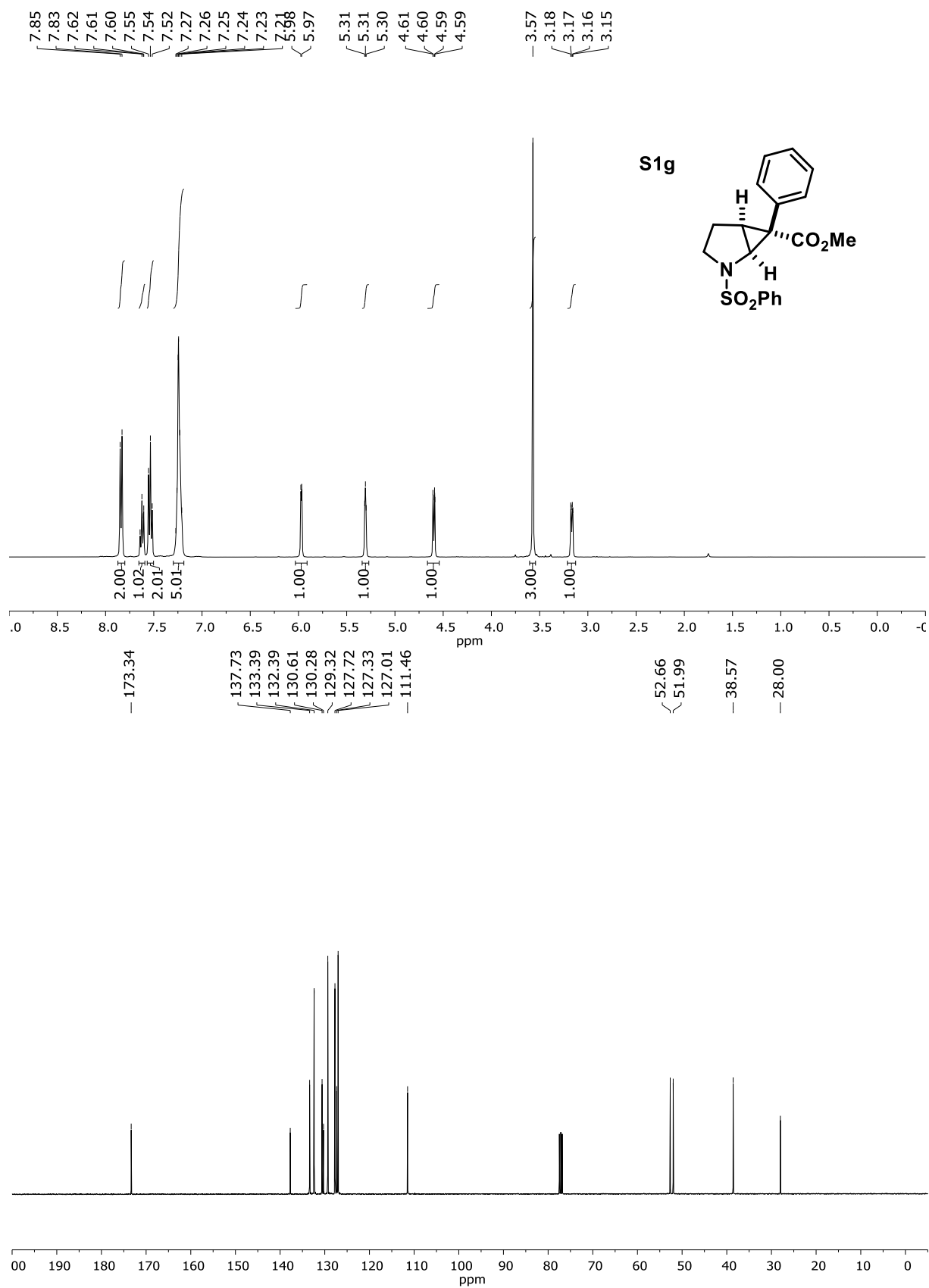


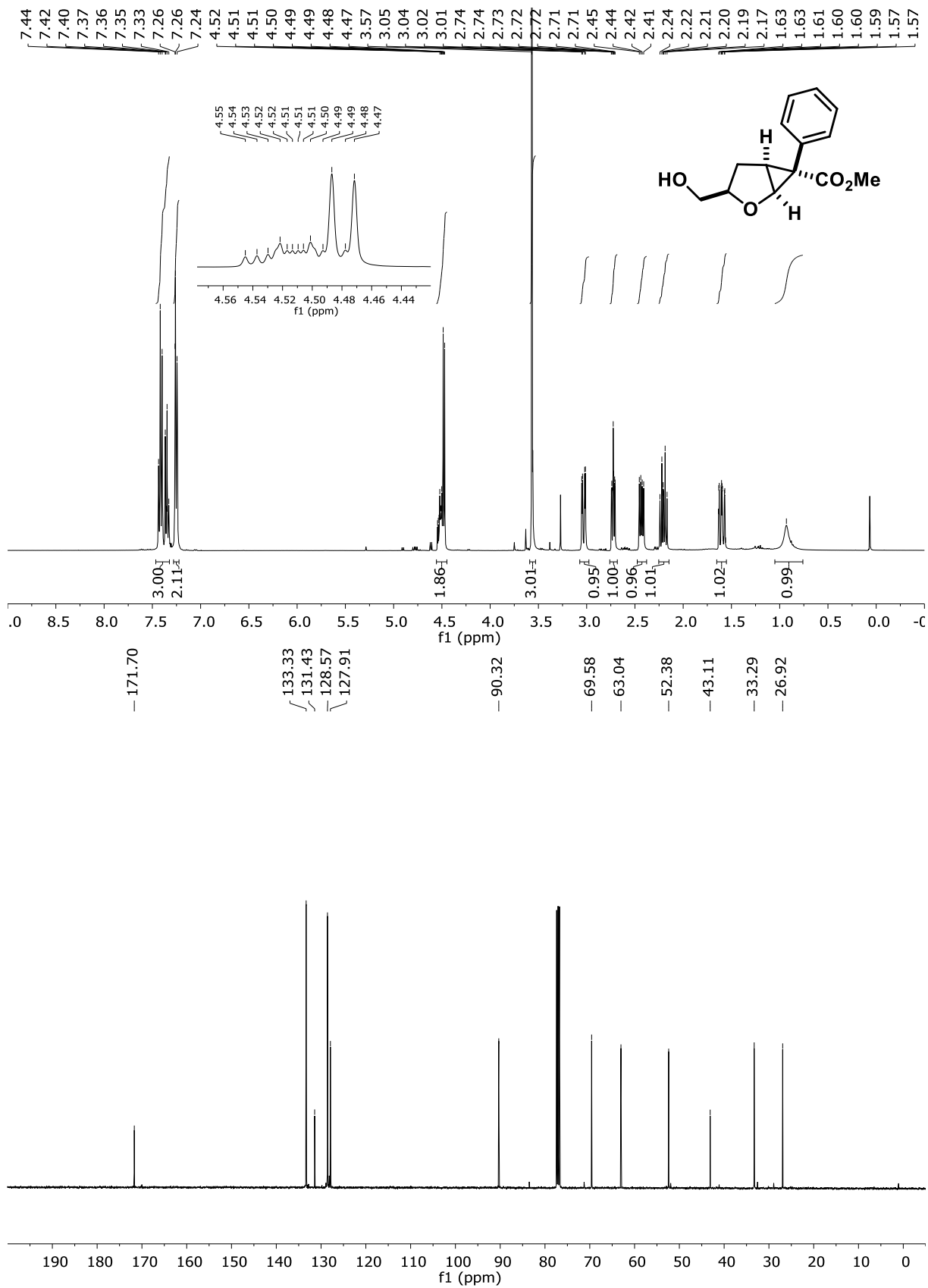


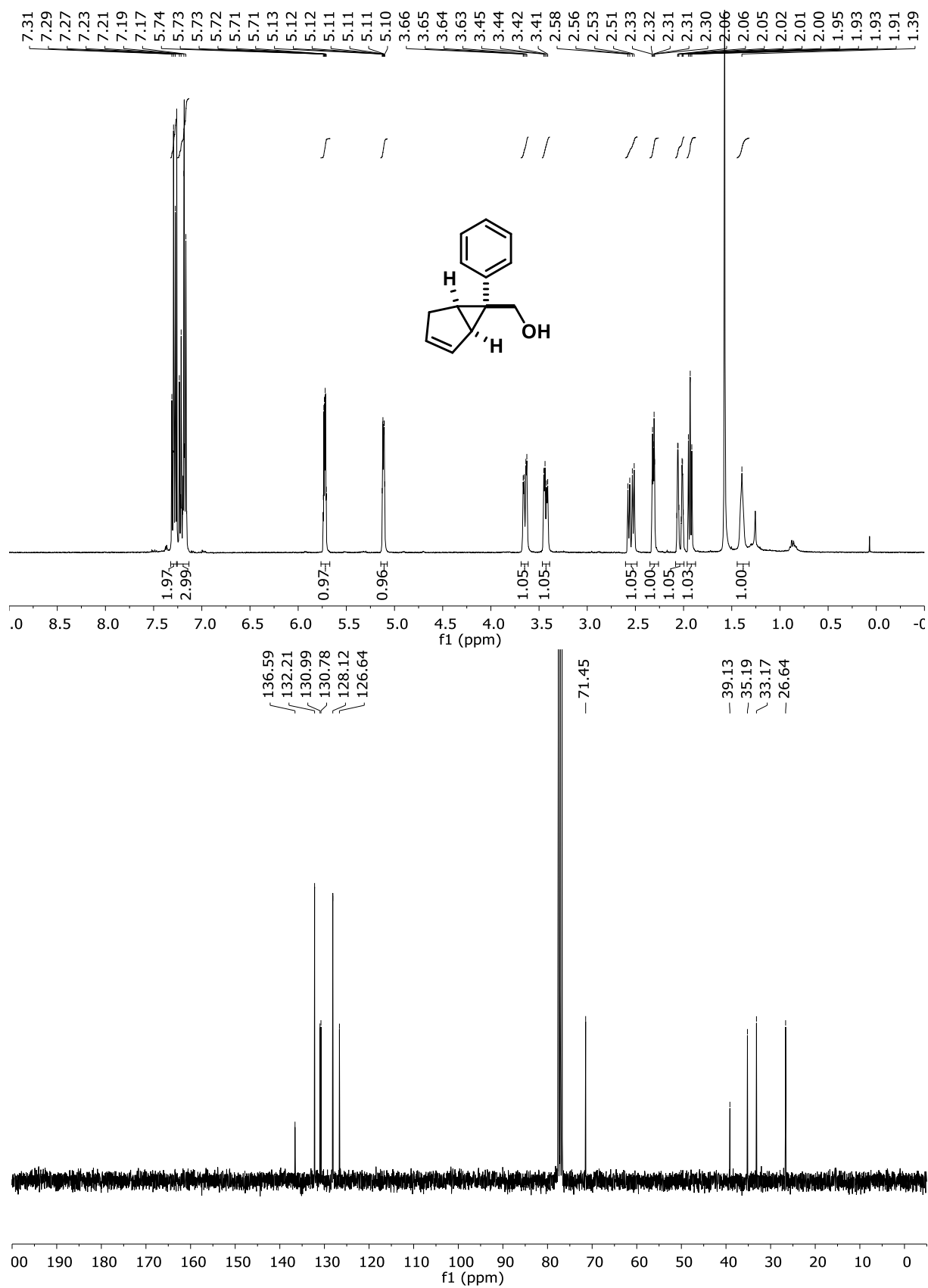












## 4.11 Literature

102. Wiberg, N.; Krieger-Hauwede, M.; Chang, J.-H., *Anorganische Chemie*. Walter de Gruyter & Co: Berlin & New York, 2017.
103. Schmidt-Rohr, K., Oxygen Is this High-Energy Molecule Powering Complex Multicellular Life: Fundamental Corrections to Traditional Bioenergetics. *ACS Omega* **2020**, *5*, 2221-2233.
104. Jones, C. W., *Applications of Hydrogen Peroxide and Derivatives*. Royal Society of Chemistry: Cambridge, 1999.
105. Schimmel&Co, Commercial and scientific notes on essential oils. *Schimmel & Co Semi-Annual Report* **1908**, 109.
106. Schenck, G. O.; Ziegler, K., Die Synthese des Ascaridols. *Die Naturwissenschaften* **1944**, *32*, 157.
107. Nelson, E. K., A Chemical Investigation of the Oli of Chenopodium. *J. Am. Chem. Soc.* **1911**, *33*, 1404-1412.
108. WorldHealthOrganization(WHO), <https://www.who.int/malaria/areas/treatment/overview/en/> **2018**, accessed 09/2019.
109. Paddon, C. J.; Westfall, P. J.; Renninger, N. S.; Newman, J. D. *et.al.*, High-level semi-synthetic production of the potent antimalarial artemisinin. *Nature* **2013**, *496*, 528-537.
110. Haynes, R. K., From Artemisinin to New Artemisinin Antimalarials: Biosynthesis, Extraction, Old and New Derivatives, Stereochemistry and Medicinal Chemistry Requirements. *Cur. Top. Med. Chem.* **2006**, *6*, 509-537.
111. Korshin, E. E.; Bachi, M. D., Synthesis of cyclic peroxides. *PATAI's Chemistry of Functional Groups* **2009**, 1-117.
112. Terentev, A. O.; Borisov, D. A.; Vil, V. A.; Dembitsky, V. M., Synthesis of five- and six-membered cyclic organic peroxides: Key transformations into peroxide ring-retaining products. *Beilstein J. Org. Chem.* **2014**, *10*, 34-114.
113. McCullough, K. J.; Nojima, M., Recent Advances in the Chemistry of Cyclic Peroxides. *Curr. Org. Chem.* **2001**, *5*, 601-636.
114. Meijere, A. d., Bonding Properties of Cyclopropane and Their Chemical Consequences. *Angew. Chem. Int. Ed.* **1979**, *18*, 809-886.
115. Li, Y.; Wang, Q.-L.; Chen, Z.; Zhou, C.-S.; Xiong, B.-Q.; Zhang, P.-L.; Yang, C.-A.; Zhou, Q., Oxidative radical ring-opening/cyclization of cyclopropane derivatives. *Beilstein J. Org. Chem.* **2019**, *15*, 256-278.
116. Wu, W.; Lin, Z.; Jiang, H., Recent advances in the synthesis of cyclopropanes. *Org. Biomol. Chem.* **2018**, *16*, 7315-7329.
117. Ebner, C.; Carreira, E. M., Cyclopropanation Strategies in Recent Total Syntheses. *Chem. Rev.* **2017**, *117*, 11651-11679.
118. Jurberg, I. D.; Davies, H. M. L., Blue light-promoted photolysis of aryldiazoacetates. *Chem. Sci.* **2018**, *9*, 5112-5118.
119. Lehner, V.; Davies, H. M. L.; Reiser, O., Rh(II)-Catalyzed Cyclopropanation of Furans and Its Application to the Total Synthesis of Natural Product Derivatives. *Org. Lett.* **2017**, *19*, 4722-4725.
120. Wimalasena, K.; Wickman, H. B.; Mahindaratne, M. P. D., Autocatalytic Radical Ring Opening of *N*-Cyclopropyl-*N*-phenylamines Under Aerobic Conditions - Exclusive Formation of the Unknown Oxygen Adducts, *N*-(1,2-Dioxolan-3-yl)-*N*-phenylamines. *Eur. J. Org. Chem.* **2001**, 3811-3817.
121. Feldman, K. S.; Simpson, R. E., Oxygenation of Substituted Vinylcyclopropanes: Preparative and Mechanistic Studies. *J. Am. Chem. Soc.* **1989**, *111*, 4878-4886.
122. Wender, P. A.; Takahashi, H.; Witulski, B., Transition Metal Catalyzed [5+2] Cycloadditions of Vinylcyclopropanes and Alkynes: A Homolog of the Diels-Alder Reaction for the Synthesis of Seven-Membered Rings. *J. Am. Chem. Soc.* **1995**, *117*, 4720-4721.
123. Jiao, L.; Yu, Z.-X., Vinylcyclopropane Derivatives in Transition-Metal-Catalyzed Cycloadditions for the Synthesis of Carbocyclic Compounds. *J. Org. Chem.* **2013**, *78*, 6842-6848.

124. Iwama, T.; Matsumoto, H.; Ito, T.; Shimizu, H.; Kataoka, T., Photochemical [3+2] Cycloaddition of 2'-Vinyl-2H-1,4-benzothiazin-3(4H)-one-2-spirocyclopropanes Catalyzed by Diphenyl Dichalcogenides. *Chem. Pharm. Bull.* **1998**, *46*, 913-917.
125. Adam, W.; Birke, A.; Cadiz, C.; Diaz, S.; Rodriguez, A., Prostanoid Endoperoxide Model Compounds: Preparation of 1,2-Dioxolanes from Cyclopropanes. *J. Org. Chem.* **1978**, *43*, 1154-1158.
126. Corey, E. J.; Nicolaou, K. C.; Shibasaki, M.; Machida, Y.; Shiner, C. S., Superoxide Ion as a Synthetically Useful Oxygen Nucleophile. *Tet. Let.* **1975**, *37*, 3183-3186.
127. Corey, E. J., The Logic of Chemical Synthesis: Multistep Synthesis of Complex Carbogenic Molecules - Nobel Lecture. *Angew. Chem. Int. Ed.* **1991**, *30*, 455-612.
128. Hamberg, M.; Svensson, J.; Wakabayashi, T.; Samuelsson, B., Isolation and Structure of Two Prostaglandin Endoperoxides That Cause Platelet Aggregation. *Proc. Natl. Acad. Sci. USA* **1974**, *71*, 345-349.
129. Nixon, J. R.; Cudd, M. A.; Porter, N. A., Cyclic Peroxides by Intramolecular Peroxymercuration of Unsaturated Hydroperoxides. *J. Org. Chem.* **1978**, *43*, 4048-4052.
130. Dussault, P.; Sahli, A.; Westermeyer, T., An Organometallic Approach to Peroxyketals. *J. Org. Chem.* **1993**, *58*, 5469-5474.
131. Tokuyasu, T.; Ito, T.; Masuyama, A.; Nojima, M., Synthesis of 3-Hydroperoxy (or Hydroxy)-substituted 1,2-Dioxanes and 1,2-Dioxepanes by the Ozonolysis of Unsaturated Hydroperoxy Acetals. *Heterocycles* **2000**, *53*, 1305-1316.
132. Payne, G. B.; Smith, C. W., Hydrogen Peroxide. III. Tungstic Acid Catalyzed Hydroxylation of Cyclohexene in Nonaqueous Media. *J. Org. Chem.* **1957**, *22*, 1682-1685.
133. Jefford, C. W.; Ferro, F.; Moulin, M. C.; Velarde, J.; Jaggi, D.; Kohmoto, S.; Richardson, G. D.; al., e., New chemistry involving 1,2,4-trioxanes related to Qinghaosu. *New Trends Nat. Prod.* **1986**, *26*, 163-183.
134. O'Neill, P. M.; Rawe, S. L.; Borstnik, K.; Miller, A.; Ward, S. A.; Bray, P. G.; Davies, J.; Oh, C. H.; Posner, G. H., Enantiomeric 1,2,4-Trioxanes Display Equivalent in vitro Antimalarial Activity Versus Plasmodium falciparum Malaria Parasites: Implications for the Molecular Mechanism of Action of the Artemisinins. *ChemBioChem* **2005**, *6*, 2048-2054.
135. Avery, M. A.; Jennings-White, C.; Chong, W. K. M., Simplified Analogues of the Antimalarial Artemisinin: synthesis of 6,9-Desmethylartemisinin. *J. Org. Chem.* **1989**, *54*, 1792-1795.
136. Dussault, P. H.; Liu, X., SnCl<sub>4</sub>-mediated reaction of ozonides with allyltrimethylsilane: formation of 1,2-dioxolanes. *Tet. Let.* **1999**, *40*, 6553-6556.
137. Baader, W. J.; Bastos, E. L., Product subclass 3: five-membered cyclic peroxides with no further heteroatoms in the ring (1,2-dioxolanes and 1,2-dioxolan-3-ones). In *Science of Synthesis*, 2009; Vol. 38, pp 345-378.
138. Singh, R.; Ishar, M. P. S., UV irradiation of arylidene-b-ionones in the presence of dioxygen: regioselective formation of stable endoperoxides. *Tet. Let.* **2003**, *44*, 1943-1945.
139. Ramirez, A.; Woerpel, K. A., Synthesis of 1,2-Dioxolanes by Annulation Reactions of Peroxycarbenium Ions with Alkenes. *Org. Lett.* **2005**, *7*, 4617-4620.
140. Lu, Z.; Parrish, J. D.; Yoon, T. P., [3+2] Photooxygenation of Aryl Cyclopropanes via Visible Light Photocatalysis. *Tetrahedron* **2014**, *70*, 4270-4278.
141. Mizuno, K.; Kamiyama, N.; Ichinose, N.; Otsuji, Y., Photo-oxygenation of 1,2-diarylcyclopropanes via electron transfer. *Tetrahedron* **1985**, *41*, 2207-2214.
142. Yedoyan, J.; Wurzer, N.; Klimczak, U.; Ertl, T.; Reiser, O., Regio- and Stereoselective Synthesis of Functionalized Dihydropyridines, Pyridines, and 2H-Pyrans: Heck Coupling of Monocyclopropanated Heterocycles. *Angew. Chem. Int. Ed.* **2019**, *58*, 3594-3598.
143. Weisser, R.; Yue, W.; Reiser, O., Enantioselective Synthesis of Furo[2,3-*b*]furans, a Spongiane Diterpenoid Substructure. *Org. Lett.* **2005**, *7*, 5353-5356.
144. Beumer, R.; Reiser, O., *beta*-Aminocyclopropanecarboxylic acids with *alpha*-amino acid side chain functionality. *Tetrahedron* **2001**, *57*, 6497-6503.

145. Schinnerl, M.; Böhm, C.; Seitz, M.; Reiser, O., New bis(oxazoline) ligands with secondary binding sites for the asymmetric cyclopropanation of furans. *Tetrahedron: Asymmetry* **2003**, *14*, 765-771.
146. Reiser, O., Catalytic Conversions of Furans and Pyrroles to Natural Products and Analogues Utilizing Donor-Acceptor Substituted Cyclopropanes as Key Intermediates. *Isr. J. Chem.* **2016**, *56*, 531-539.
147. Xu, Z.-J.; Wittlin, S.; Wu, Y., Probing the Peroxycarbenium [3+2] Cycloaddition Reactions with 1,2-Disubstituted Ethylenes: Results and Insights. *Chem. Eur. J.* **2017**, *23*, 2031-2034.
148. Joshi-Pangu, A.; Levesque, F.; Roth, H. G.; Oliver, S. F.; Campeau, L.-C.; Nicewicz, D. A.; DiRocco, D. A., Acridinium-Based Photocatalysts: A Sustainable Option in Photoredox Catalysis. *J. Org. Chem.* **2016**, *81*, 7244-7249.
149. Budde, S.; Goerdeler, F.; Floß, J.; Kreitmeier, P.; Hicks, E. F.; Moscovitz, O.; Seeberger, P. H.; Davies, H. M. L.; Reiser, O., Visible-light mediated oxidative ring expansion of anellated cyclopropanes to fused endoperoxides with antimalarial activity. *Org. Chem. Front.* **2020**, *7*, 1789-1795.
150. Jefferey, T.; David, M., [Pd/Base/QX] catalyst systems for directing Heck-type reactions. *Tetrahedron Letters* **1998**, *39*, 5751-5754.
151. Thompson, J. L.; Davies, H. M. L., Enhancement of Cyclopropanation Chemistry in the Silver-Catalyzed Reactions of Aryldiazoacetates. *J. Am. Chem. Soc.* **2007**, *129*, 6090-6091.
152. Terent'ev, A. O.; Vil', V. A.; Demchuk, D. V.; Terent'ev, A. O., Rearrangements of organic peroxides and related processes. *Beilstein J. Org. Chem.* **2016**, *12*, 1647-1748.
153. Mizuno, K.; Ichinose, N.; Otsuji, Y., Cis-Trans Photoisomerization and Photooxygenation of 1,2-Diarylcyclopropanes. Salt Effects on the Photoinduced electron Transfer Reactions. *Chem. Lett.* **1985**, 455-458.
154. Tanielian, C., Dye-sensitized photooxygenations. *Biochimie* **1986**, *68*, 797-806.
155. Mizuno, K.; Tamai, T.; Hashida, I.; Otsuji, Y.; Kuriyama, Y.; Tokumaru, K., Photooxygenation of 1, $\omega$ -Bis(diarylethenyl)alkanes via Photoinduced Electron-Transfer: Formation of 1,4-Radical Cations and Its Trapping by Molecular Dioxide. *J. Org. Chem.* **1994**, *59*, 7329-7334.
156. Tamai, T.; Mizuno, K.; Hashida, I.; Otsuji, Y., Salt Effect on the 9,10-Dicyanoanthracene-Sensitized Photooxygenation of 1,2-Diarylcyclopropanes and the Photodecomposition of 3,5-Diaryl-1,2-dioxolanes. *J. Org. Chem.* **1992**, *57*, 5338-5342.
157. Gesmundo, N. J.; Grandjean, J.-M. M.; Nicewicz, D. A., Amide and Amine Nucleophiles in Polar Radical Crossover Cycloadditions: Synthesis of  $\gamma$ -Lactams and Pyrrolidines. *Org. Lett.* **2015**, *17*, 1316-1319.
158. Mizuno, K.; Otsuji, Y., Addition and Cycloaddition Reactions via Photoinduced Electron Transfer  
Electron Transfer I. *Top. Curr. Chem.* **1994**, *169*, 301-346.
159. Schmidt, M. W.; Baldrige, K. K.; Boatz, J. A.; Elbert, S. T.; Gordon, M. S.; Jensen, J. H.; Koseki, S.; Matsunaga, N.; Nguyen, K. A.; Su, S.; Windus, T. L.; Dupuis, M.; Montgomery, J. A., General Atomic and Molecular Electronic Structure System. *J. Comput. Chem.* **1993**, *14*, 1347-1363.
160. Gordon, M. S.; Schmidt, M. W., Advances in electronic structure theory: GAMESS a decade later. In *Theory and Applications of Computational Chemistry: the first forty years*, Dykstra, C. E.; Frenking, G.; Kim, K. S.; Scuseria, G. E., Eds. Elsevier: Amsterdam, 2005; pp 1167-1189.
161. Humphrey, W.; Dalke, A.; Schulten, K., VMD - Visual Molecular Dynamics. *J. Molec. Graphics* **1996**, *14*, 33-38.
162. WorldHealthOrganization(WHO), [https://www.who.int/malaria/media/artemisinin\\_resistance\\_qa/en/](https://www.who.int/malaria/media/artemisinin_resistance_qa/en/), **2019**, accessed 10/2019.
163. Kotani, H.; Ohkubo, K.; Fukuzumi, S., Photocatalytic Oxygenation of Anthracenes and Olefins with Dioxide via Selective Radical Coupling Using 9-Mesityl-10-methylacridinium Ion as an Effective Electron-Transfer Photocatalyst. *J. Am. Chem. Soc.* **2004**, *126*, 15999-16006.

164. Lowry, M. S.; Goldsmith, J. I.; Slinker, J. D.; Rohl, R.; jr, R. A. P.; Malliaras, G. G.; Bernhard, S., Single-Layer Electroluminescent Devices and photoinduced Hydrogen Production from an Ionic Iridium(III) Complex. *Chem. Mater.* **2005**, *17*, 5712-5719.
165. Sheldrick, G. M., Crystal structure refinement with SHELXL. *Acta Cryst.* **2015**, *C71*, 3-8.
166. Dolomanov, O. V.-.; Bourhis, L. J.; Gildea, R. J.; Howard, J. A. K.; Puschmann, J., OLEX2: a complete structure solution, refinement and analysis program. *J. Appl. Cryst.* **2009**, *42*, 339-341.
167. Dery, V.; Duah, N. O.; Ayanful-Torgby, R.; Matrevi, S. A.; Anto, F.; Quashie, N. B., An improved SYBR Green-1-based fluorescence method for the routine monitoring of *Plasmodium falciparum* resistance to anti-malarial drugs. *Malar. J* **2015**, *14*, 481-486.
168. Radfar, A.; Mendez, D.; Moneriz, C.; Linares, M.; Marin-Garcia, P.; Puyet, A.; Diez, A.; Bautista, J. M., Synchronous culture of *Plasmodium falciparum* at high parasitemia levels. *nat. protoc.* **2009**, *4*, 1899-1915.
169. Pavlishchuk, V. V.; Addison, A. W., Conversion constants for redox potentials measured versus different reference electrodes in acetonitrile solutions at 25°C. *Inorganica Chimica Acta* **2000**, *298*, 97-102.
170. Lauer, M. G.; Thompson, M. K.; Shaughnessy, K. H., Controlling Olefin Isomerization in the Heck Reaction with Neopentyl Phosphine Ligands. *J. Org. Chem.* **2014**, *79*, 10837-10848.
171. Penn, L.; Shpruhman, A.; Gelman, D., Enantio- and Regioselective Heck-Type Reaction of Arylboronic Acids with 2,3-Dihydrofuran. *J. Org. Chem.* **2007**, *72*, 3875-3879.
172. Tschoerner, M.; Pregosin, P. S.; Albinati, A., Contributions to the Enantioselective Heck Reaction Using MeO-Biphep Ligands. The Case Against Dibenzylidene Acetone. *Organometallics* **1999**, *18*, 670-678.
173. Gratia, S.; Mosesohn, K.; Diver, S. T., Highly Selective Ring Expansion of Bicyclo[3.1.0]hexenes. *Organic Letters* **2016**, *18*, 5320-5323.

## 5. List of Abbreviations

Å	Angstrom	DCBA	Di(cyclohexyl) <sup>iso</sup> butylamin
Ac	Acetyl	DCM	dichloromethylene
Acr	acridinium	DIPEA	di( <sup>iso</sup> propyl)ethylamine
ADHD	<u>A</u> ttention <u>D</u> eficiency <u>H</u> yperactivity <u>D</u> isorder	ΔT	elevated temperature
ADHS	<u>A</u> ufmerksamkeits <u>d</u> efizit und <u>H</u> yperaktivitäts <u>s</u> törung	DMF	dimethylformamide
AIBN	azobis( <sup>iso</sup> butyronitrile)	DMSO	dimethylsulfoxide
aq	aqueous	dtbbpy	di <sup>tert</sup> butylbispyridin
Ar	aryl	EA	<u>E</u> lectron <u>A</u> cceptor
ATRA	Atom Transfer Radical Addition	ED	<u>E</u> lectron <u>D</u> onor
ATR-IR	<u>A</u> ttenuated <u>T</u> otal <u>R</u> eflection <u>I</u> nfr <u>a</u> red Spectroscopy	EDTA	ethylenediamintetraacetate
BDMAP	1,6-bis(dimethylamino)pyrene	ee	enantiomeric excess
Bn	benzyl	<i>e.g.</i>	<i>exempli gratia</i> = for example
Boc	<sup>tert</sup> butyloxycarbonyl	ET	Electron Transfer
Box	bisoxazolin	<i>et al.</i>	<i>et alii</i> = and others
bpy	2,2'-bipyridin	EtOAc	ethyl acetate
bpz	2,2'-bipyrazin	FT-IR	<u>F</u> ourier- <u>T</u> ransform <u>I</u> nfr <u>a</u> red Spectroscopy
<sup>n</sup> Bu	n-butyl	HOMO	<u>H</u> ighest <u>O</u> ccupied <u>M</u> olecular <u>O</u> rbital
<sup>t</sup> Bu	tert-butyl	HPLC	<u>H</u> igh <u>P</u> ressure <u>L</u> iquid <u>C</u> hromatography
dap	2,9-dianisoyl-1,10- phenanthrolin	IC50	Half Maximal <u>I</u> nhibitory <u>C</u> oncentration
Cat	Catalyst	<i>i.e.</i>	<i>id est</i> = that is
DCA	9,10-dicyanoanthracene	IET	<u>I</u> nternal <u>E</u> lectron <u>T</u> ransfer
DCC	Di(cyclohexyl)carbodiimide	LAH	<u>l</u> ithium <u>a</u> luminium <u>h</u> ydride



LED	<u>L</u> ight <u>E</u> mitting <u>D</u> iode	TGA	<u>T</u> hermogravimetric <u>A</u> nalysis
Me	methyl	TFA	trifluoroacetic acid
Mes	mesityl	THF	tetrahydrofuran
m.p.	melting point	TLC	<u>T</u> hin <u>L</u> ayer <u>C</u> hromatography
NBS	<i>N</i> -bromosuccinimide	TMS	Trimethylsilyl
NMR	<u>N</u> uclear <u>M</u> agnetic <u>R</u> esonance	Ts	4-toluenesulfonyl
NPht	<i>phthalimidyl</i>	Q	Quencher
Pg	Protecting group	Ref.	Reference
Ph	phenyl	SET	<u>S</u> ingle <u>E</u> lectron <u>T</u> ransfer
<sup><i>i</i></sup> Pr	<sup><i>iso</i></sup> propyl	UV	ultraviolet
ppy	2-phenylpyridin	vs.	<i>versus</i> = opposite to / in contrast to
R	residue	vssl.	voraussichtlich
rac	racemic		
r.t.	room temperature		
sat	saturated		
SCE	<u>S</u> tandard <u>C</u> alomel <u>E</u> lectrode		
SI	<u>S</u> upporting <u>I</u> nformation		

**6. Curriculum Vitae**



## 7. Acknowledgements

Mein Dank gilt meinem Doktorvater Prof. Dr. Oliver Reiser, der mir während meines Bachelorstudiums einen Aufenthalt an der UC Berkeley ermöglichte, unter dessen Anleitung ich meine Masterarbeit anfertigte und der mich schließlich in seine Arbeitsgruppe aufnahm und mich bei meiner Bewerbung um ein Promotionsstipendium unterstützte. Seine wertvolle konstruktive Kritik erlaubte mir persönliche und fachliche Weiterentwicklung.

Für fachliche, technische und moralische Unterstützung danke ich Herrn Dr. Peter Kreitmeier, dessen Fachkenntnis und persönlicher Einsatz die Arbeiten an dieser Dissertation ermöglichten. Auch unseren Technikern Klaus Döring, Helena Konkel, Roxane Harteis, Brigitte Eichenseher und Johannes Floss gilt mein Dank. Durch großen Einsatz trugen Dr. Peter Kreitmeier und Johannes Floß entscheidend zum Peroxid-projekt bei, wofür ich ihnen besonders dankbar bin.

Ich bedanke mich bei den Mitarbeitern der zentralen Analytik der Universität für Durchführung und Unterstützung bei der Auswertung von NMR, Massenspektroskopie und Kristallstrukturanalyse.

Beim Sekretariat des Lehrstuhls, Frau Michaela Schüle und Frau Antje Weigert, bedanke ich mich für Unterstützung und Bearbeitung von organisatorischen und bürokratischen Angelegenheiten jeglicher Art. Bei Frau Dr. Petra Hilgers bedanke ich mich für die Begleitung im Rahmen des Graduiertenkollegs Photokatalyse.

Ich danke meinen lieben Laborkollegen, die ich über die Jahre hatte – Dr. Christian Faderl, Dr. Christian Eichinger, Andreas Hartl sowie Dr. Matthias Knorn, dessen Arbeitsplatz ich zunächst übernehmen durfte. Ohne meine Kollegen hätte ich nie die Zeit durchgehalten, und wäre sicher nicht so gerne ins Labor gekommen – Danke für ein offenes Ohr, für die Geduld mit meinen Launen und die gute Zusammenarbeit & Freundschaft.

Ich danke Tobias Babl dafür, dass er seine Bachelorarbeit mit mir durchgestanden hat, und später als Doktorand zur Arbeitsgruppe stieß – ich wünsche ihm für die Zukunft alles Gute!

Ich danke meinen Forschungspraktikantinnen und Forschungspraktikanten, derer ich einige zu meinen Freunden in der Arbeitsgruppe zählen darf. Viktoria Scheidler, Carina Sonnleitner und Robert Eckl stießen als Masteranden zur Arbeitsgruppe; mit Carina konnte ich später auch für den Regensburger Halbmarathon trainieren - danke für die Motivation!

Auch allen weiteren gegenwärtigen und ehemaligen Angehörigen des Arbeitskreises Reiser gilt mein herzlicher Dank für entgegengebrachtes Vertrauen, für fachlichen Rat, für persönlichen Rat, für gemeinsames Lachen, und für so viel mehr. Danke, dass ihr mich während meiner Zeit am AK Reiser begleitet habt!

Leider habe ich während dieser Arbeit auch einen guten Freund noch aus Schultagen, Ralph, an den Krebs verloren. Ich bedauere, dass wir nicht mehr gemeinsam den Abschluss unserer jeweiligen Promotionsarbeiten feiern können. Du fehlst!

Meinen Freunden in und ausserhalb der Uni, in der Friedrich-Ebert-Stiftung, in Regensburg und wo auch immer sie sich gerade rumtreiben, danke ich für die guten Gespräche und die schöne Zeit, die wir gemeinsam hatten und haben. Danke dass ihr mein Leben lebenswert macht!

Meinem guten Freund Ulrich Sattler danke ich für ein immer offenes Ohr, seine Hilfsbereitschaft und Unterstützung, und die gemeinsamen Ausflüge zu seinem Kamerunschaf Bocki.

Besonders bedanken möchte ich mich bei meiner Freundin Natalija, für ihre Unterstützung und Motivation, und dass ich oft mit ihr zusammen lachen kann.

Zu guter Letzt bedanke ich mich bei meinen Eltern und meiner ganzen Familie, dass sie stets an mich geglaubt haben, für die bedingungslose Unterstützung und Liebe. Danke - ich weiß dass diese Arbeit nicht nur mich gefordert hat.



## 8. Declaration

Herewith I declare that this thesis is a presentation of my original work, prepared single-handedly unless otherwise noted. Contributions of others are marked clearly with reference to the literature, license or acknowledgement of collaborative research.

Ich erkläre hiermit, dass die vorgelegte Dissertationsschrift, soweit nicht anders angegeben, der Ausfluss meiner eigenen, eigenhändigen Arbeit ist. Beiträge anderer sind klar als solche gekennzeichnet unter Angabe der jeweiligen Literaturstelle oder Anerkennung der Kollaborationsleistung.

Simon Budde

Regensburg, xx.xx.2020